Mechanical and microstructural properties of different FRP composites under various environmental conditions

Milad Bazli

M.Sc. in Structural and Earthquake Engineering

A thesis submitted for the degree of Doctor of Philosophy at Monash University in 2020

Department of Civil Engineering

Copyright notice

Abstract

Use of fibre-reinforced polymer (FRP) composites is rapidly increasing in automotive, aerospace, and marine applications, as well as in civil engineering. Due to the outstanding characteristics of FRP composites, especially their corrosion resistance properties, they are known as an appropriate alternative material to the traditional steel reinforcement when used in aggressive environments and with corrosive materials. However, despite the numerous advantages of these materials, concerns still exist regarding the durability of FRPs under aggressive environments, such as alkalinity, acidic, seawater, and ultraviolet radiation (UV), as well as temperature fluctuations and hydrothermal effects. This lack of knowledge is one of the most important factors delaying the widespread acceptance of such materials as load carrying structural elements.

In this PhD thesis the mechanical and microstructural properties of various FRPs when exposed to different harsh environments and used with concrete (i.e. seawater and sea sand concrete (SWSSC)) are investigated. To study the mechanical properties of several types of FRP under environmental conditions, different mechanical tests, including three-point bending, charpy impact, compression, tensile, split-disk, and push-out, were carried out. Moreover, to investigate the microstructural properties and degradation mechanisms, scanning electron microscopy (SEM) and micro computed tomography (micro- CT) analyses were conducted. Regression models (linear Bayesian regression) and long-term performance models (using Arrhenius law) were constructed to predict short-term and long-term mechanical properties of different FRPs under different conditions. Finally, reduction factors for different environments were proposed based on the experimental results and long-term performance models.

Numerous parameters affecting the performance of FRP composites under different environmental and loading conditions were studied. The variables, in terms of FRPs, taken into account were (1) fibres type (glass, carbon and basalt), (2) fibres length and orientation, (3) fabrication type (pultrusion, filament winding and vacuum infusion process), and (4) geometrical properties of FRP composites (various sections of FRP profiles were studied). Environmental conditioning in this research were classified into three categories: (1) harsh ambient conditions, namely elevated temperatures, UV and moisture cycles, and freeze/thaw cycles; (2) alkalinity environment (i.e. using FRPs with SWSSC); (3) combination of harsh ambient environment and a SWSSC. The variables, in terms of conditioning, taken into account were (1) the time in all conditions and (2) the temperature in some conditions.

Thesis outline

This PhD thesis, is presented in three main sections. First section includes the mechanical and microstructural properties of different FRPs under harsh ambient environmental conditions. With this regard, the obtained results of various types of FRP composites performance under harsh ambient environmental conditions, including elevated temperatures, UV radiation and moisture cycles, freeze/thaw cycles with-out the presence of moisture and freeze/thaw cycles with the presence of moisture are presented. In second section, the mechanical and microstructural properties of FRPs when used in civil applications (i.e. SWSSC filled FRP tubes under seawater condition) are reported. With this regard, the bond performance between different FRP tubes and SWSSC, the bond durability under seawater, and material properties degradation of tubes when exposed to SWSSC and seawater conditions are presented. Last section includes the combination of harsh ambient environmental conditions and SWSSC environments. In this section, the behaviour of different FRP composites after exposure to UV radiation and moisture cycles and freeze/thaw cycles firstly and then to SWSSC is presented. Finally, design suggestions, in terms of reduction factors for civil applications are proposed for different FRPs under various environmental conditions. This publication-based PhD thesis, contains eleven chapters. A brief discerption for each chapter is as follow:

Chapter 1 Introduction

Briefly in this chapter, first, the research backgrounds in terms of using innovative materials in civil applications, particularly FRP composites and SWSSC as alternatives to conventional steel reinforcement and OPC-based concretes, is presented. Later, the significance of studying the durability of FRP composites is pointed out. By reviewing the literature, the available gaps regarding the durability of FRP composites under harsh environmental conditions and when used with SWSSC are highlighted. Further, the novelty of the thesis and the contribution of the research to the current literature is explained. Finally, the research objectives and program, namely conditioning procedure, mechanical tests, and microstructural analyses are introduced.

Chapter 2 Effect of thickness and reinforcement configuration on flexural and impact behaviour of GFRP laminates after exposure to elevated temperatures

Briefly, in this chapter the mechanical (i.e. flexural and impact) and microstructure properties (i.e. SEM analyses) of vacuum infusion GFRP laminates after exposure to elevated temperature are presented. The parameters investigated are the effect of fibre’s length and orientation, laminate’s thickness and exposing time. In addition, regression models are proposed to obtain the flexural and impact properties retentions.

Chapter 3 Effect of fibres configuration and thickness on tensile behaviour of GFRP laminates exposed to harsh environment

Briefly, in this chapter the mechanical (i.e. tensile) and microstructure properties (i.e. SEM analyses) of vacuum infusion GFRP laminates under (1) freeze/thaw cycles without the presence of moisture, (2) freeze/thaw cycles with the presence of moisture and (3) UV radiation and water vapour condensation cycles are presented. The parameters investigated are the effect of fibre's length and orientation, laminate's thickness and exposing time. In addition, regression models are proposed to obtain the tensile properties retentions.

Chapter 4 Effects of UV radiation, moisture and elevated temperature on mechanical properties of GFRP pultruded profiles

Briefly, in this chapter the mechanical (i.e. bending, tensile and compressive) and microstructure properties (i.e. SEM analyses) of pultruded GFRPs under UV radiation and water vapour condensation cycles are presented. The parameters investigated are the effect of profile cross section and exposing time. In addition, regression models are proposed to obtain the mechanical properties retentions.

Chapter 5 Bond-slip behaviour between FRP tubes and seawater sea sand concrete

Briefly, in this chapter the bond-slip performance between FRP (Pultruded and filament winding) tubes and seawater sea sand concrete is presented. The parameters investigated are the effect of fibres type (GFRP, CFRP and BFRP), fibres orientation, and tube thickness. Also, the quantified mechanical and chemical bond strength between the concrete and FRP tubes are presented and compared with each other. Finally, regression model is proposed to predict the bond strength between the FRP tubes and SWSSC.

Chapter 6 Bond performance between FRP tubes and seawater sea sand concrete after exposure to seawater condition

Briefly, in this chapter the durability of the bond-slip performance between FRP (Pultruded and filament wound) tubes and seawater sea sand concrete under seawater condition are presented. The parameters investigated are the effect of fibre type (GFRP, CFRP and BFRP) and time and temperature of the conditioning. The changes in bond performance compared to the reference samples are presented and the reduction factors are proposed.

Chapter 7 Durability of pultruded GFRP tubes subjected to seawater sea sand concrete and seawater environments

Briefly, in this chapter the mechanical (i.e. tensile and compressive) and microstructure properties (i.e. SEM and micro-CT analyses) of pultruded FRP tubes under SWSSC and seawater are presented. The parameters investigated are the effect of conditioning type, tube thickness, and time and temperature of conditioning. Degradation mechanisms and voids increment are investigated using microstructural analyses. Finally, the long-term performance of the tubes is predicted and the reduction factors are proposed.

Chapter 8 Durability of filament wound FRP tubes subjected to seawater sea sand concrete and seawater environments

Briefly, in this chapter the mechanical (i.e. disk-split tensile and compressive) and microstructure properties (SEM and CT X-ray analyses) of filament wound FRP tubes under SWSSC and seawater are presented. The parameters investigated are the effect of fibre type (GFRP, CFRP and BFRP), fibre orientation, and time and temperature of conditioning. Degradation mechanisms and voids increment are investigated using microstructural analyses. Finally, long-term performance of the tubes is predicted and the reduction factors are proposed.

Chapter 9 Mechanical properties of pultruded GFRP profiles under seawater sea sand concrete environment coupled with UV radiation and moisture

Briefly, in this chapter the mechanical (i.e. bending, tensile and compressive) and microstructure properties (SEM analyses) of pultruded GFRP profiles when used with SWSSC after exposure to harsh daily environmental conditions are presented. The sequence of conditioning is (1) exposing UV and water vapour condensation cycles for different periods and (2) exposing to certain time of SWSSC environment. The parameters investigated are the effect of profile cross section, conditioning type and exposing time. In addition, regression models are proposed to obtain the mechanical properties retentions.

Chapter 10 Durability of GFRP composites under seawater and sea sand concrete coupled with harsh outdoor environments

Briefly, in this chapter the mechanical (i.e. bending, tensile and compressive) and microstructure properties (SEM analyses) of pultruded GFRP profiles when used with SWSSC after exposure to harsh daily environmental conditions are presented. The sequence of conditioning is (1) exposing to freeze/thaw cycles for different periods and (2) exposing to certain time of SWSSC environment. The parameters investigated are the effect of profile cross section, conditioning type and exposing time. In addition, regression models are proposed to obtain the mechanical properties retentions.

Chapter 11 Conclusions and future works

In this section, the general conclusions found in previous chapters are presented and recommendations for the environmental reduction factors are proposed for consideration in current FRP standards and codes. Recommendations for the future studies are also presented.

The thesis outline of chapters 2 to 10 are illustrated in **Fig.A.1**.

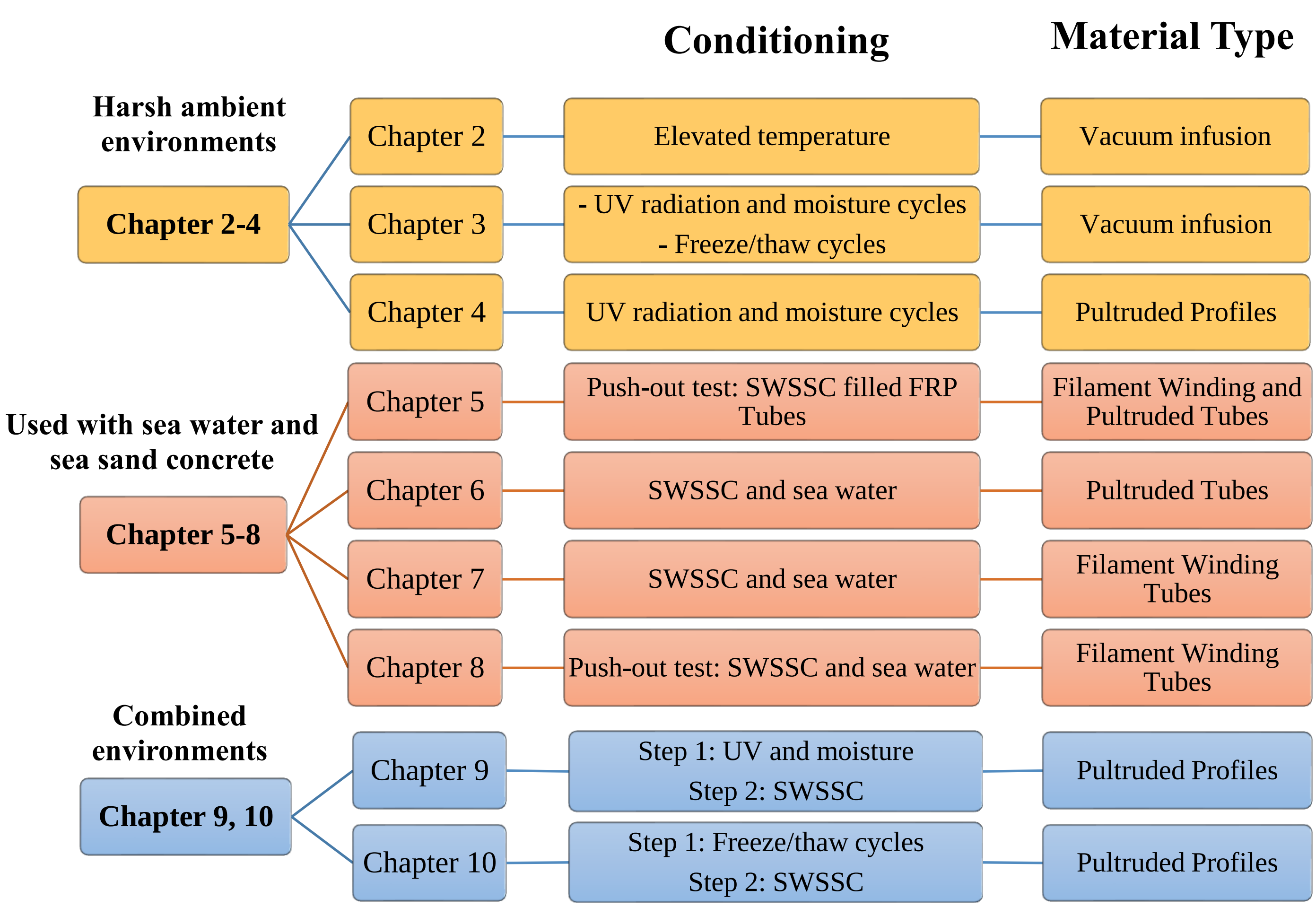

Fig. A.1: Thesis out-line of chapters 2 to 10

Note:

It should be noted that the format of this PhD thesis follows Monash University format of "Thesis including published works", in which a separate "Literature Review" chapter is not presented as each published paper includes relevant introduction and literature review itself. Because chapter 2 to chapter 10 are published journal papers, each chapter has abstract, keyword, and introduction. Based on the Monash University policy, simply photocopying the published papers as part of the thesis is not allowed. The contents in Chapters 2 to 10 are the same as those in published papers, except that the numbering of figures and tables is changed to suit each chapter. Acknowledgements of all the chapters are listed on page XX, whereas references of all the chapters are listed at the end of the thesis to avoid repetition.

Declaration

I hereby declare that this thesis contains no material which has been accepted for the award of any other degree or diploma at any university or equivalent institution and that, to the best of my knowledge and belief, this thesis contains no material previously published or written by another person, except where due reference is made in the text of the thesis.

Milad Bazli

June 2020

Publications during enrolment

Peer reviewed published journal papers:

[1] **Bazli, M.**, Ashrafi, H., Jafari, A., Zhao, X. L., Gholipour, H., & Oskouei, A. V. (2019). Effect of thickness and reinforcement configuration on flexural and impact behaviour of GFRP laminates after exposure to elevated temperatures. Composites Part B: Engineering, 157, 76-99.

[2] **Bazli, M.**, Jafari, A., Ashrafi, H., Zhao, X. L., Bai, Y., & R.K. Singh. (2020). Effects of UV radiation, moisture and elevated temperature on mechanical properties of GFRP pultruded profiles. Construction and Building Materials, 231, 117137.

[3] **Bazli, M.**, Zhao, X. L., Bai, Y., R.K. Singh, & Al-Saadi, S. (2019). Bond-slip behaviour between FRP tubes and seawater sea sand concrete. Engineering Structures, 197, 109421.

[4] **Bazli, M.**, Zhao, X. L., Bai, Y., R.K. Singh, Al-Saadi, S., & Haque, A. (2020). Durability of pultruded GFRP tubes subjected to seawater sea sand concrete and seawater environments. Construction and Building Materials, 245, 118399.

[5] **Bazli, M.**, Ashrafi, H., Jafari, A., Zhao, X. L., R.K. Singh, & Bai, Y. (2019). Effect of fibers configuration and thickness on tensile behavior of GFRP laminates exposed to harsh environment. Polymers, 11(9), 1401.

[6] **Bazli, M.**, Zhao, X. L., Raman, R. S., Bai, Y., & Al-Saadi, S. (2020). Bond performance between FRP tubes and seawater sea sand concrete after exposure to seawater condition. Construction and Building Materials, 265, 120342.

[7] **Bazli, M.**, Li, Y. L., Zhao, X. L., Raman, R. S., Bai, Y., Al-Saadi, S., & Haque, A. (2020). Durability of seawater and sea sand concrete filled filament wound FRP tubes under seawater environments. Composites Part B: Engineering, 108409.

[8] **Bazli, M.**, Zhao, X. L., Jafari, A., Ashrafi, H., Bai, Y., Raman, R. S., & Khezrzadeh, H. (2020). Mechanical properties of pultruded GFRP profiles under seawater sea sand concrete environment coupled with UV radiation and moisture. Construction and Building Materials, 120369.

[9] **Bazli, M.**, Zhao, X. L., Jafari, A., Ashrafi, H., Raman, R. S., Bai, Y., & Khezrzadeh, H. (2020). Durability of glass-fibre-reinforced polymer composites under seawater and sea-sand concrete coupled with harsh outdoor environments. Advances in Structural Engineering, 1369433220947897.

Peer reviewed conference papers

[10] **Bazli, M.**, Zhao, X. L., Bai, Y, R.K. Singh, Al-Saadi, S. (2019). Durability of pultruded GFRP tubes under sea water sea sand concrete. Seventh Asia-Pacific Conference on FRP in Structures (APFIS 2019), 1-4.

[11] **Bazli, M.**, Zhao, X. L., Bai, Y, R.K. Singh, Al-Saadi, S. (2019). Bond strength durability between FRP tubes and seawater sea sand concrete under sea water condition. Seventh Asia-Pacific Conference on FRP in Structures (APFIS 2019), 1-4.

Thesis including published works declaration

I hereby declare that this thesis contains no material which has been accepted for the award of any other degree or diploma at any university or equivalent institution and that, to the best of my knowledge and belief, this thesis contains no material previously published or written by another person, except where due reference is made in the text of the thesis.

This thesis includes 9 original papers published in peer reviewed journals. The core theme of the thesis is Structural Engineering. The ideas, development and writing up of all the papers in the thesis were the principal responsibility of myself, the student, working within the Department of Civil Engineering under the supervision of Prof. Xiao-Ling Zhao, Prof. R.K. Singh Raman and Prof. Yu Bai.

(The inclusion of co-authors reflects the fact that the work came from active collaboration between researchers and acknowledges input into team-based research.)

In the case of Chapters 2-10 my contribution to the work involved the following:

Chapter	Publication Title	Journal/Status	Nature and % of student contribution	Co-author name(s) Nature and % of Co-author's contribution	Co-author Monash student
2	Effect of thickness and reinforcement configuration on flexural and impact behaviour of GFRP laminates after exposure to elevated temperatures	Composites Part B: Engineering /Published	Developing ideas, establishing methodologies, experimental work, data analysis, write up and revision, 70%	1) Mr. Hamed Ashrafi: Developing ideas, input into manuscript, revision, 8% 2) Mr. Armin Jafari: Developing ideas, Input into manuscript, revision, 8% 3) Prof. Xiao-Ling Zhao: Developing ideas, Input into manuscript, revision, financial support, 8% 4) Mr. Hamed Gholipour: revision, 3% 5) A/Prof. Asghar Vatani Oskouei: revision, 3%	Yes
3	Effect of Fibres configuration and thickness on tensile behaviour of GFRP laminates exposed to harsh environment	Polymers/Published	Developing ideas, establishing methodologies, experimental work, data analysis, write up and revision, 70%	1) Mr. Hamed Ashrafi: Developing ideas, input into manuscript, revision, 6% 2) Mr. Armin Jafari: Developing ideas, Input into manuscript, revision, 6% 3) Prof. Xiao-Ling Zhao: Developing ideas, Input into manuscript, revision, financial support, 6% 4) Prof. R.K. Raman Singh: Input into manuscript, financial support revision, 6% 5) Prof. Yu Bai: Input into manuscript, revision, 6%	Yes
4	Effects of UV radiation, moisture and elevated temperature on mechanical properties of GFRP pultruded profiles	Construction and Building Materials/Published	Developing ideas, establishing methodologies, experimental work, data analysis, write up and revision, 70%	1) Mr. Armin Jafari: Developing ideas, input into manuscript, revision, 6% 2) Mr. Hamed Ashrafi: Developing ideas, Input into manuscript, revision, 6% 3) Prof. Xiao-Ling Zhao: Developing ideas, Input into manuscript, revision, financial support, 6% 4) Prof. Yu Bai: Input into manuscript, revision, 6% 5) Prof. R.K. Raman Singh: Input into manuscript, financial support revision, 6%	Yes
5	Bond-slip behaviour between FRP tubes and seawater sea sand concrete	Engineering Structures/Published	Developing ideas, establishing methodologies, experimental work, data analysis, write up and revision, 70%	1) Prof. Xiao-Ling Zhao: Developing ideas, Input into manuscript, revision, financial support, 15% 2) Prof. Yu Bai: Input into manuscript, revision, 6% 3) Prof. R.K. Raman Singh: Input into manuscript, financial support revision, 6% 4) Dr. Saad Al-Saadi: revision, 3%	No
6	Bond performance between FRP tubes and seawater sea sand concrete after exposure to seawater condition	Construction and Building Materials /Published	Developing ideas, establishing methodologies, experimental work, data analysis, write up and revision, 70%	1) Prof. Xiao-Ling Zhao: Developing ideas, Input into manuscript, revision, financial support, 15% 2) Prof. R.K. Raman Singh: Input into manuscript, financial support revision, 6% 3) Prof. Yu Bai: Input into manuscript, revision, 6% 4) Dr. Saad Al-Saadi: revision, 3%	No

7	Durability of pultruded GFRP tubes subjected to seawater sea sand concrete and seawater environments	Construction and Building Materials /Published	Developing ideas, establishing methodologies, experimental work, data analysis, write up and revision, 70%	1) Prof. Xiao-Ling Zhao: Developing ideas, Input into manuscript, revision, financial support, 15% 2) Prof. Yu Bai: Input into manuscript, revision, 5% 3) Prof. R.K. Raman Singh: Input into manuscript, financial support revision, 5% 4) Dr. Saad Al-Saadi: revision, 2.5% 5) Dr. Asadul Haque: revision 2.5 %	No
8	Durability of seawater and sea sand concrete filled filament wound FRP tubes under seawater environments	Composites Part B: Engineering /Published	Developing ideas, establishing methodologies, experimental work, data analysis, write up and revision, 60%	1) Dr. Yinglei-Li: establishing methodologies, experimental work, data analysis, write up and revision, 20% 2) Prof. Xiao-Ling Zhao: Developing ideas, Input into manuscript, revision, financial support, 10% 3) Prof. R.K. Raman Singh: Input into manuscript, financial support revision, 3% 4) Prof. Yu Bai: Input into manuscript, revision, 3% 5) Dr. Saad Al-Saadi: revision, 2% 6) Dr. Asadul Haque: revision 2 %	No
9	Mechanical properties of pultruded GFRP profiles under seawater sea sand concrete environment coupled with UV radiation and moisture	Construction and Building Materials/Published	Developing ideas, establishing methodologies, experimental work, data analysis, write up and revision, 70%	1) Prof. Xiao-Ling Zhao: Developing ideas, Input into manuscript, revision, financial support, 10% 2) Mr. Armin Jafari: Developing ideas, input into manuscript, revision, 4% 3) Mr. Hamed Ashrafi: Developing ideas, Input into manuscript, revision, 4% 4) Prof. Yu Bai: Input into manuscript, revision, 4% 5) Prof. R.K. Raman Singh: Input into manuscript, financial support revision, 4% 6) A/Prof. Hamed Khezrzadeh: revision, 4%	Yes
10	Durability of GFRP composites under seawater and sea sand concrete coupled with harsh outdoor environments	Advances in Structural Engineering/Published	Developing ideas, establishing methodologies, experimental work, data analysis, write up and revision, 70%	1) Prof. Xiao-Ling Zhao: Developing ideas, Input into manuscript, revision, financial support, 10% 2) Mr. Armin Jafari: Developing ideas, input into manuscript, revision, 4% 3) Mr. Hamed Ashrafi: Developing ideas, Input into manuscript, revision, 4% 4) Prof. R.K. Raman Singh: Input into manuscript, financial support revision, 4% 5) Prof. Yu Bai: Input into manuscript, revision, 4% 6) A/Prof. Hamed Khezrzadeh: revision, 4%	Yes

I have renumbered sections of published papers in order to generate a consistent presentation within the thesis.

Student: Milad Bazli Date: 30/06/2020

The undersigned hereby certify that the above declaration correctly reflects the nature and extent of the student's and co-authors' contributions to this work. In instances where I am not the responsible author I have consulted with the responsible author to agree on the respective contributions of the authors.

Main Supervisor: Prof. Xiao-Ling Zhao Date: 30/06/2020

Acknowledgements

Firstly, I would like to sincerely thank my main supervisor, Prof. Xiao-Ling Zhao, for his guidance, support and patience during my PhD adventure. His friendly attitude, together with his knowledge greatly contribute to my successful PhD completion in an exceptional time.

My deep thanks are also extended to my co-supervisors, Prof. R.K. Singh Raman and Prof. Yu Bai, for their help, supports and contributions to during my PhD candidature. I would also like to thank Dr. Saad Al-Saadi for his help and contribution on several parts of this thesis.

Thanks are given to Monash University for offering the PhD scholarships and to Australia Research Council for financial support of the project through an ARC Discovery Grant (DP160100739). I also would like to acknowledge Monash Civil Engineering Laboratory, Mr. Damian Carr of Bayside City Council for his permission to provide seawater and sea sand, Dr. Asadul Haque for conducting X-ray CT scans, Monash Centre for Electron Microscopy (MCEM), and CST composites for suppling FRP materials. My thanks are expressed to people who offered help on the experimental works, including technical staffs of Monash Civil Engineering Laboratory, Dr. Ying-Lei li, Mr. Hamed Ashrafi, Mr. Armin Jafari, and Mr. Esmaeil Pournamazian.

My deepest appreciation goes to my parents and my partner, for their love and support.

Finally, I would like to thank all individuals whose names are not mentioned here but kindly participate in this multidisciplinary thesis.

Milad Bazli

June 2020

Table of Contents

List of Figures

List of Tables

Chapter 1 Introduction

1.1 Background

In the past few decades Fibre Reinforced Polymer (FRP) composite materials are widely being used for different purposes, including automotive and aerospace applications [1, 2] as well as construction applications [3] (especially marine applications [4]). Several advantages, such as high strength and stiffness-to-weight ratios, outstanding corrosion resistance and ease of use and handling [5-7] have made them as alternatives to traditional steel reinforcements when working in damaging environments like marine settings [8].

Production of conventional concrete (about 25 billion tonnes in 2016 [9]), needs a huge amount of recourses (i.e. river sand and fresh water), which results environmental and ecological problems. Recently, as an interesting solution to prevent river sand and water shortages, seawater and sea sand concrete (SWSSC) has been proposed as an alternative to OPC-based concretes. According to the previous studies, it has been found that the mechanical properties of SWSSC, including the workability, short term (28-day) and long term compressive strengths are almost the same as the conventional OPC-based concretes [10]. It has been also reported that using geo-polymers in SWSSC will significantly reduce the concrete cracking of conventional concretes due to the alkali silica reaction (ASR) [11]. However, due to replacing fresh water and river sand in OPC-concrete with sea water and sea sand in SWSSC, and consequently presence of high chloride content, traditional steel reinforcements will significantly be corroded if used for reinforcing the concrete members [12, 13]. Therefore, FRP composites as corrosion resistant materials can also be used to overcome the corrosion problems of traditional steel reinforcement when used with SWSSC. As mentioned earlier, FRPs, which are highly resistant to chloride ions, are interesting alternatives to conventional metallic materials, which are vulnerable to electrochemical corrosion [14]. In addition to their corrosion resistance, the considerably lighter weight of FRPs, makes an enormous difference in construction sites, by easing the handling and use compared to conventional steel structures. Such advanced materials could also be used to retrofit/strengthen the existing offshore structures and infrastructures, which will significantly increase the life-span of such expensive structures. Therefore, using FRPs and geopolymer SWSSC as advanced materials in construction and particularly in offshore structures, such as piers and foundations enables the fabrication of durable and cost-effective structures and significantly decreases the CO_2 emission caused by the conventional steel and concrete production processes.

Considering the applications of FRPs in versatile conditions, they are liable to be exposed to different environmental conditions, such as elevated temperatures, moisture, UV radiation and freeze/thaw cycles. This may occur during transportation and storage as well as during their life-service on a daily basis [15, 16]. Moreover, based on the previous studies [17, 18], using FRPs with concrete (e.g. concrete filled FRP tubes), which is one the most important applications of FRPs in construction, results in degradation of FRPs' mechanical properties.

When FRPs are subjected to elevated temperatures, their mechanical properties may be degraded, which is mainly related to the resin and resin/fibre interface degradation and less to the fibre degradation [19-21]. Significant degradation of FRPs under elevated temperatures occurs when the resin glass transition temperature (T_g) is reached. This is due to state change of the resin from glassy to a rubbery, which leads to weakening the load transfer capacity between the resin and fibres. Glass transition temperature of composites varies according to resin type and fabrication process (about 50 °C - 120 °C [22]). This degradation will significantly increase when the temperature reaches the resin decomposition temperature (Td). Decomposition temperature of composites starts from about 300 °C

The mechanical properties degradation of FRPs when subjected to UV radiation is mainly related to the chemical changes of the resin. These changes include complex processes involving UV radiation and oxygen. Photochemical degradation reactions will also be involved in processes [23, 24]. It is known that the light photons interact with the molecular chains of polymers, which initiate photo degradation. The wavelength of the UV photons when they reach the surface of the earth, which is about 6% of solar radiant flux, is almost the same as the wavelength needed for dissociation the chemical bonds of many polymers, which is about 290 – 460 kJ/mole [25]. This is known as the reason for vulnerability of polymeric materials to UV radiation.

The potential degradation due to the diffusion of moisture into the FRP composites includes resin matrix swelling, cracking, plasticisation, hydrolysis and fibre/resin interface debonding. All these possible damages cause the degradation of FRP mechanical properties [26, 27].

When FRPs are subjected to subzero temperatures, resin matrix hardening and microcracks are the possible factors for mechanical properties degradation. Thermal expansion coefficient difference between the resin and fibres increases the internal stress and leads to fibre/resin debonding when subjecting to thermal variations. Therefore, one can conclude that thermal cycles at low temperatures is harsher environment for FRPs compare to constant exposure to freezing temperatures [49].

The potential degradation due to the diffusion of moisture into the FRP composites includes resin matrix swelling, cracking, plasticisation, hydrolysis and fibre/resin interface debonding. All these

possible damages cause the degradation of FRP mechanical properties [26, 27]. When FRPs are subjected to sea water, in addition to the degradation due to the moisture diffusion, blisters and solid compounds occur on their surfaces. Blisters results osmotic pressures between sea water and FRP surface, which deforms the resin, and consequently results to mechanical properties degradation [28].

Regarding the alkaline environment, when FRPs are used with concrete, various damages, in terms of resin [29], fibre [18], and fibre/resin interface deteriorations occurs [30]. Resin damages include swelling, cracking, alkaline hydrolysis, delamination, and plasticization. Moisture absorption and chemical diffusion are the main reasons for these damages [31-33]. Glass and basalt fibres damages are due to the metallic cations leaching out of the fibre's surface and breaking the Si-O-Si bonds by hydroxyl ions (etching) [34, 35]. However, in contrast to glass and basalt, carbon fibres are almost resistant to chemical environments [36]. Finally, the fibre/resin interface deterioration includes delamination, debonding and osmotic cracking [37]. It is worth mentioning that the mechanical properties degradation of FRP composites is mainly attributed to the interface damages rather than resin and fibres damages [38].

Generally, it can be concluded that FRPs are vulnerable to harsh environmental conditions. However, some conditions have higher detrimental effects on mechanical and microstructural properties and some have lesser.

Considering the above degradation mechanisms of FRP composites under harsh environmental conditions, regardless of the outstanding characteristics of such materials, their short-term and long-term performances under different environmental conditions need to be studied carefully. Therefore, in this PhD thesis, the various factors affecting the behaviour of FRPs under different environmental and loading conditions are investigated.

1.2 State of the art

In this section, literature with respect to the short-term and long-term performance of FRPs under various conditions is reviewed shortly and the available gaps are mentioned.

1.2.1 Elevated temperature

Based on the literature, studies about the FRP composites performance under elevated temperatures, are mostly focused on bars as the internal reinforcement [20, 38-42] and wraps and laminates [43-48] as external reinforcement used for retrofitting/strengthening the existing structures. The mechanical properties of FRP profiles and panels under elevated temperatures have also been investigated [49-54]. There are also some studies available on the post fire tensile [55, 56], compressive [56], flexural [56-59], and interlaminar shear [55, 56] strength of FRP composites.

According to the applications of FRPs in construction, as secondary elements (e.g. pedestrian bridge) and structural members, they may be subjected to impact loading in their life-span. Several studies have been conducted on the impact behaviour of FRPs [60] and FRP reinforced/retrofitted concrete structures [61]. However, the impact behaviour of FRP composites subjected to elevated temperatures is not studied. Moreover, research on the FRP composites performance under elevated temperatures, are carried out on samples with constant fibres length and orientation. However, it is well known that the fibre's length and orientation are important factors in FRPs strength, stiffness and impact properties. Based on the current literature, no study has been carried out to investigate such factors on the mechanical properties of FRP composites under elevated temperatures.

Regarding the FRP member thickness, it is known that the thickness has a significant effect on the flexural response of strengthened reinforced concrete (RC) members [62]. Also, regarding their behaviour under elevated temperatures, it seems that the thickness is an important factor in the deterioration level and damage penetration. This is due to the heat flux exposure time and temperature. However, studies considering the effect of FRP thickness on the mechanical properties under elevated temperatures are limited.

Therefore, considering the above facts and available research gaps, a comprehensive study to investigate the effect of fibre's length, fibre's orientation, laminate's thickness on the flexural and impact behaviour of GFRP laminates under elevated temperatures is needed.

1.2.2 Harsh ambient environments

Regarding the performance of FRP composites under harsh ambient environments, generally, existing research has shown degradation of mechanical properties after exposure to UV radiation, moisture, thermal cycles and elevated temperature [15, 63, 64]. Elevated temperatures, UV radiations, moisture, wet/dry and freeze/thaw cycles are among the aggressive environments that offshore structures will experience during their life-span. However, previous research mostly focused on the structural performance of members reinforced and/or strengthened with FRP [65-71]. Few studies are also available regarding degradation of FRP composites mechanical properties after exposing to harsh environments [39, 72, 73]. However, as mentioned earlier, previous studies are conducted on samples with constant thickness and fibres length and orientation [70, 72, 74] and the effect of thickness and fibres configuration on the durability of FRP composites under harsh ambient environments remained poorly studied. It is generally known that FRP composites have anisotropic behaviour due to coupling between the strains (direct and shear strains) [75]. Therefore, FRPs can be classified as almost orthotropic (along and normal to the member's longitudinal axes) [76] . However, the effects of fibre length and orientation on the mechanical properties of FRP composites under harsh environments have gathered very limited attentions. Therefore, FRPs with different fibres length and orientations (i.e. unidirectional, woven and chopped strand mat) have been used in this thesis.

In addition, the studies of FRPs performance under harsh ambient conditions are mostly focused on material views, and were carried out on FRP bars and laminates. However, the performance of FRP sections under such environments has received limited attention [15, 77, 78] and there is a significant lack of knowledge in these aspects of FRP commercial profiles, which are currently used for different constructional applications. The effect of freeze/thaw cycles on the performance of pultruded FRP section has been studied by Jafari et al [64]. However, no study has been conducted on the impact on FRP profiles' cross-sections on their mechanical properties when exposed to UV radiation, moisture and elevated temperature cycles.

Therefore, considering the above facts and available research gaps, comprehensive studies are needed to address the effects of fibre's length, fibre's orientation and cross section configuration on the mechanical properties of different FRP composites under harsh ambient environments.

1.2.3 FRP Using with concrete: SWSSC

1.2.3.1 Bond between FRP tubes and SWSSC

Because of several advantages, including high load-carrying capacity and appropriate seismic performance, concrete-filled tubes (CFTs) are extensively being used in civil applications, such as bridge piers, high-rise buildings and drilling platforms [79]. The bond between the concrete and the tube in composite columns, especially close to the end connections where the load transfer happens, is a critical factor [80]. Therefore, to obtain an appropriate composite action, understanding the bond-slip performance between the concrete and the tube is necessary.

There are several studies focused on the compressive behaviour of concrete filled FRP tubes under axial loads [8, 81-83]. There are also numerous studies concentrating on the bond between FRP bars and concrete [6, 13, 17, 84-86] as well as that between steel and FRP composites [87-93]. However, the studies on the bond between the concrete and FRP tubes are very limited.

On the other hand, all studies conducted on the bond between the concrete and FRP tubes were related to conventional OPC-based concrete and very limited FRP tube types. Consequently, the tube characteristics effect, including the fibre type and orientation is not addressed properly.

Therefore, considering the above facts and available research gaps, a comprehensive study is needed to address the effects of fibres type and orientation and tube thickness on the bond-slip performance between FRP tubes and SWSSC.

1.2.3.2 Bond durability between FRP tubes and SWSSC under seawater

Based on the literature, the durability of FRP composites under different environmental conditions related to civil engineering applications has been studied well [13, 18, 30, 94-98]. There are also limited studies available focusing on the durability of FRPs exposed to SWSSC under sea water condition [12, 99]. However, the bond durability between SWSSC and FRP composites under different environmental conditions, such as sea water, is not studied well.

Therefore, considering the above facts and available research gap, a comprehensive study is needed to address the bond durability between FRP tubes and SWSSC, considering different variables, such as effect of fibre type and orientation and tube fabrication method.

1.2.3.3 Durability of SWSSC filled FRP tubes under seawater

Due to the direct contact with harsh environments, such as sea water, acid rain, etc., carbon steel tubes used in CFTs are liable to be significantly corroded after long-term exposure to such harsh conditions [100]. To address this issue, using concrete-filled FRP tubes (CFFTs) has recently been proposed as an alternative to carbon steel reinforcement under aggressive environments, such as sea water [101-103]. It is worth mentioning that using corrosion-resistant FRP composites with SWSSC in coastal areas was firstly proposed by Teng [104] and has recently attracted researchers' attention.

Despite the appropriate corrosion resistant characteristic of FRP composites in coastal areas [105, 106], previous studies have shown that their durability when used with concrete (i.e. alkali environment) could be a critical issue and needs to be taken into account [95, 107, 108]. However, studies on their durability in alkaline environments are mostly related to OPC-based concretes environments [17, 109, 110]. Limited number of studies have been carried out on the durability of FRPs under SWSSC environment [12, 99, 111]. These studied mainly focused on the durability of compressive strength of

CFFTs, which do not provide sufficient information on the degradation of the FRP tube individually (i.e. individual components degradation of the tube, including fibre, resin, and fibre/resin interface). Considering the fact that when using CFFTs in marine environments, the inner and outer sides of the tubes are exposed to concrete and seawater condition, respectively, an in-depth study should be conducted to investigate the effect of this dual conditioning on the mechanical and microstructural properties of FRP tubes. However, very few studies are available in the literature with this regards [112].

Hence, to assuage this literature gap, a comprehensive study in needed to explore the durability mechanisms of different FRP tubes, when exposed to SWSSC and seawater, considering various factors, such as fibre type and orientation, tube cross section configuration and fabrication method, and time and temperature of conditioning.

1.3 Objectives

This PhD thesis focuses on the mechanical and microstructural properties of various FRP composites when exposed to SWSSC and harsh ambient environments. Mechanical tests, SEM and micro-CT analyses were used for this purpose. The objectives of this thesis were classified into five parts:

Preparing appropriate specimens

FRPs were fabricated using three different methods, including filament winding, vacuum infusion, and pultrusion, to investigate the effects of fabrication type, fibre orientation and specimen cross-section configuration.

Preparing accelerated conditioning environments

Five different simulated environmental conditions, including SWSSC, seawater, elevated temperatures, UV and water vapour cycles, and freeze/thaw cycles were used to investigate the effect of different environments.

Conducting mechanical tests

Different mechanical tests, including push-out, three-point bending, charpy impact, tensile, compression, and split-disk were conducted to investigate the mechanical properties of different FRPs under various loading and environmental conditions.

Conducting microstructural analyses

SEM and micro-CT analyses were performed to investigate the damage mechanisms and damage progression level after exposure to different environmental conditions.

Conducting statistical analyses

Analyses of variance (ANOVA), Bayesian linear regression (BLR), and long-term prediction performance (using Arrhenius law) were conducted to predict the short-term and long-term mechanical properties of FRPs under different loading and environmental conditions.

Chapter 2 Effect of thickness and reinforcement configuration on flexural and impact behaviour of GFRP laminates after exposure to elevated temperatures

Abstract

This study investigates the flexural and impact behaviour of GFRP laminates after exposure to elevated temperatures. The effect of fibre's length and orientation, laminate's and exposing time is studied. A total number of 540 tests in terms of three-point bending and Charpy impact tests were conducted to obtain the mechanical properties. In addition, SEM analyses were carried out to investigate the degradation mechanisms. Finally, statistical study was conducted to investigate the contribution of each variable and developing probabilistic models using ANOVA and linear Bayesian regression method. The results showed that generally the flexural and impact properties of GFRP laminates decreases by increasing the temperature and time of exposing as well as decreasing the laminates' thickness. It is also observed that laminates with unidirectional fibres have the best performance under elevated temperatures, while laminates with randomly distributed fibres are the most vulnerable type. The performance of laminates with woven fibres are almost between those two other types. However, all types of the laminates lost almost all their flexural strength and impact energy absorption capacity at 300 ˚C.

Key words

GFRP laminates; Elevated temperature; Bending; Charpy impact; Fibre orientation

2.1 Introduction

Fibre reinforced polymer (FRP) composites are widely used in automotive, aerospace, and marine applications as well as civil engineering projects [1, 2, 113]. due to their advantages, including lightness, high strength, ease of installation and handling, corrosion resistance, and relatively good durability, which make them appropriate alternatives to traditional materials in many applications [5, 6, 8, 114]. FRPs are also used in engineering infrastructure for the rehabilitation and strengthening of existing structures due to their unique characteristics [3, 115-117]. Among all types of fibres, including glass, carbon, aramid, and basalt, glass fibres are the most common and widely used in constructing FRP composites due to their relatively low cost (particularly compared to CFRP and AFRP) and high strength (especially compared to BFRP) [17, 118].

Despite the advantages of FRP composites, their shear strength and ductility under various loading scenarios, durability under environmental conditions, and performance under elevated conditions need to be addressed [19, 119]. For example, when FRP composites are used for rehabilitation and strengthening purposes, as well as non-structural elements or secondary structures, such as water and waste treatment plant, cooling towers, and pedestrian bridge, they may be subjected to elevated temperatures, such as fire condition [120]. However, using FRPs in applications with a high risk of fire occurrence, such as oil drilling platforms and submarines, is limited due to the poor performance of such materials when subjected to elevated temperatures [59].

In addition, the degradation of FRP composites' mechanical properties is mainly attributed to the resin and resin/fibre interface and less to the fibre itself [19-21]. The first stage of resin degradation occurs when the resin glass transition temperature (Tg) is reached (50 ˚C–120 ˚C based on the composite's resin type and fabrication process [22]), converting the resin from a glassy state to a rubbery state, which may lead to a significant reduction in the resin matrix's mechanical properties, weakening the load transfer capacity between the resin and fibre. More severe degradation occurs when the temperature reaches the resin's decomposition temperature (Td) (approximately 300 ˚C–400 ˚C) because the chemical bonds within the modular chains of resin and between the fibres break. During the final stage, at temperatures above Td, the resin may lose most of its strength and load transferring capacity due to its ignition [19, 40, 41, 121]. However, the high threshold temperature for the fibres (about 1000℃ and 2000℃ for glass and carbon fibres, respectively), may enable them to carry some load in a longitudinal direction at very high temperatures [42]. Therefore, composites subjected to severe fire conditions, even after the fire has been extinguished, may experience a considerable reduction in their mechanical properties [56].

The behaviour of FRP material used structures will be classified based on four temperature regions: (1) Temperatures below the glass transition temperature (Tg) of the resin, which can also reach to extremely high environmental temperature (e.g. 60 ˚C); (2) Temperatures above Tg, but less than the resin decomposition temperature (Td); (3) Temperature is around the decomposition temperature of resin, i.e. 300 ˚C; (4) Temperatures above 300 ˚C, which is the case for fire and post-fire cases. As most of the research in the literature are focused on either normal environmental condition (< 60 ˚C) or fire and post-fire scenarios (much higher than 300 ˚C), this paper looks at cases (1), (2) and (3) mentioned above to fill the knowledge gap on the behaviour of GFRP laminates after exposure to elevated temperatures. This temperature region may happen for some isolated fire when FRP components are at some distance from the fire.

Based on the literature, most studies that evaluated the performance of FRP composites under elevated temperatures focused on FRP bars as internal reinforcements [20, 38-42] and FRP wraps and laminates

[43-48] as external reinforcements to strengthen an existing structures. Some studies also investigated the effects of elevated temperatures on the mechanical properties of FRP profiles and panels [49-54]. A number of studies also investigated the post fire mechanical properties of FRP composites, including tensile [55, 56], compressive [56], flexural [56-59], and interlaminar shear [55, 56] strength.

Mouritz and Mathys [56] investigated the post-fire mechanical properties of GFRP composites and found that the tensile, compressive, flexural, and interlaminar shear strength of GFRPs decreased significantly (e.g., up to 80% reduction of tensile strength after exposure to a heat flux of 50 kW/m2 for 1800 seconds) when the heat flux and exposure time increased because the resin matrix burned, resulting in delamination cracking and charring. The same conclusion was obtained by Mouritz [59] on the post-fire flexural properties of epoxy, polyester, and phenolic FRP composites.

However, the impact behaviour of such materials subjected to elevated temperatures has not been studied. Moreover, the studies conducted on the mechanical properties of FRP composites under elevated temperatures are limited to one type of fibre length and orientation. However, the fibre's configuration (length and orientation) has a significant effect on the FRPs strength, stiffness, and impact properties. Fibres with a length of approximately 0.2–0.4 mm are classified as short fibres, while long fibres typically have a length greater than 1 mm [122].

Generally, FRP composites have anisotropic behaviour in the flexural and torsional deflections in FRP profiles due to coupling between the strains (direct and shear strains) [75]. However, for pultruded FRP profiles, such as FRP bars and plates, which have continuous unidirectional fibres, the coupling influence is not significant and may be neglected. Therefore, the composite may be classified as almost orthotropic (along and normal to the member's longitudinal axes) [76] . No study on the effects of fibre length and orientation on the mechanical properties of FRP composites under elevated temperatures has been conducted.

The FRP laminate's cross section (thickness and width) has a considerable effect on the flexural response of strengthened reinforced concrete (RC) members [43]. The laminate's cross section (especially the thickness) may play a key role in the deterioration level and damage penetration through the laminated thickness based on the heat flux exposure time and temperature. However, studies on the effects of an FRP laminate's cross section on the mechanical properties under elevated temperatures is very limited.

Mouritz and Mathys [56] reported less reduction in normalized tensile strength for thicker laminates due to differences in radiant heating. However, the effects of the laminate's thickness on the flexural and impact behaviour of FRPs subjected to elevated temperatures is not well studied. Therefore, this study focuses on the effects of the fibre length and orientation, laminate thickness, temperatures, and exposure time on the post-fire flexural and impact behaviour of GFRP laminates.

Therefore, to fill these gaps, this study focuses on the effect of fibre's length, fibre's orientation, laminate's thickness, temperatures, and exposure time, on the flexural and impact behaviour of GFRP laminates under elevated temperatures.

2.2 Experimental Program

This study is a part of an ongoing research program on the performance of FRP composites subjected to elevated temperatures. It focuses on the flexural and impact properties of GFRP laminates under elevated temperatures constructed using fibres of different lengths and orientations. The flexural and impact properties of GFRP laminates in terms of failure modes, damage mechanisms due to the elevated temperatures, and mechanical strength were investigated. The fibre length and orientation and laminate thickness were considered as the variables in this study. Failure modes and damages mechanism were studied through observation and using Scanning Electron Microscopy (SEM), while flexural and impact mechanical properties were obtained by conducting three-point bending and Charpy impact tests, respectively. Finally, statistical methods including Analysis of Variance (ANOVA) and linear Bayesian regression were used to investigate the variables' contribution to the results and to predict probability models for reduction ratios of mechanical properties.

2.2.1 Materials

Three types of E-glass FRP laminates, including three fibre orientations and two thicknesses, were constructed using the vacuum infusion process (VIP). VIP is mainly used for high-quality large components. However, due to its relatively high cost compared to the traditional wet lay-up method, it is appropriate for providing limited series. Briefly, VIP is conducted in the following four steps: (1) loading the reinforcement (fibres and any other components without resin) into the dry mold; (2) sealing the dry reinforcement placed in the vacuum bag using a sealant tape; (3) evacuating the air in the cavity using a high vacuum pump; (4) infusion of the resin (sucking through the vacuum) into the cavity and wetting the reinforcement (**Figure 2-1**).

Figure 2-1 Preparing large GFRP laminates using VIP

Regarding the fibre orientations and laminate textile, unidirectional, woven, and random fibres were used to construct different types of GFRP laminates (**Figure 2-2**). Continuous E-glass fibres (with 350 g/m^2 areal weight) were used to construct unidirectional laminate (UL) and woven laminate (WL), while for random oriented laminates (RL), long chopped E-glass fibres with the lengths of 25 ± 5 mm were used. Epoxy resin was the matrix used for all laminates, the thicknesses of which were 2 and 5 mm. Tensile coupon tests, based on ASTM D638−14 [63], and with a loading rate of 1 mm/min, were carried out on three identical specimens of each type of laminate to obtain their tensile mechanical properties. The tensile samples and set-up of the coupon tests are listed in **Figure 2-3**, while **Figure 2-4** shows the failure modes of each laminate type. **Table 2-1** presents the characteristics and mechanical properties of each GFRP laminates tested at ambient temperature (25 ˚C). The tensile and flexural strength of the resin matrix were 70 and 60 MPa, respectively, while its tensile elastic modulus is 5 GPa. It is needed to note that the glass transition temperature of the laminates was reported about 80 ˚C.. The possible reason for thicker laminates having higher strength than the thinner laminates is the fabrication process.

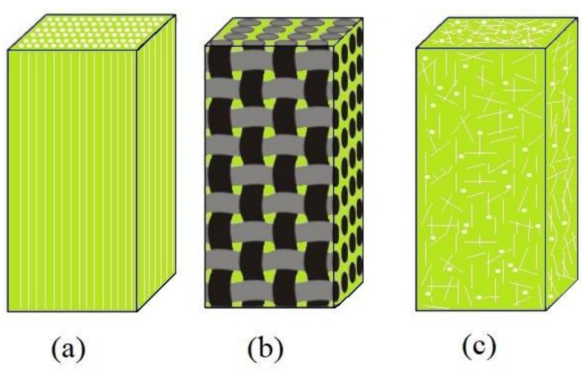

Figure 2-2 Laminate's fibre orientations: a) Unidirectional; b) Woven; c) Random oriented (chopped strands)

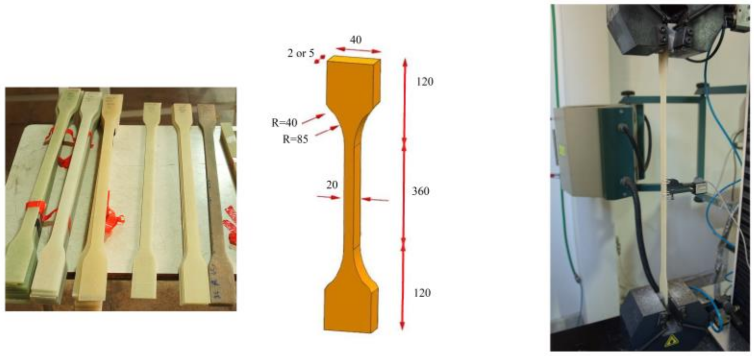

(a) (b)

Figure 2-3 Tensile coupon tests: a) Dog-bone shaped samples; b) Test set-up

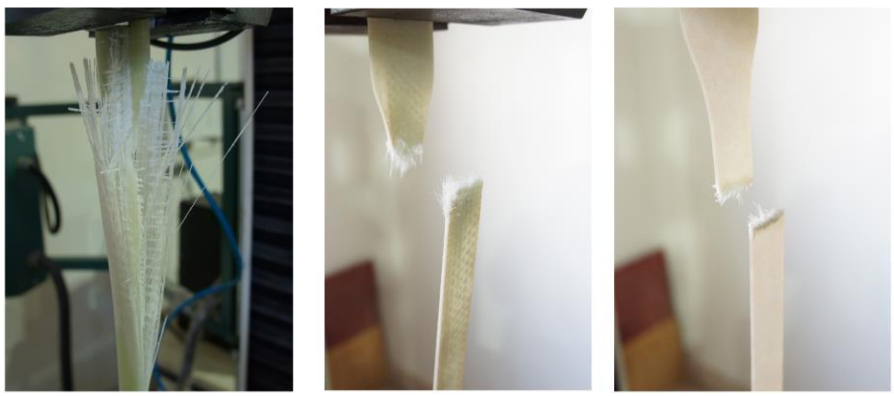

(a) (b) (c)

Figure 2-4 Tensile coupon samples' failure modes: a) UL, b) WL, and c) RL

Table 2-1 Characteristics of GFRP laminates

GFRP Laminates	Thickness (mm)	Number of layers	Fibre weight fraction (%)	Tensile strength (MPa)	Ultimate strain	Tensile Elastic modulus (GPa)
UL	2	6	70.5	633	0.020	32.1
	5	16	71.2	800	0.023	33.8
WL	2	6	65.2	275	0.022	17.8[a], 11.9[b]
	5	17	64.6	290	0.019	23.0[a], 14.5[b]
RL	2	3	41.6	177	0.018	10.0
	5	7	33.1	202	0.013	15.7

Note: WL showed essentially bilinear stress-strain curve [123]: a) Initial Elastic modulus, b) secondary chord Elastic modulus.

2.2.2 Conditioning of samples

GFRP laminates were classified into unconditioned and conditioned series. The unconditioned specimens were tested for three-point bending and Charpy impact at ambient temperature (25 ˚C) and considered as the reference. The conditioned specimens were subjected to four elevated temperatures of 60, 120, 200, and 300 ˚C (in a three-zone temperature-controlled furnace) for two different periods: 20 and 120-min. The specimens were left to cool for 24 h and then tested for three-point bending and Charpy impact. The aim of choosing these temperatures was to cover the first three cases out of four cases mentioned in the introduction section. Furthermore, 20-min exposure time was chosen to ensure that all laminate's surface temperature reaches the furnace temperature. 120-min exposure time was used to ensure that the core of the laminates reach the furnace temperature.

2.2.3 Specimens

To conduct the three-point bending and Charpy impact tests, rectangular specimens with a width of 18mm, length of 70 mm, and two thicknesses of 2 mm and 5 mm were cut from the large GFRP sheets using a water jet. **Table 2-2** summarizes the characteristics of the specimens used in this study.

Table 2-2 Specimens' characteristics

Mechanical test	Laminate Type	Time of exposing (min)	Temperatures (˚C)	Number of identical specimens	Total Number
Three-point bending	UL	20, 120	25, 60, 120, 200, 300	5	90
	WL	20, 120	25, 60, 120, 200, 300	5	90
	RL	20, 120	25, 60, 120, 200, 300	5	90
Charpy impact	UL	20, 120	25, 60, 120, 200, 300	5	90
	WL	20, 120	25, 60, 120, 200, 300	5	90
	RL	20, 120	25, 60, 120, 200, 300	5	90

2.2.4 Mechanical tests

2.2.4.1 Three-point bending

To investigate the effect of variables (glass fibre reinforcement type and sample thickness) on GFRP laminates' flexural properties subjected to elevated temperatures, three-point bending tests were conducted according to the recommendations of the ASTM D790 standard [15] with a loading rate (cross-head speed) of 3mm/min. The tests were carried out using a Zwick roll servo electric testing machine with a capacity of 150 kN. Based on the standard recommendation, and to increase the reliability of the results, 5 identical specimens were tested in each condition. **Figure 2-5** shows the three-point bending test set-up. The steel roller-type supports with span of 65 mm for all samples were used. The load and corresponding vertical displacement were recorded continuously by the testing machine.

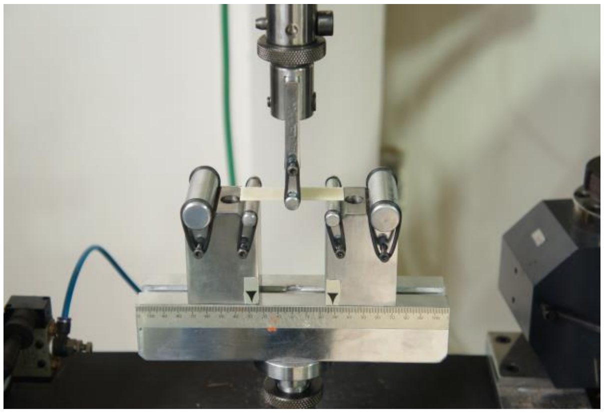

Figure 2-5 Three-point bending test set-up

2.2.4.2 Charpy impact

In order to investigate the effect of variables (glass fibre reinforcement type and sample thickness) on the impact behaviour of GFRP laminates subjected to elevated temperatures, Charpy impact tests were conducted on samples with the dimensions similar to those used for three-point bending tests using a Charpy impact testing machine. The information obtained from the Charpy impact tests includes the impact energy and material toughness, which is generally used for quality control procedures. Some recommendations in ASTM D61110-10 have been adopted in conducting Charpy impact tests. Impact energy (the energy absorbed by a sample) in the Charpy impact test is calculated based on the height variation of the pendulum before and after collision [124]. The impact velocity at the time of collision and the energy absorbed by the specimen until it was fractured can be calculated using Eq. 2.1 and Eq. 2.2, respectively, where, g = local gravity acceleration, H1 = vertical height of the striking nose, m = pendulum mass, h1 = elevation of the pendulum mass centre before collision, and h2 = elevation of the pendulum mass centre after collision.

$$V = \sqrt{2gH_1} \tag{2.1}$$

$$U = mg(h_1 - h_2) \tag{2.2}$$

In this study, the initial impact angle and the speed at the moment of contact were 149.7˚ (with respect to the vertical axis) and 5.23 m/s, respectively. Similar to the bending tests, five identical specimens were tested in each condition. **Figure 2-6** shows the Charpy impact test setup. The same span to three-point bending tests was also used for Charpy impact tests (65 mm). The collision speed, elevation of the pendulum mass before and after collision and the absorbed energy were recorded by the testing machine.

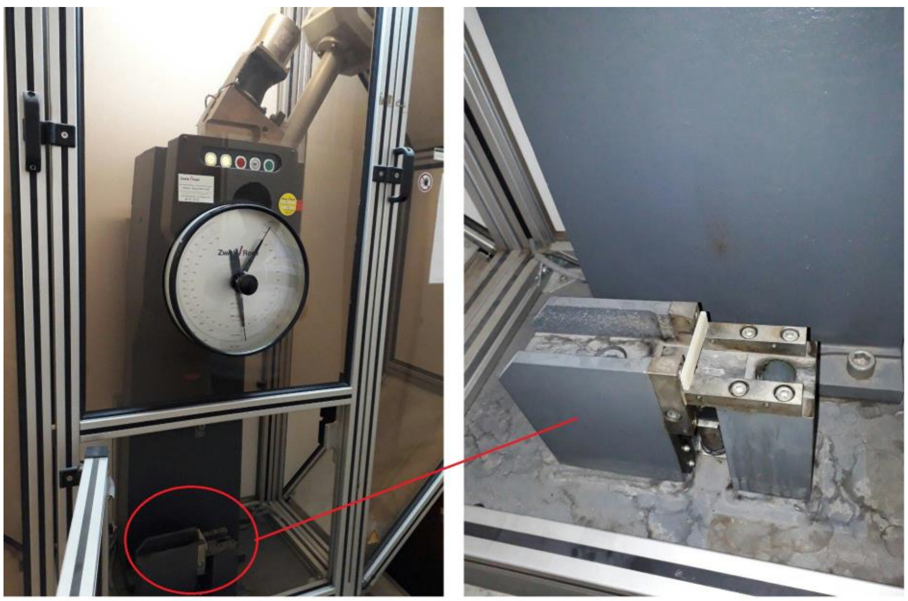

Figure 2-6 Charpy impact test: a) Testing machine, b) Test set-up

2.2.5 Scanning electronic microscopy (SEM)

To study the probable damage mechanisms including resin cracking, delamination, and fibre/matrix interface debonding of GFRP laminates after exposure to elevated temperatures and before testing, the selected samples of each condition were observed and analysed under SEM. Moreover, some samples were also observed under SEM after conducting mechanical tests to investigate the details of failure modes (debonding, delamination, crack growth, and fibre fracture) in fractured surfaces. It should be noted that all the samples were coated with 30 mm gold layer before undergoing SEM.

2.3 Results and discussion

In this section, the failure modes and mechanical test results, including three-point bending tests, Charpy impact tests, and microstructural analyses, are presented and discussed in detail. Generally, the targets are investigating the thickness and the reinforcement arrangement of GFRP laminates through a comprehensive comparison.

2.3.1 Failure modes

Failure modes of the conditioned and unconditioned GFRP laminates tested in three-point bending and Charpy impact tests are classified based on the identification code presented ASTM D 7264/D 7264M–15 [125] standard. In this classification, a three-part notation was used to identify each failure characteristics. **Table 2-3** represents the notation system used.

Table 2-3 Failure identification code [125]

First character		Second character		Third character	
Failure mode	Code	Failure area	Code	Failure location	Code
Tension	T	At loading nose	A	Top	T
Compression	C	At support nose	S	Bottom	B
Buckling	B	Between load and support nose	L	Left	L
Interlaminar shear	S	Unknown	U	Right	R
Multi-mode	M (xyz)			Middle	M
Other	O			Various	V
				Unknown	U

A four-part notation system was also used to identify the specimen. The first and second parts represent the type and thickness of GFRP laminate, respectively while the third and fourth parts stand for the temperature and time of the exposure, respectively. For an example RL-2-60-20 identifies the 2mm thickness randomly fibre distributed GFRP laminates exposed to 60 ˚C for 20-minutes. A fourth part is not considered for unconditioned specimens as they are not exposed to elevated temperatures. **Table 2-4** lists all failure modes of unconditioned and conditioned specimens tested under three- point bending. It is worth mentioning that the temperature at surface reached to that of the furnace for all specimens after 20-min exposure to the target temperature.

Table 2-4 Failure identification code of GFRP laminates after three-point bending tests

Specimen	**Failure mode**	**Specimen**	**Failure mode**	**Specimen**	**Failure mode**
UL-2-25	TAB	WL-2-25	TAB	RL-2-25	TAB
UL-5-25	TAB	WL-5-25	TAB	RL-5-25	TAB
UL-2-60-20	TAB	WL-2-60-20	TAB	RL-2-60-20	TAB
UL-2-60-120	TAB	WL-2-60-120	TAB	RL-2-60-120	TAB
UL-5-60-20	TAB	WL-5-60-20	TAB	RL-5-60-20	TAB
UL-5-60-120	TAB	WL-5-60-120	TAB	RL-5-60-120	TAB
UL-2-120-20	TAB	WL-2-120-20	M (CB)AV	RL-2-120-20	M(TC)AV
UL-2-120-120	TAB	WL-2-120-120	M (CB)AV	RL-2-120-120	M(TC)AV
UL-5-120-20	M(CT)AV	WL-5-120-20	M (CB)AV	RL-5-120-20	M(TC)AV
UL-5-120-120	M(CT)AV	WL-5-120-120	M (CB)AV	RL-5-120-120	M(TC)AV
UL-2-200-20	SLV	WL-2-200-20	M (CB)AV	RL-2-200-20	SLV
UL-2-200-120	SLV	WL-2-200-120	M (CB)AV	RL-2-200-120	SLV
UL-5-200-20	SLV	WL-5-200-20	SLV	RL-5-200-20	SLV
UL-5-200-120	SLV	WL-5-200-120	SLV	RL-5-200-120	SLV
UL-2-300-20	SLV	WL-2-300-20	SLV	RL-2-300-20	SLV
UL-2-300-120	SLV	WL-2-300-120	SLV	RL-2-300-120	SLV
UL-5-300-20	SLV	WL-5-300-20	SLV	RL-5-300-20	SLV
UL-5-300-120	SLV	WL-5-300-120	SLV	RL-5-300-120	SLV

It should be noted that all five identical specimens had almost same failure modes. Generally, the failure modes of GFRP laminates can be classified into three groups. Regarding the first group (temperatures below Tg), the failure modes did not change compared to ones tested at the ambient temperature and all specimens failed in tension zone through the fibres' rupture at loading nose (**Figure 2-7**). This was because in temperatures under Tg, the resin is not vulnerable and may maintain its mechanical properties and load transferring capacity.

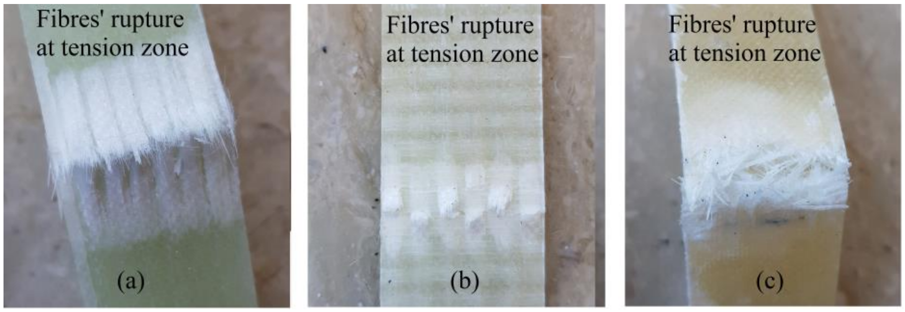

Figure 2-7 Bending failure modes at ambient and 60 ˚C: a) UL, b) WL, and c) RL

The second group is attributed to 120 ˚C, in which the temperature just passed the glass transition temperature of the epoxy resin used in this study, which was about 80 ˚C. In comparison to the first group, one can conclude that due to the mechanical degradation of the resin, for UL and RL specimens (except UL-2-120-20 and UL-2-120-20), in addition to the fibres fracture in tension zone, a local compression failure under the loading nose was observed. However, for UL-2-120-20 and UL-2-120-120, the resin characteristics degradation was not enough to change the failure mechanism compared to the unconditioned one. At this group, all woven laminates failed due to the combination of compression and fibre bulking failures as a result of resin mechanical properties degradation (**Figure 2-8**).

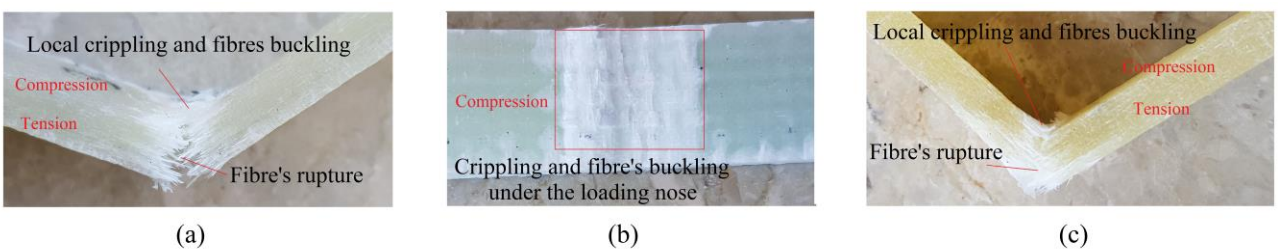

Figure 2-8 Bending failure modes at 120 ˚C: a) UL, b) WL, and c) RL

Regarding the third group (T ≥ 200 ˚C), it is observed that all the specimens (except WL with 2 mm thickness) failed through the delamination of the laminates' layers (interlaminar shear delamination). The reason for this can be addressed through the significant damages of the resin matrix during the heating process, which may lead to a significant reduction in mechanical properties of the resin and resulted a reduction in load transferring capacity between the resin and fibre and debonding of fibre and resin (**Figure 2-9**). The reason for compression and fibre buckling failure of WL-2-200-20 and WL-

2-200-120 may be a relatively lower compressive strength under the loading nose than the interlaminar shear strength of the laminates. In this case the interlaminar shear strength of the laminates, even after exposing to severe temperatures were higher than the local compressive strength of the laminates under the loading nose.

As a general observation, failures in compression zone after exposing to elevated temperatures was more likely for RL and WL rather than UL. Therefore, it can be concluded that the effect of resin strength and fibre/matrix interface, which may damage under elevated temperatures, is more significant in flexural properties when the fibres are randomly and woven distributed rather than unidirectional.

From **Table 2-5** it is also concluded that the exposure time did not change the failure mechanism. In other words, all types of GFRP laminates experienced a same failure mode in three-point bending test when exposed to a same temperature for a period of 20-min and 120-min.

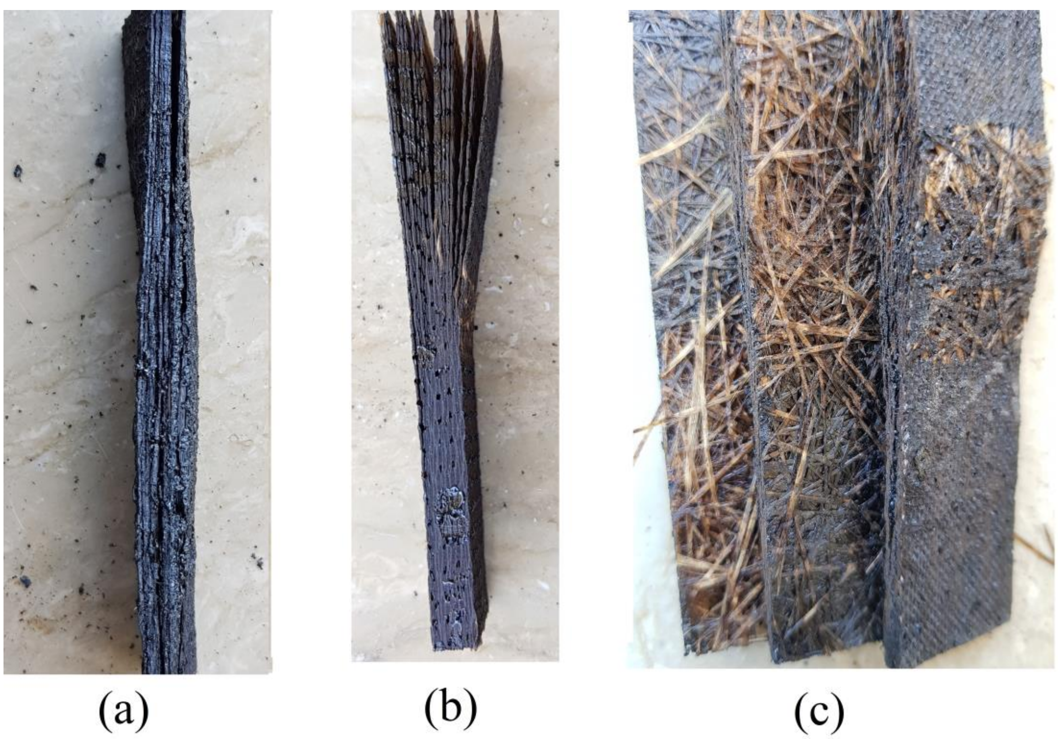

Figure 2-9 Bending failure modes at T ≥ 200 ˚C: a) UL, b) WL, and c) RL

Table 2-5 Failure identification code of GFRP laminates after Charpy impact tests

Specimen	Failure mode	Specimen	Failure mode	Specimen	Failure mode
UL-2-25	FF	WL-2-25	FF	RL-2-25	FF
UL-5-25	M(FF-D)	WL-5-25	FF	RL-5-25	FF
UL-2-60-20	FF	WL-2-60-20	FF	RL-2-60-20	FF
UL-2-60-120	FF	WL-2-60-120	FF	RL-2-60-120	FF
UL-5-60-20	M(FF-D)	WL-5-60-20	FF	RL-5-60-20	FF
UL-5-60-120	M(FF-D)	WL-5-60-120	FF	RL-5-60-120	FF
UL-2-120-20	M(FF-FP)	WL-2-120-20	FF	RL-2-120-20	FF
UL-2-120-120	FF	WL-2-120-120	FF	RL-2-120-120	TF
UL-5-120-20	M(FF-D)	WL-5-120-20	M(FF-FP-D)	RL-5-120-20	FF
UL-5-120-120	M(FF-D)	WL-5-120-120	M(FF-FP-D)	RL-5-120-120	TF
UL-2-200-20	D	WL-2-200-20	D	RL-2-200-20	D
UL-2-200-120	D	WL-2-200-120	D	RL-2-200-120	D
UL-5-200-20	D	WL-5-200-20	D	RL-5-200-20	D
UL-5-200-120	D	WL-5-200-120	D	RL-5-200-120	D
UL-2-300-20	D	WL-2-300-20	D	RL-2-300-20	D
UL-2-300-120	D	WL-2-300-120	D	RL-2-300-120	D
UL-5-300-20	D	WL-5-300-20	D	RL-5-300-20	D
UL-5-300-120	D	WL-5-300-120	D	RL-5-300-120	D

Regarding the Charpy impact test a similar trend to three-point bending tests was observed in which before 200 ˚C temperatures, generally laminates failed due to the rupture and pull-out of the fibres and sample fracture, while at temperatures of T ≥ 200 ˚C, a considerable delamination of the laminates was occurred for all types (**Figure 2-10**). It is important to note that the location of the fracture is attributed to the point that may not absorb further energy through the impact. Similar to the bending tests, all five identical specimens had almost same failure modes. **Table 2-5** lists all failure modes of unconditioned and conditioned specimens tested under Charpy impact. Where FF, FP, D, and TF refer to fibres' fracture, fibres' pull-out, delamination, and total fracture failures, respectively.

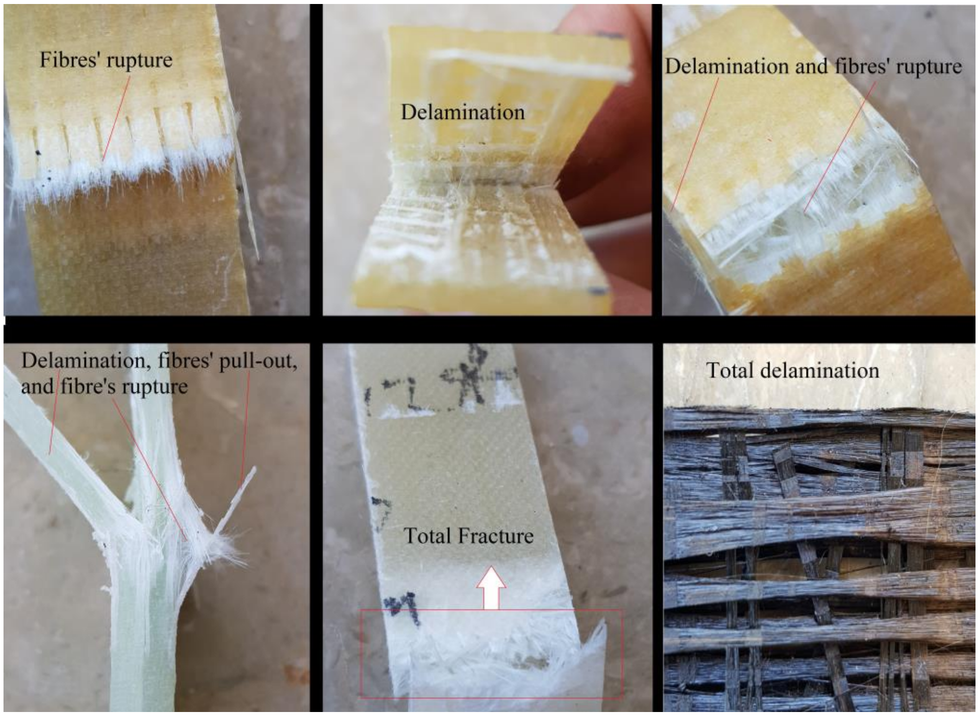

Figure 2-10 Typical failure modes observed during Charpy impact tests

2.3.2 Microstructural Analyses

In order to investigate the microstructural changes and probable damages occurred in GFP laminates after exposing to elevated temperatures, the unconditioned and some of the conditioned samples were observed under Scanning Electron Microscopy (SEM). **Figure 2-11** shows the unconditioned samples of each GFRP laminates type before any exposure. It is worth mentioning that, in order to obtain a rough surface for better gripping of the testing machine's jaws in tensile tests (which the results will be published in another paper by the authors), the last resin layer of the laminates was pressed by one layer of woven fibres and then the woven fibres layer was removed. In this case, before any damages, all laminates look like woven fibres laminate; however, it is just a surface resin layer). Therefore, recognizing the types before any damage of the surface resin is not possible. As expected, it is seen that no significant cracks and delamination on the resin matrix is observed in all laminates. It is worth mentioning that the small cracks on the resin may be due to the polishing process and handling of the sample before loading on the SEM device.

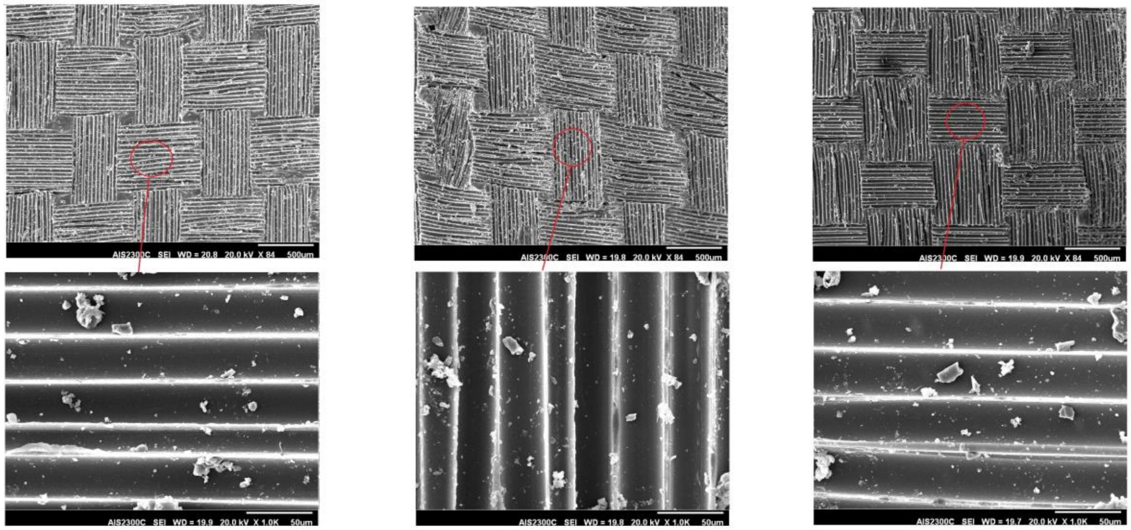

(a) (b) (c)

Figure 2-11 SEM images of unconditioned GFRP laminates: a) UL, b) WL, and c) RL

At 60 ˚C, similar to the unconditioned samples, just some small cracks were observed on the surface resin of all GFRP laminate, while at temperatures of 120 ˚C, more cracks and relatively small holes were observed on the surface resin of the specimens, which shows that the resin started to be degraded as the temperatures passed its glass transition temperature.

Figure 2-12 shows the SEM images of some selected specimens exposed to 120 ˚C. In this case, as the surface damages were not significant, similar to temperatures of 25 and 60, the differences between the different types (UL, WL, and RL) is not recognizable.

At 200 ˚C, as shown in **Figure 2-13** the surface resin started to be melted and almost was ruined in RL. Furthermore, significant damage of the resin led to the deterioration of the resin/matrix interface and caused fibre/resin debonding in some areas. From the observations, it is seen that the fibre/resin interface of UL experienced some damage and limited debonding was observed (**Figure 2-13 (a)**), while for RL a significant and obvious fibre/matrix debonding was observed in many portions of the sample (**Figure 2-13 (c)**). Regarding the WL, the fibre/resin debonding was also obvious for a large region of the sample (**Figure 2-13 (b)**). However, the damage level was not as high as RL.

At 300 ˚C the surface resin layer was extremely melted, numerous cracks at the resin matrix and significant resin/fibres debonding were seen for all types of GFRP laminates (**Figure 2-14**). In this case, due to the reaching of temperature to the Td of the resin, almost all fibres/resin interface, regardless of the type (UL, WL, RL) were debonded. From these observations, the delamination failure occurred for all specimens at 300 ˚C during three-point bending and Charpy impact tests can be confirmed, as the interface between the fibres and the resin were significantly damaged.

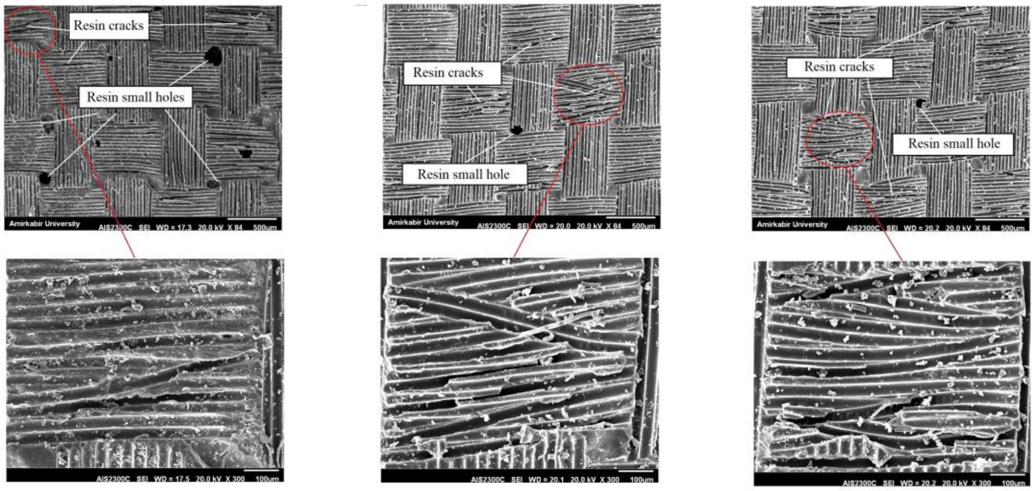

(a) (b) (c)

Figure 2-12 SEM images of selected GFRP laminates exposed 120 ˚C: a) UL-2-120-120, b) WL-2-120-120, and c) RL-2-120-120

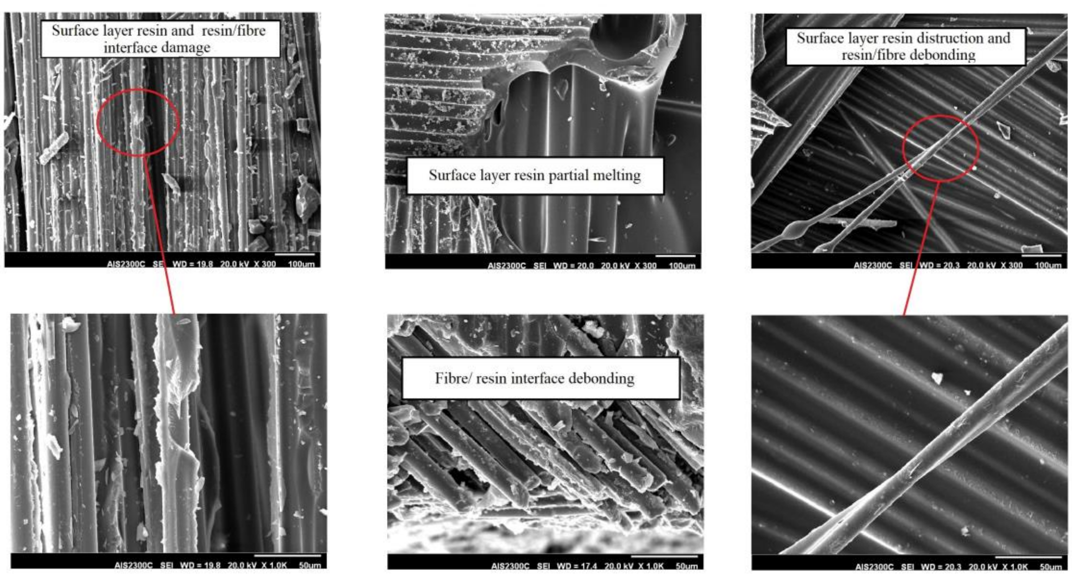

(a) (b) (c)

Figure 2-13 SEM images of selected GFRP laminates exposed 200 ˚C: a) UL-2-200-120, b) WL-2-200-120, and c) RL-2-200-120

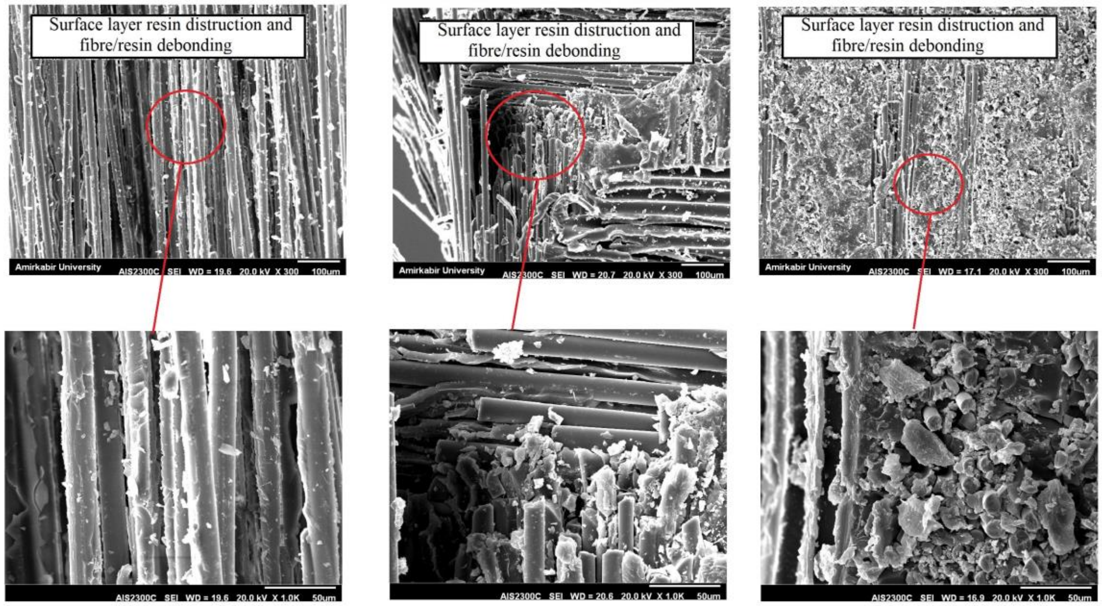

(a) (b) (c)

Figure 2-14 SEM images of selected GFRP laminates exposed 300 ˚C: a) UL-2-300-120, b) WL-2-300-120, and c) RL-2-300-120

2.3.3 Mechanical test results

2.3.3.1 Three-point bending test

Table 2-7 summarize the three-point bending test results of all conditioned and unconditioned GFRP laminates, providing the ultimate strength (Us) and retention values (R) obtained after 20-and 120-minute exposure to elevated temperatures, respectively. The typical flexural load versus mid-span displacement curves of all conditioned and unconditioned UL, WL, and RL GFRP laminates are depicted in **Figure 2-15** to **Figure 2-17**. As can be seen from these plots, the initially linear curves become nonlinear, before reaching the ultimate flexural loads (the only exception are samples at 300 ˚C). It is worth mentioning that nonlinearity is more pronounced at higher temperatures, likely due to the presence of interlaminar shear cracks in the resin matrix and delamination. Finally, as expected, most of the specimens experienced a sudden failure due to fibre fracture (which typically occurs before any other failures at lower temperatures and after delamination at higher temperatures). Moreover, at 300 ˚C, samples started to delaminate at the beginning of each test, due to which a slight load was carried with a large amount of deformation by separated (delaminated) layers.

Table 2-6 Three-point bending results after 20-min exposing

Temperature (˚C)	UL-2 mm			WL-2 mm			RL-2 mm			UL-5 mm			WL-5 mm			RL-5 mm		
	Average U_s (N)	COV (%)	R (%)	Average U_s (N)	COV (%)	R (%)	Average U_s (N)	COV (%)	R (%)	Average U_s (N)	COV (%)	R (%)	Average U_s (N)	COV (%)	R (%)	Average U_s (N)	COV (%)	R (%)
25	870	2.3	100	360	1.8	100	210	2.1	100	5500	1.1	100	2450	3.2	100	2250	0.7	100
60	830	3.1	95	345	2.5	96	187	2.6	89	5400	3.1	98	2400	4.1	98	2010	2.2	89
120	740	2.8	85	260	3.1	72	141	4.6	67	4800	3.5	87	2000	2.5	81	1580	2.6	70
200	590	5.5	67	190	4.7	52	107	4.5	51	3900	3.3	70	1350	4.2	55	1220	7.2	54
300	90	5.1	10	30	5.5	8	20	8.8	9	580	7.4	10	141	6.1	6	130	8.5	6

Table 2-7 Three-point bending results after 120-min exposing

Temperature (˚C)	UL-2 mm			WL-2 mm			RL-2 mm			UL-5 mm			WL-5 mm			RL-5 mm		
	Average U_s (N)	COV (%)	R (%)	Average U_s (N)	COV (%)	R (%)	Average U_s (N)	COV (%)	R (%)	Average U_s (N)	COV (%)	R (%)	Average U_s (N)	COV (%)	R (%)	Average U_s (N)	COV (%)	R (%)
25	870	1.8	100	360	0.8	100	210	3.1	100	5500	1.5	100	2450	2.1	100	2250	2.8	100
60	830	2.9	95	335	2.2	93	180	2.8	86	5400	2.1	98	2350	1.9	96	1995	2.4	89
120	710	3.5	82	250	4.4	69	129	3.3	61	4580	2.5	83	1790	3.5	73	1510	4.1	67
200	540	6.1	62	170	5.1	47	97	3.1	46	3750	6.3	68	1230	3.1	50	1050	4.4	47
300	69	6.8	8	18	5.5	5	10	7.2	5	440	8.8	8	105	9.1	4	95	8.9	4

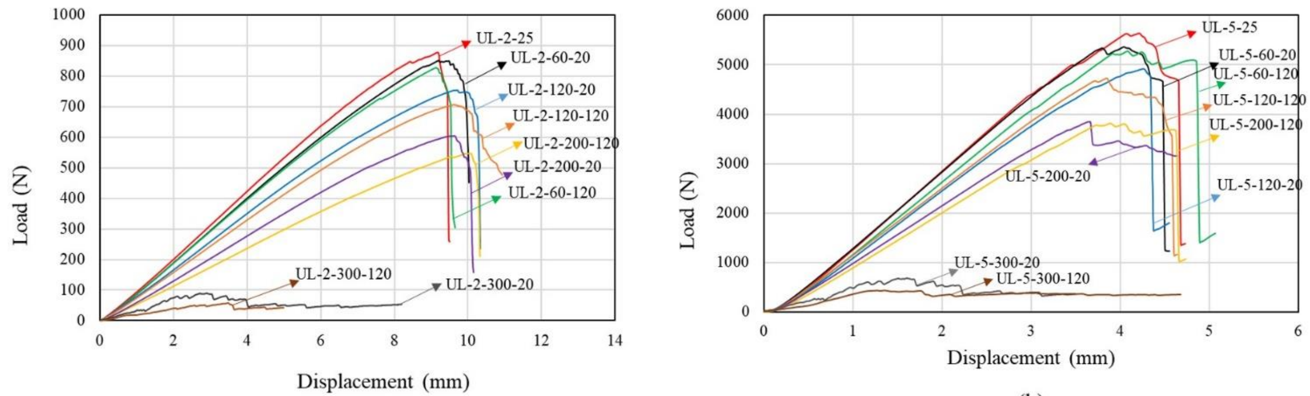

(a) (b)

Figure 2-15 Selected flexural load versus mid-span displacement curves of UL: a) 2 mm, b) 5 mm

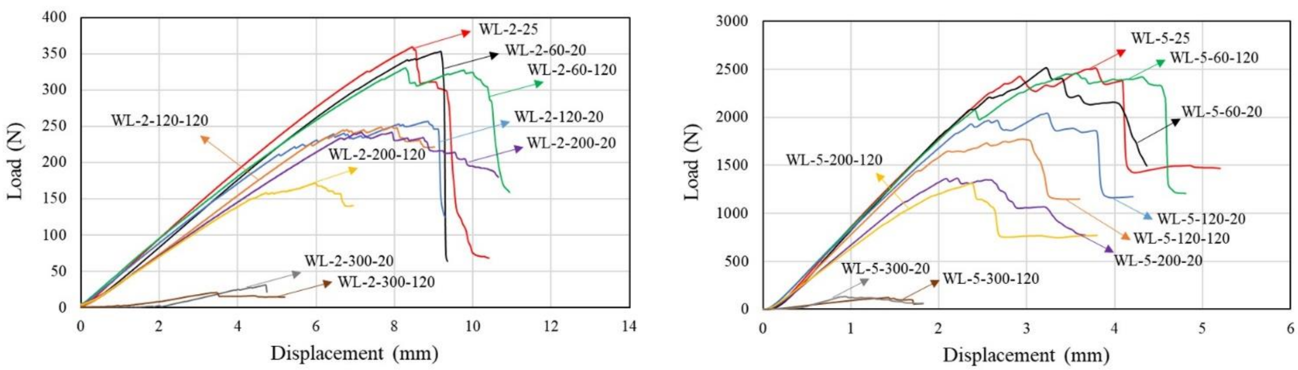

(a) (b)

Figure 2-16 Selected flexural load versus mid-span displacement curves of WL: a) 2 mm, b) 5 mm

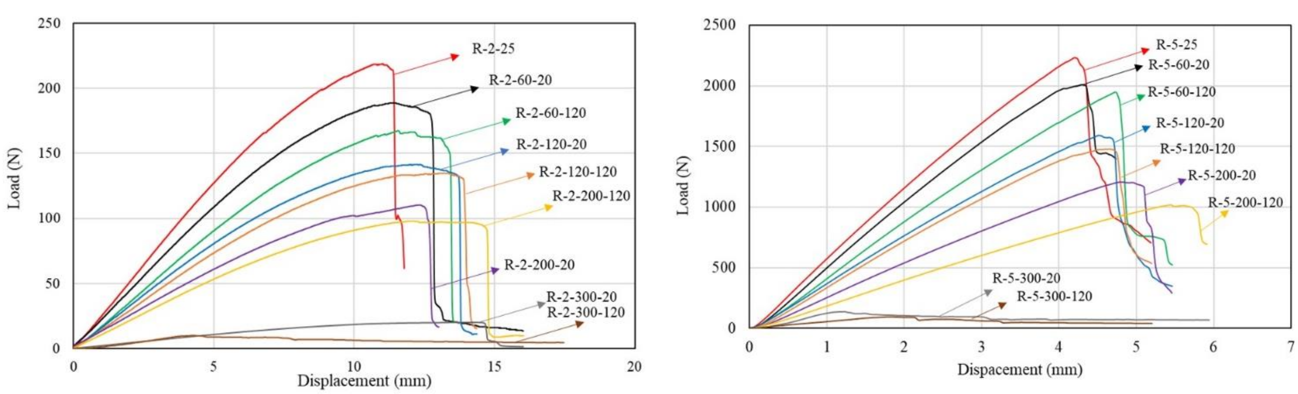

(a) (b)

Figure 2-17 Selected flexural load versus mid-span displacement curves of RL: a) 2 mm, b) 5 mm

Based on the obtained results, firstly, to investigate the effect of thickness and fibre arrangement, the flexural strength of unconditioned laminates is discussed. Then the flexural performance of each laminate will be presented and finally the retention values of each type are compared.

2.3.3.1.1 Unconditioned samples

Figure 2-18 presents the results of three-point bending tests performed on the unconditioned samples. It is evident that, irrespective of sample thickness, as expected, due to the same fibre orientation and applied tensile/compression load, UL laminates exhibit a considerably higher strength relative to WL and RL laminates. In addition, the normalized strength values depicted in **Figure 2-18 (b)** indicate that a decrease in thickness from 5 mm to 2 mm did not have a significant effect on WL strength compared to UL (as 0.45 was obtained for 5 mm and 0.41 for 2 mm laminates). However, changing the thickness in RL laminates significantly reduced the strength compared to the corresponding UL specimens (with 0.41 and 0.24 measured for 5 mm and 2 mm, respectively). This phenomenon may be due to the non-uniform fibre distribution through the sample volume. Therefore, the thickness of the composites incorporating fibres of random orientation must be taken into account when using such materials in construction.

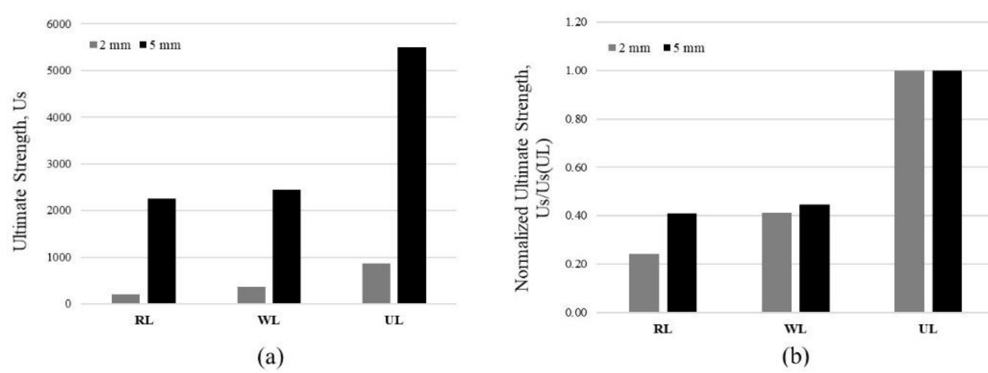

Figure 2-18 Unconditioned three-point bending results: a) Ultimate strength, b) Normalized strengths to UL ultimate strengths

2.3.3.1.2 Conditioned samples: UL

Figure 2-19 shows the three-point bending strength versus the temperatures of UL samples compared to the corresponding unconditioned specimens. As seen in **Figure 2-19 (c)**, three different behaviours can typically be observed in the retention-temperature curves of GFRP laminates. The first occurs in the 20 ˚C ≤ T ≤ 60 ˚C temperature range, in which a slight decrease (about 5%) occurred after both 20-min and 120-min exposure. Insignificant changes in resin properties in terms of molecular chains may be the main reason for this phenomenon [42]. The second portion pertains to the 60−200 ˚C range. Here, a significant reduction in laminate flexural strength was observed due to reaching the glass temperature of the resin (Tg = 80 ˚C) and changing its state from glassy to rubbery (this may reduce the load transferring capacity of the resin) [40]. Finally, the third zone spans the 200 ˚C ≤ T ≤ 300 ˚C temperature range where, as a result of reaching the resin decomposition temperature (Td ≈ 300 ˚C), the laminates may lose most (about 90%) of their load carrying capacity, whereby a slight load is sustained through the fibres [38].

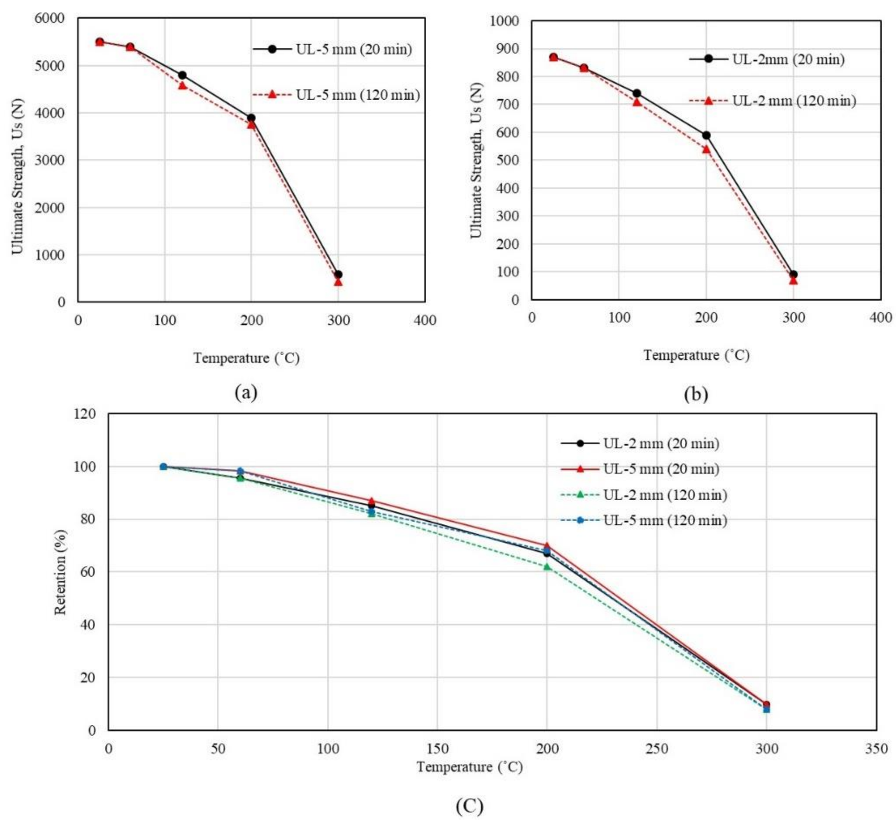

Figure 2-19 Three-point bending results of UL: (a) Ultimate strength versus temperature of 5 mm samples; (b) Ultimate strength versus temperature of 2 mm samples; (c) Retention versus temperature

In **Figure 2-19 (a)** and **Figure 2-19 (b)**, it can be seen that increasing the exposure time will generally decrease the flexural strength of GFRP laminates in the 20 ˚C ≤ T ≤ 60 ˚C temperature range. In addition, **Figure 2-19 (c)** indicates that this reduction is greater in 2 mm laminates compared to those of 5 mm thickness, as the former permit heat flux penetration earlier and more easily.

2.3.3.1.3 Conditioned samples: WL

Figure 2-20 shows the three-point bending strength versus the temperatures of WL samples compared to the corresponding unconditioned specimens. A trend similar to that observed for UL is also evident here, as 120-min exposure results in greater adverse effects relative to those noted after 20-min (the only exception is the 5 mm thick WL sample heated to 60 ˚C). Moreover, 5 mm laminates exhibit superior performance when compared to those of 2 mm thickness. Finally, the third zone observed in the curves pertaining to UL was identified in those pertaining to WL samples, whereby a slight reduction observed in the 25 ˚C ≤ T ≤ 60 ˚C temperature range is followed by a significant reduction in 60 ˚C ≤ T < 200 ˚C, and finally a catastrophic reduction at 300 ˚C.

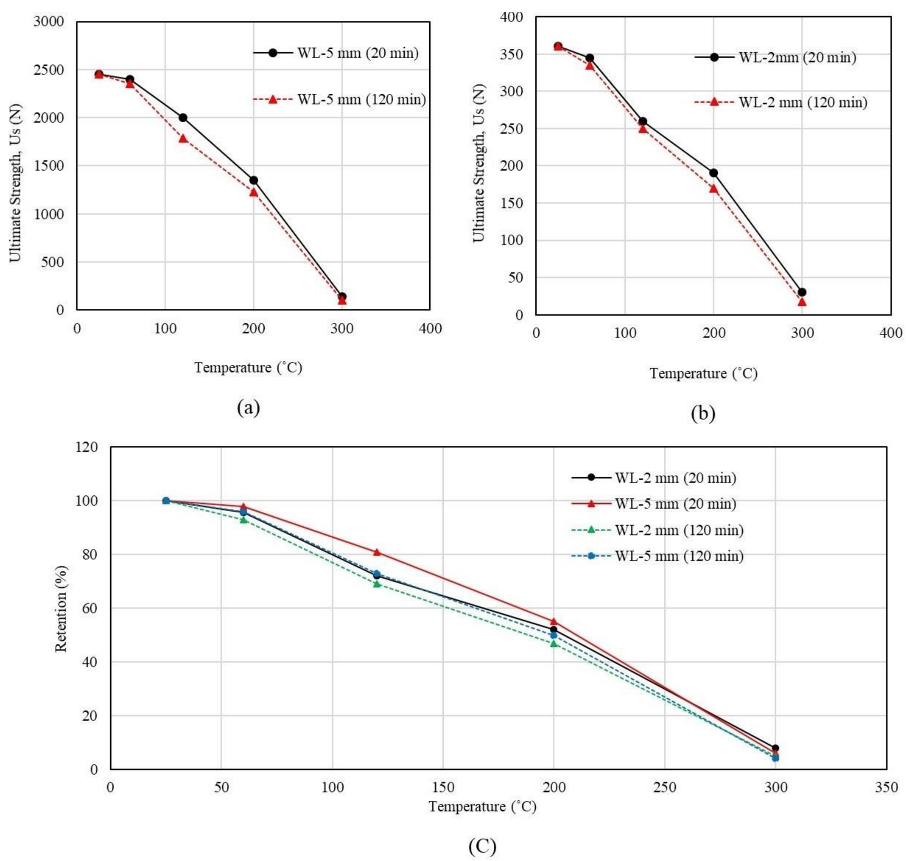

Figure 2-20 Three-point bending results of WL: (a) Ultimate strength versus temperature of 5 mm samples; (b) Ultimate strength versus temperature of 2 mm samples; (c) Retention versus temperature

2.3.3.1.4 Conditioned samples: RL

Figure 2-21 shows the three-point bending strength versus the temperatures of 20-min and 120-min exposing time of RL samples compared to the corresponding unconditioned specimens. It is seen that in contrast to the UL and WL samples, RL showed a considerable reduction even at temperature of 60 (more than 10%), which is lower than the resin Tg. This may be due to the high dependency of the RL flexural strength to the mechanical properties of the resin matrix, in which a slight resin degradation may cause a considerable reduction in laminate's strength. Moreover, based on **Figure 2-21 (c)**, the reduction rate in temperatures of 120 ˚C ≤ T ≤ 200 ˚C is less than 60 ˚C ≤ T ≤ 120 ˚C. However, the other characteristics mentioned before was also concluded for RL samples.

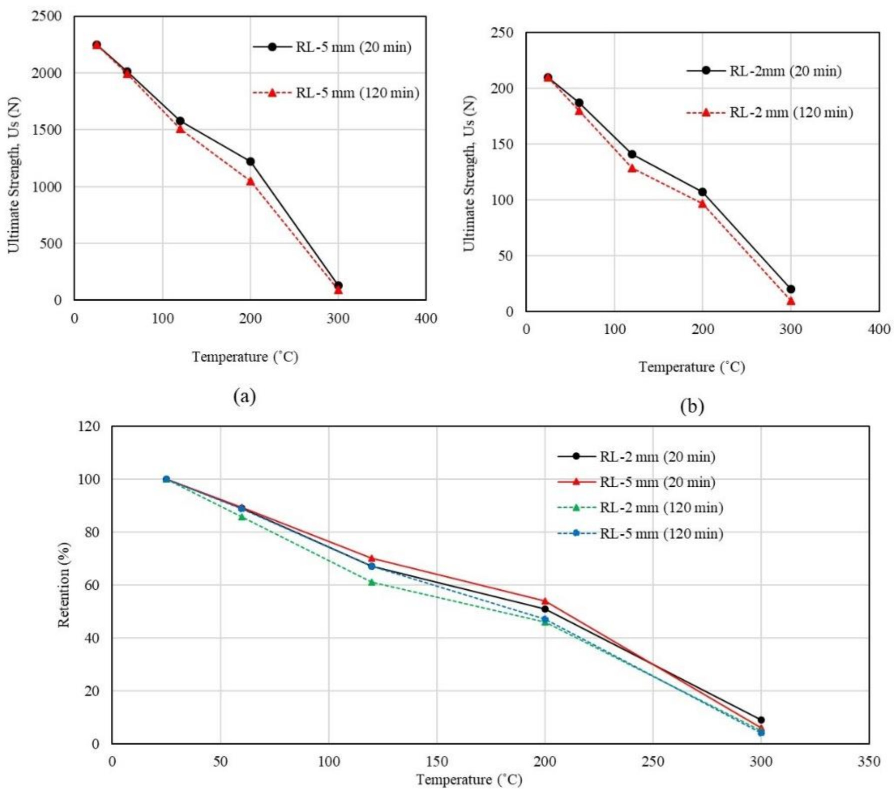

Figure 2-21 Three-point bending results of RL: (a) Ultimate strength versus temperature of 5 mm samples; (b) Ultimate strength versus temperature of 2 mm samples; (c) Retention versus temperature

2.3.3.1.5 Comparison between the UL, WL, and RL

Figure 2-22 compares the three-point bending strength versus the temperatures of three different GFRP laminates used in the present study. It is obvious in all curves that UL had the best performance between all types, while RL showed the weakest and WL was between the two. However, at very extreme temperatures (200 ˚C and 300 ˚C), RL and WL showed almost similar performance. This also was occurred for WL and UL at 60 ˚C temperature. Therefore, as a general conclusion, unidirectional fibre distributed laminates have the best flexural behaviour under elevated temperatures due to a higher contribution of the fibres in carrying the loads compared to woven and randomly distributed fibre laminates. With the same reason, WL laminates have better performance than random laminates.

Beside the types of laminates, it can be concluded that bending properties are more sensitive to the elevated temperatures (especially at very high temperatures that delamination may occur) compared to the tensile properties. The results obtained in the study of Hawileh et al. [43] confirms this fact, in which the all FRP laminates, regardless of the fibre type and resin, could retain at least 50% of their reference tensile strength after exposing to 300 ˚C for 45 min. This shows that due to early interlaminar shear failure in bending tests, the reduction factor for flexural properties must be higher than tension.

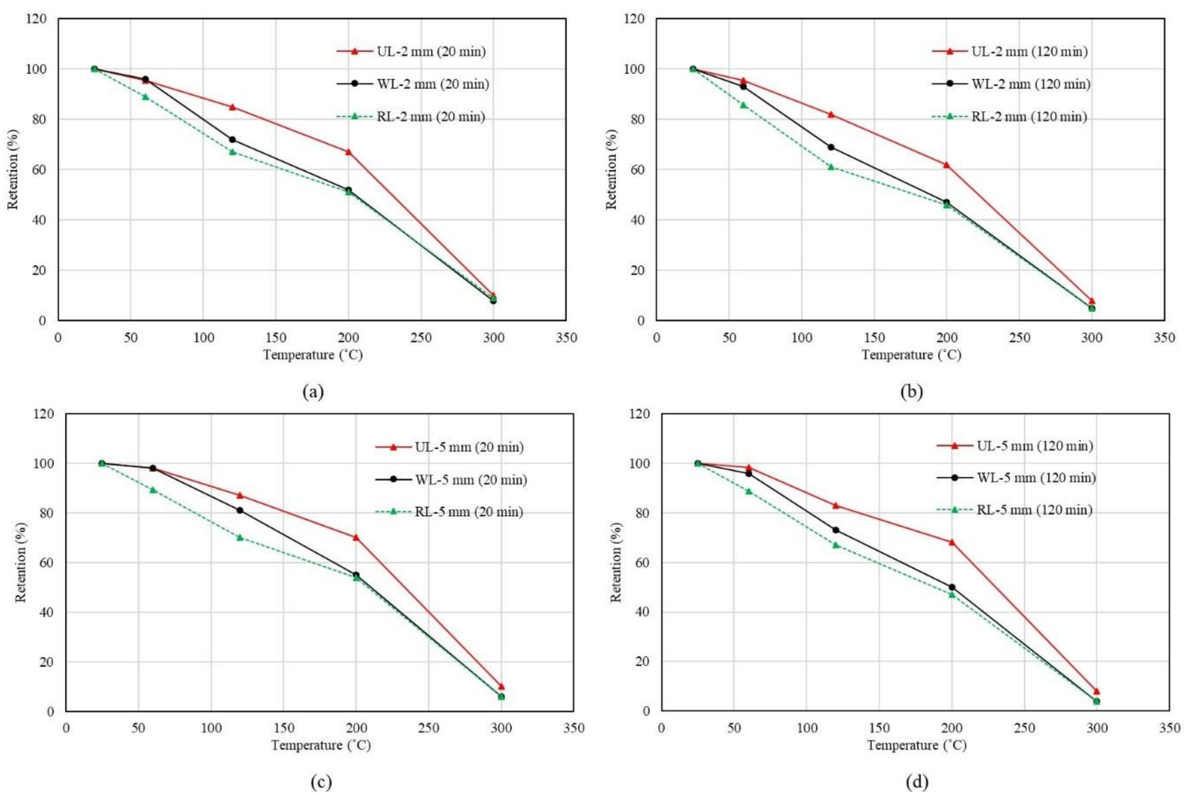

Figure 2-22 Compression between the retention-temperature curves of the GFRP laminates: (a) 2 mm laminates exposed to 20-min; (b) 2 mm laminates exposed to 120-min; (c) 5 mm laminates exposed to 20-min; (d) 5 mm laminates exposed to 120-min

2.3.3.2 Charpy impact test

It is known that the impact Charpy test is a low velocity impact, which is of great importance to investigate, especially for composite materials, in which an internal fracture may cause a significant decrease in materials performance, even if there is no obvious failure at the impacted area. A low velocity nature of the Charpy impact test may lead the specimens to be highly dependent on the fibre configuration and sample thickness [126]. It is worth mentioning that the other effective factors, such as loading velocity, fibre and matrix type, and projectile characteristics were constant in this study.

Table 2-8 and **Table 2-9** summarize the Charpy impact test results of all conditioned and unconditioned GFRP laminates in terms of ultimate strength (Us) and retention values (R) after 20-min and 120-min exposing to elevated temperatures, respectively. Similar to the bending tests, at first the effect of thickness and fibres arrangement is investigated by studying the unconditioned laminates. Then the impact behaviour of each type is discussed and finally the retention values of each type are compared with each other.

2.3.3.2.1 Unconditioned samples

Figure 2-23 presents the results of Charpy impact tests for unconditioned samples. Similar to the bending results, regardless of the laminate's thickness, UL had the best impact behaviour among all other types. In contrast to the bending, 5 mm WL revealed a relatively appropriate performance with respect to its corresponding UL (about 82%). This shows that if the thickness is appropriate, the fibres perpendicular to the load orientation may have a considerable contribution in load carrying capacity of the laminate. However, by decreasing the thickness to 2 mm, both WL and RL showed a considerable reduction in energy absorption values compared to their corresponding UL. This may show that the fibres in WL and RL could not perform properly under impact load when the thickness is relatively small.

Table 2-8 Charpy impact results after 20-min exposing

Temperature (˚C)	UL-2 mm			WL-2 mm			RL-2 mm			UL-5 mm			WL-5 mm			RL-5 mm		
	Average U_s (N)	**COV (%)**	**R (%)**	**Average U_s (N)**	**COV (%)**	**R (%)**	**Average U_s (N)**	**COV (%)**	**R (%)**	**Average U_s (N)**	**COV (%)**	**R (%)**	**Average U_s (N)**	**COV (%)**	**R (%)**	**Average U_s (N)**	**COV (%)**	**R (%)**
25	18.9	5.8	100	7.1	3.8	100	4.3	2.2	100	51	3.5	100	42.1	2.9	100	17.7	3.3	100
60	18.4	4.5	97	6.3	4.5	88	3.8	5.1	88	48.5	4.2	95	40.7	3.3	96	16.9	1.8	95
120	16.7	4.8	83	6	5.1	84	3.5	5.8	81	46.4	4.4	90	37.2	3.8	88	15.1	2.5	85
200	15.9	4.4	84	5.6	6.2	79	3.1	4.5	72	38.8	4.8	76	35.4	5.5	84	13.2	7.7	74
300	1.3	11	7	0.8	12.1	11	0.6	9.6	14	4.6	5.5	9	3	12.3	7	1.5	8.2	8

Table 2-9 Charpy impact results after 120-min exposing

Temperature (˚C)	UL-2 mm			WL-2 mm			RL-2 mm			UL-5 mm			WL-5 mm			RL-5 mm		
	Average U (kJ)	**COV (%)**	**R (%)**	**Average U (kJ)**	**COV (%)**	**R (%)**	**Average U (kJ)**	**COV (%)**	**R (%)**	**Average U (kJ)**	**COV (%)**	**R (%)**	**Average U (kJ)**	**COV (%)**	**R (%)**	**Average U (kJ)**	**COV (%)**	**R (%)**
25	18.9	2.8	100	7.1	2.6	100	4.3	3.8	100	51	2.1	100	42.1	1.8	100	17.7	2.8	100
60	16.4	4.6	86	5.6	2.9	79	3.4	4.5	79	45.3	5.6	89	38.2	5.2	90	14.9	3.2	84
120	15.5	4.4	82	5.1	3.9	72	3.2	5.5	74	42	6.2	82	33.7	5.6	80	14.2	3.2	80
200	13.8	5.3	73	4.6	6.7	65	2.9	5.9	67	36.2	6.7	71	32.9	6.9	78	12.3	4.8	69
300	1	11.1	6	0.4	12.5	5	0.5	9.8	12	4.3	12.6	8	2	10.5	5	1.4	9.6	8

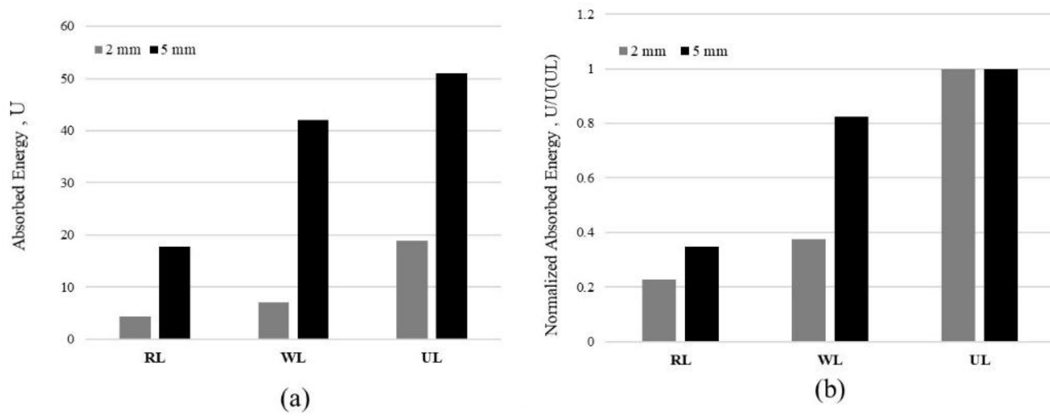

Figure 2-23 Unconditioned Charpy impact results: a) Energy absorbed, b) Normalized energy absorbed to UL energy

2.3.3.2.2 Conditioned samples: UL

Figure 2-24 shows the energy absorbed versus the temperatures of 20-min and 120-min exposing time of UL samples compared to the corresponding unconditioned specimens. As expected, increasing the exposing time decreased the absorbed energy for both 2 mm and 5 mm laminates. These reductions were slightly higher for 2 mm samples. At temperature zone of 25 ˚C ≤ T ≤ 60 ˚C, a slight decrease (about 5 %) was seen for laminates exposed to 20-min, while the reduction after exposing to 120-min was almost considerable (more than 10%). This shows that even a small internal damage (probable cracking in the resin matrix) may cause an earlier failure under impact test. At temperature zone of 60 ˚C ≤ T ≤ 200 ˚C, the absorbed energy kept reducing with an almost a similar rate for all conditions except UL-20-min at 200 ˚C. Having a higher energy absorption of UL-2-20-200 compared to UL-5-20-200 may be due to the randomness of the samples and high standard deviation of the results. At 300 ˚C, as a result of approaching to the decomposition temperature (Td) of the resin, the absorbed energy reduced significantly (about 10% compared to the corresponding unconditioned sample).

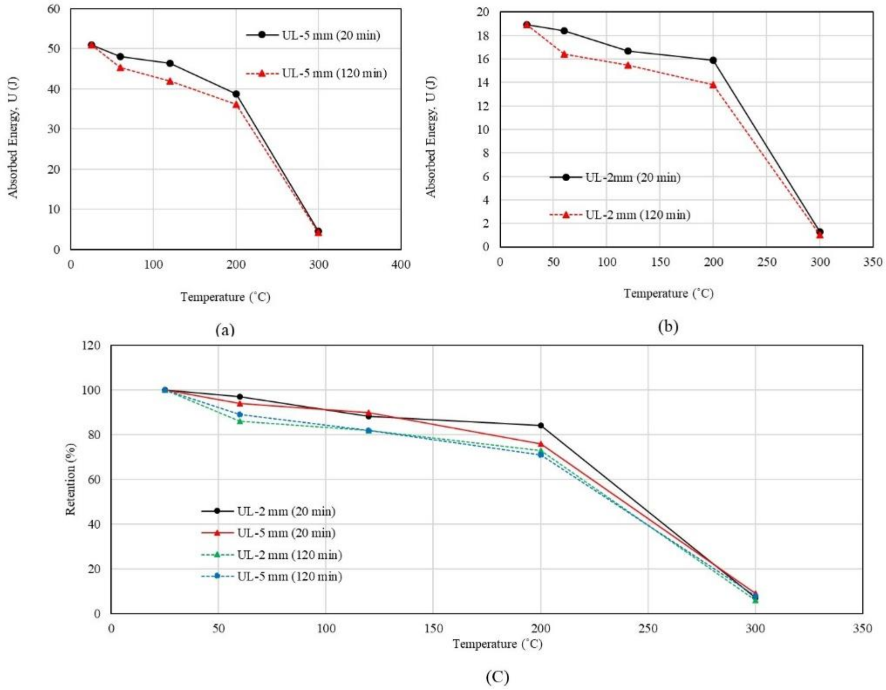

Figure 2-24 Charpy impact results of UL: (a) Absorbed energy versus temperature of 5 mm samples; (b) Absorbed energy versus temperature of 2 mm samples; (c) Retention versus temperature

2.3.3.2.3 Conditioned samples: WL

Figure 2-25 shows the energy absorbed versus the temperatures of 20-min and 120-min exposing time of WL samples compared to the corresponding unconditioned specimens. Almost the same trend to UL was observed for the reduction regime of WL. However, the reduction rate of 2 mm laminates compared to the corresponding 5 mm laminates was higher for WL than UL. As an unexpected observation, it should be noted that WL-2-60-120 lost more than 20% of its reference absorbed energy. This may be due to probable cracking in the resin matrix of some specimens when exposed to 60 ˚C, which led to an early failure during the impact tests.

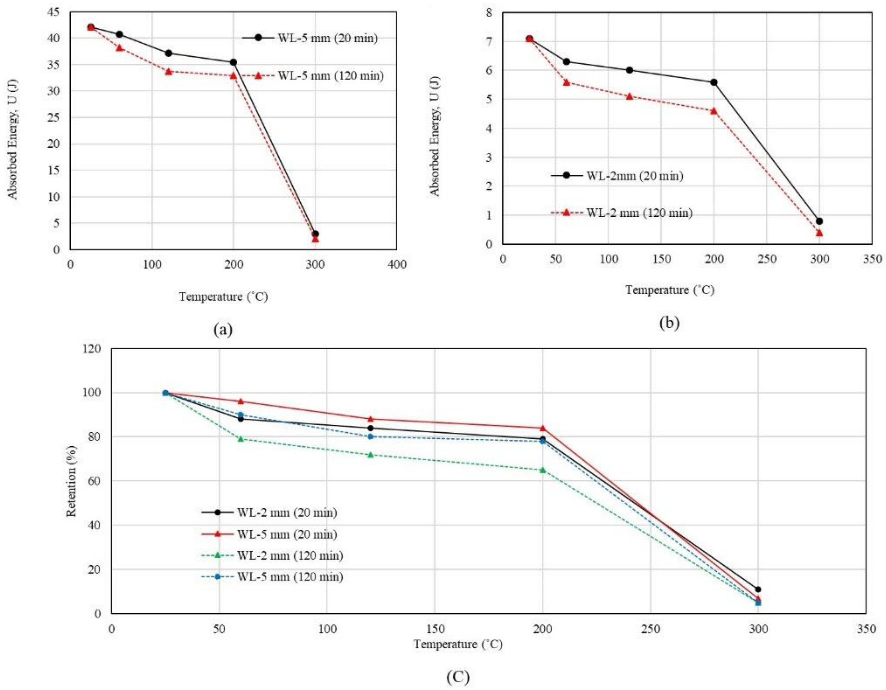

Figure 2-25 Charpy impact results of WL: (a) Absorbed energy versus temperature of 5 mm samples; (b) Absorbed energy versus temperature of 2 mm samples; (c) Retention versus temperature

2.3.3.2.4 Conditioned samples: RL

Figure 2-26 shows the energy absorbed versus the temperatures of 20-min and 120-min exposing time of RL samples compared to the corresponding unconditioned specimens. Also, a same trend was obtained in energy absorption behaviour of RL compared to WL and UL. However, compared to the previous types, all conditions (expect RL-5-20) showed a considerable decrease (more than 10% and up to 21%) in their absorbed energy values compared to their corresponding unconditioned samples. This shows that the resin degradation (micro cracks and reduction in the load transferring capacity) is more critical in impact behaviour of randomly fibre distributed laminates in comparison to the woven and unidirectional fibre laminates when subjected to elevated temperatures.

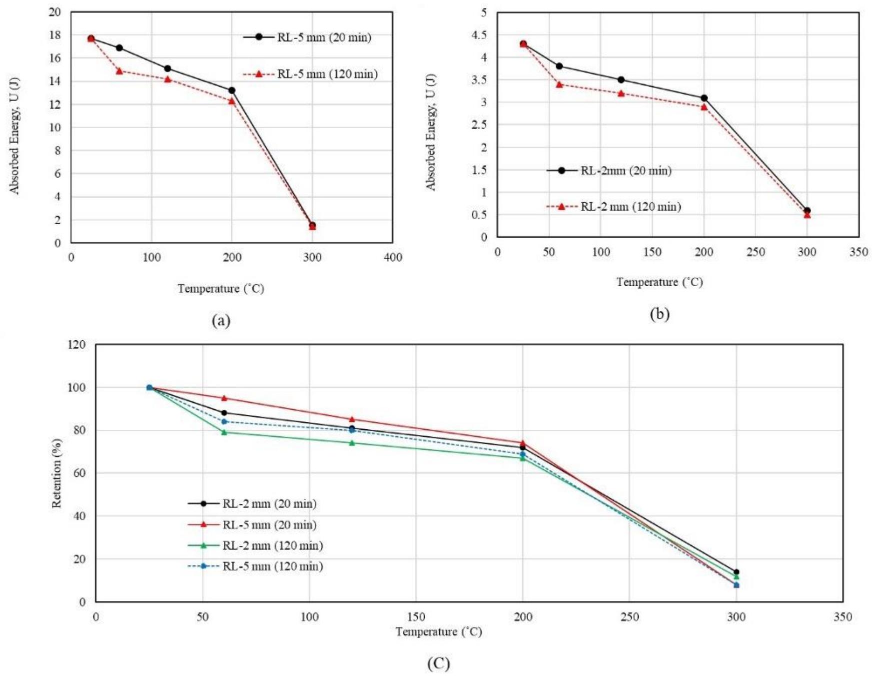

Figure 2-26 Charpy impact results of RL: (a) Absorbed energy versus temperature of 5 mm samples; (b) Absorbed energy versus temperature of 2 mm samples; (c) Retention versus temperature

2.3.3.2.5 Comparison between the UL, WL, and RL

Figure 2-27 compares the energy absorption versus the temperatures of three different GFRP laminates used in the present study. It can generally be concluded that RL, due to its high dependency to resin properties, showed the weakest and UL showed the best impact performance, while the WL was somewhere between. As is seen, at 60 ˚C, UL-2-20-60, UL-5-20-60, and WL-5-20-60 were almost resistant to this temperature (less than 5% reduction), while other types were vulnerable, even at this temperature, which is below the Tg of the resin.

By changing the temperature from 60 ˚C to 120 ˚C, all laminates experienced more reduction in terms of absorbed energy. However, the reduction rates in this range of temperatures were less than that of the bending tests. This shows that the static flexural behaviour of GFRP laminates are more sensitive to temperatures near and above Tg of the resin. It is known that at temperatures above Tg, the bond between fibre and resin may be degraded significantly. At 300 ˚C, similar to the bending tests, as a result of reaching the decomposition temperature of the resin (Td), the absorbed energy significantly reduced (about 90% reduction compared to the corresponding unconditioned sample).

At 300, all laminates lost more than 80% of their reference strength, which reveal that the bond between the fibres and the resin is significantly weakened after exposing to elevated temperature and consequently total delamination occurred for all GFRP laminates during the impact test.

General comparison between the retention-temperature curves of three-point bending and Charpy impact tests showed that in three-point bending tests laminates lost their flexural strength up to 55% at 200 ˚C, while the energy absorption capacity reduced up to 35%. This shows that a higher reduction factor for static loading at extreme temperature (i.e. 200 ˚C) must be considered than the impact loading when using FRPs. However, more experimental and numerical data is needed for better understanding the performance of such materials under static and impact loading conditions. The reason for this difference may be due to the difference of the loading condition and failure zones during three-point bending and impact tests.

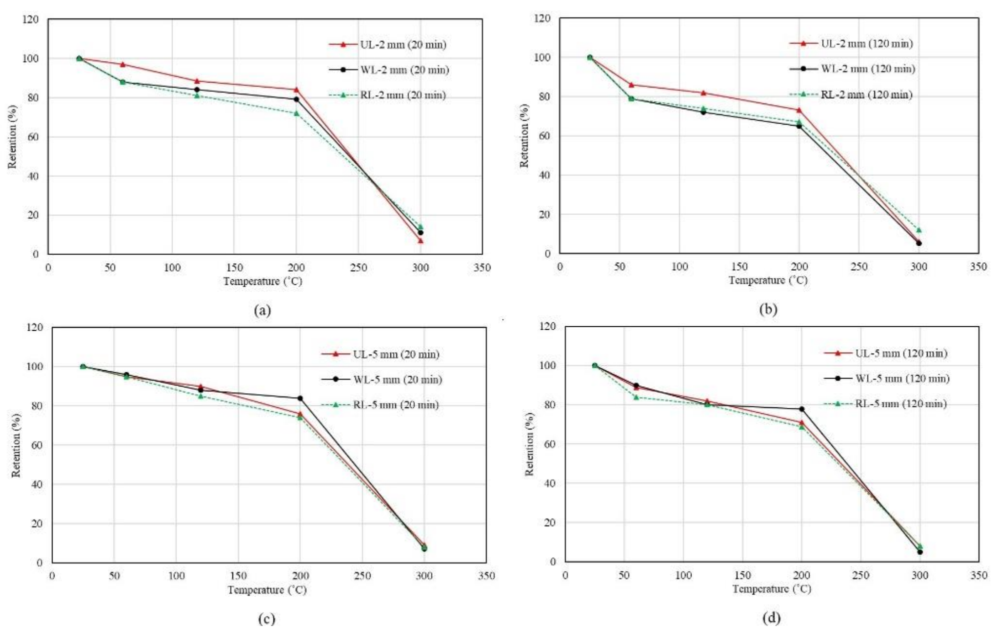

Figure 2-27 Compression between the retention-temperature curves of the GFRP laminates: (a) 2 mm laminates exposed to 20-min; (b) 2 mm laminates exposed to 120-min; (c) 5 mm laminates exposed to 20-min; (d) 5 mm laminates exposed to 120-min

2.4 Statistical analysis

2.4.1 Analysis of Variance (ANOVA)

Two-way analysis of variance (ANOVA) was conducted to investigate the effect and contribution percentage of each variable on bending and impact properties of various GFRP laminates after exposure to elevated temperatures. It is worth mentioning that as at 300 ˚C, all GFRP laminates lost almost all their strength and energy absorption capability, the ANOVA were applied on elevated temperatures up to 200 ˚C.

2.4.1.1 Three-point bending

According to three-point bending tests and ANOVA results the contribution of each parameter on the absorbed energy and its retention values are presented in **Figure 2-28** to **Figure 2-30**. At first (charts (a) and (b) of the figures), the temperature and time are the variables studied (thickness is considered as a constant parameter), while (in charts (c) and (d) of the figures), the contribution of temperature and thickness are investigated next (exposure time is considered as a constant parameter). Generally, it is seen that the effect of time and thickness on the bending properties of GFRPs exposed to elevated temperatures is not significant and can be neglected. However, it is needed to mention that the effect of time on bending properties of GFRP laminates increased by increasing the temperatures. This was obtained based on some additional ANOVA analyses performed on the temperatures higher than 60 ˚C. From these analyses the contribution of time for 2mm laminates increased from 1.4% for UL, 1% for WL, and 1% for RL (ANOVA based on all elevated temperatures) to 6%, 4%, and 5%, respectively (ANOVA based on temperatures more than 60 ˚C). In similar for 5mm laminates, the contribution of time increased from 0.9% for UL, 2% for WL, and 1.1% for RL to 5%, 7%, and 8%, respectively.

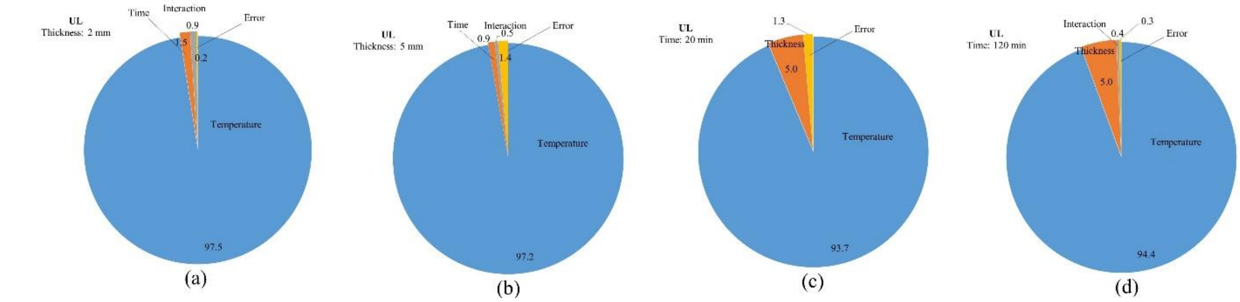

Figure 2-28 Contribution percentage of the studied variables on bending strength retention values of UL: (a) effect of temperature and time on 2 mm laminates; (b) effect of temperature and time on 5 mm laminates; (c) effect of temperature and thickness on laminates

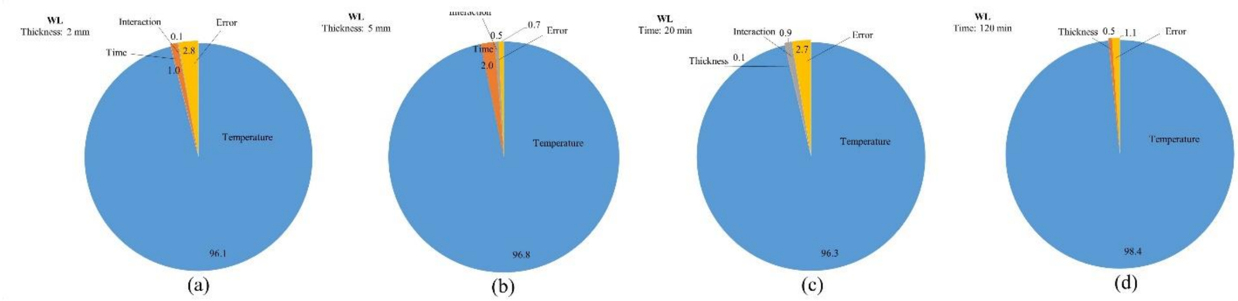

Figure 2-29 Contribution percentage of the studied variables on bending strength retention values of WL: (a) effect of temperature and time on 2 mm laminates; (b) effect of temperature and time on 5 mm laminates; (c) effect of temperature and thickness on laminates

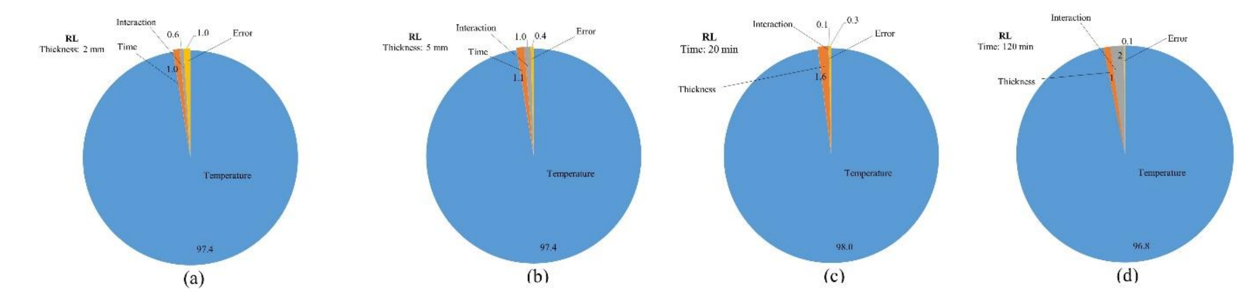

Figure 2-30 Contribution percentage of the studied variables on bending strength retention values of RL: (a) effect of temperature and time on 2 mm laminates; (b) effect of temperature and time on 5 mm laminates; (c) effect of temperature and thickness on laminates

2.4.1.2 Charpy impact

According to Charpy impact tests and ANOVA results the contribution of each parameter on the absorbed energy and its retention values are determined and presented in **Figure 2-31** to **Figure 2-33**. From the figures it is seen that the effect of temperatures is highest for RL. This again shows that the RL samples are more vulnerable to elevated temperatures due to their more dependency to the resin mechanical properties, which will be degraded by increasing the temperatures. Furthermore, the contribution of time is the lowest for. This shows that less time is needed for RL samples to be degraded under impact loading and 20-min is almost adequate for this degradation. The interaction between the variables of WL and RL were not considerable (less than 3%), which shows that in these types the variables have individual effects on impact behaviour of GFRP laminates. However, the time and temperature in 5mm UL sample and also the thickness and temperature in 120-min exposing of UL samples have dependent effects on the results. The interesting observation was for the high effect of thickness and time of exposure in **Figure 2-32 (a)** and **Figure 2-32 (d)**. These results show that the exposure time plays an important role on impact behaviour of 2 mm WL as well as thickness in 120-min exposure of 5 mm WL.

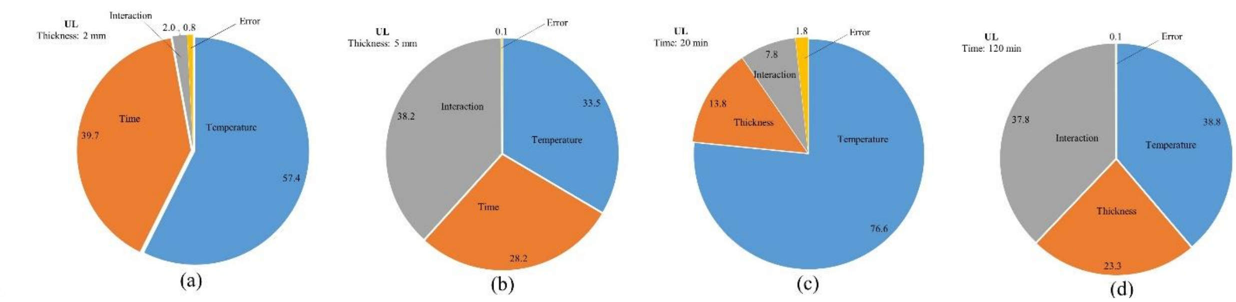

Figure 2-31 Contribution percentage of the studied variables on absorbed energy retention values of UL: (a) effect of temperature and time on 2 mm laminates; (b) effect of temperature and time on 5 mm laminates; (c) effect of temperature and thickness on laminates

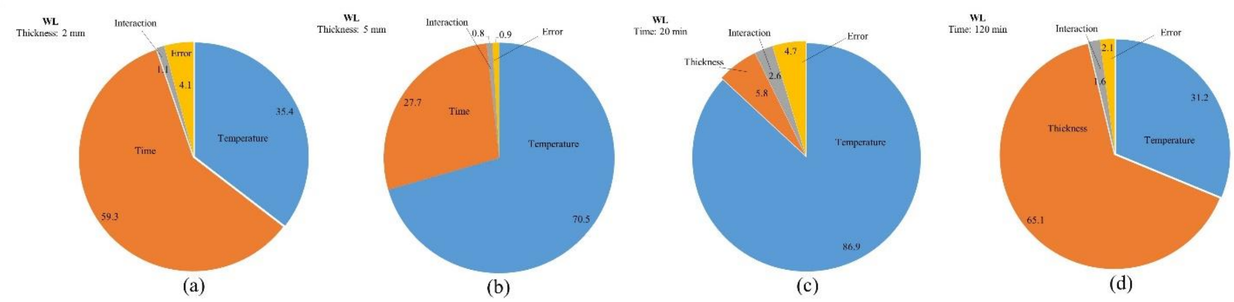

Figure 2-32 Contribution percentage of the studied variables on absorbed energy retention values of WL: (a) effect of temperature and time on 2 mm laminates; (b) effect of temperature and time on 5 mm laminates; (c) effect of temperature and thickness on laminates

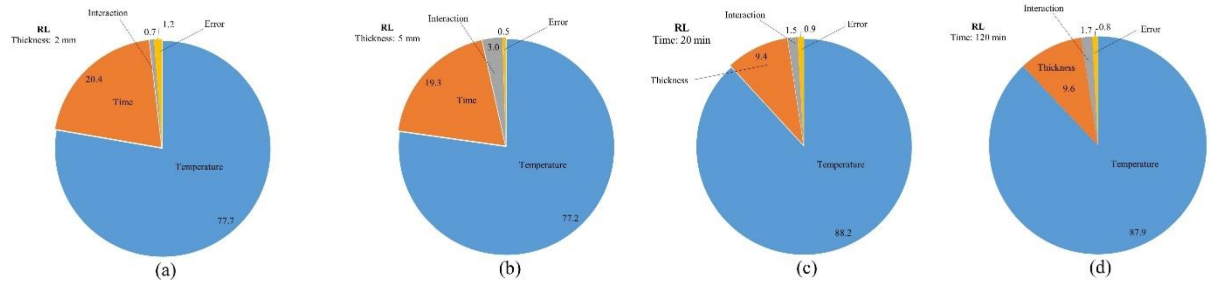

Figure 2-33 Contribution percentage of the studied variables on absorbed energy retention values of RL: (a) effect of temperature and time on 2 mm laminates; (b) effect of temperature and time on 5 mm laminates; (c) effect of temperature and thickness on laminates

2.4.2 Linear Bayesian regression

In this section probability models for tensile three-point bending and Charpy impact tests conducted on GFRP laminates after exposure to elevated temperatures were developed. The equations were based on the experimental results and ANOVA analyses using the linear Bayesian regression method.

In order to predict the best model in Bayesian regression method, stepwise deletion procedure is used. To do so, firstly it is recommended to start with a model including all variables as a comprehensive candidate. The initial predicted model in the following form can be considered in the following form:

$$F\ (x, \theta) = \sum_{i=1}^{n} \theta_i h_i(x) \tag{2.3}$$

where $F\ (x, \theta)$ is the selected deterministic model (i.e. function of the variables x and parameters θ, θ_i is the model unknown parameters, and $h_i(x)$ is explanatory functions set.

Then, based on the available data, the posterior statistics of the model parameters θ_i, and the model standard deviation, σ, will be computed.

Then, to modify the model, unimportant terms and terms that are closely correlated will be deleted and combined, respectively. With this regard, the least informative function that its coefficient θ_i has the largest posterior coefficient of variation may drop from the proposed model.

Next step is to find out whether the variables in $h_i(x)$ and $h_j(x)$ are related and these functions need to be combined. To do so, the largest correlation coefficient value between θ_i and other remaining parameters θ_k, $k \neq i$, is calculated (i.e. $\left|\rho_{\theta_i\theta_j}\right| = max_{k\neq i}|\rho_{\theta_i\theta_k}|$). If the value of $\left|\rho_{\theta_i\theta_j}\right|$is close to 1 (say larger than 0.7), it indicates that $h_i(x)$ and $h_j(x)$ are related and can be combined using:

$$\hat{\theta}_i = \mu_{\theta_i} + \rho_{\theta_i\theta_j}\frac{\sigma_{\theta i}}{\sigma_{\theta j}}\left(\theta_j - \mu_{\theta_j}\right) \tag{2.4}$$

Where μ_{θ_i} and $\sigma_{\theta i}$ are the posterior mean and standard deviation of θ_i, respectively. Now the reduced model will be assessed by calculating the posterior mean of σ and if it has not increased by an unacceptable amount, the reduced model is acceptable. Otherwise, the reduction is not desirable and the initial model must be kept.

If the reduction is accepted, the same steps will be done with the new model until the most accurate model is developed (i.e. value of $\left|\rho_{\theta_i\theta_j}\right|$is less than 0.7 (ideally less than 0.5))

The risk tools (RT) [127] software was used to derive the equations. It must be noted that the data for 300 ˚C was not used for developing the modes as the laminates could not carry appropriate loads.

It is worth mentioning that the parameters that revealed effective contribution in flexural strength and energy absorption capacity reduction based on the ANOVA analyses were used as inputs of the linear Bayesian models' variables to drive the equations.

On the basis of variable parameters, the normalized three-point bending strength and absorbed energy in Charpy impact tests of GFRP laminates after exposure to elevated temperatures can be calculated as follows:

$$R\ (\%) = a\left(\frac{1}{T^3}\right) + b\left(\frac{1}{\left(Log\left(\frac{t_1}{6}\right)\right)^{0.5}}\right) - c\left(\frac{1}{(Log(t_2))^{0.5}}\right) + d \tag{2.5}$$

where T (º K) is the temperature, t_1 (min) is the exposure time, t_2 (mm) is the thickness, and a, b, c, and d are the constants based on the laminates type. The constant values for three-point bending and Charpy impact tests are listed in **Table 2-10** and **Table 2-11**, respectively.

The R factor, the coefficient of variation (COV) of standard deviation (%), and the mean of standard deviation of the models were presented in **Table 2-12** and **Table 2-13**. The reliability of the developed model using linear Bayesian method is confirmed by these values.

Table 2-10 Constant values in Eq.1 for three-point bending tests

Specimen Type	a	b	c	d
UL	1.1224×10^7	0.039318	0.037198	0.627804
WL	1.7070×10^7	0.065736	0.046531	0.411259
RL	1.7907×10^7	0.062085	0.031416	0.331234

Table 2-11 Constant values in Eq.1 for Charpy impact tests

Specimen Type	a	b	c	d
UL	7.9974×10^6	0.11621	0.011657	0.546518
WL	8.2290×10^6	0.14028	0.100651	0.672677
RL	9.7566×10^6	0.10469	0.052822	0.585015

Table 2-12 Regression parameters for three-point bending tests model

Specimen Type	R-factor	Mean of standard deviation	Coefficient of variation of standard deviation
UL	0.94	0.0544	0.25
WL	0.95	0.0757	0.25
RL	0.99	0.0398	0.25

Table 2-13 Regression parameters for Charpy impact tests model

Specimen Type	R-factor	Mean of standard deviation	Coefficient of variation of standard deviation
UL	0.96	0.0323	0.25
WL	0.95	0.0379	0.25
RL	0.97	0.0306	0.25

A comparison of the experimental tests results and model predictions are illustrated in **Figure 2-34** and **Figure 2-35**. As is seen, good agreements between the test data and model values was obtained.

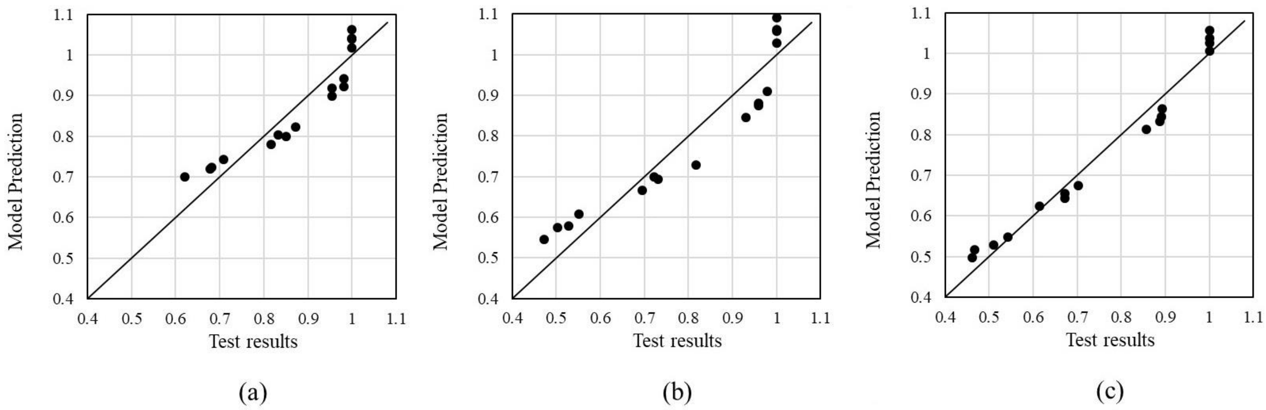

Figure 2-34 Comparison between the experimental results (average of five identical tests) and predicted values of three-point bending tests: a) UL, b) WL, and C) RL

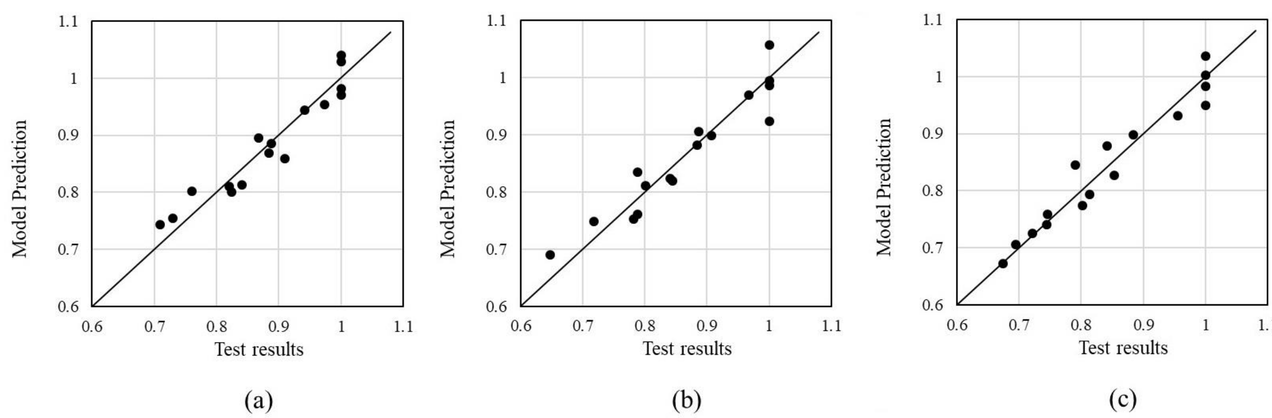

Figure 2-35 Comparison between the experimental results (average of five identical tests) and predicted values of Charpy impact tests: a) UL, b) WL, and C) RL

2.5 Conclusion

The study presents the results of different GFRP laminates performance after exposure to elevated temperatures using mechanical tests (three-point bending and Charpy impact), microstructural analyses (SEM), and statistical analyses (ANOVA and linear Bayesian regression). Regarding the obtained results, the following conclusions may be presented:

- The general failure modes in both bending and impact tests changed from the fibres rupture at tension zone (also some limited failures at compression zone) at lower temperatures to the delamination of the layers at very high temperatures.
- It was generally observed that the flexural and impact properties of GFRP laminated subjected to elevated temperatures decrease with the increase of the temperature and exposing time and decrease of the laminates thickness.
- In both bending and Charpy impact tests, GFRP laminates with unidirectional fibres showed the best performance, while the woven and randomly fibres distributed laminates were the moderate and weakest types, respectively.
- At temperatures below Tg (60 ˚C) all laminates (instead of RL) were almost resistant in terms of bending strength, while their impact properties (energy absorption capacity) decreased more than 10%. This showed that the impact performance of GFRP laminates subjected to elevated temperatures is sensitive to even a small degradation of the resin matrix.
- Reaching the temperature to glass transition temperature of the resin and above it (120 ˚C and 200 ˚C), led to a significant reduction in both bending strength and impact behaviour of the GFRP laminates. This was mainly because of the degradation of the resin matrix properties as changing its state from glassy to rubbery and consequently weakening of the load transferring capacity and the bond between the resin and fibre.
- At 300 ˚C temperature, which is close to the resin decomposition temperature, all GFRP laminates lost almost all their bending strength and energy absorption capacity under three-point bending and Charpy impact tests, respectively. This may be attributed to the breaking of the chemical bonds and modular chains of the resin, which leads to the total debonding of the resin from the fibre.
- Based on the ANOVA analyses, the effects of thickness and time of exposure are more significant in impact behaviour of GFRP laminated in comparison to the bending properties.

Chapter 3 Effect of Fibres configuration and thickness on tensile behaviour of GFRP laminates exposed to harsh environment

Abstract

The present study indicates the importance of using GFRP laminates with appropriate thickness and fibres orientation when exposed to harsh environmental conditions. The effect of different environmental conditions on tensile properties of different GFRP laminates is investigated. Laminates were exposed to three environmental conditions: (1) freeze/thaw cycles without the presence of moisture, (2) freeze/thaw cycles with the presence of moisture and (3) UV radiation and water vapour condensation cycles. The effect of fibre configuration and laminate thickness were investigated by considering three types of fibres arrangement: (1) continuous unidirectional, (2) continuous woven and (3) chopped strand mat and two thicknesses (2 and 5 mm). Microstructure and tensile properties of the laminates after exposure to different periods of conditioning (0, 750, 1250 and 2000 h) were studied using SEM and tensile tests. Statistical analyses were used to quantify the obtained results and propose prediction models. The results showed that the condition comprising UV radiation and moisture condition was the most aggressive, while dry freeze/thaw environment was the least. Furthermore, the laminates with chopped strand mat and continuous unidirectional fibres respectively experienced the highest and the lowest reductions properties in all environmental conditions. The maximum reductions in tensile strength for chopped strand mat laminates were about 7%, 32%, and 42% in the dry freeze/thaw, wet freeze/thaw and UV with moisture environments, respectively. The corresponding decreases in the tensile strength for unidirectional laminates were negligible, 17% and 23%, whereas those for the woven laminates were and 7%, 24% and 34%.

Keywords

UV; moisture; freeze/thaw cycles; unidirectional fibres; woven fibres; random fibres; chopped strand fibres; durability

3.1 Introduction

Use of fibre-reinforced polymer (FRP) composites is rapidly increasing in automotive, aerospace, and marine applications, as well as in civil engineering [2, 6, 64]. These composites have several advantages, including lightness, high strength, ease of installation and handling, corrosion resistance, and relatively good durability properties, which have made them an attractive alternative to traditional materials (i.e. steel) in many applications [7, 8, 128]. The unique characteristics of FRPs also make them useful in engineering infrastructure for the rehabilitation and strengthening of existing structures [3, 129]. However, despite their outstanding characteristics, FRPs also have disadvantages, such as low ductility, low shear strength (due to the weak mechanical performance of the resin), vulnerability to extreme temperatures and poor durability when exposed to alkaline conditions, ultraviolet (UV) radiation, freeze/thaw cycles or fluctuating hydrothermal conditions [105, 130-134]. Consequently, the use of FRP composites in non-structural elements, secondary structures, and for rehabilitation and strengthening of existing structures is limited, particularly, in situations where there are greater chances of exposure to the regular harsh environmental conditions, as well as to elevated temperatures and fires during structural service life, such as during transportation or storage [120, 135].

The current literature on the degradation of FRP composites has examined the effects of different environmental factors, including alkaline and acidic solutions [4, 12, 99, 113, 136-139], seawater [24, 99, 113, 137, 139-143], hydrothermal conditions [144-148], temperature fluctuations [72, 140, 142, 149-151], UV radiation [23-25, 39, 105, 148, 152, 153], and elevated temperatures [38, 39, 63, 105]. However, relatively fewer studies have focused on the performance of FRPs subjected to the harsh environmental conditions posed by the freeze/thaw cycles that simulate cold region climates or by the UV, moisture, and elevated temperature conditions that simulate sunny days in hot regions [64, 70, 71, 132, 154].

UV radiation is one factor responsible for the degradation of organic material, as it can break chemical bonds and initiate oxidation reactions. Although this degradation tends to be superficial and may not have any significant effect on mechanical properties of FRPs [105, 155], a combination of UV radiation and moisture, together with elevated temperature, may intensify the adverse effects of these factors [39].

The potential damage resulting from diffusion of moisture into the polymer includes resin matrix cracking, swelling, plasticisation, hydrolysis and fibre/resin interface debonding, which are the primary causes of the degradation of the mechanical properties of composites [26, 27].

Elevated temperature alone (without the presence of the moisture) is not a critical issue when it is below the glass transition temperature, Tg, of the resin (which is 80 °C for the resin of FRP used in this study) [156, 157]. The rapid degradation of FRPs due to elevated temperature starts when the temperature reaches the Tg, when the resin matrix begins to change from a glassy to a rubbery state [121, 158]. However, moisture penetration into the matrix may also be faster and deeper at elevated temperatures.

By contrast, matrix hardening (increased brittleness) and microcracks may occur when FRPs are exposed to subzero temperatures. The difference in the coefficients of thermal expansion between the resin and fibres in a composite material may also increase the internal stress in FRPs and lead to fibre/resin debonding in response to thermal variations. One conclusion, therefore, is that thermal cycles at low temperatures may be more damaging to the mechanical properties of FRPs when compared to constant exposure to freezing temperatures [159]. Further, the microcracks that can develop due to subzero temperatures may increase resin hydrolysis, plasticisation and moisture penetration into the resin matrix, thereby, further degrading the FRP mechanical properties. In other words, thermal cycling in the presence of moisture (wet cycling) can cause moisture to be absorbed and trapped in the resin cracks at higher temperatures, while subsequent freezing and expansion at low temperatures can cause crack growth and further resin/fibre debonding [154, 160, 161]. Studies on the effects of freeze/thaw cycles on the mechanical properties and degradation of FRP composites are limited [123]. Therefore, the present study investigates mechanical properties and microstructural degradation of glass fibre reinforced polymer (GFRP) composites, fabricated by vacuum infusion process, under freeze/thaw cycles (in the presence or absence of moisture).

Previous research into the effects of regular environmental factors (viz., UV radiation, moisture and thermal fluctuations) on FRP composites has mostly focused on the effects of such factors on the structural behaviour (e.g., bonding between the FRP laminate and the member substrate) of structures reinforced and/or strengthened with FRP [65-71]. Limited studies have also investigated the effects of parameters that influence the mechanical properties of the FRPs themselves after environmental exposures [39, 72, 73]. In addition, the literature related to the degradation of the mechanical properties of FRP composites subjected to harsh daily environmental conditions has mainly concentrated on only one type of fibre configuration (i.e., continuous-unidirectional fibres) [70, 72, 74]. However, other fibre characteristics, such as length and orientation, are also expected to affect the fabrication quality, mechanical properties and structural performance of FRPs [63, 162], that, in turn, can affect the degradation mechanisms and penetration and propagation of cracks, and, consequently, the mechanical properties of the composite materials after exposure to harsh environmental conditions. To the best of the authors' knowledge, the effect of fibre configuration on the durability and mechanical properties of FRP composites subjected to harsh environments remains poorly studied. Therefore, the effect of various fibre configurations is addressed in the present study by considering three types of GFRP composites: unidirectionally orientated, woven orientated, and chopped strand (randomly orientated) fibres.

The behaviour of FRP composites due to fibre orientation may be classified into two categories: (1) anisotropic behaviour for composites with fibres orientated in different directions, due to direct and shear-strain coupling effects [75] and (2) almost orthotropic behaviour for composites with unidirectional fibres, due to their negligible strain coupling effects [76].

In addition to the fibre configuration, the thickness of the composites may play an important role in determining the damage resulting from environmental agents such as moisture, UV radiation and temperature fluctuations. It is known that the effects of moisture on composites are localized to a thin sub-surface layer that is exposed to moisture. Moreover, it is well stablished that UV radiation may mostly affect the surface (outer layer) of the composites and the inner layers are generally unaffected. Therefore, the effect of exposed (damaged) layer will become more pronounced when a significant portion of the tested area is affected by the local damage zone: the thinner the sample, the greater is the chance of measuring the conditioning adverse effects [74]. However, based on the literature, the effect of specimen thickness on the mechanical properties of FRPs after exposure to harsh environmental conditions has received very limited attention [63]. Therefore, the present study will investigate this effect by considering different thicknesses of GFRP composites when exposing to environmental conditioning.

With the background described above, this experimental study investigates the effect of different parameters, i.e., the configuration of the fibres (length and orientation), specimen thickness, and number of conditioning cycles on mechanical and microstructural properties of GFRP composites after exposure to three environmental conditions: (1) UV radiation and water vapour condensation cycles, (2) freeze/thaw cycles without moisture, and (3) freeze/thaw cycles with moisture.

3.2 Experimental Description

The present study, as part of an ongoing research project on durability of FRP composites used for structural applications, focuses on the tensile properties of GFRP laminates subjected to regular harsh environmental conditions. Thin laminates were tested in tension to simulate the condition of retrofitting structural members with FRP laminates. The flexural and compressive properties of FRP composites when used as individual structural members under aggressive environments will be studied by the authors in the future.

The effects of fibre length and orientation were investigated by considering unidirectional continuous, woven continuous, and chopped strands fibres. Moreover, the thickness effect was studied using two different thicknesses. Regarding the conditioning scheme, three regimes of cycling: (1) sequential exposure of UV radiation and water vapour condensation, (2) freeze/thaw cycles with the presence of moisture (i.e., wet cycling) and (3) freeze/thaw cycles without the presence of moisture (i.e., dry cycling) were used. In order to study the effect of exposure time, three durations of cycling for each regime were used. Mechanical properties of the specimens after exposure to different periods of conditioning were investigated using tensile tests. Furthermore, scanning electron microscopy (SEM) was carried out after conditioning (both before and after mechanical tests) to study the microstructural degradation, damage progression and failure modes. Finally, in order to quantify the obtained results and contribution of each variable on the final results, statistical study, including Analysis of Variance (ANOVA) and linear Bayesian regression were carried out.

3.2.1 Materials

Specimens were produced by vacuum infusion process (VIP). Details of VIP can be found in [63]. Continuous E-glass fibres were used for laminates with unidirectional and perpendicular (0˚ and 90˚) woven fibres, while 25 ± 5 long mm E-glass fibres were used to produce randomly distributed laminates (chopped strand mat). The tensile strength, elastic modulus and density of E-glass fibres used were, 2900-3100 MPa, 70 GPa, and 2.6 g/cm^3, respectively based on the manufacturer. IN2 Epoxy Infusion Resin with tensile strength, viscosity and density of about 65.5-73.5 MPa, 200-450 mPa.s and 1.08-1.12 g/ml (all at 20 ˚C) was used. All laminates were cured in room temperature for 24 h. Moreover, laminates were kept in 50 ˚C for 8 h to complete the post curing cycle. Samples of 2 and 5 mm thicknesses were used. **Figure 3-1** shows the samples used for this study. **Table 3-1** lists the characteristics of laminates. Tensile tests were carried out by the authors to obtain the mechanical properties of the samples. The details of the test procedure are presented in section 3.2.3 and 3.2.4.

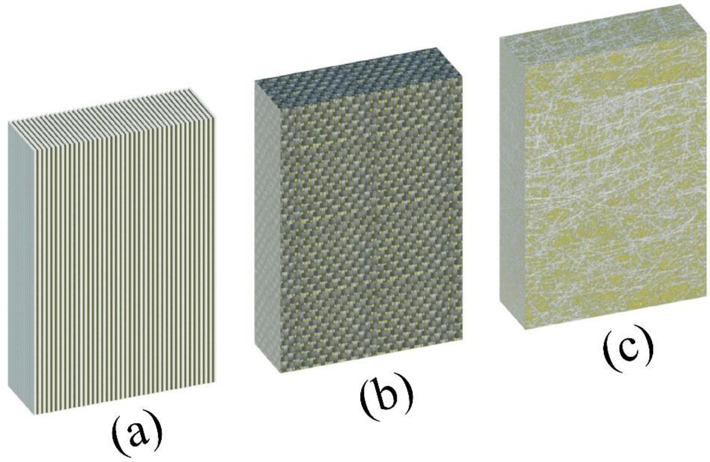

Figure 3-1 Different types of GFRP laminates used in this study: (a) Continuous unidirectional fibres, (b) Continuous woven fibres and (c) Chopped strand fibres.

Table 3-1 Characteristics of GFRP laminates constructed by VIP method.

Property	**U**		**W**		**R**	
Thickness (mm)	2	5	2	5	2	5
Number of layers	6	16	6	17	3	7
Fibre to resin ratio by volume (Fibre (%) / Resin (%))	70.5/29.5	71.2/28.8	65.2/34.8	64.6/35.4	41.6/59.4	33.1/66.9
Arial weight of each roving layer (gr/m2)	350	350	350	350	350	
Tensile Strength of single roving layer based on manufacturer data-sheet (MPa)	750-921		297-342		negligible	
Thickness of single roving layer based on manufacturer data-sheet (mm)	0.27		0.25		0.53	
Roving elongation based on manufacturer data-sheet (%)	3		2		Not-specified	
Count of yarns (threads/cm)	4.5		4 (Wrap) × 4 (Fill)		Not-specified	
Ultimate tensile strength (MPa) (mean ± standard deviation)	700 ± 5.6	872 ± 5.3	320 ± 1.8	341 ± 2.5	180 ± 2.2	246 ± 2.8
Tensile Elastic modulus (GPa) (mean ± standard deviation)	32 ± 1.1	33 ± 0.8	18 a ± 0.1, 11b ± 0.1	22.0 a ± 0.2, 15 b ± 0.1	11.0 ± 0.1	15 ± 0.2
Glass Transition Temperature, Tg (˚C)	80	80	80	80	80	80
Thermal Expansion Coefficient (10 -6 / ˚C)	0.3-0.6	0.3-0.6	0.3-0.6	0.3-0.6	0.3-0.6	0.3-0.6

Note: U=unidirectional, W=woven, R=random, W laminates have bilinear stress-strain curve [123]: a) Initial Elastic modulus, b) secondary chord Elastic modulus.

3.2.2 Environmental conditioning

Figure 3-2 shows the environmental condition schemes used in this study. From each sample type, three identical un-conditioned specimens were tested in tension and the average ultimate tensile strength was used as reference for each condition. Samples were subjected to environmental conditioning for three durations: 750, 1250 and 2000 h.

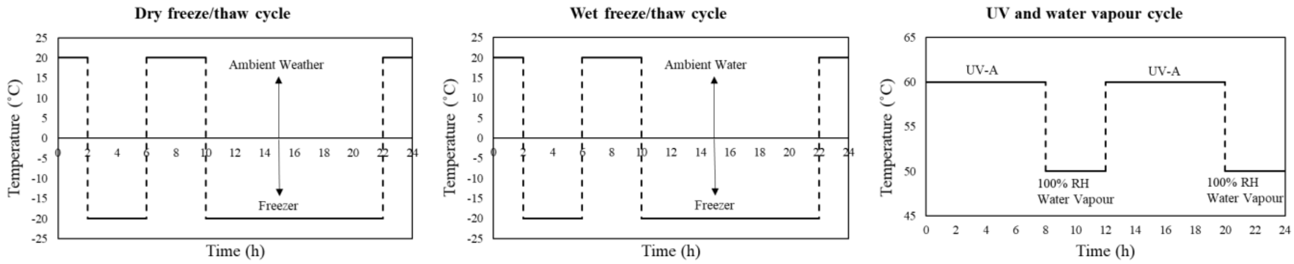

Figure 3-2 Environmental condition cycles used in this study.

It is worth mentioning that as there is no specification for the number of thermal cycles that FRPs may experience during their life-span, the number of conditioning cycles were estimated according to the standard recommendations for other non-structural and coating materials (i.e. EN 1504-4 [163] and ASTM D6944-15 [164]). In those standards maximum number of 50 cycles is recommended for a life span of 25 years. Accordingly, the maximum cycling duration of 2000 h was chosen in this study, which is a reasonable estimation for about 30 to 50 years of service life under very cold conditions.

As the first environmental conditioning, the samples were exposed to the cycles of UV radiation and water vapour condensation according to the standard, ASTM G154 [64]. As shown in **Figure 3-2**, each cycle constituted 8 h of UV-A radiation at 60 ˚C followed by 4 h of water vapour condensation at 50 ˚C with 100 % RH. A UV-A lamp with the radiation' wavelength of 340 nm, and an irradiate of 0.85 W/m2 was used to simulate a regular harsh environment of coastal areas [165].

For each dry freeze/thaw cycle, which lasted for 24 h, the samples were held for 12 h at a sub-zero temperature (-20 ˚C), followed by 4 h at the ambient temperature (20 ˚C), 4 h of subzero temperature (as a shock to maximize the conditioning effect), and finally, 4 h of ambient temperature.

For wet freeze/thaw cycling, the samples were held for 14 h at a subzero temperature (-20 ˚C), followed by 8 h of immersion in tap water at 20 ˚C. It is important to note that the temperature range (-20 ˚C to 20 ˚C) was selected according to the recommendations [150] for testing to simulate very cold regions (e.g., those in Canada).

3.2.3 Specimens

A total of 204 laminates were prepared for conditioning and mechanical tests. The length and width of all samples were 300 and 20 mm, respectively. To examine the reproducibility of data, test in each condition was triplicated. In order to prevent possible failure and slip at the ends of the sample (grip of the testing machine), two tabs were attached to the tensile samples before conducting the tests. It should be noted that tabs were attached after conditioning.

3.2.4 Tensile tests

Tensile properties of control and conditioned GFRP laminates were determined by tensile tests using a Santam servo electrical testing machine. All tensile samples were subjected to increasing load at a constant loading rate of 1.2 mm/min, until fracture. Strain was measured using an extensometer attached at the middle of the sample. **Figure 3-3** shows the tensile test set-up and the sample configuration.

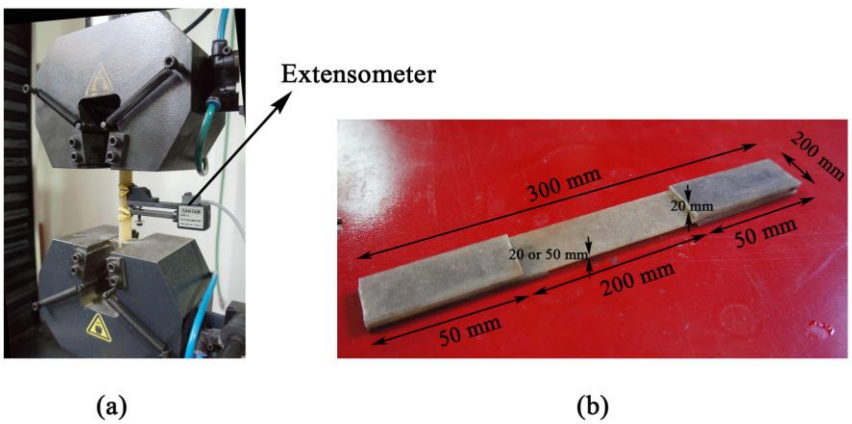

Figure 3-3 Tensile test: (a) test set-up and (b) sample configuration

3.2.5 Scanning electron microscopy (SEM)

In order to investigate the degradation mechanisms of resin matrix, fibres and their interface as well as the damage propagation (e.g., cracks configuration and fibre/matrix debonding) under different conditioning, SEM analyses were conducted on a few randomly selected samples after exposure to different freeze/thaw cycles and before mechanical tests. SEM was also carried out on the samples that were fractured in tensile tests.

3.3 Results and discussion

Degradation in GFRP and their mechanical properties, and the degradation mechanisms are discussed in this section.

3.3.1 Microstructural changes due to conditioning

To investigate the degradation mechanism of GFRP composites, the surfaces of selected laminate samples before (control) and after (conditioning) exposure to different environmental conditions were observed under SEM. **Figure 3-4** shows the control samples of each laminate type used in this study. It is noted that, in order to achieve a relatively rough surface during fabrication that was required for gripping the tensile test samples, the manufacturer used a layer of perpendicular woven fibre on the sample surface. However, this layer was removed at final stage. Therefore, as seen in **Figure 3-4**, all studied laminate types have a final woven shaped resin matrix layer (i.e., the uppermost layer does not comprise woven fibres). Therefore, all laminates, as seen in **Figure 3-3**, have just a woven shaped matrix surface (there is no woven fabric). As expected, no considerable damage (e.g., significant cracks in the resin matrix) is observed in the control samples. The holes and cracks seen in the resin matrix are attributed to sample fabrication, handling or loading.

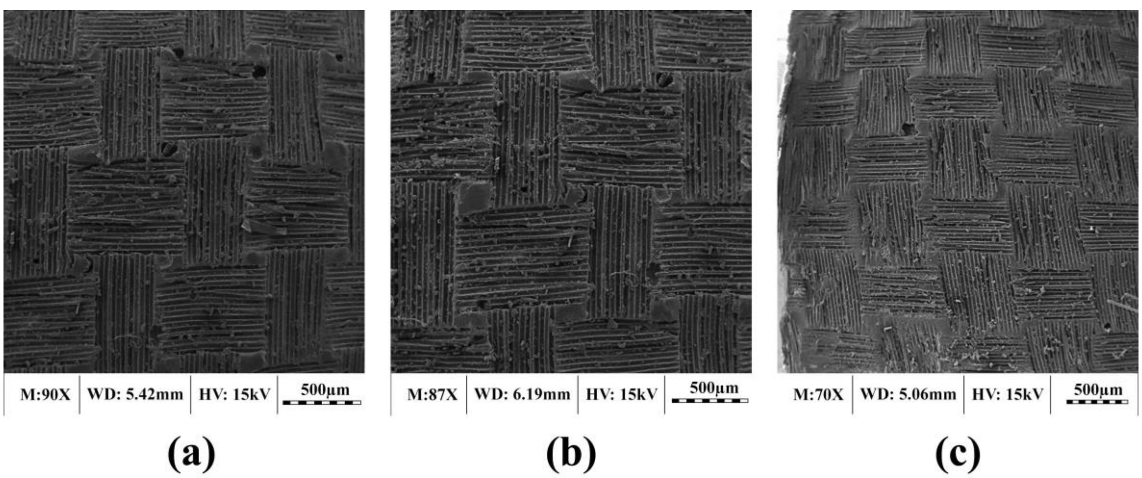

Figure 3-4 SEM micrographs of control laminates: (a) unidirectional laminate, (b) woven laminate and (c) chopped strand laminate.

Figure 3-5 shows SEM images of the selected laminates exposed to dry freeze/thaw cycles, indicating that a greater number of holes and cracks is produced with increasing number of cycles. These cracks and holes in the resin matrix may be attributed to the matrix degradation as well as the differences in the thermal expansion coefficients of fibre and resin. However, considerable fibre/resin debonding was not observed in the examined samples. It should be mentioned that UL, WL, and RL represent unidirectional, woven and chopped strand mat laminates, respectively.

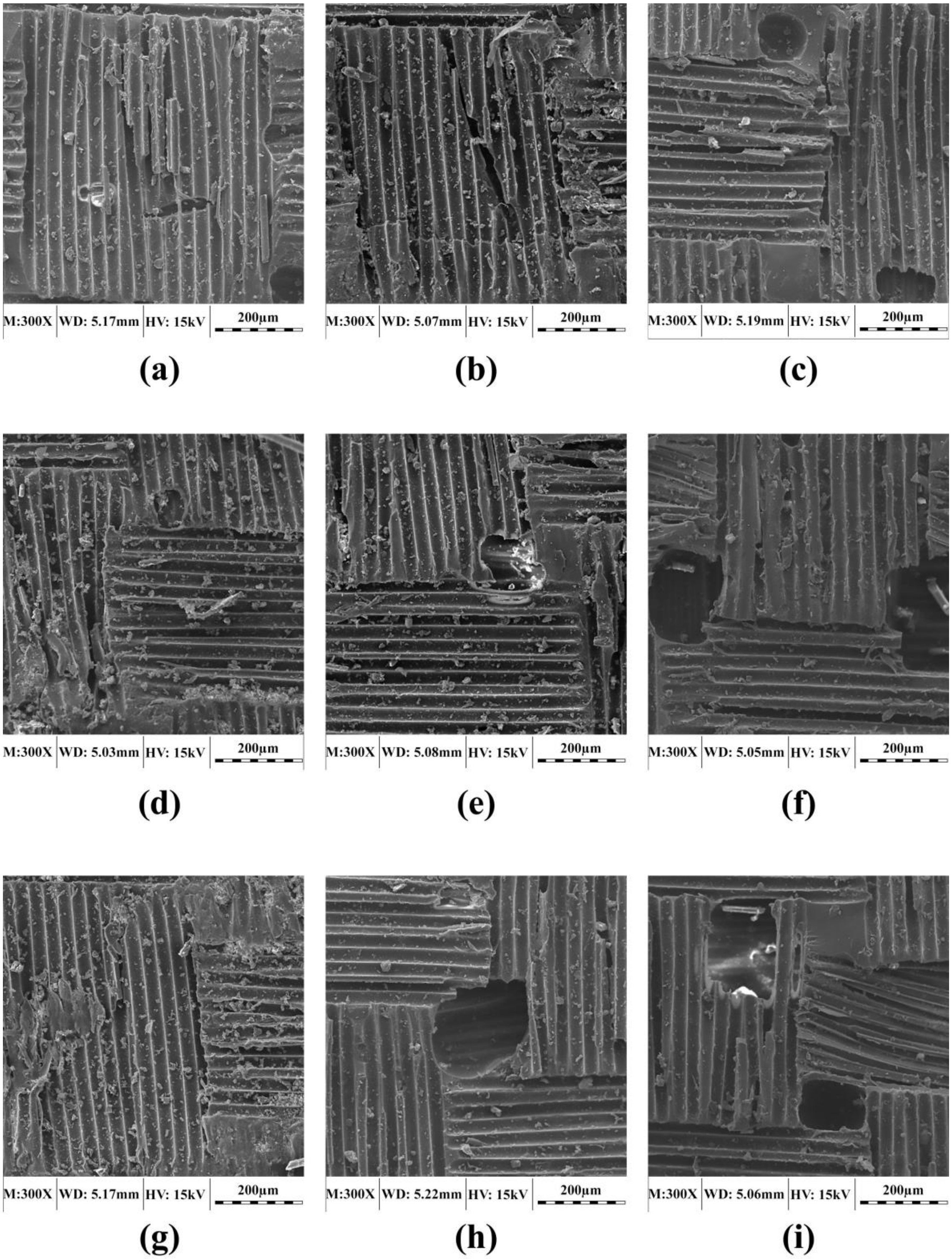

Figure 3-5 SEM micrographs of selected 2mm laminates exposed to dry freeze/thaw cycles: (a) UL exposed to 750 h cycles, (b) UL exposed to1250 h cycles, (c) UL exposed to 2000 h cycles, (d) WL exposed to 750 h cycles, (e) WL exposed to1250 h cycles, (f) WL exposed

Figure 3-6 shows SEM images of the selected laminates exposed to wet freeze/thaw cycles.

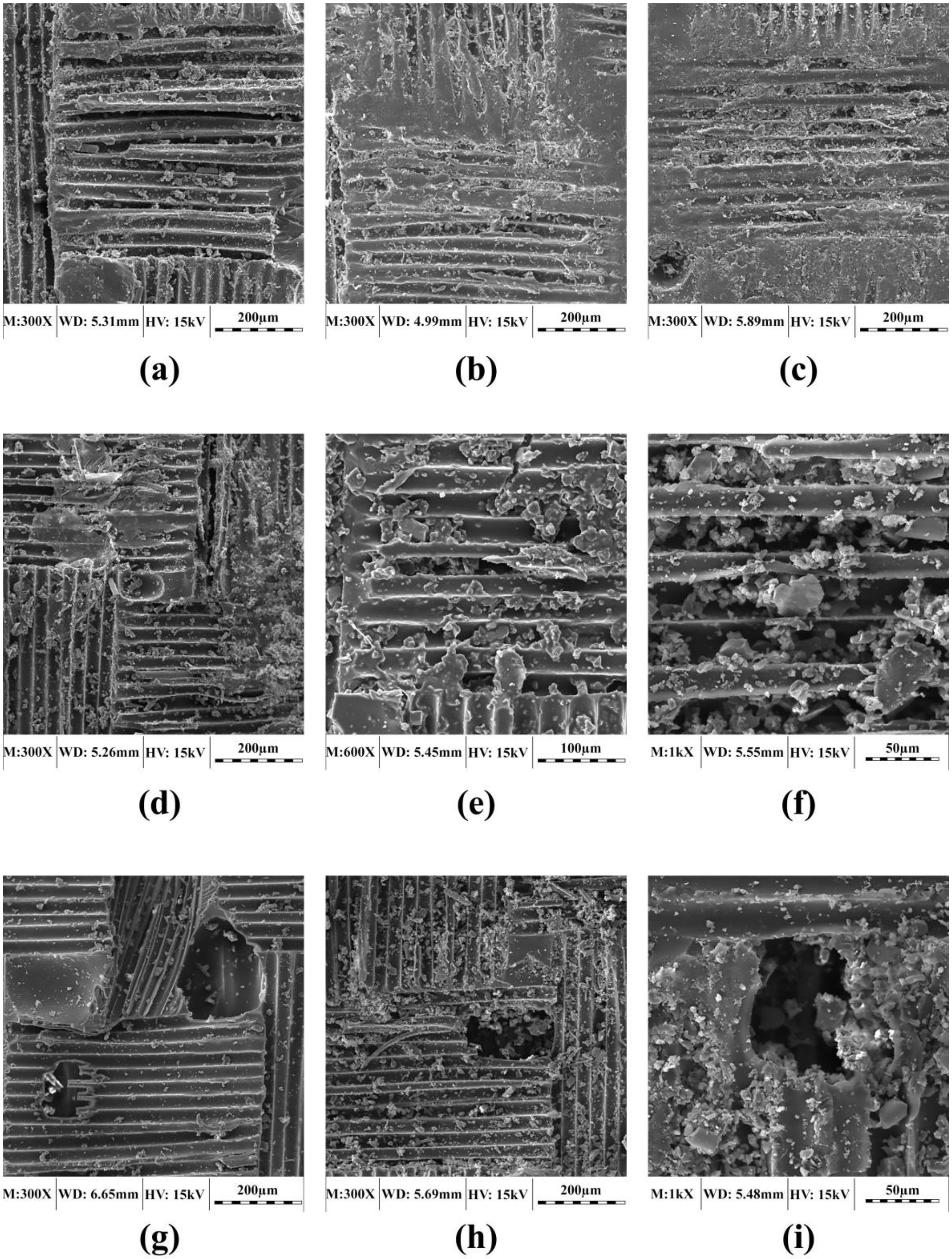

Figure 3-6 SEM micrographs of selected 2mm laminates exposed to wet freeze/thaw cycles: (a) UL exposed to 750 h cycles, (b) UL exposed to1250 h cycles, (c) UL exposed to 2000 h cycles, (d) WL exposed to 750 h cycles, (e) WL exposed to1250 h cycles, (f) WL exposed

It is also evident that increasing the number of cycles in the wet freeze/thaw condition may cause a greater damage to resin matrix, leading to fibre/matrix debonding that may degrade the composite's mechanical properties. Extensive fibre/resin debonding is seen for laminates subjected to 2000 h of wet freeze/thaw cycles. Obviously, the damage incurred in the wet cycles is more severe than to that resulting from dry cycles, which is attributed to the additional deterioration of the resin matrix due to the absorbed moisture in the wet cycle.

Figure 3-7 shows SEM images of the selected laminates exposed to UV radiation and water vapour condensation cycles that caused more pronounced cracks and holes in the resin matrix and fibre/resin debonding than the freeze/thaw cycles, indicating that UV radiation and moisture cycles represent the harshest environment. From **Figure 3-6**, it is also evident that, after exposure to 2000 h of conditioning cycles, the surface resin layer was severely damaged and the fibres were obviously exposed and debonded. Therefore, in addition to possible swelling, plasticization and cracking due to moisture, chemical changes in the resin matrix due to the processes involving UV radiation and oxygen can be distinguished as the main factors contributing to such significant deterioration of the laminates. The greater damages in the UV radiation and moisture cycles has direct bearing on the tensile test properties (as will be demonstrated later).

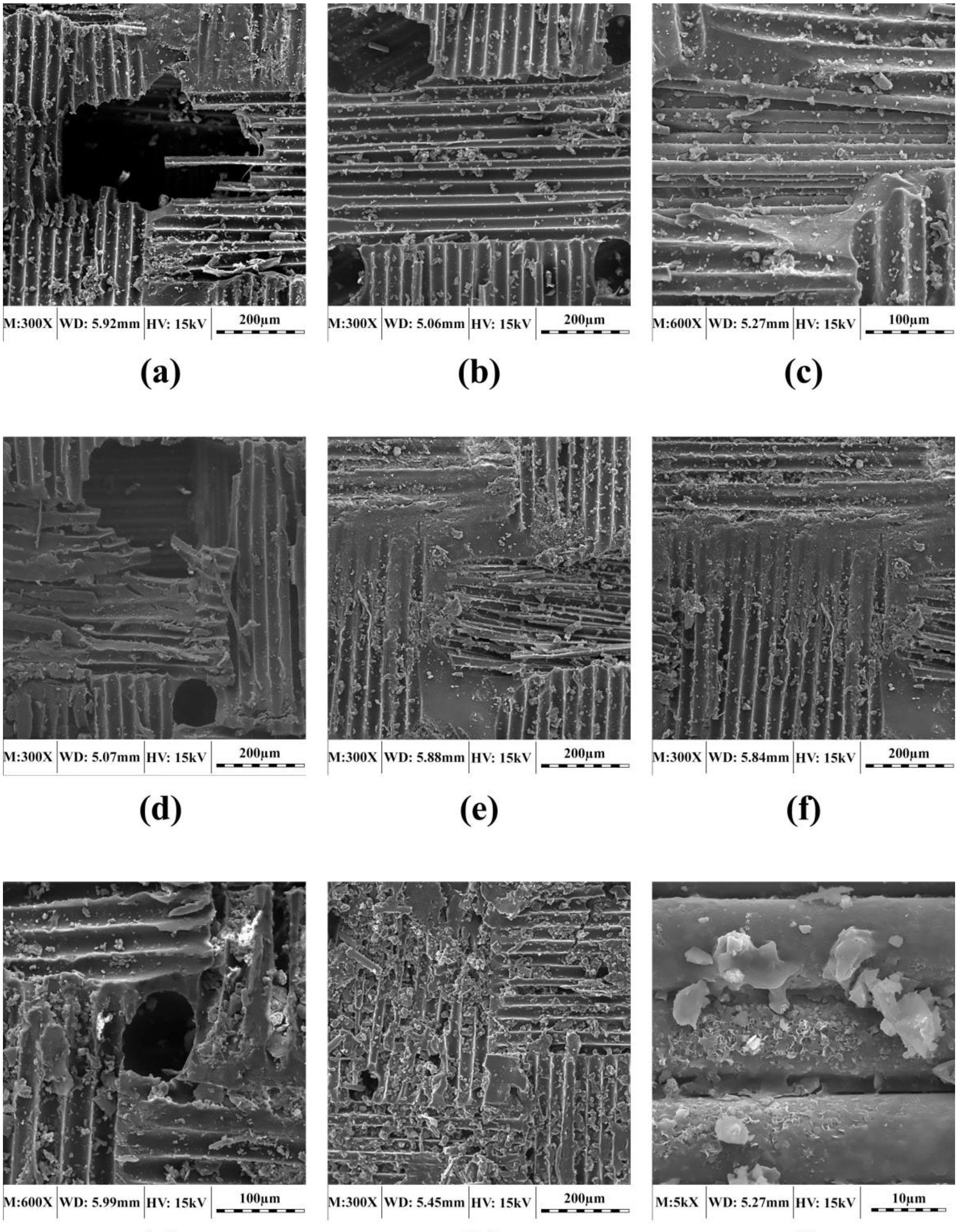

Figure 3-7 SEM micrographs of selected 2mm laminates exposed to UV and water vapour condensation cycles: (a) UL exposed to 750 h cycles, (b) UL exposed to1250 h cycles, (c) UL exposed to 2000 h cycles, (d) WL exposed to 750 h cycles, (e) WL exposed to1250 h cycles

3.3.2 Failure modes

It is noteworthy that a similar failure mode was observed in all conditioned and control samples of each laminate type. In other words, environmental conditions did not affect the failure modes of the control samples. Based on the ASTM D 3039/D 3039M [166] standard, three failure modes were observed during the tensile tests. SEM images were also taken from the fracture surface of some selected samples for a close inspection of the failure modes. **Figure 3-8 (a)** shows the typical failure mode of the unidirectional GFRP laminate. UL samples failed due to long splitting of the fibres in the gauge length of the sample. **Figure 3-8 (b)** shows the typical failure mode of the woven GFRP laminate. WL specimens failed between the gauge length of the laminates following the zigzag (angled) pattern of weaving. This failure included fracturing of the fibres orientated in the applied load direction, as well as deformation and delamination of the fibres orientated perpendicular to the applied load direction. **Figure 3-8 (c)** shows the typical failure mode of the chopped strand mat GFRP laminate. In the case of RL samples, since a significant part of the applied load is carried by the resin (a limited number of the fibres are orientated in the same direction as the load applies), both resin matrix and the fibres failed through a lateral failure at a section within the gauge length of the laminates.

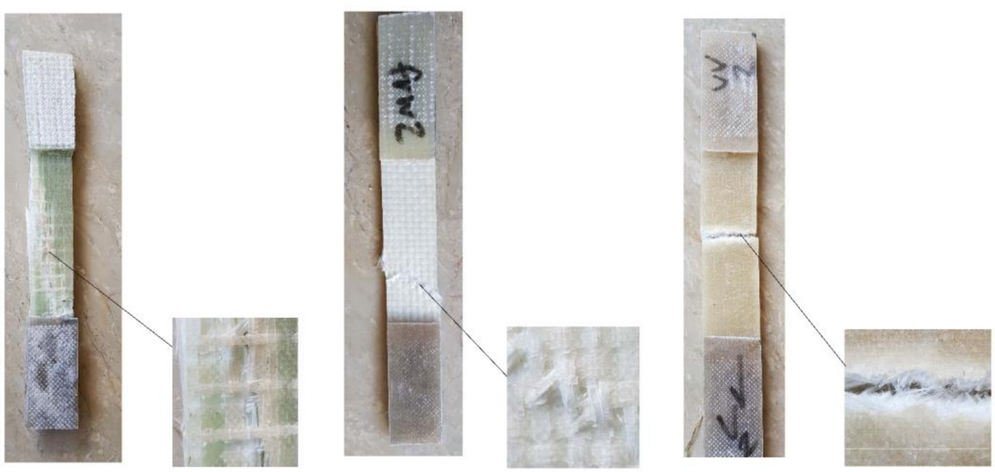

(a) (b) (c)

Figure 3-8 Typical failure modes of GFRP laminates: (a) unidirectional laminate, (b) woven laminate and (c) chopped strand laminate.

3.3.3 Tensile test results

The elastic modulus results of conditioned samples showed no significant changes compared to the control samples. In other words, the results for all samples exposed to different conditions were within the standard deviation of the control samples. The possible reason for this observation is an insignificant degradation of fibres, as the main factor in tensile elastic modulus value of FRP, due to the environments. Therefore, by considering this observation that the tensile elastic modulus of GFRP laminates are not affected by the UV radiation and freeze/thaw cycles, the tensile strength variation of such laminates will be studied in the following sections.

Table 3-2 presents the tensile test results for the control and conditioned GFRP laminates. For sample identification, a four-part notation system was used, whereby the first letter represents the fibre type, namely, U for unidirectional, W for woven, and R for random. The second and third letters denote sample thickness and time of exposure, respectively, and the last letter stands for the environmental condition, whereas FD and FW represent dry freeze/thaw and wet freeze/thaw cycles, respectively, while UV denotes the cycles of ultraviolet radiation and water vapour moisture. For example, U-2-1000-UV shows the 2 mm GFRP laminate with unidirectional fibres exposed to 1000 h of UV and water vapour cycles.

In order to investigate the effect of each parameter, first, the results for each fibre configuration will be studied, and then all laminate types will be compared with each other to find out their relative performance under different environmental condition.

Table 3-2 Test results.

Specimen	Average Ultimate Stress (MPa)	CV (%)	Retention (%)	Specimen	Average Ultimate Stress (MPa)	CV (%)	Retention (%)	Specimen	Average Ultimate Stress (MPa)	CV (%)	Retention (%)
U-2-0-FD	872.2	0.61	100.0	W-2-0-FD	320.1	0.57	100.0	R-2-0-FD	180.1	1.24	100.0
U-2-750-FD	871.5	2.39	99.9	W-2-750-FD	316.0	1.88	98.7	R-2-750-FD	178.9	2.67	99.3
U-2-1250-FD	872.0	1.29	100.0	W-2-1250-FD	305.9	2.46	95.5	R-2-1250-FD	175.4	3.37	97.4
U-2-2000-FD	864.8	2.65	99.2	W-2-2000-FD	297.3	4.32	92.9	R-2-2000-FD	167.1	4.68	92.8
U-2-0-FW	872.0	0.61	100.0	W-2-0-FW	320.1	0.57	100.0	R-2-0-FW	180.1	1.24	100.0
U-2-750-FW	756.0	3.47	86.7	W-2-750-FW	277.0	2.12	86.5	R-2-750-FW	152.0	2.21	84.4
U-2-1250-FW	728.0	4.48	83.5	W-2-1250-FW	256.0	1.33	80.0	R-2-1250-FW	135.0	4.85	75.0
U-2-2000-FW	722.0	3.96	82.8	W-2-2000-FW	244.0	3.97	76.2	R-2-2000-FW	123.0	4.89	68.3
U-2-0-UV	872.2	0.61	100.0	W-2-0-UV	320.1	0.57	100.0	R-2-0-UV	180.1	1.24	100.0
U-2-750-UV	756.6	1.84	86.8	W-2-750-UV	233.7	2.44	73.0	R-2-750-UV	118.6	1.02	65.9
U-2-1250-UV	657.5	3.63	75.4	W-2-1250-UV	228.0	2.01	71.2	R-2-1250-UV	105.0	3.67	58.3
U-2-2000-UV	634.2	5.15	72.7	W-2-2000-UV	210.0	4.17	65.6	R-2-2000-UV	104.0	4.23	57.7
U-5-0-FD	700.1	0.81	100.0	W-5-0-FD	341.6	0.72	100.0	R-5-0-FD	246.0	1.14	100.0
U-5-750-FD	695.6	2.90	99.3	W-5-750-FD	346.4	1.85	101.4	R-5-750-FD	245.3	2.09	99.7
U-5-1250-FD	696.9	2.71	99.5	W-5-1250-FD	326.8	1.97	95.7	R-5-1250-FD	238.5	2.55	97.0
U-5-2000-FD	694.6	2.54	99.2	W-5-2000-FD	322.7	3.13	94.5	R-5-2000-FD	228.5	3.61	92.9
U-5-0-FW	700.1	0.81	100.0	W-5-0-FW	341.6	0.72	100.0	R-5-0-FW	246.0	1.14	100.0
U-5-750-FW	694.0	1.54	99.1	W-5-750-FW	309.0	0.94	90.5	R-5-750-FW	217.0	1.54	88.2
U-5-1250-FW	683.0	1.88	97.6	W-5-1250-FW	299.0	2.81	87.5	R-5-1250-FW	214.0	1.84	87.0
U-5-2000-FW	661.0	2.72	94.4	W-5-2000-FW	283.0	3.07	82.8	R-5-2000-FW	201.0	3.57	81.7
U-5-0-UV	700.1	0.81	100.0	W-5-0-UV	341.6	0.72	100.0	R-5-0-UV	246.0	1.14	100.0
U-5-750-UV	652.2	3.48	93.2	W-5-750-UV	267.0	2.58	78.2	R-5-750-UV	184.6	3.35	75.1
U-5-1250-UV	653.1	2.95	93.3	W-5-1250-UV	254.0	3.55	74.4	R-5-1250-UV	168.7	4.71	68.6
U-5-2000-UV	642.0	3.29	91.7	W-5-2000-UV	244.0	3.73	71.4	R-5-2000-UV	158.0	5.85	64.2

Note: CV= coefficient of variation.

3.3.3.1 Unidirectional GFRP laminates (UL)

Figure 3-9 Retention ultimate tensile strength vs exposure period of UL: (a) dry freeze/thaw cycles, (b) wet freeze/thaw cycles and (c) UV and water vapour condensation cycles. shows the retention in ultimate tensile strength vs exposure period of unidirectional fibre laminates. It is seen that the environment of UV and moisture cycles was the most aggressive environment while dry free/thaw condition was the least damaging. The maximum reduction of UL samples was about 27% related to U-2-2000-UV. No significant change was observed for UL specimens subjected to FD (up to 1%). This shows that unidirectional GFRP laminates are resistant to freeze/thaw cycles, even without the presence of moisture. Greater reduction in tensile strength of GFRP laminates under FW cycles compared to that in FD (up to 8% for U-2-2000-FW) suggests the damaging role of moisture in degradation of FRPs. The greater resistance of the thicker samples to environmental damage may be simply due to the lesser fraction of sample thickness getting penetrated by moisture and getting damaged. For the environment of UV and moisture, it is well known that the UV radiation mostly affects the surface of the composites [39]. Hence, the greater fraction of sample thickness will be getting damaged for the thinner laminates compared than for the thicker laminates.

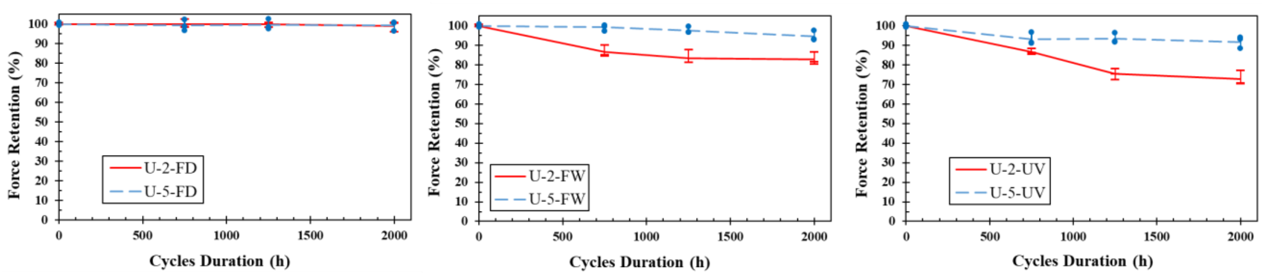

(a) (b) (c)

Figure 3-9 Retention ultimate tensile strength vs exposure period of UL: (a) dry freeze/thaw cycles, (b) wet freeze/thaw cycles and (c) UV and water vapour condensation cycles.

Figure 3-10 shows the load vs deflection curves of the control and conditioned UL laminates. As expected, FRP laminates under tensile loading showed a viscoelastic behaviour up to the failure.

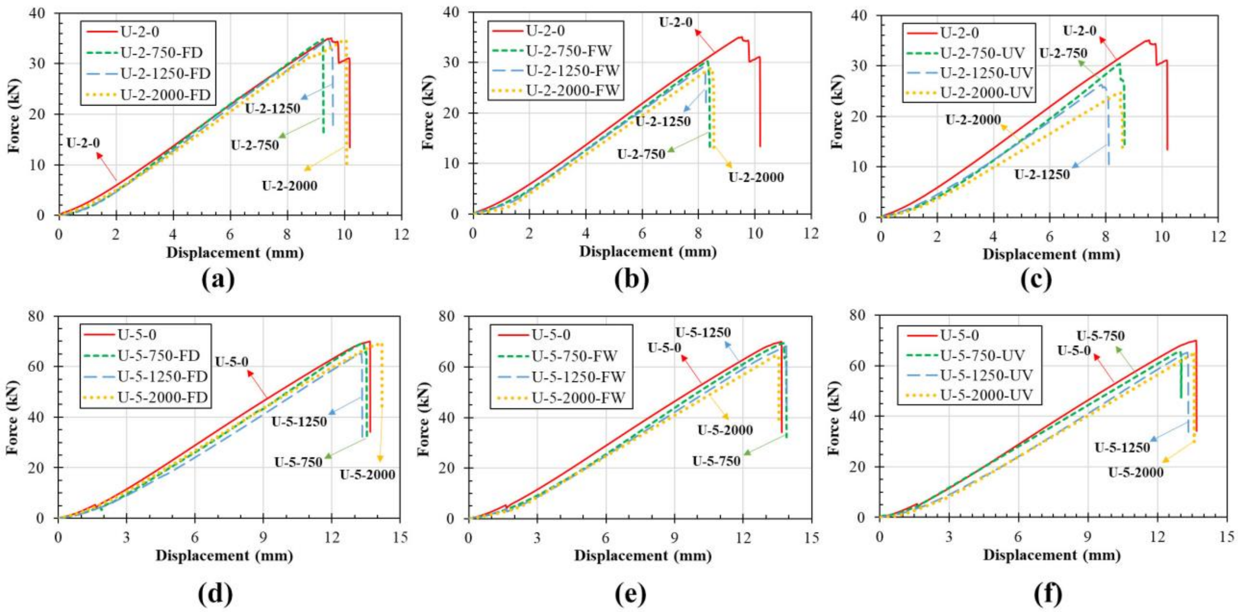

Figure 3-10 Load-deflection curve of 2mm UL laminates: (a) 2mm laminate exposed to FD, (b) 2mm laminate exposed to FW, (c) 2mm laminate exposed to UV, (d) 5mm laminate exposed to FD, (e) 5mm laminate exposed to FW and (f) 5mm laminate exposed to UV.

3.3.3.2 Woven GFRP laminates (WL)

Figure 3-11 shows the retention in ultimate tensile strength vs exposure period of woven fibre laminates. Similar to UL specimens, WL specimens experienced the highest reductions under UV and moisture environment (the maximum reduction of UV and moisture environment was 35% for U-2-2000-UV) and the lowest reductions under dry freeze thaw environment (the maximum reduction of dry freeze thaw environment was 7% for U-2-2000-FD). WL samples exposed to wet freeze/thaw cycles experienced a maximum of 24% reduction in tensile strength (**Table 3-2**). This significant difference between the reductions in the dry and wet freeze/thaw cycles confirms that the presence of moisture may considerably enhance the adverse effect of freeze/thaw cycles on the mechanical properties of FRPs. In addition to the adverse effects of moisture on composites [26, 27], freezing and expanding the moisture inside the laminates, which may cause crack growth and resin/fibre debonding [160, 161] may be another reason for this difference. Less reduction in properties of the 5 mm samples compared to the 2 mm samples is consistent with the similar findings for UL laminates (Section 3.3.3.2).

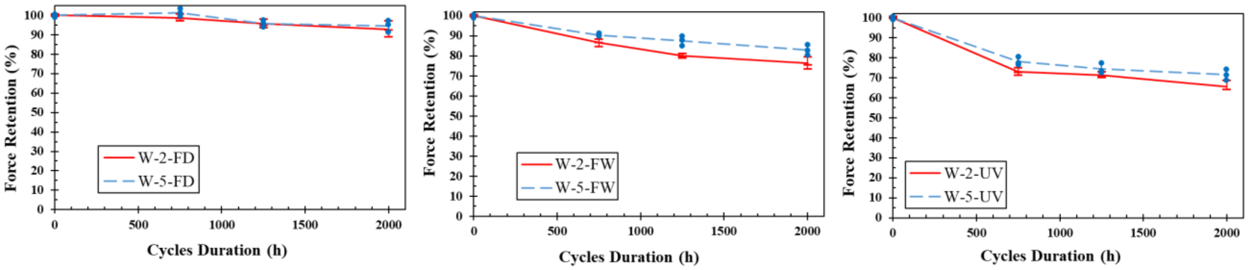

(a) (b) (c)

Figure 3-11 Retention ultimate tensile strength vs exposure period of WL: (a) dry freeze/thaw cycles, (b) wet freeze/thaw cycles and (c) UV and water vapour condensation cycles.

Figure 3-12 shows the load vs deflection curves of the control and conditioned WL laminates. Similar to UL samples, a linear elastic behaviour was observed for all control and conditioned WL samples.

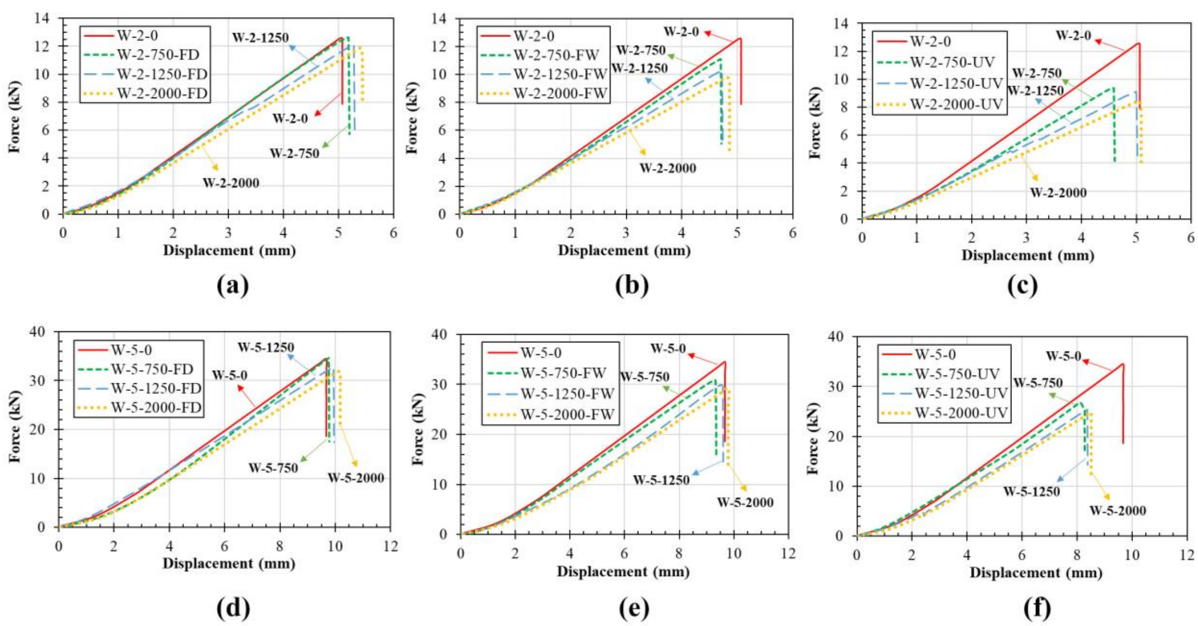

Figure 3-12 Load-deflection curve of WL: (a) 2mm laminate exposed to FD, (b) 2mm laminate exposed to FW, (c) 2mm laminate exposed to UV, (d) 5mm laminate exposed to FD, (e) 5mm laminate exposed to FW and (f) 5mm laminate exposed to UV.

3.3.3.3 Chopped strand mat GFRP laminates (RL)

Figure 3-13 shows the retention in ultimate tensile strength vs exposure period of random fibre laminates. The performance of RL samples were similar to that of UL and WL in terms of the degradation rates in different environmental conditions as well as the effect of thickness. The maximum degradation of RL laminates in each environmental condition were about 42%, 32% and 7% for R-2-2000- UV, R-2-2000-FW, and R-2-2000-FD, respectively. Considerable difference in strength reductions was observed for thicker laminates compared to the thinner ones under wet freeze/thaw and UV with moisture conditions. However, no significant difference was seen under dry freeze/thaw cycles. The maximum reductions for 5 mm laminates were about 36%, 19% and 7% for R-5-2000-UV, R-5-2000-FW, and R-5-2000-FD, respectively. This observation reveals that the moisture penetration and UV radiation effects are strongly related to the thickness, while the adverse effect of dry freeze/thaw cycles may not change considerable with changing in the sample thickness. This was also confirmed for UL and WL samples (**Table 3-2**).

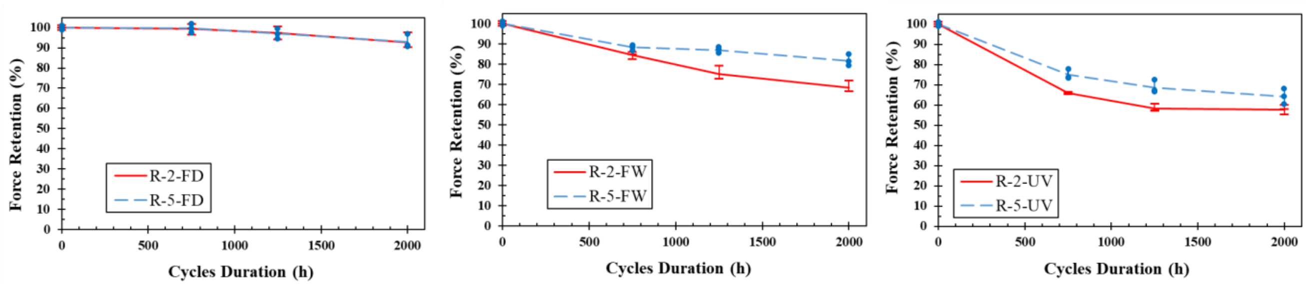

(a) (b) (c)

Figure 3-13 Retention ultimate tensile strength vs exposure period of RL: (a) dry freeze/thaw cycles, (b) wet freeze/thaw cycles and (c) UV and water vapour condensation cycles.

Figure 3-14 shows the load vs deflection curves of the control and conditioned RL laminates. Although the behaviour of RL samples, in terms of linear elastic behaviour, was the same as UL and WL, the RL samples were failed with a significantly lower sound than UL and WL specimens.

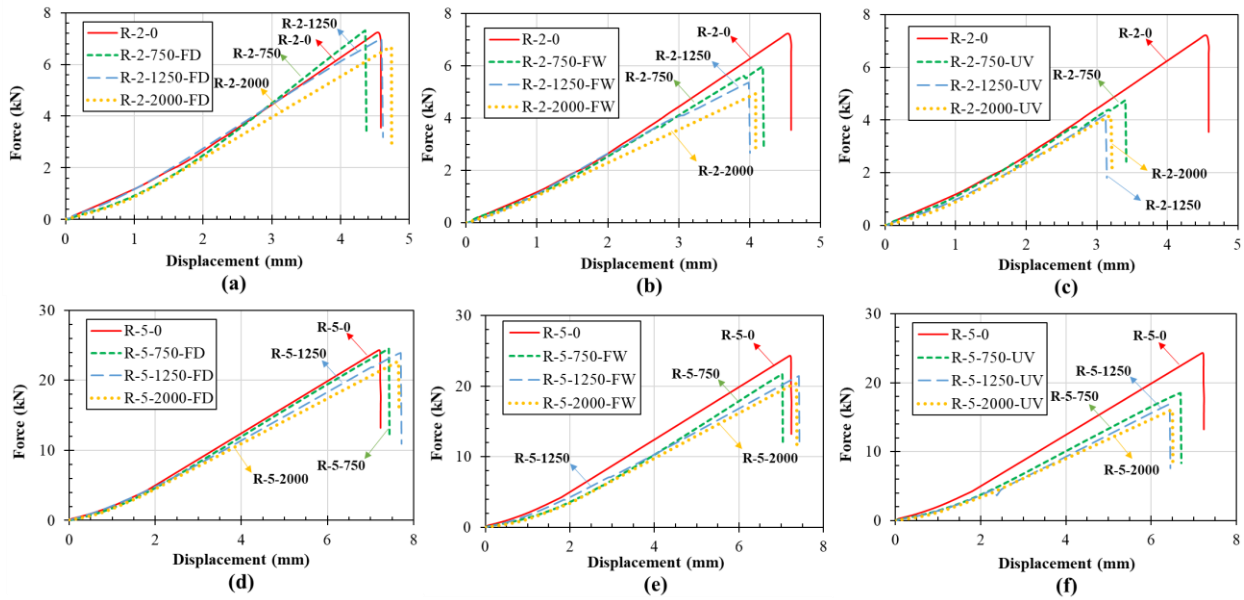

Figure 3-14 Load-deflection curve of RL: (a) 2mm laminate exposed to FD, (b) 2mm laminate exposed to FW and (c) 2mm laminate exposed to UV, (d) 5mm laminate exposed to FD, (e) 5mm laminate exposed to FW and (f) 5mm laminate exposed to UV.

3.3.3.4 Comparison between different types of GFRP laminates

Figure 3-15 compares the retention in ultimate tensile stress vs exposure period of different GFRP laminates exposed to different environmental conditioning. Among the three laminate types, generally, UL samples showed the best performance, while RL samples showed the weakest performance under different environmental conditions. In general, it can be concluded that, regardless of the type of laminates, GFRP laminates used in this study were resistant to freeze and thaw cycles without the presence of moisture (maximum reduction of 7%). The other two conditions were detrimental due to the presence of moisture, which could intensify the adverse effects of freeze/thaw and UV cycles. It is well known that the resin matrix degradation is the primary factor responsible for the degradation of FRPs' mechanical properties [21]. Therefore, the laminates with continuous unidirectional fibres are resistance against materials degradation as they have more fibres in the direction of the applied load compared to the woven and random fibre laminates. This explanation is also valid for the comparison of WL and RL. As the mechanical properties of RL are more dependent on the properties of resin matrix than WL (since more fibres are orientated in the direction of applied loads in WL than RL), the reductions in tensile strength of RL are higher than WL laminates.

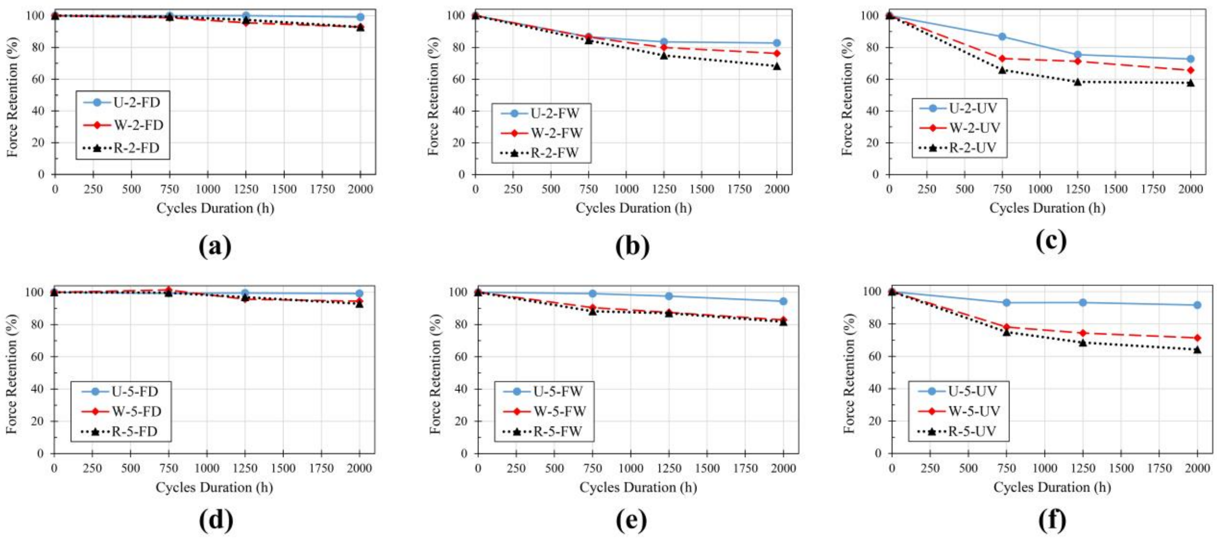

Figure 3-15 Comparison between the tensile strength reductions of GFRP laminates: (a) 2mm laminate exposed to FD, (b) 2mm laminate exposed to FW, (c) 2mm laminate exposed to UV, (d) 5mm laminate exposed to FD, (e) 5mm laminate exposed to FW and (f) 5mm laminate exposed to UV

3.3.3.5 Comparison the results with similar studies

In this section, the results of the present study are compared with those of similar studies reported by other researchers. **Table 3-3** and **Table 3-4** summarize the results of this study and some similar studies under freeze/thaw cycles and UV with moisture cycles conditions, respectively.

From **Table 3-3** and the results reported by Wu et al. [123] on flexural properties of 3.5 mm plates from a GFRP vinylester resin deck system, which was made out of two layers of fabric (each layer included fibres orientated in 0˚, 90˚, 45˚, -45˚ and random directions) subjected to freeze/thaw cycles in air and water, it can be concluded that generally, FRP composites are resistant to freeze/thaw cycles without the presence of the moisture. Wu et al. [123] also found freeze/thaw cycles carried out in the temperature range of 4.4 to −17.8°C in water do not have significant difference in loss in mechanical properties as compared to the FRPs conditioned in distilled water.

As is seen in **Table 3-4**, the results for unidirectional FRP laminates, regardless of the fabrication method, are comparable. In addition, the reductions observed for woven and chopped strand GFRP laminates were greater than the results reported for all unidirectional laminates. This comparison confirms the greater susceptibility of the FRP composites with less fibres along the applied load, i.e., the lesser the fibres in the same direction of the applied load, the higher is the strength reductions. In other words, the tensile properties of laminates with woven and chopped strand fibres are governed more by the resin properties than those of unidirectional laminates, and thus, laminates with woven and chopped strand fibres are more vulnerable under environmental conditions.

Table 3-3 Test results of the present study and other research under freeze/thaw cycles.

Reference	FRP Type	Environmental condition	Results
Present study	Vacuum infusion GFRP epoxy laminates	Dry freeze/thaw cycles from -20 ˚C to 20 ˚C	negligible, 7% and 7% reductions for 2mm unidirectional, woven and chopped strand mat laminates, respectively after 2000 h cycles
Present study	Vacuum infusion GFRP epoxy laminates	Wet freeze/thaw cycles from -20 ˚C to 20 ˚C	17%, 24% and 32% reductions for 2mm unidirectional, woven and chopped strand mat laminates, respectively after 2000 h cycles
[160]	Wet lay-up GFRP vinylester laminates.	Dry freeze/thaw cycles from -10 ˚C to 22.5 ˚C	9.1 % reduction for laminates with three layers of 0.125mm stabilized unidirectional fabric after 2400 h cycles
[160]	Wet lay-up GFRP vinylester laminates.	Wet freeze/thaw cycles (in deionized water) from -10 ˚C to 22.5 ˚C	9.6 % reduction for laminates with three layers of 0.125mm stabilized unidirectional fabric after 2400 h cycles
[167]	Wet lay-up GFRP epoxy laminates.	Dry freeze/thaw cycles from -30 ˚C to 30 ˚C	No significant change in tensile strength after 90 cycles
[154]	pultruded GFRP isophthalic polyester sheet	Dry freeze/thaw cycles from -10 ˚C to 20 ˚C	No significant change in tensile strength after 300 cycles
[154]	pultruded GFRP isophthalic polyester sheet	Wet freeze/thaw cycles from -10 ˚C to 20 ˚C	13 % reduction for 6.4 mm laminates with five roving layers (3 continuous strand mats and 2 unidirectional roving) after 300 cycles

Table 3-4 Test results of the present study and other research under UV radiation and moisture environment.

Reference	FRP Type	Environmental condition	Results
Present study	Vacuum infusion GFRP epoxy laminates	UV radiation and water vapour condensation cycles	27%, 34% and 42% reductions for 2mm unidirectional, woven and chopped strand mat laminates, respectively after 2000 h cycles
[73]	Pultruded GFRP vinylester laminates	UV radiation and water vapour condensation cycles	25% reduction for 2 mm laminates after 2000 h cycles
[77]	hand lay-up flax fabric reinforced epoxy composites	UV radiation and water spray cycles	29% reduction of 5.2 mm laminate after exposure to 1500 h cycles
[168]	Pultruded GFRP polyester/vinyl ester laminates	Combined effect of high temperature, freeze–thaw cycles, moisture and UV radiation	15.5 %, 10.4 %, and 13.9 % reduction for 2.85 mm isophthalic polyester, orthophthalic polyester, and vinyl ester laminates after six months
[169]	Pultruded GFRP polyester laminates	UV radiation and moisture cycles	21 % reduction of 5 mm laminates after exposure to 3000 h cycles

3.4 Statistical Analyses

3.4.1 Analysis of Variance (ANOVA)

To investigate the contribution percentage of each variable used in this study, namely type of the laminates, conditioning period and sample thickness in tensile strength reduction of GFRP laminates after exposure to environmental conditions, two-way ANOVA analyses were used. Two sets of analyses were carried out to investigate all variable effects. First, the type of laminates considered as the constant factor and exposing period and laminate thickness considered as variables. Next, the thickness of the laminates was considered as the constant factor and type of the laminate and exposing period were considered as the analysis variables.

The details of the procedure for ANOVA analyses can be found in [38]. Significantly high error for UL under dry freeze/thaw environment was obtained, which confirms that the laminates is less dependent to the tests variables and, as shown in tensile strength results, is resistant to the dry freeze/thaw condition. The results for both wet freeze/thaw and UV with moisture conditions revealed that the testing variable, namely thickness and exposing periods are significantly effective factors in tensile strength reductions of unidirectional GFRP laminates. However, the effect of thickness is higher in wet freeze/thaw condition than that of UV and moisture condition (46% compared to 32% contribution).

For woven and chopped strand laminates, as expected, the conditioning period is the most important factor with more than 80% contribution for all conditions. Similar to UL samples, the effect of thickness is higher under wet freeze/thaw cycles than UV and water vapour cycles (8% contribution compared to 2% for woven laminates and 13% contribution to 4% for chopped strand laminates).

For all conditions, the effect of exposing period is the main factor with the minimum of 53% contribution on the final tensile retention results. The exposing time has the lowest and highest effects on 2mm laminates under dry freeze/thaw and wet freeze/thaw conditions, respectively (53%, 87% and 82% for dry freeze/thaw, wet freeze/thaw and UV with moisture conditions, respectively). The possible reason for the low dependency of the dry freeze/thaw condition to the exposing time may be due to the less adverse effect of freeze/thaw cycles on the laminates in terms of tensile strength. However, the effect of exposing period in 5mm laminates decreased for other two conditions (55%, 55% and 53% for dry freeze/thaw, wet freeze/thaw and UV with moisture conditions, respectively). This observation may confirm the fact that due to the less ratio of the damaged layers to the testing area for 5mm laminates compared to 2mm laminates, the rate of degradation is smaller for thicker laminates with respect to the exposure time.

3.4.2 Fitting models

According to the tensile test results and ANOVA analyses, probability models were proposed using linear Bayesian regression models with the help of risk tools (RT) software [127]. Thickness and time of exposure were considered as the effective parameters on tensile strength retentions. To confirm the validity of proposed models, various regression parameters, including the regression coefficient, homoscedasticity, non-collinearity and error normality were checked for numerous models. Finally, Eq.3.1 was selected to predict the tensile strength retention of unidirectional, woven and chopped strand mat GFRP laminates after exposure to dry freeze/thaw cycles, wet freeze/thaw cycles and UV radiation and water vapour cycles conditions. It should be mentioned that, due to the large error value in ANOVA analyses of UL samples exposed to FD condition (i.e. no reductions observed for UL sample in that condition), the proposed formula does not predict the values of UL in FD condition.

$$R\ (\%) = A\left(\frac{1}{Log(T)}\right) + B\ (t^{0.33}) + c \tag{3.1}$$

Where T (h) is the exposure period; t (mm) is the laminate thickness; and A, B and C are constants based on each type of GFRP laminates. **Table 3-5** summarizes the equations' constants for each environmental condition.

Statistical parameters of linear Bayesian regression for each probability model is presented in **Table 3-6**. According to the results the reliability of the equations is confirmed. However, using more experimental data to improve the accuracy of the proposed models with considering different possible effective variables, such as materials characteristics and condition temperature is recommended. The results of tensile strength obtained from the experimental tests with the results calculated based on the fitted models for each environmental condition were compared in **Figure 3-16**. As it is seen an acceptable agreement is achieved for the predictions, which confirms the high accuracy of the proposed models.

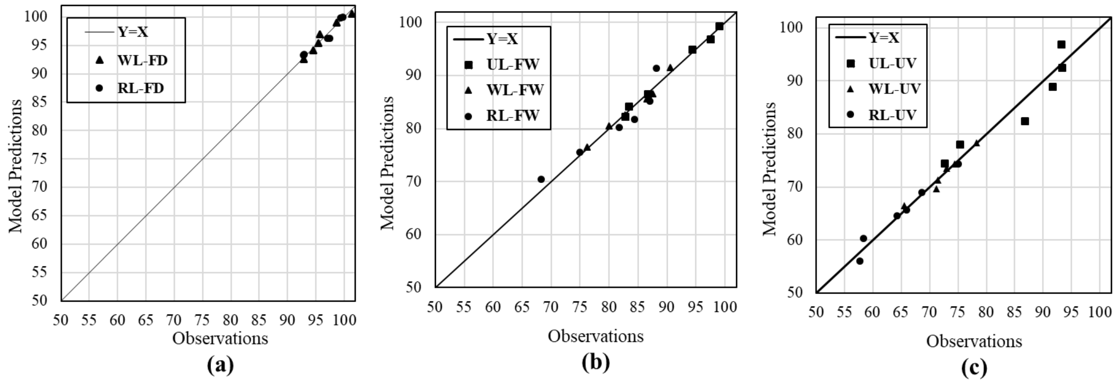

Figure 3-16 Comparison between the test results and model predictions: (a) FD, (b) FW and (c) UV.

Table 3-5 Constant values in Eq.1 for FD condition.

Specimen Type	Environmental condition	A	B	C
UL	FD	-	-	-
WL	FD	142.988	3.337	45.088
RL	FD	145.893	0.074	49.056
UL	FW	95.744	28.258	17.664
WL	FW	200.12	13.424	-0.959
RL	FW	250.179	21.657	-32.576
UL	UV	175.939	32.114	-19.254
WL	UV	1156.327	10.531	5.930
RL	UV	215.628	19.283	-33.639

Table 3-6 Bayesian regression parameters for FD condition.

Specimen Type	**Environmental condition**	**R-factor**	**Mean of standard deviation**
UL	FD	-	-
WL	FD	0.98	0.949
RL	FD	0.97	0.954
UL	FW	0.99	0.737
WL	FW	0.99	1.062
RL	FW	0.96	3.063
UL	UV	0.94	4.12
WL	UV	0.98	1.09
RL	UV	0.99	1.62

3.5 Conclusion

This study was conducted as part of a research program related to the degradation of FRP composites under environmental conditions. Future studies will focus on the durability of FRP composites when used for civil engineering applications (e.g. using with seawater sea sand concrete). In the present study the mechanical and microstructural properties of unidirectional, woven, and chopped strand mat GFRP laminates were studied using tensile tests and SEM analyses. The following conclusions were drawn based on the observations and analyses:

- The tensile elastic modulus of the GFRP laminates are not considerably affected by the UV radiation and freeze/thaw cycles.
- In all environmental conditions unidirectional and chopped strand mat GFRP laminates showed the best and the worst tensile performance, respectively, while the woven GFRP laminates performed between those two. This may be due to the amount of fibres, which are the greatest for unidirectional and the lowest for the strand laminates, in the direction of the applied load; the greater the amount of the fibres in the longitudinal direction, the less the degradation of tensile mechanical properties.
- Based on SEM analyses, cracks and holes in resin matrix increase by the exposure time. Accordingly, due to the damage growth, considerable resin/fibre interface debonding was observed when the conditioning period reached 2000 h for most of the samples exposed to different conditions.
- All three types of GFRP laminates are almost resistant against the freeze/thaw cycles without the presence of the moisture (maximum reduction was about 7%).
- Presence of moisture in freeze/thaw cycles increases the damage level of GFRP laminates due to the freezing and expanding the absorbed moisture, which leads to the crack growth and fibre/matrix debonding (e.g. maximum reduction of 32% for random fibre laminate subjected to wet freeze/thaw compared to 7% for dry freeze/thaw).
- UV radiation and water vapour condensation condition is found to be the most aggressive environment among all three environmental conditions. Maximum reductions of about 27%, 34% and 42% were found, after 2000 h exposing, for 2 mm unidirectional, woven and chopped strand mat GFRP laminates, respectively.
- The sample thickness is an important factor in tensile performance of laminates exposed to daily environmental conditioning. This is due to the fact the daily conditions mainly affect the

surface of the composites rather than the inner layers. The maximum difference in tensile strength reduction about 19 %, 6 % and 13 % were observed between 2mm and 5mm laminates after exposure to different environmental conditions for unidirectional, woven and chopped strand mat samples, respectively.

As this study shows, several factors, such as the materials characteristics and fabrication method, composites cross section (i.e. thickness), exposing time may affect the degradation level of FRP composites under daily environmental conditions. Therefore, conducting more experimental tests in order to obtain more data to better understand the performance of FRPs under such conditions and possible modelling of this influence is recommended.

Chapter 4 Effects of UV radiation, moisture and elevated temperature on mechanical properties of GFRP pultruded profiles

Abstract

The present research examines the effects of UV radiation, moisture and elevated temperature on the mechanical properties of GFRP pultruded profiles. Flexural, compressive and tensile properties of different GFRP sections were studied after they were exposed for 1000, 1500, 2000 and 3000 h to UV radiation and water vapour condensation cycles. Mechanical tests, including three-point bending, compression and tension tests, SEM analyses, and statistical studies were conducted to gather comprehensive results. The results showed that the mechanical properties of various GFRP sections generally decreased with the duration of conditioning: however, the rate of the decrease that was only slight up to 1000 h, increased rapidly during 1000-2000 h, and again it was slow during 2000-3000 h. The maximum reductions were 34%, 28% and 23% after exposure to 3000 h cycles for bending, tensile and compression tests, respectively. In the bending tests, where interlaminar shear failure controls ultimate strength, the degradation was greater compared to the situation where fibres fracture controls the failure. Further, regarding the cross-section parameter, it was concluded that the thickness and perimeter are the effective factors; the thinner the sample and the larger the perimeter, the greater is the reduction. However, the maximum effect of the cross section in terms of thickness and perimeter did not exceed 13% among all sections.

Key words

GFRP pultruded sections; Mechanical properties; Degradation mechanism; UV radiation; hydrothermal condition.

4.1 Introduction

Recent years have seen the extensive use of fibre-reinforced polymer (FRP) composite materials for a variety of purposes, including construction [3, 38] (especially for marine applications [4]), as well as automotive and aerospace applications [2]. Such usage is motivated by the various advantages of the materials, including high strength and stiffness-to-weight ratios and strong corrosion resistance [6, 7, 170]. Amongst different FRPs and fabrication methods, glass fibre reinforced polymer (GFRP) pultruded profiles are widely employed given their relatively low cost and desirable characteristics [64, 171]. Despite the numerous advantages of FRPs, however, concerns remain as to their durability under aggressive environmental conditions, such as alkalinity, acidity, seawater conditions, ultraviolet (UV) radiation, and fire [43, 99, 134, 157, 172-178]. Reservations also extend to the longevity of FRPs under changing natural conditions, such as temperature fluctuations and hydrothermal effects [8, 12, 87, 109, 113, 114, 138, 140, 142]. These aggressive situations cause adverse outcomes that may be exacerbated when accompanied with various loading conditions, such as sustained load, dynamic load and hydraulic pressure [96, 134, 179, 180]. Given these issues, the broader acceptance of FRPs as suitable materials for many practical engineering applications necessitates the collection of substantial data on their durability.

FRP composites have been used for various outdoor purposes, such as the construction of main structural members, non-structural elements and decking and bridge piers, as well as the retrofitting of existing structures. These materials are exposed to a variety of environmental conditions and are therefore regularly exposed to UV radiation, elevated temperatures and considerable moisture during transportation and storage and throughout their service life [15, 16, 128, 181].

One of the primary causes of FRP deterioration is the diffusion of moisture, which results in the swelling, plasticisation, cracking, and hydrolysis of resin, and debonding of the fibre/matrix interface [17, 27, 182, 183]. Another source of FRP degradation is UV radiation, whose effect is generally attributed to the chemical changes in constituent resin because of the series of complex processes characterising UV radiation and oxygen [23, 24] These processes may also involve photochemical degradation reactions. Photodegradation is initiated by the interaction of light photons with a polymer's molecular chains. It may also be induced by the wavelengths of UV radiation; the shorter the wavelength (which is characterised by high photon energies), the greater its potential to break a polymer's chemical bonds [106, 184]. Correspondingly, UV radiation is considered a significant factor for the vulnerability of polymeric materials primarily because of the wavelengths that UV photons possess when they reach the Earth's surface (about 6% of solar radiant flux). These wavelengths are similar to those responsible for the chemical bond dissociation of many polymers (290–460 kJ/mole) [25].

With respect to the role of elevated temperatures, FRP composites begin to be degraded when the glass transition temperature (Tg) of the materials' resin matrix is reached [63, 121, 185]. This form of damage is primarily attributed to a shift in resin state from glassy to rubbery (i.e. resin softening), which diminishes the load carrying and transferring capacity of resin [38, 156, 186, 187]. Thus, the mechanical properties of FRPs are profoundly influenced by temperature [20, 158, 171].

The degradation of polymeric materials due to UV radiation, moisture and elevated temperature accelerates when these environmental factors transpire simultaneously [168, 188].

The concurrent exposure of FRPs to UV radiation and water vapour condensation accelerates deterioration mechanisms in different ways. For instance, the rate at which moisture and chemical agents penetrate into a composite increase because of the pathways provided by microcracks that develop on surfaces exposed to UV radiation. Another mechanism is the enhancement of photo-oxidation reactions owing to the presence of moisture. Moreover, water vapour condensation may remove soluble photo-oxidation reactions products from the surfaces exposed to UV radiation, thereby creating new surfaces on which further degradation can occur [25].

Research has been conducted on the chemical, physical and mechanical properties of FRP composites subjected to UV radiation and moisture at elevated temperatures [152]. However, further studies are required to predict degradation occurrence and illuminate various real-life situations wherein UV radiation and moisture work simultaneously. The literature has expounded on damage to FRP composites upon sequential exposure to UV radiation, moisture and elevated temperature during outdoor service [15, 63], but investigations were primarily focused on material-based perspectives and conducted on FRP laminates and bars. The effects of such conditions on FRP sections have received minimal attention.

Ashrafi et al. [39] inquired into the mechanical properties of 10 mm (diameter) GFRP bars exposed to sequential cycles of UV radiation and water vapour condensation at 60°C and different durations. The authors found reductions in the properties of the materials after 3000 h of exposure in short-beam (15%), three-point bending (8%) and tensile strength (3%) tests. Sousa et al. [169] explored the degradation of small-scale polyester/vinyl-ester-GFRP coupons (cut from commercial GFRP profiles) that were naturally aged for 3.5 years in a Mediterranean climate using a UV-accelerated weathering chamber (QUV) for up to 3000 h. The researchers uncovered no significant changes in the mechanical properties of the materials under both real-world and accelerated conditions.

As previously stated, researchers have concentrated solely on the bulk material characteristics of FRP composites [15, 77, 78], yet the outermost layers of these materials are damaged mostly because of UV radiation. As regards moisture, penetration depends on several factors, such as time of exposure and profile geometry. Knowledge is markedly lacking in these aspects of the performance of FRP commercial profiles currently used for different constructional applications. No study has been devoted to the impact of UV radiation, moisture and elevated temperatures on the mechanical properties of FRP profiles with respect to their cross-section configuration. The current work is an attempt to fill this gap. The research revolved around the mechanical properties (tensile, flexural and compression) and related microstructural characterisation of various GFRP pultruded profiles subjected to different periods of sequential exposure to UV radiation and water vapour condensation.

4.2 Experimental Program

This study, as part of an ongoing investigation of on the durability of FRP composites under various environmental conditions, focuses on the mechanical properties of GFRP pultruded sections subjected to sequential cycles of UV radiation and water vapour condensation for 1000, 1500, 2000 and 3000 h. To investigate the degradation of the mechanical properties, three-point bending, tensile and compression tests were conducted on various GFRP sections. The parameters investigated in this study included the profile section type, the cross-sectional geometry and the exposure time. To assess the possible damage caused by exposure and mechanical testing, as well as the failure modes, the microstructural features of the GFRP profiles both before and after the mechanical testing were examined by means of scanning electron microscopy (SEM). Finally, statistical analyses, which included an analysis of variance (ANOVA) and linear Bayesian regression, were conducted. Using such methods, it was possible to determine each parameter's contribution and to construct probability models to predict the reduction ratios for the mechanical properties.

4.2.1 Materials

GFRP pultruded profiles in the form of various cross-sections, including I-shaped sections, circular tubes, boxes, channels and laminates, were fabricated by the manufacturer using E-glass fibres and vinylester resin (**Table 4-1**). All the profiles comprised unidirectional E-glass rovings as the inner part, a continuous strand mat as the outer layer and a very thin vinylester surface veil as the outermost layer. **Figure 4-1** presents the typical profiles used in this study. The details of the pultrusion process and the profile characteristics provided by the manufacturer are listed in **Table 4-2**. The mechanical, thermal and physical properties of the GFRP profiles are listed in **Table 4-3** and **Table 4-4**. Elephant foot buckling failure of the compressive profiles rather than failure along the length of the samples, is the possible reason for the significant difference between the compressive strength value reported by the manufacturer and obtained in this study. It should be noted that the results listed in Table 4.4, which are related to the values tested by the authors, were used for discussions later in this study.

Table 4-1 GFRP profiles cross sections characteristics

Profile Cross Section	Test Type	b (mm)	h (mm)	t (mm)	P (mm)	A (mm^2)	I_x (mm^4)	I_y (mm^4)
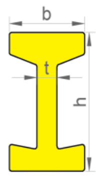	3-point bending along both principal axis	15	25.5	4	99.38	206.3	16882.4	2687.3
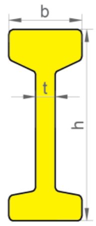	3-point bending along both principal axis	15	38.3	4	119.46	292.6	54113.2	3488.3
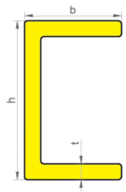	3-point bending along both principal axis	50	30	5	206.57	499.1	178632	41299.2
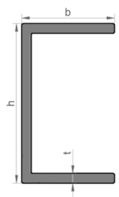	3-point bending along both principal axis	50	30	3	212.28	311.8	120702	27382
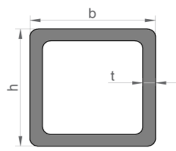	Compression	30	30	3	228	324	-	-
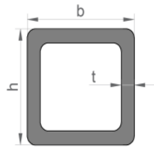	Compression	25	25	3	188	264	-	-
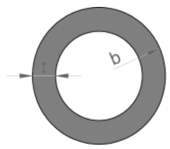	Compression	13	-	4.5	135.02	303	-	-
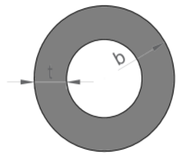	Compression	13	-	6	125.6	377	-	-
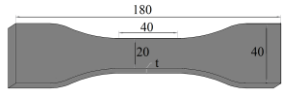	Tension	-	-	2, 5	-	40, 100	-	-

Table 4-2 Pultrusion process and Profiles characteristics (same for all sections)

Fibre Type	E-glass
Resin Type	Vinylester
Fillers (wt % of the resin)	Nano Clay (2 wt %) – Carbonate Calcium (12 wt %)
Fibre Content by volume (%)	60
Pultrusion Average Speed	0.25 m/min
Pultrusion temperature (˚C)	130 (entrance) – 170 (exit)

Table 4-3 Mechanical and physical properties of pultruded profiles (given by manufacturer)

Properties	**Value**
Average Tensile Strength Along Unidirectional Fibres (MPa)	400
Tensile Elongation at Rapture (%)	2.5
Average Flexural Strength About Major Axis (MPa)	460
Average Axial Compression Strength along (MPa)	550
Density (g/cm^3)	2
Water Absorptivity rate (%)	0.2 - 0.6
Thermal Expansion Coefficient (10^{-6} / ˚C)	4.5
Glass Transition Temperature, T_g (˚C)	100 - 105

Table 4-4 Mechanical properties of pultruded profiles (tested by the authors)

Specimen	**Mechanical properties (MPa)**			
	Tensile Strength (Unidirectional)	Axial Compressive Strength	Flexural Strength	
			about major axis	about minor axis
I-1	-	-	345	490
I-2	-	-	295	585
U-1	-	-	-	322
U-2	-	-	-	360
L-1	608		-	-
L-2	459		-	-
C1	-	248	-	-
C2	-	271	-	-
B1	-	183	-	-
B2	-	297	-	-

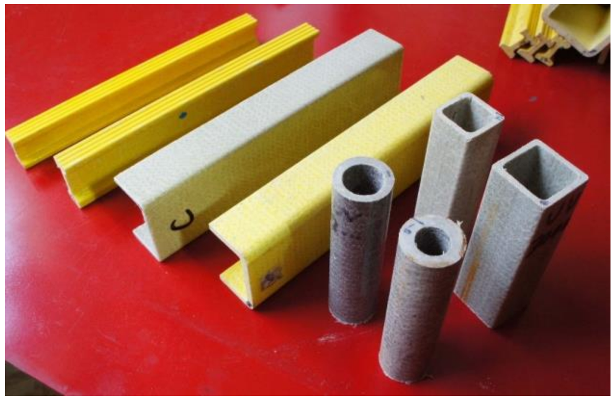

Figure 4-1 Typical pultruded sections of GFRP used in this study

4.2.2 Environmental cycles

Two sets of specimens were considered, namely an unconditioned group, which was classified as the 'reference' and tested at an ambient temperature of 25˚C, and a conditioned group, which was tested following exposure to 1000, 1500, 2000 and 3000h conditioning cycles. To simulate the harsh environmental conditions that commonly prevail in coastal areas [165], the specimens were subjected to sequential exposure to UV radiation and water vapour condensation cycles based on the ASTM G154 standard [64]. As one of the schemes, the standard recommends cycles, involving exposure to UV-A at 60˚C for 8 h followed by 4 h of condensation (100% RH) at 50˚C, as used in this study to simulate the environmental impact on composites. A PARS AZMA Co (Tehran, Iran) UV chamber was used for the conditioning. The wavelength and irradiation intensity of the UV-A lamp used in this study were approximately 340 nm and 0.85 W/m^2, respectively. **Figure 4-2** shows the UV chamber, the locations of the lamps as well as the distance between the samples and the lamps. All the samples were flipped and changed in terms of their location every 24 hours to ensure uniform UV absorption and to avoid chamber location effects. To determine the total time required to produce UV radiation equivalent to the annual outdoor UV dose in Victoria, Australia, the available data were searched and 250 MJ/m^2, as the average annual dose in Australia, was selected as the target dose. According to [189], the total amount of UV radiation emitted from the wavelengths between 295–400 mm with an irradiation intensity of 0.55 W/m^2 is approximately 222 kJ/m^2/h. Therefore, the corresponding value in the present study, with an irradiation intensity of 0.85 W/m^2, was about 343 kJ/m2/h (i.e. ((0.85/0.55)×222)). In this case, the total number of hours needed to produce UV radiation equivalent to the annual outdoor UV dose using the UV chamber with the settings applied in the present study was approximately 729 hours (i.e. (250×10^3)/343). Therefore, 1000, 1500, 2000 and 3000h exposure to artificial UV in the present study was equivalent to 1.4, 2, 2.7 and 4.1 years of exposure, respectively, to outdoor UV radiation in Australia. It is important to note that the maximum temperature during the conditioning (60˚C) was much lower that the resin glass transition temperature (i.e. approximately 100˚C). Therefore, the conditioning temperature itself would not affect the T_g of the resin and, consequently, the degradation mechanism.

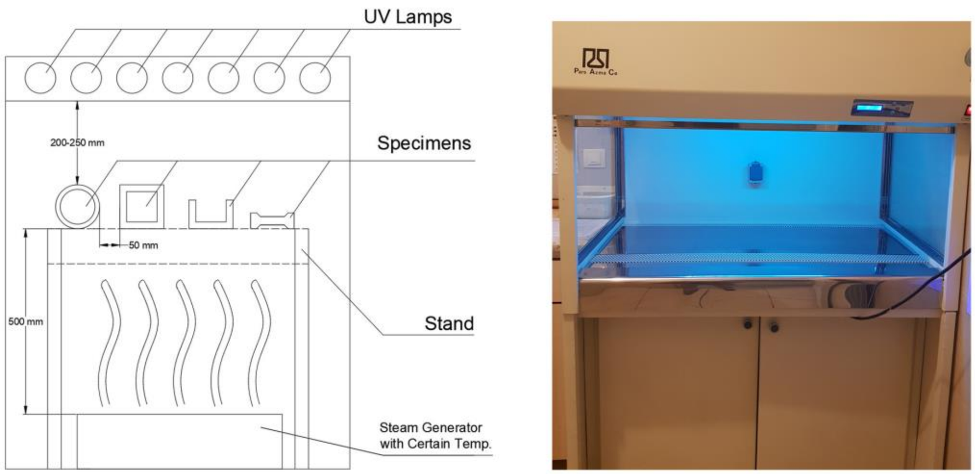

(a) (b)

Figure 4-2 UV chamber configuration: (a) Schematic and (b) Real

4.2.3 Mechanical tests

The testing setups details are presented in **Figure 4-3**.

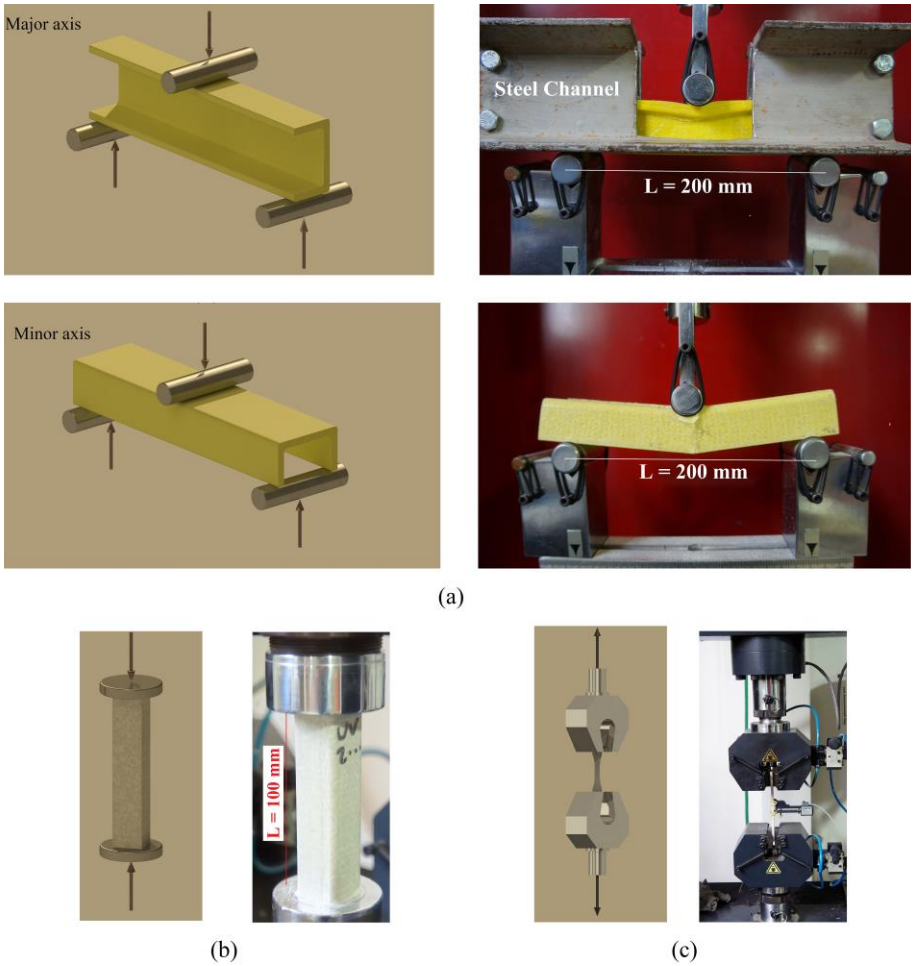

Figure 4-3 Mechanical testing set-up: (a) Three-point bending; (b) Compression; (c) Tension

4.2.3.1 Three-point bending

To investigate the flexural properties of the GFRP sections both before and after the conditioning, three-point bending tests were performed based on the recommendations contained within the ASTM D790 standard [190]. All the mechanical tests were conducted using a universal servo-electric testing machine with a loading capacity of 150 kN. The load was applied in a displacement-controlled manner with a loading rate of 1.1 mm/min. The bending sections (see **Table 4-1** for the sample sizes) were cut into 230 mm lengths using a water-jet. The sections were then tested in terms of the bending along both the minor and major axes. The span between the supports (200 mm) was maintained in all the tests was maintained in all tests to observe different failure modes for reference samples. To prevent the lateral-torsional buckling of the U-shaped channels, when conducting the bending tests along their major axis, the sections were restrained along their length using two reverse channels (made of steel). The tests were continued until either the applied load dropped to almost 50% of the specimen's maximum recorded load or the mid-span vertical displacement reached approximately 20 mm. Three identical sections were tested for each type of GFRP profile so as to ensure the statistical validity of the data.

4.2.3.2 Compression tests

To investigate the compressive properties of the GFRP sections both before and after the conditioning, compression tests were conducted by employing a loading rate of 1.1 mm/min. To prevent global buckling, the compression test specimens (see **Table 4-1** for the sample sizes) were all cut into 100 mm strips. Three identical sections were tested for each type of compressive sample.

4.2.3.3 Tensile tests

To investigate the tensile properties of the GFRP laminates (see **Table 4-1** for the sample sizes) both before and after the conditioning, tensile tests were conducted according to the recommendations contained within the ASTM D-638 standard [6] which specifies employing a loading rate of 1.2 mm/min. Three identical sections were tested for each type of tensile sample.

4.2.4 Scanning electronic microscopy (SEM)

In order to investigate the microstructural features and the mode of damages in the resin matrix, fibre, and resin/fibre interface of GFRP-pultruded profiles after conditioning, the randomly selected specimens were examined under SEM. Furthermore, the failure mechanisms of different mechanical tests were carefully examined for an improved understanding of failure under each test condition. As the FRP composites are relatively non-conducting in nature, a 30 nm thick gold layer was sputtered on the samples before SEM, to avoid possible charging and thermal damages during SEM.

4.3 Results and discussion

4.3.1 Changes in the surface colour

Figure 4-4 shows the change in appearance of GFRP after exposure for 1000, 2000, and 3000h. The colour, lustre, and smoothness have changed after exposing to UV and water vapour condensation cycles, and the changes intensify with time. It was observed that the longer the time of exposure, the more the colour and lustre of the surfaces changed. These changes were from yellow and shiny to white and pale.

Figure 4-4 Surface changes of GFRP I-shaped sections after exposure for different cycles to UV radiation and water vapour condensation

4.3.2 SEM analyses after exposure

A few selected samples were examined under SEM after the exposure but before the mechanical tests. **Figure 4-5** shows the selected reference and conditioned GFRP profiles. All samples were taken from the middle of the I1 section's web. As expected, no significant cracks or damages were observed in the reference sample, while micro-cracks and damages appeared within the resin matrix after exposure to environmental conditions. The longer the conditioning period, the greater the number of micro-cracks and damages. There were also instances of fibre/resin debonding at the surface after the 3000-h exposure, which confirms the detrimental effect of UV radiation, moisture, and elevated temperature on composites. However, more accurate analyses in terms of damage penetration rate and progress ability can be obtained using 3D scans (i.e., CT x-ray analysis) in further studies.

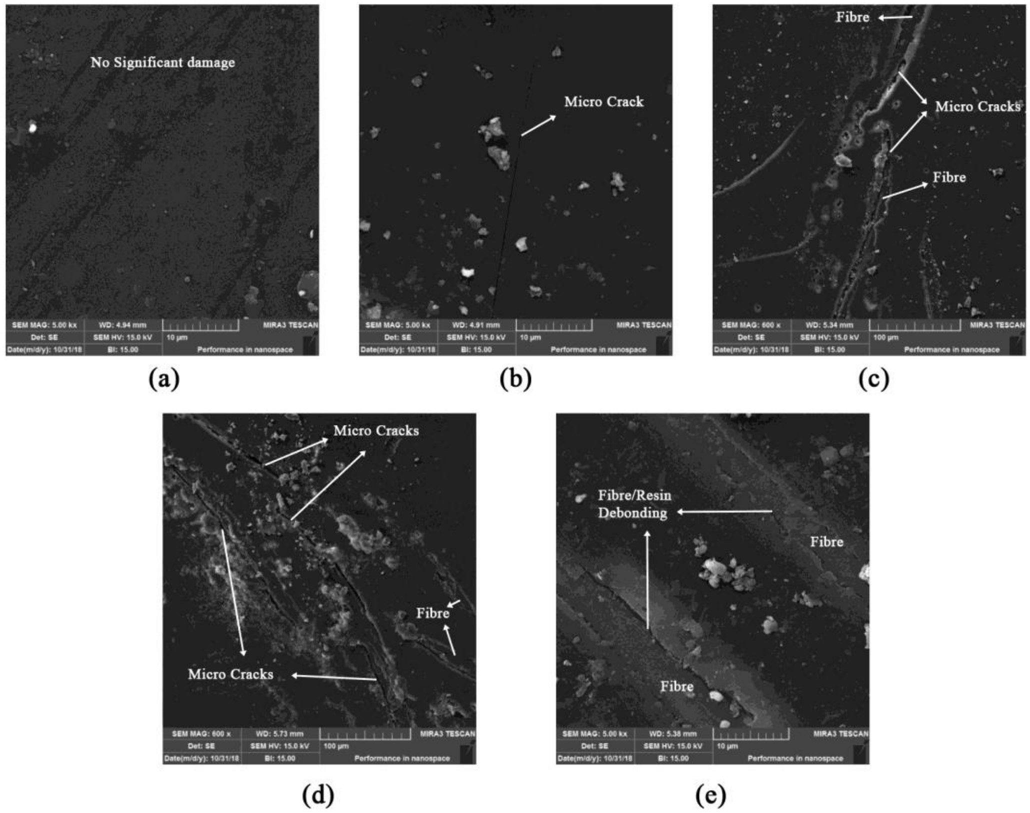

Figure 4-5 SEM images of I-1: (a) reference, (b) after 1000 h conditioning, (c) after 1500 h conditioning, (d) after 2000 h conditioning and (e) after 3000 h conditioning

4.3.3 Failure modes

It is important to note that the combination of different failure modes, possible failure mode changes over time, and randomness of the samples are some factors explains the difficulty in analysing the failure modes of bending sections. In this study, for the purpose of comparison, the dominant failure mode was considered for each section. However, the observations in this study should not be widely considered as characteristics behaviour of similar GFRP profiles.

4.3.3.1 Three-point bending

4.3.3.1.1 *I-shaped sections*

The modes of failure observed for I-shaped sections were tensile fibres fracture, web crippling, compressive fibre fractures, and resin crippling under the loading nose. However, the dominant failure mode along the major axis was the web-flange junction caused by the inter-laminar shear failure of the beam due to the local higher resin content and lower shear strength combined with a high moment of inertia. Whereas, along the minor axis, the predominant failure modes were the tensile fibre fractures and flange/web crippling. Therefore, it can be concluded that, in this case of the bending tests, the bending capacity of the I-shaped specimens may be lower than the inter-laminar shear capacity, which, in this study, led to the occurrences of fibre failure earlier than the interlaminar shear failure. In some cases, vertical cracks (shear failure) were also observed; however, this delayed failure mode was not the dominant mode of failure.

Regarding the interlaminar shear failure, the initial cracks started at the mid-span section and propagated to the end of the sections. This propagation of cracks mostly occurred on the top flange, near the middle of the web, and at the web-flange junctions. **Figure 4-6 (a)** and **Figure 4-6 (b)** illustrate the typical main failure modes observed for the reference I-shaped sections.

Regarding the conditioned specimens, the effect of conditioning on failure modes is classified into two categories: (1) no significant changes (even for 3000 h exposure) in beams tested along their minor axis; and (2) the greater the exposure time, the more significant the interlaminar shear cracks and resin crippling. In the first category, the degradation of the resin matrix and fibre/resin interface was not enough to change the dominant failure mode from fibre fractures to interlaminar shear failure. On the other hand, for bending about the major axis, the degradation of the resin matrix and consequently, the fibre/matrix interface due to the UV radiation, moisture, and temperature, was effective in increasing the possibility of interlaminar shear crack initiation and propagation. **Figure 4-6(c)** and **Figure 4-6 (d)** show the typical failure modes of conditioned I-shaped sections tested under three-point bending about the major axis. Failure of the beams tested about the minor axis (**Figure 4-6 (e-g)**) resulted in a final plastic hinge at the mid-span section for I-shaped beams.

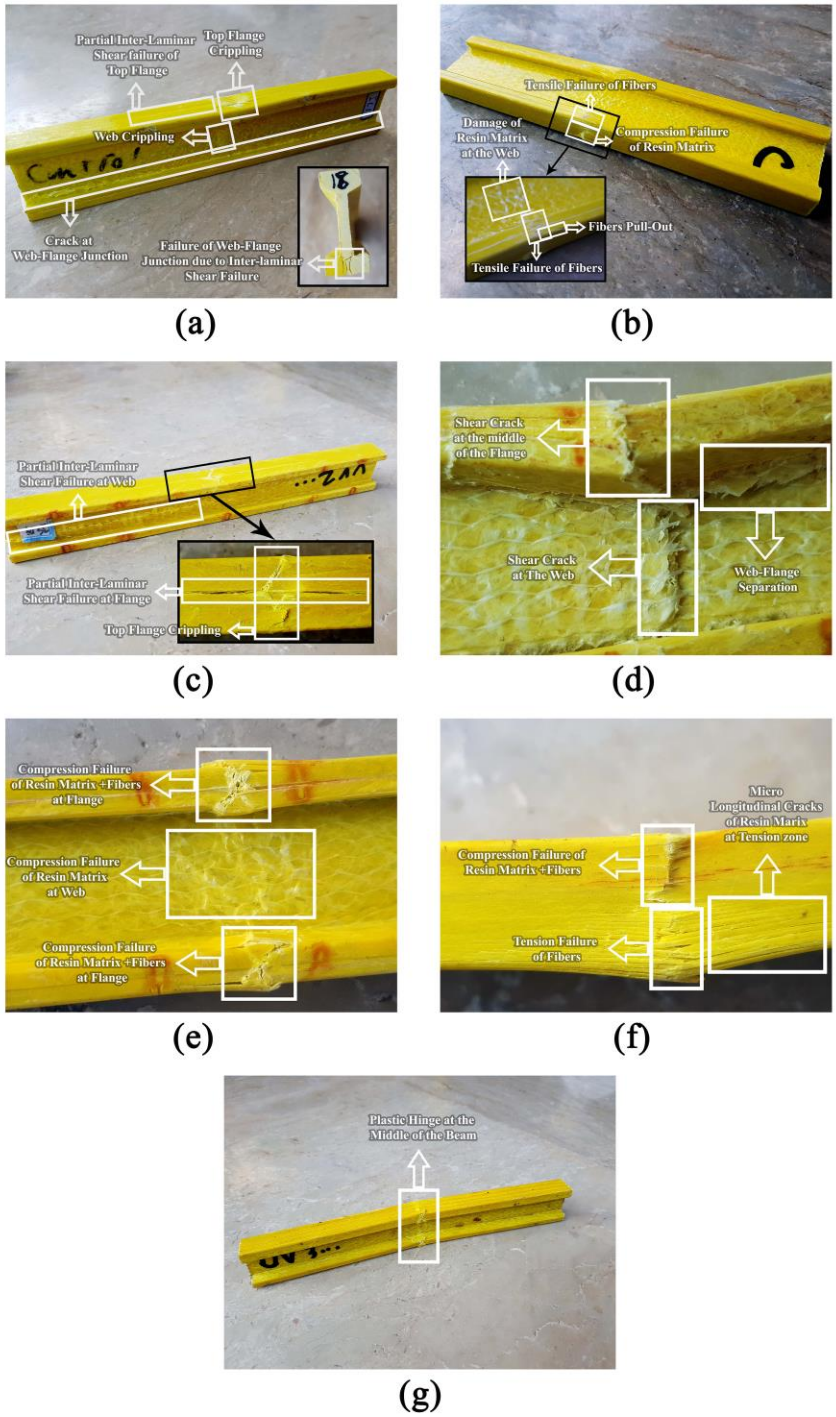

Figure 4-6 Failure modes of I-shaped sections under three-point bending tests: (a) reference about major axis; (b) reference about minor axis; (c) 2000 h conditioned about major axis; (d) 3000 h conditioned about major axis; (e) 2000 h conditioned about minor axis; (f) 3000 h conditioned about minor axis; and (g) 3000 h conditioned about minor axis

4.3.3.1.2 *Channel sections*

Similar to the I-shaped sections, unconditioned thinner channel sections failed due to fibre fractures at the tension and compression zones of the beam at mid-span when tested about their minor bending axis (**Figure 4-7 (a)** and **Figure 4-7 (b)**). However, an interesting phenomenon was observed during testing: for the thinner channel beams conditioned for more than 2000 h, the failure mode of channels changed from fibre fracture to a combination of interlaminar shear failure (web-flange junction failure) and partial fibre fracture in the tensile and compressive zones at mid-span (**Figure 4-7 (c)** and **Figure 4-7 (e)**). This shows that the conditioning (for >2000 h) that adversely affects the resin mechanical properties, and consequently, the fibre/resin interface, was adequate to decrease the interlaminar shear strength capacity of the larger channel sections up to a lower value compared to the section's bending capacity. It should be noted that micro-cracks formed in the resin matrix during conditioning might be the main reason for early initiation of the interlaminar shear cracks and their propagation. Regarding the failure of thinner channels about the major axis, similar to the I-sections, all unconditioned and conditioned specimens failed because of the interlaminar shear failure (particularly the web-flange junction failure) (**Figure 4-7 (d)**).

Moreover, due to a higher shear flow in the larger channels during the three-point bending tests about both the minor and major axes, all unconditioned and conditioned specimens failed along their web-flange junction (**Figure 4-7 (f)-Figure 4-7 (h)**).

To study the failure modes in terms of the fibres, resin matrix and resin/fibre interface, SEM analyses were conducted on the fracture surfaces of some of the tested samples. Fibre fractures in the tensile and compressive zones, interlaminar shear failure (at the flange, web, and web-flange junctions) and web/flange partial crippling failures are shown in **Figure 4-8** for both the I-shaped and channel sections tested under three-point bending about their both principal axes. As mentioned previously, due to the difference in bending behaviour between the I-shaped and channel sections about the major axis (owing to the channel's non-symmetric cross-section about the major bending axis), channel sections are more susceptible to out-of-plane deflections, which may cause variations in the applied stresses. This tendency may lead to a different mode of fibre fracture failure. Therefore, as seen in **Figure 4-8 (a)** and **Figure 4-8 (b)**, the fibre failures in the I-shaped beam are more regular, and are attributed to the fibres placed at the highest distance from the neutral axis, while the fibres of channel sections failed in an irregular manner (groups of fibres together). Moreover, the crack propagation paths of the I-shaped sections compared to the channel sections are more regular and predictable.

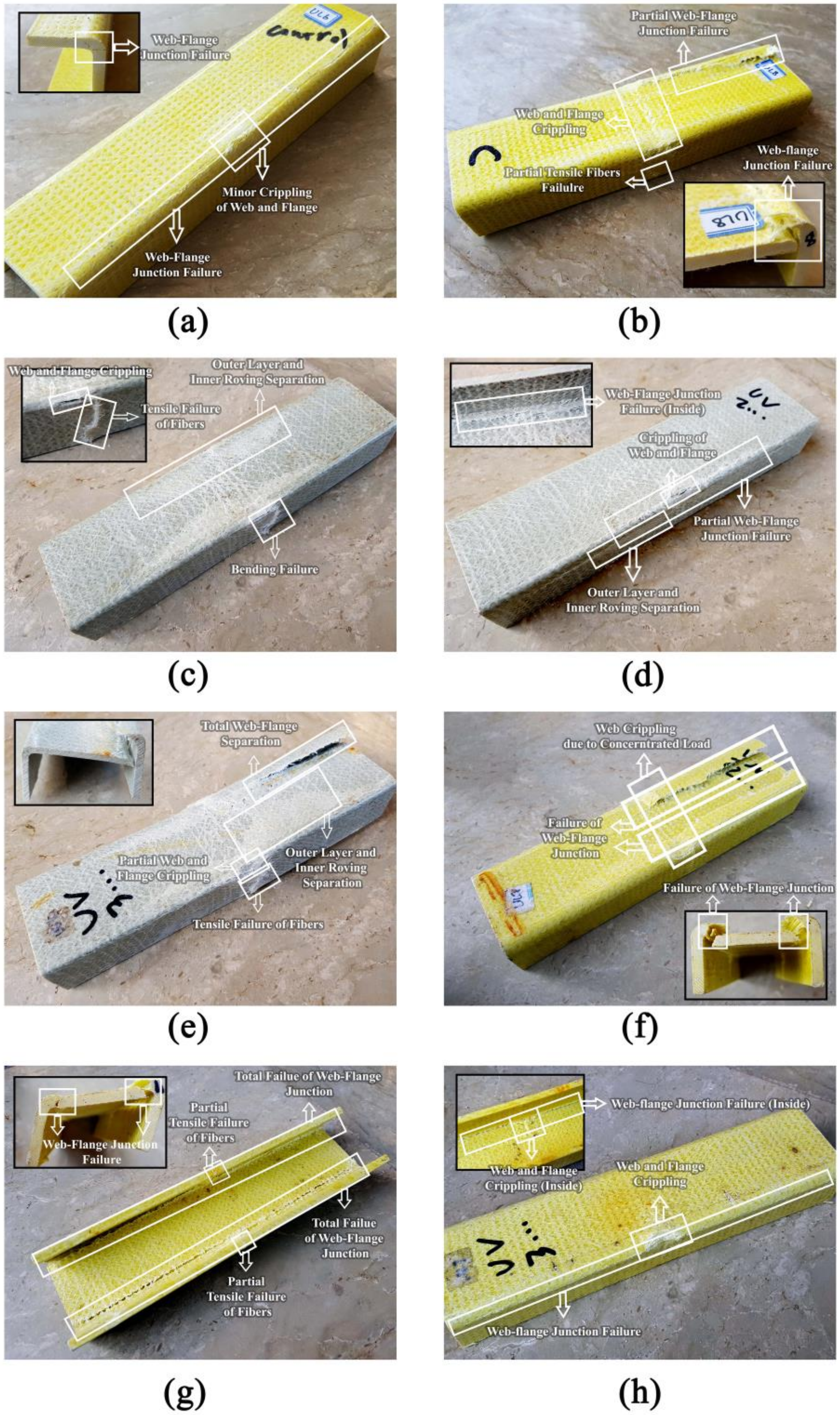

Figure 4-7 Failure modes of channel sections under three-point bending tests: (a) reference about major axis; (b) reference about minor axis; (c) 1500 h conditioned thinner channel section (U-1) about minor axis; (d) 2000 h conditioned U-1 about major axis; (e) 3000 h conditioned U-1 about minor axis; (f) 2000 h conditioned thicker section (U-2) about minor axis; (g) 3000 h conditioned U-2 about minor axis; (h) 3000 h conditioned U-2 about major axis

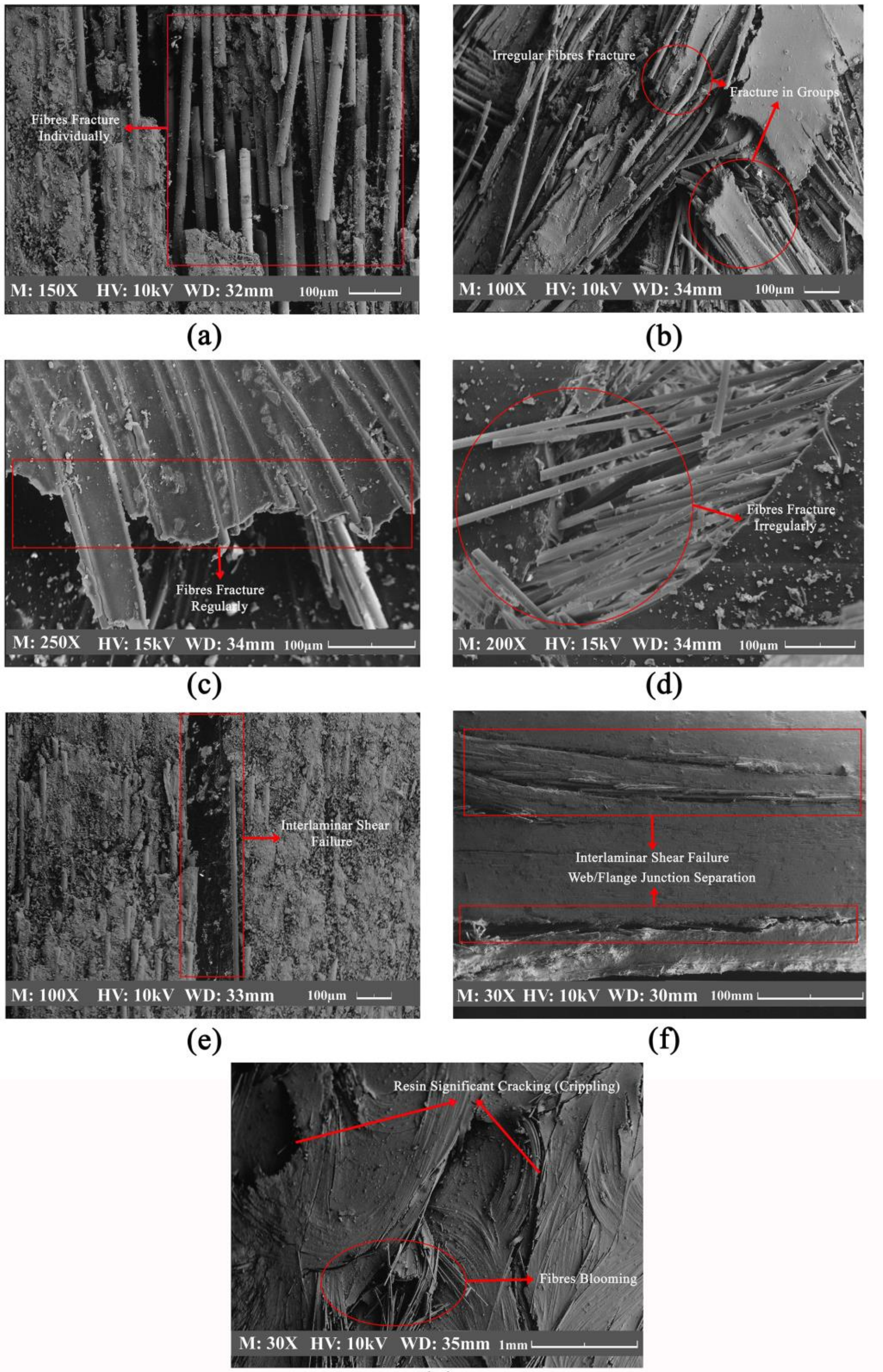

Figure 4-8 Different failure modes observed in GFRP profiles: (a) Tensile region of I-2 reference, (b) tensile region U-2 reference, (c) compression region 3000 h conditioned I-1, (d) compression region 1500 h conditioned U-1, (e) web of 2000 h conditioned I-1, (f) flange of 2000 h conditioned I-1, (g) web-flange junction of 3000 h conditioned U-2 and (h) Crippling failure of 2000 h conditioned I-2

4.3.3.2 Tensile tests

The same failure mode (long splitting) was observed for all of the unconditioned and conditioned GFRP plates during tensile tests. Therefore, it can be concluded that the UV radiation, moisture, and elevated temperatures may not affect the tensile failure mode (mainly fibre fractures) of the GFRP specimens. The reason for this could be the fact that UV radiation and moisture mostly affect the surface of the samples, and thus, in contrast to the bending tests, the degradation of the surface may not change the tensile properties of the samples significantly (since the whole sample cross-section contributes to the tensile behaviour). SEM analyses were also conducted on some tensile samples after testing. **Figure 4-9** shows the typical failure mode observed for all tensile samples and the fracture surfaces of both the control and 3000 h conditioned specimens. As is seen, no significant different is seen between both control and conditioned samples and they all failed through irregular patterns of resin failure and fibres fracture.

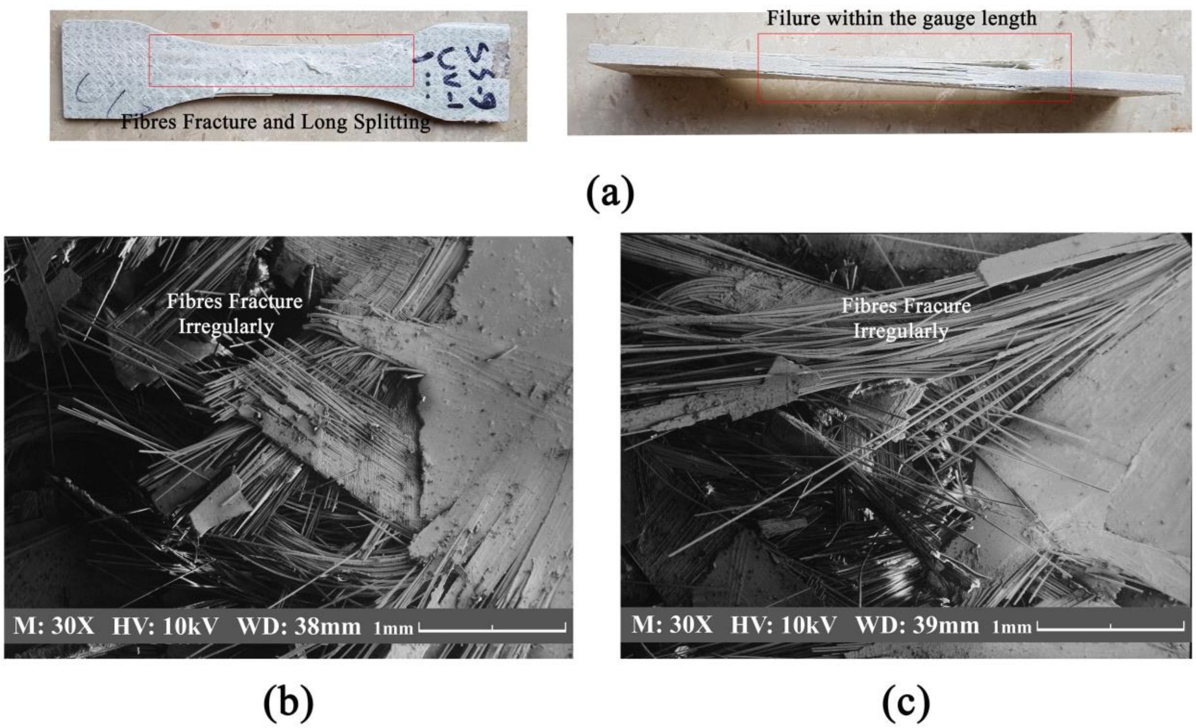

Figure 4-9 Typical failure mode of GFRP plates: (a) 1000 h conditioned sample (b) reference sample and (c) 3000 h conditioned sample

4.3.3.3 Compressive tests

As expected, like the tensile tests, due to the nature of the adverse effect (surface degradation) and test type (contribution of the entire cross-section to the load carrying capacity), a similar failure mode (elephant foot failure) was observed for all of the unconditioned and conditioned GFRP sections (boxes and tubes). **Figure 4-10** shows the typical failure mode of boxes and circular tubes that was observed for all of the compressive samples.

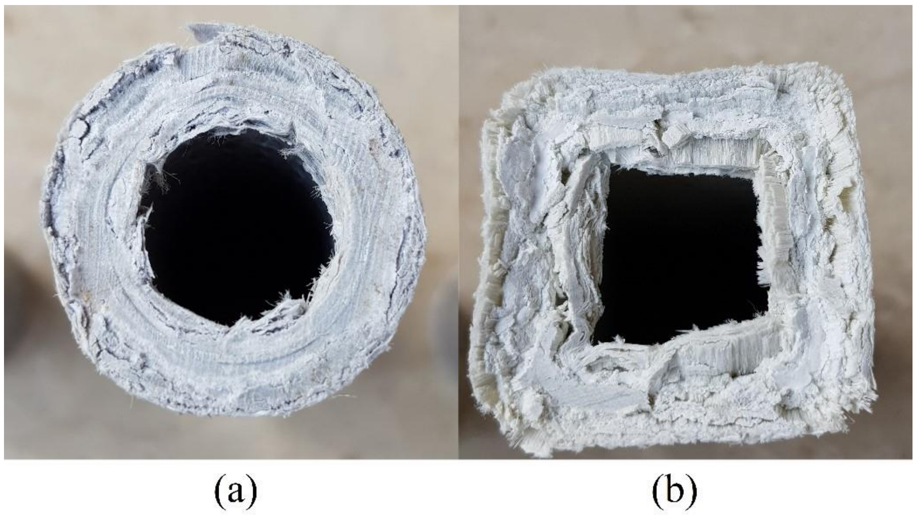

Figure 4-10 Typical failure mode of compressive sections: (a) circular tube and (b) box

4.3.4 Mechanical test results

4.3.4.1 Three-point bending test

The three-point bending test results, in terms of the average maximum load and strength retention values with corresponding coefficient of variation (CV), for both the reference and conditioned sections, are summarized in

Table 4-5. In general, the flexural strength of the GFRP pultruded profiles decreased as the number of conditioning cycles increased. However, no significant trend was observed for the maximum mid-span deflection of the specimens. To provide an in-depth analysis of the specimens, each section with different conditioning periods will first be considered and compared with its corresponding reference sample, and then the performance of all of the sections will be compared in order to investigate the effect of section type.

Table 4-5 Three-point bending test results

GFRP Section	Conditioning period	Average maximum load (N)	CV (%)	Retention (%)
I-1-W	Control	3203	1.04	100.0
	1000 h	3162	1.56	98.7
	1500 h	3058	2.34	95.8
	2000 h	2965	2.55	92.6
	3000 h	2933	3.28	91.6
I-1-S	Control	6292	0.88	100.0
	1000 h	5926	1.55	94.2
	1500 h	5182	2.65	84.2
	2000 h	4979	1.15	79.1
	3000 h	4958	3.25	78.8
I-2-W	Control	6577	1.26	100.0
	1000 h	6501	3.25	98.8
	1500 h	6312	3.33	95.5
	2000 h	5626	3.89	85.5
	3000 h	5236	4.55	79.6
I-2-S	Control	10793	2.22	100.0
	1000 h	9860	2.65	91.4
	1500 h	8841	1.25	81.9
	2000 h	7921	3.67	73.4
	3000 h	7121	4.89	66.0
U-1-W	Control	7250	0.89	100.0
	1000 h	7045	0.55	97.2
	1500 h	6290	2.25	86.8
	2000 h	6108	2.65	84.2
	3000 h	5966	3.22	82.3
U-1-S	Control	4320	2.25	100.0
	1000 h	4266	3.36	98.8
	1500 h	4025	1.25	93.2
	2000 h	3922	3.32	90.8
	3000 h	3820	4.12	88.4
U-2-W	Control	11002	1.15	100.0
	1000 h	10859	3.25	98.7
	1500 h	10522	1.33	95.6
	2000 h	9578	2.98	87.1
	3000 h	9130	2.22	83.0
U-2-S	Control	7659	1.89	100.0
	1000 h	7538	1.55	98.4
	1500 h	7150	3.26	93.4
	2000 h	6940	4.12	90.6
	3000 h	6650	2.25	86.8

4.3.4.1.1 I-shaped sections

The ultimate load retention versus the conditioning duration of the I-shaped sections for both bending tests are shown in **Figure 4-11**. As expected, the load retention decreases with increasing exposure cycle. However, the reduction is greater when bending about the major axis in comparison to the minor axis (e.g., a 22% and 34% reduction after 3000 h cycles for the major axis in comparison to a 9% and 21% reduction for the minor axis for the I-1 sections and the I-2 sections, respectively). This observation confirms that beams with interlaminar shear failure are more susceptible to environmental degradation than beams with fibre fracture failure. This might be due to the degradation of the resin matrix and, consequently, the resin/fibre interface of the GFRP sections during their exposure to environmental conditions. However, it is known that the fibres will also be affected by ultraviolet (UV) radiation [39], and this degradation may be the main reason for the reductions about the minor axis observed in the tested beams. It should also be considered that the fibres hardly would be exposed to UV radiation as they are embedded in the resin matrix (e.g. fibres in **Figure 4-5 (e)** will be exposed to UV radiation due to the surface resin leaching).

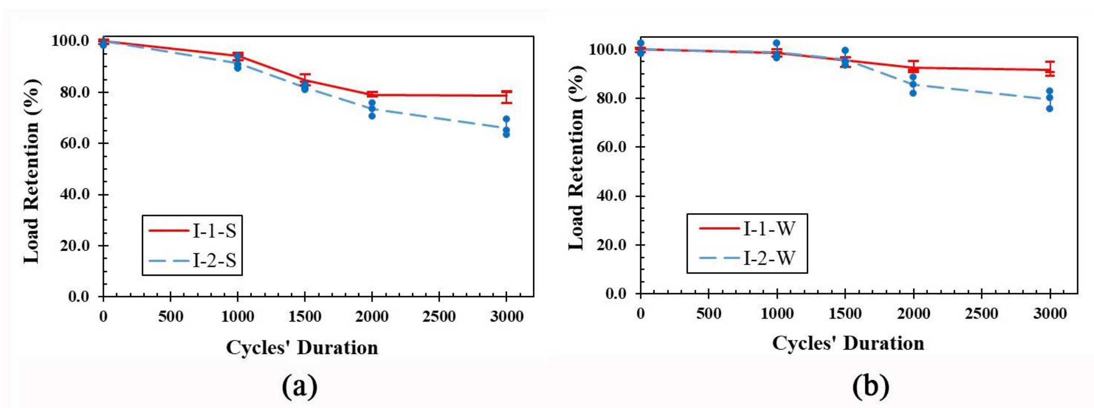

Figure 4-11 Ultimate load retention versus conditioning duration of I-shaped sections during three-point bending test: (a) about major axis and (b) about minor axis

Regarding the cross-section of the beams, it is obvious that the reductions were greater in the I-2 beams than the I-1 beams (e.g., a 7% reduction for the minor axis and a 21% reduction for the major axis for the I-1 sections after 2000 h cycles in comparison to 15% and 27% reductions respectively for the corresponding I-2 sections). Accordingly, it concluded that the section with a larger surface exposed to UV radiation and vapour condensation had a higher level of degradation and, consequently, a lower bending capacity. It should be mentioned that the thickness of both I sections was identical.

Regarding the load-deflection behaviour of the beams under the bending, the nonlinear regions of the I-sections were significantly larger under the major axis than the minor axis. This difference is attributed to the failure modes of the beams; the significant nonlinear region of the beam is related to the cracks at the resin matrix (interlaminar shear failure), which starts from the critical section (mid-span) and web-flange junction and propagates through the entire beam. However, due to fibre fractures and fewer resin cracks and fibre/resin debonding, the nonlinear region was found to be small for the beams tested about the minor axis. It was also observed that the load-displacement performance of samples did not change qualitatively with ageing.

4.3.4.1.2 Channel sections

The ultimate load retention versus the conditioning duration of the channel sections for both bending tests are shown in **Figure 4-12**. As seen, in contrast to the I-sections, the reductions were greater in the channels tested about the minor axis than the corresponding sections tested about the major axis (e.g., 18% and 17% reductions after 3000 h cycles for the minor axis in comparison to 12% and 14% reductions for the major axis for U-1 and U-2, respectively). This may be due to the change in the failure mode (from the fibre fracture to the interlaminar shear failure) during conditioning, which increases the effect that the resin and resin/fibre interface degradation has on the beam's ultimate strength.

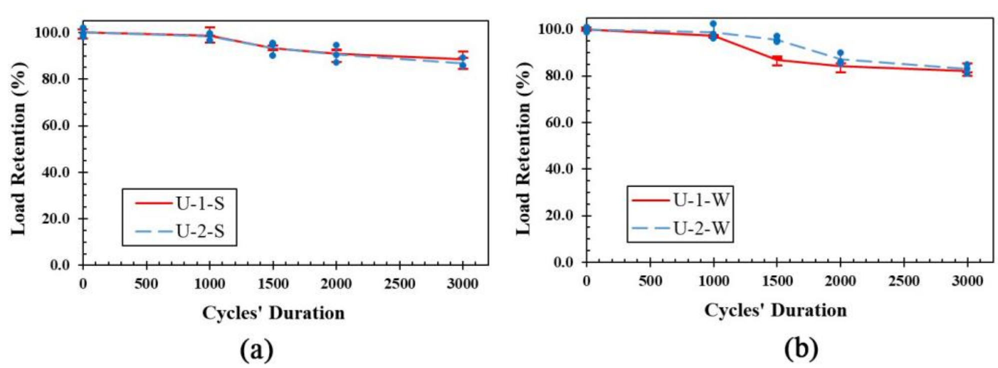

Figure 4-12 Ultimate load retention versus the conditioning duration of channel sections during three-point bending test: (a) about major axis and (b) about minor axis

Considering the cross-section of the beams, the results demonstrate that, when a beam was tested about its minor axis, the thicker section (channel 2), with a perimeter nearly identical to that of channel 1, had less reduction than the thinner section (e.g., a 14% reduction for the U-2 sections after 1500 h cycles in comparison to a 5% reduction for the U-1 sections). However, the final reduction was found to be almost the same for both sections (about 17% for 3000 h). The reductions for the beams tested about the major axis were found to be almost the same after each duration of exposure. These observations show that, due to less moisture and heat penetration, the thicker sections may be less affected by environmental conditions. However, because UV radiation and water vapour condensation mainly affect the surface of the samples, the effect of the thickness is not significant.

Regarding the load-deflection behaviour, for all conditions, no significant nonlinear behaviour (for either the fibre fracture or the interlaminar shear failure) was observed for any of the channel sections. Sudden web-flange separation due to an out of plan bending during the test about the major axis and fast crack propagation during the test under minor axis may be the possible reasons for the observed behaviour of channel sections.

4.3.4.1.3 Comparison of the sections

Figure 4-13 compares the retention versus displacement of different sections tested under three-point bending. It shows that the I-1 section exhibited the best performance among the sections, while U-1 (except at 3000 h) showed the weakest performance. These results confirm that sections with a smaller thickness and larger perimeter may experience greater material degradation (especially resin matrix degradation) after exposure to UV radiation and water vapour condensation. However, regarding the major axis, it is clear that the reduction values of the I-shaped sections were greater than those of the channels (**Figure 4-13 (a)**). This may be due to the early failure of the channels because of the eccentricity of the applied load, which may have reduced the effect of material degradation on the ultimate failure load.

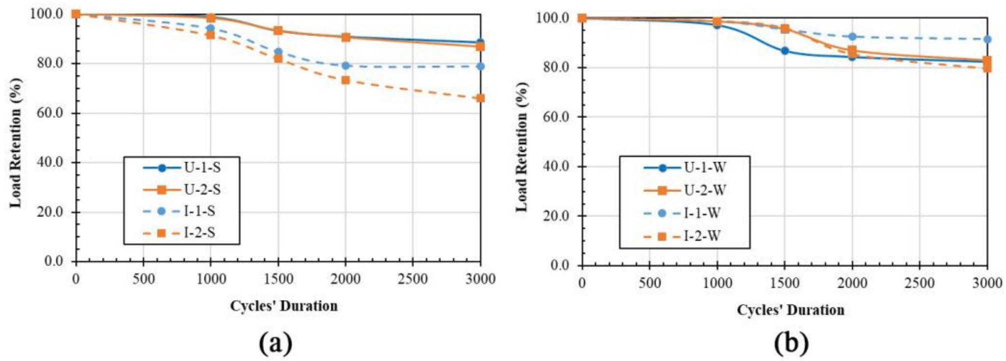

Figure 4-13 Comparison between the bending performance of different sections during three-point bending test: (a) about major axis and (b) about minor axis

4.3.4.2 Compression test

The compression test results, in terms of the maximum load for both the reference and conditioned sections, are summarised in **Table 4-6**. Like for the bending tests, it can be seen that the compressive strength of the GFRP sections decreased when the number of conditioning cycles was increased.

Table 4-6 Compression test results

GFRP Section	Conditioning period	Average maximum load (N)	CV (%)	Retention (%)
C-1	Control	60321	2.12	100.0
	1000 h	58962	3.14	97.7
	1500 h	50623	3.59	83.9
	2000 h	48518	2.58	80.4
	3000 h	47850	3.16	79.3
C-2	Control	92655	2.25	100.0
	1000 h	91512	3.55	98.8
	1500 h	85675	3.56	92.5
	2000 h	83645	4.12	90.3
	3000 h	82486	3.28	89.0
B-1	Control	43195	2.78	100.0
	1000 h	42189	3.15	97.7
	1500 h	37601	2.27	87.0
	2000 h	35028	3.68	81.1
	3000 h	33956	5.01	78.6
B-2	Control	65233	1.15	100.0
	1000 h	64925	3.12	98.5
	1500 h	55654	3.55	85.3
	2000 h	52341	4.12	80.2
	3000 h	50357	6.01	77.2

4.3.4.2.1 Circular tube sections

As illustrated in **Figure 4-10**, the tubes failed due to the local fibres buckling and resin crippling at the ends of the specimens (brooming effect). This failure starts to occur when the fibres of a tube's external layers begin to buckle due to the failure of the resin matrix under the applied compressive loads. Therefore, it can be concluded that the degradation of the tubes subjected to UV radiation and water vapour contestation (which mainly affect the external layers of the composites) is an important factor in determining the compressive strength of the tubes.

The ultimate load retention versus the conditioning duration plots for circular tube sections under compressive tests are shown **Figure 4-14**. It is clear that the ultimate strength reductions for thicker tubes were less than those for the thinner ones (e.g., 21% reduction for C-1 sections compared with 11% for C-2 sections after 3000 h cycles). Less moisture and heat penetration in the thicker tube may have caused this difference. It is worth mentioning that the surface areas that the UV light acted on were equal for both tubes.

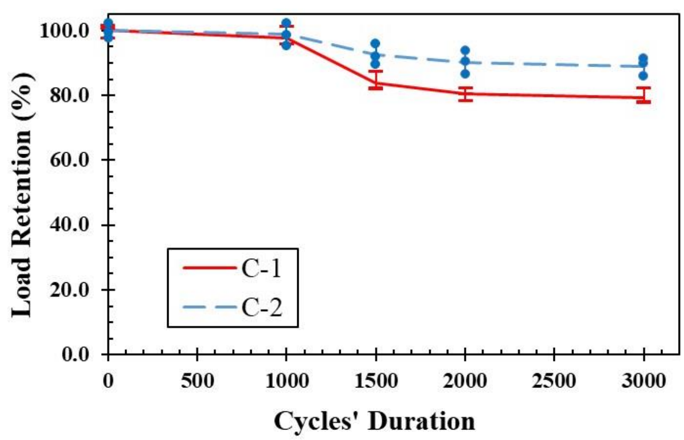

Figure 4-14 Compressive ultimate load retention versus the conditioning duration of circular tube sections during compression test

4.3.4.2.2 Box sections

The ultimate load retention versus the conditioning duration of box sections under compressive tests are shown in **Figure 4-15**. Based on the results, like in the bending tests, the sections with a larger perimeter (same thickness) subjected to environmental conditions experienced greater reductions in ultimate compressive strength. However, the differences in strength reductions between the sections with different perimeters were not significant and were within scatter of the test results, which shows that, for compression tests, the thickness is a more important factor than the section perimeter. This can be explained according to the failure mode of the compressive samples (elephant foot buckling), in which the more the outer layers' degradation, the earlier the elephant foot buckling occurs. Moreover, the 1000 h exposure time was an exception to this (**Table 4-6**). This may have been due to the sample randomness and low level of degradation after 1000 h conditioning.

Regarding the load-displacement behaviour of compressive samples, almost linear behaviour was observed for all sections during the compressive tests. Moreover, the load-displacement performance of samples did not change qualitatively with ageing.

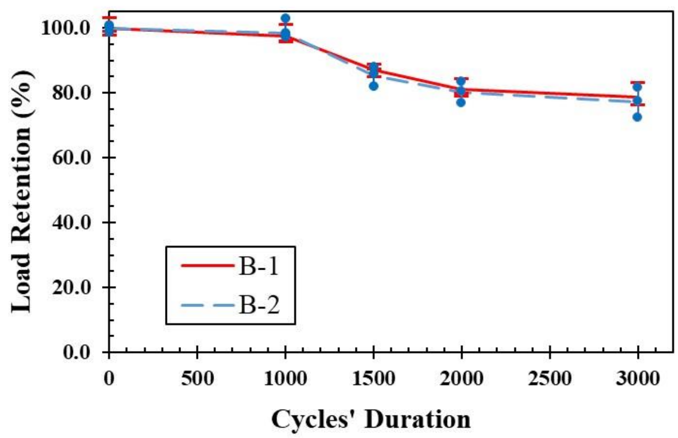

Figure 4-15 Compressive ultimate load retention versus the conditioning duration of box sections during compression test

4.3.4.2.3 Comparison of the sections

Figure 4-16 compares the retention versus displacement of different sections tested under compression. It was found that the C-2 section (the thickest section) had the best compressive performance among all the sections, while the others showed similar behaviour. This demonstrates that the thickness is an extremely important factor in the compressive behaviour of GFRP after environmental conditioning.

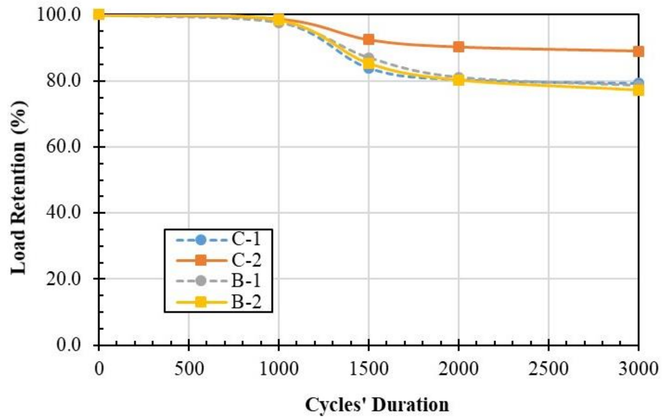

Figure 4-16 Comparison between the compressive performances of GFRP sections during compression test

4.3.4.3 Tension test

The tensile test results, in terms of the ultimate tensile load and elastic modulus for both the reference and conditioned sections, are summarised in **Table 4-7**. Both the ultimate tensile load decreased with increasing duration of conditioning cycles, whereas the elastic modulus initially increased before it decreased. As is known, the elastic moduli of FRP composites are primarily governed by the elastic moduli of the fibres, and the changes in resin properties during conditioning may not change an FRP's elastic modulus significantly. However post-curing of the resin matrix due to the temperature and UV radiation [88, 191], secondary cross-linking (through hydrogen bonding) and void occupation due to moisture absorption [192] are known to increase the stiffness of the polymers, which may explain the initial increase in the elastic moduli of GFRP laminates upon the exposure to UV radiation and water vapour condensation cycles.

As is seen in **Figure 4-17**, the adverse effect of UV radiation and water vapour condensation on the ultimate tensile load of the plates is higher for the thinner L-1 as compared to L-2. For example, after 2000 h cycles, there is a 20% reduction for L-1 sections compared to 15 % for L-2. However, it should be mentioned that after 3000 h cycles, almost the same results were observed for both L-1 and L-2, which shows that the aging time was enough for thicker laminate to reach the degradation level of the thinner one.

Comparing the results of compressive and tensile tests showed that the reductions for tensile strength are slightly higher. This could be due to the fact that in the compressive test, only the external surface of the section is exposed to UV radiation, whereas in tensile samples, both sides are in contact with

UV radiation. The other possible reason for this difference may be the different failure mechanisms and cross-sections.

Regarding the load displacement behaviour, as expected, a brittle failure with a loud sound occurred for all the laminates. In addition, the load-displacement performance of samples did not change qualitatively with ageing.

Table 4-7 Tensile test results

GFRP Section	**Conditioning period**	**Average maximum load (N)**	**C.V (%)**	**Retention (%)**	**Average elastic modulus**	**CV (%)**	**Retention (%)**
L-1	Control	28345	1.12	100.0	35	1.7	100
	1000 h	27349	1.55	96.5	40	2.4	108
	1500 h	22994	0.89	81.1	36	2.2	97
	2000 h	21332	4.23	75.3	35	3.1	94
	3000 h	20577	2.84	72.6	32	2.9	86
L-2	Control	40906	0.89	100.0	45	2.1	100
	1000 h	40760	1.12	99.6	48	2.8	106
	1500 h	38456	2.56	94.0	51	3.6	113
	2000 h	32965	3.55	80.6	41	1.8	91
	3000 h	30255	3.84	74.0	40	4.1	88

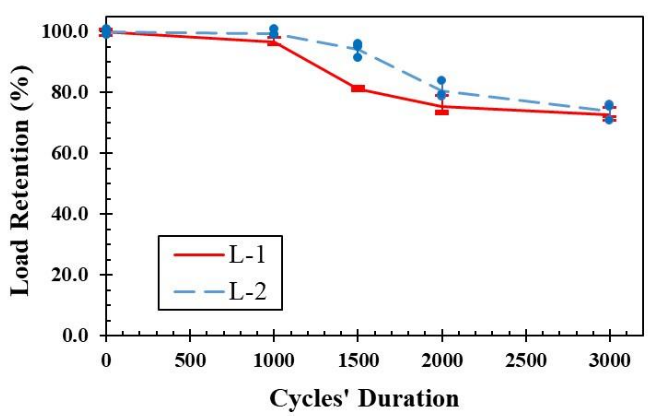

Figure 4-17 Tensile ultimate load retention versus the conditioning duration of GFRP laminates during tension test

4.4 Comparison of the results with the literature

To generate a better understanding of the variables used (environmental conditioning, conditioning period, specimen type and configuration), the results of the present study were compared with some previous research conducted by other researchers using similar conditions. It should be mentioned that, due to the lack of studies on the compressive properties of FRP composites after environmental conditioning, the comparison is only conducted for the tensile and three-point bending tests.

4.4.1 Tensile tests

It should be pointed out that most studies in the literature focus on the tensile behaviour of composites under environmental conditions. **Table 4-8** shows some results reported by researchers on the tensile performance of FRP composites after exposure to specific conditions. It can be seen that the effect of environmental conditioning on the tensile strength of FRP bars was not significant, while laminates were affected by such conditions. This may be due to the larger ratio of the exposed surface to the sample thickness in laminates compared with bars. However, the use of different materials, conditioning procedures and testing properties could be the reasons for the scatter in the results reported by different researchers. Generally, considering all the results of the present study and the results reported by the other researchers, one might conclude that tensile properties of FRP composites, regardless of the fibre and resin matrix type, are not significantly affected by UV radiation and moisture cycles. However, by using appropriate material type, sample thickness and protective layer this amount of degradation may also be avoided.

Table 4-8 Comparison between the tensile test result of the present study and similar research

Reference	FRP Type	Environmental condition	Results
-	Present study	UV radiation and water vapour condensation cycles	26% reduction of plates with the thickness of 5 mm and width of 20 mm after 3000 h cycles
[39]	Glass-fibre reinforced epoxy bars	UV radiation and water vapour condensation cycles	5% reduction of 6-mm bar after exposure to 3000 h cycles
[165]	Carbon-fibre reinforced epoxy bars	UV radiation and water spray cycles	No significant changes
[77]	flax fabric reinforced epoxy composites	UV radiation and water spray cycles	29% reduction of 25×25×5.2 mm^3 laminate after exposure to 1500 h cycles
[168]	Glass-fibre reinforced polyester/vinyl ester laminates	Combined effect of high temperature, freeze–thaw cycles, moisture and UV radiation	15.5 %, 10.4 %, and 13.9 % reduction for isophthalic polyester, orthophthalic polyester, and vinyl ester laminates (thickness of 2.85 mm) after six months
[169]	Glass-fibre reinforced polyester laminates	UV radiation and moisture cycles	21 % reduction of 5 × 25 × 300 mm laminates after exposure to 3000 h cycles

4.4.2 Three-point bending tests

As there is no specific study focused on the bending properties of FRP sections, the results of the present study are compared with the results of research conducted on FRP bars and laminates. As one selected type of the sections used in this study, I-1 beams were used for comparison. Beams tested about minor axis (due to the interlaminar shear failure) were compared with the results of short beam tests in the literature, while sections tested about the major axis were compared with the flexural results.

Table 4-9 Comparison between the bending and interlaminar shear/short beam test results of the present study and similar research

Reference	FRP Type	Environmental condition	Results
-	Present study	UV radiation and water vapour condensation cycles	22% reduction of I-1 tested about the major axis (interlaminar shear failure) after 3000 h cycles
[39]	Glass-fibre reinforced epoxy bars	UV radiation and water vapour condensation cycles	15% reduction of 10-mm bar under short beam test after exposure to 3000 h cycles
[12]	GFRP bars	simulated seawater sea sand concrete solutions	25 % reduction of 6-mm bar under interlaminar shear test after 84 days of conditioning
[169]	Glass-fibre reinforced vinylester/polyester laminates	UV radiation and moisture cycles	9 % and 7 % reductions of $5 \times 15 \times 30$ mm polyester and vinyl ester laminates, respectively after exposure to 3000 h cycles
-	Present study	UV radiation and water vapour condensation cycles	9 % reduction of I-1 tested about the minor axis (flexural failure) after 3000 h cycles
[39]	Glass-fibre reinforced epoxy bars	UV radiation and water vapour condensation cycles	8% reduction of 10-mm bar for flexural strength after exposure to 3000 h cycles
[77]	flax fabric reinforced epoxy composites	UV radiation and water spray cycles	10% flexural reduction of $100\times20\times5.2$ mm^3 laminate after exposure to 1500 h cycles
[168]	Glass-fibre reinforced polyester/vinyl ester laminates	Combined effect of high temperature, freeze–thaw cycles, moisture and UV radiation	14.8 % and 10.5 %, reduction for flexural strength of orthophthalic polyester, and vinyl ester laminates (thickness of 2.85 mm) after six months
[169]	Glass-fibre reinforced vinyl ester laminates	UV radiation and moisture cycles	13 % reduction of $5 \times 15 \times 150$ mm laminates after exposure to 3000 h cycles

Table 4-9 shows the results of some reported research in the literature. Regardless of the differences in sample type and cross-section, a good agreement is observed between the results of this study and those by other researchers. However, various parameters, such as the test and conditioning configuration, affect the final strength reduction. Generally, similar to the results of tensile strength changes from **Table 4-9**, it can be concluded that the flexural strength of FRP composites, when fibre failure occurs, is not significantly affected by the UV radiation and moisture cycles. However, this reduction increases if the failure occurs due to the interlaminar shear strength. Therefore, to reduce the adverse effects of such environments, especially when interlaminar shear strength is the possible failure mode, using appropriate cross- section and protective layer is strongly recommended to avoid considerable degradation.

For the future study, the authors will investigate the performance of degraded GFRP profiles when used with sea water sea sand concrete.

4.5 Statistical analysis

4.5.1 Analysis of Variance (ANOVA)

In order to quantify the contribution of each parameter (conditioning period and cross-section' geometry) on mechanical properties of GFRP pultruded profiles, two-way analysis of variance (ANOVA) was used. In order to have a better understanding, two life spans were considered for the ANOVA analyses: (1) up to 1500 h and (2) up to 3000 h cycles. According to test results, contributions of both conditioning period and profile type and their interaction on the ultimate strengths of the specimens are shown in **Figure 4-18** to **Figure 4-22**.

From **Figure 4-18**, it can be noted that for I-shaped sections, the effect of profile type (perimeter in this case) is negligible up to 1500 h conditioning and increase for both types of bending tests. The interaction of the conditioning period and profile type factors is significantly larger for bending about the minor axis compared to the major axis (15 % compared to 4 %). This shows that the dependency of these two factors must be taken into account when predicting the reduction strength of sections with flexural failing. Regarding the channel sections, **Figure 4-19** shows that the effect of profile type (thickness, in this case) is not an effect factor for testing about the major axis, while it is effective (especially in the short-term period) for testing about the minor axis. Early failure of the channels (out of plan bending) when testing about the major axis may be the main reason for thickness to be an ineffective factor in this case. Significant increase in the contribution value of the conditioning period for bending about the minor axis shows that web-flange junction will weaken regardless of the sections' thickness.

It is seen from **Figure 4-20** that the effect of profile type for circular tubes is significant and increase by increasing the conditioning time (from 7.5 % for duration of 0 -1500 h to 14.7 % for duration of 0 – 3000 h). However, for both durations, the effect of profile type for box sections is negligible (**Figure 4-21**). These results show that the effect of thickness is important in compressive strength reduction of FRP profiles subjected to UV radiation and moisture, while the effect of perimeter is insignificant.

Regarding the tensile strength, as is the case for circular tube sections, the effect of the profile type (thickness in this case) is an important factor; in contrast to the case for circular tubes, this effect decreases with the increase in the duration of the conditioning (from 15.8 % for a duration of 0 -1500 h to 4.2 % for a duration of 0 – 3000 h) (**Figure 4-22**). This may be due to the different failure areas of the sections in compressive and tensile tests. The tubes failed due to the local buckling of the outer fibres and the resin crippling at the external layers (the environmental conditioning affects these layers), while laminates failed due to fibres fracture and long-splitting within the whole cross-section during the tensile tests. In other words, the penetration rate of the possible damage decreases after a while. However, this assumption needs to be carefully investigated using microstructural analyses (i.e. CT X-ray analysis) in further studies.

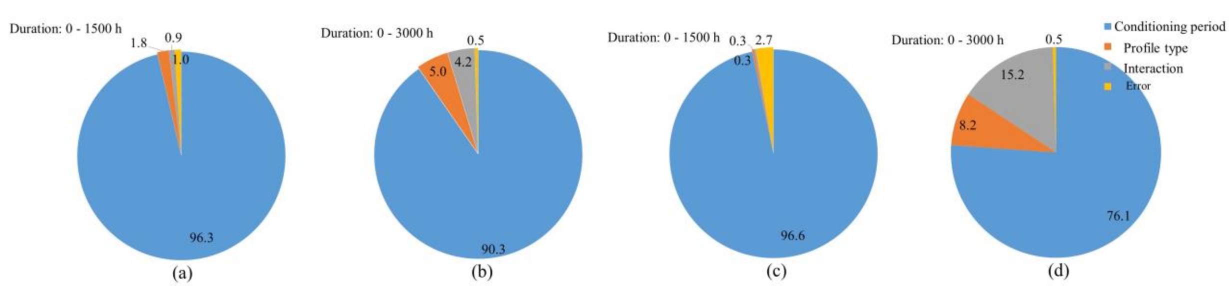

Figure 4-18 ANOVA results for I-shaped sections: (a) major axis (up to 1500 h), (b) major axis (up to 3000 h), (c) minor axis (up to 1500 h) and (d) minor axis (up to 3000 h)

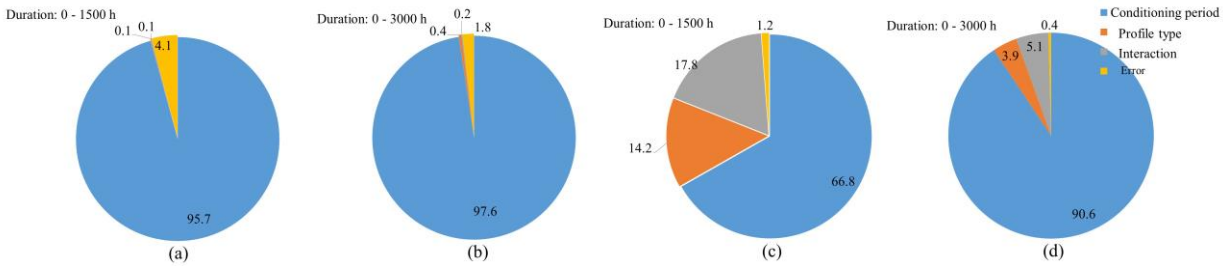

Figure 4-19 ANOVA results for channel sections: (a) major axis (up to 1500 h), (b) major axis (up to 3000 h), (c) minor axis (up to 1500 h) and (d) minor axis (up to 3000 h)

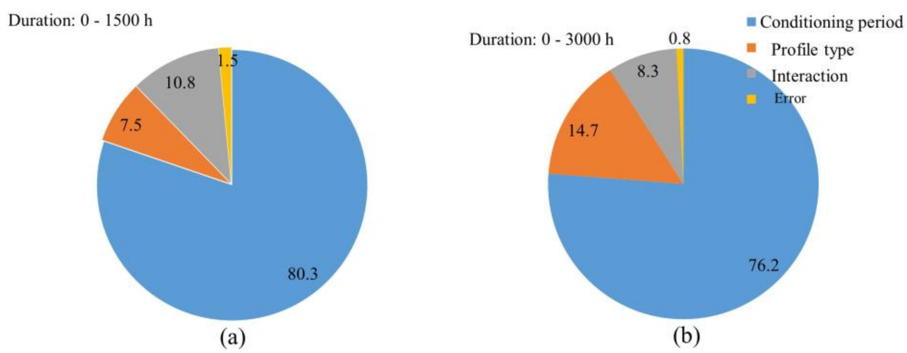

Figure 4-20 ANOVA results for circular tube sections: (a) Up to 1500 h and (b) Up to 3000 h

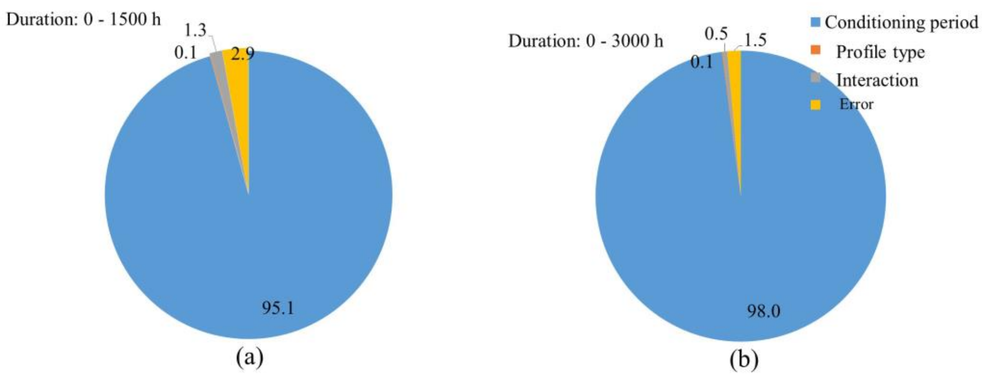

Figure 4-21 ANOVA results for box sections: (a) Up to 1500 h and (b) Up to 3000 h

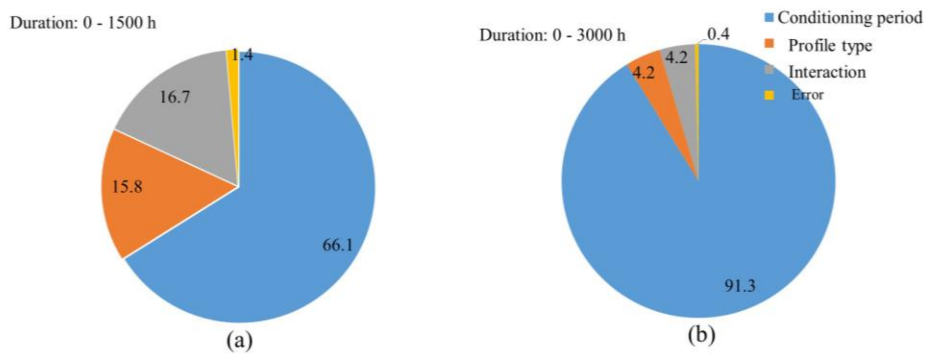

Figure 4-22 ANOVA results for laminates: (a) Up to 1500 h and (b) Up to 3000 h

4.5.2 Linear Bayesian regression

In this section, probability models are proposed using the experimental data obtained. The models are developed using linear Bayesian regression (LBR) for the different mechanical tests. Briefly, in the LBR method, at first the effective variables are identified among all the variables of the study. Next, the relationship between the test results and the effective variables is found by trying numerous models. Finally, the best model, according to the statistical factors, is proposed to predict the results. It is worth mentioning that the proposed model may be used in the case of exactly the same variables as this study and may not be used for other cases with different parameters. The aim is to predict the reduction strength of GFRP pultruded profiles after they are exposed to UV radiation and water vapor condensation cycles. For this purpose, Risk Tools (RT) software was used [193]. Effective variables, according to ANOVA analyses, were considered as the inputs. Using the selected variables, several models were tried and compared with each other in terms of the statistical indexes (i.e. homoscedasticity, non-collinearity, regression coefficient correlations and errors normality). Finally, **Eq.4.1** was selected as the most accurate model to predict the retention values of pultruded GFRP mechanical properties after exposing to different cycles of UV and water vapor condensation:

$$R\ (\%) = A\left(\frac{1}{\log(T)}\right) + B(t^2) + C\left(\frac{1}{p}\right) + D\sqrt{I_x} + E \qquad (4.1)$$

where T (h) is the period of conditioning cycles, t (mm) is the specimen thickness, p (mm) is the specimen perimeter, I_x (mm^4) is the moment of inertia about x axis, and A, B, C, D, and E are the equations' constants for each test type. **Table 4-10** lists the constants for the different tests. Additionally, the regression parameters, including the R factor, C.V. of standard deviation (SD), and mean of SD for each type of test are listed in **Table 4-11**. Although according to the values in **Table 4-10**, the reliability of the model is acceptable, more experimental data considering several different is needed in order to have a more accurate and practical formula. In **Figure 4-23** and **Figure 4-24**, the results predicted by the proposed model are compared with the results obtained from the experiments. As seen, an acceptable agreement is obtained between the obtained results and predictions.

Table 4-10 Constant values in Eq.4.1

Test Type	**A**	**B**	**C**	**D**	**E**
Three-point bending about the major axis	341.28	1.845	-18957	-0.364	186.5
Three-point bending about the minor axis	324.67	0.214	846	0	-19.2
Compression	383.90	0.455	-1774	0	-28.8
Tension	561.00	0.270	0	0	-93.6

Table 4-11 Regression parameters for Eq.4.1

Test Type	**R-factor**	**Mean of SD**	**C.V. of SD (%)**
Three-point bending about the major axis	0.96	3.08	0.26
Three-point bending about the Mainor axis	0.92	3.08	0.25
Compression	0.93	3.35	0.25
Tension	0.97	3.36	0.70

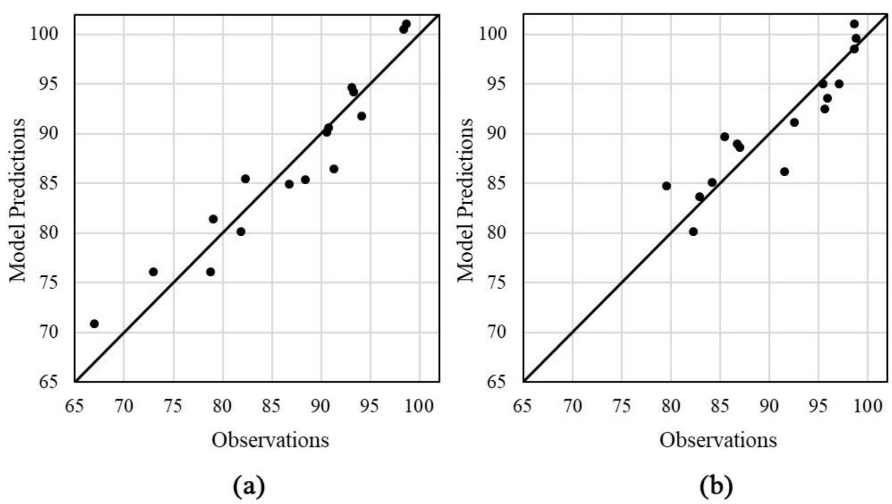

Figure 4-23 Comparison between the experimental tests and predicted values for three-point bending tests: (a) about the major axis and (b) about the minor axis

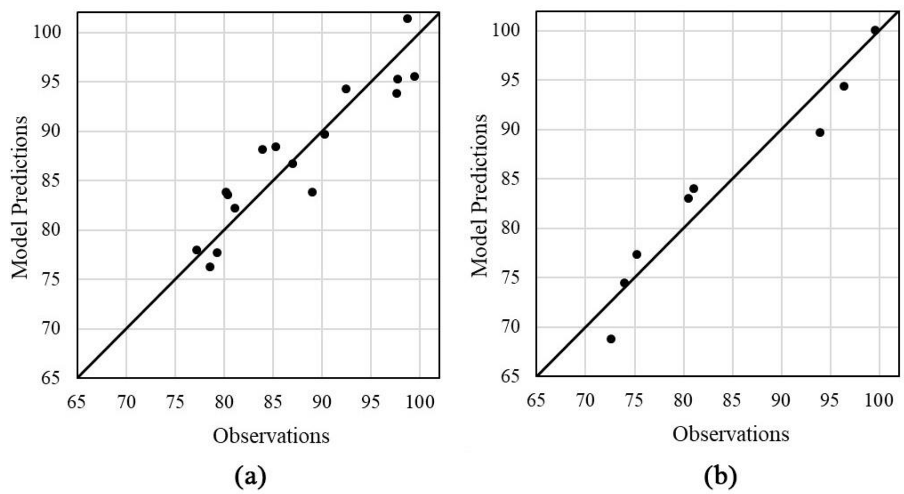

Figure 4-24 Comparison between the experimental tests and predicted values: (a) compression tests and (b) tensile tests

4.6 Conclusion

This study was a part of an ongoing research program on the performance of FRP composites subjected to different environmental conditions. The mechanical and microstructural properties of various GFRP pultruded sections after exposure to different periods of sequential UV radiation and water vapour contestation cycles were studied. Mechanical tests, including bending, compression, and tension in addition to the microstructural (SEM) and statistical analyses (ANOVA and regression), were used. The following conclusion can be drawn:

- For all tensile, compressive and bending tests, the mechanical properties of various GFRP sections deteriorated within three different regions: (1) a small rate up to 1000 h (2) highest rate up to 2000 h and (3) a rate between those two periods for 3000 h.
- The maximum strength reduction was found to be 34 %, 23 %, and 28 % after exposure to 3000 h cycles for three-point bending, compressive, and tensile tests, respectively.
- Bending samples with interlaminar shear failure mode show greater strength reductions compared to samples with fibre fracture failure.
- The profiles with lower thickness and larger perimeter show greater strength reduction.
- UV radiation and water vapour condensation cycles may not affect the tensile elastic modulus of GFRP laminates significantly.

Chapter 5 Bond-slip behaviour between FRP tubes and seawater sea sand concrete

Abstract

In the present study the bond-slip behavior between FRP tubes and seawater sea sand concrete is studied using push-out tests. Pultruded and filament winding FRP tubes with different fibre orientations and diameter-to-thickness ratios (D/t) were constructed to investigate the effect of confinement pressure on the bond behaviour. Moreover, to study the effect of fibre type, three types of FRP (i.e.; GFRP, CFRP and BFRP) were used. In addition, the mechanical and chemical bond strength of concrete filled FRP tubes were quantified and compared. CFRP and BFRP tubes showed the highest and the lowest bond strengths, respectively. Furthermore, it was concluded that the real confinement pressure of the tubes has a significant effect on the bond strength: the greater the real confinement pressure, the larger the bond strength (i.e. the tubes with smaller D/t ratio and fibres orientated in 89˚ showed greater bond strength compared to the tubes with larger D/t and different fibres orientations). Repeating the push-out test for four times, for each sample, showed that the slip starts earlier by increasing the number of repetitions, while the bond strength remained almost the same. This shows that the bond strength of tubes is mostly governed by the friction (confinement pressure) rather than the adhesion (chemical bond).

Keywords

Push-out; Concrete filled tube; Bond-slip; Seawater sea sand concrete; FRP tubes

5.1. Introduction

A massive amount of concrete production will be necessary to meet the demands of expanding industrialization and urbanization around the world. To avoid shortages of such natural resources as river sand and fresh water, as well as other ecological and environmental problems (e.g. CO2 emission) caused by current concrete production, the use of seawater and sea sand concrete (SWSSC) has been recently proposed as an attractive alternative to conventional ordinary Portland cement (OPC)-based concrete for constructional applications [8, 99]. However, due to the considerably higher amount of chloride in SWSSC, the corrosion rate of carbon steel reinforcement in concrete is much greater. To address this issue, corrosion resistant materials, namely fibre reinforced polymer (FRP) composites and stainless steels, are proposed as alternatives for corrosive environments of SWSSC [7, 8, 138]. In addition to the excellent corrosion resistance of FRP composites, these materials possess other advantages, such as high strength-to-weight ratio and high stiffness-to-weight ratio, making them ideal for a wide range of civil engineering applications [17, 39, 63, 105, 113, 162, 177, 194, 195].

When FRP composites are used in conjunction with concrete, they can provide either external confinement [3, 83, 196, 197] (e.g., concrete-filled FRP tubes, similar to those employed in the present study) or internal reinforcement [6, 17, 198]. Concrete-filled FRP tubes benefit from excellent corrosion resistance (as compared to steels) as well as high load carrying capacity [199]. Therefore, using concrete-filled FRP tubes in applications that require higher durability, such as onshore structures, offshore platforms and bridges can be an appropriate choice due to their good mechanical properties and durability [200].

The most studies conducted on the performance of concrete filled FRP (GFRP, CFRP and BFRP) tubes are concentrated on their compressive behavior under axial loads [8, 81-83]. However, there are very limited studies on the bond-slip behavior of concrete-filled FRP tubes, while numerous studies have been conducted on the bond between FRP bars and concrete [6, 13, 17, 84-86] as well as that between steel and FRP composites [87-93].

It is well known that in composite columns the interface between the inner concrete and the outer tube is a critical factor, especially near the end connections where the load transfer happens [80]. Therefore, in order to obtain a good composite action for the concrete filled FRP tubes, it is important to understand the bond mechanisms and bond-slip constitutive laws properly. The load transfers between the outer tube and inner concrete through three different bond mechanisms: (1) mechanical interlocking (macro interlocking), (2) chemical bonding, and (3) frictional resistance (micro interlocking). The macro interlocking is due to the surface irregularities resulting from the manufacturing tolerances while the frictional resistance is mainly attributed to the roughness of the tube surface. For the slip between FRP materials and concrete, the mechanical interlocking is negligible and could be neglected due to their relatively smooth surface. Therefore, frictional resistance and chemical adhesion are the main factors considered in bond strength between the FRP and concrete [201].

Yuan and Hadi [201] quantified the friction resistance and chemical adhesion between the FRP pultruded profiles and concrete, using direct shear tests, and reported the friction coefficient between 0.5 – 0.6 and adhesion stress (chemical bond strength) about 0.2 MPa when the normal stress is varied between 0.5 to 2 MPa. It is important to note that the existing bond-slip models used to evaluate the bond-slip behaviour of FRP sheet/plates bonded to concrete [109, 202, 203] or FRP bars embedded in concrete [204, 205] may not be suitable for FRP profiles such as tubes. The reason that the existing bond-slip models of FRP sheet/plate is not suitable for profiles is that to provide an adequate adhesion between the sheet/plate and concrete, a strong resin must be used between FRP sheet/plate and concrete, while there is no such resin used to bond the FRP profiles and concrete. Regarding the models of FRP bars and concrete, it should be mentioned that very high contact surface exists between the FRP profiles (e.g. I-sections, tubes) and concrete compared to that between FRP bars and concrete, may lead to a different bond-slip performance [206]. Therefore, due to these different interface properties, a comprehensive study on the bond-slip behaviour of FRP tubes with concrete is needed to propose an adequate bond-slip model.

Yuan and Hadi [206] studied the bond-slip behaviour between GFRP I-section and concrete using push-out tests and proposed a model for the GFRP I-section with a smooth surface based on their experimental results. However, the authors [36] mentioned that this model is a preliminary model and a reference for bond-slip behaviour of FRP profiles with respect to push-out test, and this model may be modified by incorporating more variables, including concrete type and compressive strength, as well as the type and shape of FRP profiles. Li et al. [207] studied the effect of concrete strength on the interfacial bonding strength of concrete filled glass fibre reinforced polymer (GFRP) tubes. The results revealed that 82 MPa concrete had lower interfacial bonding strength than the columns with 49 MPa concrete. Chen et al. [196] carried out experimental tests on the bond between flax FRP tube and coconut fibre reinforced concrete composites and showed that, the concrete was pushed out with no significant damage either on the concrete core or FRP tube when no interlocking was used.

It is important to note that all the previous studies mentioned above focused on conventional OPC-based concrete and very limited types of FRP tubes. Moreover, the effect of fibre orientation on bond-slip behavior of FRP confined concrete is not investigated. Generally, to the best authors' knowledge, there is no study on bond-slip behaviour between FRP tubes and SWSSC and the effect of tube material type and characteristics (such as fibre type and orientation), and tube D/t ratio on bond-slip behavior of concrete filled tubes is not addressed. Therefore, to fill this gap, different types of FRP tubes with different fibre orientations were adopted to investigate the bond-slip behavior of FRP tubes with SWSSC using push-out tests. The friction coefficients and chemical adhesion of each condition were obtained.

5.2. Experimental Program

A total of 36 SWSSC filled FRP (GFRP, CFRP, and BFRP) tubes using filament winding process and 6 GFRP tubes using Pultrusion process were constructed to investigate the bond-slip behavior between FRP materials and SWSSC. The effects of FRP fabrication type, fibre type, fibre orientation, and tube

D/t ratio on bond-slip performance between FRP and SWSSC were studied using push-out tests. For each specimen, the push-out tests were repeated four times. After each cycle, the specimen was inverted and tested in the same loading path (the details of the samples and test set-up are explained later). Finally, a model was proposed based on the experimental results using regression method.

5.2.1 Material properties

5.2.1.1 Sea water and sea sand concrete (SWSSC)

Similar to the previous studies conducted by some of the other authors of this paper [8, 208], an alkali activated slag concrete using seawater and sea sand was adopted in this study to achieve the desired concrete compressive strength and workability. The composition of seawater and sea sand, which were obtained from Brighton beach in Melbourne are listed in **Table 5-1** and **Table 5-2**, respectively.

Table 5-1 Chemical composition of the seawater

Material	Na	Mg	K	Cl	SO_4	SiO_2	CaO
Sea water (mg/L)	11940	1430	622	20700	3420	-	-

Table 5-2 Chemical composition of the sea sand (wt %)

Material	SiO_2	Al_2O_3	Fe_2O_3	CaO	MgO	Na_2O	K_2O	TiO_2	Cl	SO_4	PO_4
Sea sand (wt %)	96.5	0.21	0.43	1.3	0.06	0.07	0.05	0.04	0.13	0.09	0.01

Basalt with 2.95 specific gravity and 14 mm maximum size were used as the coarse aggregates. Hydrated lime slurry was added to the mix design in order to improve the workability. The slump was obtained about 164 mm. In order to obtain the concrete compressive strength, the average strength of three identical cylinders with 100 mm diameter and 200 mm height were calculated. After casting, the specimens were covered by plastic film to prevent moisture loss and were cured for 28 days. The average concrete compressive strength (f_c) after 28 days was 45 MPa. **Table 5-3** lists the SWSSC mix design used in the current study.

Table 5-3 SWSSC mix design

Concrete	Slag (kg/m^3)	Sea water (kg/m^3)	Sea sand (kg/m^3)	Coarse aggregate (kg/m^3)	Sodium meta-silicate (kg/m^3)	Hydrated lime slurry (kg/m^3)
SWSSC	360	190	830	1130	38.4	14.4

5.2.1.2 FRP (GFRP, CFRP, and BFRP) tubes

Two types of FRP fabrication methods were used in this study: filament winding and pultrusion process. Three types of fibres, namely glass, carbon and basalt were used for constructing filament winding tubes. The fibre and resin were used with the combination of 60% fibre and 40% resin by volume for GFRP and CFRP, and 70% fibre and 30% resin by volume for BFRP tubes. FRP tubes with two different fibre orientations were used in this fabrication type. In the first configuration, FRP tubes consist of continuous fibres, oriented in three different directions: 20% in the angle of 15°, 40% in angle of 40°, and 40% in the angle of 75° with respect to longitudinal axis. The second configuration consists of continuous fibres all oriented in 89°. The first configuration was used in order to provide adequate strength and stiffness, both in hoop and longitudinal directions, while the second type was used to provide significant confinement strength. The pultruded GFRP tubes were constructed using E-glass continuous fibres (0°). Epoxy and vinylester resins were used for filament winding and pultruded tubes as the matrix, respectively.

Disk-split tensile and compression tests were conducted to obtain the mechanical properties of FRP tubes in longitudinal and hoop directions. All coupon samples were cut from each size of the FRP tubes. Compression tests were carried out according to ASTM D695 [209]. The load was applied to the tubes with a rate of 0.5 mm/min in a displacement-controlled manner. For basalt filament winding tubes, rubber plates were used at the ends of the specimens to prevent end effects and local failure at contact surface of FRP tubes and loading plates (elephant foot failure). However, for other tubes, due to the desired failure modes, the compressive tests were conducted without rubber plates. Two strain gauges were attached to the tube's middle part for obtaining the compressive strains in hoop and longitudinal directions. **Figure 5-1** shows the compressive tests set-up and typical failure modes for tubes with different fibre orientations.

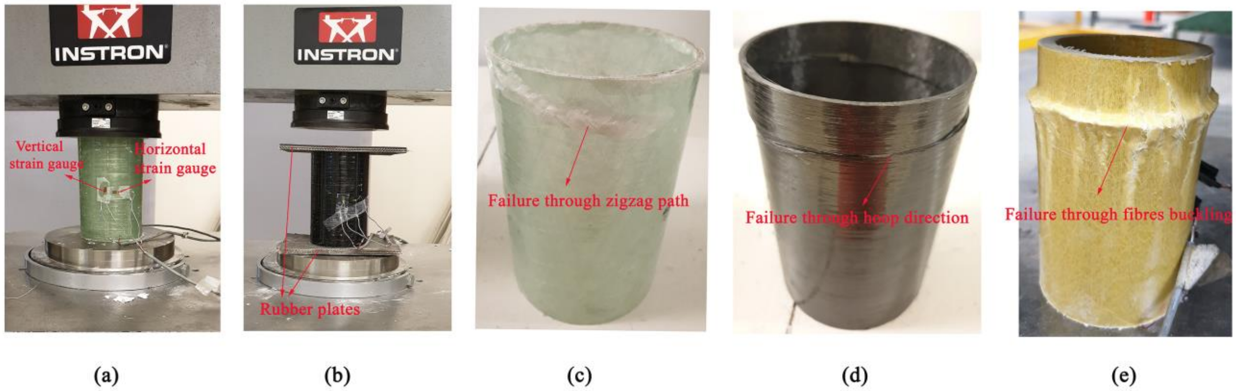

Figure 5-1 Compression test samples and set-up: (a) test set-up with-out rubber plates, (b) test set-up with rubber plates, (c) typical failure mode of tubes with multiple fibres, (d) typical failure mode of tubes with 89˚ fibres and (e) typical failure mode of pultruded tubes

Disk-split tests were conducted based on ASTM D2290 [21] standard with displacement-controlled loading at a rate of 0.5 mm/min. 20 mm rings were cut from pultruded tubes and filament winding tubes with multiple fibres, while (due to the testing machine capacity) 10 mm rings were cut from tubes with 89 º fibres. The coupon rings were mounted on testing machine by applying a high-pressure grease between the rings and steel half-disks to prevent their friction effect on the results. Two strain gauges were attached in hoop direction of each coupon ring far away from the middle gap to eliminate any bending effect. It should be noted that the hoop stress is defined as the applied load divided by the cross-sectional area of rings at the gaps. **Figure 5-2** shows the disk-split test set-up and typical failure modes for tubes with different fibres orientation.

Table 5-4 summaries the results of compression and disk-split coupon tests in terms of ultimate strengths (f_{uc} and f_{uh}), elastic modulus (E_c and E_{uh}), and ultimate strains. The results are the average of three identical specimens.

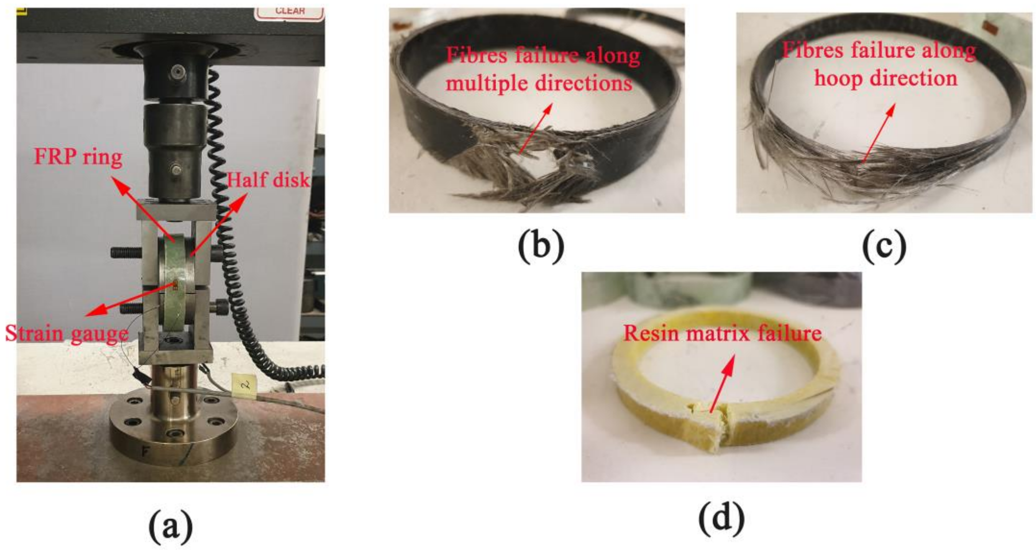

Figure 5-2 Disk- split test sample and set-up (a) test set-up, (b) typical failure mode of tubes with multiple fibres, (c) typical failure mode of tubes with 89˚ fibres and (d) typical failure mode of pultruded tubes

Table 5-4 Coupon compression and disk-split tests results

Tube Type	**Fibre Type**	**Thickness (mm)**				**Hoop direction**		
			f_{uc} (MPa)	ε_{uc} (%)	E_c (GPa)	f_{uh} (MPa)	ε_{uh} (%)	E_{uh} (GPa)
Multiple fibres Filament winding	Basalt	2.0	75.5	0.5	13.8	270.6	1.3	19.5
		4.0	83.9	0.6	13.9	281.2	1.3	21.1
	Glass	2.0	176.5	0.8	22.7	362.5	1.6	22.1
		4.0	181.3	0.8	23.0	351.3	1.5	23.5
	Carbon	2.0	174.7	0.5	33.7	501.6	0.6	79.1
		4.0	192.2	0.5	41.3	517.5	0.7	76.2
89º fibres Filament winding	Basalt	2.0	25.8	0.2	11.2	652.0	0.8	73.8
		4.0	27.0	0.2	13.0	621.7	0.9	69.2
	Glass	2.0	73.4	0.4	17.2	755.6	1.2	62.5
		4.0	69.0	0.4	16.4	647.5	0.9	69.5
	Carbon	2.0	89.6	0.5	17.2	1451.5	0.6	231.5
		4.0	87.8	0.5	17.3	1385.3	0.6	221.9
Pultrusion	Glass	8.0	381.2	0.9	42.8	19.1	0.2	10.8
		8.6	398.4	0.8	48.1	N.A	N.A	N.A

Note: f_{uc} = ultimate compressive strength, f_{uh} = ultimate hoop strength, ε_{uc} = ultimate compressive strain, ε_{uh} = ultimate compressive strain

5.2.2 Specimens

The experimental sample comprised of 42 SWSSC-filled FRP tubes fabricated using filament winding and pultrusion processes. Three identical specimens of each type were tested to examine the reproducibility of the results. The tube characteristics and dimensions are presented in **Table 5-5**. All tubes except larger pultruded samples were filled with SWSSC up to the 150 mm level (equal to 3/4 height of the tube). This deliberate initial gap (50 mm) was maintained to enable repetition of the push-out test, monitor the changes in surface roughness of the tubes and compare different effective parameters on the bond-slip behaviour. Larger pultruded tubes were completely filled with SWSSC in order to avoid the likely inaccuracy due to the large weigh of the concrete inside the tube. Therefore, only one run of push-out test was conducted for this group of the specimens. One tube from each condition (in terms of fibre type and fibre orientation) was used for roughness measurement before casting concrete. The same tube was also used for monitoring the roughness changes after each push-out cycle. **Figure 5-3** shows the specimens and their dimension details.

Table 5-5 Tubes' characteristics and dimensions

Tube Type	**Fibre Type**	**Length (L) (mm)**	**Outer diameter (D) (mm)**	**Thickness (t) (mm)**	**D/t**	**Fibre orientation angle with the axial direction**
Filament winding	Glass	200	98.0, 102.0	2.0, 4.0	49.0, 25.5	15° (20% of fibres), 40° (40% of fibres), 75° (40% of fibres)
	Carbon	200	98.0, 102.0	2.0, 4.0	49.0, 25.5	15° (20% of fibres), 40° (40% of fibres), 75° (40% of fibres)
	Basalt	200	98.0, 102.0	2.0, 4.0	49.0, 25.5	15° (20% of fibres), 40° (40% of fibres), 75° (40% of fibres)
	Glass	200	98.0, 102.0	2.0, 4.0	49.0, 25.5	89°
	Carbon	200	98.0, 102.0	2.0, 4.0	49.0, 25.5	89°
	Basalt	200	98.0, 102.0	2.0, 4.0	49.0, 25.5	89°
Pultrusion	Glass	200	94.0	8.0	11.7	0°
	Glass	330	183.7	8.6	21.3	0°

Figure 5-3 Concrete filled FRP tubes: (a) all samples, (b) typical partially filled tube and (c) schematic section of partially filled tube

5.2.3 Push-out test

The push-out tests of FRP-concrete-filled tubes were conducted using a Shimadzu machine of 300 kN capacity. The two set-ups used for conducting push-out test and the strain gauge locations are shown in **Figure 5-4**. A displacement-controlled load was applied to the concrete through a loading circular steel plate at a loading rate of 0.5 mm/min. The steel plate of a slightly smaller diameter than the inner concrete diameter was used to prevent any contact between the loading plate and the FRP tube. In order to ensure a uniform contact between the loading plate and the concrete, cement paste was used to create a flat concrete surface. Push-out test of tubes with 50 mm gap, includes 4 steps (cycles) of loading for each sample. At the first step the specimen was subjected to the monotonic static loading (0.5 mm/min) until the core concrete at the bottom end of the specimen almost reaches the end plate placed at the bottom to support the specimens (about 45-50 mm slip). After that the specimen were unloaded to zero. For the second step, the specimen was inverted and subjected to a reverse axial compression in the exactly same loading regime (monotonic static loading with the loading rate of 0.5 mm/min) until reaching the concrete core to the end plate. This testing procedure was repeated to complete the step three and four. For fully filled pultruded tubes, a steel circular tube with a slightly larger inner diameter than the FRP tube was placed under the specimen to let the concrete be pushed out. Although the inner diameter of the steel tube was larger than the core concrete diameter, the steel tube was thoroughly lubricated using grease to prevent any possible friction between the pushed-out concrete and steel tube. To measure the load transferred between the inner concrete and FRP tubes, two strain gauges were used for each specimen. The strain gauges were attached at longitudinal and circumferential directions, at mid-height on the outer side of the tube. Strain measurements were recorded using an automatic data logging system.

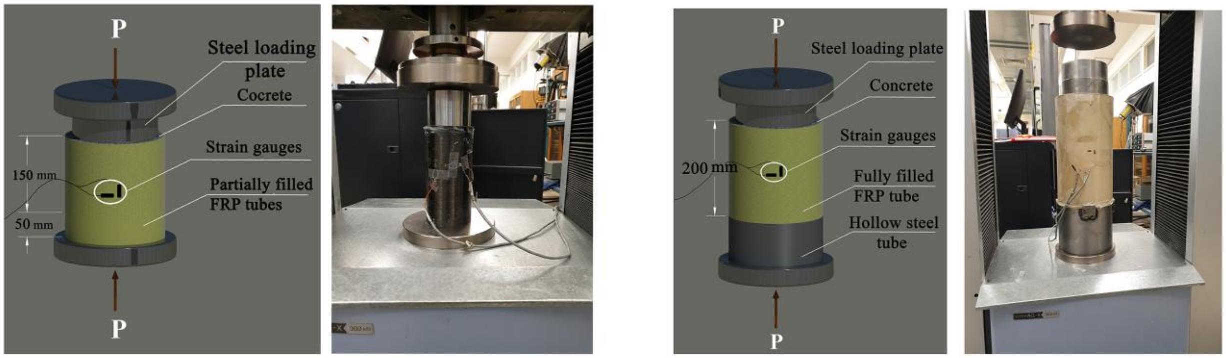

(a) (b) (c) (d)

Figure 5-4 Push-out test set-ups; partially filled specimens: (a) schematic and (b) actual; fully filled specimens: (c) Schematic and (d) actual

5.3. Results and discussion

Push-out test results, in terms of the failure modes, surface roughness of the tubes, bond strength, bond-slip curves, frictional resistance and chemical bonding are presented and discussed in detail.

5.3.1 Failure modes

Figure 5-5 shows the typical failure modes observed during the push-out tests. Three types of failure modes were observed during the push-out tests: (1) the slip between the concrete and tube as a result of breakage of the chemical bond, (2) the failure of the tubes before the slip initiation and (3) a combination of the interface failure and the tube failure, in which the tube failed after some slip occurred between the tube and the concrete. The second failure mode occurred in all 2 mm and some 4 mm FRP tubes with the fibres orientated at 89˚. This failure happened because the axial strength of the tubes was less than the bond strength (the strength corresponds to the slip initiation) between the tube and the concrete. In this case, the axial failure of the tube occurred before any slip started. Therefore, the results of this failure mode were only used for comparison between the tubes with the same failure mode. However, these results were not used for obtaining the friction and adhesion values. Each failure mode is presented in **Table 5-7** and **Table 5-8.**

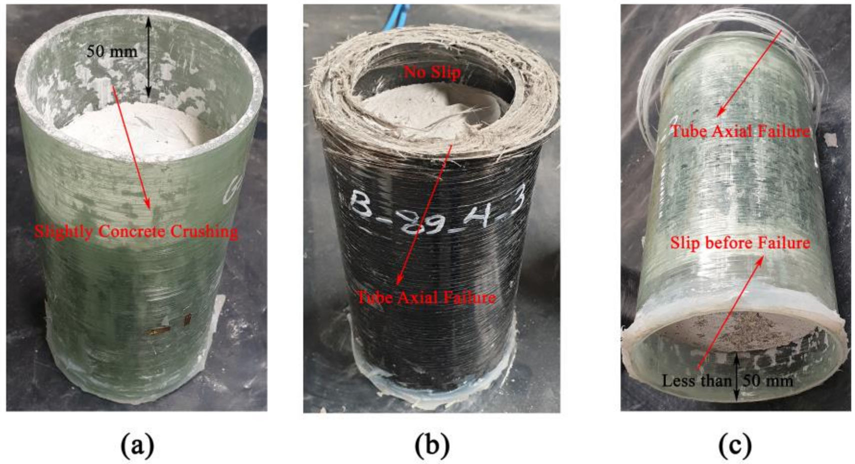

Figure 5-5 Failure modes: (a) interface failure between the tube and the concrete (4 mm GFRP with 89˚ fibres), (b) tube failure (4 mm BFRP with 89˚ fibres) and (c) combination of the interface failure and the tube failure (2 mm GFRP with 89˚ fibres)

5.3.2 Surface roughness of FRP tubes

The roughness of the FRP tube surfaces was measured in different positions before casting the concrete using Taylor-Hobson, Surtronic 3P instrument (**Figure 5-6**). R_a index (arithmetic average of surface heights measured across a surface) was used in this study to represent the roughness of the FRP tubes. Therefore, peaks and valleys on the surface of the FRP tubes, which are effective factors in friction coefficient and consequently the mechanical bond between the tube and the concrete, were captured by measuring the R_a index. As the measured R_a for all FRP tubes ranged between 2 µm and 10 µm, the sampling (ln) and evaluating lengths (lr = 5×ln) were set to 2.5 mm and 12.5 mm respectively. 15 measurements (15×12.5 mm) were conducted along the 200 mm FRP tube length for one path. Four areas of each tube yielding to 15 measurements were measured for each type of FRP tube. **Figure 5-7** shows the surface roughness topography of the different FRP tubes used in this study. As is seen, the roughness of filament winding tubes, regardless of the fibre type, is almost the same. However, the roughness of the larger pultruded GFRP tubes is less than the filament winding, while the smaller pultruded GFRP tube is rougher (i.e. the average R_a = 6.18 for larger tubes compared to R_a = 8.31 for smaller tubes). This shows that the surface roughness of the FRP tubes is mostly related to the fabrication process rather than the material type. In order to confirm that the slip occurs due to the failure of the interface between the tube and the concrete rather than the tube itself, the roughness of the tubes in some locations after each push-out cycle was measured. **Table 5-6** shows the roughness results of the different tubes after each cycle. By comparing the results of the first (before starting the test) and third cycles and the second and fourth cycles, it can be concluded that the roughness of the tubes remained almost the same and the slip does not have a significant effect on the tube surface roughness. This confirms that the slip occurs due to the failure of the interface between the concrete and the tube.

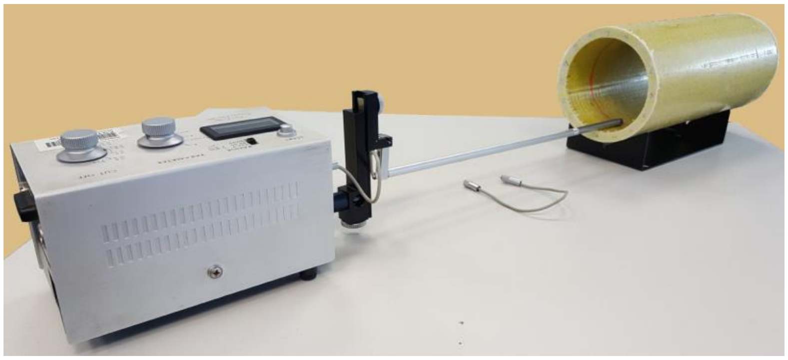

Figure 5-6 Surface roughness measurement

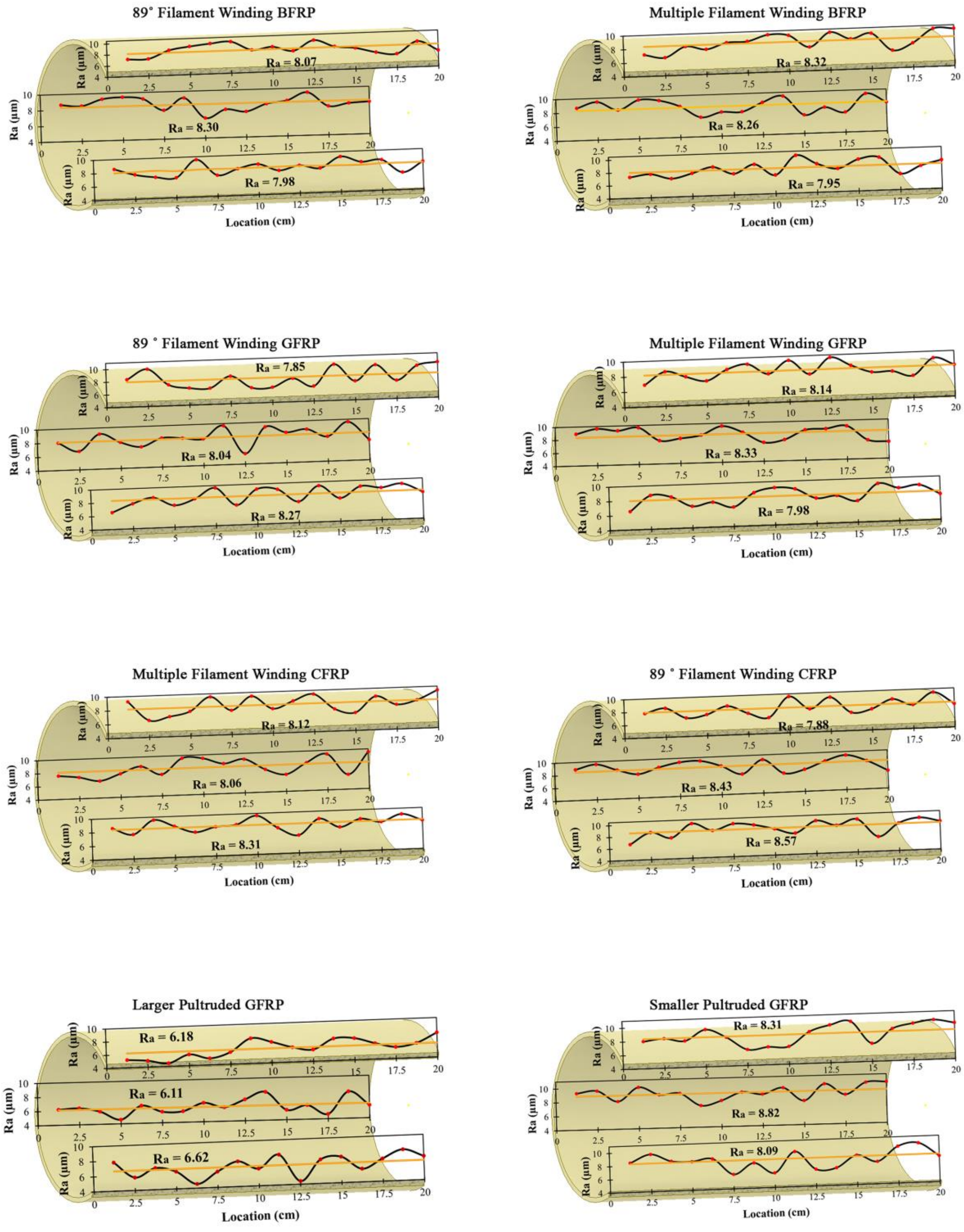

Figure 5-7 Surface roughness topography of FRP tubes

Table 5-6 Roughness of some tubes after each push-out cycle

	Cycle 1		Cycle 3		Cycle 2		Cycle 4	
Specimen	Location (mm)	Ra (µm)	Location (mm)	Ra (µm)	Location (mm)	Ra (µm)	Location (mm)	Ra (µm)
B-M-48	12.5	8.52	12.5	8.12	162.5	6.13	162.5	6.35
	25.0	9.76	25.0	8.93	175.0	6.62	175.0	6.81
	37.5	7.86	37.5	8.16	187.5	8.10	187.5	7.14
	50.0	9.96	50.0	8.53	200.0	7.51	200.0	8.95
Average	-	9.03	-	8.44	-	7.09	-	7.31
G-89-24.5	12.5	9.12	12.5	8.56	162.5	8.55	162.5	8.12
	25.0	7.19	25.0	7.70	175.0	8.89	175.0	7.95
	37.5	5.42	37.5	6.59	187.5	7.79	187.5	8.65
	50.0	7.09	50.0	6.88	200.0	8.51	200.0	8.41
Average	-	7.21	-	7.43	-	8.44	-	8.28
C-M-48	12.5	7.25	12.5	7.50	162.5	8.54	162.5	8.24
	25.0	8.12	25.0	8.51	175.0	8.31	175.0	7.93
	37.5	8.50	37.5	8.80	187.5	8.12	187.5	7.52
	50.0	8.12	50.0	8.54	200.0	9.56	200.0	8.19
Average	-	8.00	-	8.34	-	8.63	-	7.97
G-0-11.7	12.5	9.12	12.5	9.54	162.5	9.56	162.5	8.57
	25.0	8.84	25.0	9.21	175.0	8.64	175.0	9.53
	37.5	9.52	37.5	9.13	187.5	9.69	187.5	8.67
	50.0	8.13	50.0	9.55	200.0	8.92	200.0	8.12
Average	-	8.90	-	9.36	-	9.20	-	8.72

5.3.3 Push-out test results

Table 5-7 and **Table 5-8** presents the push-out test results of the concrete-filled filament winding and pultruded FRP tubes in terms of maximum bond stress, the load and corresponding displacement and the axial and hoop strain of the moment that the slip started or the first failure occurred. It is known that due to the irregular interface bond condition variation along both longitudinal and circumferential directions, unstable bonding strength in certain local area may occur. Therefore, to calculate a valid bond strength for each specimen, the average bonding strength in a finite surface area is needed. With this in mind, a uniform bond stress distribution at the concrete and FRP tube interface was considered to calculate the bond strengths of the specimens [210].

The bond stress can be calculated as follow:

$$\boldsymbol{\tau} = \frac{\mathrm{P}}{\pi D_I l_0} \tag{5.1}$$

where P is the applied axial load, D_I is the inner diameter of the tube and l_0 is the overall length of the interface.

A five-part notation system was used for specimen identification; the first letter indicates the fibre type, where C, G, and B represent carbon, glass and basalt, respectively; the second letter denotes the fibre orientation, where M shows the multiple directions (20% at the angle of 15°, 40% at the angle of 40°, and 40% at the angle of 75°) and 89 shows the tubes with all fibres orientated in 89˚; the third, fourth and fifth letters stand for the tube D/t ratio, the number of the identical test and push-out cycle number, respectively. For example, C-89-49-2-1 indicates the second cycle push-out test of the first identical specimen of CFRP tubes with D/t = 49, where the fibres are orientated at 89°. The bond stress was calculated by dividing the axial load to the inner surface area (which is in contact with the concrete) of the tube. The hoop strains (ε_h) recorded by the strain gauges were used to obtain the confinement (radial) stress (q) of the tubes using:

$$q = \frac{2F_{frp}t}{D_I} \tag{5.2}$$

where, $F_{frp} = E_h\varepsilon_h$ is the tensile stress of the FRP in the hoop direction, t is the tube thickness and D_I in the inner diameter of the tube.

It is important to note that during the push-out test, as a large lateral expansion of the concrete core is not expected, the outer FRP tube may not be activated or may be partially activated. Therefore, as the ultimate confining stress is not reached, the real confinement pressure under different conditions is used for discussion and comparison.

From **Table 5-7,** it is observed that the CFRP and BFRP tubes possessed the strongest and the weakest bond strengths, respectively, in all different conditions. Moreover, it was seen that the real confinement pressure has a significant effect on bond strength. In other words, the more the confinement, the greater is the bond strength. It is worth mentioning that the real confinement pressure of the specimens increased with the decrease in the D/t ratio of the tubes and using the fibres orientated in hoop directions. In other words, the real confinement pressure of thicker tubes is larger than that of the corresponding thinner ones. Furthermore, the real confinement pressure of the tubes with 89˚ fibres is larger than tubes with fibres orientated in multiple directions. Obviously, pultruded tubes have the lowest real confinement pressure due to the fibres being orientated in 0˚. However, it must be mentioned that the maximum load for the larger pultruded GFRP tubes was increasing constantly, but the test was terminated due to a great slip value (about 120 mm) and reaching the set-up threshold.

In order to investigate the effect of the different variables considered in this study on the bond performance of the specimens, the results will be compared with respect to the fibre type, D/t ratios and fibres orientation in the following sections.

Table 5-7 Push-out test results of filament winding FRP tubes

Specimen	Maximum bond stress (MPa)	Load correspond to slip/failure initiation (kN)	Displacement correspond to slip/failure initiation (mm)	Hoop strain correspond to slip/failure initiation (μs)	Failure mode
B-M-49-1-1	0.29	11.08	4.46	1186.00	Interface failure
B-M-49-2-1	0.27	11.81	4.19	985.00	Interface failure
B-M-49-3-1	0.23	9.05	3.85	820.00	Interface failure
Average	0.26	10.65	4.17	997.00	-
CV(%)	9.47	10.93	5.99	15.01	-
B-89-49-1-1	0.34	15.19	4.12	448.00	Tube failure
B-89-49-2-1	0.37	11.88	3.12	588.00	Tube failure
B-89-49-3-1	0.35	13.59	2.48	509.00	Tube failure
Average	0.35	13.55	3.24	515.00	-
CV(%)	3.53	9.97	20.83	11.13	-
B-M-25.5-1-1	1.04	28.57	4.01	1850.00	Interface failure
B-M-25.5-2-1	0.72	28.92	3.85	1863.00	Interface failure
B-M-25.5-3-1	0.70	28.00	3.96	1620.00	Interface failure
Average	0.82	28.50	3.94	1777.67	-
CV(%)	19.00	1.33	1.70	6.28	-
B-89-25.5-1-1	0.97	42.87	12.09	775.00	Tube failure
B-89-25.5-2-1	1.10	37.06	10.54	712.00	Tube failure
B-89-25.5-3-1	0.91	40.13	9.12	896.00	Tube failure
Average	0.99	40.02	10.58	794.00	-
CV(%)	7.98	5.93	11.46	9.62	-
G-M-49-1-1	0.36	13.88	4.08	985.00	Interface failure
G-M-49-2-1	0.27	10.83	4.03	852.00	Interface failure
G-M-49-3-1	0.23	11.53	4.13	803.00	Interface failure
Average	0.29	12.08	4.08	880.00	-
CV(%)	18.96	10.80	1.00	8.74.00	-
G-89-49-1-1	0.63	28.28	3.45	923.00	Interface failure
G-89-49-2-1	0.60	25.93	3.52	1134.00	Interface failure
G-89-49-3-1	0.71	28.86	3.36	988.00	Combined failure
Average	0.65	27.69	3.44	1015.00	-
CV(%)	7.07	4.87	1.90	8.69	-
G-M-25.5-1-1	1.34	40.25	3.33	1431.00	Interface failure
G-M-25.5-2-1	1.12	39.72	4.50	1598.00	Interface failure
G-M-25.5-3-1	1.07	39.38	3.90	1520.00	Interface failure
Average	1.18	39.78	3.91	1516.33	-
CV(%)	9.97	0.90	12.22	4.50	-
G-89-25.5-1-1	1.08	45.04	4.70	645.00	Interface failure
G-89-25.5-2-1	1.27	49.65	4.02	733.00	Interface failure
G-89-25.5-3-1	1.29	43.19	4.01	891.00	Interface failure
Average	1.21	45.96	4.24	756.33	-
CV(%)	7.80	5.91	7.61	13.46	-
C-M-49-1-1	0.68	26.69	3.56	450.00	Interface failure
C-M-49-2-1	0.56	23.24	3.85	554.00	Interface failure
C-M-49-3-1	0.68	20.85	3.45	465.00	Interface failure
Average	0.64	23.59	3.62	489.67	-
CV(%)	8.84	10.16	4.66	9.37	-
C-89-49-1-1	1.00	37.96	4.00	968.00	Combined failure
C-89-49-2-1	1.23	41.50	4.70	1121.00	Combined failure
C-89-49-3-1	1.13	42.76	4.10	887.00	Combined failure
Average	1.12	40.74	4.27	992.00	-
CV(%)	8.41	4.99	7.25	9.78	-
C-M-25.5-1-1	1.62	53.21	3.85	830.00	Interface failure
C-M-25.5-2-1	1.97	62.85	4.95	926.00	Interface failure
C-M-25.5-3-1	1.55	55.24	3.54	981.00	Interface failure
Average	1.71	57.10	4.11	912.33	-
CV(%)	10.72	7.27	14.71	6.84	-
C-89-25.5-1-1	2.36	104.58	4.85	1770.00	Tube failure
C-89-25.5-2-1	2.54	112.55	6.78	1750.00	Tube failure
C-89-25.5-3-1	2.41	106.92	5.44	1930.00	Tube failure
Average	2.44	108.02	5.69	1816.67	-
CV(%)	3.11	3.10	14.19	4.43	-

Table 5-8 Push-out test results of pultruded FRP tubes

Specimen	Maximum bond stress (MPa)	Load correspond to slip/failure initiation (kN)	Displacement correspond to slip/failure initiation (mm)	Hoop strain correspond to slip initiation or first failure (μs)	Failure Mode
G-0-11.7-1-1	0.15	3.80	1.5	26.7	Interface failure
G-0-11.7-2-1	0.11	3.90	1.42	20.2	Interface failure
G-0-11.7-3-1	0.12	3.25	1.48	25.46	Interface failure
Average	0.13	3.65	1.46	24.12	-
CV (%)	13.53	7.83	2.32	11.68	-
G-0-21.3-1-1	0.08	1.27	1.47	25.93	Interface failure
G-0-21.3-2-1	0.10	1.53	1.26	21.23	Interface failure
G-0-21.3-3-1	0.09	1.46	1.32	24.88	Interface failure
Average	0.09	1.42	1.35	24.01	-
CV (%)	9.89	7.74	6.54	8.39	-

5.3.3.1 Axial load-bond slip curves

Figure 5-8 to **Figure 5-10** show selected axial load vs displacement curves of the concrete filled FRP tubes under push-out tests. For each condition, the specimen was tested for four cycles. The axial load (F) is the load applied to the concrete from the steel circular plate. The bond slip (the slip between the inner SWSSC and the outer FRP tube) can be calculated by subtracting the displacements recorded by the testing machine from the displacement of the FRP tubes.

It is observed that for all filament winding tubes, the axial load in which the slip starts and the maximum applied load are almost the same for different cycles. Furthermore, by comparing the curves of n=1 with n=3, and the curve n=2 with n=4, it is seen that the bond-slip performance of FRP tubes is quite similar when the applied load is in the same direction. No significant changes in terms of the bond strengths is observed between n=2 and n=4. This shows that the friction coefficient is not changing significantly (because the friction coefficient is the main factor in cycle 2 and 4 as the chemical bond has already broken after cycle 1). This fact was also confirmed by measuring the surface roughness of the samples after each cycle. Regarding the cycle 1 and 3, the slightly difference, between the curves is mainly attributed to the chemical adhesion (i.e. there is no chemical adhesion in cycle 3). The fact that the slip starts earlier in other cycles than cycle 1 is also because of the same reason. These observations indicated that the mechanical interlocking was not weakened significantly after each cycle. On the other hand, as shown in section 5.3.2, the roughness of the tube surface (frictional resistance) did not change significantly after each cycle. Therefore, repeating the push-out tests may not significantly change the ultimate bond strength and the bond strength when the slip starts. This may be due to the failure at the interface between the concrete and the tube, which may not change the friction coefficient of the tubes considerably. However, as seen in **Figure 5-8**, the displacement at which the slip starts, decreases by increasing the number of cycles. The reason for this could be the expansion of the concrete (in hoop direction) during the previous cycle, which led the concrete to become already interlocked before starting the new cycle.

Regarding the smaller pultruded GFRP tubes, it is seen from **Figure 5-10** that the bond strength decreases by increasing the number of cycles. This shows that because of low real confinement pressure of the tubes the concrete will not expand in hoop direction, and thus the cracking of the concrete at the interface may gradually weaken the mechanical interlock force. This was also confirmed by very low strain readings from the strain gauges attached to the outer layer of the tubes in hoop direction. It should be noted that the larger GFRP pultruded tubes were tested just for one cycle (they were fully filled tubes). However, very small load at slip initiation for this type of tubes confirms the significant effect of confinement pressure on the bond performance of concrete filled FRP tubes.

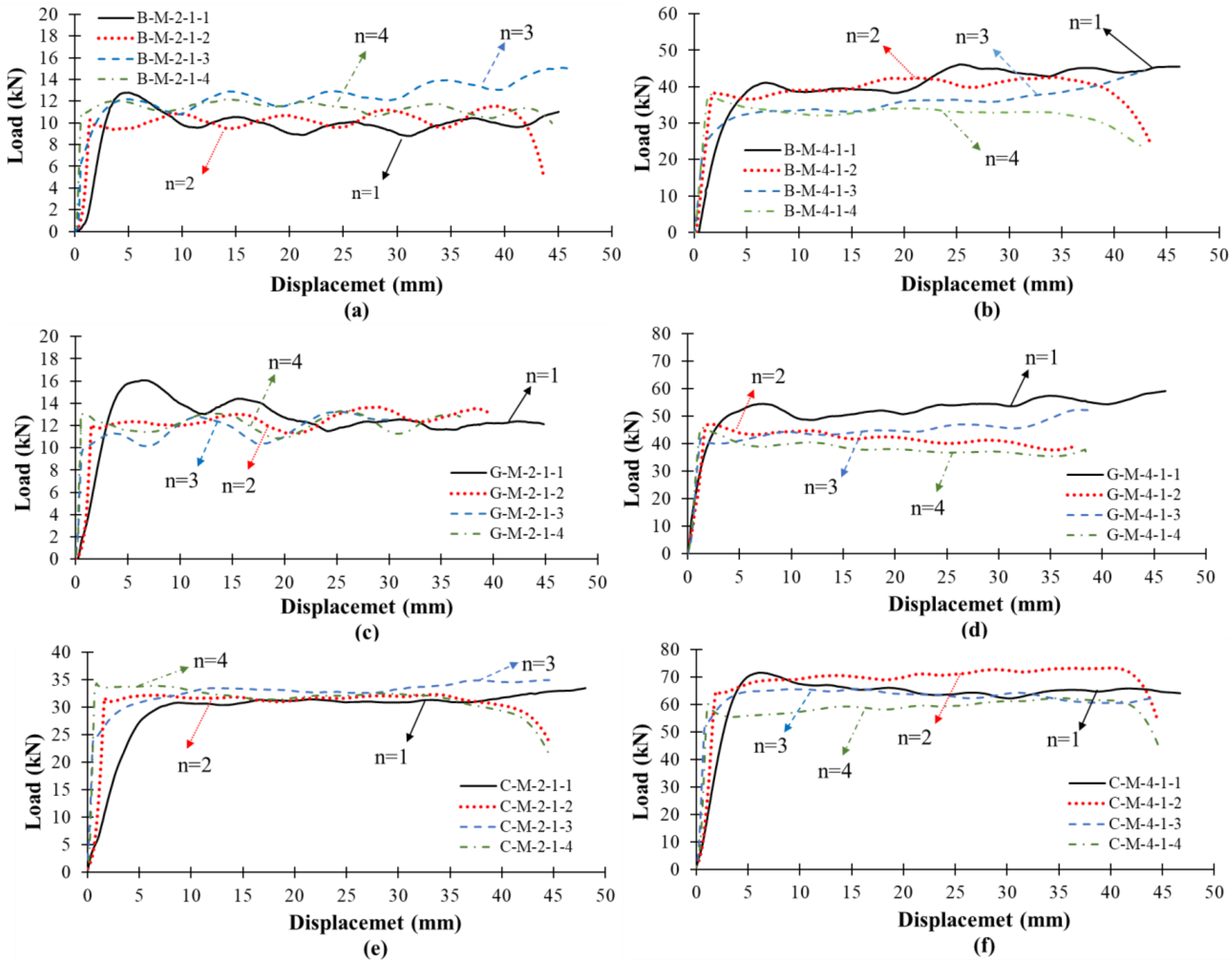

Figure 5-8 Selected axial load vs bond slip curves of filament winding with fibres in three directions: (a) 2 mm BFRP, (b) 4 mm BFRP, (c) 2 mm GFRP, (d) 4 mm GFRP, (e) 2 mm CFRP and (f) 4 mm CFRP

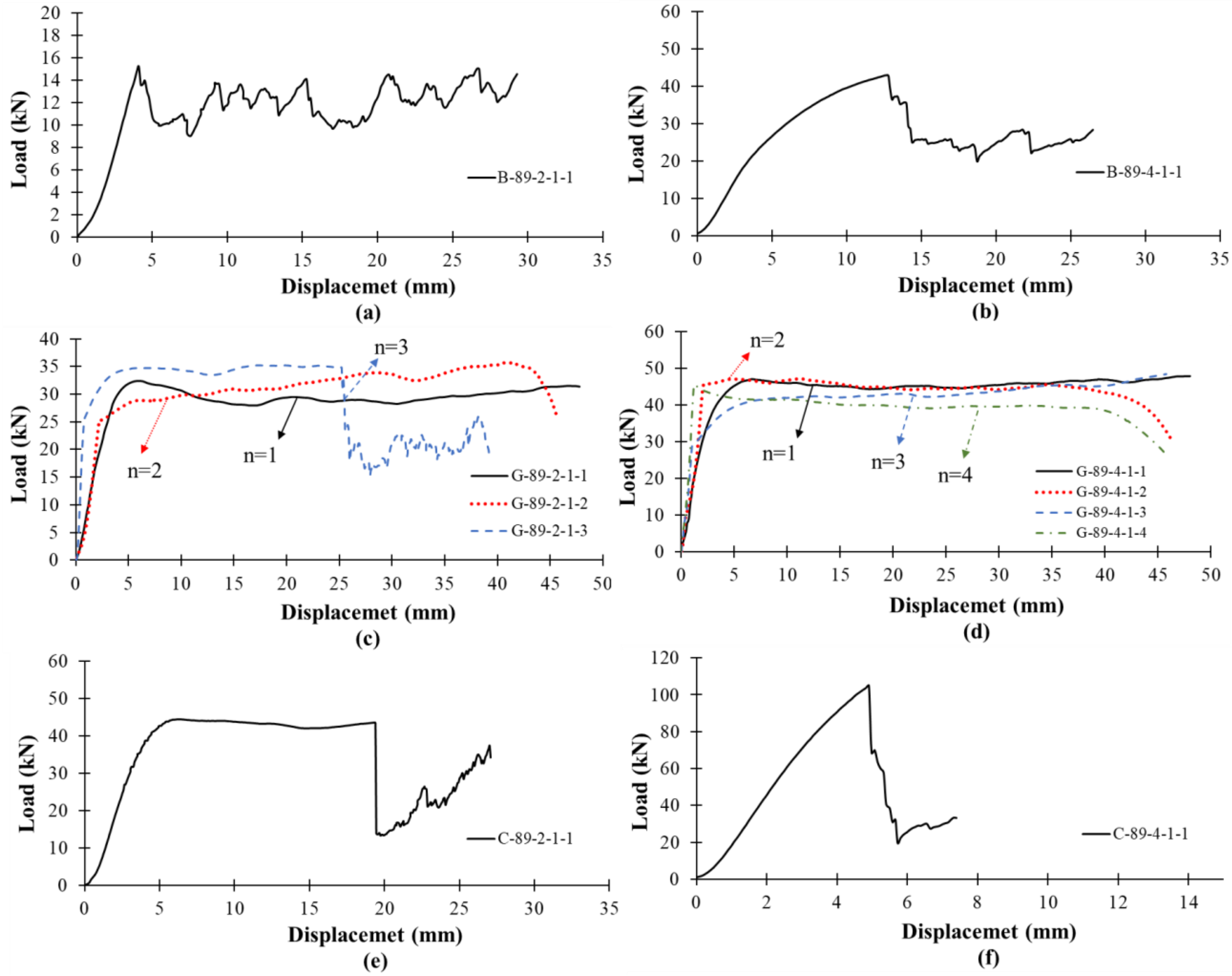

Figure 5-9 Selected axial load vs bond slip curves of filament winding with 89° fibres: (a) 2 mm BFRP, (b) 4 mm BFRP, (c) 2 mm GFRP, (d) 4 mm GFRP, (e) 2 mm CFRP and (f) 4 mm CFRP

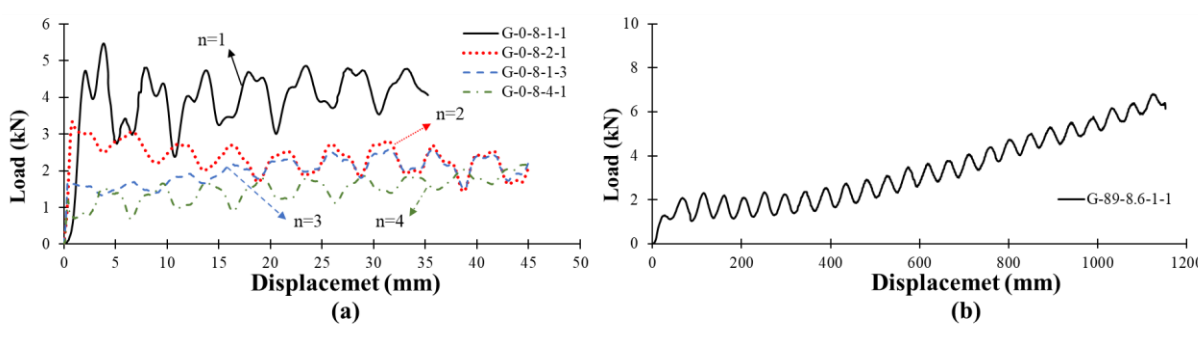

Figure 5-10 Selected axial load vs bond slip curves of pultruded GFRP: (a) 8 mm and (b) 8.6 mm

5.3.3.2 Effect of fibre type

Figure 5-11 compares the average bond strength of specimens at the moment of slip/failure initiation based on the fibre type. The values are normalized to the corresponding bond strength of CFRP tubes for comparison. It is obvious that regardless of the D/t value and fibre orientation the bond strength of the tubes with carbon fibres in all conditions are significantly higher than those with glass and basalt fibres. The bond strength of 2 mm CFRP tubes with multiple fibres is more than twice of the corresponding BFRP and GFRP tubes. 4 mm CFRP tubes also showed about 52% and 31% higher strengths compared to the corresponding BFRP and GFRP tubes, respectively. Regarding the 89˚ tubes, it can be seen that 2 mm CFRP tubes showed about 69 % and 32 % larger values than BFRP and GFRP, respectively, while 4 mm CFRP tubes showed about 59 % and 50 % larger value compared to BFRP and GFRP, respectively. It is also seen that the glass fibre tubes performed better than basalt tubes (e.g. 4% and 27% higher strengths for multiple fibres and 89˚ GFRP tubes, respectively compared to the corresponding BFRP tubes). Greater elastic modulus in the hoop direction of the carbon fibre compared to glass and basalt fibres, which leads to a greater real confinement pressure of the tubes, may be the main reason for this significant difference in bond strengths.

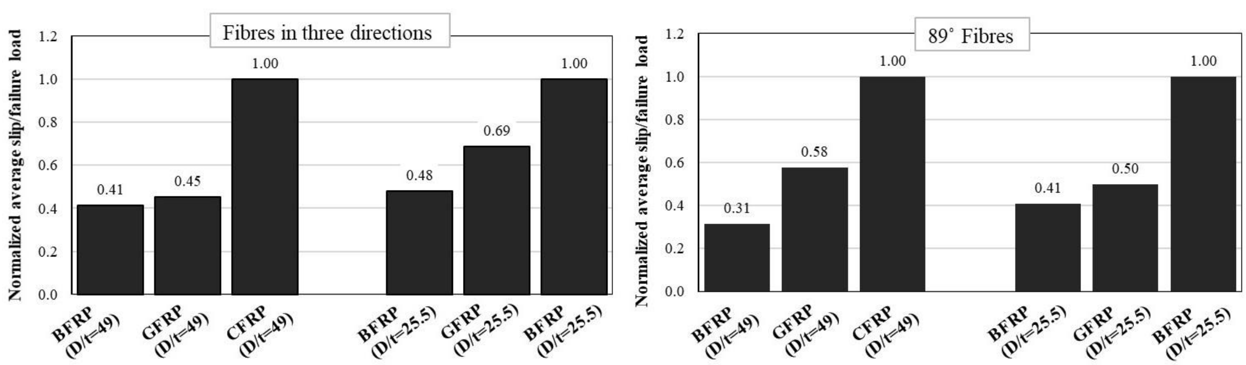

Figure 5-11 Comparison of the maximum bond strength between GFRP, CFRP, and BFRP filament winding tubes

5.3.3.3 Effect of tube D/t ratio

Figure 5-12 compares the average bond strength of specimens at the moment of slip/failure initiation based on the tube D/t ratio. The values are normalized to the corresponding bond strength of tubes with D/t = 25.5 for comparison. As expected, the tubes with D/t of 25.5 showed significantly larger bond strengths compared to the tubes with D/t = 49. These values were about 68 %, 75 % and 63 % for BFRP, GFRP and CFRP with multiples fibres, respectively. The corresponding increments for tubes with 89˚ fibres were 64 %, 47 % and 54 %. It is important to mention that the exact effect of the D/t ratio for those tubes with 89˚ fibres that the failure occurred in tubes due to the lower axial strength than the bond strength is not investigable.

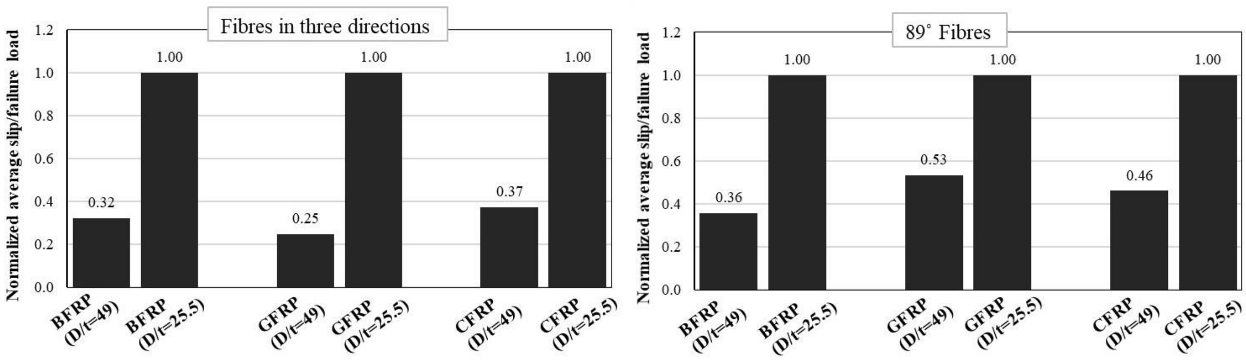

Figure 5-12 Comparison of the maximum bond strength between filament winding FRP tubes with D/t = 49 and D/t = 25.5

5.3.3.4 Effect of fibres orientation

Figure 5-13 compares the average bond strength of specimens at the moment of slip/failure initiation based on the fibres orientation. The values are normalized to the corresponding bond strength of 89˚ tubes for comparison. As expected, the fibres orientation that provides larger real confinement pressure result in greater bond strengths. Therefore, the tubes with fibres orientated in hoop direction (89˚) showed the highest bond strength than tubes with multiple fibres. As is seen, 25 %, 55 % and 43 % increases were observed for 2mm BFRP, GFRP, and CFRP tubes respectively, while the corresponding values for 4mm tubes were 27 %, 3 %, and 30 %.

It is also worth mentioning that pultruded FRP tubes with longitudinal fibres showed very small bond strength values; however, they are not presented in **Figure 5-13**, as the other factors (e.g. D/t ratio, fabrication type and surface roughness) were not the same compared to filament winding tubes). Moreover, comparing the results of pultruded tubes with filament winding tubes (**Table 5-7** and **Table 5-8**) revealed that even using thicker pultruded tubes compared to filament winding tubes did not change the significant difference between the bond strengths. This shows that the fibre orientation is one of the key factors in the bond strength of concrete filled FRP tubes.

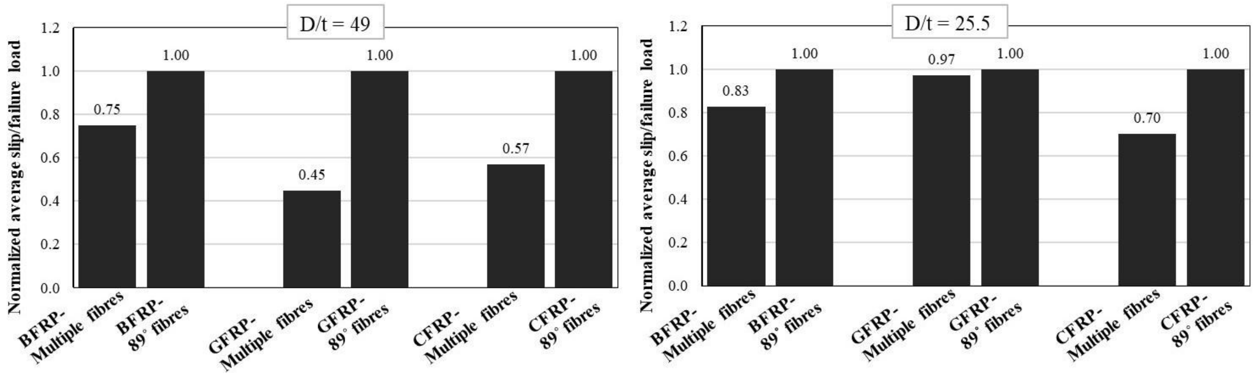

Figure 5-13 Comparison of the maximum bond strength between FRP tubes with multiple, 89° and 0° fibres orientation

5.4. Frictional resistance and chemical bonding

As the mechanical interlocking (macro interlocking) is mainly due to the surface irregularities (it can be neglected for smooth surfaces, such as the FRP tubes) [201], the bond strength between the FRP tubes and the concrete is mainly attributed to the frictional resistance and chemical adhesion. It was observed in section 5.3.2 that the roughness of the tube surfaces remained almost the same after each push-out cycle. This could also be confirmed from comparing the load-displacement curves of second and forth push-out cycles. As is seen in **Figure 5-8** and **Figure 5-9**, the loads corresponding to the slip initiation of cycles 2 and 4 were almost the same for all tubes. This shows that the roughness of the tubes and consequently, the friction coefficient (μ) remained almost constant for each tube, and thus the chemical bond (C) between the FRP tube and SWSSC can be calculated by subtracting the bond strength at slip initiation of the second cycle from the corresponding value of the first cycle. Then by using **Eq.5.3** and **Eq.5.4**, μ can be calculated from first push-out cycle [201].

$$\tau = \mu q + C \tag{5.3}$$

$$\mu = \frac{\tau - C}{\left(\frac{2F_{frp} \times t}{D}\right)} \tag{5.4}$$

where τ is the interface shear stress at slip initiation, q is the normal stress (confinement stress), C is the chemical adhesion and F_{frp} is the tensile strength of the FRP in the hoop direction at slip initiation. F_{frp} can be calculated by using the hoop strains recorded by the strain gauges and the hoop elastic modulus obtained from the disc split tensile tests. **Table 5-9** summarizes the average friction coefficient constants, average friction resistance and the average chemical bond strength for each FRP tube. It must be noted that due to the tube failure, the chemical bond of BFRP and CFRP tubes with 89º fibres were not obtained. As is seen, the chemical bond strength for all filament winding tubes are almost the same, while the corresponding value for the pultruded tube is slightly less than the others. This may be due to the final surface difference between the two fabrication processes. From **Figure 5-14** it can be seen the fibres are totally embedded in the resin matrix and therefore, for filament winding tubes the chemical bonds form between the concrete and the epoxy resin. However, the glass fibres in the surface of the pultruded tube are visible, and thus the chemical bond forms between the concrete and both resin matrix and glass fibres. Regarding the friction coefficient values, it is seen that all filament tubes have quite similar μ, which shows the high accuracy during the fabrication process of the tubes. However, as expected, the friction coefficient of pultruded tube is larger than filament winding tubes, as a result of the difference in the surface finish (as seen in **Figure 5-14**).

Table 5-9 Frictional and adhesion resistance of different tubes

Specimen	μ	Friction resistance, $\mu\sigma$ (MPa)	Adhesion, *C* (MPa)
B-M-49*	0.17	0.24	0.103
B-M-25.5	0.17	0.64	0.105
G-M-49	0.22	0.27	0.093
G-M-25.5	0.26	0.89	0.119
C-M-49	0.26	0.47	0.108
C-M-25.5	0.20	1.28	0.115
G-89-49	0.20	0.64	0.096
G-89-25.5	0.22	1.03	0.106
G-0-11.7	0.37	0.10	0.080

* = the D/t ratio of the tubes

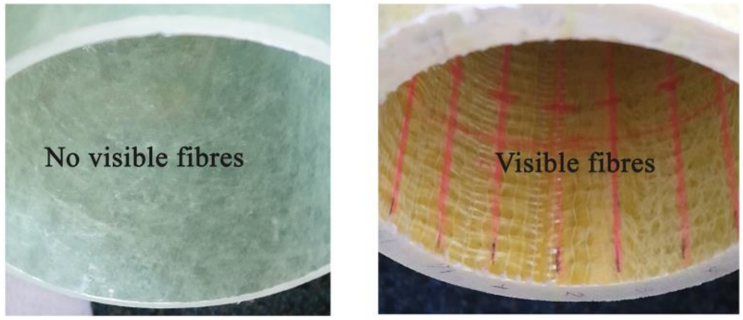

(a) (b)

Figure 5-14 Surface finishing of FRP tubes: (a) filament winding (b) pultruded

5.5. Comparison of results with other research

In this section, in order to investigate some of the other factors that may affect the bond-slip behaviour between concrete and FRP tubes, such as concrete type and other type of fibres than those used in the present study, some of the present study results are compared with similar research results reported by other researchers. However, as there are limited number of studies available in the literature focusing on push-out tests, a comprehensive comparison could not be obtained. **Table 5-10** presents the bond stress values of some FRP-concrete filled tubes tested under push-out. As no carbon and basalt fibres were tested in the literature, only the results of glass fibres in the present study are compared. As is seen, by comparing the results of [207] with 4mm tubes of the present study, the importance of the fibre direction will be confirmed: the more the fibres in the hoop directions, the greater is the bond strength. From comparing the results of [211], [212], [196] and the present study, the importance of the tube D/t ratio on the bond strength is confirmed. It is seen that, similar to the results obtained in the current study, the bond strength significantly increased by increasing the D/t ratios. For example, in [211] increasing the ratio from 8.8 to 13 increased the bond strength by 27 % and using 6 layers of fabrics in [212] instead of 4 layers in [196], increased the bond strength about 100%. However, in order to have a better comparison to achieve a comprehensive conclusion regarding the effect of various factors, more experimental data is needed.

Table 5-10 Push-out test results of the present study and other research

Reference	**FRP Type**	**Concrete type**	**Fibre orientation angle with the axial direction**	**D/t**	**Results**
[207]	E-glass	Normal to very high strength	54˚	22.3	0.42 MPa to 0.62 MPa
[211]	E-CR glass	Normal concrete	55˚	13 and 8.8	2.08 MPa for tubes with D/t = 13 and 2.64 MPa for tubes with D/t = 8.8
[212]	Flax	Coir fibre-reinforced	Warp and weft directions (0º and 89º)	100 mm / (6 layers of flax fabrics)	0.63 MPa
[196]	Flax	Coconut fibre reinforced	Warp and weft directions (0º and 89º)	100 mm / (4 layers of flax fabric)	0.31 MPa
Present study	Glass	SWSSC	Three directions (15º, 40º and 75º)	49, 25.5	0.29 MPa for D/t = 49 and 1.18 MPa for D/t = 25.5
Present study	Glass	SWSSC	89º	49, 25.5	0.65 MPa for D/t = 49 and 1.21 MPa for D/t = 25.5
Present study	Glass	SWSSC	0º	11.7	0.13 MPa

5.6. Bond strength model

Currently there is no practical model for the shear resistance of the bond strength of concrete-filled FRP tubes, which considers different effective factors. Therefore, based on the experimental results of the present study, a model is proposed using Bayesian linear regression method [213] to predict the bond strength between the SWSSC and FRP tubes considering different effective factors. It is known that, generally, the bond strength between the concrete and the tube can be calculated from **Eq.5.3**. As it was seen during push-out tests, different factors, such as the fibres orientation and cross-sectional geometry of FRP tubes are effective factors in obtaining the normal stress (q). Therefore, by considering the chemical adhesion and frictional coefficient as the main constant of the **Eq.5.3**, the effective parameters for calculating the normal stress (confinement stress) of FRP tubes must be obtained. In order to investigate the effective variables, two-way analysis of variance (ANOVA) was conducted for different testing conditions. Finally, the following model was found to be the most appropriate model based on the regression indexes (i.e. non-collinearity, homoscedasticity, regression coefficient correlations, and errors normality):

$$\tau\ (MPa) = \left(-0.1129\frac{D}{t} - 1.673\,\frac{E_h+E_c}{E_h} + 9.648\right)\mu\ + C \qquad (5.5)$$

where D, t, E_h, E_c, μ, and C (MPa) are the tube outer diameter, thickness, elastic modulus in hoop direction, compressive elastic modulus, friction coefficient, and chemical adhesion (see **Table 5-9**) between the FRP tube and the concrete, respectively. The regression parameters were obtained about 0.95, 0.1581, and 0.59 for R factor, coefficient of variation of standard deviation, and mean of standard deviation, respectively, which all confirms the accuracy of the proposed model. It is worth noting that the proposed formula may be improved in terms of accuracy and considering more effective variables by using more experimental data in the future. **Figure 5-15** compares the obtained push-out results with the model predictions. As can be seen, a good agreement is obtained.

Since the samples used in the present study is short (due to the relative size exposed to air), drying shrinkage is much more than a long pile or column. On the other hand, the diameter of the samples is small compared to full scale structures, which means under the same shrinkage strain more separation will happen in the larger CFFT making bond lower. Therefore, the results of the present study may not be directly used in full scale concrete filled FRP tubes with-out considering the size effect.

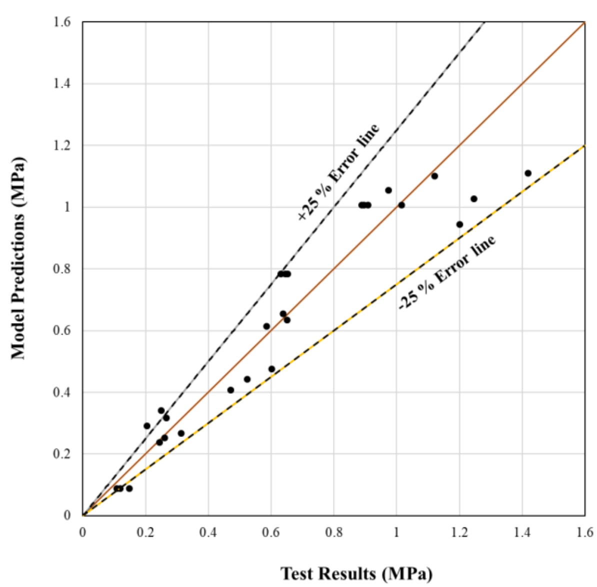

Figure 5-15 Comparison between the test results and model predictions

5.7. Conclusions

As a part of an ongoing research program on using FRP composites with SWSSC, this study presents the bond-slip behaviour between various FRP tubes and SWSSC under push-out tests. The bond strength, surface roughness, frictional resistance and chemical bond of concrete filled FRP tubes were studied. Statistical analyses were also conducted to investigate the contribution of different factors on push-out test results and propose practical models for predicting the bond strength. The following conclusions can be drawn based on the obtained results:

- CFRP and BFRP tubes possessed the strongest and the weakest bond strengths, respectively, in all different conditions.
- Decreasing the D/t ratio of the tubes increases the bond strength significantly when the confinement is adequate (i.e. for pultruded FRP tubes with low real confinement pressure, using thick tube may not have a significant effect on the bond strength).
- Using fibres orientation that increase the real confinement pressure of FRP tubes is an appropriate solution for enhancing the bond-slip performance of concrete filled FRP tubes; filament winding tubes with 89˚ fibres (if the adequate axial strength is provided) showed the best performance while pultruded FRP tubes (0 ˚ fibres) showed the weakest.
- Observing an almost the same roughness after each cycle of the push-out test, confirms that failure of the interface between the concrete and the tube is the main reason of the slip.
- The chemical bond (adhesion) resistance were obtained about 0.093 - 0.115 MPa for filament winding and 0.08 for pultruded tubes, while the friction coefficients were found between 0.17 to 0.26 for filament winding and 0.37 for pultruded tube.

This study reveals that fibres type, fibres orientation, tube surface roughness, and tube D/t ratio are some of the factors affecting the bond-slip behaviour of FRP-concrete filled tubes. However, more experimental data is needed to better understand and possible modelling of such behaviour. Future tests are being conducted to investigate the bond-slip behaviour between FRP and SWSSC after exposure to harsh environment.

Chapter 6 Bond performance between FRP tubes and seawater sea sand concrete after exposure to seawater condition

Abstract

In this study the durability of the bond between different FRP tubes and seawater sea sand concrete (SWSSC) under sea water condition is investigated. Concrete filled pultruded GFRP tubes and filament winding GFRP, CFRP and BFRP tubes were exposed to 25 °C and 40 °C seawater for 1, 3 and 6 months. Push-out tests were carried out to study the bond performance of concrete filled FRP (CFFT) tubes. The bond strength changes compared to the reference samples, in terms of the mechanical and chemical bonds, were calculated. The results showed that for most of the conditions the maximum bond strength of the tubes increased due to the conditioning, however, the bond strength at the chemical adhesion breaking moment decreased by the conditioning. On the other words, the friction coefficients of the samples increased due to conditioning, while the chemical adhesion decreased.

Key words

Seawater sea sand concrete; seawater; concrete filled FRP tubes; bond strength; chemical bond; durability.

6.1. Introduction

Using seawater and sea sand concrete (SWSSC) can effectively reduce the resource shortage of fresh water and river sand and address the ecological and environmental problems due to the over-exploitation of such materials used in ordinary Portland cement (OPC)-based concrete [99, 214, 215]. Furthermore, using supplementary cementitious materials (e.g. fly ash, slag, silica fume, metakaolin) in SWSSC reduces the cracking due to the expansion produced by alkali silica reaction (ASR) in conventional OPC-based concrete; though the mechanical properties of SWSSC are found to be almost same as those of the conventional Portland concrete [10, 11]. Furthermore, as a result of using geo-polymers (e.g. slag and fly ash), the probability of cracking due to the expansion caused by alkali silica reaction (ASR) in conventional OPC-based concrete considerably reduces. However, if the traditional carbon steel were to be used as reinforcement in SWSSC environments, they will suffer unacceptably high corrosion rate due to the considerably higher chloride content in SWSSC concrete than that in traditional concrete [12, 216]. Therefore, corrosion-resistant materials such as stainless steel and fibre-reinforced polymer (FRP) can be used as reinforcement for SWSSC to replace carbon steel [106, 208, 217].

In the past few years, FRPs have been increasingly used in numerous civil engineering applications [3, 129, 218], especially in severe corrosive environments [87, 183, 219]. FRPs superior characteristics include high strength/stiffness-to-weight ratio, great durability performance and ease of fabrication and handling [17, 63, 64, 73, 162, 220]. One of these applications is using concrete-filled FRP tubes as the main structural member, such as in bridge piers, in which a great strength and stiffness will be provided with appropriate fibre orientations [221, 222].

Carbon FRP (CFRP), aramid FRP (AFRP), and glass FRP (GFRP) composites are known as the conventional FRP materials used in construction applications. Recently, basalt FRP (BFRP) composites have emerged as an attractive alternative to conventional FRP materials due to their relatively low cost (particularly, compared to CFRP), extensive sources of raw materials and environmental friendliness [223]. However, due to the limited studies conducted on the performance of BFRP composites, especially as reinforcing materials for concrete, their durability in service life is still an unsolved issue [224].

The mechanical properties of concrete-filled FRPs (GFRP, CFRP, and BFRP), especially in terms of using normal and high-strength concrete, have been reported in literature [81, 82, 225]. Recently, the compressive behaviour of SWSSC-filled FRP tubes was studied by Li et al [8, 83, 208]. However, very limited studies have been carried out on the bond-slip behaviour of concrete-filled FRP tubes [103, 196, 207].

It is generally known that the bond strength between the inner concrete and the outer tube plays a critical role in transferring the load from the outer tube to the inner concrete. This bond strength is explained by three different mechanisms: (1) chemical bonding, (2) macro interlocking and (3) frictional resistance (micro-interlocking) [226]. The micro- and macro-interlocking, which are related to the roughness of the tube surface and surface irregularities due to the manufacturing process respectively, can cause mechanical interlocking of the concrete with the tube [227]. Regarding concrete filled FRP tubes (CFFTs), because the surfaces of FRP and concrete are relatively smooth, the mechanical interlocking could be neglected, the bond strength is mainly governed by the chemical adhesion and the friction [201].

Based on the literature, in contrast to the bond-slip behaviour of FRP sheet/plates bonded to concrete [109, 202, 203] and FRP bars embedded in concrete [6, 17, 205, 228], the studies on the bond-slip behaviour of FRP profiles (i.e. I-section and tube) with concrete are very limited. It should be noted that according to [103], the bond strength between SWSSC and untreated circular FRP ranges from 0.26 MPa to 1.71 MPa for different fibres type and tubes configurations, while much higher values for bond strength between ribbed FRP bars and concrete/SWSSC (from 4.76 MPa to 23.02 MPa) have been reported in the literature [204, 229].

Yuan and Hadi [29] presented a model for bond-slip behaviour of GFRP I-section with a smooth surface and concrete using push-out tests. The effect of concrete compressive strength (normal concrete up to very high-strength concrete) on interfacial bond strength between GFRP tubes and concrete was studied by Li et al. [207]. Chen et al. [196] conducted push-out tests (using different methods) to study the bond between flax FRP tube and concrete. Recently, Bazli et al. [103] studied the bond-slip behaviour of different FRP tubes (GFRP, CFRP, and BFRP) with SWSSC and investigated the effect of fibre type, fibre orientation, way of fabrication, and tube thickness on the bond strength using push-out tests. Results from the studies conducted on the bond performance of CFFTs generally showed that the fibre type and orientation, tube thickness and all other factors that affect the confinement strength of the tubes as well as the concrete compressive strength are important factors in the bond strength of CFFTs.

Regardless of the many advantages of using FRP composites in civil applications, especially in marine environments, previous studies on the durability of such materials have demonstrated that alkaline environments are detrimental to the mechanical properties of FRP composites (particularly GFRP and BFRP) [230]. The degradation involves fibre damage [18], resin degradation [29], and fibre/matrix interface debonding [30]. This detrimental effect may weaken the interfacial bond performance between the concrete and FRP tube on concrete-filled FRP tubes, which may have adverse effects on the load transfer mechanism between them. Moreover, seawater penetration may also affect the chemical adhesion and frictional coefficient of the tubes. Regarding the bond between FRP bar and concrete, since the chemical adhesion is significantly small compared to the friction and interlocking, it can be neglected in stress transferring mechanism [204]. However, in CFFTs (in order to have a composite action between the tube and concrete) and bonded joints [231] (due to using resin for the adhesion), chemical adhesion is an important factor in the bond strength between FRP element and concrete. Studying the environmental effects on the chemical adhesion degradation on bonded joints have shown that weakening the chemical adhesion may even change the failure mode from within concrete to within the interface [232]. However, the degradation of the chemical adhesion between the FRP tube and concrete (bond between the FRP composite and concrete with-out any resin between the two materials) as well as the frictional coefficient changes under the environmental conditions, such as seawater is not studied yet.

Based on the literature, the durability of FRP composites (GFRP, CFRP, and BFRP) under different environmental conditions related to civil engineering applications, especially under the normal concrete and seawater environments, has been studied well [13, 18, 30, 94-98]. However, there are very limited studies conducted on the durability of FRPs exposed to SWSSC under seawater condition [12, 99] and to the best of authors' knowledge, the interfacial bond durability between the concrete and FRP tubes under different environmental conditions, such as seawater, has not been studied.

It is important to note that although previous research has shown that FRPs are considerably resistant against degradation in seawater and moisture [141, 144, 233], their corrosion resistance in alkaline environment is compromised [94].

With the knowledge gaps as identified above, a comprehensive study is conducted as a part of an ongoing research on the performance of FRP composites used with SWSSC under different loading and environmental conditions to investigate the bond durability of FRP tubes and SWSSC under seawater condition. A series of push-out tests were carried out to investigate the effect of fibre type (GFRP, CFRP and BFRP), fibre orientation and tube fabrication process (i.e. pultrusion and filament winding) exposure time and temperature on bond-slip behaviour between FRP tubes and SWSSC after exposing to seawater condition.

6.2. Experimental Program

This study is a part of an ongoing study conducted on the performance of using FRP composite as a corrosion-resistant material to replace the carbon steel, and SWSSC as an alternative for OPC-based concrete under seawater conditions. **Table 6-1** explicitly describes the difference between the current paper and relevant work published in the literature [8, 103, 196, 200, 207, 211, 212]. It can be seen from **Table 6-1** that frictional coefficient and chemical adhesion were not studied in the existing literature on bond performance between FRP tubes and concrete [196, 207, 211, 212] except in the previous study by the authors [8, 103]. The current study is an extension of [8, 103] by considering the exposure to harsh environment, i.e. seawater at ambient temperature and 40^{o}C. Previous work on FRP tubes under seawater exposure [200] only focused on compressive strength of FRP tubes rather than bond behaviour. shows summarises the main details of the relevant research and this paper. In order to investigate the bond strength degradation between FRP tubes and SWSSC, push-out tests were carried out on 54 SWSSC-filled FRP (GFRP, CFRP, and BFRP) tubes made through a filament winging process and 18 GFRP tubes through pultrusion. The results obtained were used to investigate the changes in bond strength, frictional coefficients and chemical adhesions.

Table 6-1 Contribution of the relevant research in the literature and the present study

Study	Environment	Fibres type	Concrete type	D/t ratio	Fibres orientations	Bond strength	Frictional coefficient	Chemical adhesion	Compressive strength
[103]	No conditioning	C/G/B FRP	SWSSC	49, 25.5	Multiple, 0 ° and 89 ° orientations	✓			
Present	Seawater	C/G/B FRP	SWSSC	25.6	Multiple, 0 ° and 89 ° orientations	✓			
[200]	Seawater	C/G/B FRP	SWSSC	33.3, 16.6	Multiple orientations				✓
[207]	No conditioning	GFRP	Normal to very high strength concretes	22.3	54°	✓			
[211]	No conditioning	GFRP	Normal concrete	13, 8.8	55°	✓			
[212]	No conditioning	FFRP[1]	Coir fibre-reinforced	100 mm / (6 layers of flax fabrics)	Warp and weft directions (0º and 89º)	✓			
[196]	No conditioning	FFRP	Coconut fibre reinforced	100 mm / (4 layers of flax fabric)	Warp and weft directions (0º and 89º)	✓			

Note: 1: Flux fibre reinforced polymer

6.2.1. Material properties

6.2.1.1. Sea water and sea sand concrete (SWSSC)

For casting the concrete, alkali-activated slag was used with sea sand and sea water. The mix design used in this study to construct SWSSC was similar to one used in [8, 103] (**Table 6-2**). Sea water and sea sand provided from Brighton beach in Melbourne, with the characteristics listed in **Table 6-3** and **Table 6-4,** were used. The shell particle content of the sea sand was about 3%. More details of the sea sand properties, including particle size distribution (PSD) and fineness modulus (FM) can be found in [8]. For coarse aggregates, 14 mm maximum particle size basalt aggregates with the specific gravity of 2.95 were used. In order to achieve a desirable workability, hydrated lime slurry was added to the mix design, and as a result, a slump value of 160 mm was obtained. Six identical standard cylinders (diameter of 100 mm and height of 200 mm) were constructed and tested after 28 days to obtain the concrete compressive strength. An average value of 45 MPa was obtained for concrete compressive strength (f_c).

Table 6-2 SWSSC mix design

Concrete	**Slag (kg/m^3)**	**Sea water (kg/m^3)**	**Sea sand (kg/m^3)**	**Coarse aggregate (kg/m^3)**	**Sodium meta-silicate (kg/m^3)**	**Hydrated lime slurry (kg/m^3)**
SWSSC	360	190	830	1130	38.4	14.4

Table 6-3 Chemical composition of the seawater of Brighton beach

Material	**Na**	**Mg**	**K**	**Cl**	**SO_4**
Sea water (mg/L)	11940	1430	622	20700	3420

Table 6-4 Chemical composition of the sea sand of Brighton beach

Material	**SiO_2**	**Al_2O_3**	**Fe_2O_3**	**CaO**	**MgO**	**Na_2O**	**K_2O**	**TiO_2**	**Cl**	**SO_4**	**PO_4**
Sea sand (wt %)	96.5	0.21	0.43	1.3	0.06	0.07	0.05	0.04	0.13	0.09	0.01

6.2.1.2. FRP (GFRP, CFRP, and BFRP) tubes

The FRP tubes used in this study were made using filament winding and pultrusion methods. For filament winding FRP tubes, three types of fibres (GFRP, CFRP, and BFRP) were used. The fibre and resin volumetric percentages were 60% and 40%, respectively, for CFRP and GFRP tubes and 70% and 30%, respectively, for BFRP tubes. It is worth mentioning that more accurate comparison in terms of the fibres effect could be achieved if all the tubes had the same fibre to resin ratio. However, due to the fabrication requirement BFRP tubes had a different ration than CFRP and GFRP tubes To provide both longitudinal and hoop strength and stiffness, continuous fibres were oriented in 15° (20% of fibres), 40° (40% of fibres), and 75° (40% of fibres) directions. For pultruded FRP tubes, E-glass continuous fibres orientated in the longitudinal direction, were used. The resin used for filament winding and pultruded tubes were epoxy and vinyl ester, respectively. **Table 6-5** summarises the mechanical properties of the FRP tubes used in this study. Where f_{uh}, and f_{uc} are the ultimate hoop and compressive strengths, respectively; E_h and E_c are the hoop and compressive Elastic modulus, respectively and ε_{uh} and ε_{uc} are the ultimate hoop and compressive strains, respectively. The details of the coupon tests conducted on FRPs used can be found in [103].

Table 6-5 Coupon test results of FRP tubes [103]

Tube Type	Fibre Type	Thickness (mm)	Axial direction			Hoop direction		
			f_{uc} (MPa)	ε_{uc} (%)	E_c (GPa)	f_{uh} (MPa)	ε_{uh} (%)	E_h (GPa)
Filament winding	Basalt	4.0	83.9	0.6	13.9	281.2	1.3	21.1
	Glass	4.0	181.3	0.8	23.0	351.3	1.5	23.5
	Carbon	4.0	192.2	0.5	41.3	517.5	0.7	76.2
Pultrusion	Glass	8.0	381.2	0.9	42.8	19.1	0.2	10.8

6.2.2. Specimens

A total number of 72 SWSSC-filled FRP tubes were constructed and tested under push-out tests at different times. The unreliability of the results was reduced by using the average value of three identical specimens tested for each condition. **Table 6-6** lists the characteristics of the specimens used in the present study. SWSSC were poured into the tubes up to 3/4 tube height (i.e. 150 mm). The reason for leaving the 50 mm gap was to making the repetition of the push-out test possible for a specific specimen. As a result, the effects of surface roughness changes (after each repetition) and chemical bond breaking after the first test on the bond-slip performance of FRP tubes could be investigated. **Figure 6-1** the specimen configuration.

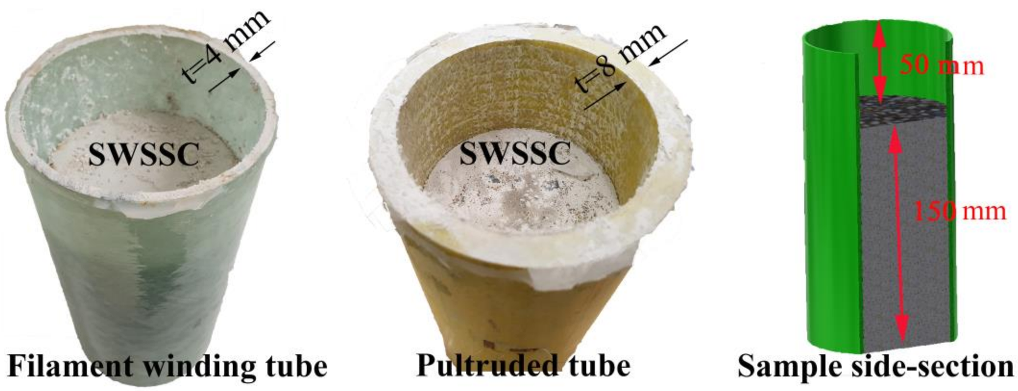

Figure 6-1 Concrete filled FRP tubes used for push-out tests

Table 6-6 Specimens' characteristics

Tube Type	Fibre Type	Length (L) (mm)	Outer diameter (D_o) (mm)	Thickness (t) (mm)	Fibre Orientation
Filament winding	Glass	200	102	4	15° (20% of fibres), 40° (40% of fibres), 75° (40% of fibres)
	Carbon	200	102	4	15° (20% of fibres), 40° (40% of fibres), 75° (40% of fibres)
	Basalt	200	102	4	15° (20% of fibres), 40° (40% of fibres), 75° (40% of fibres)
Pultrusion	Glass	200	94	8	0°

6.2.3. Environmental condition

In order to investigate the durability of bond strength between the FRP tubes and SWSSC under sea water condition, FRP concrete-filled tubes were fully immersed in seawater conditions for 1, 3 and 6 months. Ambient (25 °C) and 40 °C temperatures were used to study the effect of the temperature. The chambers were totally insulated with plastic sheets and plastofoam to avoid moisture evaporation. The temperature of the chambers was kept constant (i.e. 25 °C in one chamber and 40 °C in the other chamber) during the conditioning periods using thermocouples and thermometers. **Figure 6-2** shows the sample preparation and conditioning process used in the present study.

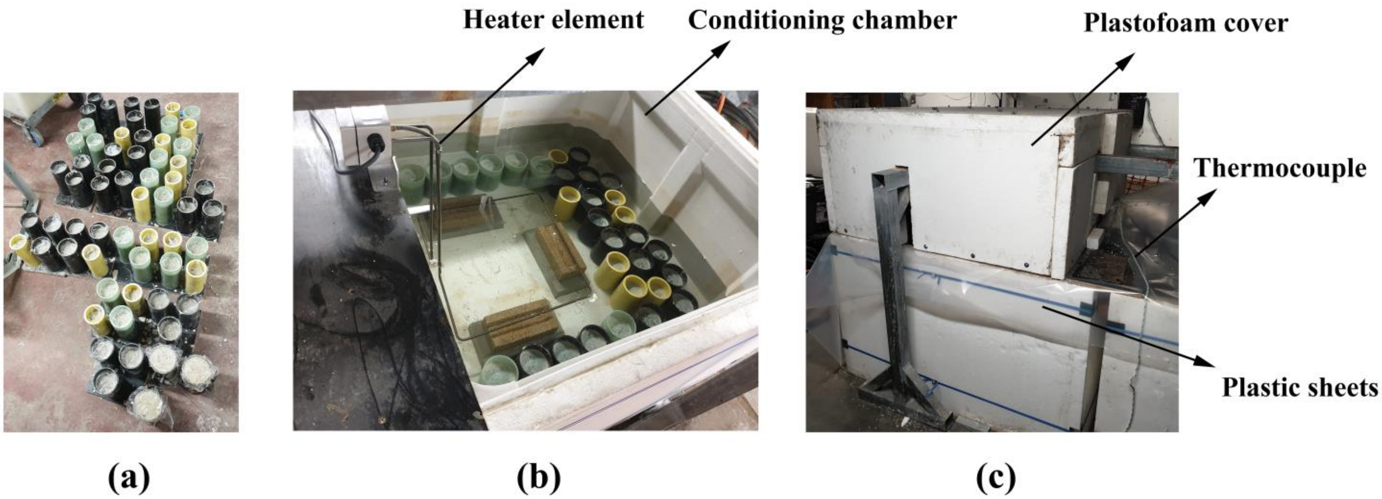

Figure 6-2 Experiment process: (a) sample preparation, (b) environmental chamber and (c) insulating and temperature controlling systems

6.2.4. Push-out test

For conducting push-out tests, a Shimadzu machine with the loading capacity of 300 kN was used. The load was applied to the concrete at a loading rate of 0.5 mm/min through a steel plate, which had a slightly smaller diameter than the inner concrete. This was provided to ensure that the load is only applied to the concrete through the steel plate. For obtaining a uniform contact between the steel plate and the concrete, the surface of the concrete was flatted using cement paste. A circular steel plate was also used at the bottom of the specimens as a support. Each sample was tested under push-out for 4 times. For the first test, monotonic static axial compression loading was applied to the sample until the concrete reached the bottom end plate (displacement about 50 mm). Then, the sample was unloaded to zero. For the second test, the sample was inverted and reverse axial compression loading with the same loading protocol was applied until the concrete reached the bottom end plate. Finally, the third and fourth tests were conducted similar to test one and two. Similar procedure to [234] was used to conduct push-out tests in the present study. Two strain gauges were attached to each sample to measure the load transfer from the inner concrete to the tubes in hoop direction. The strain gauges were attached to the outer layer of the FRP tubes at two levels: 75 mm away from one end (middle height of the concrete filled part in first and third cycles), 75 mm away from the other end (middle height of the concrete filled part in second and fourth cycles). An automatic data logger was used to record the data obtained from strain gauges. The locations of the strain gauges and test set-up are shown in **Figure 6-3**.

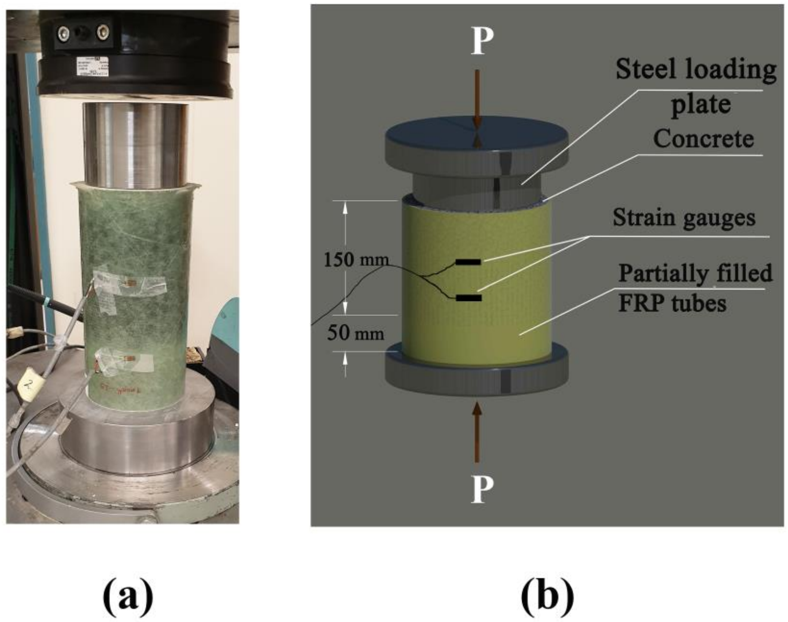

Figure 6-3 Push-out test setup: (a) real setup (b) schematic setup

6.3. Results and discussion

In this section the results and corresponding discussions regarding the failure modes, load-displacement curves and chemical and frictional bond strengths of CFFT specimens will be presented.

6.3.1. Failure modes

During push-out tests of reference [103] and conditioned samples, three typical failure modes were occurred: (1) interface failure, in which slip occurs between the concrete and the tube with-out any failure at the tube surface and (2) interface failure accompanied with damages occurred at inner side of the tubes and (3) the combination of failure mode 2 accompanied with the tube failure (this failure mode just occurred for two conditions of pultruded tubes). **Figure 6-4** shows the typical failure modes observed during push-out tests. All control samples and a few conditioned samples were failed due to the first mode. However, most of the conditioned samples experienced the second failure mode. The reason for this failure mode changing is the inner surface tube swelling due to the seawater penetration, which increases the interlocking between the concrete and the tube, and consequently the frictional resistance and decreases the bearing capacity of the tube. Increasing the friction coefficient between the tube and the concrete and decrease in bearing capacity of the tube lead to tube surface crushing due to concrete slipping. The tube crushing was more significant for samples exposed to longer period and higher temperature of conditioning. It is worth mentioning that the significant increment in frictional resistance between pultruded tubes and SWSSC (due to the surface swelling) when exposed to 6 months led to the tube failure during the push-out tests. In other words, due to the large frictional coefficient and low confinement strength of pultruded tube, the applied confinement pressure resulted the failure of the tube (see **Figure 6-4(b)**). The failure mode of each specimen has been presented in **Table 6-7** and **Table 6-8.**

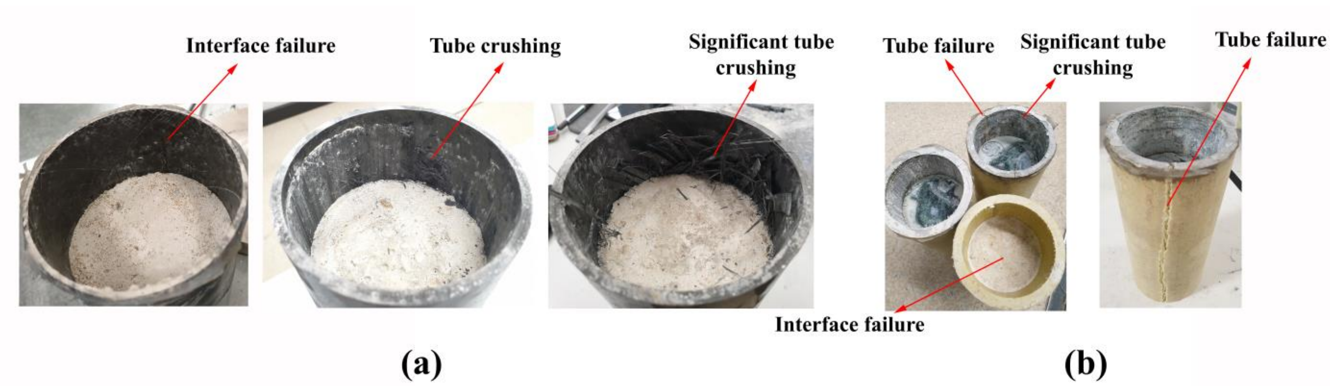

Figure 6-4 Typical failure modes observed during push-out tests: (a) filament winding tubes (b) pultruded tubes

6.3.2. Push-out test results

Table 6-7 and **Table 6-8** summarise the results of push-out tests for reference and conditioned samples. In these Tables, each sample is identified with four notations; the first letter is related to the fibre type (i.e. B, G and C are the abbreviations of basalt, glass and carbon fibres); the second letter is related to the fabrication method (i.e. F and P are the abbreviations of filament winding and pultrusion methods); and the third and fourth letters represents the temperature and time of the conditioning, respectively. For instance, B-F-40-3 represents the filament winding basalt tube subjected to 3 months of 40 °C seawater condition.

According to [200], the compressive strength of SWSSC when exposed to seawater may increase up to 50 % after 6 months exposure to 40 °C of seawater. However, because no cracks appeared in the concrete during all push-out tests of the specimens, the effect of concrete compressive strength increment on the bond strength could be ignored. In order to investigate the effect of conditioning, both maximum bond strength and bond strength corresponds to chemical bond breaking moment are presented. It is important to note that the irregular changes in the bond condition at the interface along both circumferential and longitudinal directions results unstable bond strength at specific local areas [210]. Therefore, in the present study, **Eq. 6.1** was used to calculate the bond strength, in which the bond stress is assumed to be uniformly distributed at the interface. In **Eq.6.1**, P, D_I and l_o, are the axial load, tube inner diameter and interface overall length, respectively.

$$\tau = \frac{P}{\pi D_I l_o} \tag{6.1}$$

From **Table 6-7** and **Table 6-8,** it can be observed that generally the maximum bond strength of all tubes exposed to seawater condition increased compared to the corresponding reference sample. As mentioned earlier, in one hand, the swelling of the tubes inner surface results the friction resistance increment between the tubes and the concrete. On the other hand, resin matrix swelling will decrease the bearing capacity of the tube. However, due to the final increment of the ultimate bond strength, one can conclude that the positive effect of former is higher than the negative effect of latter. In order to quantify the swelling level of tubes in different conditions, methods, such as laser scanning and computed tomography (CT) X-ray scanning may be used in future studies.

Considering the failure modes of the samples (interface failure or tube surface crushing) and the fact that the adverse effect of swelling and degradation of the tube due to the seawater and SWSSC and conditions on the bond strength was not significant, one could conclude that, in terms of the bond performance, normal concrete could be safely replaced by SWSSC with adequate compressive strength.

It is noted that the increase in the maximum bond strength is significantly higher for pultruded tubes in comparison to filament winding tubes. This suggests that the solution penetration and consequently the tube surface swelling of the pultruded tubes were higher than filament winding tubes. The different resin (i.e. epoxy resin used for filament winding tubes and vinylester resin used for pultruded tubes), fabrication process (final surface treatments may be different in different fabrication processes), and diameter to thickness ratio could be the possible reasons for this fact.

By comparing the stress values corresponding to the chemical bond breaking, it is seen that in most cases, the chemical bond of the conditioned samples has been broken earlier than the corresponding reference samples. Suggesting the chemical adhesion is decreased due to the conditioning. However, the contribution of the mechanical bond at the moment of chemical bond breaking must be calculated to confirm the fact that whether the chemical adhesion has been reduced. The results for G-P-25-1 and

G-P-40-6 show that the contribution of the mechanical bond at the moment of chemical bond breaking is significant (i.e. the stress corresponding to the chemical adhesion breaking increased in these conditions compared to the reference sample). The changes of the friction coefficients and the chemical adhesions will be presented and discussed in details later in this paper.

6.3.3. Axial load-displacement curves

In order to the study the bond performance of SWSSC filled FRP tubes under seawater condition, the load-displacement curves of the samples are presented in two sections: (1) the first cycle of the reference and conditioned samples to investigate the effect of time and temperature of conditioning on the bond performance and (2) all four cycles of each condition to investigate the effect of frictional coefficient variations on the bond performance.

Figure 6-5 shows selected first cycle of the axial load-displacement curves of the conditioned samples and their corresponding reference sample. As is seen, generally the bond strength of all filament winding and pultruded tubes increases due to the conditioning. However, the trend of the bond strength changes after the slip initiation (i.e. nonlinear region of the curves) is not the same for different conditions. Regarding the reference samples, due to the interface failure, the tube surface roughness does not change significantly (i.e. the kinetic frictional coefficient remains almost the same). Therefore, the bond strength of the samples has small fluctuations during the slippage stage. However, for conditioned samples, due to the mechanical interlocking increment (i.e. increase in confinement force) and tube surface crushing during the slippage stage (i.e. the kinetic frictional coefficient increment), the bond strength of the specimens increases by increasing the slip values. It is also observed that the trend of the increment for samples exposed to higher temperature and longer periods is higher than samples exposed to lower temperature and shorter periods. It is also observed that the BFRP and CFRP tubes showed higher trend of bond strength increment compared to the GFRP tubes. Different failure modes observed for these samples can be used to explain the reason for this observation. As is seen in **Table 6-7**, most of the BFRP and CFRP tubes exposed to higher temperature and longer periods failed due to the significant tube surface crushing, while the tube crushing of all GFRP samples and those samples of BFRP and CFRP that were exposed to lower temperature and shorter periods was not significant. Therefore, the higher the slip value, the more the mechanical interlocking and the tube crushing, and thus the larger the confinement force and kinetic frictional coefficient and as a result the higher the bond strength.

The only exceptions in terms of the bond-slip performance among all samples were G-P-25-6 and G-P-40-6. The reason for this behaviour is the tube failure due to the high confinement pressure and low confinement strength of the tubes, which led to the bond strength reduction during the push-out test (see **Figure 6-4(b)**).

Figure 6-6 shows selected load-displacement curves of different cycles for each sample. As seen for all filament winding tubes, during the first cycle, the bond strength increases by increasing the slip value. This shows that the kinetic frictional coefficient of the samples increases by increasing the slip value. In other words, the surface roughness of the tubes due to reaction of SWSSC with FRP results in surface crushing that causes increased interlocking between the tube surface and the concrete, and consequently higher bond strength. Moreover, the load corresponding to the slip initiation moment for cycles 2 to 4 is larger than that for the first cycle, suggesting that the frictional coefficient at the end of the first cycle is considerably greater. However, the bond strength fluctuations during the slipping period in push-out tests of cycle 2 to 4 are not significant (i.e. almost horizontal line for the nonlinear region of the load-displacement curve). In other words, the kinetic frictional coefficient of the tube remains almost the same for cycles 2 to 4 in contrast to cycle 1. Therefore, one can conclude that the bond strength of FRP tubes increases by increasing the slip value in cycle one, while no further increment in the bond strength is obtained in cycles 2 to 4. Furthermore, similar performance of tubes in different cycles suggests that the bond-slip performance of filament winding tubes does not change significantly with repeating the push-out tests.

Regarding the pultruded tubes, both bond strength increasing trend and decreasing trend were observed during the first cycle of push-out tests. This behaviour is attributed to the development of a relatively rougher surface of pultruded tubes in comparison to filament winding tubes during the fabrication process. As a result, the interface deterioration because of the slip may overcome the frictional coefficient increment, causing the bond strength reduction. However, for all cases, the bond strengths of pultruded tubes decreased by increasing the push-out cycles. This shows the fact that changes of the frictional coefficient do not change the bond strength of pultruded tubes significantly as they have very low confinement strength. Therefore, lower confinement pressure and greater surface deterioration will occur at higher cycles. In general, it can be concluded that the bond performance of thinner tubes with higher confinement strength (more fibres orientated in hoop direction) is significantly better than thicker tubes with lower confinement strengths (more fibres orientated in longitudinal direction).

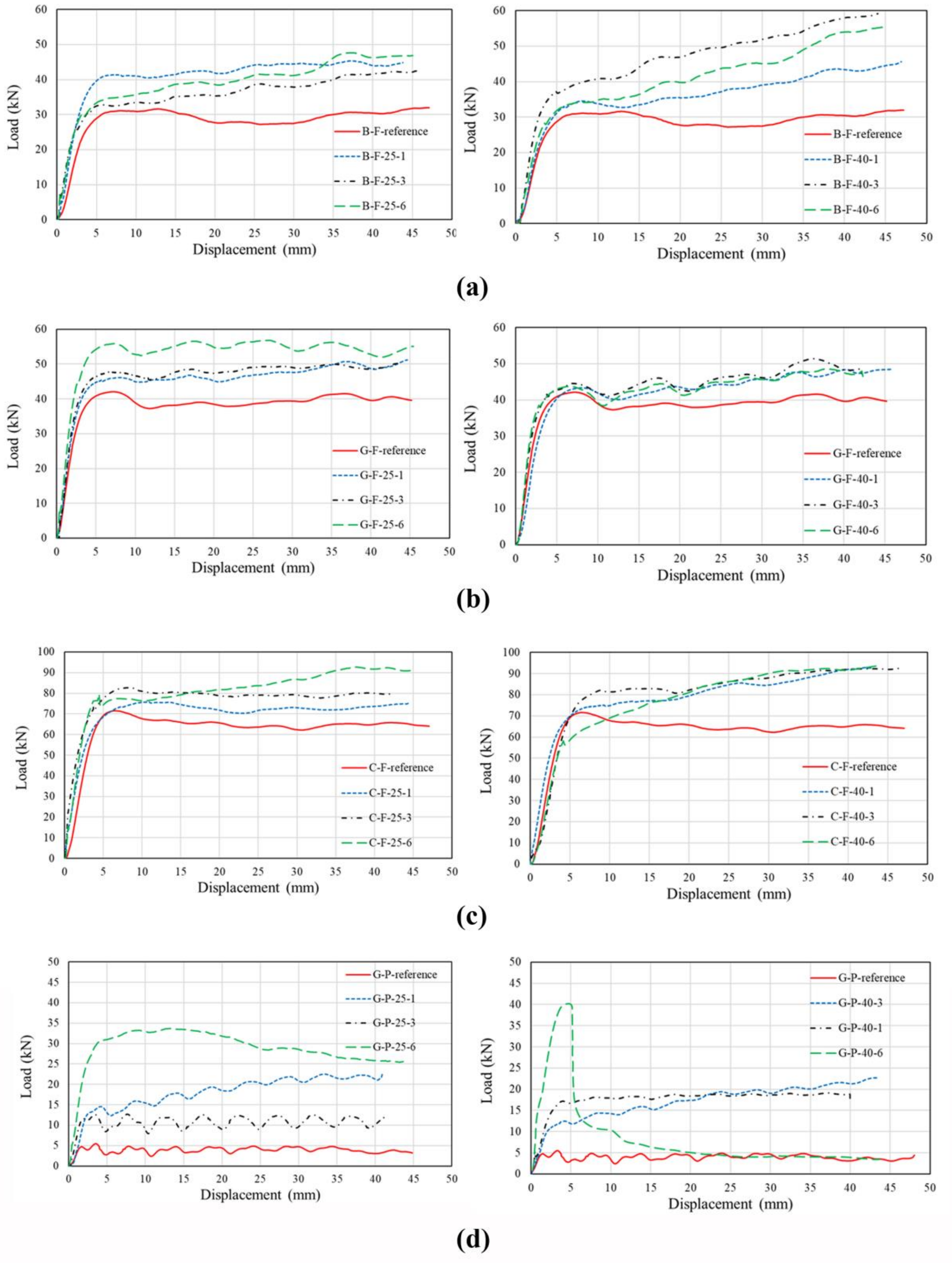

Figure 6-5 First cycle push-out load-displacement curves: (a) BFRP filament winding tubes, (b) GFRP filament winding tubes, (c) CFRP filament winding tubes, and (d) GFRP pultruded tubes

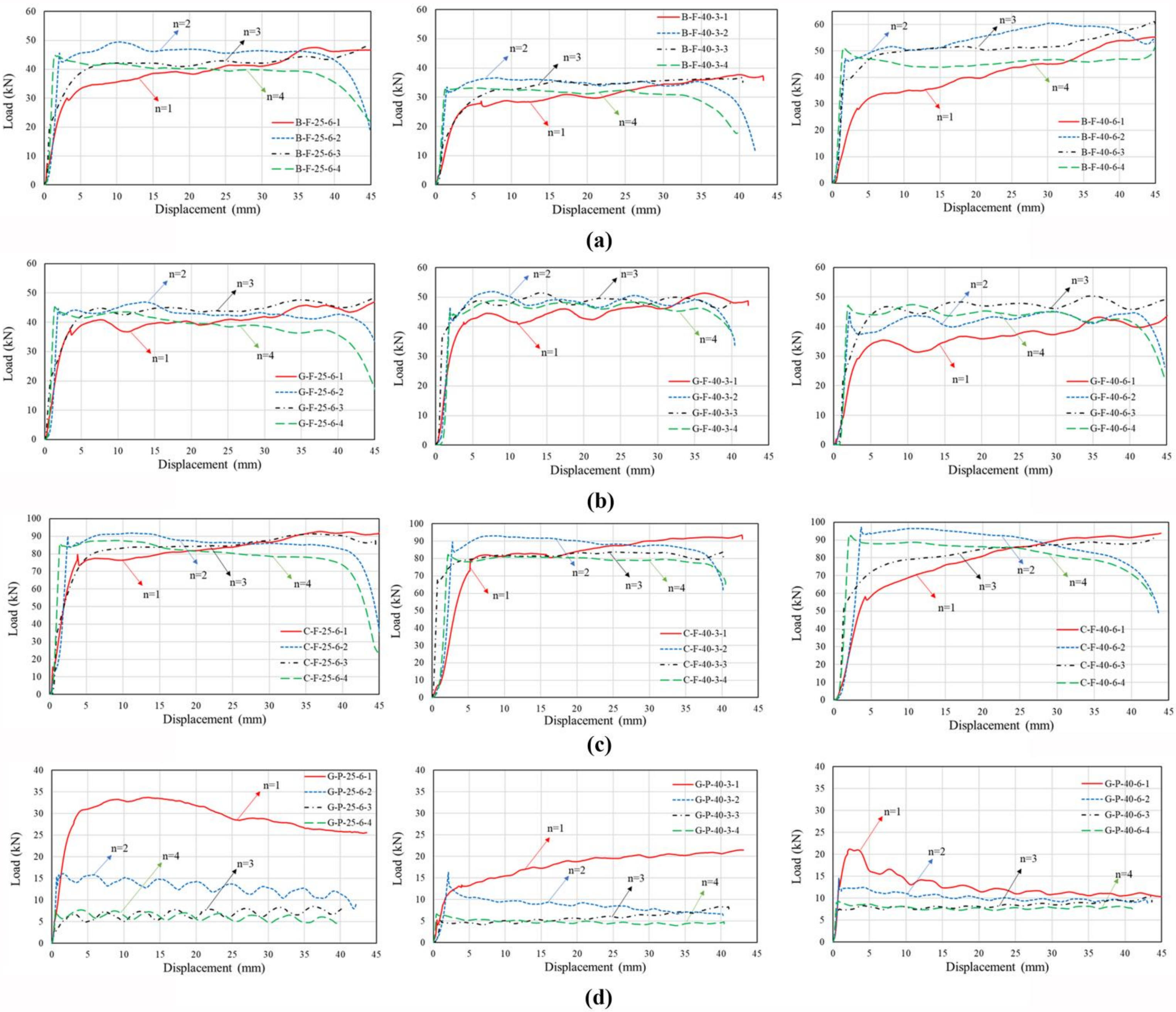

Figure 6-6 push-out load-displacement curves of different cycles: (a) BFRP filament winding tubes, (b) GFRP filament winding tubes, (c) CFRP filament winding tubes, and (d) GFRP pultruded tubes

Table 6-7 Push-out test results of filament winding tubes

Specimen	Maximum stress (MPa)	Stress corresponds to chemical bond breaking	Failure mode
B-F-reference CV(%)	0.82 19.01	0.64 1.33	Interface failure
B-F-25-1 CV(%)	1.1 20.0	0.14 6.75	Interface failure + tube crushing
B-F-25-3 CV(%)	1.08 3.20	0.17 6.92	Interface failure + tube crushing *
B-F-25-6 CV(%)	1.0 4.3	0.17 3.93	Interface failure + tube crushing *
B-F-40-1 CV(%)	1.0 4.5	0.08 3.94	Interface failure + tube crushing
B-F-40-3 CV(%)	1.02 21.96	0.09 17.08	Interface failure + tube crushing *
B-F-40-6 CV(%)	1.3 2.0	0.09 31.09	Interface failure + tube crushing *
G-F-reference CV(%)	1.18 9.82	0.90 0.90	Interface failure
G-F-25-1 CV(%)	1.2 1.4	0.13 10.87	Interface failure + tube crushing
G-F-25-3 CV(%)	1.19 4.16	0.13 15.59	Interface failure + tube crushing
G-F-25-6 CV(%)	1.2 8.1	0.15 6.79	Interface failure + tube crushing
G-F-40-1 CV(%)	1.2 6.3	0.10 9.16	Interface failure + tube crushing
G-F-40-3 CV(%)	1.18 2.52	0.10 12.51	Interface failure + tube crushing
G-F-40-6 CV(%)	1.2 13.3	0.09 3.23	Interface failure + tube crushing
C-F-reference CV(%)	1.71 10.75	1.29 7.27	Interface failure
C-F-25-1 CV(%)	2.0 11.8	0.30 10.77	Interface failure
C-F-25-3 CV(%)	1.77 4.27	0.43 13.45	Interface failure + tube crushing
C-F-25-6 CV(%)	2.0 8.2	0.36 4.42	Interface failure + tube crushing *
C-F-40-1 CV(%)	1.9 8.7	0.13 5.97	Interface failure + tube crushing *
C-F-40-3 CV(%)	1.89 8.23	0.14 18.29	Interface failure + tube crushing *
C-F-40-6 CV(%)	2.1 8.0	0.14 28.04	Interface failure + tube crushing *

Note: * = specimens with significant tube crushing

Table 6-8 Push-out test results of pultruded tubes

Specimen	Maximum stress (MPa)	Stress corresponds to chemical bond breaking	Failure mode
G-P-C	0.13	0.10	Interface failure
CV(%)	13.42	7.83	
G-P-25-1	0.59	0.11	Interface failure + tube crushing
CV(%)	44.51	18.67	
G-P-25-3	0.43	0.09	Interface failure + tube crushing
CV(%)	10.86	39.23	
G-P-25-6	0.81	0.05	Interface failure + tube crushing * + tube failure
CV(%)	34.55	29.91	
G-P-40-1	0.45	0.09	Interface failure + tube crushing *
CV(%)	15.99	47.91	
G-P-40-3	0.60	0.09	Interface failure + tube crushing *
CV(%)	2.04	41.46	
G-P-40-6	0.84	0.36	Interface failure + tube crushing *+ tube failure
CV(%)	35.65	16.33	

6.3.4. Bond strength parameters

It is known that the bond strength between FRP composites and concrete are governed through both frictional resistance and chemical adhesion before any slip occurrence and chemical bond breaking and only frictional resistance after chemical bond breaking. Therefore, **Eq.6.2** to **Eq.6.4** can be used to calculate the bond strength at different stages during push-out tests. Where τ, μ_s, μ_k, q, and C are the bond stress, static frictional coefficient, kinetic frictional coefficient, normal stress between the surfaces (i.e. confinement stress in this study) and chemical bond stress, respectively. **Eq.6.2** is used before chemical bond breaking. After chemical bond breaking and before slip initiation **Eq.6.3** is used to calculate the bond strength and finally the bond strength after slip initiation is obtained using **Eq.6.4**. It is important to note that the slip happening after the chemical bond breaking is negligible, and thus the frictional coefficient is still static until an obvious slip is observed. **Figure 6-7** shows a typical load-displacement curve of conducted push-out test, in which the regions for the validity of the equations are clarified. The starting point of the stage 2 (chemical bond breaking moment) is attributed to the sudden drop in load-axial displacement curve and the ending point of the stage two is exactly when the nonlinear region of the load-axial displacement starts.

$$\tau = \mu_s q + C \tag{6.2}$$

$$\tau = \mu_s q \tag{6.3}$$

$$\tau = \mu_k q \tag{6.4}$$

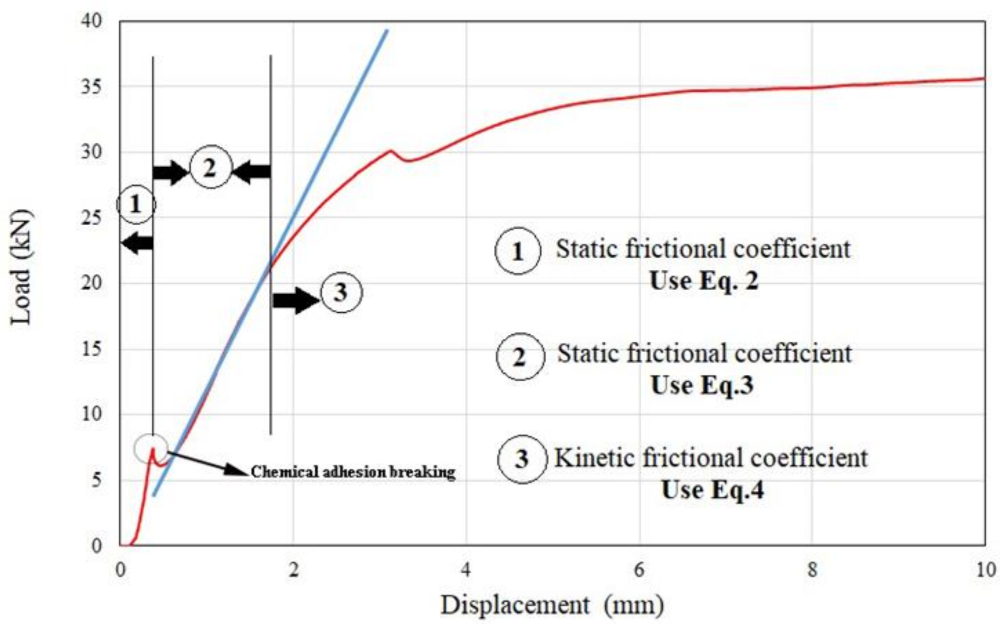

Figure 6-7 Validity regions of Eq.6.2 to Eq.6.4 in load-displacement curve of the push-out test

In this study, the following procedures have been used for calculating the bond strength parameters at different stages:

(1) Calculation of static frictional coefficient: the bond strength of the specimen at the moment after the chemical bond breaking and before the slip initiation (i.e. linear region of the load-displacement curve) was calculated using **Eq. 6.1**. Then, F_{frp} corresponds to that moment was obtained using $F_{frp} = E_h \times \varepsilon_h$, where ε_h is the hoop strain recorded by the strain gauge in hoop direction and E_h is the hoop elastic modulus of the tubes. It should be mentioned that the elastic modulus of the tubes is assumed to remain constant after exposing to environmental conditions [200]. Next, the confinement stress, q, was calculated using **Eq. 6.2**:

$$q = \frac{2F_{frp} \times t}{D_i} \tag{6.5}$$

where F_{frp}, t, and D_i are the FRP tube tensile strength in the hoop direction, tube thickness and tube inner diameter, respectively. Finally, μ_s was calculated using **Eq. 6.3**.

(2) Calculation of the chemical adhesion: firstly, the bond strength of the specimen corresponds to the moment of chemical bond breaking (i.e. the sudden drop in load-displacement curve (see **Figure 6-7**)) was obtained using **Eq. 6.1**. Then, F_{frp} corresponds to the to the moment of chemical bond breaking was obtained. Next, the confinement stress corresponds to the moment of chemical bond breaking was calculated using **Eq. 6.5**. Finally, the chemical bond for each tube was calculated using **Eq. 6.2.**
In this paper, the changes of the frictional coefficients due to the conditioning will be presented first, and then the chemical adhesion variations will be addressed

6.3.4.1.Frictional coefficients (μ)

Regarding the reference samples, the frictional coefficients for all CFRP, GFRP, and BFRP remained almost the same after push-out tests. This was due to the interface failure mode occurred for all samples. More details regarding the values of μ for reference samples can be found in [103]. However, as it was confirmed by the failure modes and the maximum bond strength results, it can be inferred that the μ of conditioned samples changes due to environmental conditioning and the variation of the μ during the push-out test (i.e. after slip initiation) is significantly larger than reference samples. To clarify this fact, the variation of frictional coefficient during push-out test for the reference and two conditioned samples of basalt tubes were calculated and shown in **Figure 6-8.** It should be noted that the starting point of the curves is the chemical adhesion break moment for each sample and the ending point is the end of push-out test. As is seen, the average static frictional coefficient conditioned samples are larger than the reference sample. As mentioned earlier, swelling of the tube surface, and consequently increment the mechanical interlocking between the tube and the concrete is the main reason for this difference. It is also observed that the kinetic frictional coefficient of conditioned samples changes by increasing the slip value. Crushing the tube surface due to the slip is the main reason for the change of the kinetic frictional coefficient. As expected and due to the interface failure of the reference sample, no significant fluctuation in the frictional coefficient was observed for reference sample. It is worth mentioning that the slight reductions in frictional coefficients before considerable variations is attributed to the transformation of the frictional coefficient from static to kinetic.

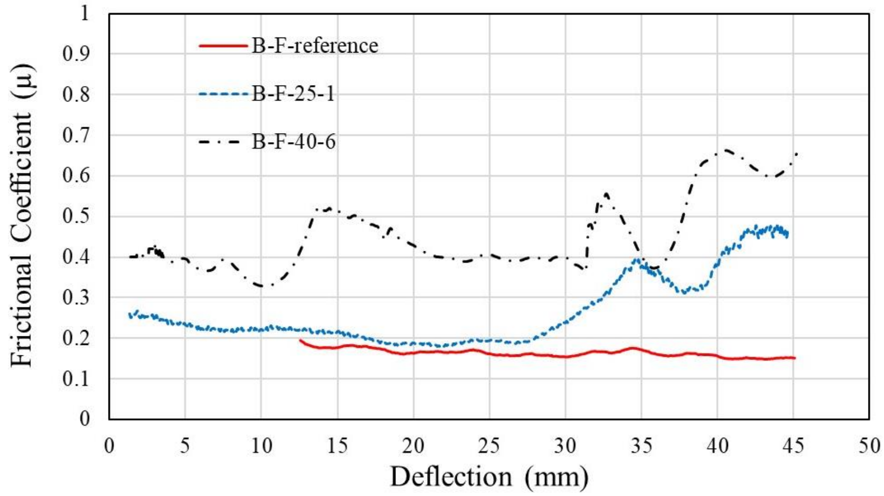

Figure 6-8 Frictional coefficient changes during push-out test

Table 6-9 compares the average μ_s values of reference and conditioned samples. As expected, the μ_s values increased due to the conditioning. However, the increment of μ for carbon tubes is significantly less than glass and basalt tubes. This shows that the solution penetration and consequently the surface deformation of carbon tubes were the least amongst all other types.

Table 6-9 Average μ_s values of reference and conditioned samples

Specimen	μ_s	**CV (%)**	**Specimen**	μ_s	**CV(%)**
B-F-reference	0.18	4.54	**C-F-reference**	0.20	16.33
B-F-25-1	0.25	21.20	**C-F-25-1**	0.22	6.68
B-F-25-3	0.58	30.29	**C-F-25-3**	0.26	28.19
B-F-25-6	0.33	16.98	**C-F-25-6**	0.22	9.11
B-F-40-1	0.44	29.68	**C-F-40-1**	0.21	12.70
B-F-40-3	0.34	5.05	**C-F-40-3**	0.23	13.91
B-F-40-6	0.39	17.69	**C-F-40-6**	0.29	29.91
G-F-reference	0.26	12.56	**G-P-reference**	0.37	13.18
G-F-25-1	0.36	5.77	**G-P-25-1**	0.39	31.27
G-F-25-3	0.55	27.09	**G-P-25-3**	0.70	35.52
G-F-25-6	0.79	8.76	**G-P-25-6**	0.80	27.5
G-F-40-1	0.39	7.76	**G-P-40-1**	0.62	19.89
G-F-40-3	0.33	38.77	**G-P-40-3**	0.70	4.67
G-F-40-6	0.44	15.07	**G-P-40-6**	0.72	1.52

6.3.4.2. Chemical adhesion (C)

It is known that a solution may disrupt the hydrogen bonding between the epoxy resin and the concrete, and consequently weaken the adhesion between the composite and the concrete. However, the level of degradation is related to the strength of interfacial adhesion: The weaker the interfacial adhesion, the lesser the hydrogen bonding, and thus the lesser the adverse effect of solution [235]. In order to calculate the chemical adhesion for different samples, the static frictional coefficients obtained (see **Table 6-9)** and the bond stress and confinement pressure of the moment before chemical bond breaking were substituted in **Eq.6.2**. **Table 6-10** compares the average chemical adhesion (C) of reference and conditioned samples. From the results, it is seen that in most cases (all conditions except carbon tubes exposed to 25 °C, which remained almost the same as the reference samples) the chemical adhesion decreased due to the environmental conditioning, which confirms the adverse effect of solution on the adhesion between the FRP and concrete. Moreover, by comparing the results of samples exposed to 40 °C with the samples exposed to 25 °C, it can be observed that the reductions in chemical bond of samples exposed to higher temperature are larger than lower temperature. However, there is no obvious trend between the time of conditioning and chemical bond degradation within the investigated durations and conditions.

Table 6-10 Average C values of reference and conditioned samples

Specimen	*C* (MPa)	CV (%)	Specimen	*C* (MPa)	CV (%)
B-F-reference	0.105	4.29	**C-F-reference**	0.115	3.55
B-F-25-1	0.092	21.19	**C-F-25-1**	0.125	5.17
B-F-25-3	0.097	6.25	**C-F-25-3**	0.123	10.11
B-F-25-6	0.102	16.60	**C-F-25-6**	0.127	9.84
B-F-40-1	0.070	10.70	**C-F-40-1**	0.068	19.24
B-F-40-3	0.077	25.79	**C-F-40-3**	0.079	30.53
B-F-40-6	0.063	13.94	**C-F-40-6**	0.074	17.57
G-F-reference	0.120	8.33	**G-P-reference**	0.106	4.49
G-F-25-1	0.090	7.07	**G-P-25-1**	0.072	20.85
G-F-25-3	0.077	24.76	**G-P-25-3**	0.064	25.40
G-F-25-6	0.095	33.03	**G-P-25-6**	0.061	6.83
G-F-40-1	0.064	4.24	**G-P-40-1**	N.A.	-
G-F-40-3	0.061	22.03	**G-P-40-3**	0.070	25.69
G-F-40-6	0.077	19.61	**G-P-40-6**	0.079	4.15

6.4. Bond strength model

In previous study on the bond performance of SWSSC filled FRP tubes by the authors of this paper [103], the following regression model was proposed to predict the bond strength at the moment of slip initiation:

$$\tau\ (MPa) = \left(-0.1129\frac{D}{t} - 1.673\frac{E_h+E_c}{E_h} + 9.648\right)\mu\ + C \tag{6.6}$$

Where D, t, E_h, E_c μ, and C are the tube outer diameter (mm), tube thickness (mm), elastic modulus in hoop direction (GPa), axial compressive elastic modulus (GPa), static frictional coefficient, and chemical bond (MPa). However, regarding the conditioned samples, the chemical bonds breaks at very early stages, and thus the confinement force can be neglected for most of the samples. Furthermore, due to the changes in frictional coefficient and interlocking between the tube and concrete the constant regarding the term related to the tube confinement will vary for different tube (i.e. in push-out test the outer FRP tube is partially activated to confine the concrete). Therefore, **Eq. 6.6** will change to **Eq. 6.7** for conditioned samples:

$$\tau\ (MPa) = \left(-0.1129\frac{D}{t} - A\frac{E_h+E_c}{E_h} + 9.648\right)\mu \tag{6.7}$$

where A is the regression coefficient related to the confinement force of each tube. **Table 6-11** lists the values of A and R^2 factor for different filament winding and pultruded tubes. As is seen the value of A for CFRP tube is very close to the constant value in **Eq. 6.7** (i.e. 1.511 compared to 1.673). The reason for this is that the frictional coefficient of CFRP tubes did not change significantly due to the conditioning, and thus the tube confinement contribution to the push-out test is almost the same. However, the frictional coefficients of BFRP and GFRP tubes changed due to the conditioning and resulted in different A values in **Eq. 6.7**. **Figure 6-9** compares the results of the bond strength corresponding to slip initiation obtained from experimental tests and **Eq. 6.7** for each tube. Although a good agreement is achieved between the predicted and the test results, more experimental data is needed to increase the accuracy and reliability of the proposed model.

Table 6-11 Regression parameters of tubes

Tube type	***A***	***R*²**
Filament winding BFRP	3.364	0.87
Filament winding GFRP	2.7925	0.93
Filament winding CFRP	1.5109	0.95
Pultruded GFRP	1.5803	0.78

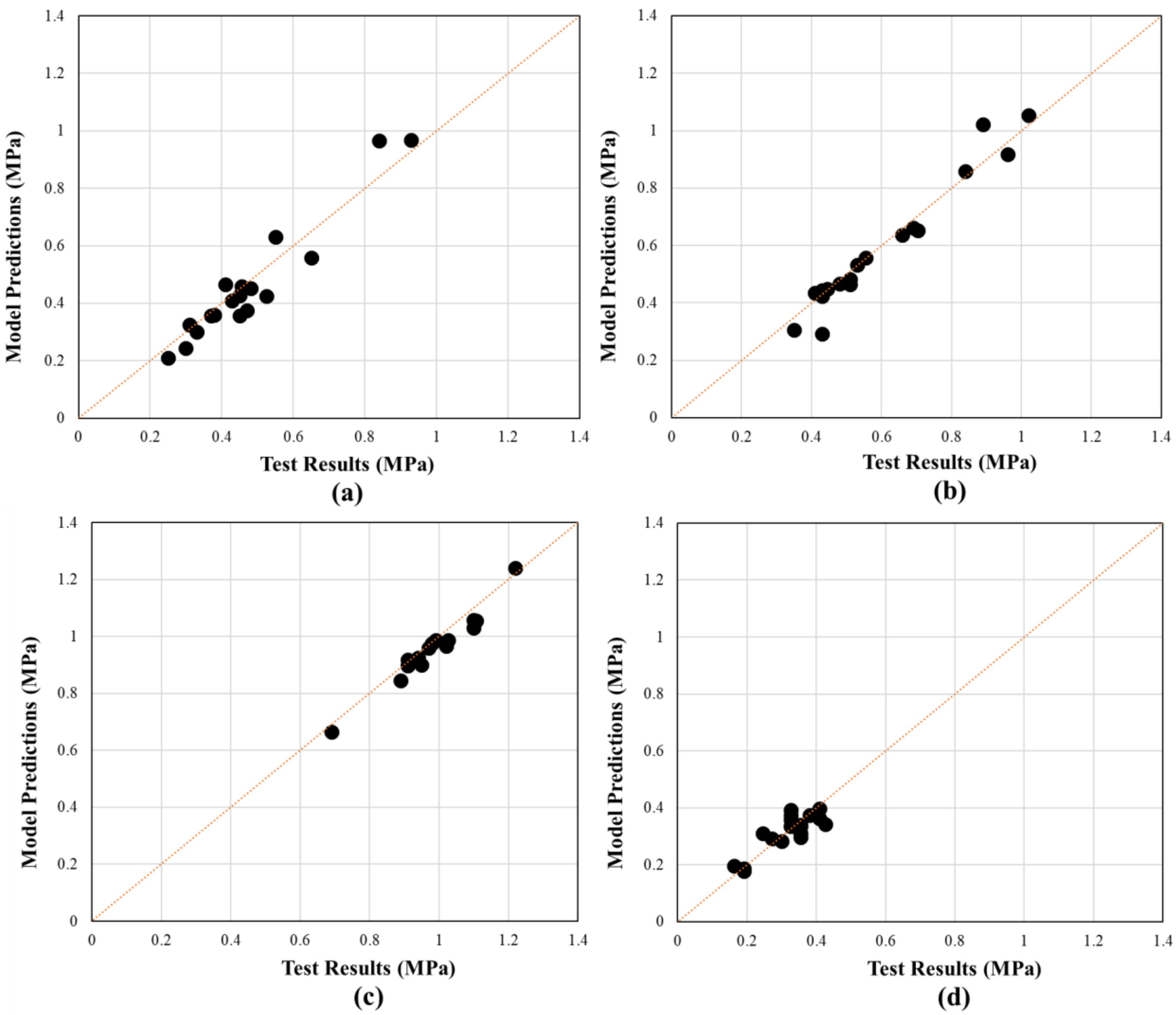

Figure 6-9 Bond strength (corresponding to the slip initiation) comparison between the experimental results and model predictions: (a) filament winding BFRP, (b) filament winding GFRP, (c) filament winding CFRP, and (d) pultruded GFRP tubes

6.5. Conclusion

This study was conducted to investigate the durability of the bond performance between different FRP tubes and sea water sea sand concrete under seawater condition. Push-out tests were carried out to study the changes in the bond strength as well as the frictional resistance and chemical adhesion between the tubes and the concrete. Based on the results obtained, the following conclusions are presented:

- In terms of the bond-slip performance of concrete filled FRP tubes, OPC-based concretes may simply be replaced with SWSSC with appropriate compressive study.
- Surface swelling of the tubes due to solution penetration increases the mechanical interlocking, and consequently the maximum bond strength between FRP tube and SWSSC.
- Failure mode during the push-out test may change from the interface failure in reference samples to the interface failure accompanied with tube inner surface crushing.
- Pultruded tubes exposed to higher temperature and longer period may also fail due to the tube failure because of relatively high applied confinement force (as a result of frictional coefficient increment) and low confinement strength.
- Due to the tube surface crushing during the slip period, the variations of kinetic frictional coefficient of conditioned samples are significantly higher compared to the reference samples.
- Seawater solution deteriorates the chemical adhesion between the FRP tube and SWSSC.

This study reveals that although the chemical adhesion between the FRP tubes and SWSSC under sea water condition reduces slightly, the maximum bond strength and the bond corresponds to slip initiation change in the range of the reference sample. Therefore, it can be concluded that, in terms of the bond performance, FRP concrete filled tubes are almost resistant to seawater environment.

Chapter 7 Durability of pultruded GFRP tubes subjected to seawater sea sand concrete and seawater environments

Abstract

This paper presents a study on the durability of pultruded GFRP tubes subjected to seawater sea sand concrete (SWSSC) and seawater environments. Environmental conditions, time and temperature of conditioning, and the tube thickness were the studied parameters. Tensile and compressive strength tests were conducted to investigate the mechanical properties of tubes after conditioning. SEM and micro-CT were used to investigate the microstructural properties, degradation mechanisms and damage levels. Finally, models were proposed to predict the mechanical properties of GFRP tubes under different conditions using Bayesian linear regression method. The results showed that SWSSC is significantly harsher condition for GFRPs compared to seawater. A reduction factor is recommended for tensile strength and compressive strength of GFRP tubes exposed to SWSSC and seawater environments.

Keywords

Seawater sea sand concrete; pultruded GFRP tube; Durability; Concrete filled FRP tube; harsh environments

7.1. Introduction

Resource shortage of fresh water and river sand owing to the widespread industrialization and urbanization can be mitigated by using seawater and sea sand concrete (SWSSC), which has recently been proposed instead of conventional ordinary Portland cement (OPC)-based concrete [8, 9, 99, 236]. In addition to the environmental [9] and economic advantages [237], the mechanical properties of SWSSC have been found to be similar to OPC-based concrete, in terms of workability, short term (28-day) and long term compressive strengths [10]. Moreover, cracking of conventional OPC-based concrete caused by the expansion triggered by the alkali silica reaction (ASR) is significantly reduced through the use of geo-polymers (e.g. slag and fly ash) in SWSSC [11]. However, in light of the presence of chloride ions in SWSSC, conventional carbon steel reinforcement are susceptible to rapid corrosion [208]. In addition, steel reinforcement may be corroded if used in the form of conventional reinforced-concrete (RC) members being subjected to harsh environments, such as sea water [17, 238]. This steel corrosion will adversely affect the performance and ductility of members, which then reduces the life and performance of the steel RC structures [239]. To avoid the high rate corrosion of carbon steel used as a reinforcement for SWSSC under sea water condition, corrosion resistant materials, such as fibre reinforced polymers (FRPs) and stainless steels have been proposed as attractive alternatives [128, 208]. In addition to the non-corrodibility properties of FRP materials, several other advantages, such as high strength-to-weight ratio, high stiffness-to-weight ratio and ease of installation and handling have encouraged the use of such materials in several applications [38, 63, 73, 113, 162, 183]. Among the different types of FRP composites, glass-fibre-reinforced polymers (GFRPs) are increasingly being used by civil engineers and the construction industry at large due to their relatively low cost and comparable durability/mechanical properties when compared to other FRP types (CFRP, AFRP, and BFRP) [6, 64].

Concrete-filled tubes (CFTs), due to several advantages, such as high load-carrying and appropriate seismic performance, are extensively used in constructions, including bridge piers, high voltage transmission tower, drilling platforms and high-rise buildings [79]. It is a known fact that owing to the direct contact between the outer tubes of CFTs with harsh environmental agents, such as seawater, acid rain and so on, carbon steel tubes are vulnerable to significant corrosion after long-term exposure to these environments [100]. Notably, concrete-filled FRP tubes (CFFTs) have recently been used to overcome the corrosion problems accompanied with normal steel reinforcement under harsh environments, including seawater [101-103].

Many studies have been conducted on the mechanical properties of CFSTs under corrosive environments [240-242]. Furthermore, the currently available research literatures on CFFTs are confined to their load-carrying capacity and ductility under different loading conditions [8, 208, 243, 244]. However, their durability under environmental conditions, such as sea water, have not been well documented or studied [245]. With this backdrop, it is important to mention that although FRP composites are regarded as appropriate corrosion resistant materials in marine environments [105, 106], their durability under alkaline environments (concrete pore solution) remains debatable and hence, must be considered as a critical issue [95, 107, 108]. Fibre [18], resin [29], and fibre/resin interface [30] may be damaged due to the detrimental effects of the alkaline conditions. These degradations may have adverse effects on the long-term mechanical properties of FRP tubes and should be thoroughly investigated. It should be noted that most studies on the durability of FPR materials in alkaline environments are associated with OPC-based concretes [17, 109, 110] and that very limited studies on the durability of FRPs exposed to SWSSC environments have been carried out [4, 12, 99]. The use of SWSSC with corrosion-resistant FRP composites in marine environments has recently been attracting researchers' attention.

Boumarafi et al. [239] conducted experimental tests to investigate the effect of harsh environments (immersion in water, saline, and alkali solutions and exposure to the freeze/thaw cycles) on the compressive strength of CFFTs. Their results showed that CFFTs experienced the highest degradation in a salt solution environment (immersion in the salt solution and exposure to 200 freeze-thaw cycles led to a 9% reduction in compressive strength at 28 days). However, it was generally concluded that CFFTs were almost resistant to aggressive environments and might constitute an appropriate alternative to conventional steel in aggressive alkali environments such as SWSSC. Micelli and Myer [246] found that GFRP-confined cylinders immersed in NaCl solution experienced a moderate decrease (about 20%) of ultimate compressive strength, while this value did not change significantly for CFRP-confined cylinders.

It is worth mentioning that the compressive strength reduction of CFFTs does not provide sufficient information on the degradation at the level of FRP tube and its individual components, such as fibre, resin, and fibre-resin interface. Admittedly, the inner side of FRP tubes was exposed to concrete and the outer side to marine environments, i.e. seawater condition. Therefore, an in-depth study is required on the degradation mechanism to assess the service life of FRP-reinforced structures in harsh environments. However, very few literature is available on the durability of mechanical properties of FRP tubes' when exposed to both concrete (or simulated concrete solution) and seawater and degradation mechanisms [112].

Robert and Fam [112] reported 11% and 21% reduction in hoop strength of filament-wound GFRP tubes filled with concrete after exposure to salt solution for 12 months at temperatures of 23 °C and 50 °C, respectively.

However, to the best of the authors' knowledge, there are no reports on the durability of FRP pultruded tubes exposed to both SWSSC and seawater environments. Hence, to assuage the knowledge gap, this research deals with the durability mechanisms of pultruded GFRP tubes, filled with simulated SWSSC, and exposed to artificial seawater solution. The long-term behaviour of GFRP tubes under such environment was predicted with the Arrhenius relation theory.

7.2. Experimental Program

The research primarily focusses on the mechanical properties and long-term performance of FRP composites used together with SWSSC, as alternatives for conventional steel reinforcement and OPC-based concrete, under aggressive marine environment. In this regard, a comprehensive investigation is undertaken to determine the durability of pultruded GFRP tubes by exposing them to SWSSC and sea water (inside and outside the tube, respectively). For comparison purpose, the tubes were also exposed to both seawater (i.e., seawater, both inside and outside) and SWSSC solution (i.e., SWSSC solution, both inside and outside). Therefore, the variables used in the study are: environmental conditions, tube geometry, time, and temperature of the exposure.

Tensile and compression tests were conducted on 228 pultruded GFRP samples, to investigate the changes of mechanical properties before and after exposure to environmental conditions. Further, scanning electron microscopy (SEM) and X-ray micro-Computed Tomography (micro-CT) were used to study the microstructural properties of GFRP composites exposed to SWSSC and sea water. Finally, based on the experimental results obtained from accelerated tests, using Arrhenius relation theory, the long-term mechanical properties of GFRP pultruded tubes under SWSSC and sea water condition was predicted.

7.2.1. Material properties

Two different sizes of circular GFRP tubes, fabricated through pultrusion process using unidirectional E-glass fibres and vinyl ester resin, were used in this study. A very thin vinylester surface veil were used as the outermost layer of the tubes. All tubes comprised of continuous fibres uniformly oriented along their lengths. The smaller tube had an outer diameter of 63 mm and thickness of 4 mm, respectively, while the larger one had 94 mm diameter and 8 mm thickness. The fibre to resin fraction constituted about 60% to 40% by volume, respectively. **Table 7-1** shows the material properties (tensile and compressive strength and modulus) of the GFRP tubes. More details regarding the material properties of pultruded tubes can be found in [247].

Table 7-1 Material properties of GFRP tubes

Outer diameter (mm)	**Thickness (mm)**	**f_{ut} (MPa)**	**f_{uc} (MPa)**	**E_{ut} (GPa)**	**E_{uc} (GPa)**
63	4	472	345	33	35
94	8	514	342	34	34

7.2.2. Environmental conditions

In the present work, seven different environmental conditioning were investigated for the durability of GFRP tubes. **Table 7-2** summarizes the environments used in this study. In environments 1-3, the real condition of SWSSC-filled FRP tubes when subjected to seawater was simulated, while the other conditions were used for comparison purposes: SWSSC both on inner and outer surfaces (environments 4 and 5) represents the most severe condition, whereas seawater both on inner and outer surfaces (environments 6 and 7) as the least severe condition.

Table 7-2 Conditioning environments

Number	**Conditioning environment**	**Inside the tube**	**Outside the tube**	**Temperature (˚C)**
1	CS-25	SWSSC	Seawater	25
2	CS-40	SWSSC	Seawater	40
3	CS-60	SWSSC	Seawater	60
4	CC-25	SWSSC	SWSSC	25
5	CC-60	SWSSC	SWSSC	60
6	SS-25	Seawater	Seawater	25
7	SS-60	Seawater	Seawater	60

Elevated temperatures were used for accelerating the degradation process. Although the conditioning temperatures are far below the glass transition temperature (T_g) of the GFRP tubes resin matrix (above 100 ˚C), it is unknown if such temperature will cause significant degradation on the mechanical properties of the sample. The conditioned samples were tested after 1, 3 and 6 months of exposure. The chemical composition used for simulating SWSSC in this study was 2.4 g/l sodium hydroxide (NaOH), 19.6 g/l potassium hydroxide (KOH), 2 g/l calcium hydroxide ($Ca(OH)_2$), and 35 g/l sodium chloride (NaCl). The pH of the solution was measured to be about 13.4. The mass concentrations of NaOH, KOH, and $Ca(OH)_2$ were considered based on previous studies by some of the authors of this paper [12, 248] to simulate normal SWSSC. To simulate the seawater environment, 35 g/l NaCl was mixed with distilled water. In order to keep the pH of the seawater constant during exposure, the seawater was replaced often to prevent alkaline ion build-up (and their penetration through the internal environment). The pH monitoring (resolution of 0.01 pH at 25 °C) was conducted continuously to ensure that the seawater pH is kept constant in the range of 7.5 - 8.4.

7.2.3. Specimens

The specimens were classified into two groups - unconditioned (control) and conditioned. The control samples were tested to obtain the reference results. To simulate a real condition of concrete-filled FRP tubes (conditions 1-3 in **Table 7-2**), a dual exposure environment, without any leakage of the internal solution to the external surface and vice versa, was needed. To achieve this, a petri dish was used to seal one end of the tubes using an epoxy resin as the base. Then, the SWSSC solution was filled inside the tubes and the other end was further sealed. Finally, the GFRP tubes sealed on either end were placed in a temperature-controlled water bath containing simulated seawater for different durations (1, 3 and 6 months). For conditions 4-6, the samples were directly immersed in simulated SWSSC/seawater solutions. The procedure of preparing specimens for conditioning is illustrated in **Figure 7-1.**

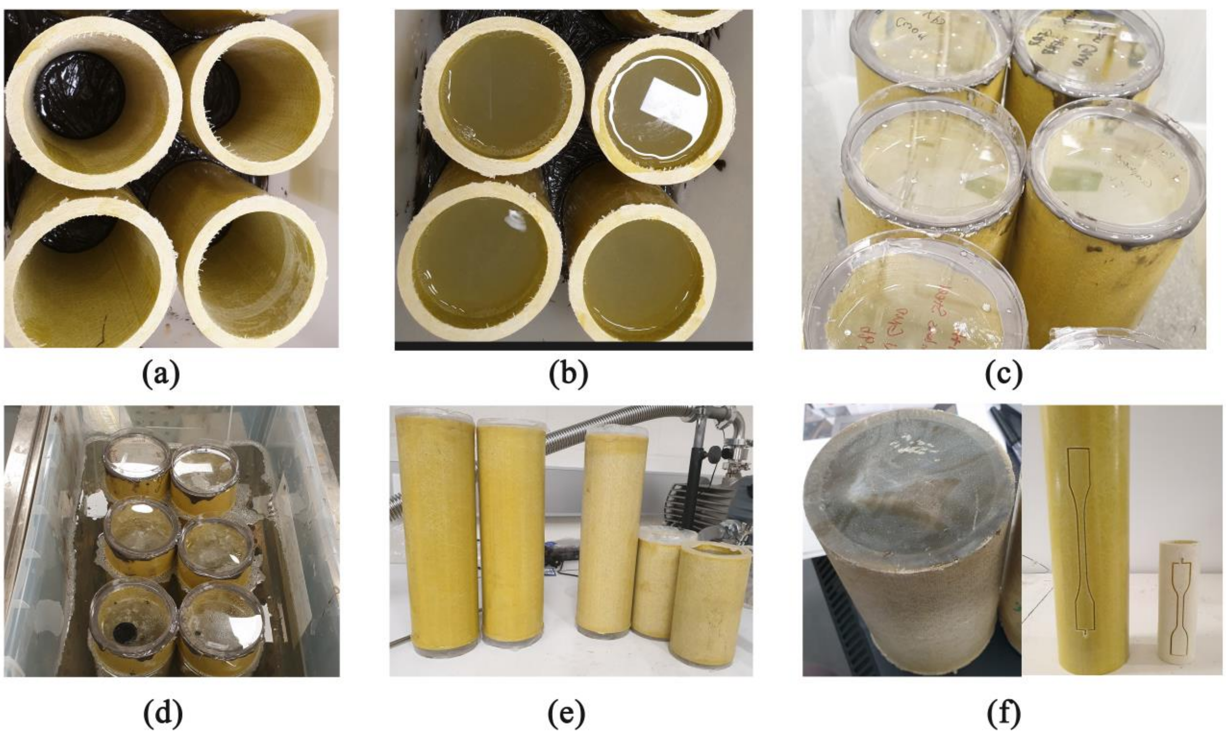

Figure 7-1 Specimen preparation and conditioning procedure: (a) Sealing on side of the tubes, (b) pouring the solution inside the tubes, (c) sealing the other side of the tubes, (d) pouring the solution in the container for outer environment, (e) taking out the samples on target periods and (f) preparing coupons microstructural and mechanical tests

7.2.4. Mechanical tests

Compressive and tensile strengths of pultruded tubes after exposure to SWSSC and seawater were studied using compression and tensile tests. It is worth mentioning that the hoop strength of pultruded tubes is negligible due to the fibres oriented unidirectionally in longitudinal direction. Therefore, the hoop tensile strength of the samples is not studied in this research. However, the hoop tensile strength of SWSSC filament wounded FRP tubes with different fibres orientation under seawater condition, will be addressed in future study by the authors.

7.2.4.1 Compression tests

Compression tests were conducted to investigate the degradation of compressive strength and modulus properties of GFRP pultruded tubes exposed to environmental conditions. To examine the reproducibility of results, three identical samples of each type of GFRP tubes were tested for control and conditioned situations. An Instron 600 kN universal testing machine with the loading rate of 0.5 mm/min was used for conducting the compression tests. In each test, a strain gauge was attached at the centre to obtain strains in longitudinal directions. The thickness, inner diameter, and length of compressive samples were 8 mm, 94 mm, and 200 mm for larger tubes and 4 mm, 63 mm, and 100 mm for smaller tubes, respectively.

Figure 7-2 shows compression test sample dimensions and the compression test set-up.

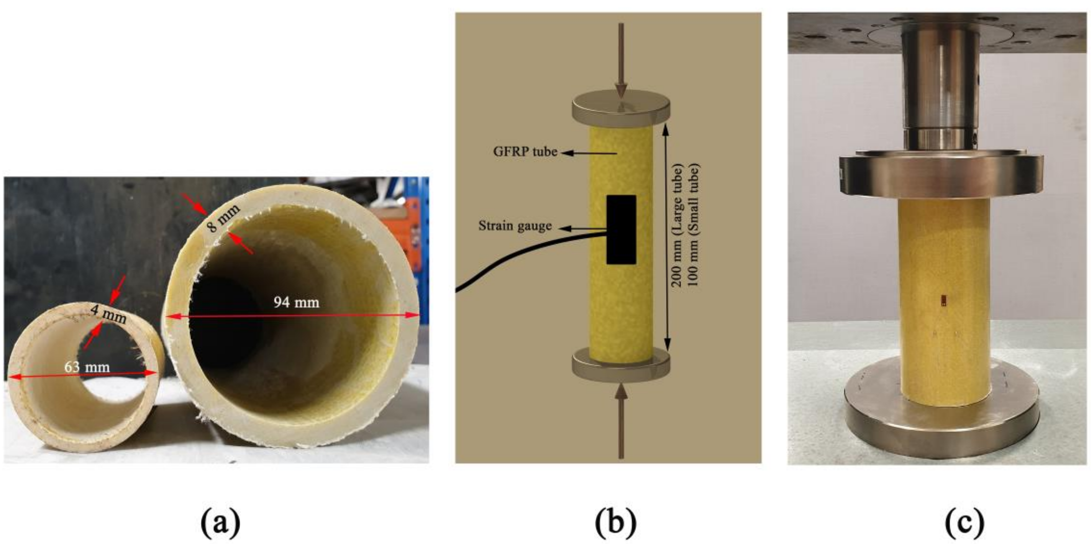

Figure 7-2 Sample configuration and compression test set-up: (a) Tubes cross-section dimensions; compression test set-up: (b) schematic, (c) actual

7.2.4.2 Tensile tests

Instron 100 kN universal testing machine with the loading rate of 0.5 mm/min was used for conducting tensile tests. Tensile coupon samples were cut from each of the control and conditioned tubes. Three identical samples were tested for each condition. As the coupons were cut from circular tubes, they were curved, and hence, aluminium gripping pieces were used to prevent any failure or slip at upper and lower jaws. A strain gauge was installed on the outer side of the sample to obtain strain in longitudinal direction. **Figure 7-3** shows the tensile coupon sample and test set-up.

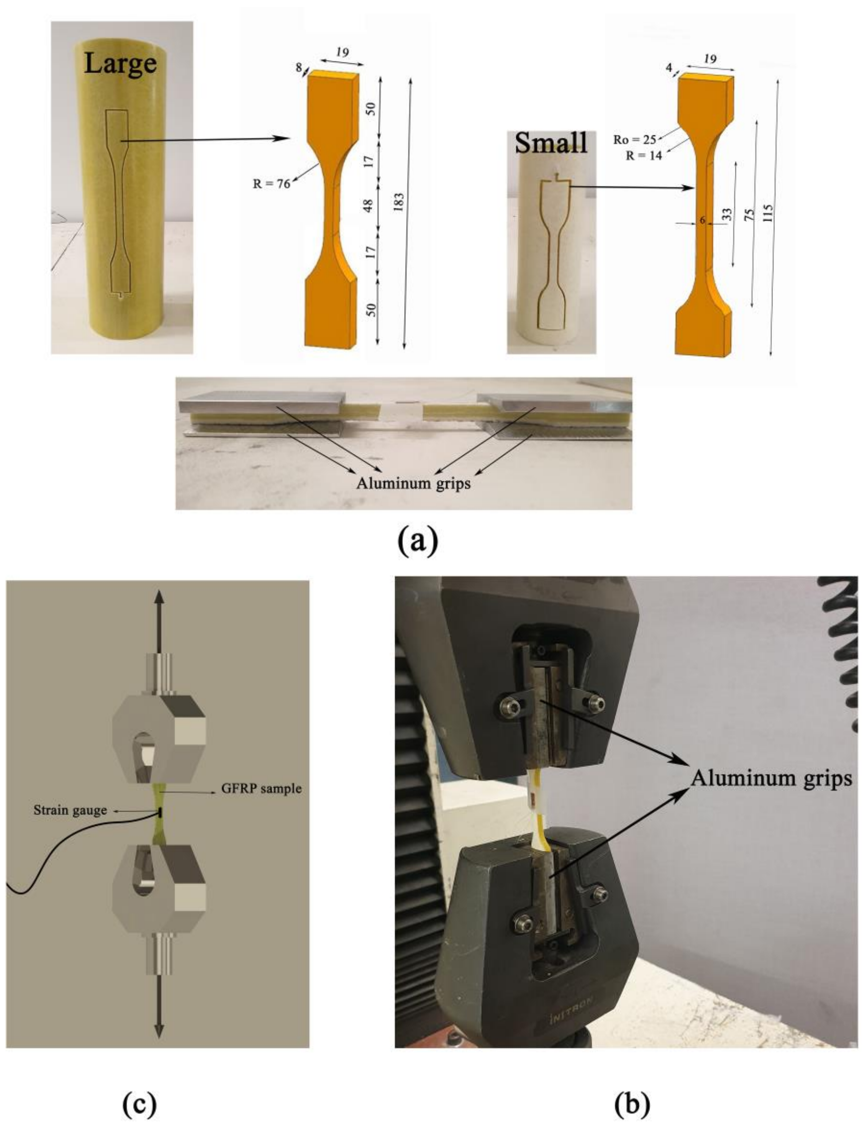

Figure 7-3 Sample configuration and tensile test set-up: (a) Tensile coupons dimensions; tensile test set-up: (b) actual and, (c) schematic

7.2.5. Microstructural analysis

To study the degradation mechanism of GFRP pultruded tubes exposed to SWSSC and seawater conditions, SEM and micro-CT analysis were conducted at different time periods. The high resolution JOEL7001 SEM and Zeiss Xradia 520 Versa micro-CT were used for visualisation and 3D imaging analysis of the tubes from its edges through the centre. The analysis was conducted through the depth of the tubes to investigate the penetration capability of each exposure condition and level of degradation. Liquid nitrogen fracturing methods were used to prepare samples for microstructural analysis.

7.3. Results and discussion

In this section, failure modes, mechanical and microstructural properties of GFRP tubes before and after conditioning are discussed.

7.3.1 Surface appearance change

Figure 7-4 shows the appearance changes of GFRP tubes after 1, 3 and 6 month exposure to different environmental conditions. As is seen, the inner and outer sides of all tubes changed in terms of colour, lustre and smoothness. These changes are more obvious when the tubes were exposed to a SWSSC environment compared to a seawater environment. Furthermore, difference is seen between the samples exposed for different duration and at different conditioning temperatures: the longer the duration or higher the temperature, the greater is the intensity of change in surface colour and lustre. As is seen in **Figure 7-4**, with increasing duration/temperature, the colour and lustre of the sample changed from yellow and shiny to white and pale (these changes are much more pronounced in SWSSC than in seawater). Moreover, due to the absence of the protective layer on the inner surface of the tubes for the harsher environments (i.e., SWSSC with higher conditioning time and temperature), the surface resin matrix suffered leaching, as result, the surface fibres became visible. Further discussions regarding the microstructural properties of the samples and chemical reactions will be presented later in this paper.

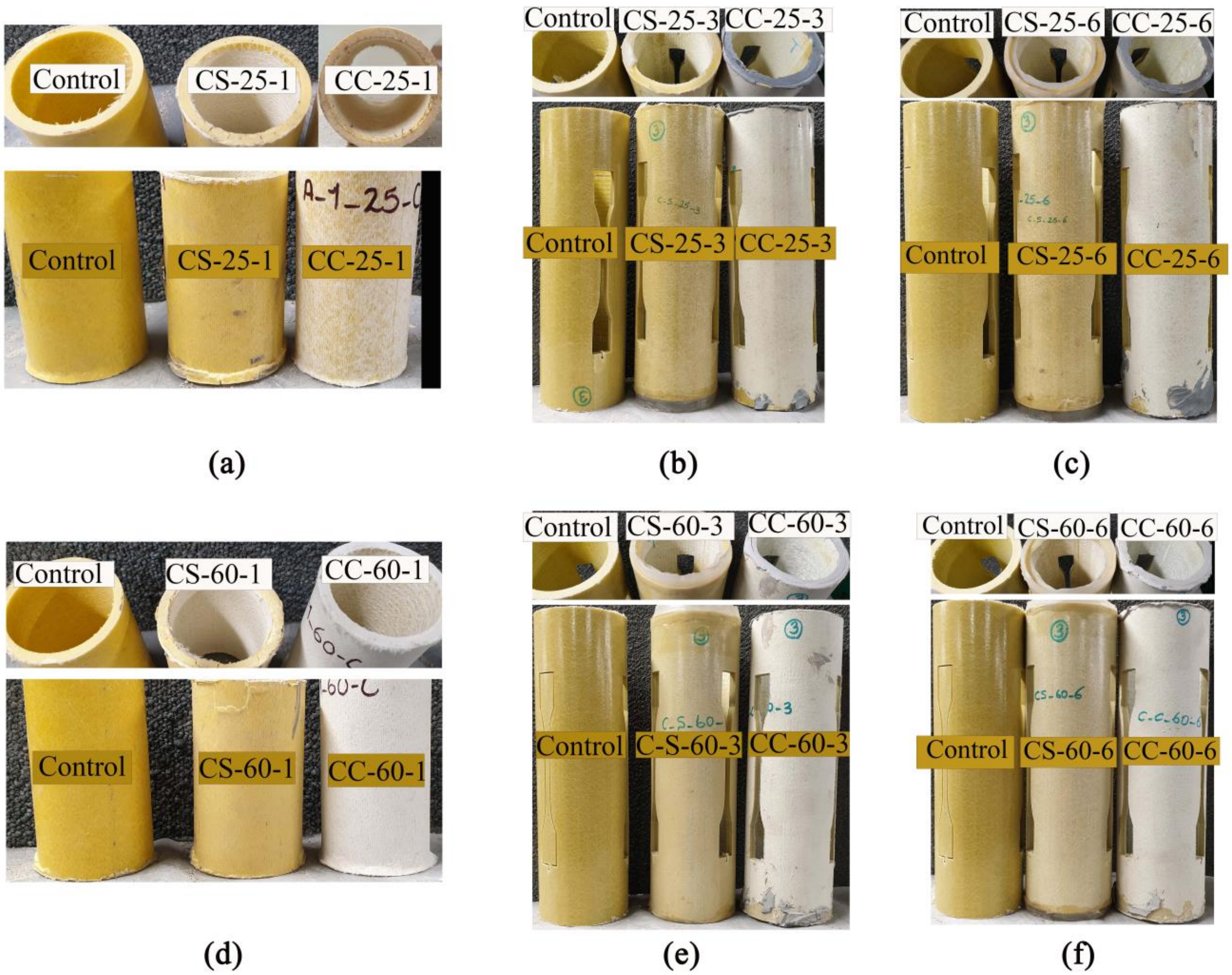

Figure 7-4 Specimens surface changes after conditioning: (a) 1-month conditioning at 25 ºC, (b) 3-months conditioning at 25 ºC (c) 6-months conditioning at 25 ºC, (d) 1-month conditioning at 60 ºC, (e) 3-months conditioning at 60 ºC (f) 6-months conditioning at 60 ºC

7.3.2 SEM analyses

In order to investigate the degradation mechanism (morphological changes) and damage level in terms of the cracks/micro cracks in the resin matrix, resin/fibre debonding (interface degradation) and fibre damage, a few selected samples before and after exposure to different conditions were examined under SEM. To avoid mechanical damages due to sample preparation for SEM (i.e., using grinding and polishing), all SEM samples were fractured after being exposed to liquid nitrogen. After liquid nitrogen fracturing, samples were coated by a thin layer of conductive carbon to prevent the sample charging. **Figure 7-5** compares the inner and outer surfaces of conditioned GFRP tubes. Damages are seen in **Figure 7-5a** and **Figure 7-5c**, including resin leaching, significant resin/matrix debonding and fibre damage on the surface exposed to SWSSC environment. Fibre damages include pitting, corrosion products (plate-shaped), cracks and corrosion shells (porous and amorphous structures). These observations are similar to the degradation mechanisms reported by Guo et al. [249].

Regarding the surface of the samples exposed to seawater solution, at the early stage (1 month conditioning), microcracks, blisters and solid compounds were observed in the matrix (**Figure 7-5b** and **Figure 7-5d**). By increasing the time and temperature of the conditioning (comparing **Figure 7-5a** and **Figure 7-5b** with **Figure 7-6a** and **Figure 7-6b**), progression of the cracks led to more resin/fibre debonding. This may be due to more solution penetration into the resin matrix as a result of crack growth. Therefore, the development of the continues cracks and resin/matrix debonding due to the harsher conditions (i.e. alkaline environments, elevated temperature and longer conditioning time), may provide more chance for the solution to penetrate further into the resin matrix and consequently cause more degradation in mechanical properties. Similar observations were reported by Bazli et al [17].

By comparing the surface of the samples exposed to seawater with the samples exposed to SWSSC (e.g. **Figure 7-5a** and **Figure 7-5c** compared to **Figure 7-5b** and **Figure 7-5d**), one can simply conclude that the SWSSC environment in significantly harsher than the seawater.

Comparing **Figure 7-6c** with **Figure 7-6d** reveals that although the solution is the same for both inner and outer sides, the degradation of the inner side was significantly higher than the outer side. The reason for this difference is a protective layer which applied on the outer layer of pultruded tubes during the fabrication process. Based on the observations of the present study, it will be beneficial to apply a protective layer also on the inner side of the tubes, particularly when using the tubes with concrete.

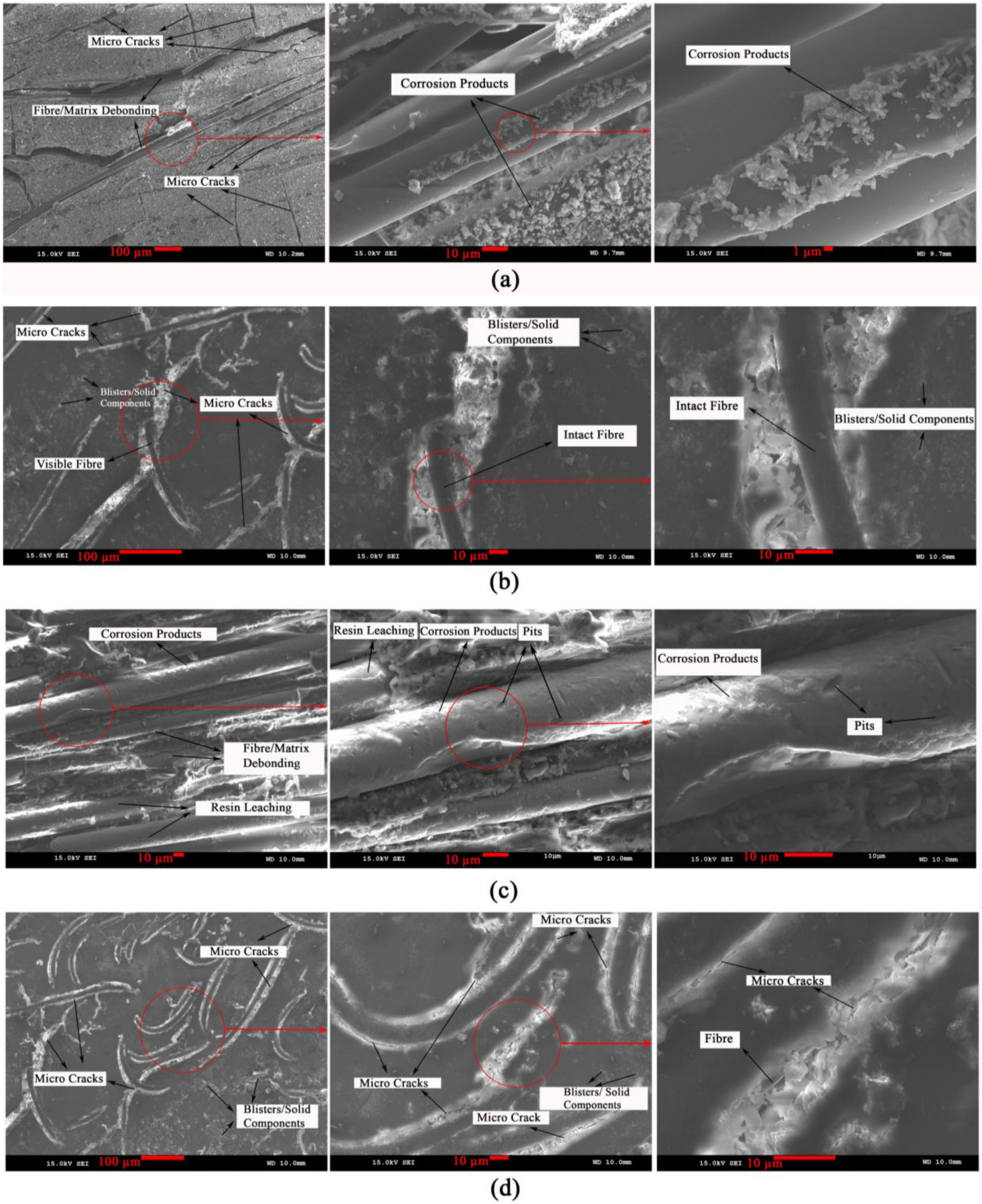

Figure 7-5 Specimens exposed to CS condition: (a) inner side of CS-4-25-1, (b) outer side of CS-4-25-1 (c) inner side of CS-8-60-1 and (d) outer side of CS-8-60-1

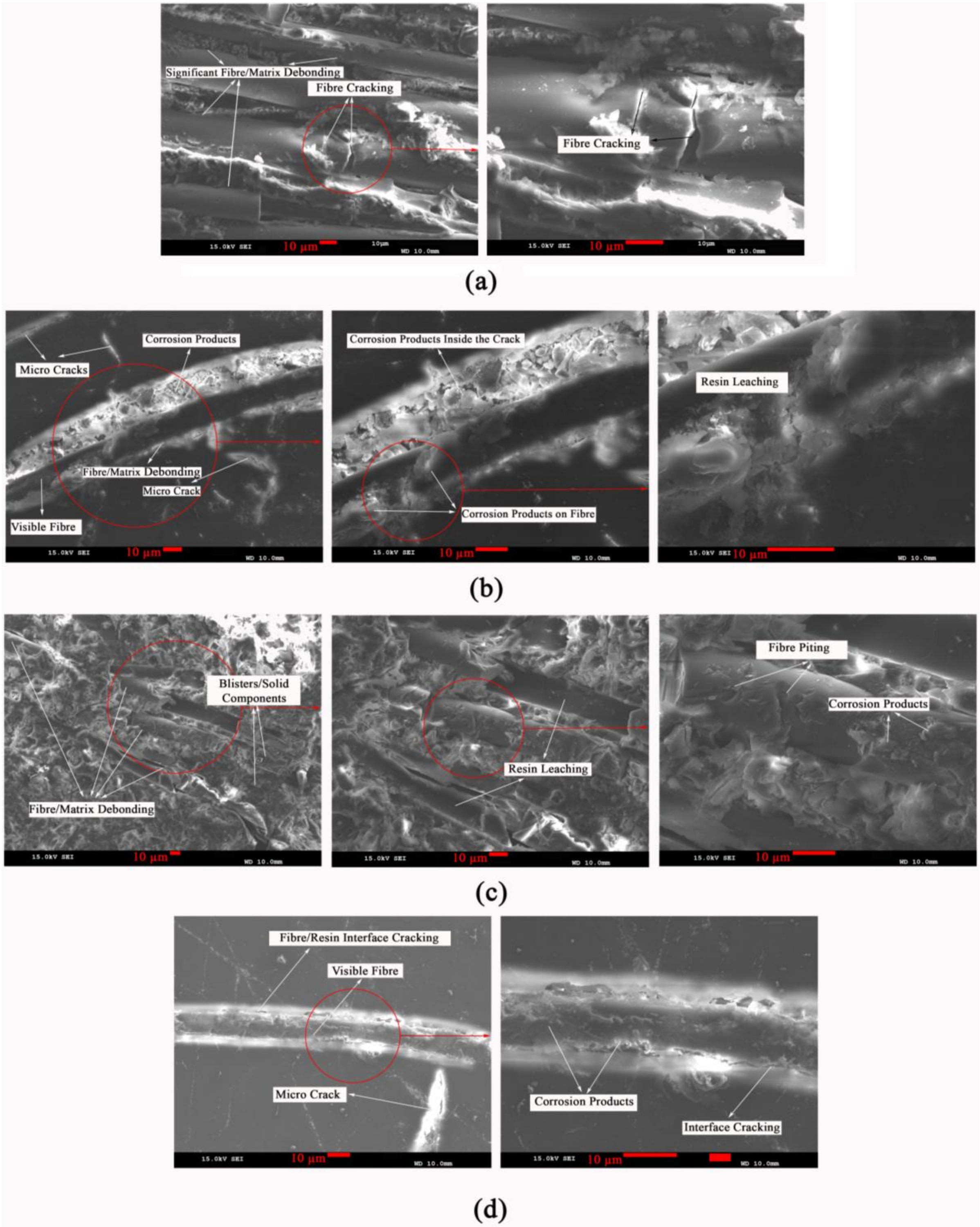

Figure 7-6 Specimens exposed to CS and SS conditions: (a) inner side of CS-4-25-6, (b) outer side of CS-4-25-6 (c) inner side of SS-8-60-6 and (d) outer side of SS-8-60-6

7.3.3 Micro-CT imaging

In order to study the degradation level of GFRP tubes exposed to SWSSC and seawater environments, three samples were analysed using micro-CT imaging at 2.94 voxel size. One reference sample and two samples that were exposed to 6 months of CS conditions at 25 ˚C and 60 ˚C were selected. The volume fracture of fibres, resin and void for different sections were measured using image processing. MATLAB codes and Avizo commercial software were used for image processing. The process includes three steps. In the first step 2D projections of samples were reconstructed by using XRM Reconstructor software. **Figure 7-7** shows the 3D images of samples. As is seen severe degradation in terms of fibre/resin debonding is observed on the side of the tube that was exposed to SWSSC. As expected, the degradation level decreases by increasing the distance from the edges due to the less solution penetration. In step two, to map the degradation variations, five sub volumes (1.47 mm × 1.47 mm × 2.94 mm) were extracted from each sample (see **Figure 7-7a**) and were analysed to obtain the ratios of fibres, resin and voids.

Figure 7-8 shows one of the outputs of the conducted image processing. The results of analyses, in terms of the volume ratios, are summarized in **Figure 7-8**. It can be seen that the volume of the resin decreases and the volume of the voids increases when sample were subjected to SWSSC and seawater condition for all sections. Moreover, the volume of the voids increases by increasing the conditioning temperature. These observations confirm the degradation of GFRPs, in terms of the resin leaching, fibre damages and fibre/matrix debonding, due to the solution penetration into the sample as discussed previously. It is known that the chemical reactions and resin swelling are the main factors in breaking the chemical bonds and physical bonds between the fibre and the resin [99]. Therefore, the more is the solution absorption, the more is the degradation (void volume).

It can be seen that the volume of the resin decreases and the volume of the voids increases when sample were subjected to SWSSC and seawater condition for all sections. Moreover, the volume of the voids increases by increasing the conditioning temperature. These observations confirm the degradation of GFRPs, in terms of the resin leaching, fibre damages and fibre/matrix debonding, due to the solution penetration into the sample as discussed previously. It is known that the chemical reactions and resin swelling are the main factors in breaking the chemical bonds and physical bonds between the fibre and the resin [99]. Therefore, the more is the solution absorption, the more is the degradation (void volume).

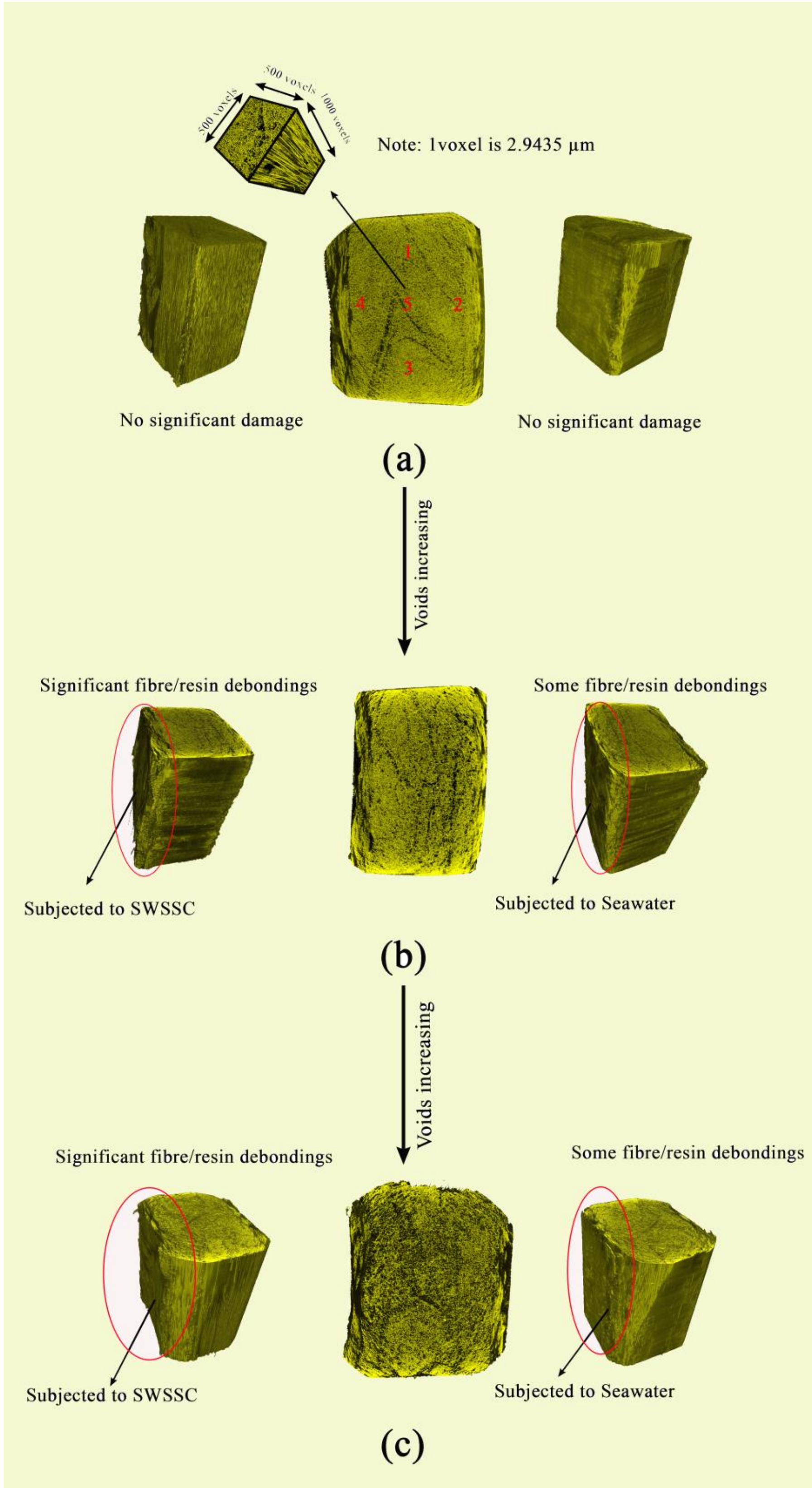

Figure 7-7 3D images of samples: (a) 4mm reference sample, (b) CS-4-25-6 and (c) CS-4-60-6

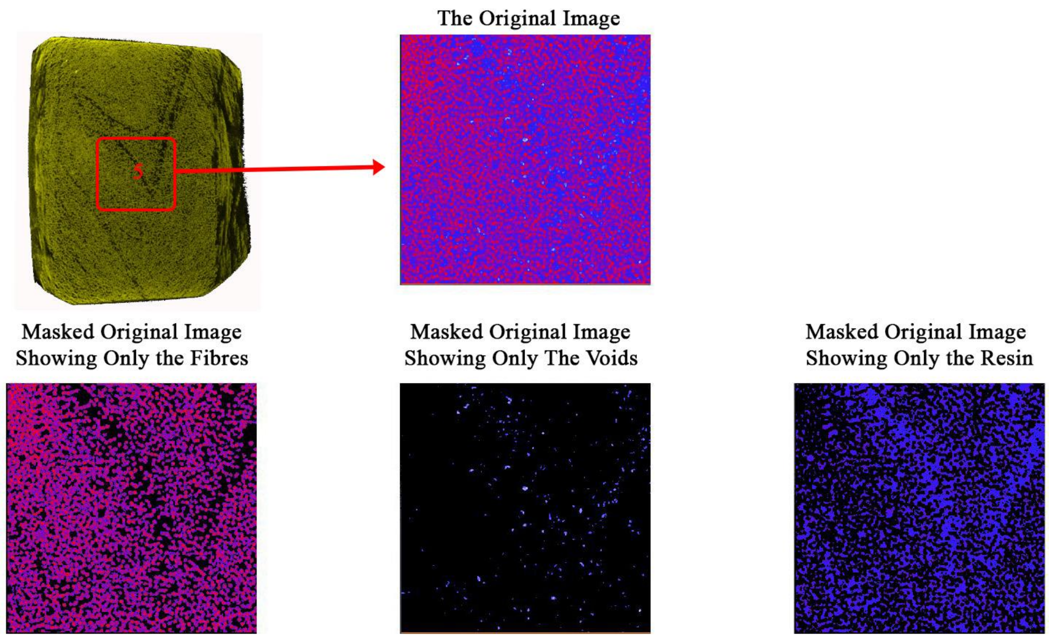

(a)

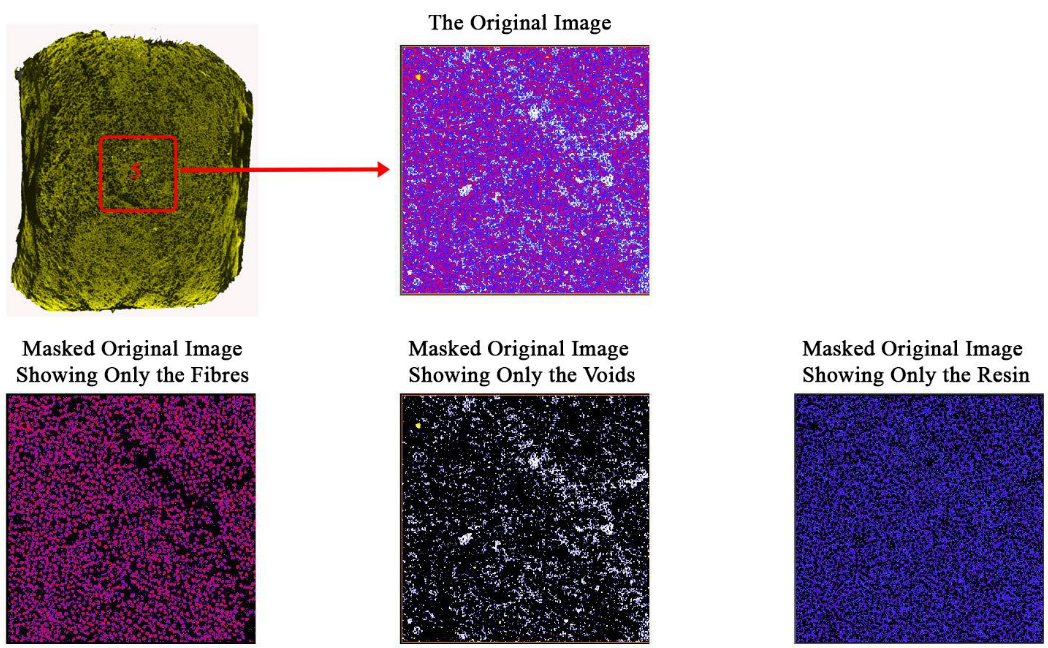

(b)

Figure 7-8 Output of one analysed image of section 5: (a) reference sample and (b) CS-4-60-6

Table 7-3 Volume fraction calculated from X-ray CT images

Section	Specimen	Fibre (%)	Resin (%)	Void (%)
1	Reference	53.7	46.02	0.28
	CS-25-6	61.72	32.9	5.38
	CS-60-6	58.57	35.83	5.6
2	Reference	50.71	48.37	0.91
	CS-25-6	56.8	33.37	9.83
	CS-60-6	55.14	38.44	6.42
3	Reference	56.92	42.76	0.32
	CS-25-6	64.48	31.3	4.16
	CS-60-6	56.16	37.64	6.2
4	Reference	62.21	35.86	1.93
	CS-25-6	59.96	30.47	9.57
	CS-60-6	52.88	35.4	11.72
5	Reference	61.02	36.37	2.61
	CS-25-6	61.79	28.85	9.36
	CS-60-6	55.27	34.13	10.6

7.3.4 Failure modes

Figure 7-9 shows the typical tensile failure modes. The main failure mode for tensile samples was SGV based on failure mode codes provided in ASTM D3039 [17], in which , S represents the long splitting failure mode type, G stands for the gauge failure area and V shows the various failure locations. However, as is seen in **Figure 7-9**, samples exposed to SWSSC environments failed firstly due to the delamination of outer layers (which were directly exposed to the solutions) and then fibre fracture. However, the main failure mode of control samples and those exposed to seawater was fibre fracture. Significant reduction of interlaminar shear strength due to SWSSC solution penetration is the main reason for delamination of layers subjected to SWSSC before fibre fracture. In case of samples subjected to seawater environment, earlier occurrence of fibre fracture than the layer delamination shows that the interlaminar shear strength reduction due to the seawater solution penetration was not enough to change the failure mode when compared to the control samples. These observations confirm that SWSSC environment as the most aggressive condition that led to the significant fibre/matrix interfacial degradation/debonding (see **Figure 7-5a**, **Figure 7-5c** and **Figure 7-6a**) and consequently interlaminar shear strength reduction. It was also observed that the delamination of the outer layers was more severe when samples were subjected to 60 ˚C compared to 25 ˚C. In other words, more layers were delaminated before the fibre fracture at 60 ˚C. This observation suggests that more solution is penetrated into the resin matrix as a result of crack growth at the higher temperature, which leads to more layers to be degraded.

It should be mentioned that similar failure modes were observed for both thinner and thicker tubes. However, the ratio of delaminated layers to the sample thickness (in samples exposed to SWSSC solutions) was higher for thinner tubes compared to that for the thicker ones.

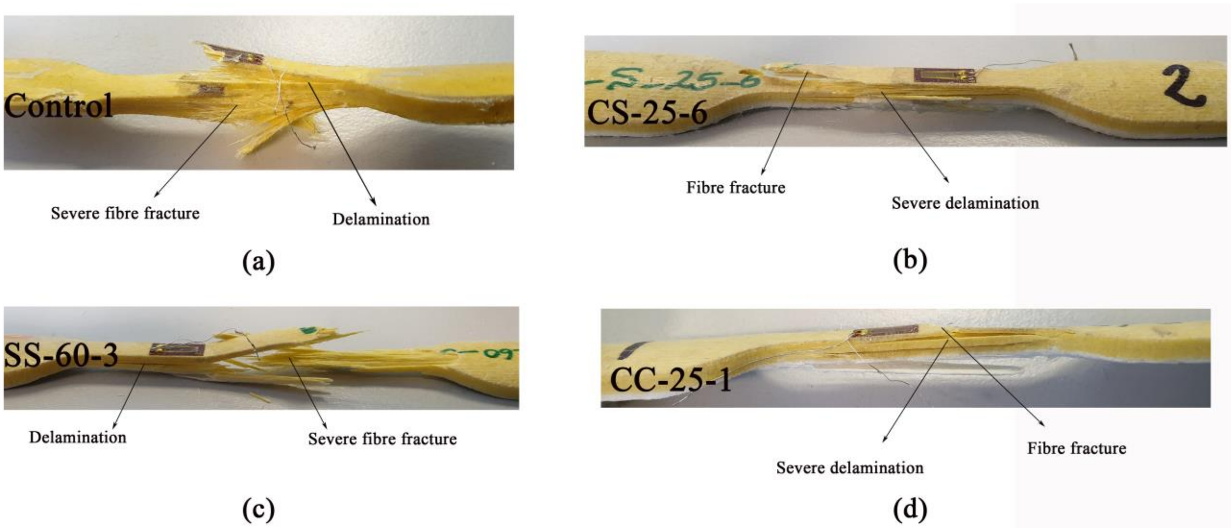

Figure 7-9 Tensile test typical failure modes: a) More fibre fracture (main failure mode) and less delamination, (b) combined failure mode, (c) more fibre fracture (main failure mode) and less delamination and (d) less fibre fracture and more delamination (main failure mode)

In contrast to the tensile samples, different failure modes were observed for control and conditioned compressive samples. **Figure 7-10** shows the typical failure modes observed during the compressive tests. All control samples failed because of the local buckling along the tube height or due to the combination of local buckling near the tube ends and longitudinal cracks along the tube length. In most cases the failure modes of the samples exposed to SS environments, regardless of the time and temperature of exposure, were almost the same as the corresponding control samples. This shows that the adverse effect of seawater solution was not adequate to change the failure modes of GFRP tubes under compression. However, limited number of SS and most of CS and CC samples failed due to the local buckling of the tube at the contact surface (elephant foot buckling) rather than tube local buckling and longitudinal cracks along their height. This may be due to the significant resin matrix degradation under SWSSC, which caused the resin frittering away under the loading plates and consequently buckling of the fibres at the sample ends. It is also observed that for CC and CS samples, increasing the time and temperature of exposure leads the elephant foot buckling failure to be more severe and the most dominant failure mechanism.

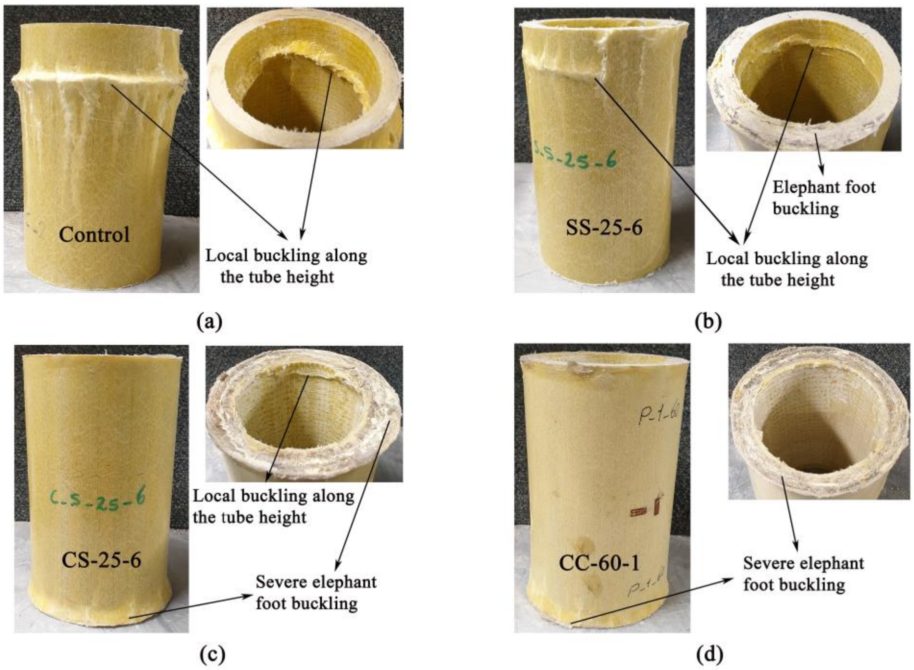

Figure 7-10 Compressive test typical failure modes : (a) Buckling along the height, (b) combination of buckling along the height (main failure mode) and elephant foot buckling (c) combination of buckling along the height and elephant foot buckling (main failure mode) and (d) elephant foot buckling

7.3.5 Mechanical test results

Table 7-4 and **Table 7-5** present the compression and tension test results of control and conditioned specimens in terms of ultimate stress, elastic modulus and the retention values, respectively. In order to identify the samples, a four-part notation system was used. The first letter represents the environmental condition. The second letter indicates the thickness of the tubes. The third and fourth letters stand for the conditioning temperature and the time (in months). For example, CS-8-60-1 indicates the GFRP tube of 8 mm thickness exposed for one-month to SWSSC as the inner solution and seawater as the outer solution at 60˚C.

To consider the effect of all variables, including the environmental conditions, conditioning temperature, conditioning time and tube thickness on the mechanical properties of GFRP pultruded profiles, the tests results were compared with respect to each variable.

Table 7-4 Compression test results

Specimen	Average ultimate compressive stress (MPa)	CV (%)	Retention (%)	Average compressive elastic modulus (GPa)	CV (%)	Retention (%)
Control (8 mm)	341.9	1.1	100.0	34.3	5.0	100.0
CC-8-25-1	174.0	2.3	50.9	33.7	3.7	98.1
CC-8-25-3	141.0	4.8	41.2	33.3	6.2	97.1
CC-8-25-6	108.7	4.9	31.8	32.7	5.2	95.1
CC-8-60-1	111.3	3.9	32.5	27.7	10.4	80.6
CC-8-60-3	97.1	6.1	28.4	26.7	7.7	77.7
CC-8-60-6	71.5	8.3	20.9	22.7	9.1	66.0
SS-8-25-1	253.3	3.7	74.1	36.0	4.5	104.9
SS-8-25-3	244.6	0.9	71.6	34.3	2.7	100.0
SS-8-25-6	229.5	3.9	67.1	32.7	6.3	95.1
SS-8-60-1	263.7	4.3	77.1	27.7	7.4	80.6
SS-8-60-3	257.3	5.6	75.2	28.0	5.8	81.6
SS-8-60-6	225.8	3.4	66.0	25.7	8.0	74.8
CS-8-25-1	181.9	4.6	53.2	33.7	5.0	98.1
CS-8-25-3	160.0	3.6	46.8	37.0	5.8	107.8
CS-8-25-6	109.6	8.7	32.1	30.3	12.7	88.3
CS-8-40-1	179.4	4.2	52.5	30.3	6.1	88.3
CS-8-40-3	131.9	5.2	38.6	30.7	3.5	89.5
CS-8-40-6	108.7	2.6	31.8	28.3	2.9	82.5
CS-8-60-1	171.1	3.7	50.0	32.0	2.6	93.2
CS-8-60-3	120.0	2.5	35.1	30.3	8.2	88.3
CS-8-60-6	100.1	12.1	29.3	22.3	14.8	65.0
Control (4 mm)	342.7	3.3	100.0	35.0	1.3	100.0
CC-4-25-1	161.5	2.7	47.1	33.0	2.5	94.3
CC-4-25-3	113.7	3.8	33.2	33.0	6.2	94.3
CC-4-25-6	90.6	3.2	26.4	35.0	9.4	100.0
CC-4-60-1	99.8	10.8	29.1	30.0	8.2	85.7
CC-4-60-3	94.6	4.6	27.6	32.0	9.0	91.4
CC-4-60-6	71.0	7.2	20.7	23.0	14.2	65.7
SS-4-25-1	249.8	5.3	72.9	35.0	3.6	100.0
SS-4-25-3	231.9	4.3	67.7	31.0	8.0	88.6
SS-4-25-6	203.7	1.7	59.4	36.0	7.3	102.9
SS-4-60-1	246.4	2.8	71.9	26.3	4.8	74.3
SS-4-60-3	225.6	5.1	65.8	29.0	4.3	82.9
SS-4-60-6	203.1	6.3	59.3	28.0	4.5	80.0
CS-4-25-1	213.5	8.3	62.3	34.0	2.4	97.1
CS-4-25-3	160.4	9.9	46.8	31.0	9.1	88.6
CS-4-25-6	98.1	9.8	28.6	30.0	10.3	85.7
CS-4-40-1	200.8	7.3	58.6	31.3	3.1	89.4
CS-4-40-3	139.8	5.6	40.8	30.7	2.6	87.7
CS-4-40-6	104.5	8.4	30.5	26.3	4.1	75.1
CS-4-60-1	200.2	13.2	58.4	30.0	5.7	85.7
CS-4-60-3	118.3	6.0	34.5	27.0	8.0	77.1
CS-4-60-6	99.8	5.0	29.1	21.0	5.9	60.0

Table 7-5 Tension test results

Specimen	Average ultimate tensile stress (MPa)	CV (%)	Retention (%)	Average Tensile elastic modulus (GPa)	CV (%)	Retention (%)
Control (8 mm)	514	3.5	100.0	34.3	6.0	100.0
CC-8-25-1	413	2.7	80.4	33.3	3.7	97.1
CC-8-25-3	401	6.9	78.0	31.3	1.5	91.3
CC-8-25-6	353	8.5	68.7	28.0	5.8	81.6
CC-8-60-1	340	8.0	66.0	24.7	5.1	71.8
CC-8-60-3	301	3.8	58.5	27.3	7.5	79.6
CC-8-60-6	252	10.5	49.1	25.0	8.6	72.9
SS-8-25-1	500	2.6	97.1	34.3	2.7	100.1
SS-8-25-3	510	2.1	99.1	35.0	2.3	102.0
SS-8-25-6	493	2.1	95.8	33.3	1.4	97.2
SS-8-60-1	491	2.4	95.5	33.0	2.5	96.2
SS-8-60-3	478	1.6	93.0	34.3	1.4	100.1
SS-8-60-6	456	3.0	88.7	31.7	1.5	92.3
CS-8-25-1	489	1.5	95.1	33.7	5.0	98.2
CS-8-25-3	488	8.1	94.9	34.0	4.8	99.1
CS-8-25-6	475	3.5	92.3	30.5	8.2	88.9
CS-8-40-1	470	4.1	91.5	32.3	5.2	94.7
CS-8-40-3	454	5.6	88.3	30.5	1.6	88.9
CS-8-40-6	441	3.9	85.9	30.7	4.2	89.5
CS-8-60-1	439	7.9	85.4	29.5	1.7	86.0
CS-8-60-3	420	3.1	81.7	28.7	4.4	83.6
CS-8-60-6	397	4.4	77.3	29.0	4.9	84.5
Control (4 mm)	462	9.7	100.0	33.7	3.7	100.0
CC-4-25-1	311	1.0	67.3	32.0	4.4	95.0
CC-4-25-3	301	1.0	65.2	32.7	2.9	96.9
CC-4-25-6	295	7.3	63.8	32.0	2.6	95.0
CC-4-60-1	288	9.1	62.3	31.7	5.4	94.0
CC-4-60-3	250	11.2	54.1	26.3	1.8	78.1
CC-4-60-6	185	7.5	40.0	26.7	3.5	79.1
SS-4-25-1	458	2.8	99.0	33.7	3.7	99.9
SS-4-25-3	459	5.1	99.3	32.7	1.4	96.9
SS-4-25-6	430	3.3	93.1	33.0	2.5	97.9
SS-4-60-1	362	11.4	78.3	33.0	2.5	97.9
SS-4-60-3	354	4.6	76.6	33.3	1.4	98.9
SS-4-60-6	332	3.2	71.7	31.3	4.0	93.0
CS-4-25-1	343	6.6	74.2	31.3	5.4	93.0
CS-4-25-3	310	5.6	67.0	30.7	3.1	91.0
CS-4-25-6	297	2.6	64.2	31.7	6.5	94.0
CS-4-40-1	318	5.6	68.9	30.5	3.1	90.5
CS-4-40-3	301	2.9	65.1	31.7	3.6	94.0
CS-4-40-6	296	4.4	64.1	30.3	7.6	89.9
CS-4-60-1	307	4.3	66.4	30.0	2.7	89.0
CS-4-60-3	310	3.0	67.1	28.0	7.7	83.1
CS-4-60-6	289	4.1	62.4	28.3	9.3	84.1

7.3.5.1 Effect of environment

Figure 7-11 compares the average ultimate compressive strength and elastic modulus retention of GFRP tubes based on the environmental conditions. It can be seen that the adverse effect of SWSSC condition is significantly higher than the seawater (e.g., 79 % reduction in compressive strength of CC-4-60-6 compared to 41 % reduction of SS-4-60-6). The fact that alkaline environment is a harsher environment than the seawater for FRP composites was also concluded by other studies [113]. It is generally known that the physical and chemical reactions between the resin matrix and the fibres due to the fluid diffusion and consequent increase in sample's volume are the main reasons for the degradation of GFRP's mechanical properties. However, the level of damage is strongly related to the type of solution and the solution penetration. When FRPs are exposed to seawater solution, blisters and solid compounds are created on the surfaces of a sample (see **Figure 7-5b**, **Figure 7-5d** and **Figure 7-6c**). These compounds, which are the results of reactions between the active metals in seawater and soluble compounds of FRP, provide osmotic pressure (between the sample surface and the sea water), which may lead to resin deformation [28]. This phenomenon may lead to degradation in the mechanical properties of FRPs when exposed to seawater conditions. However, similar to the results of the present study, it is also reported in the literature that this degradation of FRP under seawater is not significant [183]. In contrast to seawater, GFRPs are strongly vulnerable to alkaline solutions. The following phenomena may occur during the exposure of FRP composites to an alkaline solution (e.g., SWSSC): (1) degradation of the resin mechanical properties due to the hydrolysis of the polymer chains, network swelling and hydrogen bond relaxation/formation between the solution and the polymer molecules [250], (2) degradation (detachment) of the resin/fibre interface due to the migration of H_2O and $Ca(OH)_2$ at the interface (noted that the $Ca(OH)_2$ crystal growth significantly damage the interface (see **Figure 7-5a** and **c** and **Figure 7-6a**) [251] and (3) swelling and deterioration of the fibres due to the chemical attacks [252, 253]. With these in mind, one can simply conclude that the alkaline environment is significantly harsher environment than the seawater for GFRP composites. This was also confirmed by comparing the results under different conditions in **Figure 7-11**.

Regarding the compressive elastic modulus, it is seen that compared to the compressive strength, the elastic modulus of the tubes, in most conditions, is not significantly affected by the environmental conditions. In addition, in contrast to the strength variations, a constant trend for the elastic modulus variation in different conditions was not observed. This unpredictable variation could be explained by the fact that the elastic modulus of pultruded tubes along the fibre direction is more related to the fibres and less to the resin matrix. Therefore, as the degradation of fibres under different environmental conditions may not be significant [99], the main reason for the elastic modulus degradation will be due to the resin matrix degradation.

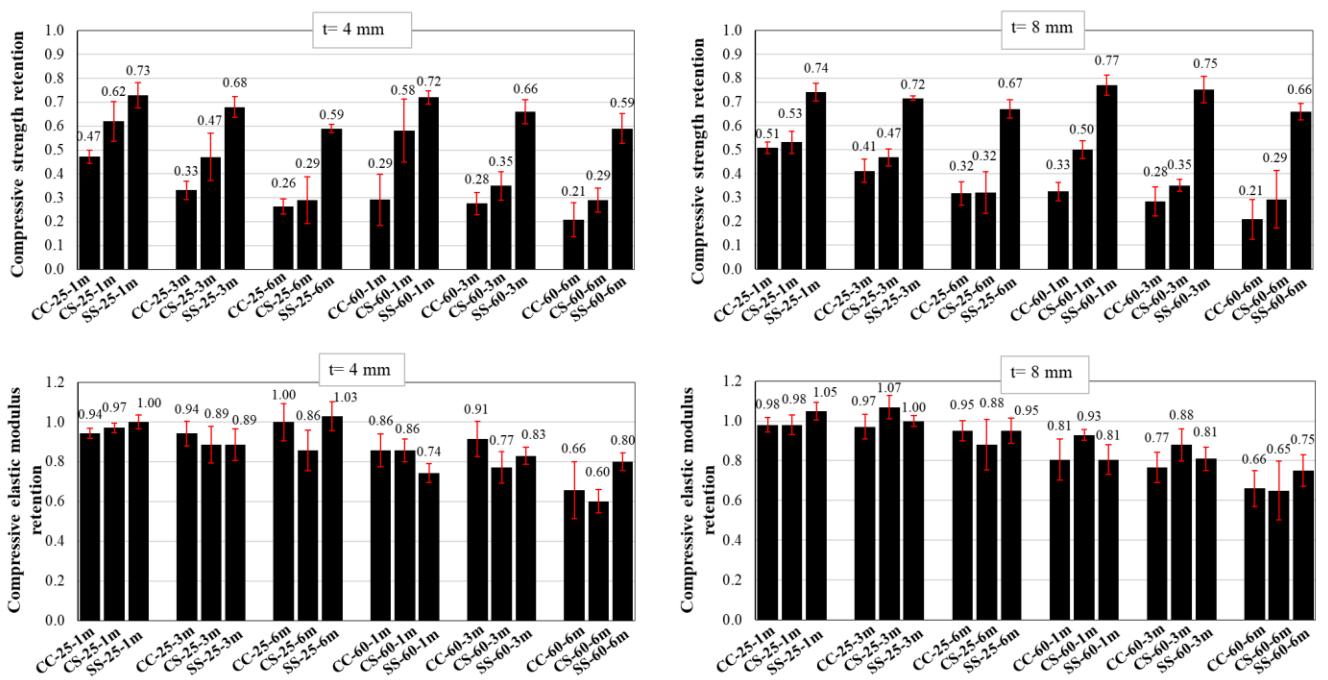

Figure 7-11 Comparison of the compressive strength and elastic modulus between CC, CS and SS conditions

Figure 7-12 compares the average ultimate tensile strength and elastic modulus retention of GFRP tubes based on the environmental conditions. Similar to the compressive results, it is seen that the strength reduction of the samples exposed to SWSSC environment is significantly higher than that for the samples exposed to seawater (e.g., 60 % reduction in tensile strength of CC-4-60-6 compared to 28 % reduction of SS-4-60-6). However, the ultimate tensile strength reductions of specimens are significantly lower than the corresponding compressive strength (e.g., 60, 38 and 28% reductions in tensile strength of CC-4-60-6, CS-4-60-6 and SS-4-60-6, respectively compared to 79, 71 and 41% corresponding reductions in compressive strength). To understand the reason for this difference, it is worth noting that during the tensile tests, fibres may continuously carry loads in the applied loading (longitudinal) direction, while during the compression tests, the degradation of the resin matrix and consequently the resin/fibre interface may lead to the buckling of the fibres and early failure of the specimens. Even so, the degradation of the resin matrix and resin/fibre interface reduced the overall tensile strength of the tubes due to the load transferring reduction between the resin and fibres [39]. Regarding the tensile elastic modulus, almost the same trend as the tensile strength variation is observed. However, the reduction rates and level of dependency of the tensile elastic modulus of the samples after exposure to different environments are significantly lower than that of strength reductions.

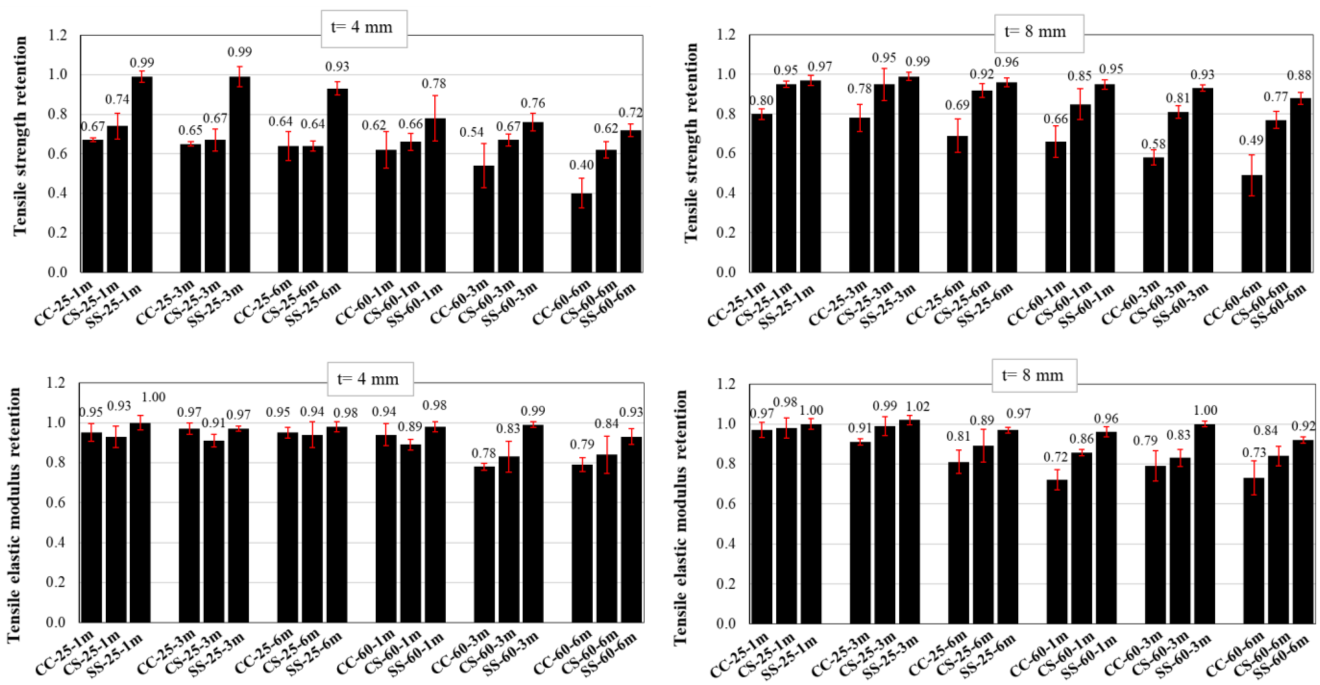

Figure 7-12 Comparison of the tensile strength and elastic modulus between CC, CS and SS conditions

7.3.5.2 Effect of conditioning temperature

Figure 7-13 compares the average ultimate compressive strength and elastic modulus retention of GFRP tubes based on the conditioning temperature. As expected, in most cases (except the two conditions of SS for 8 mm tubes) the compressive strength degradation of specimens at 60 ˚C is higher than that of specimens at room temperature. The reason for slightly higher strength reduction of those two conditions may be due to the randomness of the specimens. Regarding the elevated temperature, two major effects on the composites can be counted: (1) thermal gradient between the components and (2) viscosity increment [159]. Therefore, due to the higher moisture absorption of the composites at elevated temperatures, consequences, such as plasticization and hydrolysis (which may decrease T_g of the polymer) and higher probability of fibre/matrix debonding may occur [113]. Therefore, as a result of higher moisture absorption in specimens exposed to 60 ˚C compared to ambient temperature, especially during early staged of conditioning, higher reductions in compressive strengths were observed. The strength reduction difference between the different temperatures is more obvious in CC and CS compared to SS. This shows that alkaline solution penetration through the thickness of the samples is more critical than the seawater penetration.

As is seen in **Figure 7-13**, the compressive elastic modulus reduction in all tubes exposed at 60 ºC is higher than that of the corresponding ones at 25 ºC. The higher moisture absorption along with the probable reduction of the T_g [254], which consequently leads to the degradation of the resin matrix mechanical properties of tubes exposed at 60 ºC compared to 25 ºC may be counted as the possible reasons for this reduction variations.

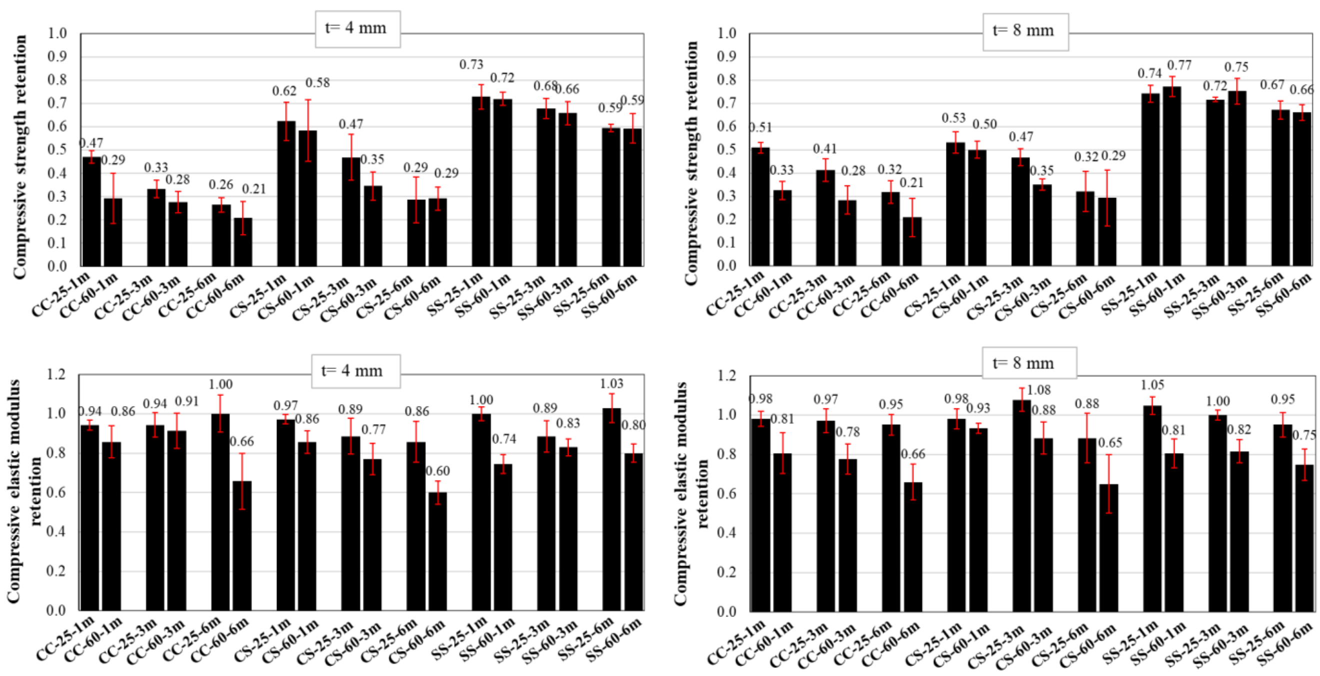

Figure 7-13 Comparison of the compressive strength and elastic modulus between 25 ºC and 60 ºC conditions

Figure 7-14 compares the average ultimate tensile strength and elastic modulus of GFRP tubes based on the conditioning temperature. As expected, similar to compressive results, reductions of the samples exposed to higher temperature is greater than the ambient for all different conditions. Regarding the variations in tensile elastic modulus, the same trend compared to the tensile strength results was observed for most of the cases.

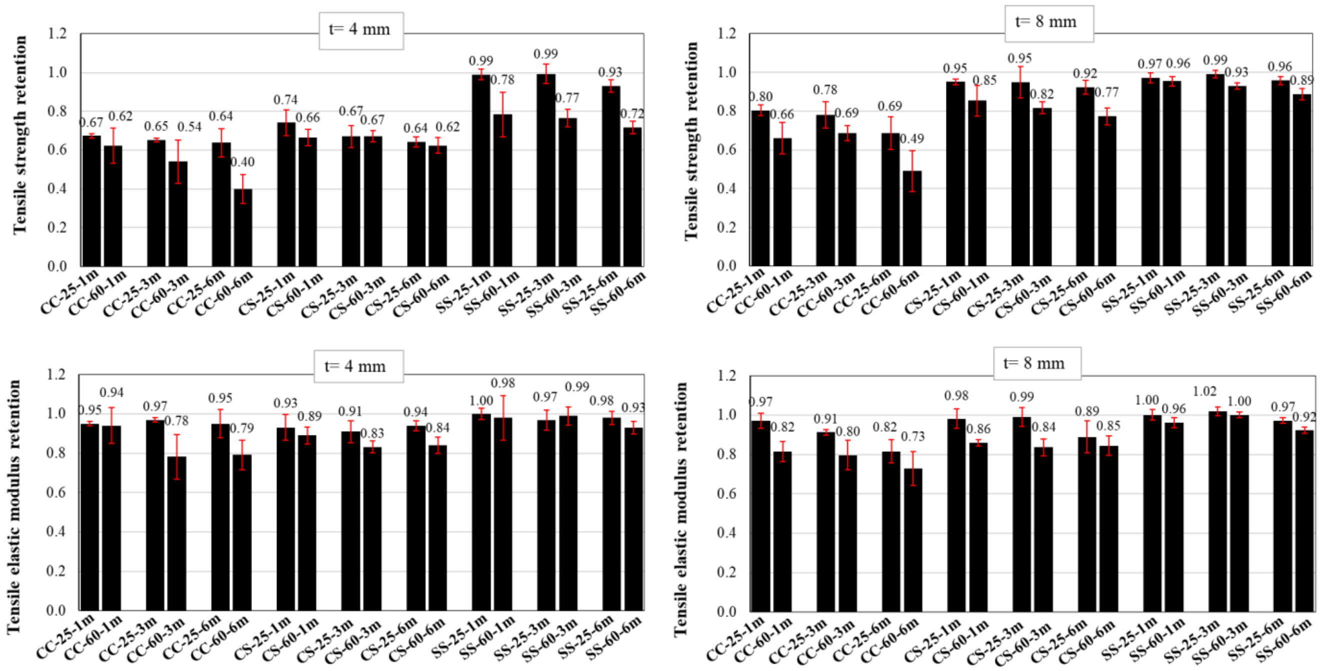

Figure 7-14 Comparison of the tensile strength and elastic modulus between 25 ºC and 60 ºC conditions

7.3.5.3 Effect of conditioning time

Figure 7-15 compares the average ultimate compressive strength and elastic modulus retention of GFRP tubes based on the conditioning time. As expected, it is seen that the compressive strength reduction increases with the time of conditioning for all environmental conditions. However, regarding the compressive elastic modulus variation, this reduction did not happen for all conditions. This shows the lower dependency of the elastic modulus compared to the compressive strength to the environmental conditions. The reason for this different trend in elastic modulus values could be the possible post curing of the resin [255] and/or the randomness in the sample properties.

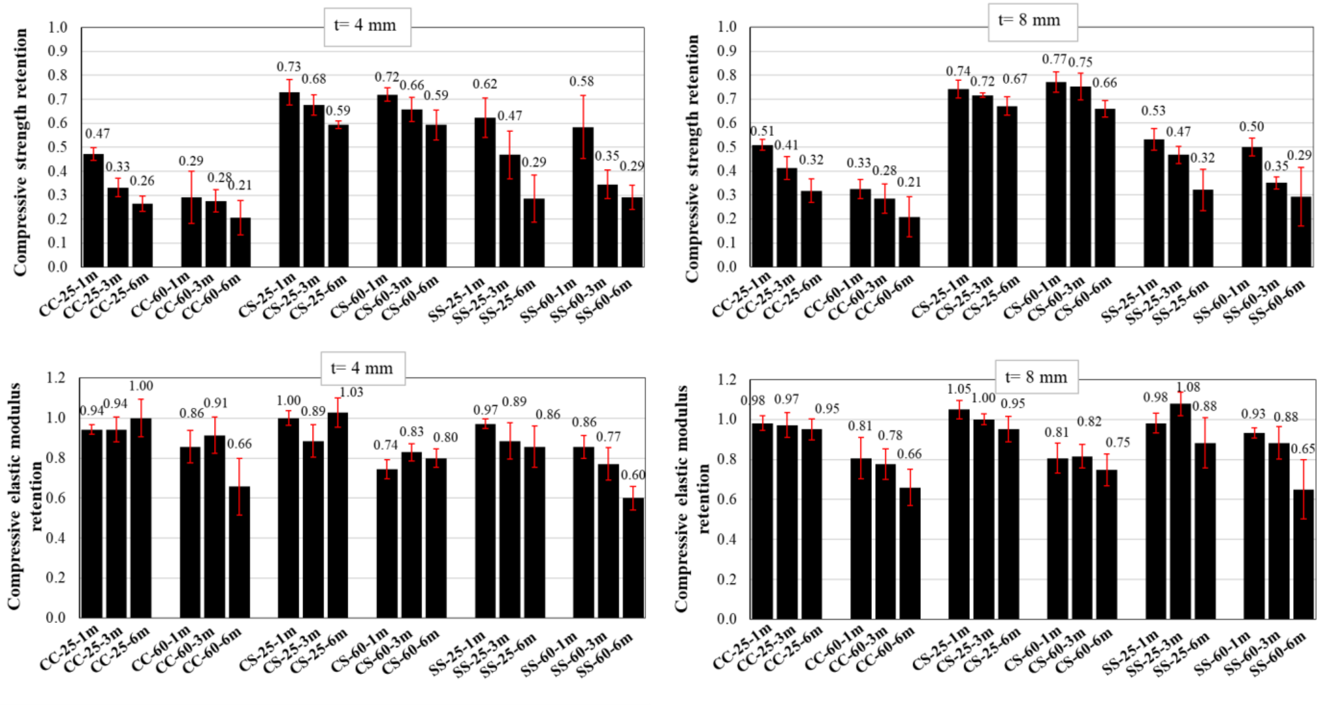

Figure 7-15 Comparison of the compressive strength and elastic modulus between 1, 3 and 6 month of conditioning

Figure 7-16 compares the average ultimate tensile strength and elastic modulus of GFRP tubes exposed for different conditioning times. As is seen for all conditions except two, the greater the time of exposure, the higher is the strength reduction. However, the reduction rate due to the time increment seems to be lower in tensile strength compared to the compressive strength. This also confirms that the tensile properties of GFRP tubes are less vulnerable to environmental conditioning compared to the compressive properties. Similar to the compressive elastic modulus variations, due to the possible post curing of the resin and/or the randomness in the sample properties, no recognizable trend in tensile elastic modulus variations based on the conditioning time, was observed.

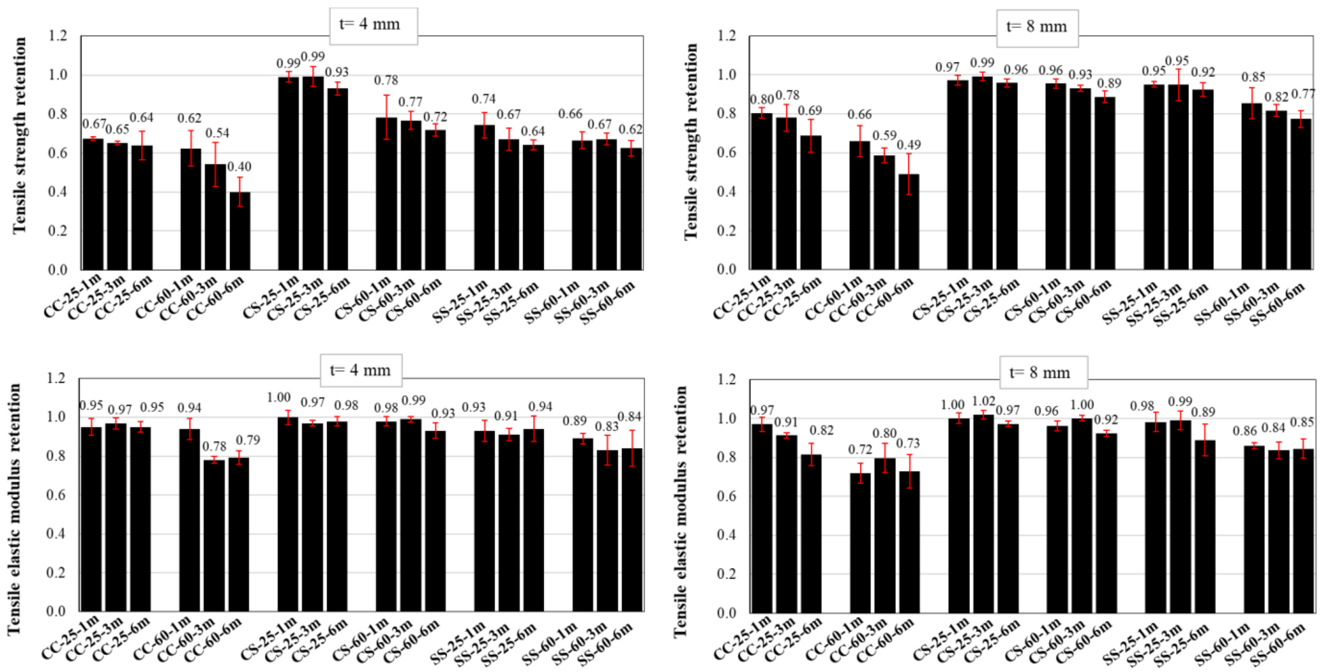

Figure 7-16 Comparison of the tensile strength and elastic modulus between 1, 3 and 6 month of conditioning

7.3.5.4 Effect of thickness

Figure 7-17 compares the average ultimate compressive strength and elastic modulus retention of GFRP tubes based on the tube thickness. It is seen for all cases, except one-month conditioning in CS (which may be due to the sample randomness and high CV%), the compressive strength reduction values under different environments are greater in 4 mm tubes compared to 8 mm. The greater strength reduction of the thinner tubes compared to the thicker tubes may be due to the greater fraction of tube thickness getting penetrated by solution and getting degraded. Regarding the elastic modulus variations, it can be seen that no specific trend regarding the effect of the tube thickness can be specified. This shows that the thickness of the samples may not have significant effect on the compressive elastic modulus variation of GFRP tubes exposed to different environmental conditions.

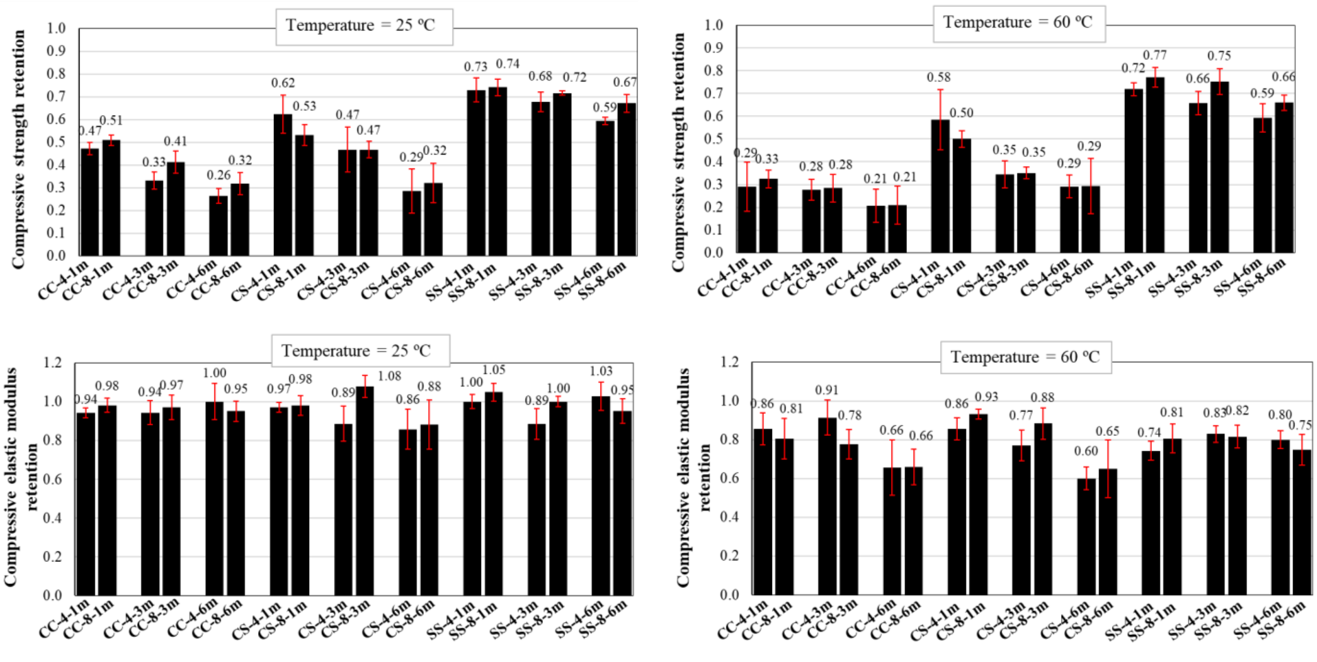

Figure 7-17 Comparison of the compressive strength and elastic modulus between 4 mm and 8 mm tubes

Figure 7-18 compares the average ultimate tensile strength and elastic modulus of GFRP tubes of different thicknesses. As is seen, similar to the compressive strength variations, in all cases (except one-month conditioning in SS at 25º C), the tensile strength reduction values under different environments are larger in 4 mm tubes than in the 8 mm tubes. The reason for the un-expected observation of tubes exposed to 25 º C seawater for 1 month, may be due to the low adverse effect of that environment (the reduction values are within the CV% domain). No specific trend regarding the tensile elastic modulus variations reveals that the tube thickness may not have a significant effect on the tensile elastic modulus GFRP tubes exposed to different environmental conditions.

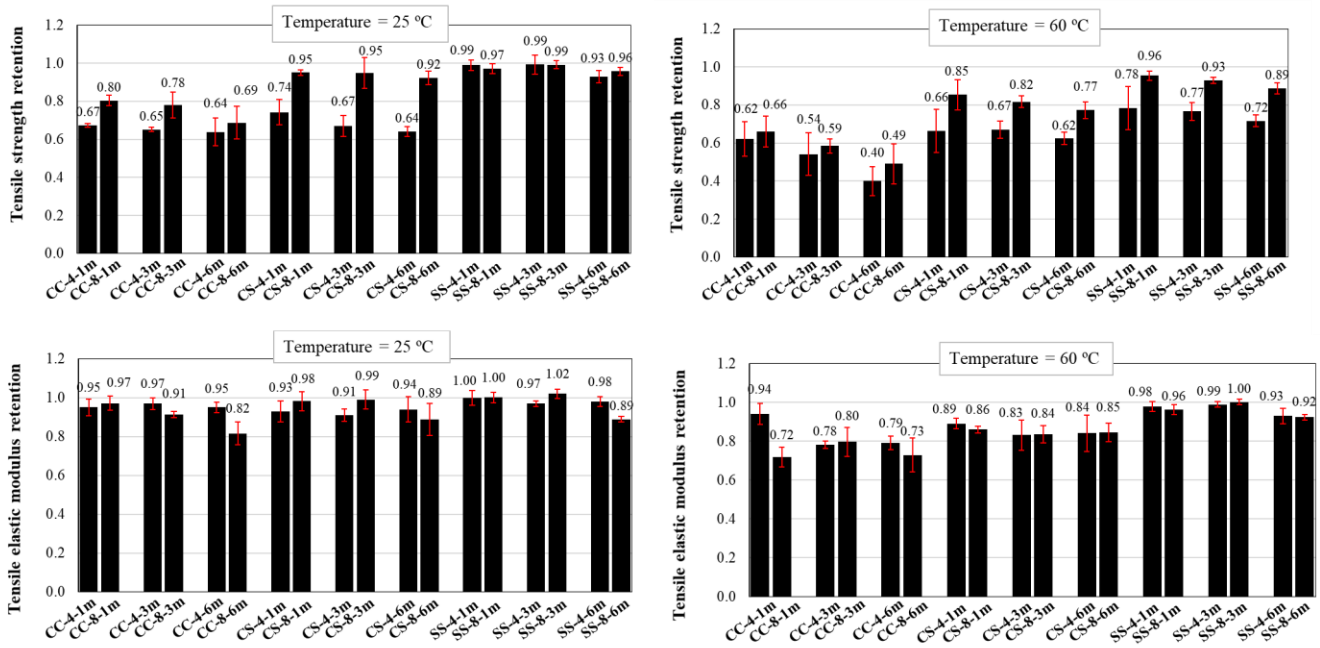

Figure 7-18 Comparison of the tensile strength and elastic modulus between 4 mm and 8 mm tubes

7.4. Comparison of results with relevant research

To better understand the adverse effect of SWSSC and seawater on the mechanical properties of GFRP composites, some of the results observed in the present study is compared with those reported by other researchers regarding different environmental conditions. However, as there are very limited number of studies focused on the durability of GFRP profiles (i.e. most of the studies are focused on the coupon samples), a widely comparison, especially for compressive properties may not be achieved. **Table 7-6** and **Table 7-7** list the tensile and compressive properties results of different GFRP composites after exposing to different environmental conditions, respectively. It is generally seen, that a significant tensile and compressive strengths reduction is observed when samples exposed to alkali environments, especially at elevated temperatures. Regarding the seawater condition, based on the reported data, it can be concluded that salt may not increase the adverse effect of water solution considerably. Moreover, CFRP composites are significantly more resistant to the environmental conditioning than GFRP and BFRP do. However, because of various differences in test and conditioning parameters in different studies, such as material mechanical properties, thickness, time and temperature conditioning, an accurate comparison may not be achieved.

Table 7-6 Comparison between the tensile test result of the present study and similar research

Reference	FRP Type	Sample thickness (mm)	Environmental condition	Results
Present study	GFRP vinylester pultruded tubes	4	CC, CS and SS at 25 ºC and 60 ºC for 6 months	37 %, 36% and 7 % reductions in tensile strengths at 25 ºC, and 60 %, 38% and 29 % at 60 ºC for CC, CS and SS, respectively 5 %, 6% and 2 % reductions in tensile modulus at 25 ºC, and 21 %, 16% and 7 % at 60 ºC for CC, CS and SS, respectively
[24]	GFRP vinylester pultruded coupons (cut from rectangular tube)	5	demineralised water and salt water at 60 ºC	38 % and 21 % reductions in tensile strength and elastic modulus after 18 months of immersing in water, respectively. 29 % reduction in tensile strength after 9 months and 5 % reduction in elastic modulus after 18 months of immersing in saltwater, respectively.
[256]	Unidirectional CFRP, GFRP and BFRP epoxy pultruded sheets	NA	Water, alkaline (normal concrete) and salt solutions at 55 ºC for 66 days	15 %, 33 % and 18 % reductions in tensile strength of BFRP subjected to water, alkaline and salt solutions, respectively. 19 %, 29 % reductions in tensile strength of GFRP subjected to water and alkaline solutions, respectively. No significant changes in tensile strength CFRP composites No significant changes in elastic modulus of all composites
[257]	Unidirectional CFRP epoxy pultruded sheets	1.2	Distilled water and alkaline (normal concrete) solution with pH = 12.4 for 2 years at ambient temperature	1.49% and 6.34% reductions in tensile strength and 1.15% and 4.35% reductions in tensile modulus for distilled water and alkaline solution, respectively
[258]	Unidirectional GFRP vinylester pultruded coupons	6.4	de-ionized water at 25 ºC for 380 days	29 % and 23 % reductions in tensile strength and elastic modulus, respectively

Table 7-7 Comparison between the compressive test results of the present study and similar research

Reference	FRP Type	Sample thickness (mm)	Environmental condition	Results
Present study	GFRP vinylester pultruded tubes	4	CC, CS and SS at 25 ºC and 60 ºC for 6 months	74 %, 71% and 41 % reductions in compressive strengths at 25 ºC, and 79 %, 71% and 41 % at 60 ºC for CC, CS and SS, respectively
[113]	GFRP vinylester pultruded tubes	8	Sea water at 20 ºC and 60 ºC and alkaline (normal concrete) solution with pH = 13.6 for 5 months	20 %, 27 % and 41 % reductions in compressive strengths for 20 ºC seawater, 60 ºC seawater and alkaline solutions, respectively
[259]	A three-cell GFRP isophthalic polyester pultruded profile		Alkaline solution at 20, 40, and 60°C with pH = 13.4 for 18 months	About 45%, 60 % and 85 % reductions in compressive strengths for 20 ºC, 40 ºC and 60 ºC, respectively

7.5. Long-term performance prediction of GFRP tubes

In order to predict the long term performance of FRP composites, following models were proposed by other researchers, based on the Arrhenius theory [260] and assuming the degradation mechanism as the fibre/matrix interface debonding [4, 94, 96]:

$$Y = 100\exp(-\frac{t}{\tau}) \tag{7.1}$$

$$Y = (100 - Y_{\infty})\exp(-\frac{t}{\tau})+Y_{\infty} \tag{7.2}$$

where Y is the mechanical properties retention (%); t is the exposing time; τ is regression fitting parameter; and $Y\infty$ is the mechanical properties retention (%) at exposing time of infinity.

Between the proposed models, **Eq. 7.2** was found to be successfully used to predict the long-term compressive and tensile strengths retention of GFRP pultruded tubes exposed to SWSSC and seawater environments. Therefore, in this study, the results of accelerated short-term tests of tubes exposed to SWSSC as the inner condition and seawater as the outer condition were analysed according to **Eq. 7.2** to predict the long-term performance of such materials when used with SWSSC under seawater environment. Similar to [4], four locations in Canada were selected as the target places for predictions.

Briefly, the prediction procedure for each specimen type (e.g. tensile strength retention of 8 mm tubes) include four steps. Step 1 is finding regression fitting parameter, τ, for different temperature. For this purpose, **Eq. 7.2** is fitted to the test results for each temperature (**Figure 7-19**). It should be mentioned that Y∞ value obtained through fitting the results of 60 ˚C is used for 25 ˚C and 40 ˚C for each condition. The results are shown in **Table 7-8.**

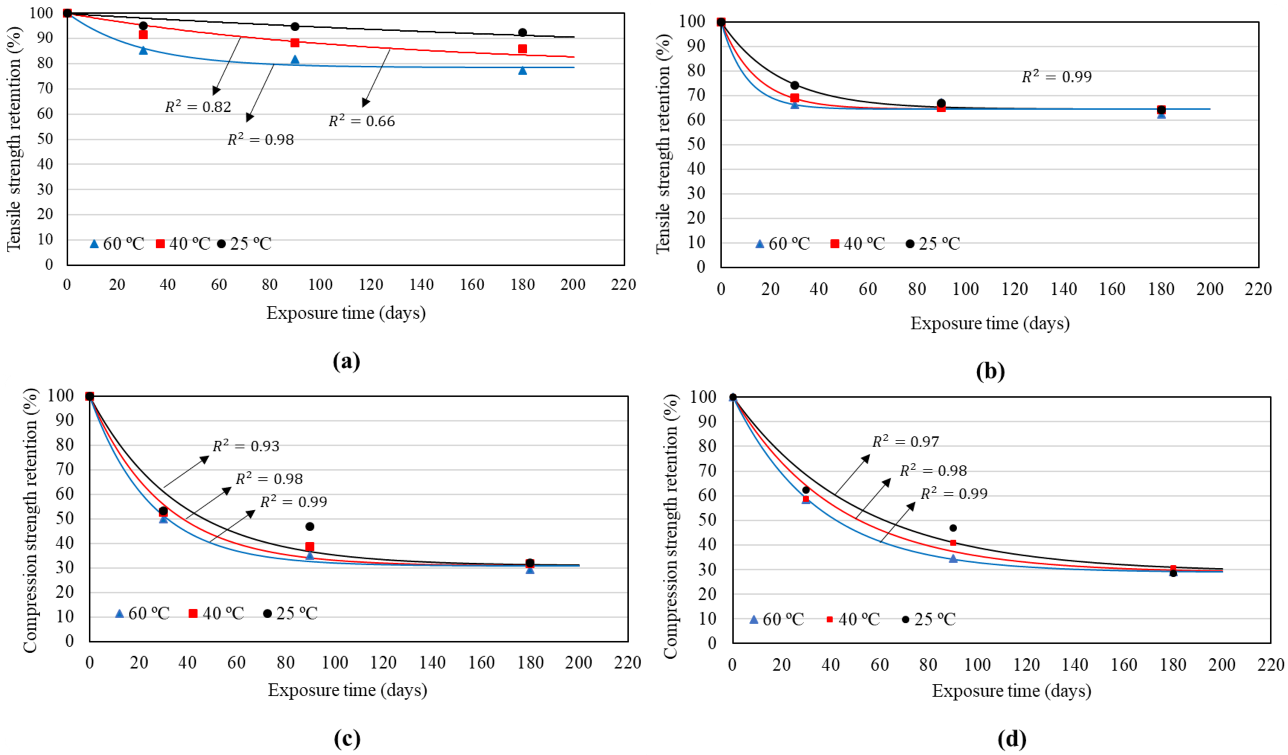

Figure 7-19 Fitted curves using Eq.2: (a) 8 mm tensile samples exposed to CS, (b) 4 mm tensile samples exposed to CS, (c) 8 mm compressive samples exposed to CS and (d) 4 mm compressive samples exposed to CS

Step 2 is to find $\frac{E_a}{R}$ (the slope of Arrhenius plots) for each specimen type, where E_a is the activation energy and R is the universal gas constant. For this purpose, the logarithm of time (ln(t)) needed for the retention (%) of samples to reach a certain value (i.e. 95%, 90%, 85% and 80% in this paper) at different exposure temperatures versus 1000/T (1/K) is drawn. In order to obtain ln (t) at different temperatures, **Eq. 7.2** with τ values from **Table 7-8** is used. The slope of the parallel diagrams is $\frac{E_a}{R}$ for each sample type.

Figure 7-20 shows the Arrhenius plots and $\frac{E_a}{R}$ for each specimen type. **Table 7-9** compares the results of $\frac{E_a}{R}$ values obtained in the present study with the values reported by other researchers for different material types and environments. Different values of $\frac{E_a}{R}$ represent different degradation rate and possibly different degradation mechanisms [98]. Various factors, such as profile type (i.e. FRP bars or FRP sections), fibre and resin matrix type, fabrication method, environmental temperature and conditions may be some possible reasons for these differences. It should be mentioned that no similar research was found in the literature regarding the prediction of the compressive properties of FRP composites.

Table 7-8 Regression coefficients in Eq. 7.2

Specimen type	Temperature (˚C)	τ	Y∞
8 mm- Tensile samples	25	349.19	78.63
	40	121.22	78.63
	60	28.95	78.63
4 mm- Tensile samples	25	23.93	64.56
	40	14.32	64.56
	60	10.17	64.56
8 mm- Compressive samples	25	36.44	30.68
	40	29.75	30.68
	60	24.78	30.68
4 mm- Compressive samples	25	50.94	28.84
	40	42.65	28.84
	60	34.73	28.84

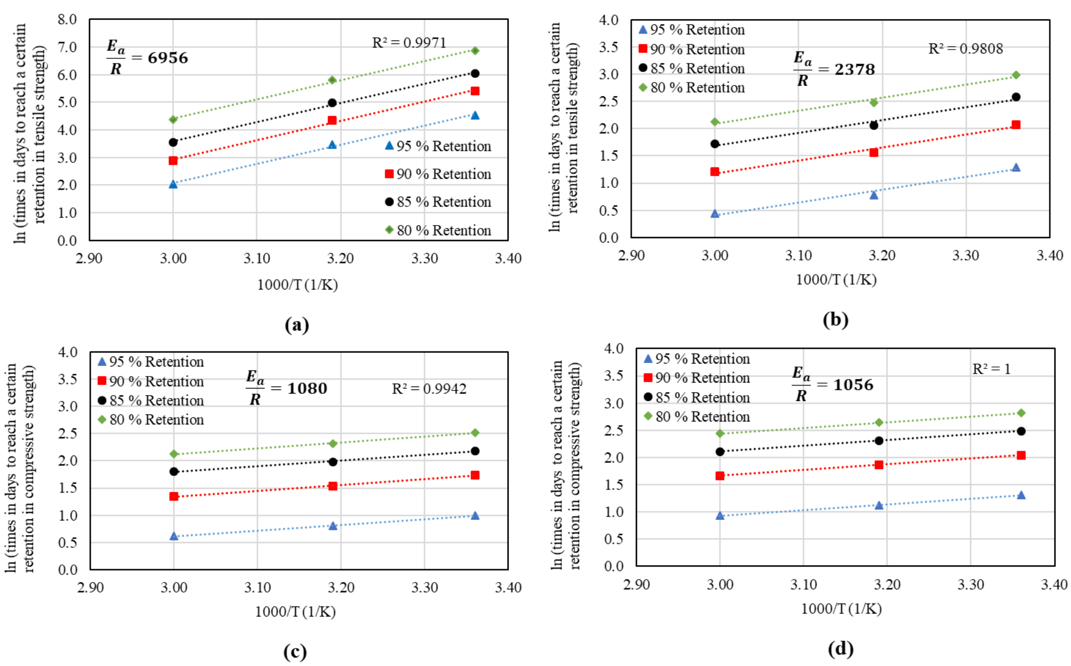

Figure 7-20 Arrhenius plots (a) 8 mm tensile samples exposed to CS, (b) 4 mm tensile samples exposed to CS, (c) 8 mm compressive samples exposed to CS and (d) 4 mm compressive samples exposed to CS

Table 7-9 Comparison between the Ea/R results of the present study and similar research in the literature

Reference	**FRP Type**	**Environmental condition**	**Model Used**	**Ea/R**
Present study	GFRP pultruded tubes	normal SWSSC and seawater	Eq.2	6956 for 8 mm tubes 2378 for 4 mm tubes
Wang et al. **[4]**	BFRP bars	high performance SWSSC	Eq.1 and Eq.2	8039 for Eq.1 9369 for Eq.2
Wang et al. **[99]**	BFRP bars	normal SWSSC	Eq.1	11567
Chen et al. **[98]**	Two types of GFRP bars	normal and high performance concrete solutions	Eq.1	4890 for type1 and 1420 for type 2
Wu et al. **[96]**	BFRP bars	alkaline solution	Eq.1	7519

Step 3 is to find the time shift factor (TSF) using **Eq. 7.3**:

$$TSF = \exp[\frac{E_a}{R}(\frac{1}{T_0} - \frac{1}{T_1})] \quad (7.3)$$

where T_0 is the lower temperature (mean temperature of each four locations in Canada in this study) and T_1 is the higher temperature (exposure temperature in this study). **Table 7-10** lists the TSF of each four locations in Canada with T_0 as their annual mean temperature.

Table 7-10 TSF for GFRP tubes exposed to SWSSC and seawater solutions

Specimen type	**Temperature**	**Ea/R**	**TSF**			
			Waterloo Creek Bridge (9.9 ˚C)	Hall's Harbor Wharf (7.6 ˚C)	Chatham Bridge (4.6 ˚C)	Crowchild Trail Bridge (3.9 ˚C)
8 mm- tensile samples	25	6957	3.48	4.25	5.56	5.92
	40	6957	10.64	13.02	17.02	18.13
	60	6957	40.44	49.47	64.67	68.90
4 mm- tensile samples	25	2378	1.53	1.64	1.80	1.84
	40	2378	2.24	2.40	2.63	2.69
	60	2378	3.54	3.79	4.16	4.25
8 mm- Compressive samples	25	1080	1.21	1.25	1.31	1.32
	40	1080	1.44	1.49	1.55	1.57
	60	1080	1.78	1.83	1.91	1.93
4 mm- Compressive samples	25	1056	1.21	1.25	1.30	1.31
	40	1056	1.43	1.48	1.54	1.55
	60	1056	1.75	1.81	1.88	1.90

At the last step, master curves are drawn by fitting **Eq. 7.2** to the transformed results. Transformed results, which are obtained by multiplying the TSF with the corresponding exposure times at different temperatures, and the fitted curves are shown in

Figure 7-21 for each condition. The results are shown in **Table 7-11**. ACI 440.1R-06 recommends an environmental reduction factor of 0.7 for GFRP bars embedded in concrete. As is seen in

Figure 7-21a (using model 2) 8 mm GFRP tubes do not reach below 70 % of their tensile strengths in all four locations in Canada (i.e. the maximum reduction is about 22 %) in their lifetime. This shows that the reduction factor proposed in ACI 440.1R-06 is conservative for thicker GFRP tubes. For thinner GFRP tubes, it can be seen that the tensile strength of GFRP tubes may drop 30 % at the early conditioning periods (i.e. just after 2 to 3 months of conditioning). However, the maximum reduction for all four locations converge to about 35 % (i.e. a reduction factor of 0.65) for the whole lifetime. In this case, the ACI 440.1R-06 factor may slightly underestimate the reduction. Regarding the compressive strengths, a significant reduction factor (about 0.3) should be considered for both thinner and thicker GFRP tubes if the failure mode is the same as the present study.

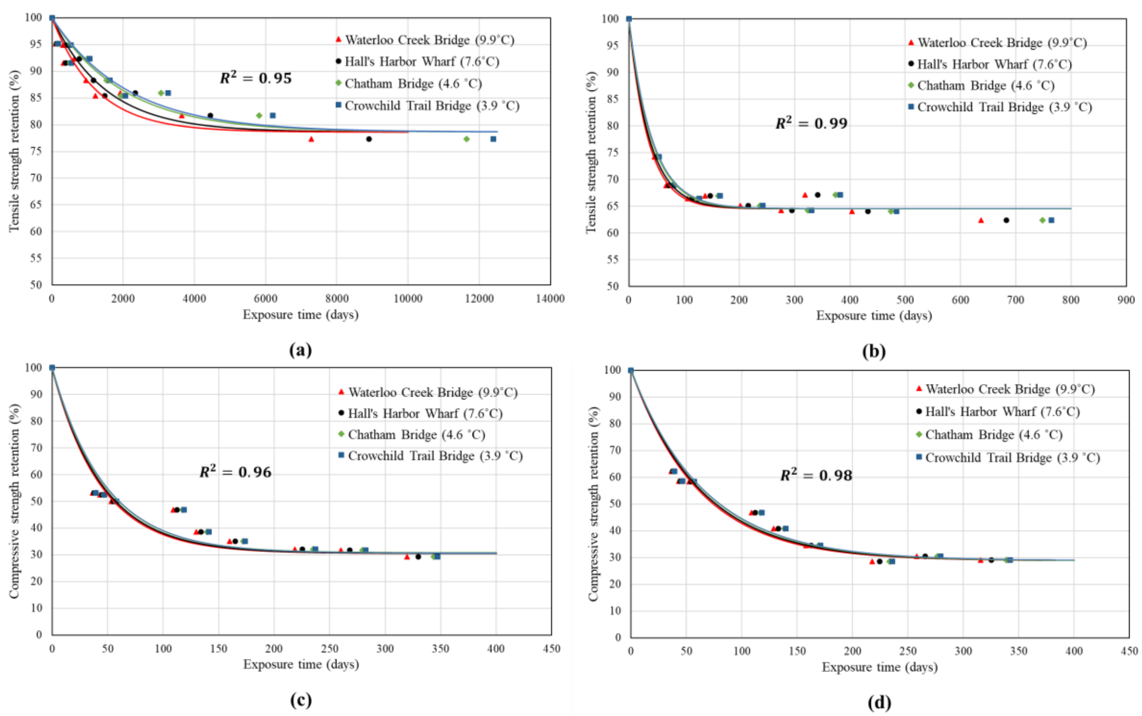

Figure 7-21 Master curves of GFRP tubes exposed to SWSSC and seawater solutions: (a) 8 mm tensile samples, (b) 4 mm tensile samples, (c) 8 mm compressive samples and (d) 4 mm compressive samples

Table 7-11 Regression coefficients in Eq. 7.2 for master curves

Specimen type	**Structure (mean annual temperature ˚C)**	**τ**	**Y∞**
8 mm- Tensile samples	Waterloo Creek Bridge (9.9 ˚C)	1236.0	78.6
	Hall's Harbor Wharf (7.6 ˚C)	1512.0	78.6
	Chatham Bridge (4.6 ˚C)	1977.0	78.6
	Crowchild Trail Bridge (3.9 ˚C)	2106.0	78.6
4 mm- Tensile samples	Waterloo Creek Bridge (9.9˚C)	34.9	64.6
	Hall's Harbor Wharf (7.6 ˚C)	37.3	64.6
	Chatham Bridge (4.6 ˚C)	40.9	64.6
	Crowchild Trail Bridge (3.9 ˚C)	41.8	64.6
8 mm- Compressive samples	Waterloo Creek Bridge (9.9˚C)	43.7	30.7
	Hall's Harbor Wharf (7.6 ˚C)	45.1	30.7
	Chatham Bridge (4.6 ˚C)	47.0	30.7
	Crowchild Trail Bridge (3.9 ˚C)	47.5	30.7
4 mm- Compressive samples	Waterloo Creek Bridge (9.9˚C)	61.2	28.8
	Hall's Harbor Wharf (7.6 ˚C)	63.1	28.8
	Chatham Bridge (4.6 ˚C)	65.7	28.8
	Crowchild Trail Bridge (3.9 ˚C)	66.4	28.8

7.6. Conclusions

The present study is part of an ongoing project with the aim of using FRP composites, as corrosion resistant reinforcement materials in seawater sea sand concrete. The mechanical and microstructural properties of pultruded GFRP tubes after exposure to artificial SWSSC and seawater conditions were studied using tensile and compressive tests, SEM and micro-CT-X. Following conclusions are drawn:

- SWSSC environment is a considerably harsher condition for GFRPs compared to seawater. The mechanical properties of GFRP tubes decreases with increase in time and temperature of the conditioning. The mechanical properties reduction of thicker specimens under different environments is lesser than thinner samples. The maximum ultimate compressive strength reductions of 79, 71 and 34% were observed for 8- mm GFRP tubes after exposure to of SWSSC for 6 months (both inside and outside conditions), SWSSC (inside condition) and seawater (outside condition), and seawater (both inside and outside conditions) at 60 ºC respectively. The maximum ultimate tensile strength reductions of 51, 23 and 21% were observed for GFRP tubes after exposure to 6 months of CC, CS and SS at 60 ºC respectively.

- Elastic modulus of GFRP tubes, compared to the mechanical strengths, is significantly less affected by the environmental conditions (i.e., maximum tensile elastic modulus reduction about 28% compared to maximum tensile strength reduction about 60% among all the samples). Tensile properties of GFRP tubes under harsh environments shows lower reductions compared to compressive properties (i.e., maximum tensile strength reduction about 60 % compared to maximum compressive strength reduction about 80% among all the samples).
- Microstructural studies show that GFRP composites experience various damages, including resin cracking, resin leaching, significant resin/matrix debonding and fibre damage when exposed to SWSSC condition. However, the main morphology observations of tubes exposed to seawater solution are microcracks in the resin matrix, blisters and solid components and limited fibre/resin debonding.
- Micro-CT imaging shows that the voids percentage, especially near the areas exposed to SWSSC solution, increases considerably (e.g. from 0.25-2.162% in the reference sample to 5.6-11.72% in one of the samples exposed to 60 °C SWSSC and seawater for 6 months).
- In this study, based on the accelerated test data and long-term performance prediction of the tensile and compressive strength results, a reduction factor between 0.65-0.88 (based on the specimen thickness) is recommended for tensile strength of GFRP tubes exposed to SWSSC and seawater environments during their service life. Regarding the compressive strength reduction factor, if the failure mode of the tubes changed to elephant buckling, a reduction factor about 0.3 may be considered.

Chapter 8 Durability of seawater and sea sand concrete filled filament wound FRP tubes under seawater environments

Abstract

Using fibre reinforced polymer (FRP) composites together with seawater and sea sand concrete (SWSSC) in coastal areas will overcome the environmental issues of using ordinary concrete and corrosion problems of conventional steel reinforcements. The present research investigates the mechanical properties of different SWSSC filled FRP tubes after exposure to seawater. Glass, carbon, and basalt filament wound FRP tubes were filled with SWSSC and exposed to seawater for different exposure durations at different temperatures. A total number of 567 Hoop tension and compression tests were carried out after conditioning to investigate the mechanical properties degradation of the tubes. In addition, scanning electron microscopy (SEM) and micro computed tomography (micro-CT) analyses were conducted on representative samples to study the degradation mechanisms and damage progression. Finally, the long-term mechanical performance of SWSSC filled tubes under seawater was predicted based on Arrhenius theory and using the experimental data. According to the test data, generally, the samples with multiple fibres direction showed better durability compared to the tubes with fibres oriented in hoop directions. Moreover, carbon tubes experienced the smallest degradation while glass and basalt tubes showed almost the same range of degradation.

Keywords

Seawater and sea sand concrete; FRP; filament winding; durability; Mechanical properties; SEM; micro-CT

8.1. Introduction

Production of conventional concrete demands use of huge amounts of river sand and fresh water, which can cause environmental and ecological problems, as well as the sand and water shortages created by the massive demand. To address these issues, seawater and sea sand concrete (SWSSC) could be an attractive alternative to conventional concretes, especially in coastal areas [261]. In SWSSC, fresh water and river sand are replaced with their sea-based equivalents [237, 262]. By using geo-polymers in SWSSC, namely slag and fly ash, the alkali silica reaction (ASR) and its accompanied probable cracking, common in traditional concretes, is highly reduced [11, 216]. Furthermore, previous research has shown that the mechanical properties of SWSSC are almost identical to those of the conventional concretes [10, 263]. SWSSC can be used as one of the main materials in structural supports, however, the corrosion resistance of traditional steel reinforcements will be unacceptably poor due to the high chloride content in seawater [12, 13]. To address the corrosion concern, particularly in the aggressive environments like marine settings, researchers have suggested using fibre-reinforced polymer (FRP) composites as corrosion-resistant materials instead of traditional steel [7, 8, 128, 183, 220]. FRP composites offer several other outstanding characteristics, such as high strength/stiffness-to-weight ratio, ease of fabrication and handling, and nonmagnetic properties [63, 113, 218, 229]. Carbon, glass, aramid, and basalt are different types of fibres used in FRP composites. Among these four types, basalt FRP (BFRP) composites have attracted attention recently due to their unique characteristics, such as the abundance of raw materials available to produce BFRP, its environmental friendliness, and its relatively low cost when compared to carbon FRP (CFRP) [103, 264].

In spite of the advantages of FRP as concrete reinforcements in marine environments, they are reported [17, 113] to be vulnerable when exposed to alkali environments (particularly concrete environments). Therefore, it is deemed necessary to investigate the durability of FRPs when used as reinforcement for reinforced-concrete (RC) structures [130, 265]. The degradation mechanisms of FRP composites under aggressive environments, such as alkaline, acidic, and seawater settings, include the deterioration of the resin matrix [29], fibre damage [18], and the weakening of the fibre/resin interface [30]. Types of damage caused by resin matrix degradation include swelling, delamination, plasticization, cracking, and alkaline hydrolysis (in polyester and vinyl ester); such damages may occur due to moisture absorption and chemical diffusion [31-33, 266]. Glass/basalt-fibre damage is caused when metallic cations leach out of the fibre surface and when the Si-O-Si bond is broken by hydroxyl ions (etching) [34]. However, the degradation rate of basalt fibre is higher due to the chemical reaction between aluminium, iron and magnesium contents of basalt with alkali and chloride in concrete environments [249]. It is generally accepted that carbon fibres are generally resistant to chemical environments [36]. Finally, the deterioration of the fibre/resin interface is caused by matrix osmotic cracking, delamination, and interfacial debonding [37]; the interface deterioration is the main reason why the mechanical properties of FRP composites degrade in aggressive environments [38].

Many studies have investigated the durability and long-term performance of FRP composites under different environmental conditions, such as harsh daily conditions, alkaline, acidic, and seawater contexts [18, 71, 73, 106, 113, 256, 267-271]. Most of these studies have examined the durability of FRP composites in alkaline environments created by traditional concrete (ordinary, Portland cement-based concrete) [17, 113]. There are a very limited number of studies available on the durability of FRP composites in SWSSC environments [4, 12, 99, 230].

The concrete-filled FRP tube (CFFT) is one among many construction applications of FRP composites used in corrosive environments (e.g., coastal areas such as bridge piers, drilling platforms, and high-rise buildings) to overcome the corrosion problems related to concrete-filled steel tubes (CFSTs) [101, 102]. Recently, many researchers have been attracted to the idea of using SWSSC with FRP composites tubes because the two are compatible materials that are both suitable for marine environments; this idea was first presented by Teng [104].

The studies conducted on CFFTs, and particularly the SWSSC-filled tubes, primarily focused on their short-term mechanical properties [113, 272-274]. However, to the best knowledge of the authors, their durability under environmental conditions has gathered very limited attentions [200, 230, 275]. Among these studies, those on the durability of CFFT compressive strength could not provide sufficient knowledge in terms of the FRP tube individual components (i.e. in the level of macro, including the mechanical properties of the tubes and micro, including the degradation mechanisms). Robert and Fam [275] investigated the long-term performance of CFFTs subjected to a salt solution and showed that filament-wound glass FRP (GFRP) tubes lost 11% and 21% of their hoop strength after exposure for 365 days to the solution at 23 °C and 50 °C, respectively. More recently, Bazli et al. [230] studied the tensile and compression strengths and modulus degradation of pultruded GFRP tubes after exposure to SWSSC and seawater environments. Based on the accelerated test results and long-term prediction models, tensile strength reduction factor between 0.65 to 0.88 (with respect to tube thickness) and compressive strength reduction factor about 0.3 were proposed by the authors for SWSSC pultruded GFRP tubes expose to seawater.

Despite these studies, the literature would suggest that there are still several factors, such as the fabrication process, fibres types, and fibres orientation that may have effect on the durability of CFFTs under seawater, which have not been studied yet. To address the existing research gap, this study focuses on the degradation of the mechanical properties of different filament wound FRP tubes (GFRP, CFRP, and BFRP), specifically, tubes with two different fibre orientations that are filled with SWSSC (inner side environment) and subjected to seawater (outer side environment).

8.2. Experimental Program

This study is a part of a comprehensive research project that examines the performance and durability of FRP composites as an alternative material for conventional steel reinforcement subjected to corrosive environments, including SWSSC and seawater. In the present study, the durability of FRP filament wound tubes exposed to SWSSC as the inner condition and seawater as the outer condition was studied. With this regard, a comprehensive experimental study was carried out by conducting a total number of 567 mechanical tests. GFRP, CFRP, and BFRP tubes with two different fibres orientation were constructed, and then filled with SWSSC and exposed to seawater. The tubes were exposed for 1, 3, and 6 months at the ambient (23 ºC), 40 ºC, and 60 ºC. After conditioning, mechanical tests, including split-disk tensile and compression tests, were carried out to investigate the degradation of FRP tubes in both hoop and longitudinal directions. Furthermore, SEM and micro computed tomography (micro-CT) analyses were conducted on some selected specimens at different times to investigate the degradation mechanisms. Finally, the long-term performance of FRP tubes' mechanical properties under the environmental condition was predicted using accelerated experimental results based on the Arrhenius law.

8.2.1 Materials

8.2.1.1 FRP tubes

In this study, filament wound FRP tubes were used to construct the CFFTs. The tubes were made of epoxy resin and continuous fibres (glass, carbon, and basalt) oriented in two patterns: (1) 20% in 15°, 40% in 40°, and 40% in 75° to provide the appropriate strength and stiffness in both the longitudinal and hoop directions; (2) 100% in 89° to investigate the effect of fibre orientation. The fibre and resin were mixed with the volumetric percentage ratios of 60% to 40%, respectively, for CFRP and GFRP, and 70% to 30%, respectively, for BFRP tubes. The average mechanical properties of FRP coupon tests are used as "reference" in this paper.

8.2.1.2 Seawater sea sand concrete (SWSSC)

There are several studies in the literature that the real condition of concrete environment has been simulated by alkaline solution (dissolving chemical compositions in distilled water), which contains the same chemical compositions of the targeted concrete type. However, due to faster movement of OH^- ions in a solution compared to a fresh/hardened concrete, the degradation level of FRPs in simulated concrete solution may be higher than that of the real concrete environment [5]. Therefore, both real SWSSC and simulated solution were used to investigate the effect of using solution instead of real concrete.

Alkaline activated, slag based, seawater and sea sand concrete (SWSSC) was used to fill the FRP tubes. The concrete mixture is: slag (360 kg/m^3), seawater (190 kg/m^3), sea sand (830 kg/m^3), coarse aggregate with maximum size of 14 mm (1130 kg/m^3), sodium meta-silicate (38.4 kg/m^3) and hydrated lime slurry (14.4 kg/m^3). A total of three batches of concrete were casted for specimens and the 28-day strengths were 37.3 MPa, 35.5 MPa, and 39.8 MPa for GFRP, CFRP and BFRP specimens, respectively. The seawater and sea sand used to cast the concrete were collected from Brighton beach in Melbourne, Australia.

Simulated normal SWSSC environment was prepared similar to previous studies [12, 230] by dissolving 35 g/l sodium chloride ($NaCl$), 19.6 g/l potassium hydroxide (KOH), 2.4 g/l sodium hydroxide ($NaOH$), and 2 g/l calcium hydroxide ($Ca(OH)_2$) in distilled water. The average measured pH of the SWSSC solution was about 13.4. It should be noted that the pH of the slag based SWSSC may be slightly lower than the cement-based SWSSC due to the high content of the slag. However, in order to compare the results [4, 12, 230, 249] with the previous studies, the same compositions were used to simulate SWSSC in the present study.

8.2.2 Specimens

In order to study the durability of filament wound FRP tubes filled with SWSSC under seawater, a total of 567 samples were tested under compression and split-disk tests. Two sets of samples were prepared: (1) samples filled with SWSSC and (2) samples filled with simulated SWSSC solution.

8.2.2.1 Specimens constructed with SWSSC

SWSSC-filled double-skin FRP tubes, which consisted of two concentric FRP tubes that sandwiched the concrete between the tubes. As a result, the inner surface of the outer tube and the outer surface of the inner tube experienced the SWSSC environment, i.e., same as the one experienced by a FRP tube fully filled with SWSSC. Therefore, the results inner tubes in double-skin specimens can be applied to fully filled specimens. The influence of corrosive environments combinations (inner seawater and outer concrete vs. inner concrete and outer seawater) can also be examined by comparing the performance of inner and outer tubes. **Figure 8-1** shows the structure of the of the double skin SWSSC FRP tube. The dimensions of the double-skin tubes are summarised in

Table 8-1, where D_i is outer diameter of inner tube, t_i is inner tube thickness, D_o is outer diameter of outer tube and t_o is outer tube thickness.

The specimens were classified into two groups: conditioned and unconditioned (reference) samples. With respect to conditioned samples, the 250 mm high SWSSC-filled double-skin FRP tubes were first prepared and cured at ambient temperature for 28 days. Then, the long FRP tubes were cut to be ready for conditioning. The concrete-filled GFRP and BFRP tubes were cut into 20 mm wide disks by diamond saws. The width for CFRP disks was 8 mm due to the limited capacity of test apparatus.

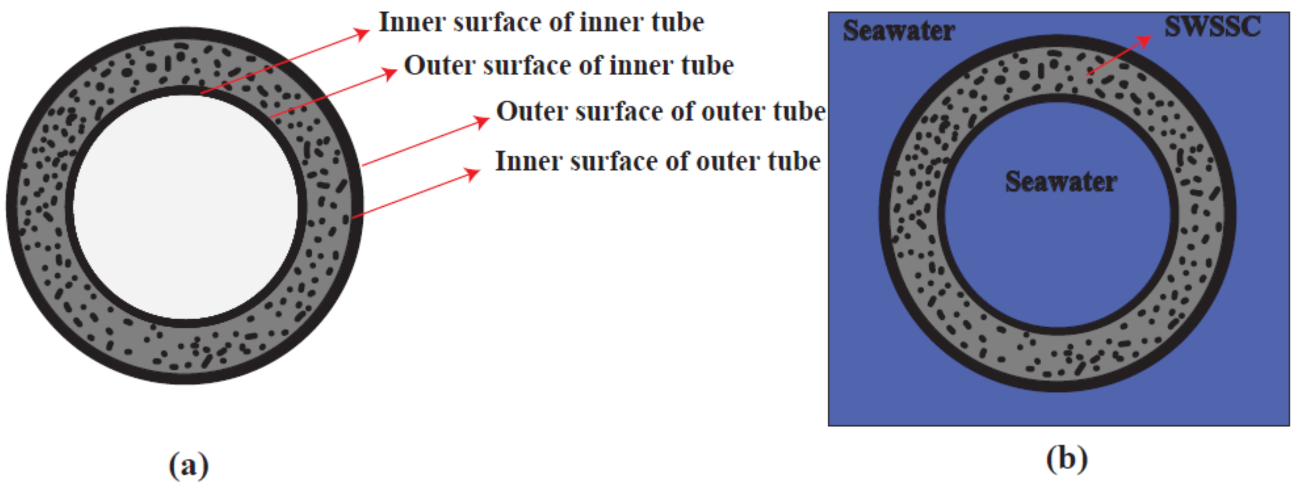

Figure 8-1 Configuration of the double skin SWSSC FRP tube: (a) before conditioning, and (b) after conditioning

Table 8-1 Dimensions of filament wound FRP tubes

FRP type	Inner tube		Outer tube	
	D_i (mm)	t_i (mm)	D_o (mm)	t_o (mm)
CFRP	99.9	2.8	158.1	2.8
GFRP	100.2	2.9	158.0	3.0
BFRP	100.0	2.9	157.7	2.7

8.2.2.2 Specimens constructed with simulated SWSSC solution

With respect to this set of samples, long FRP tubes that were cut into 250 mm, were fully filled with simulated SWSSC solution as the inner side condition. For this purpose, firstly, the FRP tube was sealed in one end with petri dish using epoxy resin. Then, SWSSC solution was poured inside the tube and the other end was sealed as well. After conditioning, for compressive tests, all types of tubes were cut into 50 mm. However, in order to conduct split-disk tensile tests, similar to double-skin samples, BFRP and GFRP tubes were cut into 20 mm wide disks and 8 mm for CFRP. The dimensions of the tubes used for fully filled samples are the same as inner tubes mentioned in

Table 8-1.

8.2.3 Environmental conditions

8.2.3.1 Specimens constructed with SWSSC

The degradation was conducted by fully immersing the samples into 3.5% NaCl solution (i.e. artificial seawater) in a beaker. For comparison purpose, some samples were also immersed in distilled water. The beakers containing specimens and solutions were placed in water tanks with temperature control and plastic films were fixed on the top of the beakers to avoid the evaporation of water. Samples were conditioned at three temperatures, including ambient temperature (23 °C), 40 °C and 60 °C for three immersion durations: 30, 90 and 180 days. The maximum aging temperature (i.e. 60 °C) was selected based on ACI 440.3R and CSA S806 standard recommendations [276]. 60 °C is much lower than the resin glass transition temperature, and it is believed that the degradation mechanisms are the same for the three temperatures.

After each period, three specimens were removed from the test vessels (beakers) and the sandwich concrete was removed for the split-disk tests.

8.2.3.2 Specimens constructed with simulated SWSSC solution

The 250 mm tubes, which were filled with SWSSC solutions were immersed in artificial seawater and exposed at the temperatures for durations as those for the double-skin samples. It is worth mentioning that the pH of the seawater solution was monitoring continuously to ensure no solution leakage occurred from inside the tubes into the seawater. **Figure 8-2** shows the details of the specimens prepared for each condition.

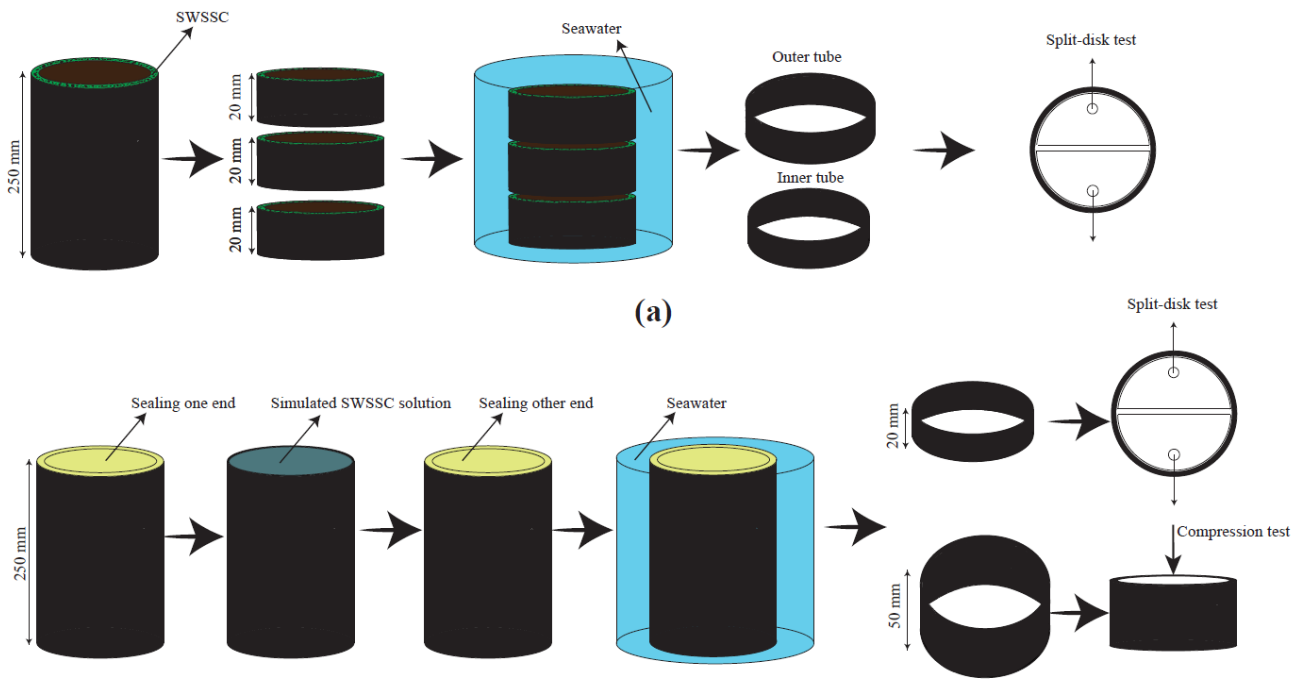

Figure 8-2 Experiments procedure: (a) double skin tubes: casting concrete, cutting the cured samples in several rings, conditioning, and knocking out the concrete for disk-split tests; and (b) fully filled tubes: sealing one end, pouring simulated SWSSC into the tube, sealing the other end, conditioning, and cutting the conditioned samples for mechanical tests

Table 8-2 summaries the type of specimens, conditioning details and the type of mechanical tests for each condition. It should be mentioned that three identical tests were conducted for each condition and the average result are used for discussions and conclusions. In total, 522 conditioned samples and 45 unconditioned samples were tested in this study.

Table 8-2 Specimens, conditioning, and test details

Specimen type	SWSSC type	Environment	Tube type	Duration (days)	Temperature (ºC)	Fibres orientation	Mechanical test	Number of specimens
double skin	fresh concrete	seawater	C/G/B FRP	30, 90, 180	23, 40, 60	multiple [1]	split-disk	162
		distilled water	G/B FRP	30, 90, 180	60	multiple	split-disk	36
fully filled	simulated solution	seawater	C/G/B FRP	30, 90, 180	23, 40, 60	multiple, 89 º	split-disk, compression	324
Total number of specimens	-	-	-	-	-	-	-	522

Note: 1: fibres in three different directions mentioned in section 8.2

8.2.4 Mechanical tests

8.2.4.1 Split-disk tests

After reaching each time target, split-disk test was then conducted on three wide disks of conditioned specimens from each of the FRP tubes (20 mm disks of GFRP and BFRP and 8 mm disks of CFRP) to obtain the mechanical properties in hoop direction. Unconditioned FRP rings with the same width of that conditioned specimens were also tested to get the reference properties. The split-disk tests were conducted according to ASTM D2290 standard [277] at a loading rate of 1 mm/min. In order to minimize the local bending effect near the split region, the diameter of the half disks used were almost the same (slightly smaller) as the inner diameter of the tubes. Two strain gauges were attached in the hoop directions at a considerable distance from the middle gaps. The reason of attaching strain gauges far from the gap was to minimise the influence of the local bending on tensile strain values. To minimise the friction between the FRP disks and the steel half-disk, a high-pressure grease was used. **Figure 8-3(a)** shows the test set-up, specimen configuration, and position of strain gauges.

8.2.4.2 Compression tests

After reaching each time target, three 50 mm wide disks of unconditioned specimens and three 50 mm wide disks of fully filled conditioned tubes, from each of the FRP tubes in **Table 8-2**, were tested in compression. Shimadzu 300 kN testing machine with a loading rate of 0.5 mm/min was used to conduct compression tests. It should be noted that, because of small thickness and relatively low axial strength of BFRP and GFRP tubes to prevent the effect of surface unevenness and local failure at the tube ends, 7mm thickness rubber plates were used at both ends of these tubes for compressive tests. To obtain the compressive elastic modulus a strain gauge was attached at mid-height of each sample in the applied load direction. **Figure 8-3 (b)** shows the compressive test set-up.

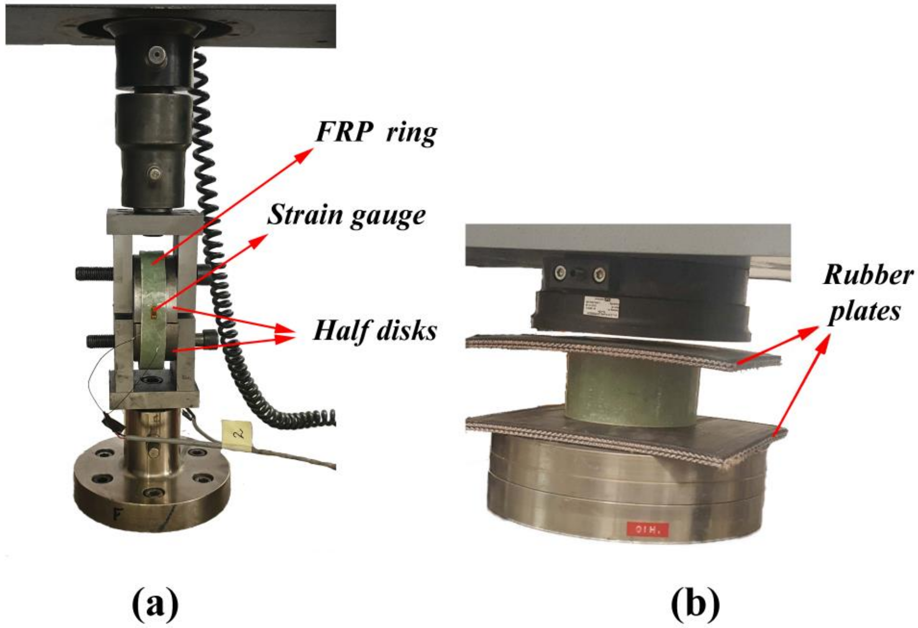

Figure 8-3 Mechanical test set-ups: (a) Disk-split tension test; and (b) Compression test

8.2.5 Analysis of microstructural degradation

The detrimental effects of alkaline ions (in terms of SWSSC) and seawater on the fibres, resin matrix, and fibre/resin interface of the filament wound FRP tubes were studied using high-resolution JOEL7001 scanning electron microscopy (SEM) and Zeiss Xradia 520 Versa X-ray micro computed tomography (micro-CT). Energy-dispersive X-ray spectroscopy (EDS) was also used for chemical characterisation of FRP samples after exposure. The tubes were analyzed using observation and image processing through their depth (from the edges toward their centers). The samples were cut from the exposed specimens at different periods and were ground and polished. Liquid nitrogen fracturing method was also used in preparation for the microstructural examination.

8.3. Results and discussion

In this section, the physical and microstructural changes as well as failure modes and mechanical test results are presented and discussed in detail.

8.3.1 Visual observations

Figure 8-4 shows the samples before and after exposure to environmental conditions. As shown in **Figure 8-4**, with the increase of aging time and temperatures, the colour of GFRP turns from light green to blue-green and slightly brown, CFRP turns from shining black to deep black and BFRP changes from black to slightly brown due to the presence of iron in BFRP. After exposure to seawater and sea sand concrete, it is found that the matrix of G/C/B-FRPs is partly damaged and the fibres are revealed is some cases. The degradation level of each type will be discussed in detail later on microstructural examination section.

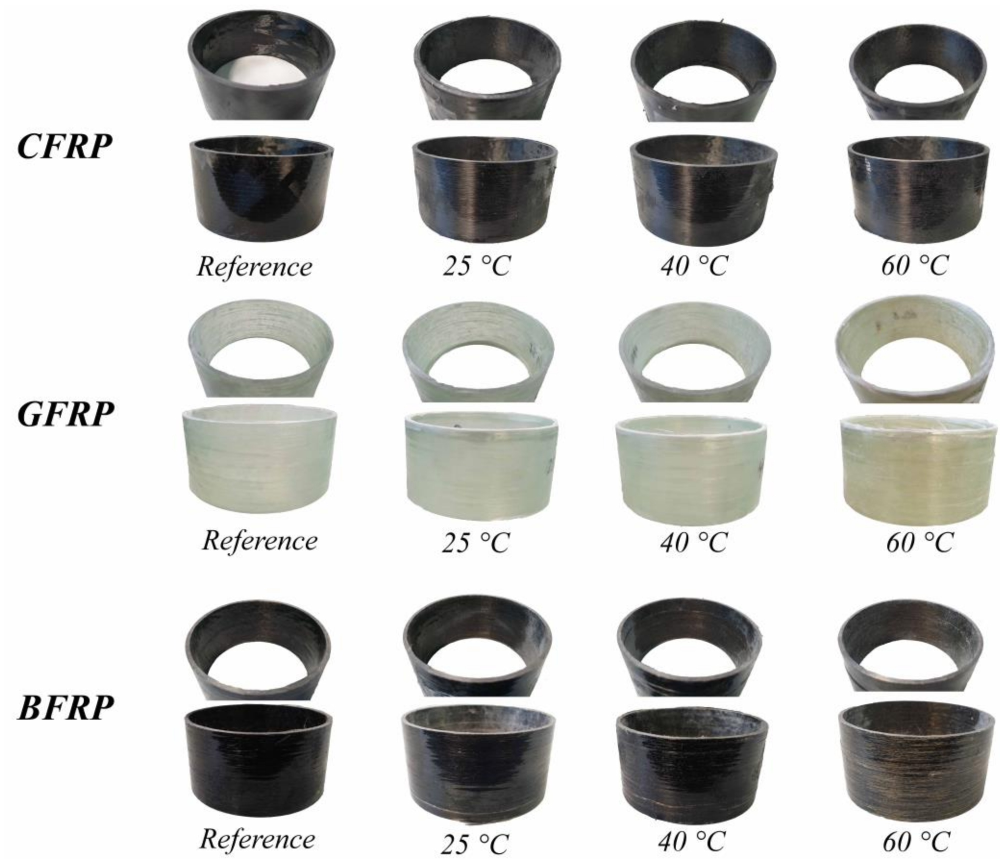

Figure 8-4 Appearance changes of the FRP tubes after 6 months of conditioning

8.3.2 Microstructural analyses

8.3.2.1 SEM

In order to study the degradation mechanisms in terms of fibres, resin, and fibre/resin interface, some samples were examined under SEM. It is worth mentioning that Guo et al. [249] studied the degradation of the same FRP tubes used in the present study during exposure to SWSSC using SEM analyses. Therefore, some of the images used in this section are related to that study. Both inner and outer surfaces of the samples exposed to SWSSC and seawater, cross-sections near the sample edges, and fracture surface were examined under SEM to comprehensively understand the damage mechanisms in different conditions.

As is seen in **Figure 8-5,** the cross-section of GFRP and CFRP samples exposed to 60 °C saltwater and real SWSSC for 180 days showed no significant damages in terms of resin cracking. However, cracks (i.e., white lines in **Figure 8-5**) are found in both sides (sides in contact with both SWSSC and saltwater) of conditioned BFRP samples. The cracks pass around the fibers indicating the interphase between matrix and fibres is degraded by the aggressive environments. With respect to samples exposed to 60 °C saltwater and simulated SWSSC solution for 180 days, it is observed that SWSSC simulated solution can degrade both the resin matrix and also the fibers in GFRP and BFRP samples (

Figure *8-6* **(b)** and **(c)**). However, similar to real SWSSC condition, no significant damage was observed in CFRP samples (

Figure *8-6***(a)**). Therefore, based on the evaluations of the cross-sectional microstructures, BFRP shows the poorest durability performance, while the CFRP shows the best durability.

To evaluate the microstructure of fibres before and after aging, the fracture surface of FRP samples were further examined, in which a thin strip of FRP was fractured after exposure to liquid nitrogen. The fracture surfaces of aged FRP samples, from both set of specimens, which were exposed to 60 °C SWSSC /simulated SWSSC solution and saltwater for 180 days, were carefully examined. As is seen in **Figure 8-7,** no obvious damages were found on fibers related to samples exposed to real SWSSC. However, Guo et al. [249] observed obvious fiber damages, such as pitting and cracking in GFRP and BFRP (**Figure 8-8**) tubes after 6 months of conditioning at 60 °C. Similar damages were observed by Bazli et al. [230] in pultruded GFRP composites when exposed to simulated SWSSC for the same duration and at the same temperature. The reactions between the alkali-ions and silicate in glass/basalt fibers, causing network destruction and its gradual dissolution, are suggested to be the main reason of the corrosion shell formation on fibers in alkali environment [278, 279].

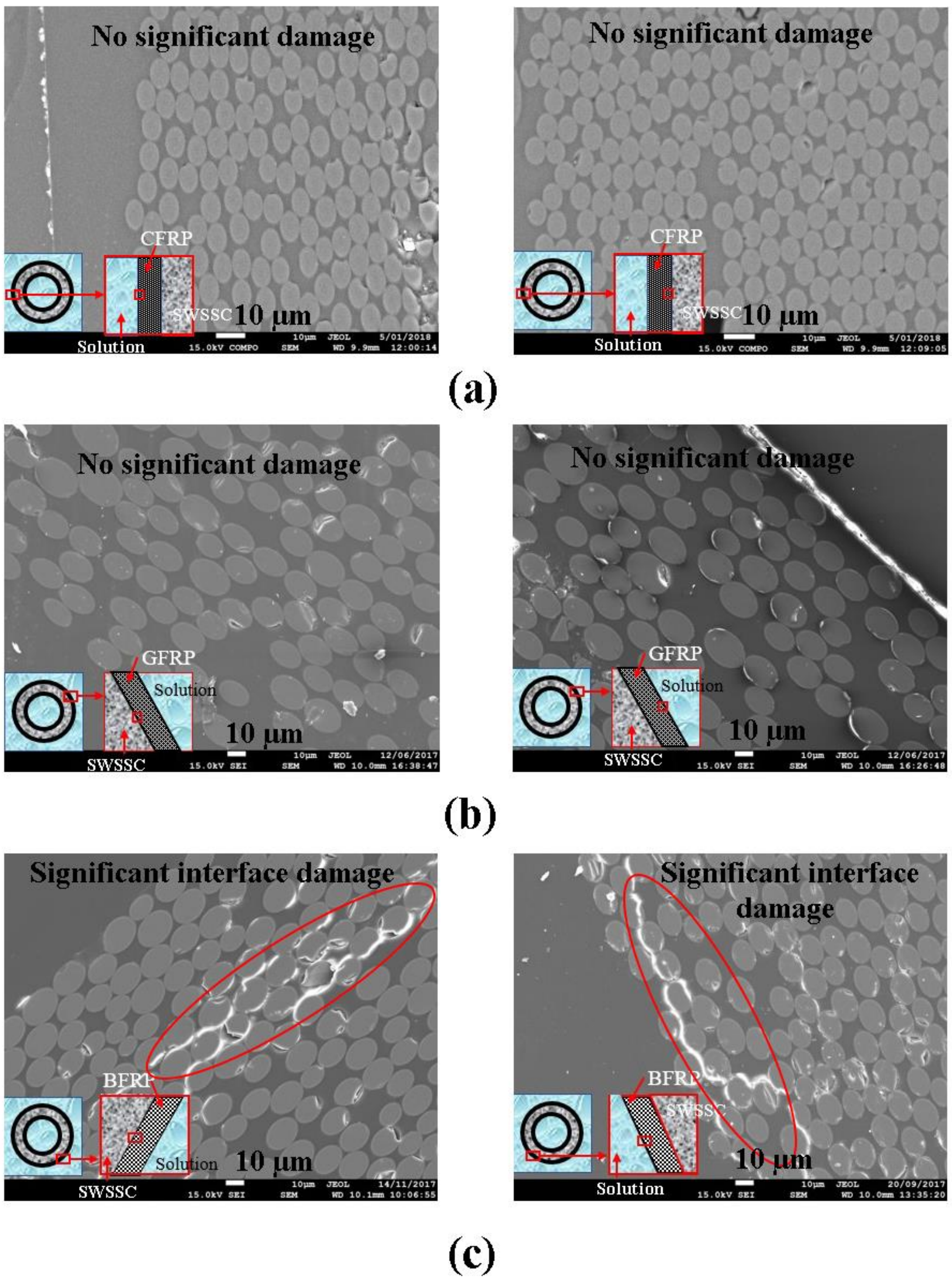

Figure 8-5 Cross-sectional images of double skin FRP tubes after exposing to 60 °C saltwater for 180 days; (a) CFRP; (b) GFRP; and (c) BFRP

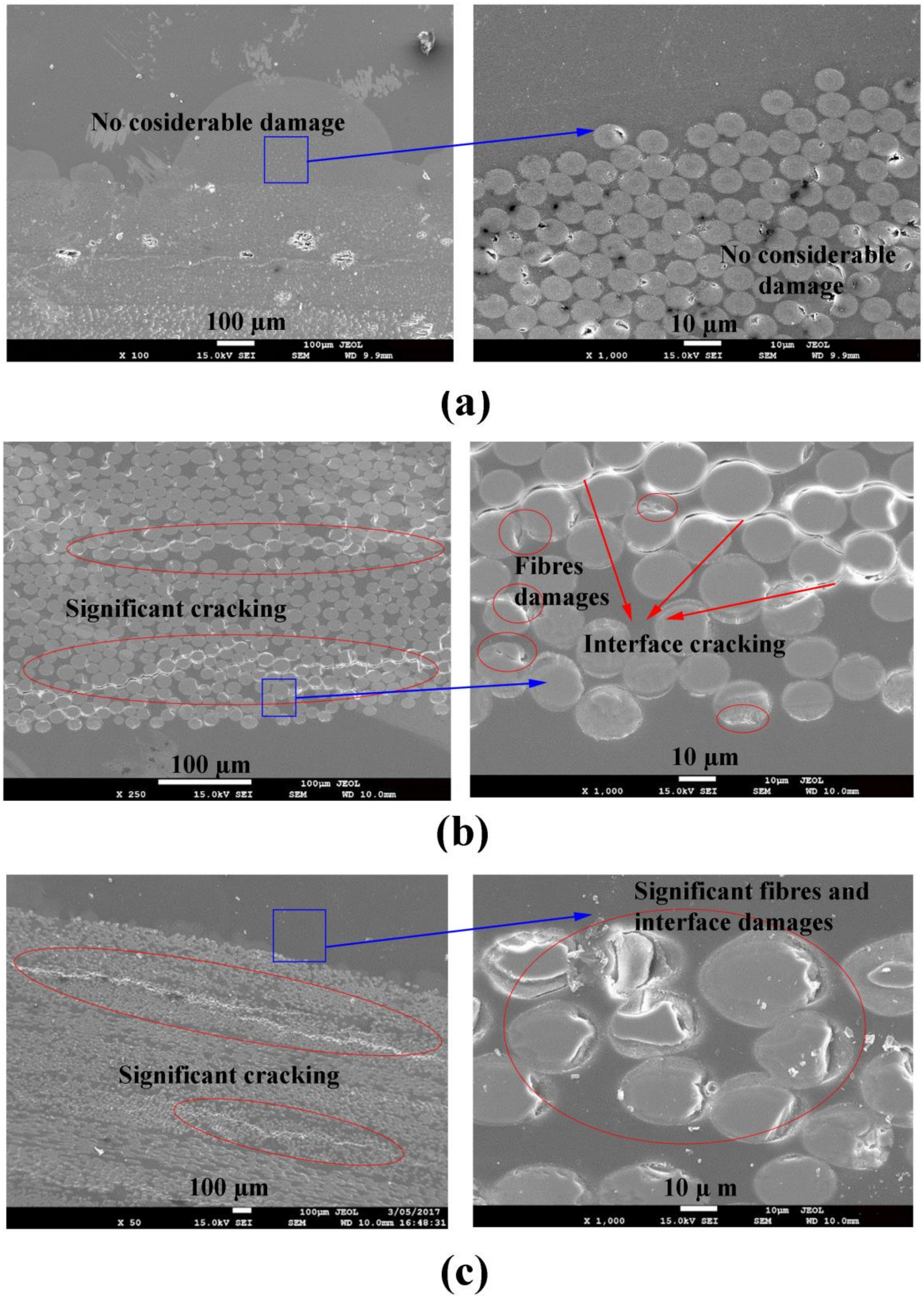

Figure 8-6 Cross-sectional images of FRP after exposing to 60 °C simulated SWSSC and saltwater for 180 days; (a) CFRP; (b) GFRP; and (c) BFRP [249]

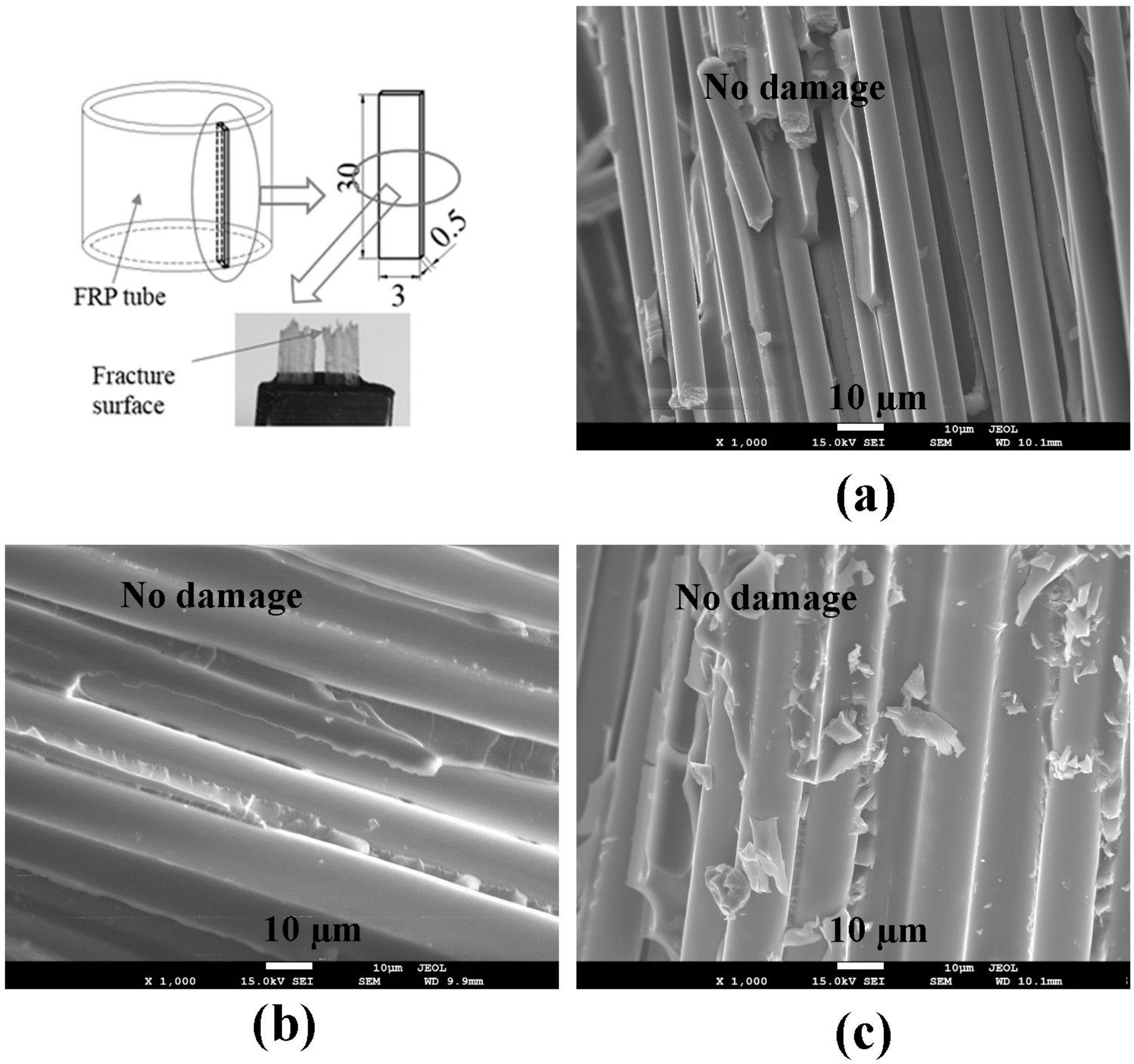

Figure 8-7 Fracture surface of double skin FRP tubes after exposing to 60 °C saltwater for 180 days: (a) CFRP; (b) GFRP; and (c) BFRP

The expansion of corrosion shells leads a local stress in the matrix and consequently fibre/resin interface debonding and exfoliation from fibres. The chemical reaction resulting the formation of corrosion shell is shown in **Eq. 8.1**. **Eq. 8.2** also shows the silicate network subsequent destruction and gradual dissolution [279-281].

$$\equiv Si - OR + (H^{+} + OH^{-}) \rightarrow \equiv Si - OH + ROH \tag{8.1}$$

$$\equiv Si - O - Si \equiv +(R^{+} + OH^{-}) \rightarrow \equiv Si - OH + RO - Si \tag{8.2}$$

The corrosion shells formed become thicker by the time of exposure and moves through the fibre core. These reactions and movements will result insoluble compounds (i.e. calcium, iron, titanium, magnesium and zirconium) to be remained [280]. Different mechanical properties between the fibre and the corrosion shell will facilitate the exfoliation process of BFRP and GFRP fibres. Regarding the fibres pitting (i.e. localized attack), reduction of the fibre local diameter will decrease the load bearing capacity of the BFRP and GFRP fibres [249]. However, as is seen in (**Figure 8-8(b)** and **(c)**), these degradations are significantly more in BFRP samples compared to GFRP samples. The possible reason could be the difference in aluminium, iron and magnesium contents which react with the chloride ions existing in seawater and simulated SWSSC.

Regarding the aluminium, the following reactions occur when fibres are subjected to simulated concrete/SWSSC:

Firstly, in an alkaline environment, the aluminium oxide dissolves according to the following reaction [282]:

$$Al_2O_3 + 2OH^-(adsorbed) \rightarrow 2AlO_2^-(aqueous) + H_2O \quad (8.3)$$

Next, aluminium ions will react with the chloride ions exist in SWSSC according to **Eq. 8.4** [283]. The formed soluble oxychloride complexes are then leached into the simulated SWSSC solution.

$$Al^{+3} + 2Cl^- + 2OH^- \rightarrow Al(OH)_2Cl_2^- \quad (8.4)$$

With similar set of reactions, the magnesium also dissolves in the SWSSC solution [282].

Regarding the iron existing in basalt fibres, the following reactions occur when basalt fibres are subjected to simulated SWSSC: Firstly, as a result of ferric iron hydrolysis in an aqueous environment, ferric hydroxide forms [284]:

$$Fe^{+3} + 3OH^- \rightarrow Fe(OH_3)_{(aq)} \quad (8.5)$$

It is worth mentioning that this hydrolysis will occur with higher rate in alkaline solution [285].

Next, the following set of reactions occur in the presence of chloride ions [286]:

$$Fe^{+3}{}_{(aq)} + Cl^{-}{}_{(aq)} \leftrightarrow Fe(H_2O)Cl^{+2}{}_{(aq)} \tag{8.6}$$

$$Fe(H_2O)Cl^{+2}{}_{(aq)} \leftrightarrow FeCl^{+2}{}_{(aq)} \tag{8.7}$$

$$FeCl^{+2}{}_{(aq)} + Cl^{-}{}_{(aq)} \leftrightarrow FeCl_{2\,(aq)}^{+} \tag{8.8}$$

$$FeCl_{2\,(aq)}^{+} + Cl^{-}{}_{(aq)} \leftrightarrow FeCl_{3(aq)} \tag{8.9}$$

The considerable amount of iron oxide in basalt fibres leads to a higher solution uptake of BFRP and thus higher degradation levels. This was explained in [285] by showing the relation between the osmotic coefficient in an NaCl solution and the molal concentration of $FeCl_2$.

Therefore, the difference in aluminium, magnesium and iron contents (refer to [249] for the amount of each component) which react with the chloride ions existing in seawater and simulated SWSSC are the main reasons for the different degradation levels of GFRP and BFRP samples.

Regarding the CFRP samples, as expected, no significant damage was observed in carbon fibers and fiber/resin interface (**Figure 8-8(a)**). This confirms the fact that carbon fibres are resistance to environmental condition regardless of the exposure solution and conditioning time and temperature.

Based on the results of double skin samples, after exposure at 60 °C to saltwater for 180 days, degradation of the interphase was only found in BFRP and no degradation of fibers was observed for all FRP types. However, clear strength loss is found for all FRPs (will be discussed in section 8.3.4), which are 46%, 15% and 42% for hoop strengths of GFRP, CFRP and BFRP, respectively. Therefore, the microstructure change of aged FRP becomes observable only when serious degradation occurs (e.g., in simulated SWSSC environment). Therefore, it may not be reliable to evaluate the strength reduction of FRPs only by checking its microstructure through SEM.

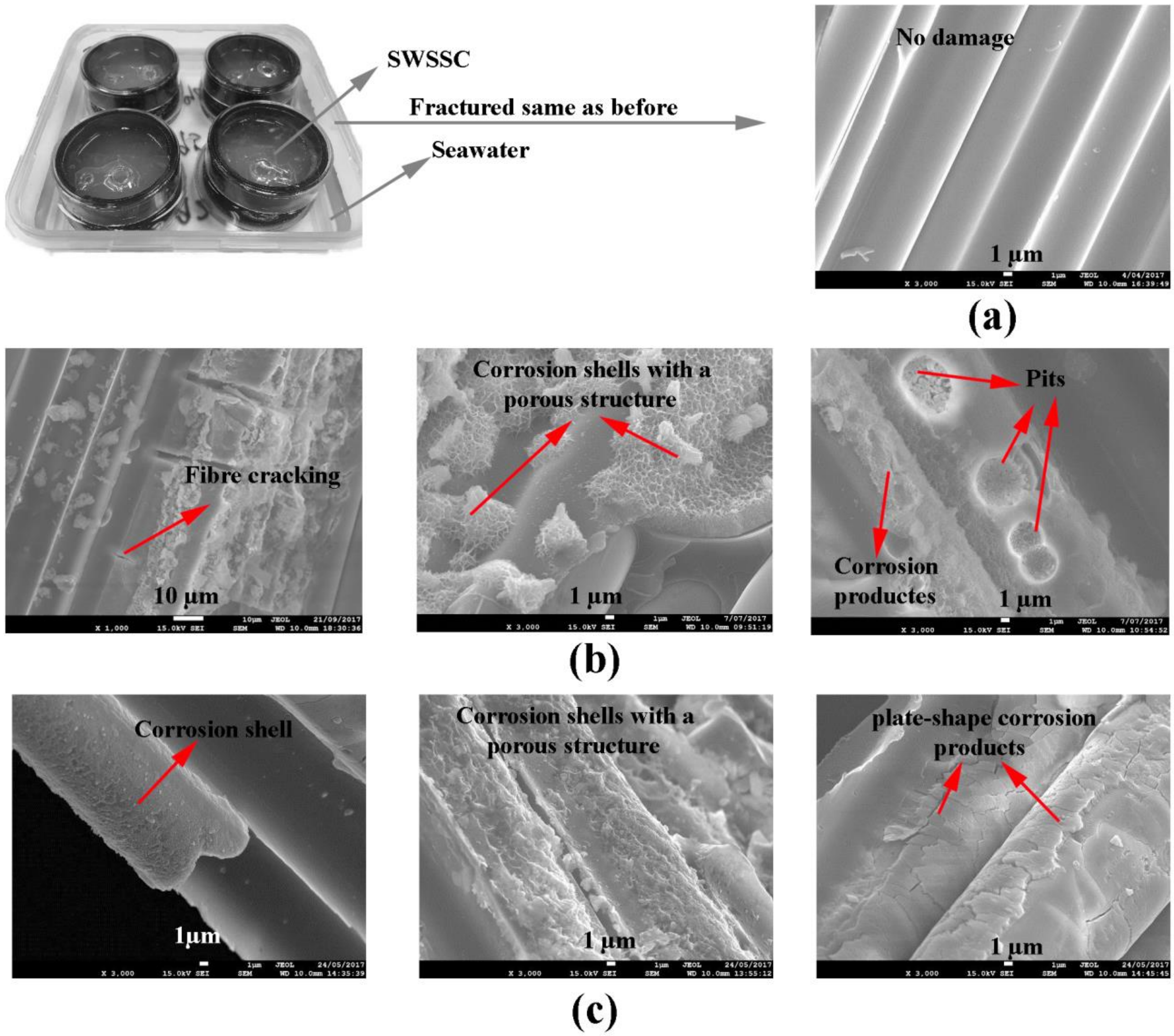

Figure 8-8 Fracture surface of FRP tubes after exposing to 60 °C simulated SWSSC and saltwater for 180 days: (a) CFRP; (b) GFRP; and (c) BFRP [249]

The chemical composition of the matrix was also analysed by Energy-dispersive X-ray spectroscopy (EDS). Since the same type of epoxy was adopted as the matrix in GFRP, CFRP and BFRP, only GFRP samples, including unconditioned and aged samples after 180 days of exposure at 40 °C or 60 °C to saltwater, were examined in the present study. The chemical composition (in percentage) is summarised in **Table 8-3**, which is an average result after analysing several points located near the sample edges. As shown in **Table 8-3**, the chemical composition of epoxy does not change significantly after aging. This shows the chemical stability of epoxy resin. This finding is in agreement with the existing understanding that the epoxy is not affected by hydrolysis due to its lack of ester group in molecular structures [36]. **Table 8-3** also indicates that the Chloride (Cl^-) concentration in aged samples is slightly higher than the concentration in unconditioned samples, which is probably caused by the ingress of Cl^- from saltwater to matrix.

Table 8-3 Chemical composition of matrix before and after aging (%)

Specimen	Number of locations selected for EDS	C	O	Si	Cl
G-Ref	5	82.1±0.5	16.5±0.3	0.2±0.07	1.1±0.23
G-T40D6-S-O	3	80.5±1.0	17.8±1.5	0.1±0.05	1.5±0.40
G-T60D6-S-O	3	80.9±0.8	17.7±0.8	0.0±0.05	1.3±0.04

8.3.2.2 Micro CT

As discussed earlier and observed in the SEM images of FRP tubes filled with simulated SWSSC and subjected to seawater solutions, significant damages in terms of fibre, resin and interface occurred after a certain period of conditioning. The amount of voids percentage in FRPs as a result of resin cracking and leaching could be used as an index to evaluate the degradation level of such materials under harsh environmental conditions. In order to achieve this, three conditioned samples and their references were imaged using the micro-CT at 3.38-micron pixel size. Subsequently, these images were analysed and compared to establish the relative degradations incurred. XRM Reconstructor software was used for 3D reconstructions using the 2D projections of the scanned samples. In order to map the degradation level through the thickness of the samples, from each sample, four sub volumes with dimensions of 1.47 mm×1.47 mm×2.94 mm were selected. The height of each sub volume is the same from the centre of the scanned sample. The width of each sub volume is considered from the edge to the centre of the tube thickness. For each sub volume the average percentage of fibres, resin, and voids in different segments were obtained using image analyses. Avizo commercial software and MATLAB codes were used with this regard. **Figure 8-9** shows the 3D scanned image of reference and one conditioned sample from each tube type. As is seen, significant damage in BFRP sample was observed, while GFRP and CFRP showed less degradations. These observations were already confirmed by the SEM images. By comparing the side of the samples that was exposed to SWSSC solution with the side exposed to seawater, it is clearly seen that the degradation is higher in former compared to the latter.

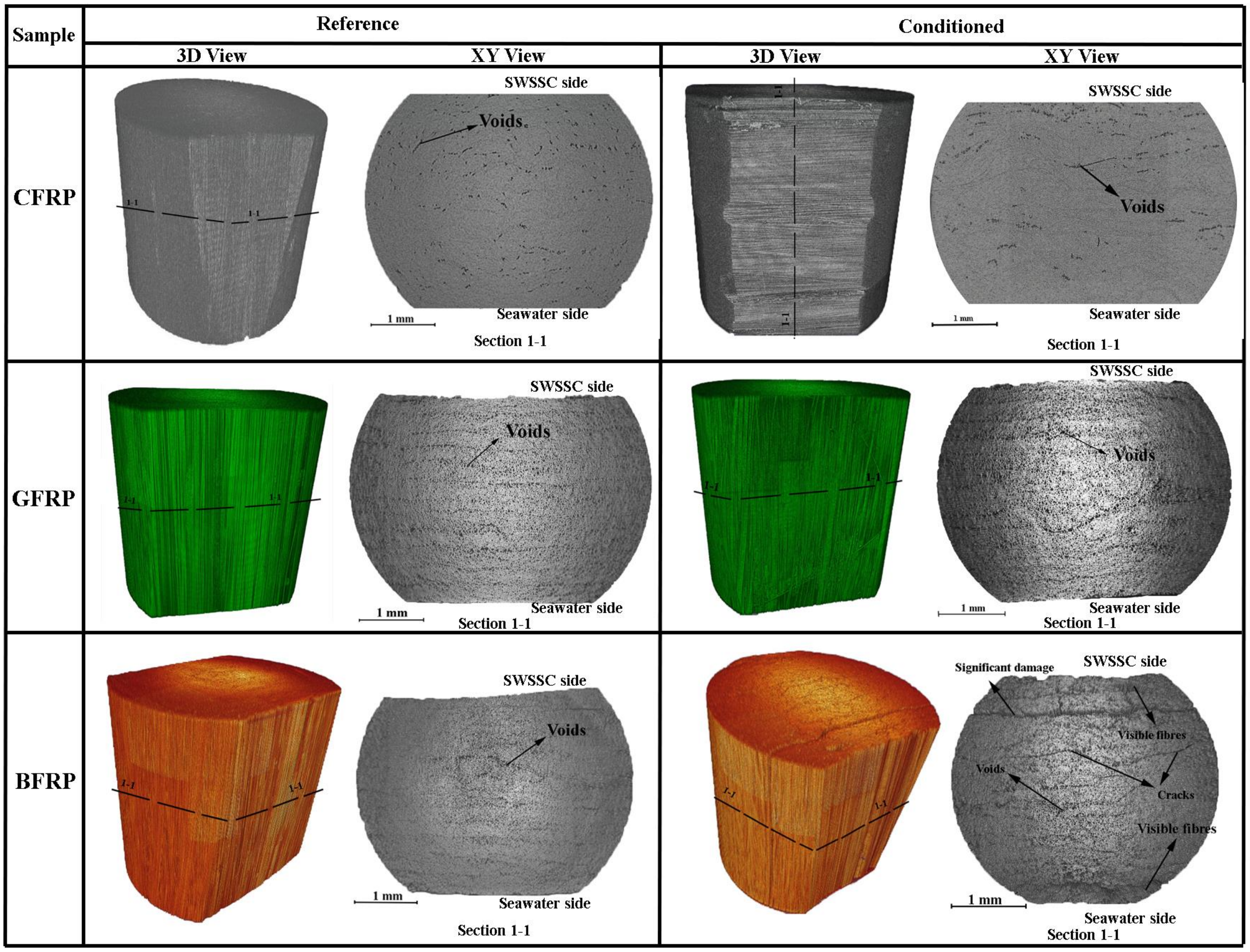

Figure 8-9 3D images of scanned reference samples and samples exposed to 60 °C simulated SWSSC and seawater for 6months

Figure 8-10 shows the image processing out-put of a segment in one sub volume of reference and conditioned sample. In order to obtain the percentage of the components, colour images related to each sub volume, were generated using Avizo software. The colour images are used as input to a MATLAB in-house produced code that enables calculation of the percentage of fibres, resin and voids. A colour image, which is also known as an RGB image is an image in which each pixel is identified by three values: one each for the red, green, and blue components of the pixel scalar. Each RGB colour image, is divided into its three colour planes (red, green and blue).

The interval number of quantization in gray scale image processing is represented by gray levels. 8-bit storage is the most commonly used storage method. In an 8-bit gray scale image, there are 256 gray levels, and each pixel can have an intensity ranging from 0 to 255, with 0 being black and 255 being white [287].

Similarly, in the present study, the resulting monochromatic image is scaled in the range 0-255. After scaling, each material corresponds to a specific section of the gray-level values histogram in one of the colour planes, therefore it can be identified and isolated. In order to do so, binarization via thresholding is performed. Thresholds are selected so that the generated binary images identify the pixel corresponding to the fibres, resin, and voids.

The results related to different sub volumes of each sample are summarised in **Table 8-4.** It is observed that amount of voids in CFRP samples did not change considerably after 6 months of exposure at 60 °C (average increment about 2.6 (%) compared to the voids percentage of reference sample), while both GFRP and BFRP tubes showed about 32 (%) and 22 (%) voids increment, respectively compared to their corresponding reference sample. The void morphology of the samples could be used to explain the reason for these observations. As is seen in **Table 8-4**, in conditioned GFRP sample, the percentage of the fibres remained almost the same, while the resin percentage decreased about 2%. This shows that the resin leaching (interface cracking) and microcracks are the main reasons of the void increment. However, in conditioned BFRP sample, the percentage of the fibres decreased about 3%, while the resin percentage remained almost the same in comparison to the reference sample. This shows that the significant cracking (see **Figure 8-9**), interface degradation and fibres damages were the main reasons of void increment in BFRP sample. These observations also confirm the fact that the CFRP tubes are less vulnerable to harsh environments compared to GFRP and BFRP tubes.

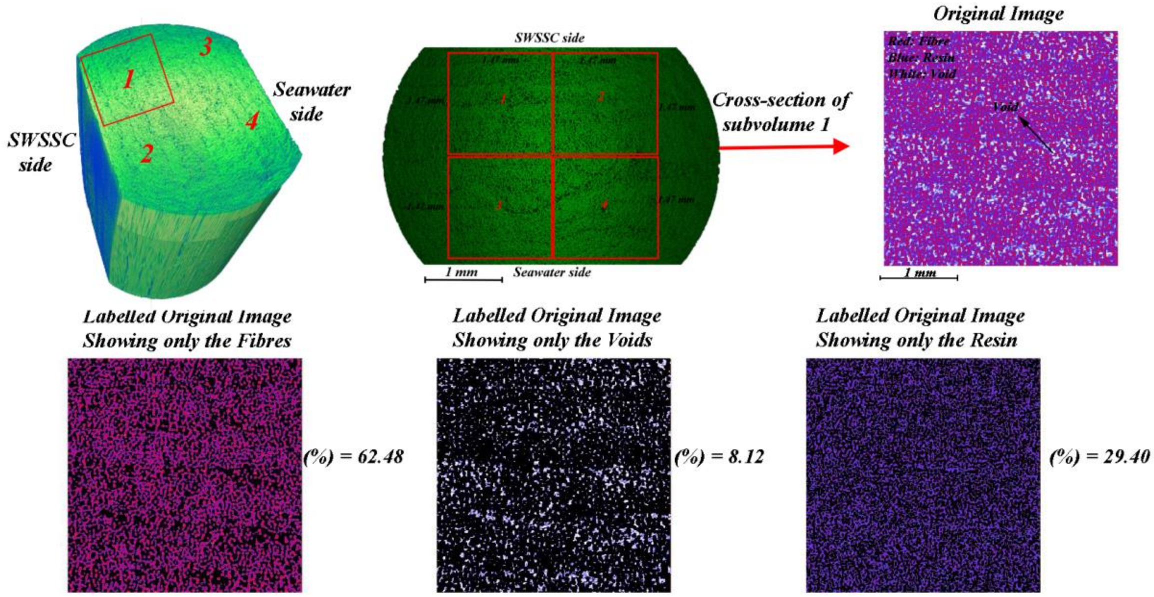

Figure 8-10 Image processing procedure of one sub-volume of GFRP sample

Table 8-4 Image processing results of scanned samples

Specimen	C-Ref			C-T60-D6			G-Ref			G-T60-D6			B-Ref			B-T60-D6		
	Fibres (%)	Resin (%)	Voids (%)	Fibres (%)	Resin (%)	Voids (%)	Fibres (%)	Resin (%)	Voids (%)	Fibres (%)	Resin (%)	Voids (%)	Fibres (%)	Resin (%)	Voids (%)	Fibres (%)	Resin (%)	Voids (%)
Sub volume 1	58.71	33.87	7.42	58.72	34.08	7.20	62.48	29.41	8.12	65.57	26.10	10.78	72.49	23.20	8.33	72.28	17.04	10.68
Sub volume 2	60.79	32.31	6.90	59.17	33.29	7.54	64.84	27.11	8.05	60.23	29.65	10.12	70.38	21.50	8.12	68.70	20.44	10.86
Sub volume 3	63.63	29.81	6.56	59.71	33.70	6.59	64.53	27.44	8.03	62.30	27.74	9.96	70.90	20.47	8.63	70.43	20.40	9.17
Sub volume 4	58.70	35.29	6.01	63.68	30.06	6.26	64.45	27.01	8.54	63.12	25.86	8.57	68.47	20.55	6.96	67.67	23.13	9.20
Average	60.46	32.82	6.72	60.32	32.78	6.90	64.08	27.74	8.19	63.12	26.10	10.78	71.26	21.43	8.01	68.93	21.32	9.74

8.3.3 Failure modes

Figure 8-11 shows the typical failure modes observed in compression and hoop tensile tests. As is seen, no significant changes were observed in compressive reference and conditioned samples: tubes with 89 fibres were failed along the tube height and through the resin/fibre interface fracture, while samples with multiple fibres direction failed due to the local buckling in multiple directions. Also, the failure mode of both tensile reference and conditioned tubes with multiple fibres was the same and it was fibres fracture. However, as is seen in **Figure 8-11(d)**, the failure mode of tensile tubes with 89° fibres changed from fibres fracture in reference samples to the combination of fibres fracture and delamination in conditioned sample. It is worth mentioning that the longer the time and the higher the temperature of the conditioning, the greater is the delaminated layers. The reason for this failure mode change is the significant interface degradation due to the solution penetration through the sample thickness.

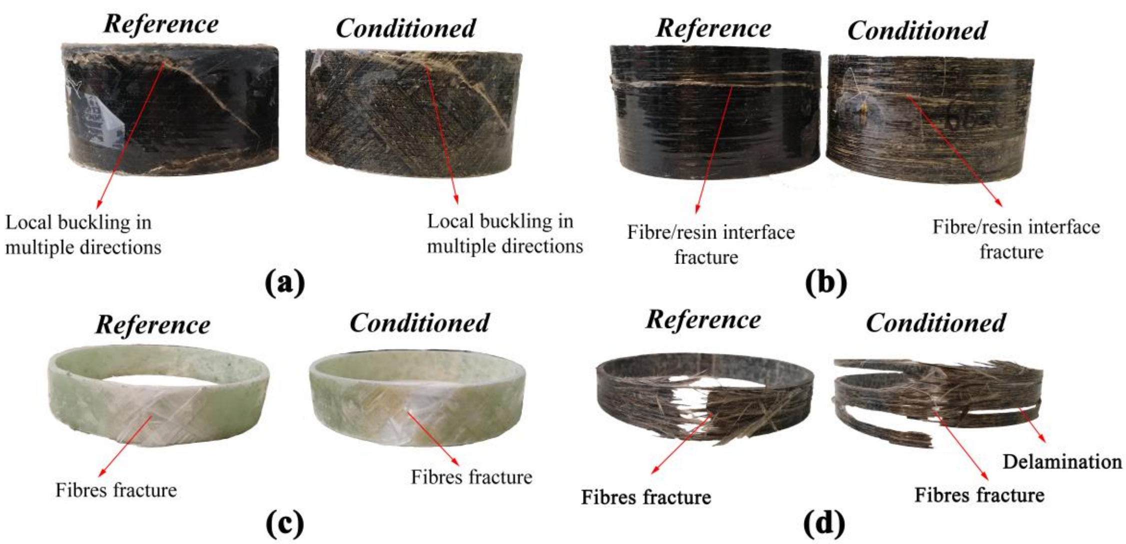

Figure 8-11 Typical failure modes observed in reference and samples exposed to 60 °C simulated SWSSC and seawater for 6months (: (a) Compressive BFRP sample with multiple fibres; (b) (a) Compressive BFRP sample with 89° fibres; (c) Tensile GFRP sample with multiple fibres; and (d) Tensile BFRP sample with 89° fibres

8.3.4 Mechanical test results

8.3.4.1 Split-disk tensile

Split-disk test was conducted on FRP rings to obtain the strength and Young's modulus in hoop direction. The nomenclature of double skin specimens is: FRP type ("G" for GFRP, "C" for CFRP and "B" for BFRP) - Temperature ("T23", "T40" and "T60" for 23, 40 or 60 °C), duration ("D1", "D3" and "D6" for 30, 90 and 180 days) - solution type ("S" for saltwater and "D" for distilled water) - ring type ("I" for inner ring and "O" for outer ring); "Ref" refers to reference specimens without aging. The labelling rule of fully filled specimens is: FRP type – fibres orientation ("M" and "89" for multiple and hoop directions)- Temperature – duration.

8.3.4.1.1 Double-skin samples

The experimental results of double-skin samples are summarised in **Table 8-5**. **Figure 8-12** shows the typical stress-strain curves of double-skin samples (inner tubes). As expected, after aging, both strength and Young's modulus, which is determined according to ASTM D2290 [288], decrease to some degrees depending on the aging time and aging temperatures. The degradation of Young's modulus is much slower than the strength degradation. It is observed that the degradation process of FRP tends to slow down with the increase of aging time. No obvious difference is observed in terms of the hoop strength retention of inner rings and outers rings. Therefore, the environment combinations do not affect the durability behaviour of FRP and the same design theory can be applied to both outer tubes and inner tubes of SWSSC-filled double-skin tubular columns in a marine environment. Based on the strength retention data of GFRP, distilled water is slightly more aggressive than saltwater. As suggested by Guo et al. [24], sodium chloride (NaCl) in SWSSC or seawater does not worsen the durability issue of FRP and it even has some beneficial effects.

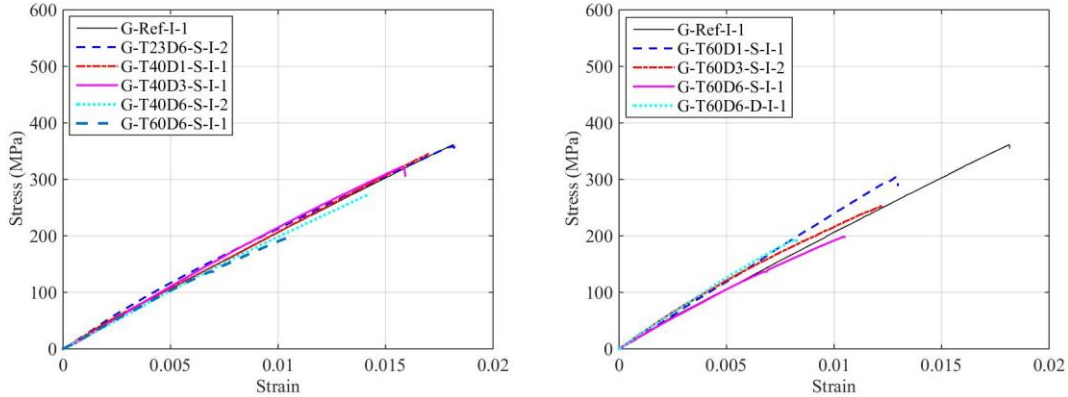

(a)

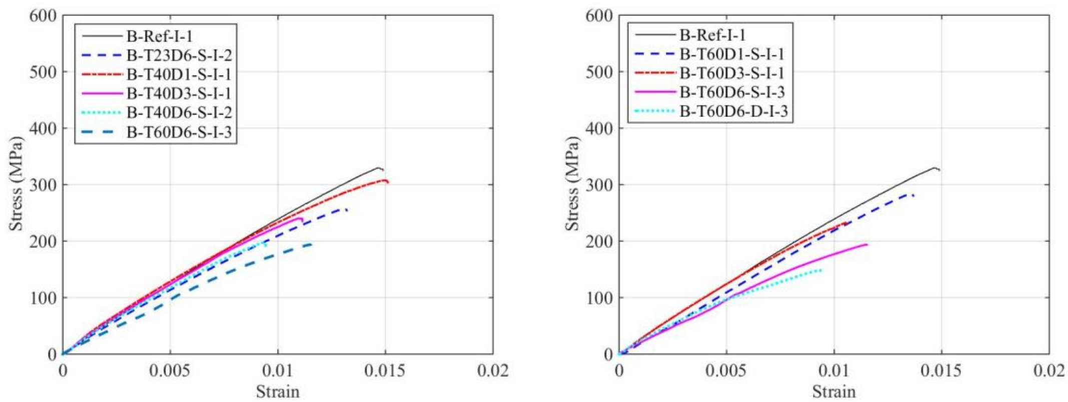

(b)

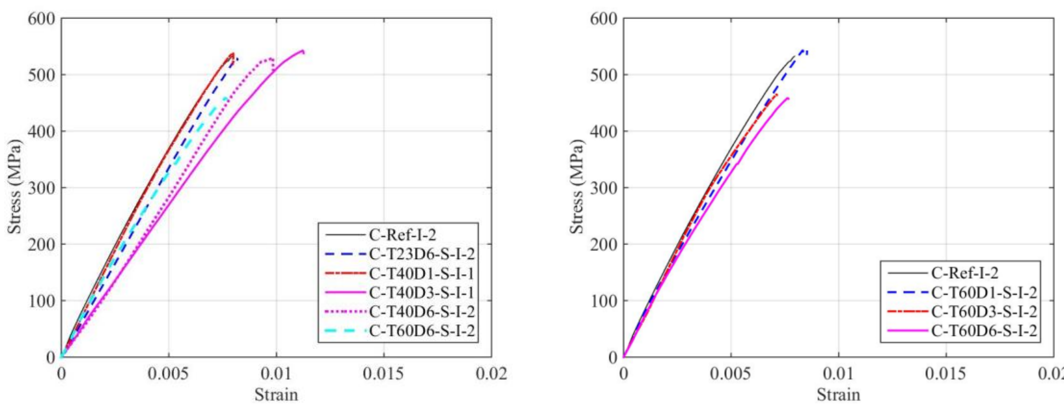

(c)

Figure 8-12 Typical stress-strain curves: (a) GFRP inner ring; (b) BFRP inner ring; and (c) CFRP inner ring

Regarding the effect of fibres type, it was seen that CFRP has significantly superior durability performance than GFRP or BFRP, which is in agreement with past studies [289]. BFRP behaves similar to GFRP at 60 °C, but more strength loss is observed for BFRP at 23 and 40 °C indicating BFRP performs worst among the three FRP types. After 180 days of exposure at room temperature (i.e., 23 °C), the average strength reduction of GFRP, CFRP and BFRP are 9.7%, 5.1% and 25.6% respectively. The experimental data of [275], in which the GFRP rings were exposed to ordinary concrete (inner) and 3.5% NaCl solution (outer) simultaneously, show less strength reduction than the corresponding GFRP specimens in the present study. Since NaCl does not affect the durability significantly and the solution alkalinity caused by concrete are almost similar, the less strength loss is mainly attributed by the manufacture quality and laminate structure of GFRP tubes.

Young's modulus is derived from stress-strain curve and the error may be introduced due to the non-uniform curvature of rings and bending effect. Therefore, the Young's modulus data show much greater scattering than the strength data and the variation trend is not very clear. In order to overcome the aforementioned shortcomings, the stiffness (K) of FRP ring is also reported in

Figure 8-13**,** which shows less scattering. The stiffness is defined as the slope of a linear stress-displacement curve, in which the displacement is recorded by the test machine. Generally speaking, the Young's modulus and stiffness decrease after aging but the extents of reduction are significantly less than that of strength. The maximum stiffness reductions are 10%, 3% and 9% for GFRP, CFRP and BFRP, respectively. Two reasons may attribute to the unnoticeable change of Young's modulus and stiffness: (a) the modulus mainly depends on the modulus of fiber and the influence of matrix degradation is not obvious due to its much lower modulus but the strength of FRP depends on fibers, matrix and their interphase; and (b) the damages on FRP are local and they mainly affect the strength as the weakest cross-section determines the strength whilst the modulus depends on the overall performance of a specimen. It is necessary to mention that in some cases (e.g., GFRP outer ring after 30-day aging) a slight stiffness increase is observed and this is probably caused by the post-curing of resin. It should be noted that the elastic modulus changes of fully filled samples were also unnoticeable in both hoop and compression tests, and thus the results of the modulus changes are not presented for these conditions.

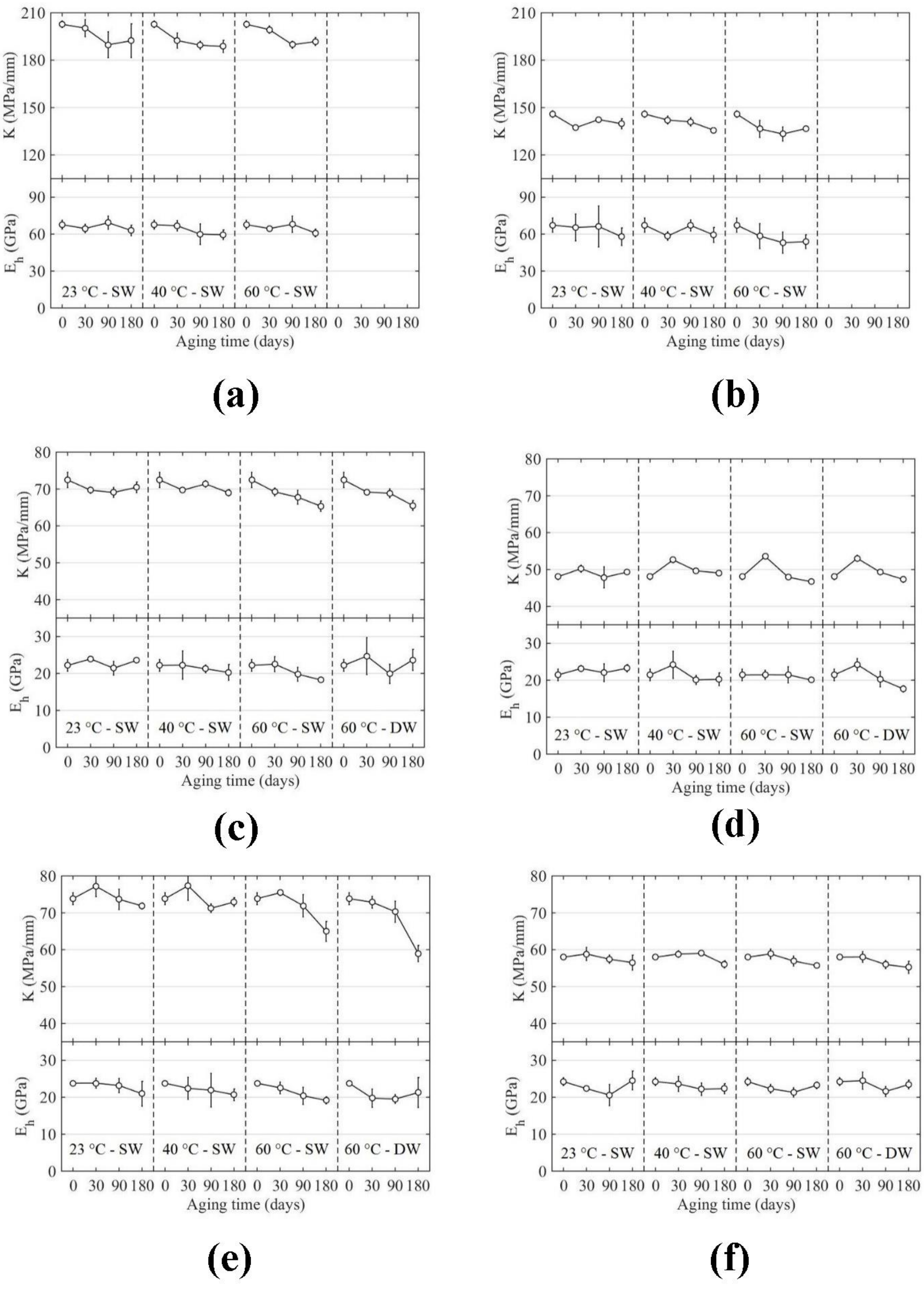

Figure 8-13 Stiffness (K) and Young’s modulus (Eh) od double skin tubes: (a) CFRP inner; (b) CFRP outer; (c) GFRP inner; (d) GFRP outer; (e) BFRP inner; and (f) BFRP outer

Table 8-5 Experiment results of split-disk test of double-skin samples

Specimen	Strength Retention (%)	CV (%)	Elastic modulus retention (%)	CV (%)	Specimen	Strength Retention (%)	CV (%)	Elastic modulus retention (%)	CV (%)
C-Ref-I	100.0	2.8	100.0	5.3	C-Ref-O	100.0	4.0	100.0	8.6
C-T23D1-S-I	99.2	1.4	95.4	5.3	C-T23D1-S-O	100.6	1.7	97.2	16.7
C-T23D3-S-I	98.5	2.5	102.4	7.6	C-T23D3-S-O	95.5	0.6	98.4	25.2
C-T23D6-S-I	98.0	2.5	93.1	6.8	C-T23D6-S-O	91.8	1.7	86.0	12.3
C-T40D1-S-I	98.9	0.7	98.7	6.3	C-T40D1-S-O	96.5	3.1	86.9	6.0
C-T40D3-S-I	98.5	2.3	88.6	14.0	C-T40D3-S-O	91.4	-	99.6	6.7
C-T40D6-S-I	94.3	5.6	87.9	6.6	C-T40D6-S-O	89.2	4.9	88.1	10.3
C-T60D1-S-I	96.7	2.8	95.3	3.3	C-T60D1-S-O	93.3	3.2	86.8	17.3
C-T60D3-S-I	85.6	0.8	100.4	9.9	C-T60D3-S-O	78.5	1.2	78.9	16.4
C-T60D6-S-I	86.9	3.1	90.0	5.1	C-T60D6-S-O	82.7	0.6	80.1	10.4
G-Ref-I	100.0	3.9	100.0	7.2	G-Ref-O	100.0	7.3	100.0	7.5
G-T23D1-S-I	99.5	2.3	107.7	2.1	G-T23D1-S-O	98.1	1.1	108.4	3.4
G-T23D3-S-I	91.2	3.3	96.4	8.9	G-T23D3-S-O	93.1	3.5	102.8	10.9
G-T23D6-S-I	93.3	4.1	105.9	0.9	G-T23D6-S-O	87.4	2.0	108.4	4.3
G-T40D1-S-I	93.2	4.5	100.5	17.0	G-T40D1-S-O	100.5	2.9	113.1	15.3
G-T40D3-S-I	89.9	2.6	95.9	4.7	G-T40D3-S-O	88.7	1.7	93.9	6.0
G-T40D6-S-I	73.6	9.7	91.4	10.3	G-T40D6-S-O	79.9	3.5	94.9	8.4
G-T60D1-S-I	82.2	1.2	101.4	8.9	G-T60D1-S-O	86.2	1.7	100.5	5.6
G-T60D3-S-I	69.4	3.0	89.2	9.6	G-T60D3-S-O	67.3	2.5	100.5	10.2
G-T60D6-S-I	52.6	2.4	82.4	3.8	G-T60D6-S-O	55.5	6.1	93.9	2.5
G-T60D1-D-I	81.9	2.6	111.3	20.2	G-T60D1-D-O	88.4	1.5	113.1	6.6
G-T60D3-D-I	57.3	2.8	89.6	13.1	G-T60D3-D-O	58.0	2.5	94.9	10.3
G-T60D6-D-I	52.7	0.2	106.8	12.2	G-T60D6-D-O	48.1	4.3	82.2	5.1
B-Ref-I	100.0	2.6	100.0	1.3	B-Ref-O	100.0	1.3	100.0	4.5
B-T23D1-S-I	99.5	1.7	100.0	5.5	B-T23D1-S-O	96.6	7.6	92.1	3.1
B-T23D3-S-I	87.9	3.4	97.5	8.2	B-T23D3-S-O	85.6	1.3	85.1	14.1
B-T23D6-S-I	75.8	2.0	87.8	16.3	B-T23D6-S-O	73.0	2.9	101.7	10.2
B-T40D1-S-I	96.2	2.0	94.1	13.4	B-T40D1-S-O	85.5	6.6	97.5	8.5
B-T40D3-S-I	71.5	2.4	92.0	21.0	B-T40D3-S-O	73.9	2.8	91.7	7.7
B-T40D6-S-I	62.5	4.0	87.0	7.7	B-T40D6-S-O	60.5	2.0	92.1	6.3
B-T60D1-S-I	85.3	3.7	94.5	7.1	B-T60D1-S-O	82.3	5.1	92.1	5.4
B-T60D3-S-I	69.3	3.1	85.7	11.3	B-T60D3-S-O	67.5	7.2	88.0	6.1
B-T60D6-S-I	60.3	3.5	80.7	4.7	B-T60D6-S-O	56.6	4.5	95.9	3.9
B-T60D1-D-I	80.1	4.2	83.2	12.6	B-T60D1-D-O	78.0	4.7	101.2	9.4
B-T60D3-D-I	63.6	1.2	81.9	6.2	B-T60D3-D-O	60.2	5.8	89.3	6.0
B-T60D6-D-I	48.8	5.9	89.5	19.2	B-T60D6-D-O	51.2	5.2	97.1	5.1

8.3.4.1.2 Fully-filled samples

The experimental results of fully-filled samples are summarized in **Table 8-6**. Similar to double-skin tubes, the degradation process of tubes exposed to simulated SWSSC tends to slow down with the increase of aging time and also CFRP showed the best performance while the BFRP showed the poorest in terms of hoop strength retention. However, higher strength reductions of samples exposed to simulated SWSSC compared to the corresponding double-skin samples (**Figure 8-14**) confirms the fact that due to the higher and faster OH^- ions movement in a simulated concrete solution in comparison to real concrete environment [5], simulated SWSSC solution is more aggressive than real SWSSC. Therefore, it can be concluded that using the simulated concrete solution instead of real concrete in accelerated environmental tests will overestimate the degradation in hoop tensile strength of FRPs.

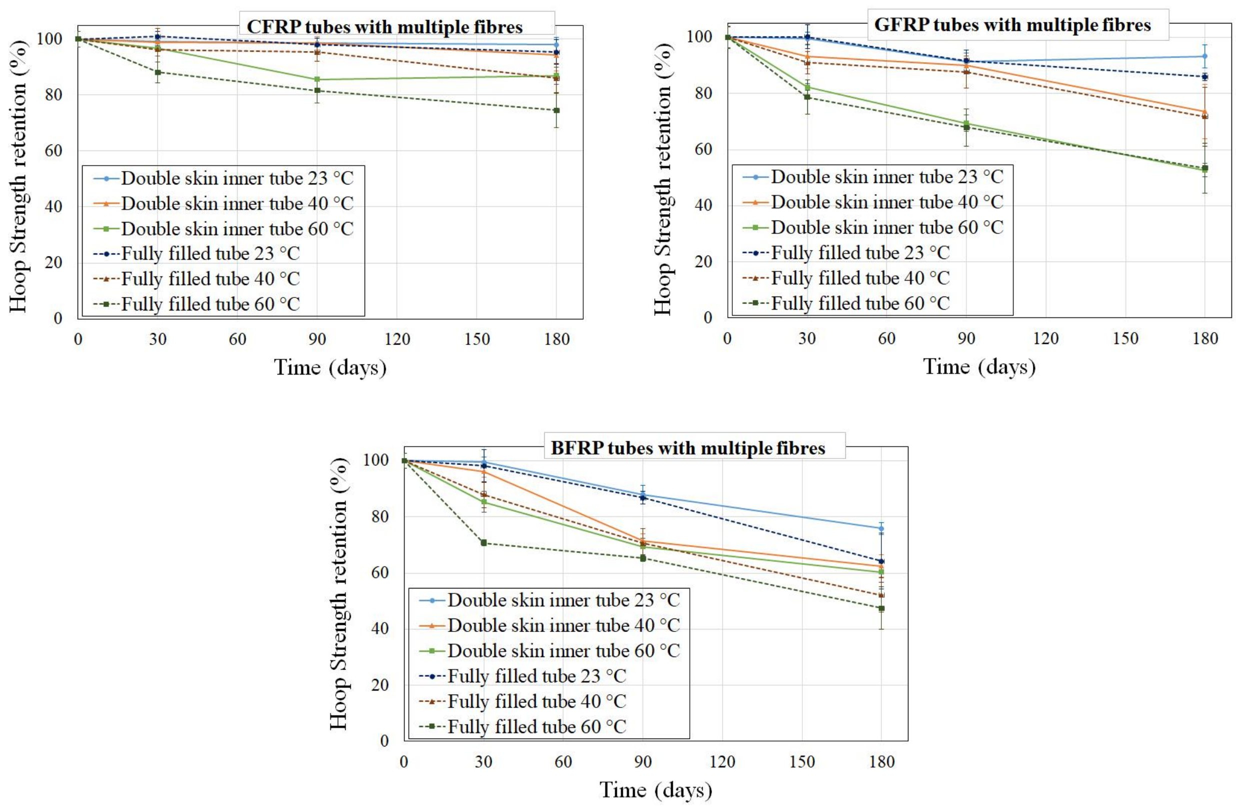

Figure 8-14 Hoop tensile strength retention versus conditioning time of double skin and fully filled samples

By comparing the results of tubes with multiple directions with the ones with 89° directions, one can conclude that the performance of tubes with multiple fibres was better. The possible reason for this observation could be the significant interface degradation between the fibres and resin which results in weakening of the resin capability to transfer the applied load to the fibres. Therefore, it should be noted that although FRP tubes with more fibres oriented in hoop directions show better confinement strength, they may be significantly vulnerable to the harsh environments if adequate amount of fibres is not available in other directions as well. In other words, when fibre/resin interface damage occurs at one direction of FRP tubes with multiple direction, loads can still be carried by fibres oriented in other directions. However, when fibre/resin interface debonding occurs at FRP tubes with fibres all oriented in hoop direction, damage propagates fast in the direction of the fibres and leads to the tube failure.

Generally, the hoop tensile strength reduction of FRP tubes may reduce the hoop strength of concrete filled FRP tubes. In other words, degradations of FRP tubes in hoop direction leads to a decrease in confinement strength of concrete filled FRP tubes. With this regard, [200] reported 35% and 54% hoop strength (i.e. FRP rupture strength in compressive tests) reductions of SWSSC filled GFRP and BFRP tubes, respectively after exposure to 3.5% NaCl solution at 40 °C for 6 months. Moreover, the strength reduction of SWSSC filled CFRP tubes were found insignificant. By comparing the results of the present study with the results reported in [200], one can conclude that the hoop strength reduction of columns was faster than that in FRP tubes. This confirms that the strength degradation of concrete filled FRP columns is mainly related to the deterioration of FRP tubes.

Table 8-6 Experiment results of split-disk test of fully-filled samples

Specimen	Strength Retention (%)	CV (%)	Specimen	Strength Retention (%)	CV (%)	Specimen	Strength Retention (%)	CV (%)
C-M-Ref	100.0	2.8	G-M-Ref	100.0	3.8	B-M-Ref	100.0	2.6
C-M-T23D1	100.9	1.9	G-M-T23D1	100.2	4.2	B-M-T23D1	98.1	5.9
C-M-T40D1	96.3	7.6	G-M-T40D1	91.0	4.0	B-M-T40D1	87.9	4.6
C-M-T60D1	88.2	3.7	G-M-T60D1	78.7	6.0	B-M-T60D1	70.7	1.0
C-M-T23D3	98.0	2.4	G-M-T23D3	91.6	3.8	B-M-T23D3	86.8	2.2
C-M-T40D3	95.3	3.2	G-M-T40D3	87.7	5.7	B-M-T40D3	70.6	5.3
C-M-T60D3	81.6	4.5	G-M-T60D3	67.9	6.6	B-M-T60D3	65.3	1.2
C-M-T23D6	95.3	4.4	G-M-T23D6	85.9	1.3	B-M-T23D6	64.2	10.0
C-M-T40D6	86.0	5.2	G-M-T40D6	71.7	10.4	B-M-T40D6	52.1	6.1
C-M-T60D6	74.6	6.1	G-M-T60D6	53.4	8.8	B-M-T60D6	47.5	7.6
C-89-Ref	100.0	1.4	G-89-Ref	100.0	0.7	B-89-Ref	100.0	0.9
C-89-T23D1	92.0	10.1	G-89-T23D1	82.4	4.9	B-89-T23D1	77.0	3.9
C-89-T40D1	84.3	6.5	G-89-T40D1	75.0	4.0	B-89-T40D1	68.9	5.0
C-89-T60D1	79.3	3.6	G-89-T60D1	65.5	4.3	B-89-T60D1	66.0	7.4
C-89-T23D3	83.3	1.0	G-89-T23D3	67.9	9.3	B-89-T23D3	69.0	2.1
C-89-T40D3	84.9	7.6	G-89-T40D3	65.5	4.8	B-89-T40D3	64.3	2.8
C-89-T60D3	78.4	5.1	G-89-T60D3	59.2	3.4	B-89-T60D3	61.6	5.5
C-89-T23D6	72.4	7.3	G-89-T23D6	40.8	7.6	B-89-T23D6	54.4	4.6
C-89-T40D6	52.7	6.3	G-89-T40D6	40.6	11.2	B-89-T40D6	44.3	6.8
C-89-T60D6	48.3	2.9	G-89-T60D6	30.7	9.6	B-89-T60D6	25.1	15.8

8.3.4.2 Compression

Compression test was conducted on 50 mm FRP rings to obtain the mechanical properties in longitudinal direction. The experimental results are summarised in **Table 8-7**. As is seen, similar to split-disk tests, CFRP tubes showed the best compressive performance amongst all types of tubes, while significantly higher reductions were observed in BFRP and GFRP tubes. Moreover, the compressive strength reductions of tubes with 89° fibres were more than that of tubes with multiple fibres. The failure modes observed in **Figure 8-11** could be used to explain this observation. It is well known that the fibre/resin interface damages are the main reason of FRP mechanical properties under environmental conditioning. Therefore, the adverse effect of resin/fibre interface degradation on the compressive properties of tubes with resin/fibre interface fracture (i.e. tubes with 89° fibres) is higher than that of tubes with local buckling failure (i.e., tubes with multiple direction fibres).

By comparing the mechanical test results, it can be concluded that FRP tubes with fibres oriented in different directions have better durability than that of tubes with fibres oriented just in hoop direction. Similar to the hoop tensile results, in tubes with fibres all oriented in hoop direction, an early fibre/resin interface damage will lead to the fibre/resin debonding progression in the hoop direction, which consequently results to the early tube failure. In contrast, the tubes with multiple fibres, will still carry loads in various directions even if damages occur in one direction. Therefore, one can conclude that, although more fibres oriented in hoop direction will increase the confinement strength of concrete filled FRP tubes, the low axial strength and fibre/resin debonding along the hoop direction after environmental conditioning will lead to an early tube rupture and consequently the failure of the concrete filled FRP tube.

Table 8-7 Experiment results of compression test of fully-filled samples

Specimen	Strength Retention (%)	CV (%)	Specimen	Strength Retention (%)	CV (%)	Specimen	Strength Retention (%)	CV (%)
C-M-Ref	100.0	1.9	G-M-Ref	100.0	2.0	B-M-Ref	100.0	2.4
C-M-T23D1	100.7	2.3	G-M-T23D1	97.6	2.8	B-M-T23D1	90.2	2.9
C-M-T40D1	100.7	2.1	G-M-T40D1	87.8	5.6	B-M-T40D1	88.6	5.8
C-M-T60D1	100.2	8.6	G-M-T60D1	85.1	3.8	B-M-T60D1	87.9	5.3
C-M-T23D3	99.6	3.6	G-M-T23D3	92.8	1.6	B-M-T23D3	89.3	3.5
C-M-T40D3	98.2	4.7	G-M-T40D3	87.3	9.2	B-M-T40D3	89.3	10.0
C-M-T60D3	93.2	1.9	G-M-T60D3	83.9	6.3	B-M-T60D3	87.1	1.5
C-M-T23D6	99.1	3.1	G-M-T23D6	73.5	5.3	B-M-T23D6	77.6	7.3
C-M-T40D6	94.1	2.1	G-M-T40D6	68.0	10.1	B-M-T40D6	74.5	3.8
C-M-T60D6	87.7	3.0	G-M-T60D6	59.1	6.9	B-M-T60D6	63.6	4.0
C-89-Ref	100.0	3.0	G-89-Ref	100.0	2.0	B-89-Ref	100.0	5.0
C-89-T23D1	95.7	10.2	G-89-T23D1	90.4	6.0	B-89-T23D1	93.2	6.7
C-89-T40D1	98.6	1.0	G-89-T40D1	81.3	5.6	B-89-T40D1	88.1	9.0
C-89-T60D1	97.8	4.2	G-89-T60D1	74.2	9.7	B-89-T60D1	76.0	8.6
C-89-T23D3	96.0	10.7	G-89-T23D3	81.4	4.3	B-89-T23D3	86.8	5.1
C-89-T40D3	95.7	1.5	G-89-T40D3	69.3	11.8	B-89-T40D3	78.2	3.2
C-89-T60D3	93.4	2.2	G-89-T60D3	72.2	12.9	B-89-T60D3	65.2	5.7
C-89-T23D6	74.2	11.8	G-89-T23D6	70.9	7.9	B-89-T23D6	79.5	14.9
C-89-T40D6	69.6	8.5	G-89-T40D6	66.9	8.6	B-89-T40D6	77.8	11.7
C-89-T60D6	62.0	13.6	G-89-T60D6	51.2	9.9	B-89-T60D6	55.3	5.0

8.4. Long-term prediction of mechanical properties

In order to predict the long-term performance of SWSSC filled FRP tubes under seawater, Arrhenius model [156, 158, 260] was used. Based on the behaviour of composites in accelerated aging tests, researchers proposed the following models to predict the mechanical strength retention:

$$Y = a\log(t) + b \tag{8.10}$$

$$Y = 100\exp(-\frac{t}{\tau}) \tag{8.11}$$

$$Y = (100 - Y_{\infty})\exp(-\frac{t}{\tau}) + Y_{\infty} \tag{8.12}$$

where Y (%) represents the retention of the composite mechanical properties; Y_{∞} (%) is the retention of the mechanical properties after infinite exposure time; t is the exposure time; a and b are the regression constants; τ is fitted parameter. **Eq. 8.10**, has some limitations. For instance, it is only a test data phenomenological representation and does not consider the degradation mechanism of the materials. However, the degradation mechanism of **Eq. 8.11** and **Eq. 8.12** is assumed to be fibre/matrix interface debonding. Although, the failure mode of some samples changed after conditioning, in the present study, the degradation mechanisms of all samples are assumed to be the resin/fibre interface degradation, and thus the results of all samples were used for log-term predicting models.

Eq. 8.11 was used in this study since the retention values of the mechanical properties after 6 months of conditioning did not converge (i.e. $Y\infty$). The targets used for the prediction models were selected according to the previous research [4, 230] and related to four locations in Canada. Briefly, the following steps were performed to predict the long-term mechanical performance of different SWSSC-filled FRP tubes under seawater condition: (1) fitting **Eq. 8.11** to the mechanical test results in order to obtain τ (regression fitting parameter) for each temperature in a particular tube type; (2) constructing Arrhenius plots for each tube type in order to obtain $\frac{E_a}{R}$ (the slope of Arrhenius plots) for each tube, where E_a and R are the activation energy and the universal gas constant, respectively. With this regard, ln(t) versus 1000/T (1/K) is drawn, were t is the time in days for a sample to reach a certain retention value at the corresponding exposure temperature and T is the exposure temperature. It should be noted that ln(t) values are obtained using **Eq. 8.11** with τ value found in previous step. It is known that the different degradation rate and mechanisms will result different $\frac{E_a}{R}$ values [98]. There are several factors, such as materials type, cross-section configuration, fabrication type, conditioning duration and temperatures that may affect the $\frac{E_a}{R}$ value of different sample; (3) finding the time shift factor (TSF) using the following **Eq.**:

$$TSF = \exp[\frac{E_a}{R}(\frac{1}{T_0} - \frac{1}{T_1})] \tag{8.13}$$

where the lower temperature, T_0 is the target temperature (in this study mean annual temperature of one of the locations in Canada) and the higher temperature, T_1, is the exposure temperature in this study; (4) finally, constructing master curves by fitting **Eq. 8.11** to the transformed results. To obtain the transformed results, the exposure time at each temperature is multiplied by the corresponding TSF calculated in previous step. Master curves constructed for each tube condition for both split-disk and compression mechanical properties are shown in **Figure 8-15** and **Figure 8-16**, respectively. For more details regarding the long-term prediction procedure the readers may refer to [4, 230]. Based on the constructed curves, reduction factors could be recommended for each tube type. However, it is worth mentioning that according to the previous studies [4, 230], the retention values of the FRP composites may converge after a certain time of exposure. Therefore, the prediction values beyond the range of regression data could be extremely overestimating in some conditions. Hence, the short-term reduction factor, based on the range of data for the target locations are proposed in **Table 8-8**. As is seen, a significantly high reductions factors are proposed for tubes with 89° fibres for a relatively short period, while longer periods with smaller reduction factors (especially for CFRP tubes) are proposed for tubes with multiple fibres. Therefore, using tubes with multiple fibres direction under aggressive environments are recommended rather than tubes with 89° fibres. Similar to the BFRP and GFRP tubes used in the present study, relatively high reduction factors were reported by researchers for BFRP and GFRP tubes and reinforcing bars when exposed to concrete environment. By using **Eq. 8.12**, Bazli el. [230] proposed tensile reduction factor of 0.4 and 0.65, respectively, for GFRP pultruded tubes exposed to simulated SWSSC (both inner and outer condition of the tube) and simulated SWSSC (inner condition) and seawater (outer condition). Wang et al. [4] reported a reduction factor of 0.67, using **Eq. 8.12**, for the life-span (i.e. $Y\infty = 0.67$) of BFRP bars when exposed to high performance SWSSC. They also reported a reduction factor of 0.7 after 10.6-19.6 years of conditioning by using **Eq. 8.11**. In another study by Davalos et al. [94] the long-term retention ($Y\infty$) of GFRP bars in concrete environment was reported as 45% for GFRP bars. The results of the present study and those reported in the literature, confirm the fact the BFRP and GFRP composites are vulnerable to alkaline environment, and thus proper design considerations need to be taken into account when using them together with concrete.

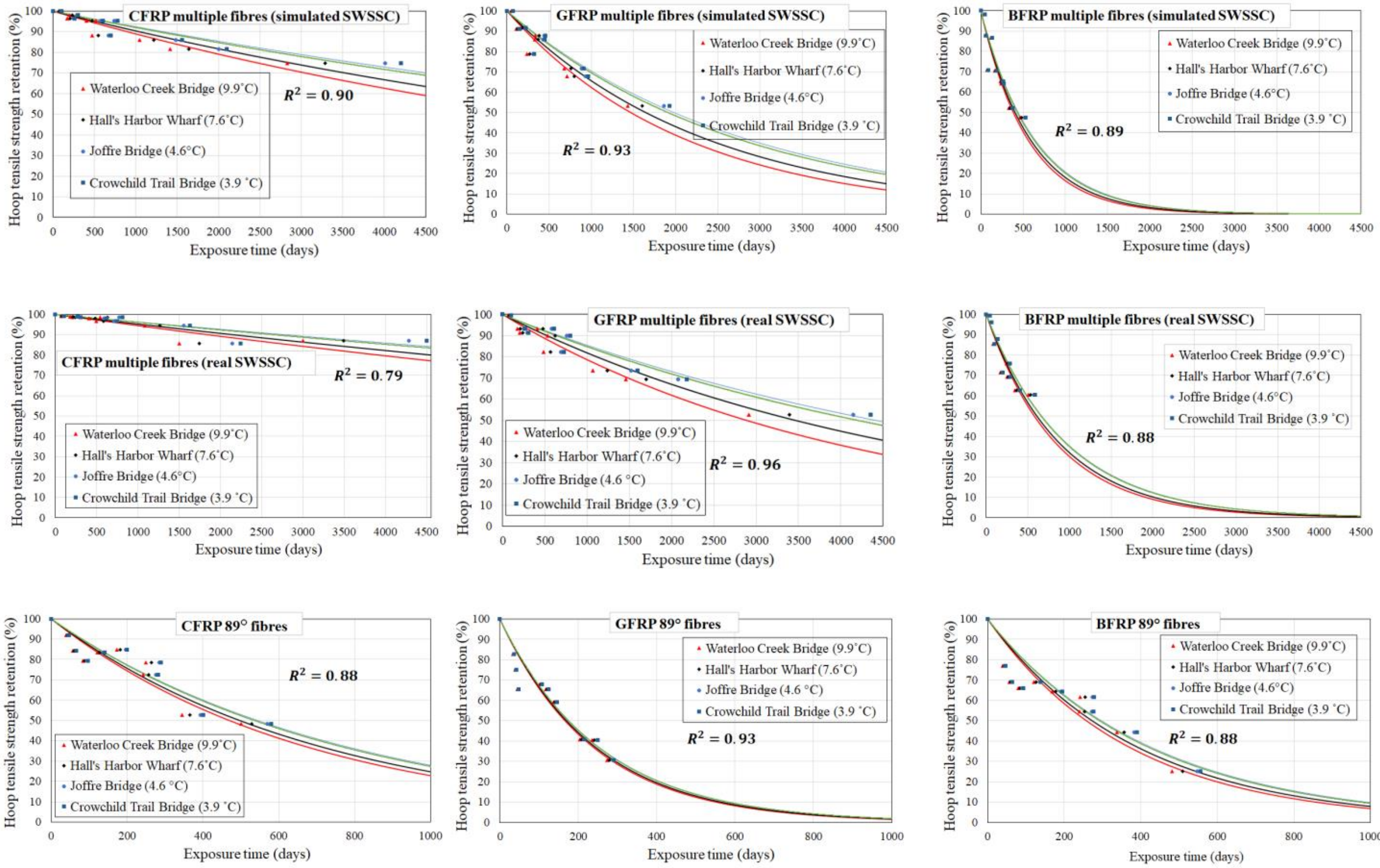

Figure 8-15 Long-term prediction: master curves constructed for each tensile tube subjected to SWSSC and seawater environment

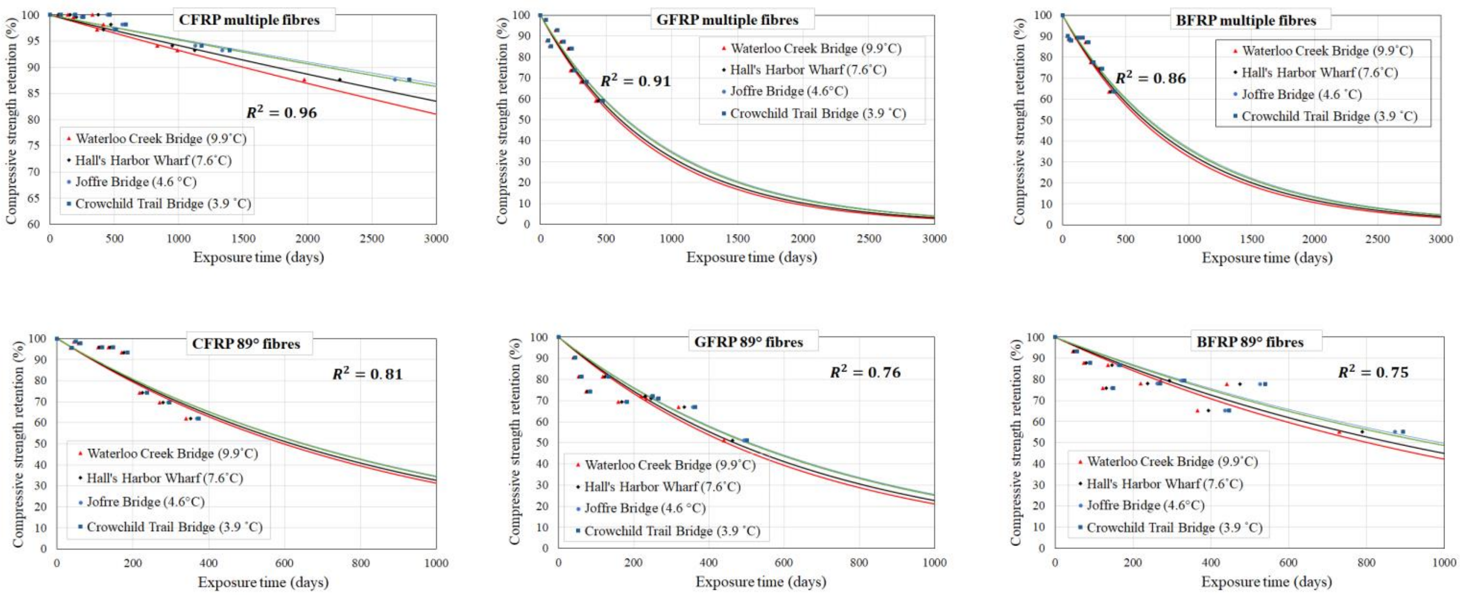

Figure 8-16 Long-term prediction: master curves constructed for each compressive tube subjected to SWSSC and seawater environment

In order to compare the tensile and compressive strength retentions of each FRP tube after conditioning, the proposed reduction factors related to a similar duration time for both compression and tension curves were compared in **Table 8-9**. For this purpose, firstly, between the compression and tension prediction master curves, the one which has the shorter period range is selected. As a reference point, the upper bound of the Waterloo Creek Bridge location was used. Then the reduction factor of the other curve, corresponding to the same duration of the previous curve was obtained. As is seen in **Table 8-9**, the compressive performance of all tubes except GFRP tubes with multiple fibres was better than hoop tensile performance. This observation reveals that the hoop tensile strength of FRP tubes, especially tubes with all fibres oriented in hoop direction, are more vulnerable to the SWSSC environmental conditions than that of compressive strength. It is important to note that, in previous study conducted by Bazli et all, it was shown that the compressive strength of pultruded FRP tubes are more vulnerable to SWSSC environment that longitudinal tensile strength [230].

Table 8-8 Short-term reduction factors for different tubes

Specimen	Fibres orientation	Mechanical properties					
		Hoop tensile strength (real SWSSC)		Hoop tensile strength (simulated SWSSC)		Compressive strength	
		Short-term period range (years)	Reduction factor	Short-term period range (years)	Reduction factor	Short-term period range (years)	Reduction factor
CFRP	multiple	8.2 - 12.3	0.84	7.74 - 11	0.72	5.4 - 7.6	0.88
	89°	-	-	1.37 - 1.6	0.48	0.9 - 1.0	0.69
GFRP	multiple	8.0 - 11.9	0.5	3.9 - 5.3	0.51	1.2 - 1.3	0.6
	89°	-	-	0.75 - 0.8	0.31	1.2 - 1.3	0.51
BFRP	multiple	1.4 - 1.6	0.54	1.26 - 1.4	0.43	1 - 1.15	0.66
	89°	-	-	1.3 - 1.5	0.27	2.0-2.40	0.53

Table 8-9 Comparison the compressive and hoop tensile strengths short-term reduction factors in Waterloo Creek Bridge (9.9 °C)

FRP tube type	Fibre orientation	Duration (days)	Tension RF	Compression RF
BFRP	multiple	367	0.51	0.66
	89 °	482	0.27	0.66
GFRP	multiple	438	0.81	0.60
	89 °	273	0.32	0.65
CFRP	multiple	1975	0.79	0.87
	89 °	352	0.59	0.66

8.5. Conclusion

As part of the research program of using seawater and sea sand concrete with FRP composites for construction applications, this study addresses the durability of different SWSSC-filled filament wound FRP tubes under seawater. Both mechanical performance and microstructural characteristics were investigated using compression tests, split-disk tests, SEM analyses and micro-CT analyses. Based on the test results and microstructural analyses, the following conclusions could be drawn:

- Considerable hoop strength reductions were observed for FRP tubes after aging. Regarding strength degradation, CFRP performs much better than GFRP, whereas GFRP shows superior durability performance than BFRP. The stiffness and Young's modulus of FRP in hoop direction do not degrade obviously and the maximum stiffness reduction after exposing to 60 °C seawater for 180 days is less than 10%.
- Simulated SWSSC environment is a relatively harsher condition than real SWSSC environment, and thus the durability results under simulated concrete environment is more conservative. For instance, the hoop tensile strength reductions of BFRP tubes after exposing to 60 °C seawater for 180 days are 52% and 40 % for simulated and real SWSSC conditions, respectively.
- Regarding the samples exposed to real SWSSC condition and seawater, no obvious microstructure changes in fibres or fiber/matrix interphase of CFRP and GFRP tubes occurs, while for BFRP tubes, the interface are degraded in some levels. However, significant interface degradation and also fibres damages occur in BFRP and GFRP tubes after exposure to simulated SWSSC and seawater environments. CFRP tubes remains intact also in this environment.

- FRP tubes with multiple fibre directions show better durability performance in both compressive and hoop strength retention compared to the tubes with fibres oriented in hoop directions. For instance, the hoop tensile strength reduction of BFRP tubes with multiple fibres after exposing to 60 °C seawater for 180 days is 52%, while the corresponding value is 40 % for BFRP with 89 ° fibres.
- Based on the micro-CT analyses, the percentage of voids in CFRP tubes does not change considerably after 6 months conditioning at 60 °C, while both GFRP and BFRP tubes show about 32 (%) and 22 (%) voids increment, respectively. Therefore, the amount of voids could be considered as an important factor in mechanical properties reduction of FRPs under harsh environments.
- Based on the long-term prediction results, using FRP tubes with all fibres oriented in 89^{o} is not recommended as their mechanical properties may significantly reduce (e.g. hoop tensile strength reduction factor of 0.27 after only 1.3 years' exposure to the condition) in long-term, while tubes, specially CFRP tubes, with fibres oriented in multiple directions could retain adequate strengths during their life-time performance.

Chapter 9 Mechanical properties of pultruded GFRP profiles under seawater sea sand concrete environment coupled with UV radiation and moisture

Abstract

In this research, the mechanical properties of various glass fibre reinforced polymer (GFRP) pultruded profiles exposed to seawater sea sand concrete (SWSSC) and its combination with UV radiation and water vapour condensation were studied. The effect of different conditions, duration of conditioning, and the profile cross-section configuration on the mechanical properties were investigated. Three-point bending, tension, and compression tests were carried out to obtain the mechanical properties, including flexural, tensile and compressive strengths and tensile elastic modulus. Furthermore, in order to scrutiny the mechanisms and extent of damage, scanning electron microscopy (SEM) was carried out on the test samples before and after the exposures. Finally, regression models were derived according to the experimental data to describe the mechanical properties of profiles after exposure to the aggressive environments used in this study. The maximum reductions of about 30 %, 33 % and 46 % were observed in three-point bending, tensile and compressive tests, respectively amongst all samples when exposed for 90 days to simulated SWSSC. These reductions increased for the same sections to 52 %, 47 %, and 50 % when the GFRP profiles were pre-exposed for 3000 h to UV radiation and moisture before immersion for 90 days to SWSSC.

Keywords

Pultruded GFRP profile; Mechanical properties; Durability; Seawater sea sand concrete (SWSSSC); UV

9.1. Introduction

Industrialisation and urbanisation necessitate increasing use of ordinary Portland cement (OPC)-based concrete that requires considerable amounts of freshwater and river sand, and hence, causes serious concern about resource shortages [8]. Due to the environmental issues and negative impacts on river ecosystems (i.e. navigation and flood control) caused by extraction of river sand, countries, such as China has recently issued some restrictions on sand-mining from particular places (e.g. Yangzi River) [9]. Therefore, the shortage of river sand and such restrictions, have led to the use of sea sand and crushed stone fine aggregates in some countries. UK's marine aggregates industry is an example with this regard. There are several successful infrastructures projects, such as, the city expansion in Singapore, the airport in Hong Kong, and the Middle East reclamation projects, in which sea sand has been used as a raw material in construction [9, 290, 291]. However, some limitations in particular places will also apply when using sea sand, which needs to be considered when using sea sand in concrete.

Therefore, it is highly attractive, for the constructions, at least in the coastal areas, conventional concrete can be replaced by seawater sea sand concrete (SWSSC) in which seawater and sea sand are used instead of freshwater and river sand, respectively [8, 99]. More details regarding the current developments and future opportunities of using SWSSC in construction application can be found in [9].

Recent studies have shown that the mechanical properties of SWSSC, including its workability and short-term and long-term compressive strength, are comparable to OPC-based concrete [10].

However, it is important to note that when SWSSC is used with conventional carbon steels as reinforcements, the steel will be significantly corroded due to the high chloride contents of seawater [12, 216]. Using corrosion-resistant materials, such as fibre-reinforced polymer (FRP) and stainless steel, has been recently proposed to address this issue [106, 208]. With this regard, several studies have been conducted to investigate the structural short-term and long-term performance of such hybrid structures under various loading and environmental conditions [13, 230, 249, 292-295].

FRP composites have many applications in different areas, such as the civil engineering construction [3, 4, 103, 129, 130], and aerospace and automotive industries [1, 2, 220]. High strength, high stiffness, low weight, corrosion resistance and ease of usage are some of the advantageous characteristics of FRPs [5-7, 170] that have made them an interesting alternative to traditional steel reinforcement, especially in corrosive areas [183, 268].

Although FRP composites have many advantages, some issues, such as low shear strength [73], vulnerability to high temperatures [38, 63, 162] and aggressive environments [113, 268] prevent them from being widely used in construction applications [73]. There are several studies on the durability of different FRP composites under various environmental conditions, such as alkaline (i.e., when used with concrete), acidic, seawater, ultraviolet (UV) radiation and thermal cycles [18, 106, 113, 128, 256, 267]. The degradation of FRPs under these conditions are attributed to damages to the resin, in terms of swelling, delamination hydrolysis and plasticization [29], chemical attack of the fibres in terms of metallic cations leaching and chemical bonds breaking [18] (except for carbon fibres, which are resistant to chemical environments), and deterioration of the fibre-resin interface (in terms of delamination, debonding and osmotic cracking) [30].

In various applications, FRPs with concrete may be regularly subjected to elevated temperature, moisture and UV radiation throughout their life [39]. Furthermore, before their actual use, FRP composites may also be exposed to harsh environments during storage and transportation. Previous studies have suggested the FRP composites to be vulnerable to alkaline environments [18, 113] while they are resistant to harsh daily conditions [64, 73]. However, there is little information on the effect of the prior exposure of FRPs to UV radiation and hydrothermal cycles before they are deployed for actual concrete construction. Such prior exposure may initiate surface discontinuities and defects that may accelerate the degradation process during the subsequent exposure to alkaline environments.

Prediction of the mechanical properties of composite materials have always been a challenging research topic both from theoretical [296, 297], and experimental [113, 298] perspectives. The deterioration in mechanical properties of FRP composites when they are used as reinforcement for concrete (i.e., in alkaline environments) is a considerably investigated topic for conventional OPC-based concrete [18, 30, 94-98]. Though the use of FRP composites as reinforcement for SWSSC is a relatively recent concept, but because of its attractive industrial implications, there have been considerable studies on the durability of FRPs in SWSSC environments [12, 99]. However, the studies on the durability of FRP in SWSSC have generally focused on the concrete-filled FRP tubes (CFFTs) [200, 230, 248, 249] and FRP reinforcing bars [4, 12, 99, 137, 299-301]. The performance of other commonly employed FRP profiles (such as I-shaped, channel, box, etc.) has not been investigated for their use in SWSSC. There is a need to address this significant knowledge gap.

Regarding the role of UV radiation and hydrothermal effects on the FRP composites mechanical properties, the reported studies have investigated FRP laminates [39, 106] and reinforcing bars [39, 165]. Recently, Bazli et al. studied the effect of UV and moisture on the pultruded GFRP profiles mechanical properties [73]. However, the combined effect of a harsh daily environment and SWSSC has not yet been addressed.

Therefore, in order to address the knowledge gaps described earlier, this study investigated the mechanical properties of various pultruded GFRP profiles after exposure to SWSSC alone as well as its combination with UV radiation and moisture cycles.

9.2. Experimental Program

The present study investigated the flexural, tensile and compressive properties of different pultruded GFRP profiles after exposure to a simulated SWSSC environment and a combination of SWSSC environment with UV and moisture cycles. The profiles were tested under three-point bending, tension and compression. The effects of conditioning time and the cross-section configuration of the profiles in different environmental conditions were studied. To study the damage mechanisms and degradation level, some samples were selected and examined under a scanning electron microscope (SEM) before and after a specific level of conditioning.

9.2.1. Materials

To study the effect of cross-section configuration, several sections were selected: two types of I-shaped sections and channels as flexural samples, two types of circular tubes and boxes as compressive samples and two types of laminates as tensile samples. **Table 9-1** shows the cross-section characteristics of the different profiles used in this study, where P, A, I_x, and I_y are the cross-section perimeter, area, moment of inertia about the x-axis, and moment of inertia about the y-axis, respectively. All the profiles were fabricated using continuous E-glass as fibres and vinylester as the resin. It should be noted that all the profiles had a strand mat layer and a thin surface veil in addition to the inner unidirectional roving part. **Figure 9-1** shows the typical pultruded GFRP profiles used in this study. **Table 9-2** lists the characteristics of the profiles reported by the manufacturer. More details regarding the GFRP profiles used in this study can be found in [73].

Table 9-1 GFRP cross-section profiles

Cross-section profile	Cross-section name	b (mm)	h (mm)	t (mm)	P (mm)	A (mm^2)	I_x (mm^4)	I_y (mm^4)
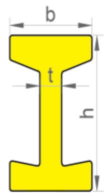	I1	15	25.5	4	99.38	206	16882	2687
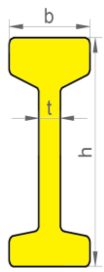	I2	15	38.3	4	119.46	293	54113	3488
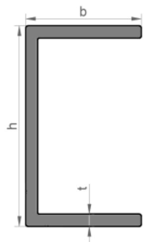	U1	50	30	3	212.28	312	120702	27382
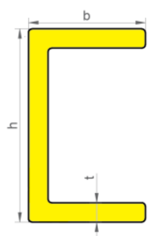	U2	50	30	5	206.57	499	178632	41299

Table *9-1* Continued

Cross-section profile	Cross-section name	b (mm)	h (mm)	t (mm)	P (mm)	A (mm^2)	I_x (mm^4)	I_y (mm^4)
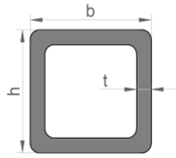	B1	25	25	3	188	264	-	-
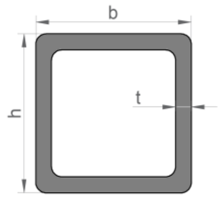	B2	30	30	3	228	324	-	-
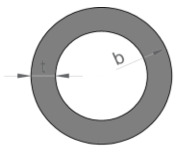	C1	13	-	4.5	135.02	303	-	-
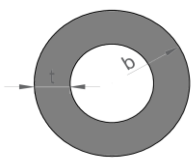	C2	13	-	6	125.6	377	-	-
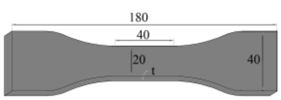	L	-	-	2, 5	-	40, 100	-	-

Table 9-2 Pultrusion process and Profiles characteristics

Properties	**Values**
Fillers (wt % of the resin)	Nano Clay (2 wt %) – Carbonate Calcium (12 wt %)
Fibre content by volume (%)	60
Pultrusion average speed	0.25 m/min
Pultrusion temperature (˚C)	130 (entrance) – 170 (exit)
Average tensile strength (MPa)	400
Tensile elongation at rapture (%)	2.5
Average flexural strength about major axis (MPa)	460
Average axial compression strength (MPa)	550
Density (g/cm^3)	2
Water absorptivity rate (%)	0.2 - 0.6
Thermal expansion coefficient (10^{-6} / ˚C)	4.5
Glass Transition Temperature, T_g (˚C)	100 - 105

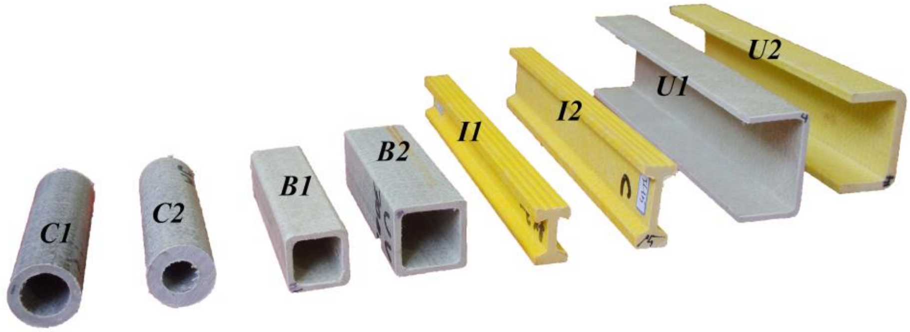

Figure 9-1 Typical GFRP pultruded profiles used in this study

9.2.2. Environmental conditioning

Three sets of samples were tested. The first set, the “reference”, is consisted of the control samples that were tested at ambient temperature and without any prior conditioning. The second set consists of the samples exposed to the simulated SWSSC solution. The third set consists of the samples that were first exposed to UV and moisture cycles for different periods and then subjected to the simulated SWSSC.

The real conditions of SWSSC environment were simulated by using 35 g/l sodium chloride (NaCl), 19.6 g/l potassium hydroxide (KOH), 2.4 g/l sodium hydroxide (NaOH), and 2 g/l calcium hydroxide ($Ca(OH)_2$) in this study (further details regarding the simulation of SWSSC environment can be found in [249]).

Four hr of UV-A at 60˚C followed by 4 hrs of water vapour condensation at 50 ˚C is one of the ASTM G154 standard [64] schemes used to simulate the daily harsh environments that FRPs may experience (especially in coastal areas) during storage, transportation, and/or service life. The UV-A lamps used had a 340 nm wavelength and 0.85 W/m^2 irradiation intensity (more details regarding the UV lamp’s characteristics, chamber configuration, and simulation parameters can be reached in [73]). **Table 9-3** shows the details of the conditioning environments and the number of samples tested in each set.

Table 9-3 Different environmental conditions and number of specimens tested in each condition

Environmental condition	I1	12	U1	U2	B1	B2	C1	C2	L	Total Number
Control	6	6	6	6	3	3	3	3	6	42
30 days SWSSC	-	-	-	-	3	3	-	3	-	9
90 days SWSSC	6	6	6	6	3	3	3	3	6	42
1000 h cycles + 30 days SWSSC	-	-	-	-	3	3	-	3	-	9
3000 h cycles + 30 days SWSSC	-	-	-	-	3	3	-	3	-	9
1000 h cycles + 90 days SWSSC	6	6	6	6	3	3	3	3	6	42
3000 h cycles + 90 days SWSSC	6	6	6	6	3	3	3	3	6	42
Total	24	24	24	24	21	21	12	21	24	195

9.2.3. Mechanical tests

A Santam universal testing machine with 150 kN maximum loading capacity was used to carry out all mechanical tests. **Figure 9-2** shows the details of mechanical test set-ups. The details of each mechanical test are presented in the following sections.

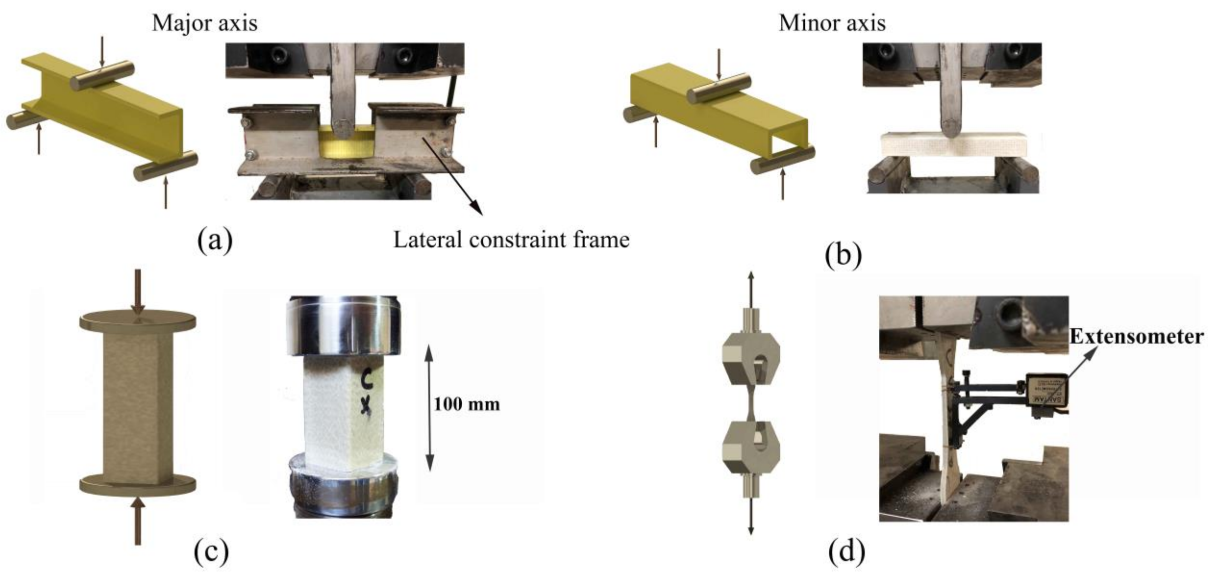

Figure 9-2 Mechanical test set-ups: (a) Three-point bending about the major axis, (b) three-point bending about the minor axis, (c) compression, and (d) tension

9.2.3.1 Three-point bending

All flexural samples had 230 mm lengths. A constant span of 200 mm between two supports was used in this study to achieve various failure modes for different sections. To reach a comprehensive understanding of the flexural properties of GFRP profiles after conditioning, bending tests were carried out on both the major and minor axes for each sample. The loading rate used in bending tests was 1.1 mm/min. Tests were terminated when the applied load dropped to about 70 % of the maximum experienced load or the sample mid-span deflection was about 20 mm. Two reverse steel channels (see **Figure 9-2(a)**) were used to prevent flexural samples from lateral movements (i.e., lateral-torsional buckling). Details regarding the lateral buckling of pultruded profiles can be found in [302]. To examine the reproducibility and validity of the results, in most cases, triplicate, and in some cases, duplicate tests were carried out for each condition, and the averaged results were used.

9.2.3.2 Compression tests

All compressive samples were cut into 100 mm lengths in order to prevent global buckling. Similar to three-point bending tests, the loading rate used in compression tests was 1.1 mm/min. The results used for discussion are the average of the three identical tests in each condition.

9.2.3.3 Tensile tests

ASTM D3039/D3039M-17 [303] recommendations were used to conduct tensile tests. The configuration of tensile samples can be found in **Table 9-1.** The load was applied at the rate of 1.2 mm/min in tensile tests. The results used for discussion are the average of three identical tests for each condition.

9.2.4. Scanning electron microscope (SEM)

SEM analyses were conducted on selected samples before conditioning and after different periods of conditioning to investigate the damage mechanisms in terms of resin, fibres, and resin/fibre interface and damage level regarding the resin matrix cracking, and resin/fibre debonding. The samples were cleaned of any dust and then coated with a very thin layer of gold metal to avoid blurry images that can be caused due to a lack of electronic conductivity and charging.

9.3. Results and discussion

In this section, the results of the conditioning and mechanical tests, in terms of the profile appearance change, SEM analyses, failure modes, and bending, tension and compression tests are presented and discussed in detail.

9.3.1 Visual inspection after conditioning

The surface appearance of the reference pultruded GFRP profile with samples exposed to UV and moisture cycles conducted in [73], and samples exposed to SWSSC, UV, and moisture cycles followed by the simulated SWSSC conducted in this study is compared in **Figure 9-3**. As is seen, after exposure to the only UV and moisture cycles, the surface appearance in terms of the colour and lustre changed from just yellow and very shiny to whiter, less yellow, paler, and less shiny with increasing duration of conditioning. However, upon exposure, the simulated SWSSC for 90 days, the colour of the sample surface changed completely from yellow to white. This shows that the protective thin surface veil was destroyed and SWSSC is a significantly harsh condition for GFRP composites.

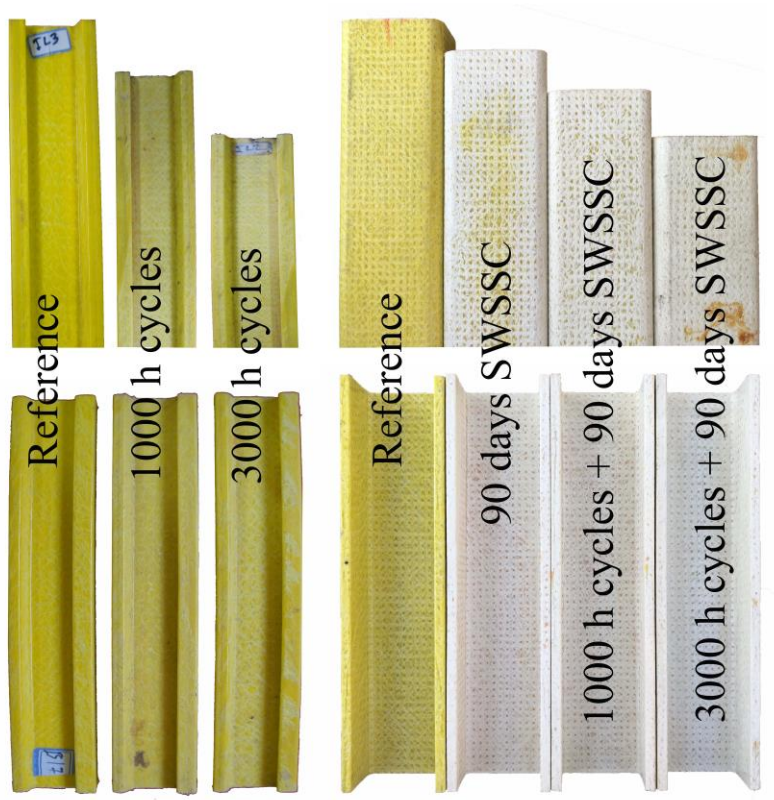

Figure 9-3 Appearance changes of the samples after exposure to different environments

9.3.2 **SEM analyses**

The selected SEM images of the reference sample with the samples exposed to UV and water vapour condensation cycles [73] and those exposed to UV and water vapour condensation cycles followed by exposure to simulated SWSSC, are compared in **Figure 9-4** and **Figure 9-5**, respectively. All the SEM samples were taken from I-shaped sections and were cut from the middle part of the web. By comparing the sample exposed to UV and vapour cycles with the reference sample, damage occurred from micro-cracks for shorter periods (i.e., 1000 h and 2000 h of exposure) and micro-cracks and some resin/fibre debonding for longer periods (3000 h of exposure).

The matrix cracks when samples are exposed to simulated SWSSC compared to the condition of only UV and vapour cycles are considerably longer and wider (**Figure 9-4** compared to **Figure 9-5**). To explain the reason, it is important to understand whether further penetration of the solution into the initial cracks contributes to the crack growth and consequent damage progression. Regarding the specimens exposed to SWSSC (**Figure 9-5**), significant damages in terms of resin matrix cracking, resin leaching, fibres pitting and cracking, and fibre/resin debonding were observed. Guo et al. [249] also reported similar damage mechanisms of FRPs when exposed to the SWSSC environment. However, due to the significant adverse effect of simulated SWSSC on the surface of the GFRP sample surface, it was not feasible to distinguish the exclusive damages caused due to different exposure conditions, i.e., the samples exposed to only SWSSC and SWSSC combined with UV and water vapour (i.e., distinguishing features between **Figure 9-5(a)** to **Figure 9-5(b-d)**).

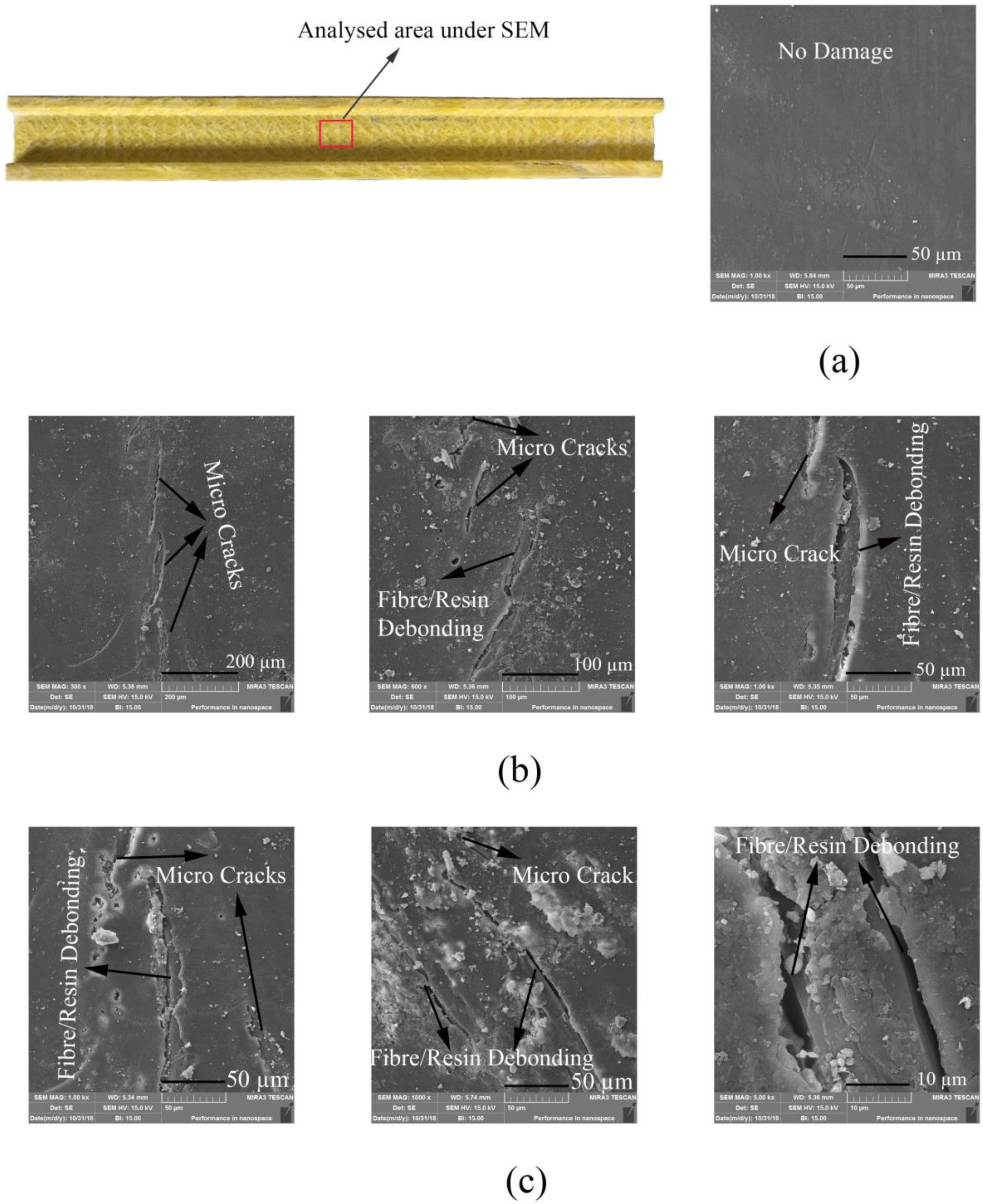

Figure 9-4 SEM images of UV and water vapour condensation cycles environment conducted in [73]: (a) Reference, (b) 1000 h cycles, (b) 1000 h cycles, and (c) 3000 h cycles

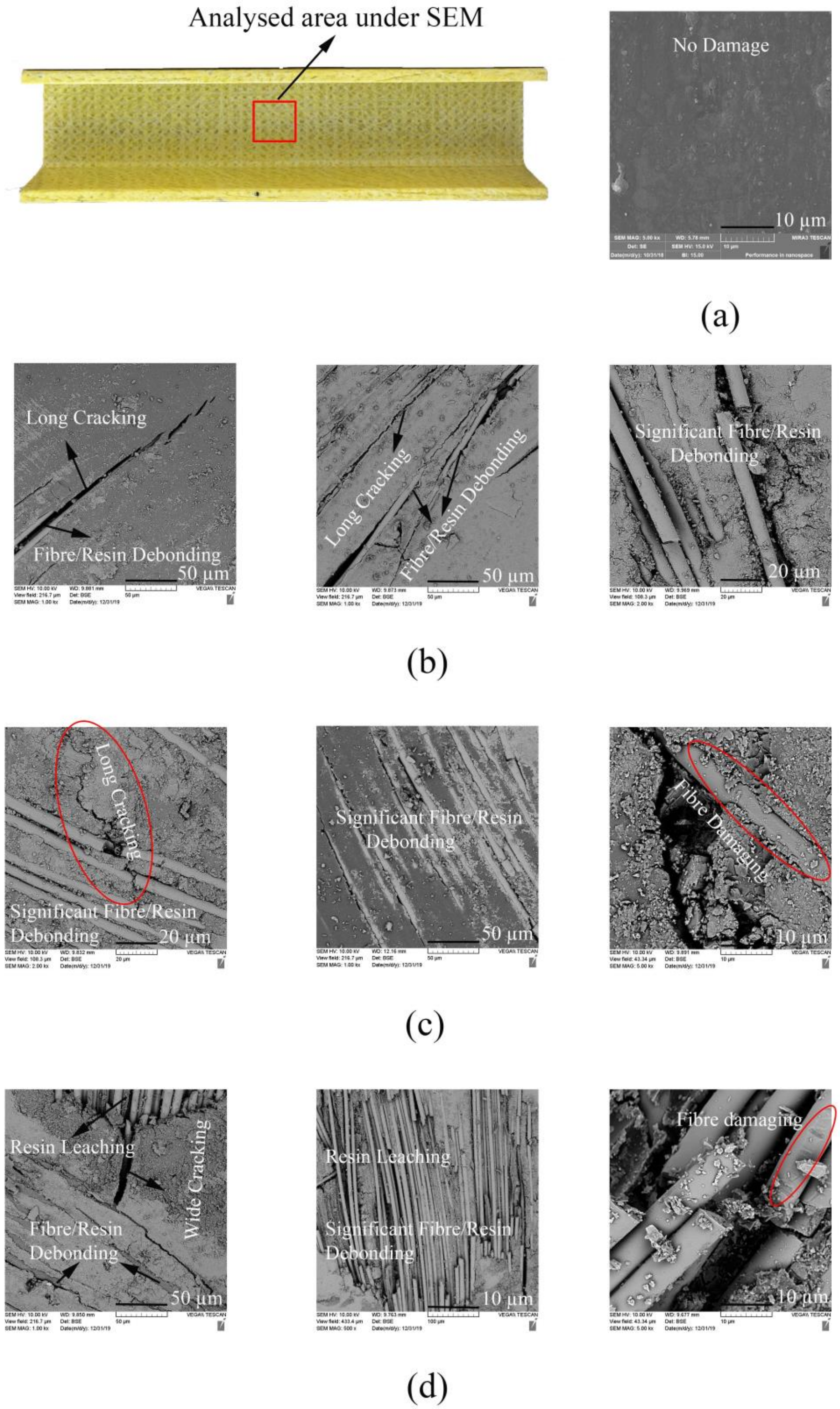

Figure 9-5 SEM images of environments conducted in this study: (a) Reference, (b) 90 days immersing in SWSSC, (c) 1000 h UV and vapour cycles followed by 90 days immersing in SWSSC, (d) 3000 h UV and vapour cycles followed by 90 days immersing in SWSSC

9.3.3 Failure modes

In this section, the failure modes of reference and conditioned GFRP profiles under different mechanical tests are discussed in detail. The combined failure modes were observed during bending tests. However, in this study, in order to compare the failure modes of reference and conditioned samples, the dominant failure mode of each condition was considered.

9.3.3.1 Three-point bending

9.3.3.1.1 I-shaped sections

The failure modes of selected reference and conditioned flexural I-shaped sections tested about their major axis are shown in **Figure 9-6**. It is seen (**Figure 9-6(a)**) that the dominant failure modes of the reference samples tested about the major axis were web cracking/crippling (i.e., web crushing and/or web buckling) and cracking at the web-flange junction (i.e., web-flange separation). Details regarding the web crippling behaviour of pultruded profiles can be found in [304]. It should be noted that due to the concentrated load, a partial failure was also observed under the loading nose; however, this was not the dominant failure mode. The high moment of inertia and concentrated load are the main reasons for the web crippling failure of the I-shaped sections [305]. Also, the high moment of inertia and low shear strength are the reasons for the interlaminar shear failure at the web-flange junction before the fibres fracture when sections are tested about their major axis.

The obvious difference observed between the failure modes of reference and samples exposed to the damaging environments, including the simulated SWSSC, was the location of the interlaminar shear failure. Regarding the reference samples, the web/flange junction separation (**Figure 9-6(a)**) was observed in all samples, while conditioned samples failed due to the interlaminar shear cracks at various locations of the flange and the web (**Figure 9-6(b)**). However, for both cases, the crack that was started at mid-span propagated toward the sample end. Significant degradation of the fibre/resin interface due to the conditioning is the main reason this earlier failure mode was observed in degraded samples. The other difference between the reference and conditioned samples was the sound at the moment of failure. Conditioned samples were failed with significantly lower noise compared to the reference sample at the moment of failure. This indicates that in conditioned samples, the initial cracks were already present due to the conditioning and just propagated under the loading, while in reference samples, the cracks were initiated during the test.

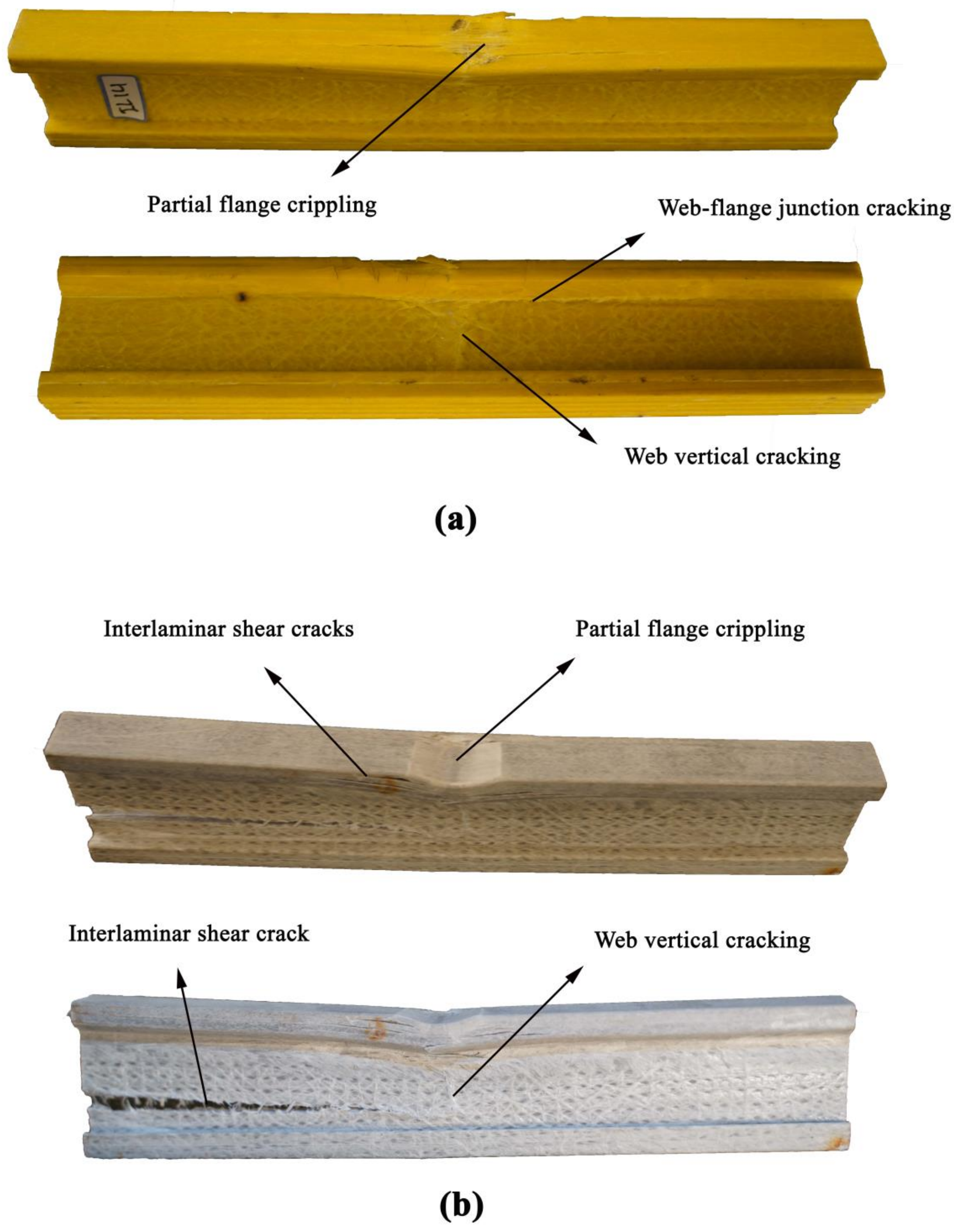

Figure 9-6 Typical failure modes observed in three-point bending tests about the major axis of I-shaped sections: (a) reference sample, and (b) sample exposed to 3000 h UV and moisture cycles followed by 90 days of SWSSC immersing

The failure modes of the selected reference and conditioned flexural I-shaped sections tested about their minor axis are shown in **Figure 9-7** shows. Regarding the reference samples (**Figure 9-7(a)**) tested about their minor axis, fibre failure in tension zone and resin failure and fibre buckling in the compression zone at mid-span were the dominant failure modes observed. In some cases, vertical web cracking was also observed after the dominant failure mode. However, as this failure mode was a delayed failure after the dominant failures, it was not considered in the discussion. The low moment of inertia, and consequently the low bending capacity, is the main reason for this type of failure. In other words, the bending capacity of I-shaped sections tested about their minor axis is lower than their interlaminar shear strength, and thus, flexural failure (i.e., fibre failure at the most critical section) occurs earlier than interlaminar shear failure. Observing different failure modes in bending about the major and minor axes prompted the study of the effect of different conditioning scenarios. Therefore, it is expected that the degradation of samples tested on their major axis is mainly related to the resin and resin/fibre interface degradation, while the fibre degradation also affects the samples tested about the minor axis.

As expected, due to the type of failure modes observed in the samples tested about the minor axis (flexural failure rather than interlaminar shear failure), no significant difference was observed between the reference samples and the conditioned samples (**Figure 9-7(a)** compared to **Figure 9-7(b)**). Therefore, it can be concluded that the degradation of the interlaminar shear strength due to the conditioning was not severe enough changing the failure mode (i.e. from flexural failure to interlaminar shear failure).

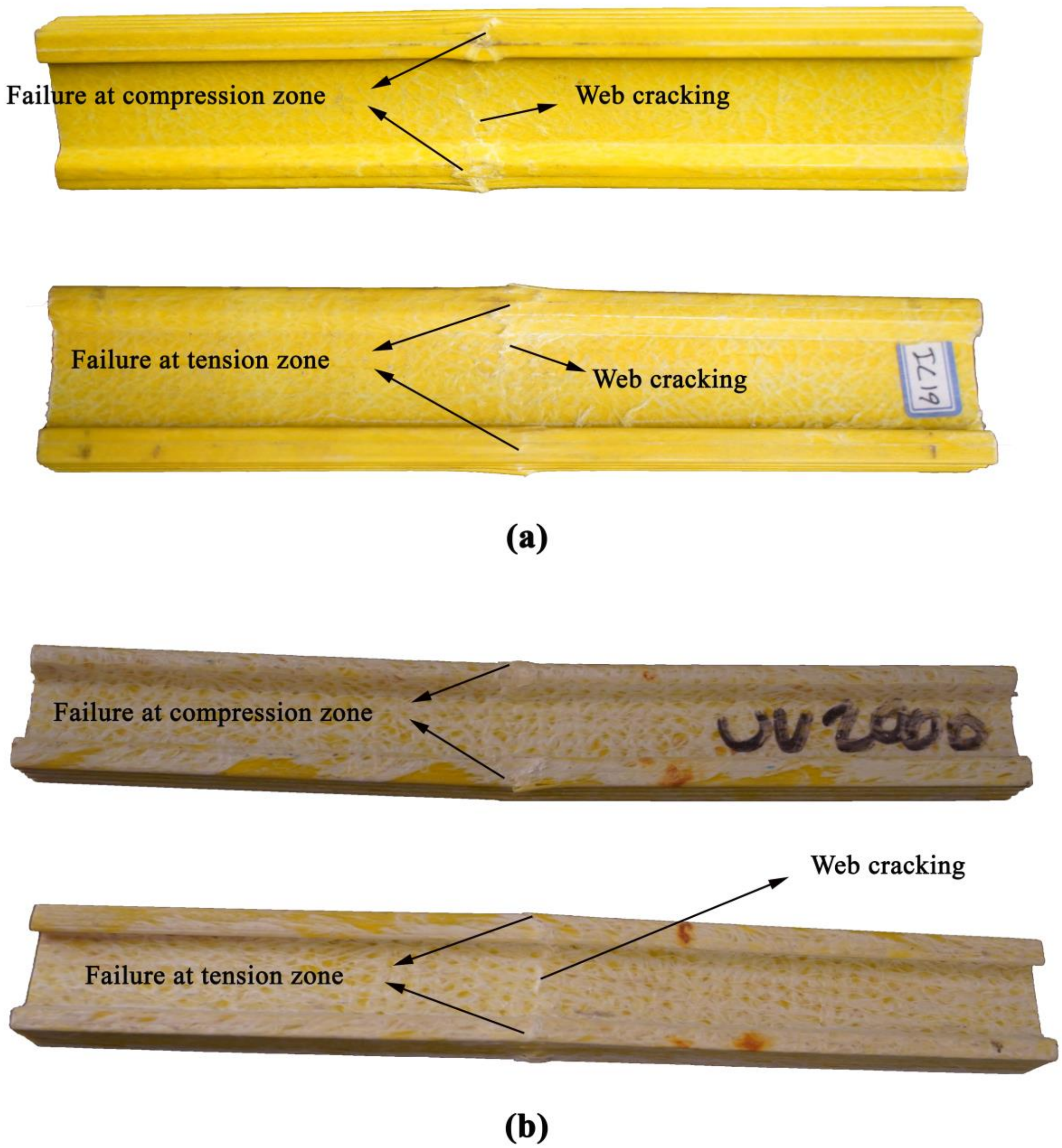

Figure 9-7 Typical failure modes observed in three-point bending tests about the minor axis of I-shaped sections: (a) reference sample, and (b) sample exposed to 2000 h UV and moisture cycles followed by 90 days of SWSSC immersing

9.3.3.1.2 Channel sections

The failure modes of selected reference and conditioned channel sections tested about their major axis are shown in Figure 9-8 shows. Similar to the I-shaped sections, the dominant failure modes observed in the reference channel sections tested about their major axis were the web/flange junction cracking and web cracking/crippling (**Figure 9-8(a)**). However, in channel sections, due to the out-of-plane moment during the bending test, the top flange was completely separated from the web, and this failure was more critical (especially for larger sections) than the web cracking/crushing.

The locations of the interlaminar shear cracking (i.e., longitudinal cracking perpendicular to the direction of the concentrated load) were the main difference observed between the reference and conditioned samples tested about the major axis. The crack was only at the web-flange junction in the reference samples (**Figure 9-8(a)**), while multiple longitudinal cracks along the flange and web-flange junction (**Figure 9-8(b)**) were observed during the test of the sample exposed to conditions including SWSSC. This again confirms the significant resin/fibre interface degradation and, consequently, the interlaminar shear strength reduction of the profiles after exposure to an SWSSC environment. Similar to I-shaped sections, much lower noise during the failure of conditioned samples compared to the reference samples was the other difference in failure modes about the major axis.

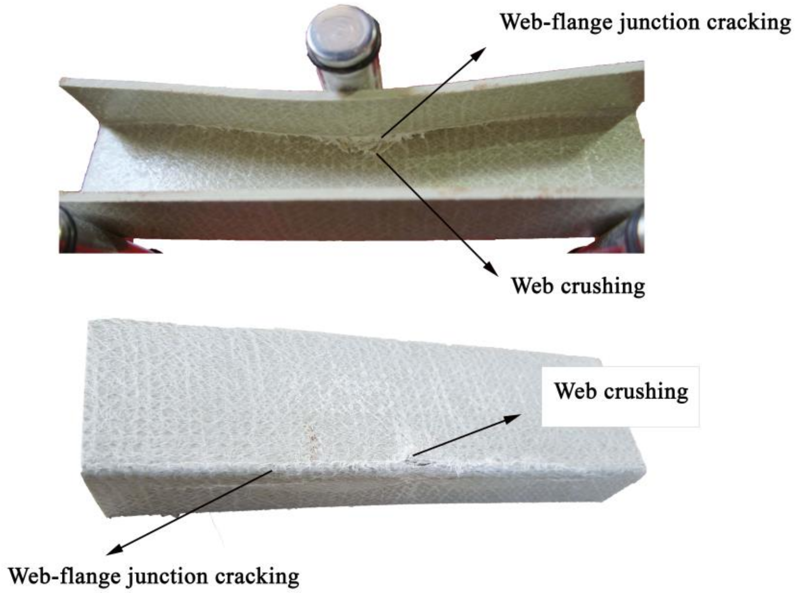

(a)

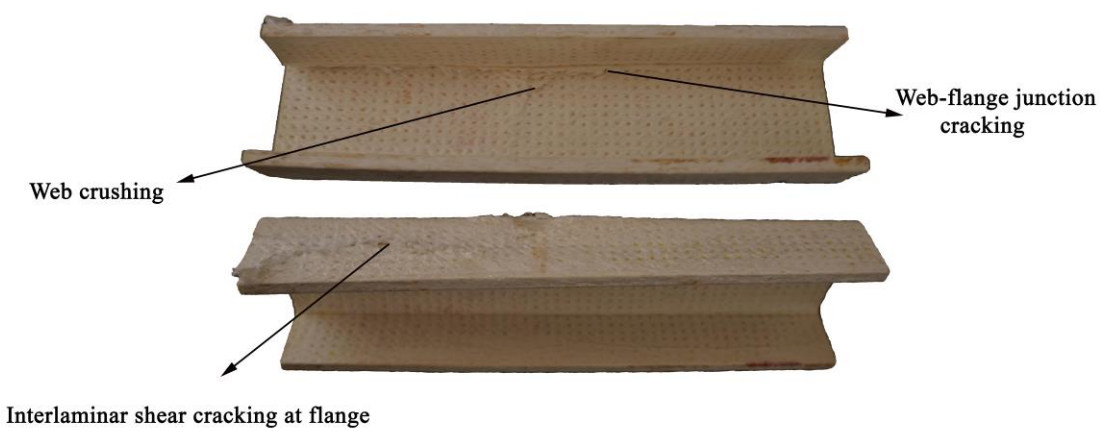

(b)

Figure 9-8 Typical failure modes observed in three-point bending tests about the major axis of channel sections: (a) reference sample, and (b) sample exposed to 2000 h UV and moisture cycles followed by 90 days of SWSSC immersing

The failure modes of the selected reference and conditioned channel sections tested about their minor axis are shown in **Figure 9-9**. As is seen in **Figure 9-9(a)**, unconditioned channels tested about their minor axis failed due to the combination of flexural failure (i.e., fibres fractured in the tension zone and resin failure and fibres buckling in the compression zone at mid-span) and web-flange junction cracking. However, the failure mode of the channels subjected to an SWSSC environment changed to web/flange junction cracking accompanied by crippling at the compression zone (**Figure 9-9(b)**). No fibre fractures at the tension zone were observed during the test of conditioned channels about the minor axis. This shows that the fibre/resin interface degradation was significantly high that changed the dominant failure mode (i.e., from fibres fracture to interlaminar shear failure).

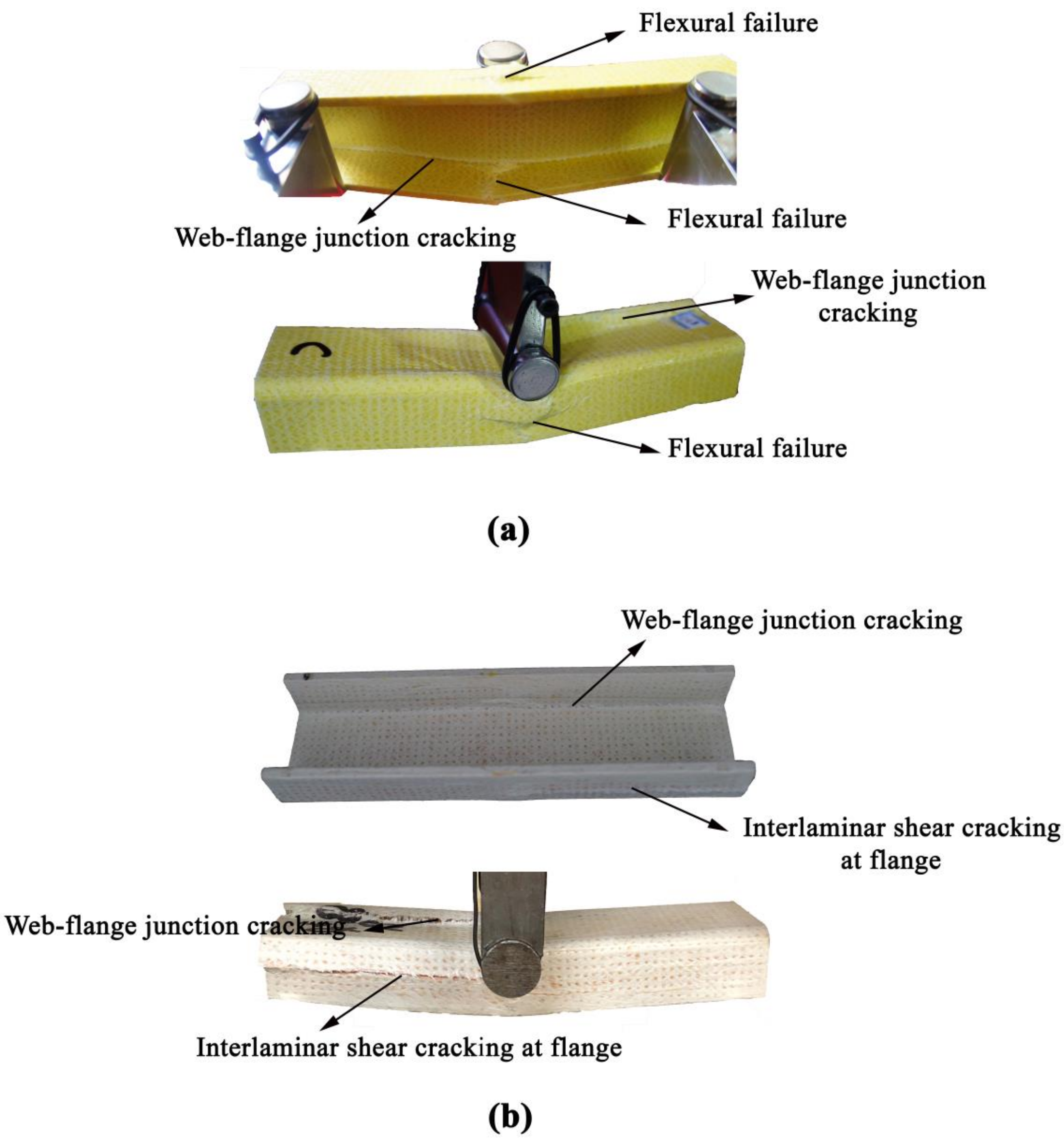

Figure 9-9 Typical failure modes observed in three-point bending tests about the minor axis of channel sections: (a) reference sample, and (b) sample exposed to 2000 h UV and moisture cycles followed by 90 days of SWSSC immersing

9.3.3.2 Tensile tests

The failure modes of the selected reference and conditioned samples are shown in **Figure 9-10**. The reference samples (both 2-mm and 5-mm laminates) failed due to the longitudinal splitting in various locations along the gauge area. In this case, fibre fracture was the dominant cause for the laminate's failure. However, the failure mode changes from the more fibre fracture along the gauge length in reference samples to more laminate layer delamination in samples exposed to conditions, including SWSSC. The reason for this failure change is the interlaminar shear strength reduction of the laminates due to the penetration of the simulated SWSSC throughout the thickness of the samples. Therefore, the delamination of the laminate layers occurs earlier than the fibre fracture during tensile tests of conditioned samples. It is worth mentioning that the failure mode observed in the previous study [73] regarding the tensile samples exposed to just UV and moisture cycles, exhibited same phenomenon. This indicates that SWSSC environment can be categorised as a significantly harsher condition than UV and vapour cycles. In fact, UV and moisture cycles mainly affect the samples surface, while the simulated SWSSC penetrates deeper into the sample and dramatically degrades the resin and fibre/resin interface.

Regarding the effect of thickness, the only difference between the failure modes of 2 mm and 5 mm laminates after the exposure to environments, including the simulated SWSSC, was the ratio of layers delaminated to the laminate thickness (obviously, the thicker the laminate, the smaller is the ratio).

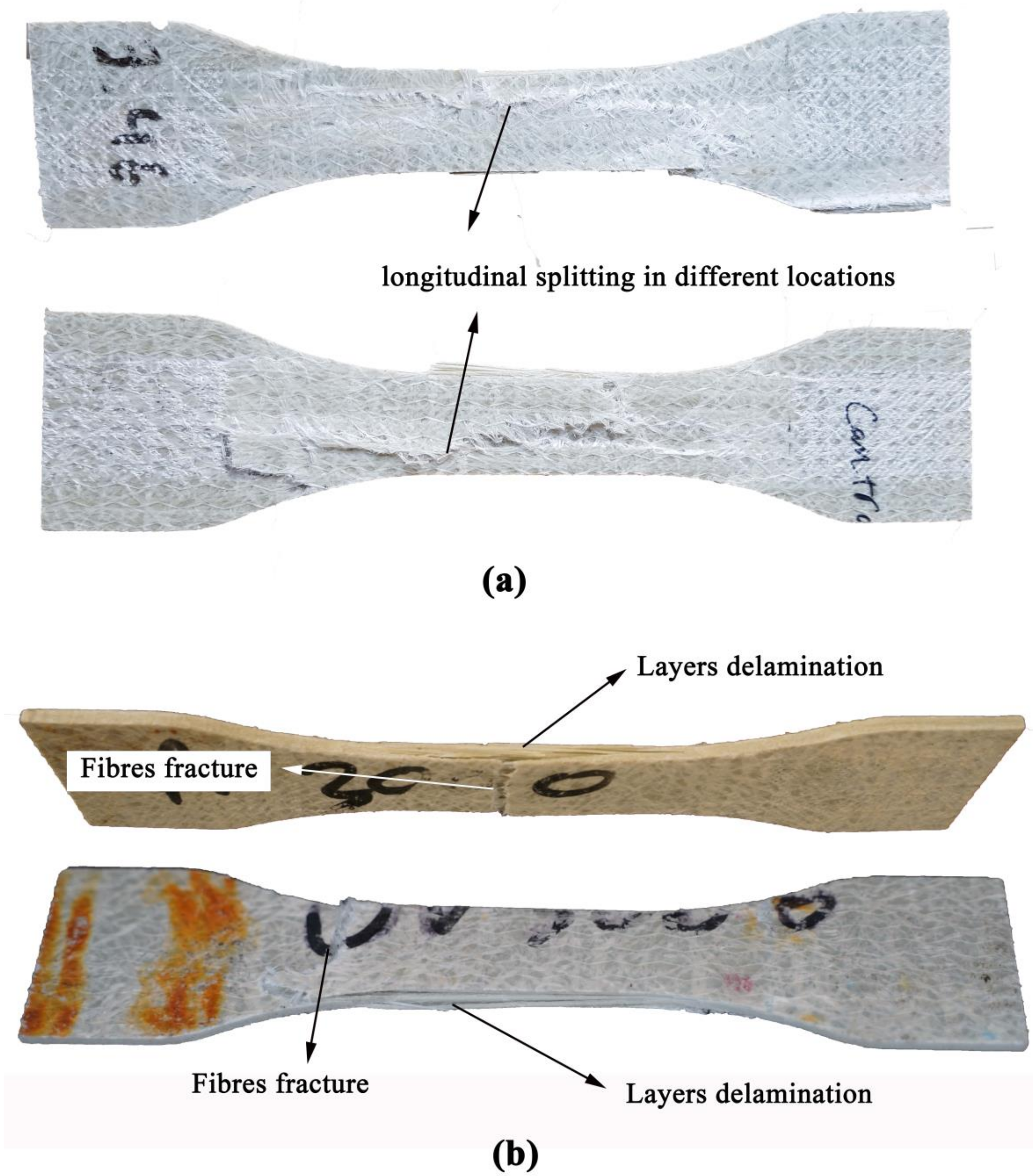

Figure 9-10 Typical failure modes observed in tensile tests: (a) reference sample, and (b) sample exposed to 3000 h UV and moisture cycles followed by 90 days of SWSSC immersing

9.3.3.3 Compressive tests

All reference and conditioned samples, regardless of the section type and conditioning environment, failed due to the elephant foot buckling (i.e., local buckling at the contact surface between the tube and the loading plate). Relatively low strength of the resin causes the resin to be frittered away at the contact surface, which results in the local buckling of the fibres at the end of compressive samples. Therefore, it can be inferred that the degradation of the resin matrix and the fibre/resin interface are the main reasons responsible for the compressive degradation in the mechanical properties of pultruded GFRP tubes in the present study. The typical failure mode observed for compressive samples is shown in **Figure 9-11**. It should be mentioned that no failure was observed on the side surface of the samples.

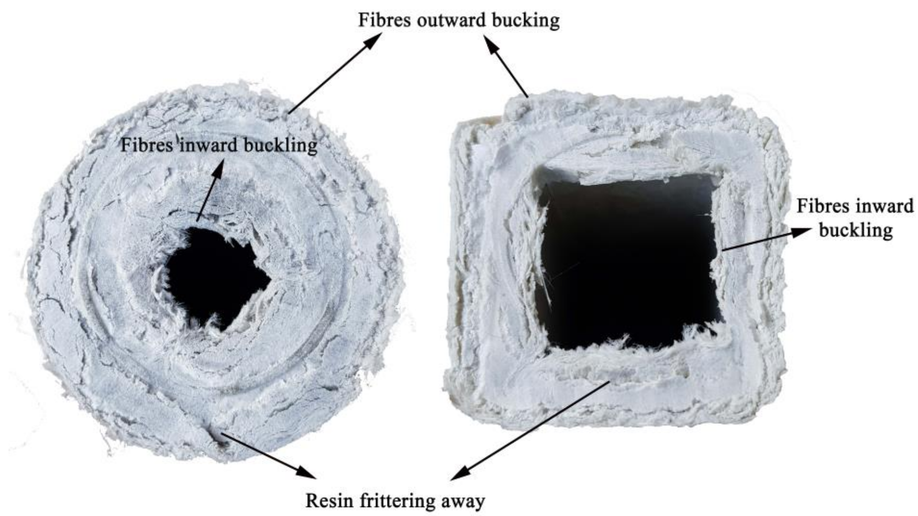

Figure 9-11 Typical failure mode of compressive samples

9.3.4 **Mechanical test results**

9.3.4.1 Three-point bending test

The bending results are presented in **Table 9-4.** In **Table 9-4,** samples are identified with two letters. The first letter represents the profile type (same as **Table 9-1**) and the second letter refers to the type of bending test (i.e., S represents strong (major) axis and W, the weak (minor) axis).

It is generally observed that the flexural strength of GFRP tubed tested under three-point bending about both major and minor axes decreased considerably under SWSSC and combined SWSSC and UV with water vapour cycles conditions. However, in order to determine the effect of different variables, firstly, the effect of different environments on the same section will be studied and later the results of different sections in the same environment will be compared with each other to investigate the effect of cross-section configuration.

Table 9-4 Three-point bending test results

Specimen	Conditioning type	Maximum load (N)	CV (%)	Retention (%)
I1-S	Control	6292	0.8	100
	90 days SWSSC	5012	3.7	79.6
	1000 h cycles + 90 days SWSSC	4561	3.2	72.4
	3000 h cycles + 90 days SWSSC	4182	1.9	66.4
I1-W	Control	3203	1.04	100
	90 days of SWSSC	2565	2.9	80.1
	1000 h cycles + 90 days SWSSC	2434	6.3	76.2
	3000 h cycles + 90 days SWSSC	2139	2.6	66.8
I2-S	Control	10793	2.22	100
	90 days of SWSSC	7578	3.58	70.2
	1000 h cycles + 90 days SWSSC	6744	4.12	62.4
	3000 h cycles + 90 days SWSSC	5223	4.8	48.3
I2-W	Control	6577	1.26	100
	90 days SWSSC	4853	5.2	73.7
	1000 h cycles + 90 days SWSSC	4419	4.57	67.2
	3000 h cycles + 90 days SWSSC	4321	3.2	65.7
U1-S	Control	4320	2.25	100
	90 days SWSSC	3727	3.12	86.3
	1000 h cycles + 90 days SWSSC	3752	3.3	86.9
	3000 h cycles + 90 days SWSSC	3335	4.7	77.2
U1-W	Control	7250	0.9	100
	90 days SWSSC	5131	6.5	70.7
	1000 h cycles + 90 days SWSSC	4815	1.8	66.4
	3000 h cycles + 90 days SWSSC	4277	5.4	59.0
U2-S	Control	7659	1.89	100.0
	90 days SWSSC	7161	4.4	93.5
	1000 h cycles + 90 days SWSSC	6631	4.1	86.6
	3000 h cycles + 90 days SWSSC	6622	5.3	86.7
U2-W	Control	11002	1.1	100
	90 days SWSSC	8658	2.7	78.6
	1000 h cycles + 90 days SWSSC	8062	1.5	73.2
	3000 h cycles + 90 days SWSSC	7529	6.3	68.4

9.3.4.1.1 Effect of different environments

The ultimate flexural strength retention of each section under different environmental conditions is compared in **Figure 9-12**. It is seen for all conditions, the combined environment of UV and vapour cycles with SWSSC is the most aggressive of all environmental conditions. This shows that the initial degradation in terms of micro-cracks and some resin/fibre debonding due to the UV and vapour cycles (see [73] for a detailed discussion) accelerate the degradation process of GFRP profiles when exposed to simulated SWSSC. Early penetration of the solution into the existing cracks (see **Figure 9-4**) will result in a wider crack, and consequently, more solution penetration, more resin leaching and more fibre/resin debonding (see **Figure 9-5**). In other words, UV and vapour cycles affect the outer layers of the profiles [73], in which the simulated SWSSC can penetrate through the cracks and voids, into the thickness of the samples and affect more layers of the profiles [230].

Regarding the samples exposed to combined conditions. As expected, for all samples except U2-S (in this condition, the reductions were the same for 1000 h and 3000 h exposures), the final flexural strength reduction of the samples exposed to 3000 h as the first conditioning is higher than that for sample exposed for 1000 h. This is due to the more initial cracks and fibre/resin debonding of samples exposed to 3000 h compared to 1000 h [73], which leads to higher final reduction after exposure to SWSSC. The possible reason for the different results observed in U2-S compared to other conditions can be explained by the failure mode of these sections. As mentioned earlier, channels tested about the major axis, due to the load eccentricity from the channel shear centre, fail earlier in comparison to the condition that the load is applied at the shear centre. Therefore, the degradation effect on the flexural strengths of channels tested about their strong axis is reduced to this phenomenon. Therefore, the reduction values will be close in different conditions, and thus the randomness of the samples will affect the results.

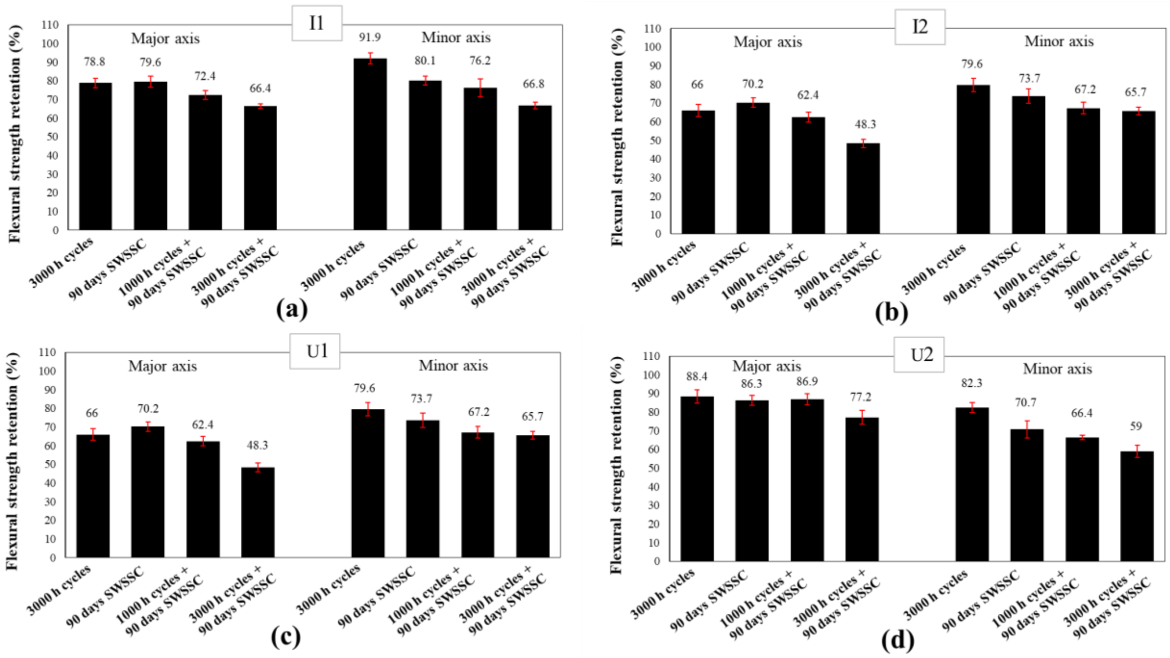

Figure 9-12 Comparison between the flexural strength retentions with respect to the conditioning environment: (a) Cross-section profile I1, (b) cross-section profile I2, (c) cross-section profile U1, and (d) cross-section profile U2

9.3.4.1.2 Effect of bending axis

The ultimate flexural strength retention of the profiles tested about the strong axis with the profiles tested about the weak axis is compared in **Figure 9-13**. Generally, for I-shaped sections, higher reductions in flexural strength were observed for samples tested about their major axis compared to the minor axis. To explain the reason, different failures observed during bending tests about both axes should be taken into account. The results reveal that samples that failed due to interlaminar shear (bending about the major axis) have experienced larger flexural strength reductions compared to samples that failed due to fibres fracture (bending about the minor axis). This confirms that resin degradation and, consequently, resin/fibre interface degradation is the main reason for the mechanical properties' degradation of FRP composites. Therefore, as these degradations significantly affect the interlaminar shear strength of GFRP profiles, more reductions are observed for samples with shear failure modes compared to the samples failed because of the fibres fracture. However, considering the reductions in bending about the weak axis, one can still conclude that the SWSSC environment is also detrimental to glass fibres (see **Figure 9-5(c)** and **(d)**).

Regarding the channel sections, in contrast to I-shaped sections, the flexural strength reductions of the channel profiles tested about the weak axis showed higher reductions in comparison to the samples tested about the major axis. As mentioned earlier, channels tested about the strong axis, due to the load eccentricity from the channel shear centre, fail earlier in this study in comparison to the condition that the load is applied at the shear centre. Therefore, the degradation effect on the flexural strengths of channels tested about their major axis is reduced due to this phenomenon.

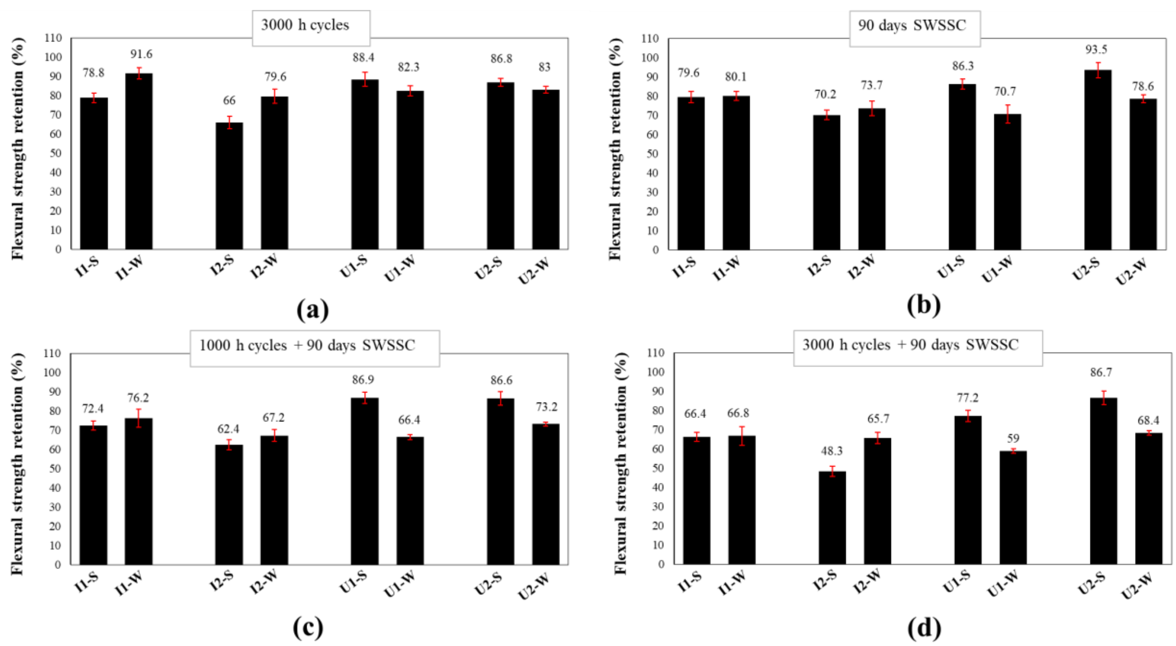

Figure 9-13 Comparison between the flexural strength retentions with respect to bending axis (S refers to Strong (major) axis, whereas W refers to Weak (minor) axis): (a) 3000 h cycles, (b) 90 days SWSSC, (c) 1000 h cycles + 90 days SWSSC, and (d) 3000 h cycles + 90 days SWSSC

9.3.4.1.3 Effect of cross-section configuration

The ultimate flexural strength retention of the GFRP profiles with respect to the configuration of the profiles cross-section is compared in **Figure 9-14**. Comparing the results of I-shaped sections shows that the performance of I1 sections in terms of the flexural strength about both weak and strong axes under different environmental conditions was better than the I2 section. This shows that profiles with a greater perimeter-to-thickness ratio (P/t) may experience more degradation. The same conclusion can be drawn by comparing the results of channel sections. As is seen in **Figure 9-14**, U1 with a smaller thickness (larger p/t ratio) showed larger reductions than U2 with the greater thickness (smaller p/t ratio). However, due to the same reason as mentioned earlier about the channels' failure mode, U2-S when exposed to 1000 h cycles and 90 days immersion compared to the corresponding U1-S sample showed a slightly higher reduction.

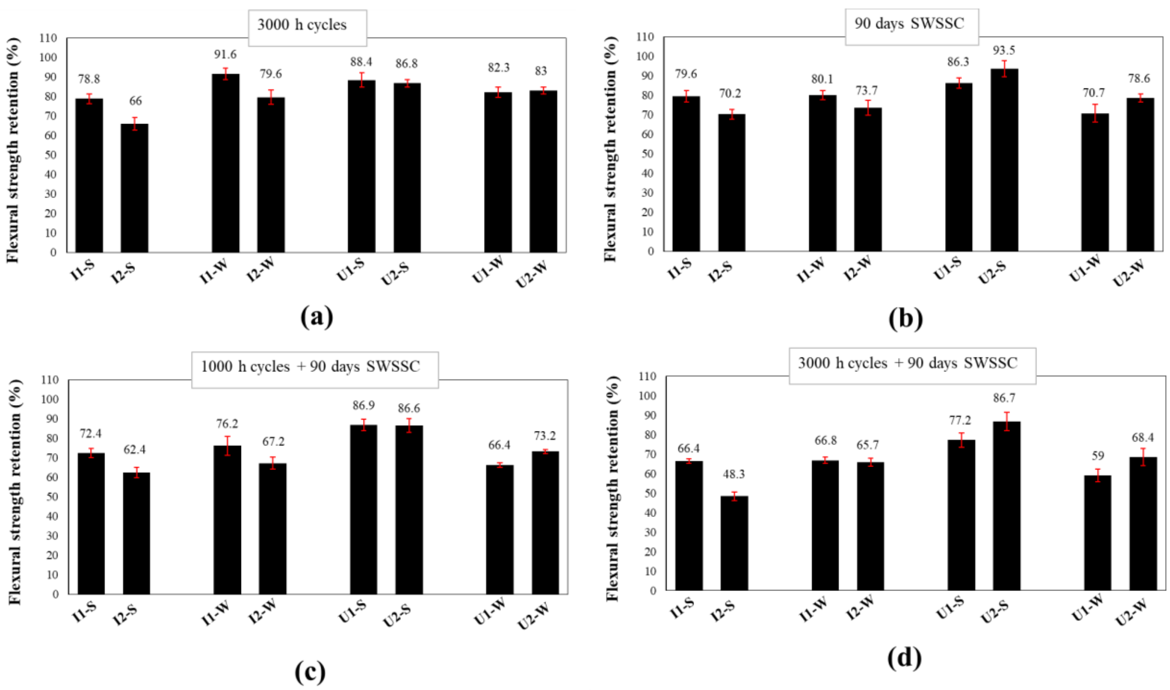

Figure 9-14 Comparison between the flexural strength retentions with respect to the profile cross-section configuration: (a) 3000 h cycles, (b) 90 days SWSSC, (c) 1000 h cycles + 90 days SWSSC, and (d) 3000 h cycles + 90 days SWSSC

9.3.4.2 Tensile test

The tensile test results of reference and conditioned samples are presented in **Table 9-5** and **Table 9-6.** It is generally observed that the tensile properties of GFRP laminates decreased considerably under SWSSC and combined SWSSC and UV with water vapour cycling conditions. Similar to the three-point bending tests, at first, the effect of different environments on the same section and then the effect of laminate thickness under each environment will be presented.

Table 9-5 Tensile strength test results

Laminate thickness	Conditioning type	Maximum Load (N)	CV (%)	Retention (%)
2 mm	Control	28345	1.12	100
	90 days SWSSC	19055	3.5	67.2
	1000 h cycles + 90 days SWSSC	15873	5.1	56.1
	3000 h cycles + 90 days SWSSC	15020	5.4	53.0
5 mm	Control	40906	0.89	100
	90 days SWSSC	30231	2.3	73.9
	1000 h cycles + 90 days SWSSC	25972	4.2	63.5
	3000 h cycles + 90 days SWSSC	23764	4.2	58.1

Table 9-6 Tensile elastic modulus test results

Laminate thickness	Conditioning type	Elastic modulus (GPa)	CV (%)	Retention (%)
2 mm	Control	35.0	1.7	100
	90 days SWSSC	29.7	1.4	84.9
	1000 h cycles + 90 days SWSSC	28.4	1.1	81.1
	3000 h cycles + 90 days SWSSC	28.1	2.3	80.3
5 mm	Control	45.0	2.1	100
	90 days SWSSC	36.1	1.8	80.2
	1000 h cycles + 90 days SWSSC	37.3	2.2	82.9
	3000 h cycles + 90 days SWSSC	36.4	1.5	80.9

9.3.4.2.1 Effect of different environments

The ultimate tensile strength retention of each laminate under different environmental conditions is compared in **Figure 9-15**. Similar to bending tests, samples subjected to the combined environment of UV and vapour cycles with SWSSC experienced the highest tensile strength reductions. A similar reduction of 2 mm laminates when exposed to 1000 h and 3000 h UV and vapour cycles followed by SWSSC, shows that the adverse effect of 1000 h cycles was significant for 2 mm laminates to aid further degradation by SWSSC.

The results of the elastic modulus of GFRP laminates indicate that regardless of the type of conditioning and thickness of the samples, about 20% reduction was observed for all samples compared to their corresponding reference sample. The reductions of the elastic modulus were generally less than the strength of the laminates. To explain the reason, it should be mentioned that the elastic modulus of FRP composites is more governed by the fibres and less by the resin. Therefore, the degradation of the fibres due to the simulated SWSSC penetration affects the elastic modulus of the samples more than the degradation of the resin matrix. On the other hand, the resin degradation, and consequently, the fibre/resin interface are important factors in tensile strength reductions. Therefore, as the fibres are less affected than the resin and interface during conditioning, one can conclude that the tensile elastic modulus of GFRP laminates is less affected under environmental conditions in comparison to the tensile strength.

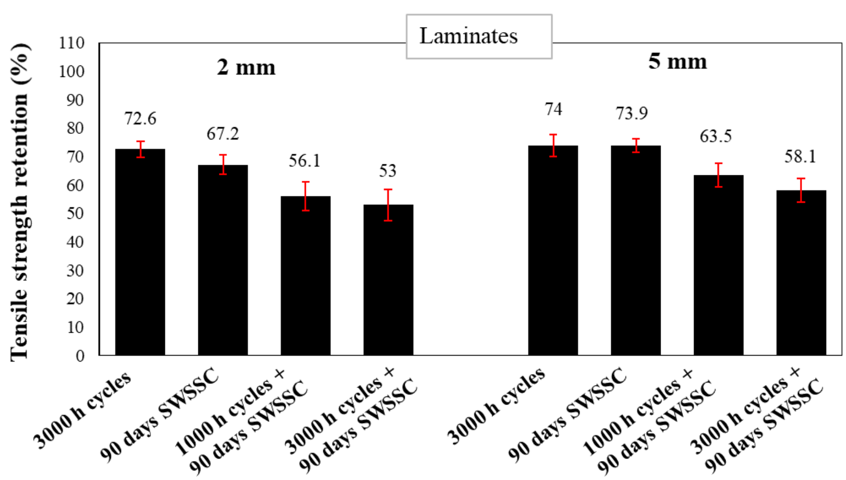

Figure 9-15 Comparison between the tensile strength retentions with respect to the conditioning environment

9.3.4.2.2 Effect of laminate thickness

The ultimate tensile strength retention of the GFRP laminates with respect to their thickness is compared in **Figure 9-16**. It is clearly seen that the degradation of thinner laminate is higher than the thickener one in all environmental conditions. The reason can be explained by considering the fact that the volume fracture of the thinner laminate that was affected due to the conditioning is greater than that of the thicker laminate. Therefore, the more the damage progression, the greater is the degradation in the mechanical properties.

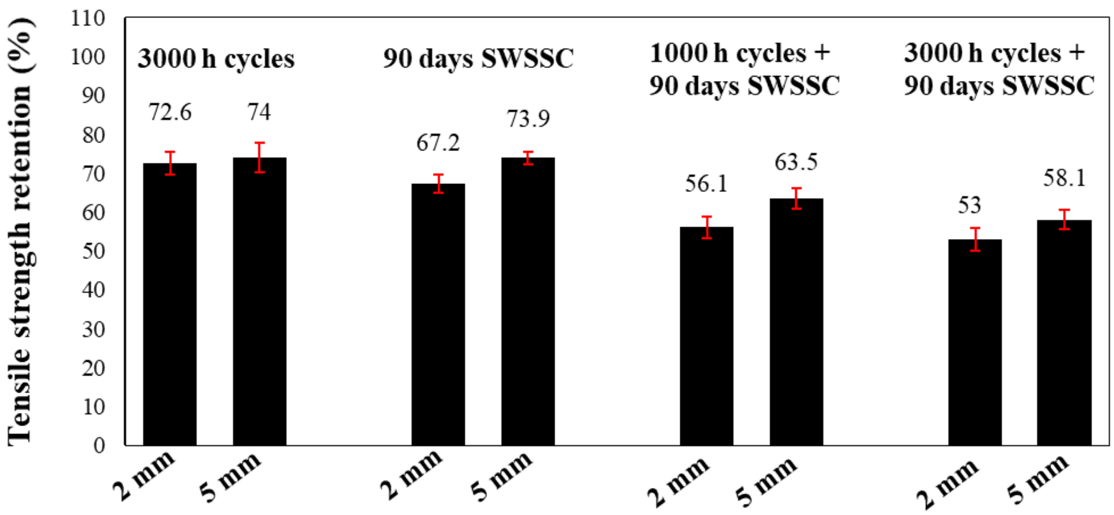

Figure 9-16 Comparison between the tensile strength retentions with respect to the laminate thickness

9.3.4.3 Compression test

The compressive test results are presented in

Table 9-7. As expected, the compressive strengths of all GFRP profiles decreased significantly under SWSSC and combined UV with water vapour cycles with SWSSC conditions.

Table 9-7 Compression test results

Specimen	Conditioning type	Maximum load (N)	CV(%)	Retention (%)
B-1	Control	43195	2.8	100
	30 days SWSSC	30668	5.3	71.0
	1000 h cycles + 30 days SWSSC	28940	4.4	67.2
	3000 h cycles + 30 days SWSSC	26780	4.7	62.3
	90 days SWSSC	25053	5.1	57.8
	1000 h cycles + 90 days SWSSC	23325	8.5	54.2
	3000 h cycles + 90 days SWSSC	23325	5.1	55.6
B-2	Control	65233	1.2	100
	30 days SWSSC	43053	7.3	66.0
	1000 h cycles + 30 days SWSSC	41749	2.8	64.2
	3000 h cycles + 30 days SWSSC	41749	6.2	64.0
	90 days SWSSC	35225	3.6	54.1
	1000 h cycles + 90 days SWSSC	34573	5.3	53.0
	3000 h cycles + 90 days SWSSC	32616	6.7	50.0
C-1	Control	60321	2.1	100
	90 days SWSSC	36192	6.8	60.0
	1000 h cycles + 90 days SWSSC	34825	5.2	57.7
	3000 h cycles + 90 days SWSSC	34503	7.1	57.2
C-2	Control	92655	2.3	100
	30 days SWSSC	69491	9.5	75.0
	1000 h cycles + 30 days SWSSC	66711	8.4	72.4
	3000 h cycles + 30 days SWSSC	62078	3.4	67.0
	90 days SWSSC	61152	6.4	66.0
	1000 h cycles + 90 days SWSSC	56898	5.8	61.4
	3000 h cycles + 90 days SWSSC	58768	5.1	63.4

9.3.4.3.1 Effect of different environments

The ultimate compressive strength retention of each profile under different environmental conditions is compared in **Figure 9-17**. As is seen, in most cases, a similar trend to the other mechanical properties in terms of the strength reductions under different environmental conditions was observed. However, the strength reductions of combined 3000 h cycles followed by 90 days of immersion were very close (even less in some conditions) to 1000 h cycles followed by 90 days of immersion. The sample randomness and lower effect of cycles conditioning compare to immersion are the possible reasons for this observation. Comparing the results of samples exposed for 30 days to SWSSC with the samples exposed for 90 days to SWSSC reveals that damage level increases by increasing the time of exposure.

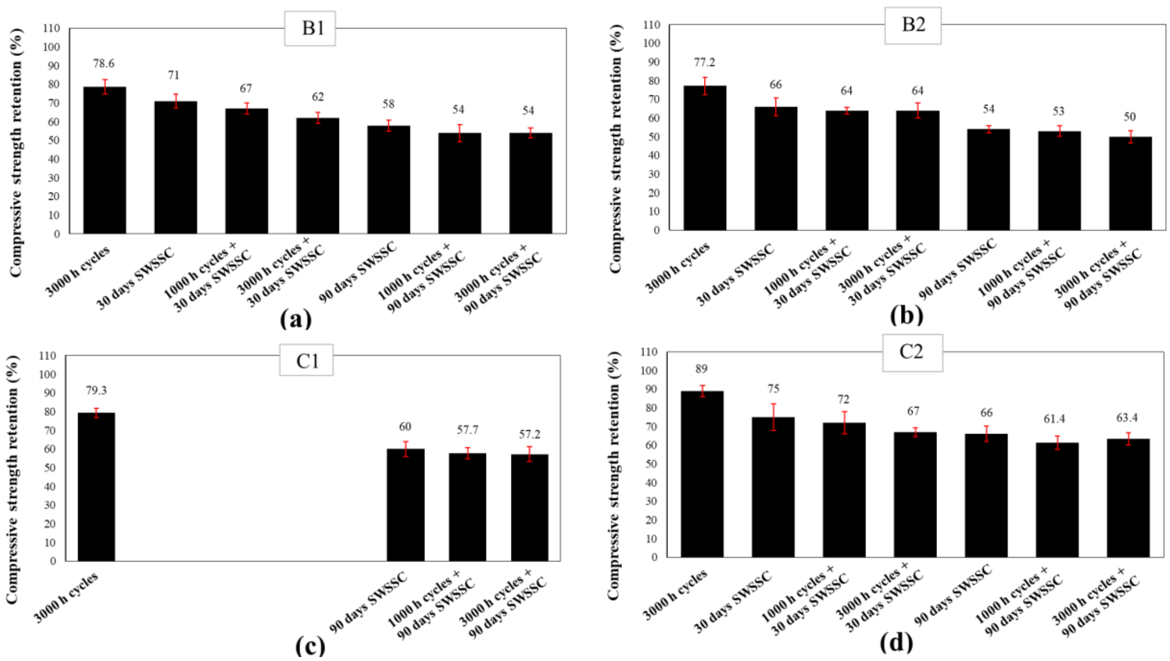

Figure 9-17 Comparison between the compressive strength retentions with respect to the conditioning environment: (a) Cross-section profile B1, (b) cross-section profile B2, (c) cross-section profile C1, and (d) cross-section profile C2

9.3.4.3.2 Cross-section configuration

The ultimate compressive strength retention with respect to the configuration of the profiles cross-section is compared in **Figure 9-18**. Comparing the results of B1 and B2 sections show that similar to the bending results, generally, samples with a higher ratio of perimeter-to-thickness (P/t) experience more degradation (i.e., B2, except for one condition showed more reductions than B1). The earlier occurrence of local buckling due to the degradation of the resin and interface for the section with a higher p/t ratio could be the reason for this observation. Higher reductions of C1 compared to C2 also confirm that a thicker sample (smaller p/t ratio) shows less degradation than the thinner sample (larger p/t ratio). More damage progression through the thickness of the thinner profiles is the main reason for this observation.

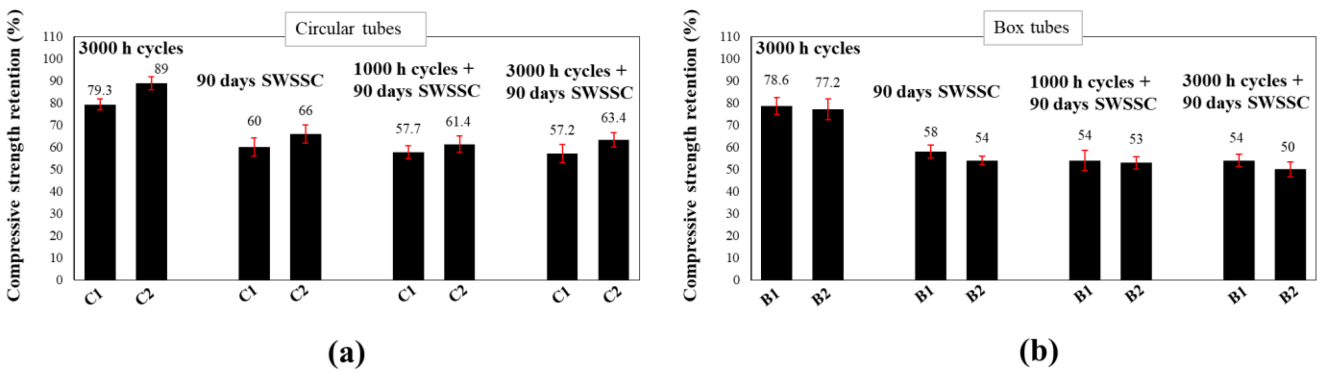

Figure 9-18 Comparison between the compressive strength retentions with respect to the profile cross-section configuration: (a) Circular tubes and (b) box tubes

9.4. Comparison of the results with literature

The degradation of GFRP profiles exposed to the environmental conditions in this study (on the role of UV and moisture cycles and alkaline solutions) are compared with the corresponding results reported in the literature. However, it should be noted that the studies conducted on the durability of GFRP sections, especially compressive profiles, are very limited and more experimental tests are still needed to achieve a comprehensive understanding of the mechanical performance of such materials under different environmental conditions. **Table 9-8** compares some results of flexural, tensile, and compressive properties of vinylester pultruded GFRP profiles under different environmental conditions, including UV, moisture and alkaline conditions, obtained in the present study with the results reported in the literature. Based on the results, it can be confirmed that alkaline environments are significantly harsher conditions than UV and moisture. Significant reductions (typically, between 30% to 50%) in all mechanical properties when exposed to alkaline environments (both normal concrete and SWSSC) reveal that a high reduction factor needs to be taken into account when using GFRP composites with concrete.

Table 9-8 Comparison of the results of the present study with some similar research in the literature

Reference	FRP Type	Environmental condition	Results
Present study	Vinylester GFRP pultruded profiles	90 days immersion in normal SWSSC (ambient temperature and pH=13.6)	Maximum reductions of 30 %, 33 %, and 48 % in flexural, compressive, and tensile strength, respectively
Present study	Vinylester GFRP pultruded profiles	3000 h cycles of UV radiation and water vapour condensation cycles followed by 90 days immersion in SWSSC	Maximum reductions of 52 %, 47 %, and 64 % in flexural, compressive, and tensile strength, respectively
[73]	Vinylester GFRP pultruded profiles	3000 h cycles of UV radiation and water vapour condensation cycles	Maximum reductions of 22 %, 27 % and 23 % in in flexural, tensile, and compressive strengths, respectively.
[169]	vinylester GFRP laminates	3000 h cycles of UV radiation and moisture cycles	13 % reduction in flexural strength of 5 × 15 × 150 mm laminates
[113]	Vinylester GFRP pultruded profiles	147 days immersion in normal concrete solution (ambient temperature and pH=13.6)	Maximum reductions of 44 % and 41 % in flexural and compressive strengths of I-shaped and circular tubes, respectively.
[230]	Vinylester GFRP pultruded tubes (4 mm thickness)	90 days immersion in normal SWSSC (ambient temperature and pH=13.6)	Maximum reductions of 53 % and 35 % in compressive strength and tensile strength, respectively.

9.5. Regression analysis

Considering the experimental data and the analyses of variance (ANOVA), time of conditioning to each environment condition and the sample thickness were the effective factors in tensile strength retention. In addition to these parameters, the sample cross-section perimeter was found to be an effective factor in compressive strength retention and bending strength retention about the minor axis values. Finally, regarding the bending strength about the major axis, all the mentioned parameters and also the moment of inertia about the major axis, I_x, was the effective parameter in retention values. With these in mind, linear Bayesian regression (LBR) was used to develop predicting models of the pultruded GFRP profiles mechanical properties retention under the harsh conditions used in this study. Bazli et al. [73] proposed the following model to predict the mechanical properties of the same profiles used in this study under the environmental condition of UV and moisture cycles:

$$R\ (\%) = A\left(\frac{1}{\log(T)}\right) + B(t^2) + C\left(\frac{1}{p}\right) + D\sqrt{I_x} + E \tag{9.1}$$

where T, t, p, and I_x are the time of cycles (h), sample thickness (mm), cross-section perimeter (mm), and moment of inertias about the major axis (mm^4), respectively. A to E constants are the regression coefficients of each mechanical test, which were obtained based on the experimental data. A similar approach was used in this study. However, the first term has been substituted with a new term to consider the effects of each conditioning period and their interaction. Therefore, **Eq.9.2** is proposed to predict the mechanical properties retention of pultruded GFRP profiles after exposure to the harsh environmental conditions used in the present study:

$$R\ (\%) = A\left(\frac{T_1 + T_2^{1.5}}{T_2^{1.1}}\right) + B(t^2) + C\left(\frac{1}{p}\right) + D\sqrt{I_x} + E \tag{9.2}$$

where T_1 and T_2 are the time of UV and moisture cycles (h) and the time of SWSSC immersing (h), respectively. A to E are the regression constants according to the experimental data. **Table 9-9** lists the regression values for all mechanical tests. The statistical regression parameters are also listed in **Table 9-10. Figure 9-19** compares the experimental test data and predicted values using **Eq.9.2**. According to **Table 9-10,** values and **Figure 9-19**, the accuracy and validity of the proposed model could be confirmed. However, more experimental data considering more variables are needed to achieve a more comprehensive prediction model.

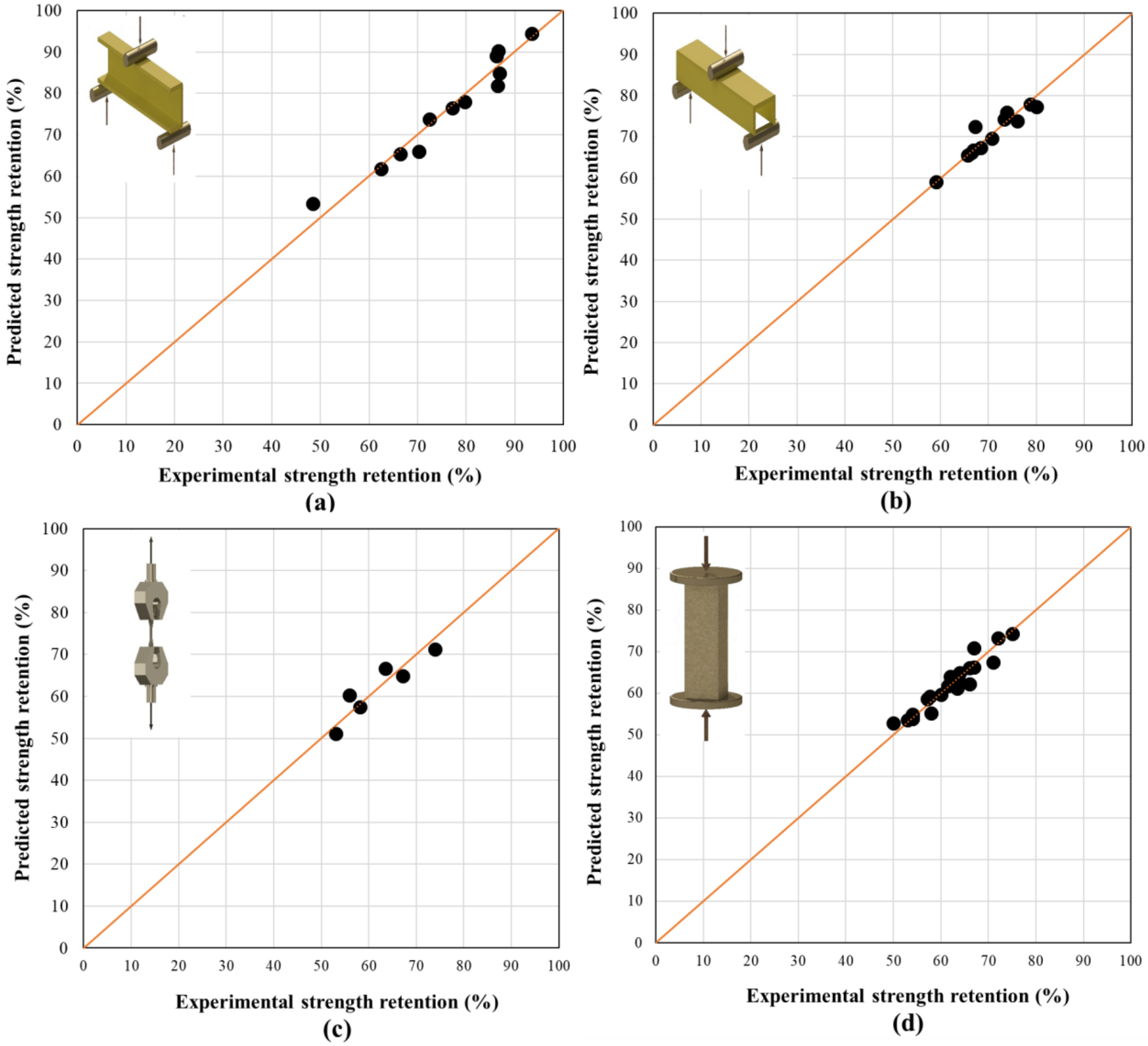

Figure 9-19 Comparison of strength retention between experimental and predicted values using Eq. (2): (a) three-point bending about the major axis (b) three-point bending about the minor axis, (c) tensile test, and (d) compression test

Table 9-9 Regression model constants in Eq.9.2

Test Type	**A**	**B**	**C**	**D**	**E**
Three-point bending about the major axis	-19.4161	4.00536	-36452.6	-0.716973	892.506
Three-point bending about the minor axis	-16.3450	0.50582	765.697	0	413.996
Compression	-1.58798	0.10780	1511.1	0	80.4770
Tension	-21.3446	0.30634	0	0	523.953

Table 9-10 Regression parameters for Eq.9.2

Test Type	R-factor	Mean of SD	C.V. of SD (%)
Three-point bending about the major axis	0.98	3.699	0.4082
Three-point bending about the Mainor axis	0.94	2.506	0.3535
Compression	0.96	2.150	0.1961
Tension	0.93	3.862	-

Note: SD = standard deviation

9.6. Conclusions

As part of an ongoing research project focusing on the performance of using seawater sea sand concrete (SWSSC) together with FRP as reinforcement, the present study investigates the mechanical and microstructural properties of various pultruded GFRP profiles subjected to SWSSC environment and its combination with UV radiation and moisture. Different mechanical tests were conducted to study the mechanical properties. SEM analyses were carried out to investigate the microstructural changes. Based on the experimental results and microstructural analyses, the following conclusions can be presented:

- The vulnerability of GFRP composites in the SWSSC environment is significantly greater than that in UV and moisture cycles.
- Profiles exposed to UV radiation and moisture cycles followed by SWSSC immersing experience more reductions in their mechanical properties in comparison to profiles subjected to SWSSC alone. Initial surface disruptions/degradation of GFRP due to the UV and moisture cycles aiding the penetration by the SWSSC environment and facilitating crack growth is the possible reason for this observation.
- The microstructural damage mechanisms of GFRP profiles exposed to only UV radiation and moisture cycles mostly include microcracks and rarely fibre/resin debonding. However, significant resin matrix cracking, resin leaching, fibres pitting and cracking and fibre/resin debonding are the damage mechanisms of samples exposed to conditions including SWSSC.
- The maximum flexural, tensile and compressive strengths of different pultruded GFRP exposed for 3000 h of UV and moisture cycles followed by 90-day immersion in simulated SWSSC are about 52%, 47%, and 50%, respectively.
- Profiles with higher cross-section perimeter-to-thickness ratios show grater reductions in mechanical properties in under harsh conditions.

- Flexural profiles that show interlaminar shear failure during bending test, experience higher strength reductions in comparison to the profiles that fail due to fibres fracture. The reason is the significantly larger degradation of the resin/fibre interface compared to the fibres themselves under aggressive environments.
- Tensile elastic modulus of GFRP laminates is less affected by aggressive environments than tensile strength (e.g., maximum elastic modulus reduction of 20% compared to strength reduction of 47 % for laminates exposed to3000 h of UV and water vapour condensation cycles followed by 90-day immersion in SWSSC).
- According to ANOVA and regression analyses, duration of UV and moisture exposure, sample cross-section configuration (i.e., the moment of inertia, thickness, and perimeter) are effective factors in mechanical properties durability of pultruded GFRP profiles under SWSSC coupled with UV radiation and moisture.

Chapter 10 Durability of GFRP composites under seawater and sea sand concrete coupled with harsh outdoor environments

Abstract

This paper presents an investigation on the durability of different glass fibre reinforced polymer (GFRP) composites when subjected to harsh outdoor conditions, including freeze/thaw cycles, ultraviolet (UV) radiation and moisture, as well as when used with seawater sea-sand concrete (SWSSC) for construction applications. To achieve this, the effects of a number of parameters, including the environment of exposure, exposure time, profile cross-section configuration and fibres orientation, on the mechanical properties of different GFRP composites were studied. To investigate the degradation of the mechanical properties, three-point bending, compression and tension tests were conducted on both reference and conditioned samples. Moreover, scanning electron microscopy (SEM) analyses were performed to examine the contribution of microstructural deterioration to the damage mechanisms of the conditioned composites. Finally, the test results were used to develop empirical regression models to predict the level of retention of mechanical properties of different composites under different environmental conditions. The findings showed the maximum flexural, compressive and tensile strength reductions to be 35%, 48% and 37%, respectively, with regards to the pultruded profiles exposed for 3000 h to freeze/thaw cycles followed by 90 days of SWSSC immersion, while the flexural strength reductions recorded for the vacuum infused samples subjected to 2000 h of freeze/thaw cycles followed by 90 days of SWSSC immersion were 28%, 72% and 56% for the unidirectional, woven and chopped-strand mat laminates, respectively.

Key words

GFRP; Durability; Seawater sea sand concrete; Freeze/thaw cycles; UV cycles; Moisture.

10.1. Introduction

Mechanical properties of composite materials in both theoretical [296, 297], and experimental [304] perspectives is a challenging research. The advantages of using fibre-reinforced polymer (FRP) composites have led to their wider use in various construction [3, 4], and automotive and aerospace applications [1, 2]. Among these advantages are corrosion resistance, high strength and a high stiffness-to-weight ratio [5-7]. However, in their varying applications, FRP composites are likely to be subjected to various environmental conditions during their storage, transportation and particularly long-term service life [15, 128, 181, 306]. For instance, moisture [183, 307, 308], thermal cycles [64, 106], UV radiation [73, 309], elevated temperature [63, 162, 310], as well as alkali and acidic environments [17, 113] are just some of the harsh environmental conditions in which FRP composites are implemented. Therefore, numerous prior studies have investigated the short- and long-term durability of different FRP composites under various environmental conditions [113, 267, 311, 312].

Based on the findings of these studies, it is generally believed that the degradations of the mechanical properties of FRP composites under most conditions, including seawater, thermal cycles and UV radiation, are not dramatic [106, 183, 313]; however, considerable reductions (except in carbon fibre reinforced polymer (CFRP)) in the mechanical properties of FRP composites have been reported when they are used in concrete (i.e. an alkaline environment) [95, 107, 108]. Glass- and basalt fibres damages are caused by metallic cations leaching out of the fibre's surface and breaking Si-O-Si bond by hydroxyl ions [34, 35]. With respect to carbon fibres, it is generally accepted that such fibres are almost resistant to harsh environments [36]. In the present study, GFRP composites, as one of the common FRPs, are used.

Generally, the damage mechanisms of a FRP composite concerns the fibres [18], the resin [29], and the fibre/resin interface [30]. Additionally, the environmental conditions can be divided into two categories. First, conditions such as UV radiation, elevated temperatures (i.e., at temperatures lower than the resin's glass transition temperature) and thermal cycles (e.g. freeze/thaw cycles). These parameters cause microcracks and resin/matrix debonding that are limited to the surface of the composites (rather than penetrating deep into the matrix) [106], Second, conditions such as moisture that cause damage, including matrix cracking, hydrolysis, plasticisation and swelling, as well as fibre/resin debonding, are capable of propagating into the inner layers of the composites [27, 314]. In the latter case, the level of damage and its progression are strongly dependent on the type of fibre and resin, type of solution as well as on the time and temperature of the conditioning. Based on the application and the area of usage, FRP composites may be subjected to either the first or the second category of condition, or their combination.

With regard to the applications of FRP composites in the field of civil engineering, due to their superior structural characteristics, they are mainly used as reinforcements for concrete members [170] as well as for external bonding/wrapping purposes for the rehabilitation and strengthening of existing structures, non-structural members and secondary members [129, 130]. Further, in terms of their area of usage, as FRP composites are highly resistant to corrosion, and hence, an alternative to traditional steel reinforcement, they are mainly used in corrosive conditions, for example, marine environments [315, 316]. Based on this characteristic, recently, the use of FRP composites with seawater and sea sand concrete (SWSSC) in marine environments has been proposed by Teng [317, 318].

The application of geo-polymer-based SWSSC as a replacement for ordinary Portland cement (OPC)-based concrete not only serves to overcome resource shortages (i.e., freshwater and river sand) but also significantly reduces the raised environmental impacts (e.g., carbon dioxide (CO_2) emissions) associated with the production of cement used in ordinary Portland cement (OPC) concrete [103, 319, 320]. Moreover, when geo-polymers such as slag and fly ash are used in the production of SWSSC, its short- as well as long-term characteristics are comparable to those of OPC-based concrete, while there is an additional benefit, i.e., the adverse effects of the alkali–silica reaction (ASR) can be significantly reduced [10, 11]. However, as mentioned above, FRP composites are vulnerable to alkaline environments and, thus, their durability when used with SWSSC still needs to be carefully addressed [321]. With this regard, GFRP pultruded profiles which could be used together with concrete in many applications, such as concrete filled FRP tubes [230], bridge decks [322], and laminates for retrofitting RC structures [323] may experience mechanical strength reductions when used with concrete. Therefore, their durability performance when used with SWSSC as a new hybrid structure needs to be addressed.

The durability of FRP composites in alkaline environments has been thoroughly studied, with a focus on normal and high-performance OPC-based concrete environments, and long-term prediction models have been proposed to assess the mechanical properties [113, 269, 324-326]. Yet, only a very few studies have focused on the durability of different FRP composites in an SWSSC environment [4, 12, 99, 249, 300, 301, 327]. Moreover, these studies on the durability of FRP composites in SWSSC have mainly focused on FRP bars [4, 12, 99, 137] and tubes [200, 249, 327, 328] (i.e., FRP-composite-reinforced beams and concrete-filled FRP tubes). However, the mechanical properties durability of other types of FRP composite configurations (e.g., FRP-composite-pultruded profiles and different FRP laminates) for different applications under such harsh conditions also need to be addressed. The effects of several factors associated with the material levels, such as the FRP fabrication method, cross-section configuration and fibre length and orientation, on the durability of FRP composites in harsh environments are not yet well understood.

Recently, Jafari et al. [64] studied the mechanical properties of different pultruded GFRP sections pre-exposed to freeze/thaw cycles. They reported the maximum flexural, compressive and tensile strength reductions to be 17%, 26% and 14%, respectively, after the cycles for 3000 h. Bazli et al. [73] used the same pultruded profiles and reported reductions in maximum flexural, compressive and tensile strength of 27%, 23%, and 14%, respectively, after 3000 h of UV exposure and water vapour condensation cycles. The effect of SWSSC and its combination with UV radiation and water vapour condensation on the mechanical properties of the same profiles was also studied by Bazli et al. [262]. The flexural, compressive, and tensile strength of different profiles decreased by up to 30%, 33%, and 46%, respectively, after 90 days of pre-immersion in the SWSSC solution at ambient temperature. The corresponding reductions reached up to 52%, 47%, and 50% after exposure to 3000 h UV and water vapour condensation followed by 90 days of immersion in SWSSC solution at ambient temperature.

The latest study showed that the initial degradation resulting from UV exposure and moisture (e.g., in the case of storage and transportation before being used with concrete) causes greater reductions in an alkaline environment compared to the cases without any initial exposure. Therefore, the initial degradation of FRPs during fabrication, storage and transportation before being used with concrete in construction applications, and the combined effects of outdoor conditions and alkaline environment during the service life of the composite structure must be taken into account.

Subzero temperatures may result in resin hardening and microcracks formation, whereas thermal cycles at low temperatures may cause resin/fibre debonding. This happens due to the different thermal expansion coefficients between the types of fibre and resin, which causes internal stress [159]. This initial degradation may accelerate the level of FRP damage when used with concrete, particularly SWSSC. Considering these facts and the abovementioned studies, the durability of pultruded profiles under the combination of freeze/thaw cycles and SWSSC environment was investigated in this study.

Regarding the effect of fibres length and orientation, Bazli et al. [106] investigated the tensile properties of GFRP laminates with unidirectional, woven, and chopped strand mat fibres after exposure to UV and water vapour condensation and freeze/thaw cycles. They concluded that the laminates with unidirectional fibres perform the best, while the laminates with random fibres showed the weakest performance under harsh outdoor environmental conditions. However, the effects of fibre configuration under SWSSC conditions and under the combined effects of outdoor environmental characteristics have not been studied yet. Based on the previous studies, the SWSSC environment [262, 328] significantly affects the fibre/resin interface, and thus the effects of fibres length and orientations seems to be an important factor that must be considered under such environmental conditions.

This experimental study is conducted to fill the knowledge gaps in the performance of different GFRP composites when exposed to outdoor harsh environments and SWSSC. The experimental conditions were selected on the basis of earlier studies by some of the authors of this article. For comparison purposes, similar specimens and/or environmental conditions to previous studies were used in the present study. This study serves to fill some of the crucial knowledge gaps in the earlier studies. Accordingly, **Table 10-1** represents the types of specimens, the environmental conditions and the mechanical tests employed in each study. The aim of this study was to investigate the durability of different pultruded GFRP profiles and vacuum-infused GFRP laminates with different fibre orientations under SWSSC environment and its combinations with harsh outdoor conditions. A series of three-point bending, compression, and tensile tests were conducted to study the mechanical properties while scanning electron microscopy (SEM) analyses were conducted to investigate the damage level and mechanisms after exposure to environmental conditions.

Table 10-1 Previous research conducted by the authors and the contribution of the present study to the program

Study	GFRP type		Environmental condition						Mechanical tests		
	Pultruded profiles [1]	Vacuum infused	UV+ moisture cycles	Freeze/thaw cycles	SWSSC	SWSSC + seawater	SWSSC + UV and moisture	SWSSC + Freeze/thaw	Three-point bending	Tension	Compression
Ref [64]	✓			✓					✓	✓	✓
Ref [73]	✓		✓						✓	✓	✓
Ref [230]	✓				✓	✓				✓	✓
Ref [262]	✓		✓		✓		✓		✓	✓	✓
Present study	✓							✓	✓	✓	✓
Ref [106]		✓	✓	✓						✓	
Present study		✓			✓		✓	✓	✓		

Note: 1: The profiles used in Ref [230] were tubes, while in all other studies various sections similar to the present study have been used.

10.2. Experimental Program

GFRP pultruded profiles with ten different cross-sections and vacuum-infused GFRP laminates with three different fibre configurations were used to study the effect of cross-section fibre configuration on mechanical properties of GFRP composites under harsh environments. As a distinct difference from the authors' previous study on the performance of pultruded profiles under SWSSC [262], the samples in this study were exposed to freeze/thaw cycles followed by SWSSC immersion, and the results were compared with previous research. The vacuum-infused laminates were subjected to three different exposure conditions: (1) immersion in SWSSC, (2) UV and water vapour condensation cycles followed by immersing in SWSSC, and (3) freeze/thaw cycles followed by immersing in SWSSC. Pultruded profiles were subjected to three-point bending tests about both minor and major axes, compression, and tension, while vacuum-infused laminates were tested in three-point bending. To study the microstructural properties, the damage mechanisms and degradation level of both pultruded and vacuum-infused specimens were analyzed using SEM.

10.2.1. Materials

Pultruded profiles with nine different cross-sections, including two types of each I-shaped, channel, circular tube, rectangular hollow tube (box), and laminate were used. All profiles included an inner section of continuous E-glass roving and vinylester resin, an outer layer of strand mat, and a very thin surface veil as the outermost layer. Vacuum-infused laminates with epoxy resin and three different E-glass fibres configurations were employed, including continuous unidirectional, continuous unidirectional and perpendicular (0° and 90°) woven, and 25 ± 5 mm long chopped strands (i.e., randomly distributed fibres) were also used in this study. For comparison, the pultruded sections were the same as those used in [64, 73, 262] and vacuum infused laminates were similar to those in [63, 106]. Cross-sections of pultruded profiles are shown in **Figure 10-1**. **Table 10-2** and **Table 10-3** also lists the material properties of pultruded profiles and vacuum infused laminates, respectively.

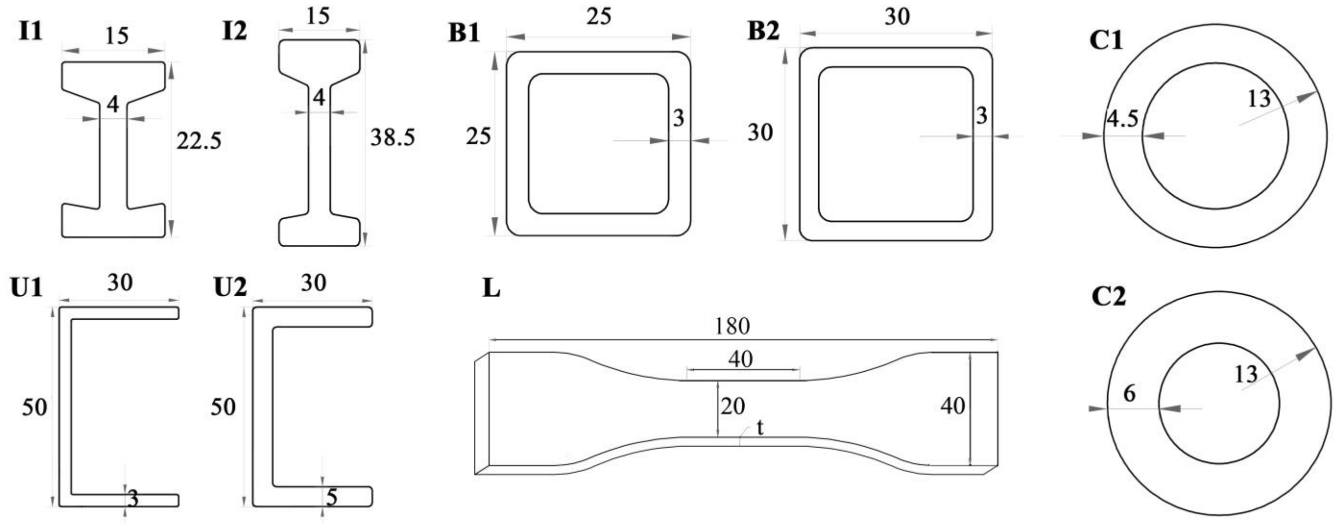

Figure 10-1 Pultruded GFRP profiles cross-sections used in this study (dimensions in mm)

Table 10-2 Pultrusion process and pultruded profiles characteristics

Properties	Values
Fillers (wt % of the resin)	Nano Clay (2 wt %) – Carbonate Calcium (12 wt %)
Fibre content by volume (%)	60
Pultrusion average speed	0.25 m/min
Pultrusion temperature (˚C)	130 (entrance) – 170 (exit)
Average tensile strength (MPa)	400
Tensile elongation at rapture (%)	2.5
Average flexural strength about the major axis (MPa)	460
Average axial compression strength (MPa)	550
Density (g/cm^3)	2
Water absorptivity rate (%)	0.2 - 0.6
Thermal expansion coefficient (10^{-6} / ˚C)	4.5
Glass Transition Temperature, T_g (˚C)	100 - 105

Table 10-3 Vacuum infused laminates characteristics

Fibres type	Thickness (mm)	Layers number	Fibre content (%)	Ultimate tensile strength (MPa)	Glass transition temperature, T_g (˚C)	Thermal expansion coefficient (10^{-6} / ˚C)
Unidirectional	5	16	71.2	800	80	0.3-0.6
Woven	5	17	64.6	290	80	0.3-0.6
Random	5	7	33.1	202	80	0.3-0.6

10.2.2. Environmental conditioning

In this study, pultruded profiles were exposed for different durations of freeze/thaw cycles followed by exposure to simulated SWSSC solution at the ambient temperature. Regarding the vacuum infused laminates, in addition to the test conditions for the pultruded profiles, samples were also exposed to two other conditions: (1) only simulated SWSSC solution at ambient temperature and (2) cycles of UV and water vapour condensation followed by exposure to simulated SWSSC solution at ambient temperature. According to [249], SWSSC real environment was simulated by dissolving the constituent chemicals in distilled water. Chemicals used were sodium chloride (35 g/l), potassium hydroxide (19.6 g/l), sodium hydroxide (2.4 g/l), and calcium hydroxide (2 g/l). It should be noted that ASTM D1141-98 [329] recommendation is used to prepare artificial seawater for simulated SWSSC solution.

In order to simulate the harsh out-door conditions, current standards/codes recommendations were used. The cycling scheme of UV and moisture was used based on ASTM G154 standard [330] to simulate hot coastal regions. A cycle including 8 hours exposure to UV-A at 60 °C followed by 4 hours water vapour condensation (100% RH) at 50 °C, was selected for this study to simulate the harsh environment. Lamps with the wavelength of 340 nm and irradiation intensity of 0.85 W/m^2 were used. Further details regarding the UV and moisture cycle used can be found in [73].

In many standards/codes, such as ASTM D6944-15 [331] and EN 1504-2 [332], a life span of 25 years with 50 thermal cycles has been considered for non-structural materials. Therefore, 120 cycles (i.e. 3000 h period of conditioning in the present study) may be a reasonable estimate for 50 years life-span of structural GFRP profiles in very cold regions. Each freeze/thaw cycle included 12 h at −20 °C followed by 4 h at 20 °C, 4 h at −20 °C and again 4 h of 20 °C. The temperature variations in the freeze/thaw cycle (i.e., −20 to 20 °C) were simulate to those in a typical cold coastal regions, as suggested in [150]. Further details regarding the freeze/thaw cycles used can be found in [106].

Laboratory cycles used in the present study is shown in **Figure 10-2.** The harsh outdoor environmental conditions were simulated by laboratory cycles similar to those in [73, 106]. A total number of 156 conditioned samples were tested and compared with the reference samples. The number of each sample type and the corresponding mechanical test and environmental conditions are summarized in **Table 10-4.**

Table 10-4 Environmental conditions, samples type, and number of identical tests used in this study

Environmental condition	**I1**	**I2**	**U1**	**U2**	**B1**	**B2**	**C1**	**C2**	**L**	**UL**	**WL**	**RL**	**Total Number**
Control	6	6	6	6	3	3	3	3	6	3	3	3	51
30 days SWSSC	-	-	-	-	-	-	-	-	-	3	3	3	9
90 days SWSSC	-	-	-	-	-	-	-	-	-	3	3	3	9
1000 h freeze/thaw cycles + 30 days SWSSC	-	-	-	-	3	3	-	3	-	3	3	3	18
3000 h freeze/thaw cycles + 30 days SWSSC	-	-	-	-	3	3	-	3	-	3	3	3	18
1000 h freeze/thaw cycles + 90 days SWSSC	6	6	6	6	3	3	3	3	6	3	3	3	51
3000 h freeze/thaw cycles + 90 days SWSSC	6	6	6	6	3	3	3	3	6	3	3	3	51
Total number	18	18	18	18	15	15	9	15	18	21	21	21	207

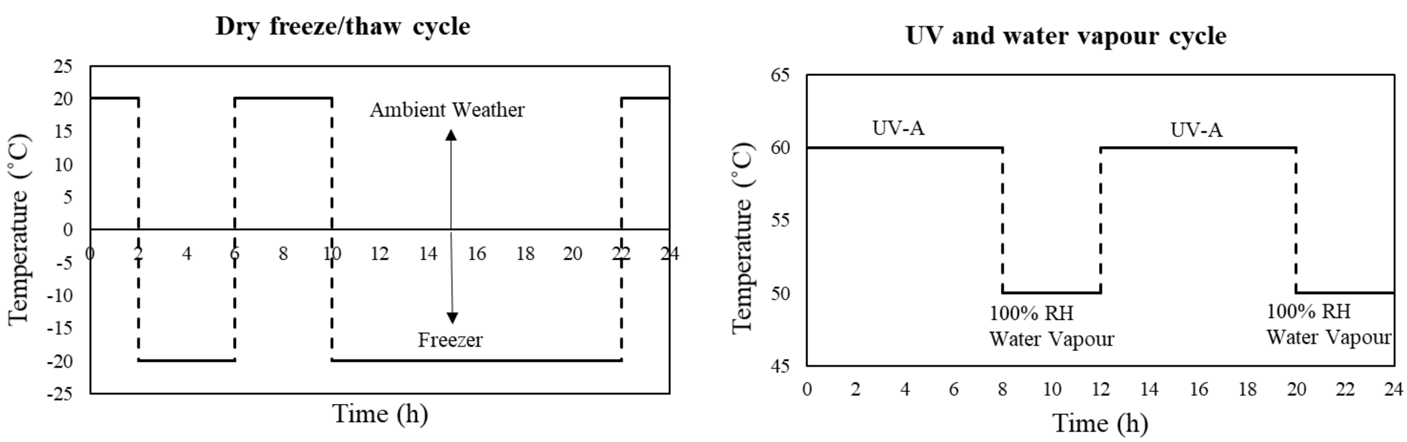

Figure 10-2 One cycle regime for each out-door condition

10.2.3. Mechanical tests

Three-point bending, compression, and tensile tests were carried out using a 150 kN Santam universal testing machine.

Pultruded flexural profiles were cut into the lengths of 230 mm and tested about both major and minor axes under three-point bending with a 200 mm constant span. The reason for selecting this test configuration was to investigate both shear failure (major axis) and bending failure (minor axis). Vacuum infused laminates were also cut and tested in the same test configuration (i.e., 230 mm length and 200 mm span) of pultruded samples. The loading rate used for all bending tests was 1.1 mm/min. Pultruded compressive profiles were cut in heights of 100 mm and tested in compression with a loading rate of 1.1 mm/min. The height was selected to prevent the global buckling of the profiles. Dog-bone shaped pultruded tensile laminates (see **Figure 10-1**) were tested in tension with a loading rate of 1.2 mm/min. Details of the test set-ups can be found in [73]**.**

In this study, for each condition, three identical tests were carried out, and the average result was used for discussion.

10.2.4. Scanning electron microscope (SEM) analysis

SEM examinations were performed on selected reference and conditioned pultruded and vacuum infused samples to investigate the level and mechanisms of degradations. For comparison, samples were extracted from the same location of reference and conditioned specimens. In order to prepare samples for SEM analyses, after cleaning any dirt and dust off the surface, a thin layer of conductive gold metal was coated on each sample to prevent charging and thermal damage that can cause a blurry image.

10.3. Results and discussion

In this section, appearance changes, microstructural properties and mechanical test results of conditioned samples will be presented, discussed and compared with the corresponding reference samples.

10.3.1 Visual inspection of GFRP composites after conditioning

Figure 10-3 compares the surface appearance changes of pultruded profiles exposed to freeze/thaw cycles [64] and those exposed to freeze/thaw cycles followed by immersion in SWSSC, with the reference profiles. The appearance changes of vacuum infused laminates after exposure to freeze/thaw cycles, UV and water vapour cycles, freeze/thaw cycles followed by immersion in SWSSC, and UV and water vapour cycles followed by immersion in SWSSC are also revealed in **Figure 10-4**. As is seen in **Figure 10-3**, no considerable change in terms of the surface colour and gloss was observed in pultruded GFRP samples exposed to only freeze/thaw cycles. However, the surface of pultruded GFRP exposed to freeze/thaw cycles followed by immersion in SWSSC changed from shiny yellow to pale and almost white. This shows leaching and disappearing of the protective surface layer due to the SWSSC solution.

Regarding the vacuum infused laminates, because no protective layer was used during the fabrication process, the surface colour changes of such samples were not as severe as the pultruded ones. However, as is seen in **Figure 10-4**, the surface of the samples exposed to the combined outdoor cycles and SWSSC solution is darker than those exposed to only harsh outdoor cycles.

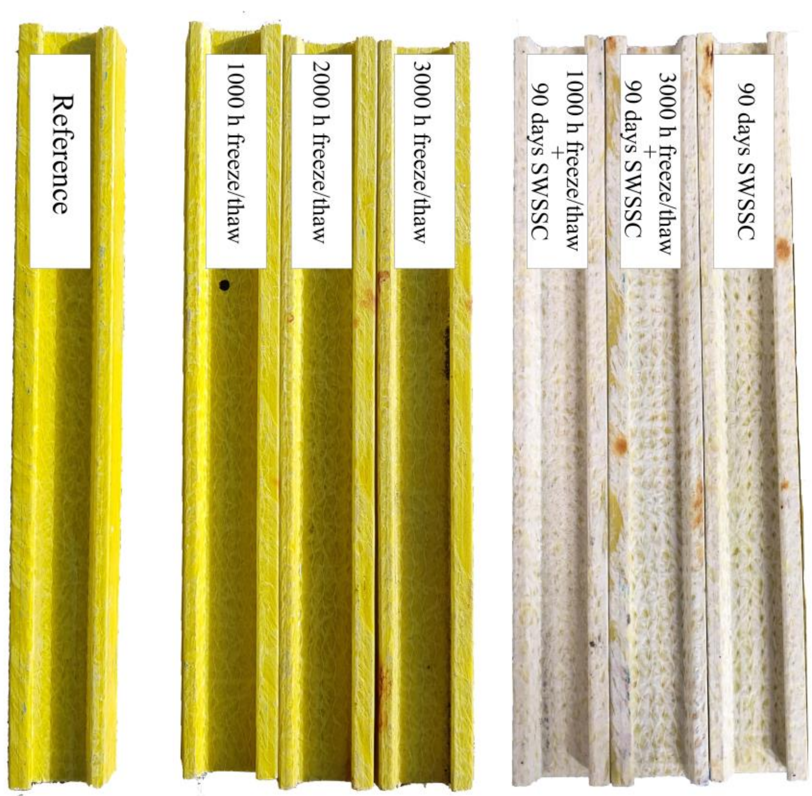

Figure 10-3 Surface changes of pultruded profiles after conditioning

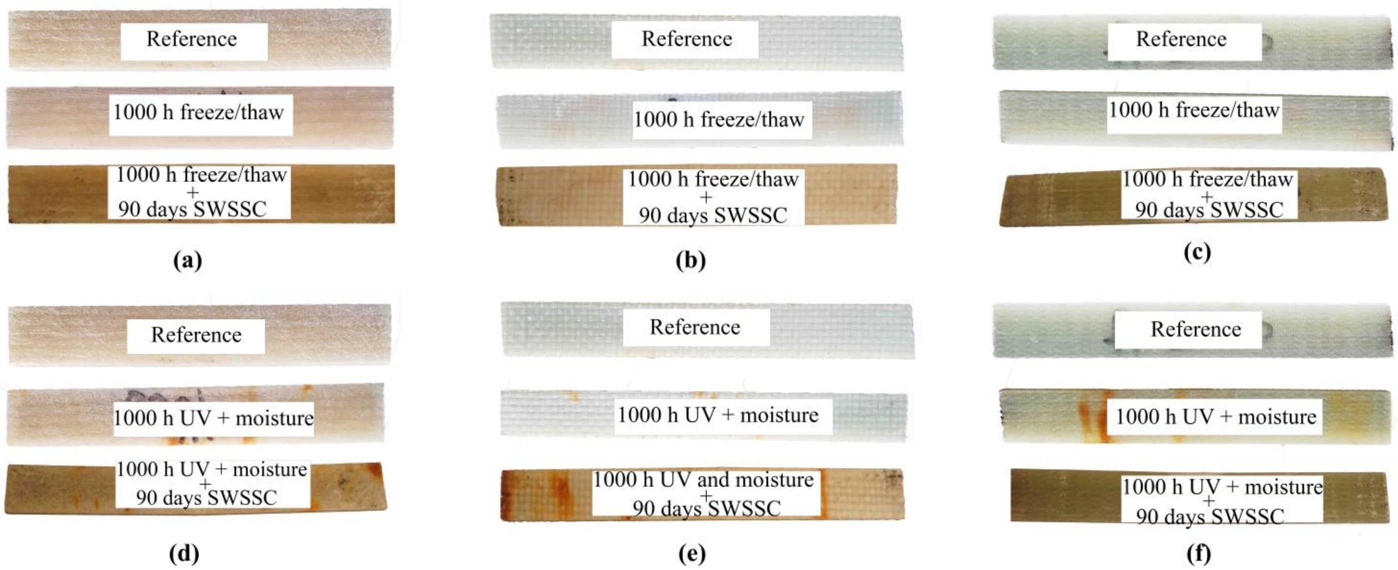

Figure 10-4 Surface changes of vacuum infused laminates after conditioning: (a) Random fibres laminates exposed to Freeze/thaw and SWSSC, (b) woven fibres laminates exposed to Freeze/thaw and SWSSC, (c) unidirectional fibres laminates exposed to Freeze/thaw and SWSSC, (d) Random fibres laminates exposed to UV-moisture and SWSSC, (e) woven fibres laminates exposed to UV-moisture and SWSSC, and (f) unidirectional fibres laminates exposed to UV-moisture and SWSSC

10.3.2 Microstructural analyses

In order to investigate the microstructural properties of the conditioned GFRP composites in terms of the damage mechanisms and degradation level, some pultruded and vacuum infused samples were observed under SEM. The analyzed pultruded samples were taken from the centre of the I-shaped profiles. **Figure 10-5** shows the SEM images of reference and pultruded samples exposed to freeze/thaw cycles [64], SWSSC solution [262], and freeze/thaw cycles followed by SWSSC solution. As is seen in **Figure 10-5(b)**, some micro-cracks and micro-holes in the surface resin matrix are the main damages due to the freeze/thaw cycles. Resin hardening and internal stress increase due to the different thermal expansion coefficient of glass fibres compared to the resin are the main reasons for the development of such defects [159]. Because the adverse effects of SWSSC solution on the surface of the pultruded samples were significantly high, the SEM images of the samples exposed to only SWSSC (**Figure 10-5(c)**) and the combined freeze/thaw cycles and SWSSC (**Figure 10-5(d)**) are not distinguishable.). Samples exposed to both the conditions suffered significant resin cracking, resin leaching and fibre/resin debonding. Moreover, fibre damages, including crushing and peeling, were also observed.

Resin damages due to the solution uptake are leaching, swelling, short-term plasticization and long-term hydrolysis, as a result of an attack on the matrix ester groups [333], while the formation of corrosion shells on the fibres are the main reason of fibres and interface degradations in alkaline solutions. Corrosion shells are formed as a result of chemical reactions between the silicate in fibres and alkali-ions [249, 280, 281]. These reactions lead to silicate network destruction and dissolution. The growth of corrosion shells consequently results in the fibre/resin debonding: the more the corrosion shell expansion, the greater the possibility of interface debonding [249].

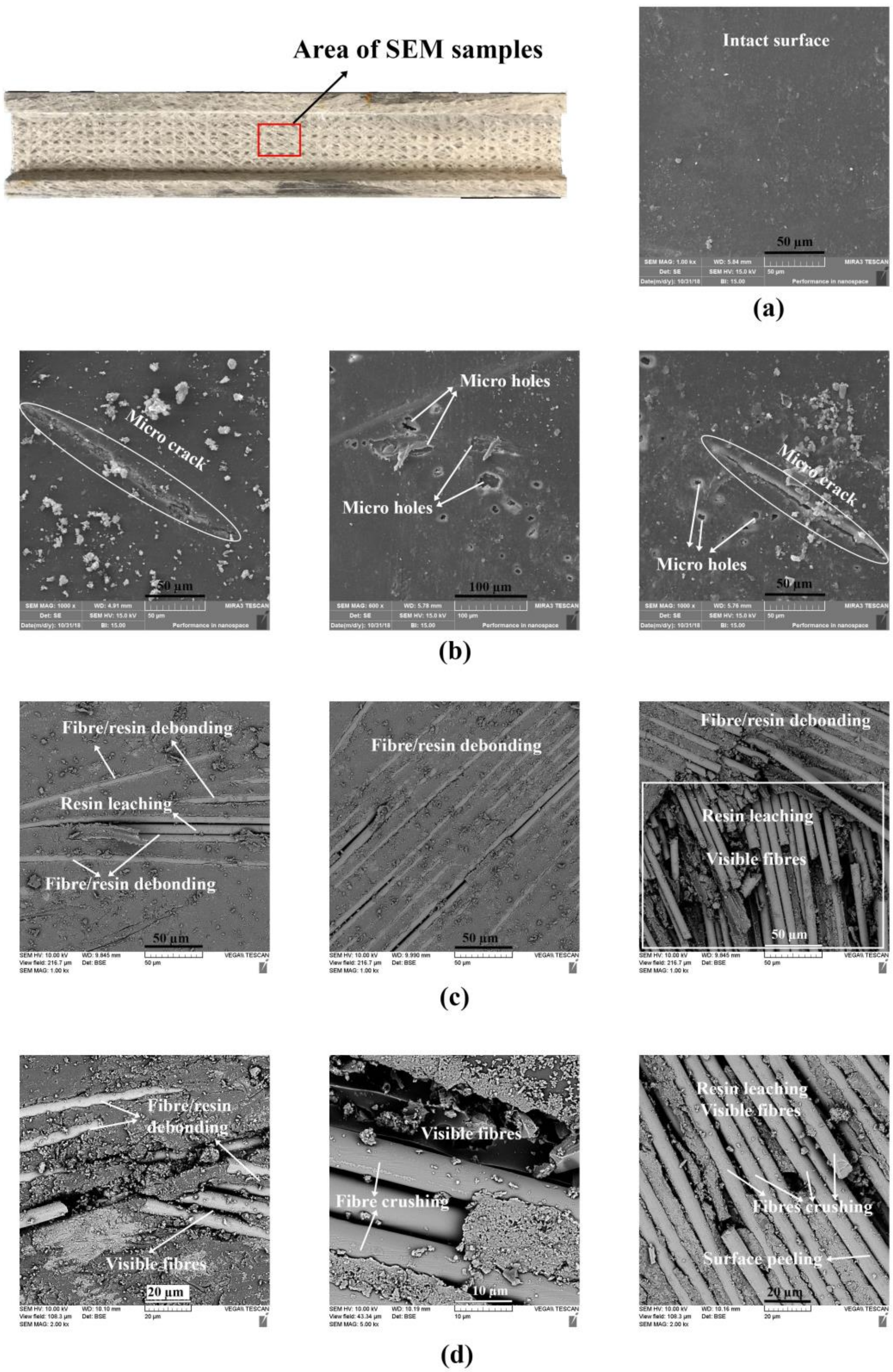

Figure 10-5 SEM images of pultruded profiles: (a) reference, (b) samples exposed to only freeze/thaw cycles, (c) samples exposed to only SWSSC solution, and (d) samples exposed to freeze/thaw cycles followed by SWSSC solution

Figure 10-6 and **Figure 10-7** show the SEM images of reference and vacuum infused samples laminates exposed to freeze/thaw cycles [106], UV and water vapour cycles [106], and freeze/thaw or UV and moisture cycles followed by SWSSC solution.

Similar to pultruded samples, micro cracks and micro-holes were the main damages of vacuum infused samples under freeze/thaw cycles (**Figure 10-6(b)**). However, cracks and holes are more pronounced in samples under UV and moisture cycles compared to freeze/thaw cycles (compare **Figure 10-7(b)** to **Figure 10-6(b)**). Moreover, some fibre/matrix debonding was also observed in UV and moisture conditions (**Figure 10-7(b)**). This difference shows that the outdoor condition of UV and moisture cycles is a harsher than the freeze/thaw cycles to GFRP composites. Regarding the samples exposed to conditions including SWSSC, it is seen that the surface resin layer is significantly damaged (as wide cracks and huge holes developed), and consequently fibres are exposed, and in some cases, deboned from the surrounding resin (**Figure 10-6(c)** and **Figure 10-7(c)**).

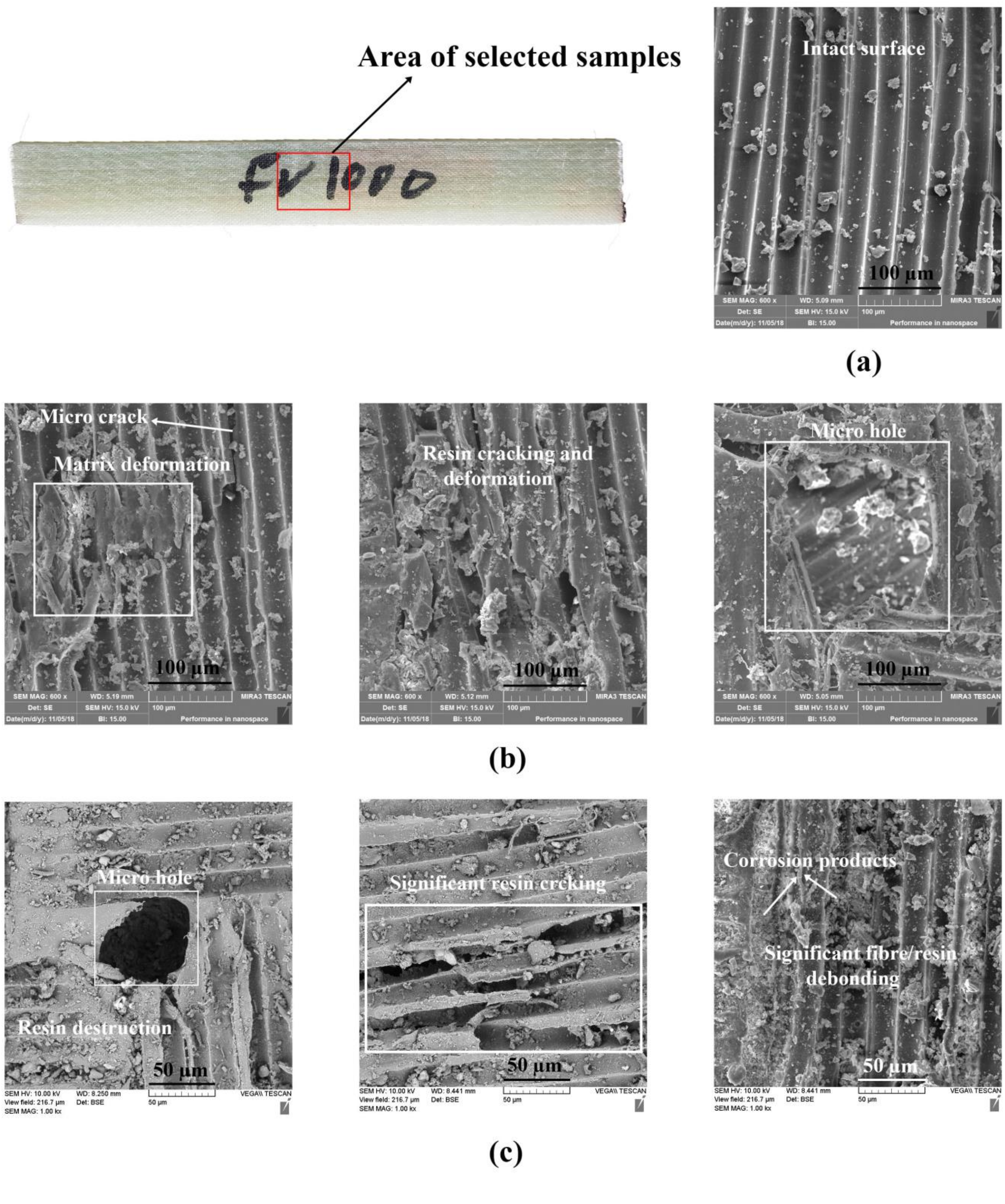

Figure 10-6 SEM images of vacuum infused laminates: (a) reference, (b) samples exposed to only freeze/thaw cycles, (c) samples exposed to freeze/thaw cycles followed by SWSSC solution

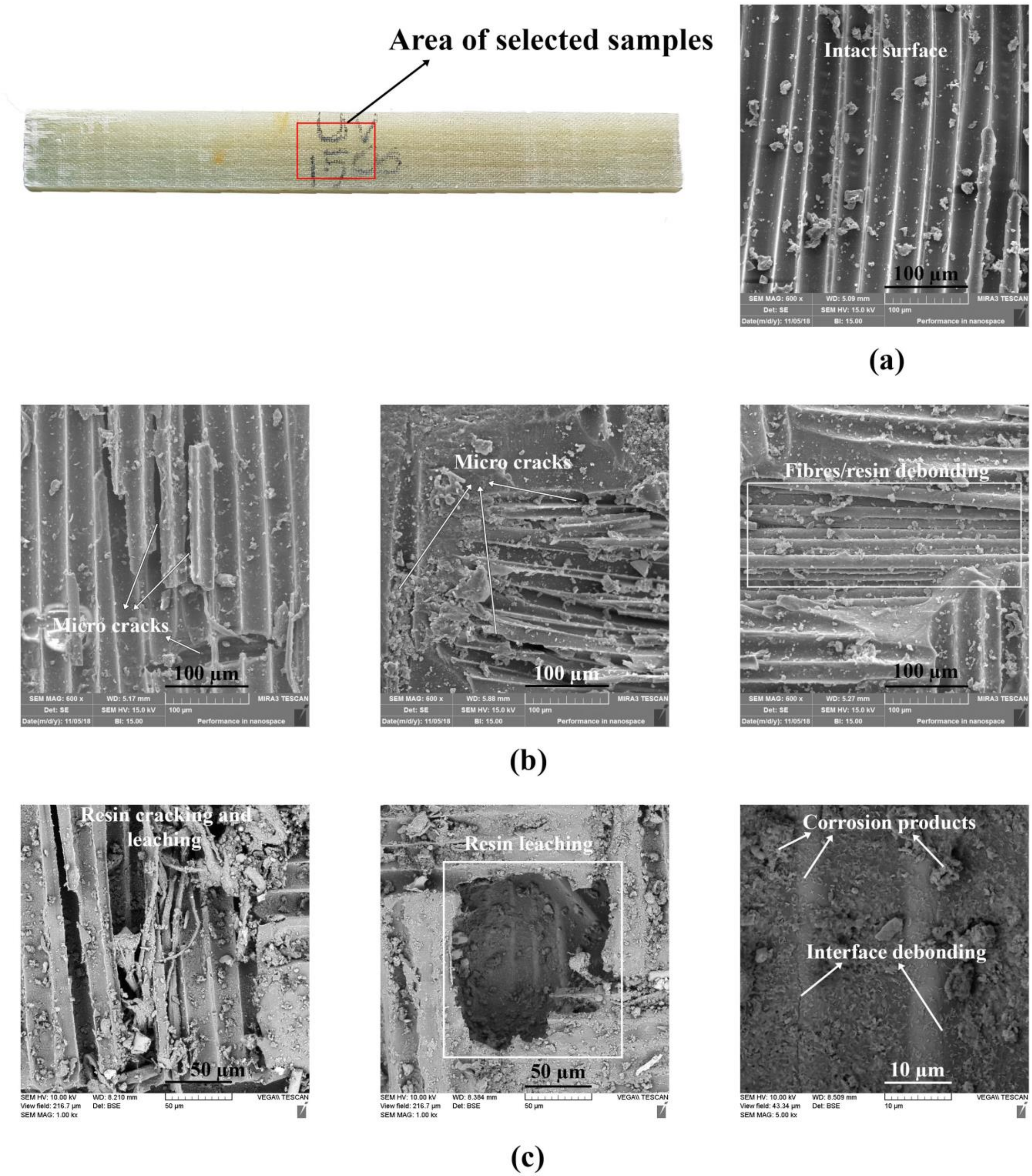

Figure 10-7 SEM images of vacuum infused laminates: (a) reference, (b) samples exposed to only UV and moisture cycles, (c) samples exposed to UV and moisture cycles followed by SWSSC solution

10.3.3 Mechanical test results

10.3.3.1 Failure Modes

Table 10-5 lists the typical dominant failure modes observed in reference and conditioned flexural pultruded profiles. It is important to clarify that freeze/thaw cycles did not affect the failure modes observed (i.e., the same failure modes were observed in samples exposed to SWSSC solution [262] with or without prior exposure to freeze/thaw cycles. Therefore, in **Table 10-5,** all samples were divided into two groups: reference and conditioned. **Figure 10-8** shows the typical failure modes observed in three-point bending, compression, and tension tests of pultruded profiles.

Table 10-5 Failure modes observed in pultruded profiles under bending

Bending axis	**Specimen**	**Tensile fibres fracture**	**Compressive fibres buckling**	**Interlaminar shear cracks**		**Web**		**Resin crippling**	
				web/flange junction	Web and/or flange	Vertical cracking	Crushing	Under the loading nose	At supports
Major	I-reference			✓		✓		✓	
	U-reference			✓			✓		
	I-conditioned			✓	✓	✓		✓	
	U-conditioned			✓	✓		✓		
Minor	I-reference	✓	✓			✓		✓	
	U-reference	✓	✓	✓				✓	
	I-conditioned	✓	✓			✓		✓	✓
	U-conditioned			✓	✓				✓

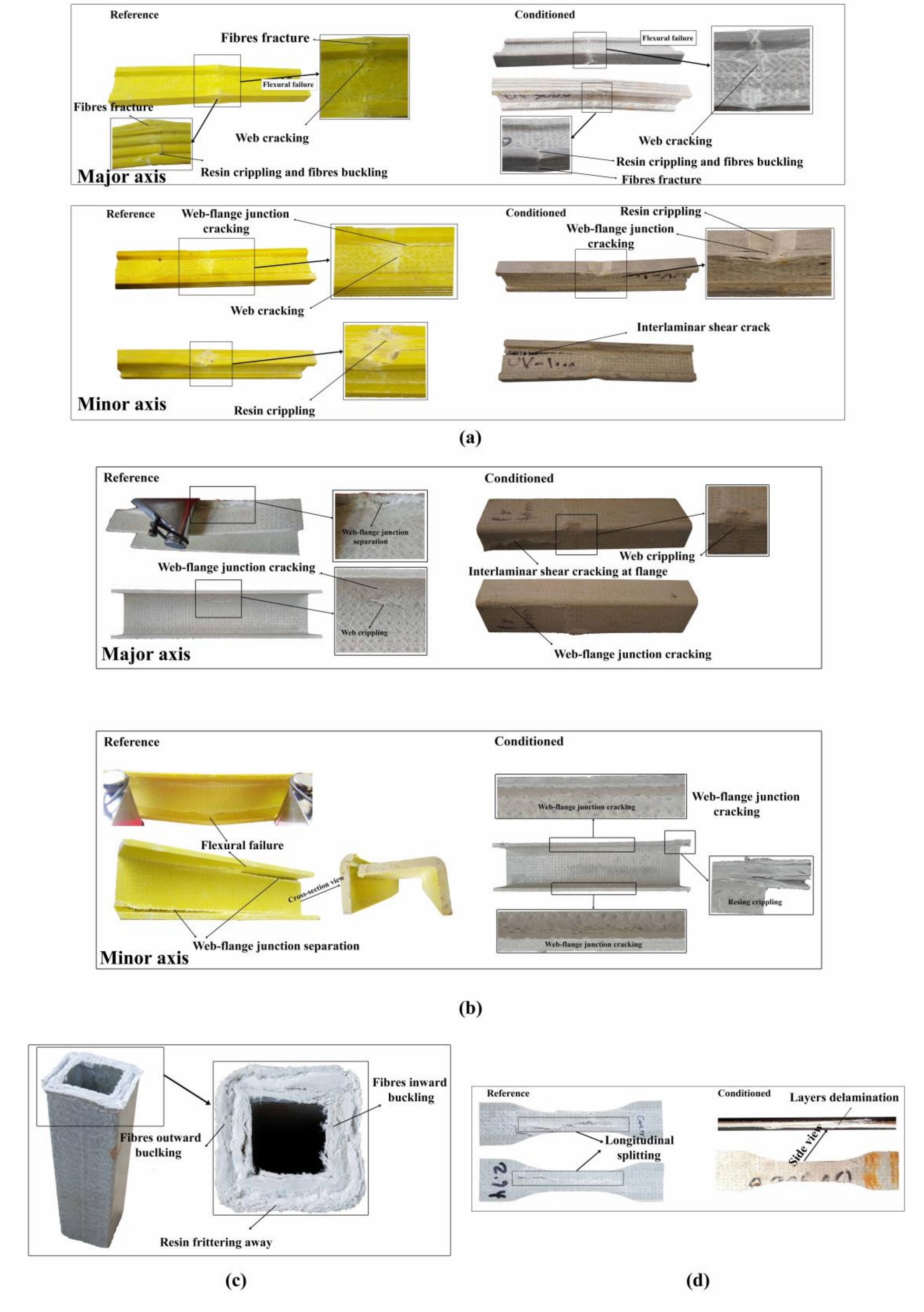

Figure 10-8 Typical failure modes observed in pultruded I-shaped sections: (a) about minor axis and (b) about major axis

As seen in **Table 10-5**, regarding the flexural samples, the difference observed between the reference and conditioned sections when tested about their major axis was the interlaminar shear crack locations. Significant degradation at the resin-fibre interface due to the SWSSC environment was the main reason that interlaminar shear cracks occurred at different locations at the web and flange of conditioned samples, rather than only at web-flange junction in the reference samples. However, when the profiles were tested about their minor axis, the failure mode of channel sections changed from combination of flexural failure and web-flange junction separation in reference samples to only web-flange junction separation in conditioned samples while no change was observed in the I-shaped samples. This reveals that, in contrast to the I-shaped sections, the resin/fibre interface degradation was adequate to change the failure mode of channel sections.

As the elephant foot buckling was the dominant failure mode of the compressive reference sample, interface degradation due to conditioning caused the elephant foot buckling to occur earlier than any other failure mode, and thus, conditioned samples also failed due to the same type of buckling. For tensile samples, as seen in **Figure 10-8**, fibre fracture was the dominant failure mode for the reference samples, while delamination between the laminate layers was the dominant failure mode for the conditioned samples. Resin matrix degradation, and consequently, the resin-fibre interface degradation, led to this failure mode change.

Detailed discussions regarding the pultruded profile failure modes under harsh environments can be found in [262].

Figure 10-9 shows the typical failure modes observed in reference and conditioned vacuum infused laminates. As is seen in **Figure 10-9(b)**, the failure mode of conditioned woven laminates changed from flexural failure (i.e., tensile fibre fracture, compressive fibre buckling and resin crippling) in the reference samples to laminate layer delamination in the conditioned samples. However, the failure modes of unidirectional and chopped strand laminates did not change after conditioning (**Figure 10-9(a)** and **(c)**). This shows that the interface strength between the layers of woven laminates was significantly decreased due to the fibre-resin interface degradation, which resulted in the delamination failure mode to occur earlier than the fibre fracture.

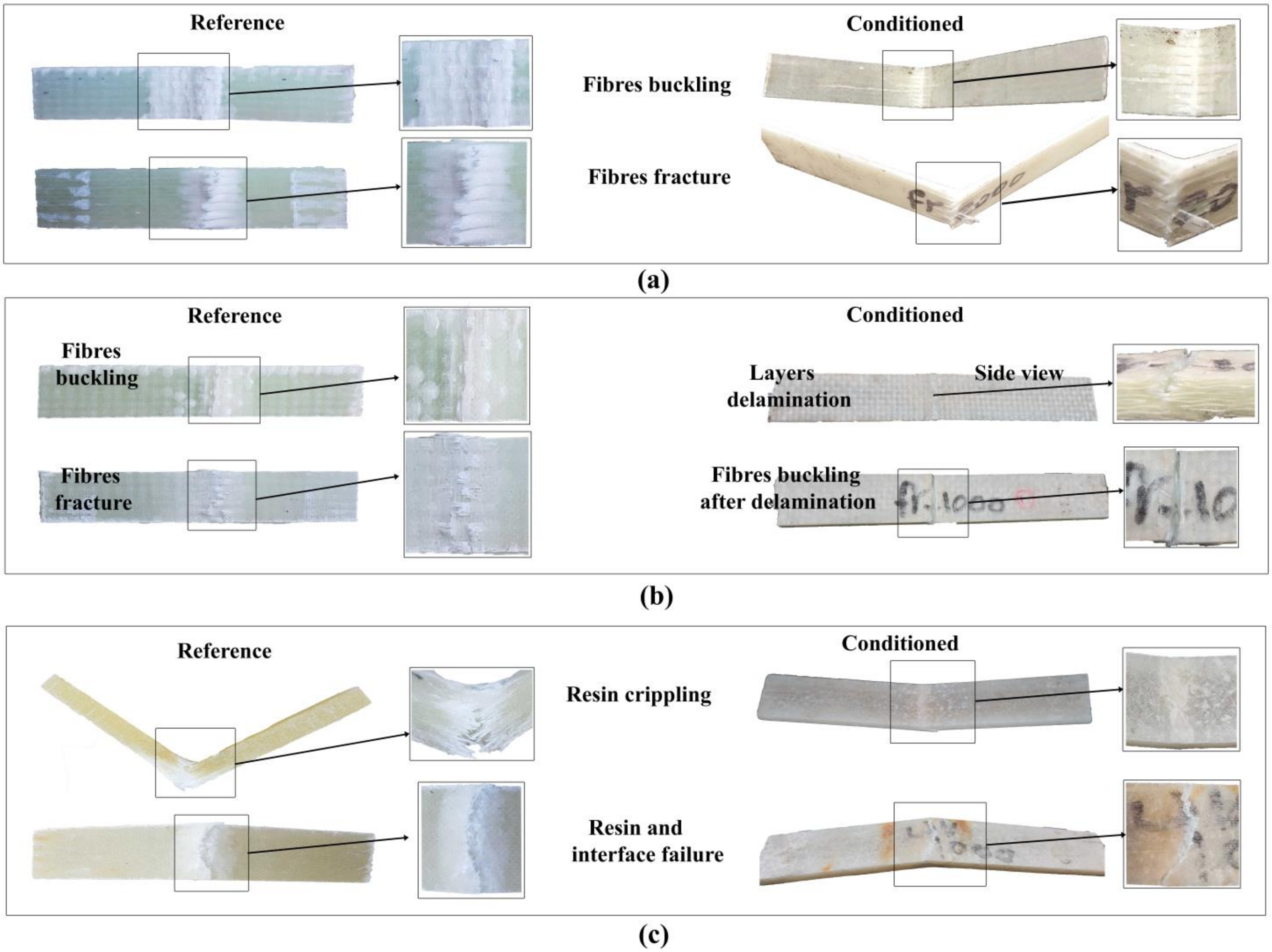

Figure 10-9 Typical failure modes observed in reference and conditioned vacuum infused laminates: (a) unidirectional, (b) woven, and (c) chopped stand

10.3.3.2 Three-point bending

Bending test results of pultruded profiles and vacuum infused laminates are presented in **Table 10-6** and **Table 10-7**, respectively. The identification system used includes two terms: the first term represents the sample type, and the second term represents the axis of the bending test (i.e., S and W represent the principal strong and weak axis, respectively). The results of pultruded profiles subjected to only the SWSSC solution reported in [262] are also presented in **Table 10-6** for comparison purposes. In addition, the flexural strength retention versus the environmental condition of pultruded and vacuum infused samples are presented in **Figure 10-10** and **Figure 10-11**, respectively.

Table 10-6 Three-point bending test results of pultruded profiles

Specimen	**Conditioning type**	**Maximum load (N)**	**CV (%)**
I1-S	Control	6292	0.8
	90 days SWSSC [262]	5012	3.7
	1000 h freeze/thaw + 90 days SWSSC	4782	5.1
	3000 h freeze/thaw + 90 days SWSSC	5248	4.4
I1-W	Control	3203	1.0
	90 days SWSSC [262]	2565	2.9
	1000 h freeze/thaw + 90 days SWSSC	2498	4.6
	3000 h freeze/thaw + 90 days SWSSC	2477	3.1
I2-S	Control	10793	2.2
	90 days SWSSC [262]	7578	3.6
	1000 h freeze/thaw + 90 days SWSSC	6891	5.6
	3000 h freeze/thaw + 90 days SWSSC	7373	4.2
I2-W	Control	6577	1.3
	90 days SWSSC [262]	4853	5.2
	1000 h freeze/thaw + 90 days SWSSC	4880	3.1
	3000 h freeze/thaw + 90 days SWSSC	4565	3.9
U1-S	Control	4320	2.3
	90 days SWSSC [262]	3727	3.1
	1000 h freeze/thaw + 90 days SWSSC	3621	4.4
	3000 h freeze/thaw + 90 days SWSSC	3654	4.1
U1-W	Control	7250	0.9
	90 days SWSSC [262]	5131	6.5
	1000 h freeze/thaw + 90 days SWSSC	5012	5.2
	3000 h freeze/thaw + 90 days SWSSC	4758	4.2
U2-S	Control	7659	1.9
	90 days SWSSC [262]	7161	4.4
	1000 h freeze/thaw + 90 days SWSSC	6746	6.1
	3000 h freeze/thaw + 90 days SWSSC	6610	5.2
U2-W	Control	11002	1.1
	90 days SWSSC [262]	8658	2.7
	1000 h freeze/thaw + 90 days SWSSC	7578	3.2
	3000 h freeze/thaw + 90 days SWSSC	7823	5.6

Table 10-7 Three-point bending test results of vacuum infused laminates

Specimen	Condition type	Ultimate load (N)	CV (%)
Unidirectional laminates	Control	3377	1.1
	30 days SWSSC	3017	3.2
	90 days SWSSC	2435	2.5
	1000 h freeze/thaw + 30 days SWSSC	3004	4.1
	2000 h freeze/thaw + 30 days SWSSC	2967	3.2
	1000 h freeze/thaw + 90 days SWSSC	2477	2.8
	2000 h freeze/thaw + 90 days SWSSC	2452	2.3
	1000 h UV and moisture + 30 days SWSSC	2354	4.2
	2000 h UV and moisture + 30 days SWSSC	2305	3.4
	1000 h UV and moisture + 90 days SWSSC	2133	1.9
	2000 h UV and moisture + 90 days SWSSC	2087	2.8
Woven laminates	Control	1504	1.8
	30 days SWSSC	465	3.2
	90 days SWSSC	431	3.8
	1000 h freeze/thaw + 30 days SWSSC	471	2.8
	2000 h freeze/thaw + 30 days SWSSC	466	4.6
	1000 h freeze/thaw + 90 days SWSSC	402	5.1
	2000 h freeze/thaw + 90 days SWSSC	429	2.1
	1000 h UV and moisture + 30 days SWSSC	417	1.9
	2000 h UV and moisture + 30 days SWSSC	366	3.7
	1000 h UV and moisture + 90 days SWSSC	321	2.5
	2000 h UV and moisture + 90 days SWSSC	295	4.3
Chopped strand mat laminates	Control	1381	2.1
	30 days SWSSC	775	1.8
	90 days SWSSC	705	2.9
	1000 h freeze/thaw + 30 days SWSSC	788	3.2
	2000 h freeze/thaw + 30 days SWSSC	783	3.8
	1000 h freeze/thaw + 90 days SWSSC	662	4.1
	2000 h freeze/thaw + 90 days SWSSC	613	3.3
	1000 h UV and moisture + 30 days SWSSC	701	4.2
	2000 h UV and moisture + 30 days SWSSC	655	4.9
	1000 h UV and moisture + 90 days SWSSC	515	3.1
	2000 h UV and moisture + 90 days SWSSC	417	5.2

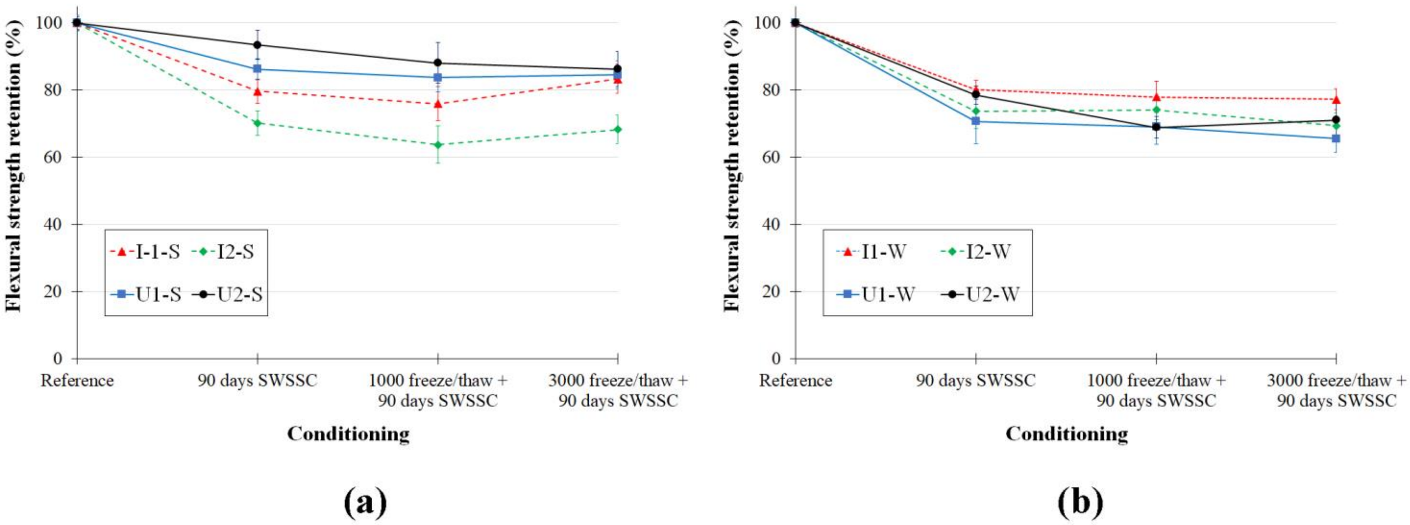

Figure 10-10 Flexural strength retention versus the conditioning of pultruded profiles: (a) tested about the major axis, and (b) tested about the minor axis

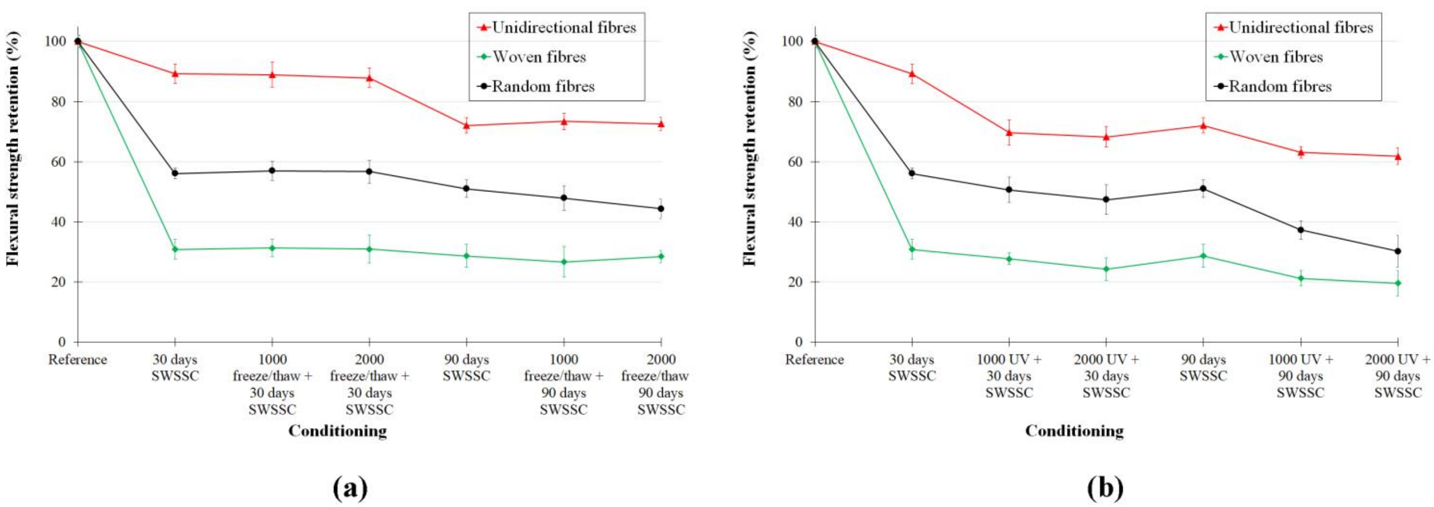

Figure 10-11 Flexural strength retention versus the conditioning of vacuum infused laminates: (a) SWSSC immersion and freeze/thaw cycles, and (b) SWSSC immersion and UV cycles

Regarding the pultruded profiles, in contrast to the initial adverse effect of UV radiation and water vapour condensation cycles reported in [262], the effect of freeze-thaw cycles before exposure to SWSSC is not significant (the maximum flexural strength difference between the samples exposed to only SWSSC and samples pre-exposed to freeze-thaw cycles before exposure to SWSSC is about 8%, while this difference is about 22% between the samples subjected to UV and moisture cycles [262]). This shows that the initial degradation of GFRP composites due to the pre-exposure to the freeze-thaw cycles is not significant in comparison to that due to exposure to UV and moisture cycles (see **Figure 10-5 (b)**). In fact, the final flexural strength of samples exposed to the combined freeze-thaw cycles and SWSSC solution were nearly the same as the samples exposed to only SWSSC solution. These observations also confirm that GFRP composites' resistance to the freeze-thaw cycles, and exposure of the profiles to such condition before or during their use with concrete in construction applications is not a serious concern.

A trend similar to those reported in [73, 262] for the effect of profile cross-section configuration and bending axis was observed in the present study. For detailed discussion the readers may refer to [262].

From **Figure 10-11**, it is obvious that the laminates with unidirectional fibres show the best flexural performance among all vacuum infused samples under all the environmental conditions investigated in this study. However, surprisingly, the woven laminates performed weaker than the chopped strand mat laminates. Failure modes observed in each type of laminate can explain the trend in flexural strength results. As was mentioned earlier, the dominant failure mode of conditioned woven laminates during bending tests was the delamination between the layers in the tensile zone. Therefore, the fibre-resin interface degradation significantly affects the flexural strength of conditioned woven laminates. In other words, the interface strength degradation between the layers of woven laminates was severe enough to change the failure mode from fibre fracture (in the reference samples) to delamination (in the conditioned samples).

However, as the dominant failure mode of unidirectional and chopped strand laminates (i.e., fibre fracture at tension zone and resin failure and fibres buckling at compression zone) did not change after the conditioning, the flexural strength degradation of these laminates was less than that of the woven laminates. This indicates that the number of layers used during the hand-made fabrication process of GFRP laminates and the interface strength of each individual layer are important factors in the flexural behaviour of such laminates under harsh environments, especially environments including solutions that can affect the interface significantly.

10.3.3.3 Compression

The compression test results of pultruded profiles are presented in **Table 10-8.** Also, the compressive strength retention versus the environmental condition of pultruded samples are presented in **Figure 10-12**. Similar to the bending test results, it was generally observed that the initial freeze/thaw cycles have very little effects on degradation of a profile's compressive strength after exposure to SWSSC solutions (the maximum compressive strength difference between the samples exposed to only SWSSC and those pre-exposed to freeze/thaw cycles followed by SWSSC is about 8 %). Regarding the effect of profiles cross-section, the trend was similar to those reported in the previous studies. Readers may refer to [73, 262] for the details.

Table 10-8 Compression test results of pultruded profiles

Specimen	Conditioning type	Maximum load (N)	CV (%)
B-1	Control	43195	2.8
	30 days of SWSSC [262]	30668	5.3
	1000 h freeze/thaw + 30 days SWSSC	31324	4.3
	3000 h freeze/thaw + 30 days SWSSC	30124	6.2
	90 days SWSSC [262]	25053	5.1
	1000 h freeze/thaw + 90 days SWSSC	25285	5.5
	3000 h freeze/thaw + 90 days SWSSC	24986	4.7
B-2	Control	65233	1.2
	30 days of SWSSC [262]	43053	7.3
	1000 h freeze/thaw + 30 days SWSSC	42145	5.3
	3000 h freeze/thaw + 30 days SWSSC	41465	4.3
	90 days SWSSC [262]	35225	3.6
	1000 h freeze/thaw + 90 days SWSSC	37125	6.2
	3000 h freeze/thaw + 90 days SWSSC	36349	5.1
C-1	Control	60321	2.1
	90 days SWSSC [262]	36192	6.8
	1000 h freeze/thaw + 90 days SWSSC	34267	5.5
	3000 h freeze/thaw + 90 days SWSSC	31490	6.1
C-2	Control	92655	2.3
	30 days of SWSSC [262]	69491	9.5
	1000 h freeze/thaw + 30 days SWSSC	65756	7.2
	3000 h freeze/thaw + 30 days SWSSC	66125	6.3
	90 days SWSSC [262]	61152	6.4
	1000 h freeze/thaw + 90 days SWSSC	60321	5.3
	3000 h freeze/thaw + 90 days SWSSC	58239	7.1

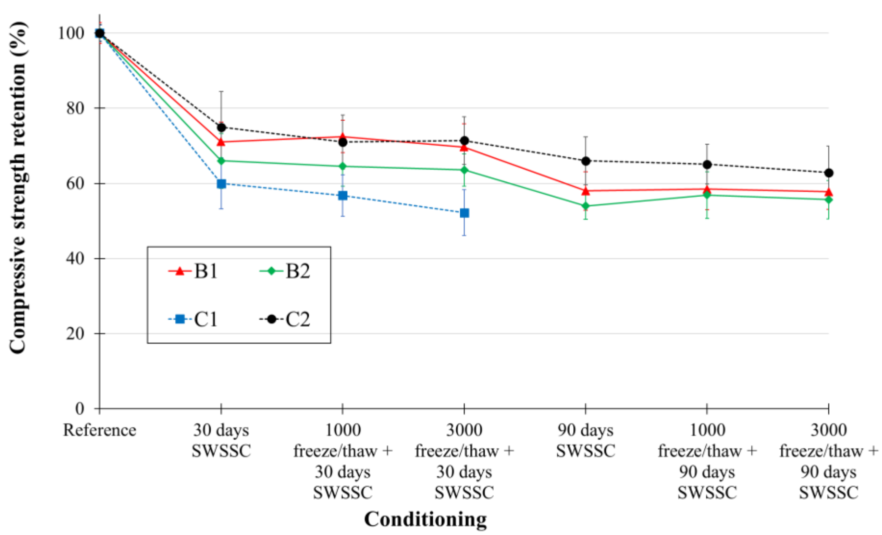

Figure 10-12 Compressive strength retention versus the conditioning of pultruded profiles

10.3.3.4 Tension

Tension test results of pultruded laminates are presented in **Table 10-9** and the tensile properties retention versus the environmental condition curves are shown in **Figure** 10-13 Tensile properties retention **versus the conditioning** of pultruded laminates: (a) strength retention, and (b) elastic modulus retention**.** The maximum tensile strength difference between the samples exposed to only SWSSC and those pre-exposed to freeze/thaw cycles followed by SWSSC is about 5 %, while no significant difference in elastic modulus was observed between the samples exposed to the two conditions, again confirming resistance of the pultruded profiles to any degradation due to any prior exposure to the freeze/thaw cycles. Moreover, as expected, the tensile strength degradation of thinner laminates was greater (e.g., 37 % reduction in 2 mm thick laminates compared to 31 % reduction in 5 mm laminates when exposed to 3000 h of freeze/thaw cycles followed by 90 days of SWSSC immersion). It was also observed that the elastic modulus reductions under harsh environments were significantly smaller than the corresponding strengths values. The fact that fibres, the main component responsible for elastic modulus of composites materials, are less affected by the environment compared to the resin, can explain this observation. Detailed discussions regarding the effect of laminate thickness on the tensile properties of pultruded profiles under harsh environments can be found in [73, 262].

Table 10-9 Tensile properties of pultruded laminates

Laminate thickness	Conditioning type	Maximum Load (N)	CV (%)	Elastic modulus (GPa)	CV (%)
2 mm	Control	28345	1.12	35.0	1.7
	90 days SWSSC [262]	19055	3.5	29.7	1.4
	1000 h freeze/thaw +90 days of SWSSC	18933	4.1	28.2	2.6
	3000 h freeze/thaw + 90 days of SWSSC	17976	5.2	29.3	3.7
5 mm	Control	40906	0.89	45.0	2.1
	90 days SWSSC [262]	30231	2.3	36.1	1.8
	1000 h of freeze/thaw + 90 days SWSSC	28350	5.1	39.9	4.4
	3000 h of freeze/thaw + 90 days SWSSC	28100	4.2	37.1	3.6

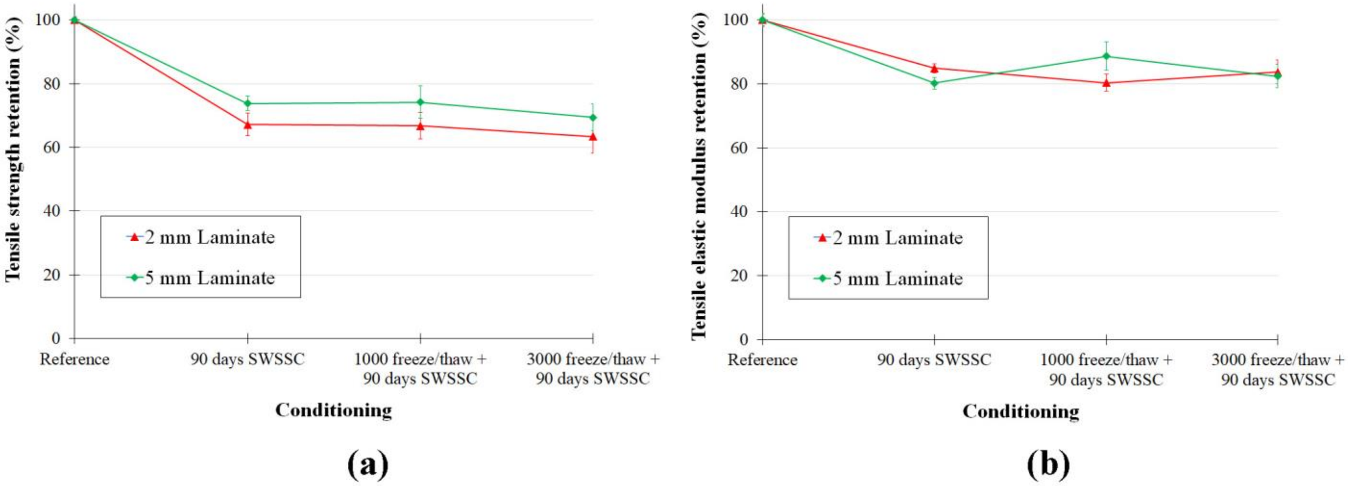

Figure 10-13 Tensile properties retention versus the conditioning of pultruded laminates: (a) strength retention, and (b) elastic modulus retention

10.4. Comparison with previous work

As suggested by **Table 10-1**, similar specimens were tested under different environments in previous research. The maximum mechanical strength reductions under different conditions are compared in **Table 10-10.** As is seen, between the harsh outdoor conditions and SWSSC, generally, 90 days immersion in SWSSC is more damaging to GFRP composites compared to 3000 h of cycles of UV and moisture and further 3000 h of cycles of freeze/thaw cycles. In addition, in most cases samples exposed to freeze/thaw cycles exhibit less declines compared to samples exposed to UV and moisture cycles. However, in channel sections tested about the major axis and B1 sections, the reductions were slightly higher in freeze/thaw cycles compared to UV and moisture. This could be explained by the failure modes of such samples, in which the failure occurs before the samples reach their ultimate capacity (i.e., out of plane failure in channel sections and elephant foot buckling of compressive samples). The results of samples exposed to only SWSSC and samples exposed to SWSSC after prior exposure to out-door environments show that initial exposure to UV and moisture will affect the final degradation of the GFRP profiles. However, freeze/thaw cycles are largely ineffective in causing any serious damage. Comparing the samples exposed to freeze/thaw cycles followed by SWSSC immersion with samples exposed to UV and moisture cycles followed by SWSSC immersing, one can conclude that the latter is more aggressive environment. This confirms that the initial degradation of samples exposed to UV and moisture was higher than that due to freeze/thaw cycles. Accordingly, the final ultimate reductions of samples exposed to UV and moisture were higher.

Table 10-10 Comparison between the previous studies and the present study on the maximum mechanical strength reductions of pultruded GFRP profiles subjected to different conditions

Profile	**UV + moisture cycles [73]**	**Freeze/thaw cycles [64]**	**SWSSC [230, 262]**	**SWSSC + UV and moisture [262]**	**SWSSC + Freeze/thaw**
I1					
Three-point bending (major axis)	21%	17%	21%	34%	17%
Three-point bending (minor axis)	9%	8%	20%	33%	23%
I2					
Three-point bending (major axis)	34%	17%	30%	52%	32%
Three-point bending (minor axis)	21%	2%	26%	34%	31%
U1					
Three-point bending (major axis)	12%	14%	14%	23%	16%
Three-point bending (minor axis)	18%	19%	29%	41%	35%
U2					
Three-point bending (major axis)	13%	16%	7%	14%	14%
Three-point bending (minor axis)	17%	9%	22%	32%	29%
B1					
Compression	22%	26%	42%	44%	42%
B2					
Compression	23%	14%	46%	50%	44%
C1					
Compression	21%	-	40%	43%	48%
C2					
Compression	11%	-	34%	37%	37%
8 mm tubes					
Compression	-	-	59%	-	-
L1					
Tension	28%	14%	33%	47%	37%
L2					
Tension	26%	9%	26%	42%	31%

Note: All SWSSC conditions are 90 days immersing in ambient temperature and out-door cycles duration is 3000h.

The maximum mechanical strength reductions of vacuum infused laminates under different conditions are also compared in **Table 10-11.** As is seen, laminates exposed to elevated temperature above laminate matrix's glass transition temperature, T_g, showed higher reductions compared to harsh out-door environments (i.e. UV-moisture and freeze/thaw cycles). Moreover, the UV and water vapor cycles at an elevated temperature (i.e. 60 ºC) caused significantly higher reductions compared to freeze/thaw cycles. These show that the mechanical properties of polymers are significantly susceptible to degradation at elevated temperatures near and above T_g, while they are almost resistant to freezing temperatures. Regarding the laminates exposed to conditions including SWSSC solution, one can conclude that vacuum infused laminates are significantly vulnerable to such environments. In addition, initial exposure to UV and moisture cycles leads to higher final degradation (i.e. higher reductions in laminates exposed to UV and moisture cycles followed by SWSSC immersing compared to only SWSSC immersion), while initial exposure to freeze/thaw cycles seems to cause insignificant damage.

Table 10-11 Comparison between the previous studies and the present study on the maximum mechanical strength reductions of vacuum infused laminate exposed to different environmental conditions

Profile	**UV+ moisture cycles [106] [1]**	**Freeze/thaw cycles [106] [1]**	**Elevated temperature [2] [63, 218]**	**SWSSC**	**SWSSC + UV and moisture**	**SWSSC + Freeze/thaw**
UL						
Tensile	8%	No reduction	20%	-	-	-
Three-point bending	-	-	17%	28%	28%	38%
WL						
Tensile	29%	6%	29%	-	-	-
Three-point bending	-	-	27%	71%	80%	72%
RL						
Tensile	36%	7%	47%	-	-	-
Three-point bending	-	-	33%	49%	70%	56%

Note: 1: The duration of all out-door condition cycles was 2000 h**; 2:** the condition is 120 min exposure to 120 ºC.

10.5. Proposed models

In this section, using the experimental results, regression models are proposed to obtain the mechanical properties of GFRP composites under harsh environmental conditions. With this regard, the following steps were performed: (1) A two-way Analysis of Variance (ANOVA) was conducted on different variables of the study; (2) Based on the ANOVA results, the effective parameters that showed considerable contributions on the final strength retention of GFRP composites were identified; (3) Several regression models (i.e. linear Bayesian regression) were tried to predict the strength retention of the samples using the selected parameters; (4) finally, according to the regression statistical parameters (e.g. regression coefficient correlations, homoscedasticity, non-collinearity, and error normality), the best predicting model was proposed. Bazli et al. [262] proposed the following model to predict the mechanical properties of GFRP pultruded profiles exposed to UV radiation and water vapour condensation as the outdoor condition followed by SWSSC solution immersing (i.e., immersing in ambient temperature similar to the present study):

$$R\ (\%) = A\left(\frac{T_1+T_2^{1.5}}{T_2^{1.1}}\right) + B(t^2) + C\left(\frac{1}{p}\right) + D\sqrt{I_x} + E \tag{10.1}$$

where T_1 and T_2 are the UV and moisture cycles time and immersing time in SWSSC (h) solution, respectively and t, p, and I_x are the sample thickness (mm), cross-section perimeter (mm), and moment of inertia (mm^4) about the x-axis (major axis), respectively. A to E are the regression parameters according to the experimental data. The same equation is used for this study. As the initial exposure to out-door conditions has changed to freeze/thaw cycles in this study, the regression coefficients will change accordingly. **Table 10-12** summarizes the regression constants and parameters of **Eq.10.1** for different mechanical tests. **Figure 10-14** shows the comparison between the experimental test results and prediction values using **Eq.10.1.** It is worth mentioning that the proposed model is valid for pultruded profiles with the cross-section configuration, time and temperature of conditioning within the range of the present study.

Table 10-12 Regression constants and parameters of Eq.10.1

Test Type	**A**	**B**	**C**	**D**	**E**	**R factor**	**Mean of standard deviation**
Pultruded profiles							
Three-point bending (major axis)	-1.435	3.530	-31525.3	-0.638	454.6	0.96	3.343
Three-point bending (minor axis)	-7.161	0.271	1279.6	0	216.1	0.87	2.836
Compression	-1.564	0.185	326.4	0	87.4	0.92	1.397
Tension	-6.649	0.231	0	0	210.2	0.96	0.353
Vacuum Infused laminates							
UL	-2.217	0	0	0	121.1	0.99	0.939
WL	-0.426	0	0	0	37.3	0.92	0.828
RL	-1.227	0	0	0	74.5	0.93	2.318

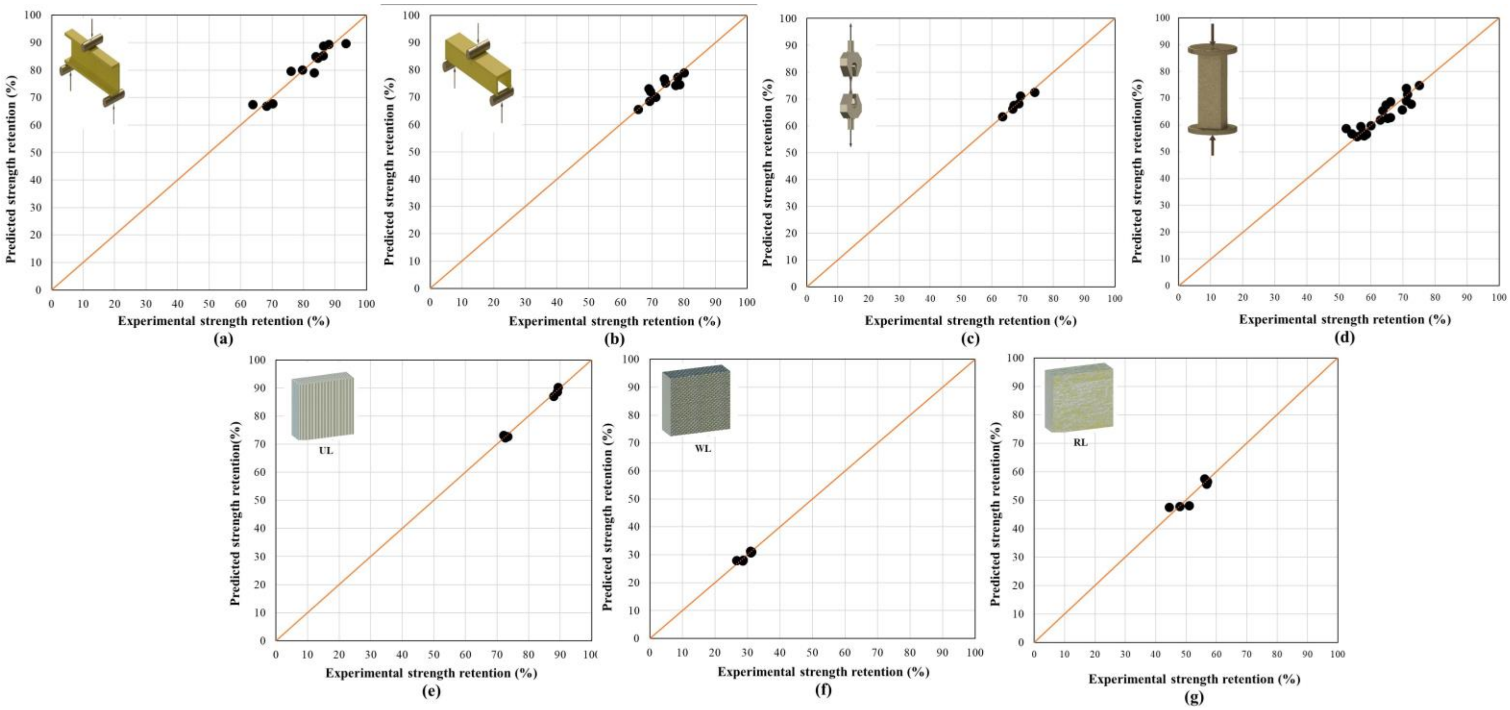

Figure 10-14 Comparison of strength retention between experimental and predicted values using Eq. (1): (a) three-point bending about major axis, (b) three-point bending about major axis, (c) tension, (d) compression, (e) three-point bending of unidirectional vacuum infused laminates, (f) three-point bending of woven vacuum infused laminates, and (g) three-point bending of chopped strand vacuum infused laminates

10.6. Conclusions

As part of the research project about using SWSSC with FRP composites in coastal areas, this study addresses the durability of pultruded GFRP composites subjected to freeze/thaw cycles followed by SWSSC solution and vacuum infused GFRP laminates subjected to SWSSC solution and its combination with freeze/thaw or UV and water vapour cycles. Mechanical tests, including three-point bending, compression, and tension, were used to investigate the mechanical properties of GFRP composites after conditioning. In addition, the microstructural properties of conditioned samples were investigated using SEM analyses. The following conclusions can be reported based on the observations and test results:

- SWSSC environment significantly affects the mechanical properties of different GFRP composites; the adverse effect is higher for pultruded profiles with interlaminar shear failure compared to fibres fracture (e.g. 30 % and 26 % reductions, respectively in bending strengths about major and minor axis of I2 samples after 90 days immersing in SWSSC).

- Degradation of flexural strength of vacuum infused woven laminates under the conditions including SWSSC solution is significantly higher than that of unidirectional and chopped strand mat laminates (e.g. maximum reductions of 80% in WL compared to 70% in RL and 38 % in UL after 2000 h exposure to UV and moisture followed by 90 days immersing in SWSSC); however, chopped strand mat laminates exhibit the weakest performance under the condition of only outdoor cycles.
- Initial exposure to freeze/thaw cycles does not have a significant effect on the final degradation of samples exposed to SWSSC solutions. In other words, the samples exposed to SWSSC solution have almost the same mechanical properties reduction in comparison to the samples exposed to freeze/thaw cycles followed by the SWSSC solution.
- In contrast, to freeze/thaw cycles, vacuum infused laminates exposed to UV and water vapour condensation cycles followed by SWSSC immersing show lower flexural strength in comparison to the samples exposed to only SWSSC solution.
- Microstructural analyses of samples exposed to outdoor conditions mainly show microcracks and micro-holes on the surface, the density of which is higher in the case of UV and moisture exposure. Therefore, if samples are exposed to SWSSC solution, the initial degradation due to the outdoor condition may lead to earlier solution penetration through the initial cracks, and thus faster damage progression, which the effect is less significant in freeze/thaw exposure.
- Microstructural analyses of samples exposed to conditions, including the SWSSC solution, show significant damages in terms of surface resin cracking and leaching, interface debonding, and fibres crushing.
- Pultruded profiles showed maximum reductions of 35 %, 48 %, and 37 % in flexural, compressive, and tensile strength, respectively, after exposure to 3000 h of freeze/thaw cycles followed by 90 days immersing in SWSSC solution.
- The mechanical performance of pultruded profiles with a lower ratio of perimeter to thickness (p/t) under harsh environments is better than that of profiles with a higher ratio.
- Vacuum infused laminates with unidirectional, woven, and chopped strand fibres showed maximum flexural reductions of 28 %, 72 %, and 56 %, respectively, after exposure to 3000 h of freeze/thaw cycles followed by 90 days immersing in SWSSC solution. The corresponding values after exposure to 3000 h of UV and water vapour cycles followed by 90 days immersing in SWSSC solution were 38 %, 80 %, and 70 %, respectively.

Chapter 11 Conclusions and future works

11.1. Conclusions

In this PhD thesis the mechanical and microstructural properties of different FRP composites under different environmental conditions have been investigated. Glass, carbon, and basalt fibre reinforced polymers with different fibres orientation, fabricated through different methods, including pultrusion, vacuum infusion, and filament winding were used. Several cross-sections have been considered. Samples were exposed to various conditions, including seawater and sea sand concrete (SWSSC), seawater, elevated temperatures, UV radiation and moisture cycles, freeze/thaw cycles and the combination of SWSSC and harsh outdoor environments for different periods. Mechanical tests, including three-point bending, compression, tension, push-out, and split-disk tensile tests have been carried out to investigate the short-term and long-term mechanical properties' durability of such materials in different environments. Scanning electron microscopy (SEM) and micro computed tomography (micro- CT) analyses were also conducted to investigate the damage mechanisms and degradation levels of samples exposed to harsh environmental conditions.

Based on the mechanical test results the short-term/long-term reduction factors for different FRP composites under different environmental conditions are proposed in **Table 11-1**. It is worth mentioning that based on the push-out test results, the bond strength between FRP tubes and SWSSC does not change after exposure to 6 months seawater environment, and thus no reduction factor is proposed for this condition. Moreover, the combined exposure to harsh-out door environment and SWSSC results showed that the effect of initial exposure to harsh out-door conditions (i.e. UV and moisture cycles and freeze/thaw cycles) may not have a significant effect on the degradation level of GFRP composites when subjected to SWSSC. Therefore, no reduction factors also are proposed for these environments.

Table 11-1 can be used by the researchers and engineers to enhance their understanding about the degradation level of different FRP composites in various environmental conditions, including extreme temperatures, harsh ambient environmental conditions, using with concrete in construction applications and combinations of these environments. In addition, the data of this thesis, particularly the reduction factors presented in **Table 11-1** could be used to provide more accurate and detailed reduction factors for FRP composites in design codes and standards as the current recommendations regarding the reduction factors mostly are not separated for each environment and mostly are related to FRP bars.

The key conclusions drawn after the comprehensive study on the mechanical and microstructural properties of different FRP composites when subjected to various environmental conditions can be summarised as follow:

- At temperatures below Tg, GFRP composites are almost resistant to elevated temperatures. Reaching the temperature to glass transition temperature of the resin and above slightly above it, a significant reduction in mechanical properties of GFRP composites occurs. At temperature close to the resin decomposition temperature, GFRP composites may lose almost all their bending strength and energy absorption capacity under three-point bending and Charpy impact tests and most of their tensile strength.
- GFRP composites are almost resistant against the freeze/thaw cycles without the presence of the moisture. Presence of moisture in freeze/thaw cycles increases the damage level of GFRP composites due to the freezing and expanding the absorbed moisture, which leads to the crack growth and fibre/matrix debonding. UV radiation and water vapour condensation condition is found to be the most aggressive environment among all out-door harsh environmental conditions used in this thesis.
- FRP composites with interlaminar shear failure mode show greater strength reductions compared to samples with fibre fracture failure mode. Moreover, specimens with lower thickness and larger perimeter show greater strength reduction under aggressive environments.
- In concrete filled FRP tubes, decreasing the diameter/thickness ratio of the tubes increases the bond strength significantly when the confinement is adequate. In addition, using fibres in an orientation (i.e. more fibres in hoop direction) that increase the confinement strength of FRP tubes is an appropriate solution for enhancing the bond-slip performance of concrete filled FRP tubes.
- Although the chemical adhesion between the FRP tubes and SWSSC under seawater condition degrades slightly, the maximum bond strength and the bond corresponds to the slip initiation vary in the range of the reference sample. Therefore, it is concluded that, in terms of the bond performance, FRP concrete filled tubes are almost resistant to seawater environment.
- Microstructural studies, including SEM and micro-CT analyses show significant damages, including resin cracking, resin leaching, resin/matrix debonding and fibres damages in GFRP and BFRP composites when exposed to SWSSC condition. However, the main morphology observations of tubes exposed to seawater are microcracks in the resin matrix, blisters and solid components. Moreover, the voids percentage, especially near the areas exposed to SWSSC solution,

increases considerably in both GFRP and BFRP composites. These observations together with dramatic mechanical properties degradations confirm the fact that SWSSC environment is a significant harsh condition for GFRP and BFRP composites. However, the degradation level of CFRP composite from both mechanical and microstructural points of view are significantly lesser than that of GFRP and BFRP composites. This confirms the superior performance of CFRP composites under aggressive environments compared to other types of FRP composites.

- Regarding SWSSC filled FRP tubes, using FRP tubes with all fibres oriented in hoop direction (i.e. 89°) is not recommended as their mechanical properties may significantly reduce in long-term due to the significant fibre/resin interface degradation, while tubes, with fibres oriented in multiple directions could retain adequate strengths during their life-time performance.
- GFRP pultruded profiles exposed to UV radiation and moisture cycles followed by SWSSC environment experience more reductions in their mechanical properties in comparison to specimens subjected to SWSSC alone. Initial surface disruptions/degradation of GFRP due to the UV and moisture cycles aiding the penetration by the SWSSC environment and facilitating crack growth is the possible reason for this observation. However, the difference is not significant.
- Samples exposed to SWSSC condition have almost the same mechanical properties reduction in comparison to the samples exposed to freeze/thaw cycles followed by the SWSSC condition. Therefore, initial exposure to freeze/thaw cycles does not have a significant effect on the final degradation level of samples exposed to SWSSC environment.
- Fibres orientation and composite thickness are important factors when studying the durability performance of FRP composites under different environmental conditions. Based on the application of the composite structure and the type of the applied loads, the appropriate fibres orientation and specimen thickness could be considered according to the results reported in this PhD thesis.

Table 11-1 Reduction factors proposed for different FRP composites under various environmental conditions

Specimen	Fabrication type	Fibres orientation	Environmental condition	Mechanical properties							
				Hoop tensile strength		Tensile strength		Compressive strength		Flexural strength	
				Range (years)	Reduction factor	Range (years) or (Temperatures °C)	Reduction factor	Range (years)	Reduction factor	Range (years) or (Temperatures °C)	Reduction factor
BFRP tube	Filament winding	multiple	real SWSSC and SW[1]	1.40 - 1.60	0.54	-	-	-	-	-	-
		multiple	simulated SWSSC and SW	1.26 - 1.40	0.43	-	-	1.00-1.15	0.66	-	-
		89°	simulated SWSSC and SW	1.30 - 1.50	0.27	-	-	2.00-2.40	0.53	-	-
GFRP tube	Filament winding	multiple	real SWSSC and seawater	8.00 - 11.90	0.50	-	-	-	-	-	-
		multiple	simulated SWSSC and SW	3.90 - 5.30	0.51	-	-	1.20 - 1.30	0.60	-	-
		89°	simulated SWSSC and SW	0.75 - 0.80	0.31	-	-	1.20 - 1.30	0.51	-	-
	Pultruded tube	Unidirectional (0°)	simulated SWSSC	-	-	Life-span	0.40	Life-span	0.20	-	-
			simulated SWSSC and SW	-	-	Life-span	0.65	Life-span	0.30	-	-
CFRP tube	Filament winding	multiple	real SWSSC and SW	8.20 - 12.30	0.84	-	-	-	-	-	-
		multiple	simulated SWSSC and SW	7.74 - 11.00	0.72	-	-	5.40 - 7.60	0.88	-	-
		89°	simulated SWSSC and SW	1.37 - 1.60	0.48	-	-	0.90 - 1.00	0.69	-	-
GFRP [2] Profiles	Pultruded profiles	Unidirectional (0°)	UV and moisture cycles	-	-	Life-span	0.86	Life-span	0.77	Life-span	0.66
		Unidirectional (0°)	Freeze/thaw cycles	-	-	Life-span	0.86	Life-span	0.74	Life-span	0.81
GFRP laminate	Vacuum infused	Unidirectional (0°)	UV and moisture cycles	-	-	Life-span	0.72	-	-	-	-
		woven (0° and 90°)	UV and moisture cycles	-	-	Life-span	0.65	-	-	-	-
		Random fibres	UV and moisture cycles	-	-	Life-span	0.57	-	-	-	-
GFRP laminate	Vacuum infused	Unidirectional (0°)	Wet freeze/thaw cycles	-	-	Life-span	0.82	-	-	-	-
		woven (0° and 90°)	Wet freeze/thaw cycles	-	-	Life-span	0.76	-	-	-	-
		Random fibres	Wet freeze/thaw cycles	-	-	Life-span	0.68	-	-	-	-
GFRP laminate	Vacuum infused	Unidirectional (0°)	Freeze/thaw cycles	-	-	Life-span	1.00	-	-	-	-
		woven (0° and 90°)	Freeze/thaw cycles	-	-	Life-span	0.92	-	-	-	-
		Random fibres	Freeze/thaw cycles	-	-	Life-span	0.92	-	-	-	-
GFRP [3] laminate	Vacuum infused	Unidirectional (0°)	Elevated temperatures	-	-	025-70 °C	0.91	-	-	025-70 °C	0.95
		Unidirectional (0°)	Elevated temperatures	-	-	70 - 120 ° C	0.76	-	-	70 - 120 ° C	0.82
		Unidirectional (0°)	Elevated temperatures	-	-	120- 200 °C	0.68	-	-	120- 200 °C	0.62
		Unidirectional (0°)	Elevated temperatures	-	-	Around 300 °C	0.43	-	-	Around 300 °C	0.08
GFRP laminate	Vacuum infused	woven (0° and 90°)	Elevated temperatures	-	-	25 -70 °C	0.76	-	-	25 -70 °C	0.93
		woven (0° and 90°)	Elevated temperatures	-	-	70 - 120 ° C	0.69	-	-	70 - 120 ° C	0.69
		woven (0° and 90°)	Elevated temperatures	-	-	120- 200 °C	0.54	-	-	120- 200 °C	0.47
		woven (0° and 90°)	Elevated temperatures	-	-	Around 300 °C	0.29	-	-	Around 300 °C	0.05
GFRP laminate	Vacuum infused	Random fibres	Elevated temperatures	-	-	25 -70 °C	0.64	-	-	25 -70 °C	0.86
		Random fibres	Elevated temperatures	-	-	70 °C - 120 °	0.46	-	-	70 °C - 120 °	0.61
		Random fibres	Elevated temperatures	-	-	120- 200 °C	0.35	-	-	120- 200 °C	0.46
		Random fibres	Elevated temperatures	-	-	Around 300 °C	0.07	-	-	Around 300 °C	0.05

Note: 1: seawater; 2: the flexural strength reduction factors of pultruded GFRP profiles are proposed based on [64]; 3- the tensile strength reduction factors of vacuum infused laminates are proposed based on [218]

11.2. Future work

According to the works completed during this PhD thesis, the following recommendations are outlined for consideration in in future research on durability performance of FRP composites when used with seawater sea sand concrete and/or subjected to various harsh outdoor environments:

Environmental condition point of view:

(1) Investigating the performance of the samples when exposed to real life environmental condition, i.e. exposure tests outside laboratory.

(2) Increasing the exposure duration for those environments that the strength retention did not converge to a certain value in order to propose a reduction factor for the life-span of the materials when subjected to such environmental condition.

(3) Considering different environmental conditions than those used in this thesis, such as high-performance seawater and sea sand concrete, acidic environment and wet/dry cycles.

(4) Considering the combined environmental conditions with wider range of conditions and exposure time in order to understand the quantitative effect of each environmental condition.

Mechanical properties point of view:

(5) Studying the other mechanical properties, such as impact and fatigue performance of FRP composites after exposure to similar environmental conditions.

(6) Performing different enhancement methods, such as using protective layers for enhancing the durability and increasing the surface roughness for enhancing the bond-performance between FRP and concrete.

Microstructural point of view:

(7) Conducting standard chemical and electrochemical tests, such as Fourier-transform infrared spectroscopy (FTIR), X-Ray Diffraction (XRD), and electrochemical impedance spectroscopy (EIS) on conditioned samples to investigate the degradation level and mechanisms in FRP composites and investigate the correlation between the obtained results and mechanical test results.

(8) More detailed study on the damage progression within the thickness of the sample using micro-CT analyses on the conditioned samples. Different exposure duration and temperature could be considered to obtain a comprehensive understanding regarding the degradation level and damage rate changing according to the type, time and temperature of the conditioning.

Computational point of view:

(9) Numerically studying the performance of composite structures. The materials properties of FRP composites under different environmental conditions reported in this thesis could be used as inputs for modelling the structures constructed, reinforced, or strengthened with FRPs.

(10) Using all the experimental data reported in this thesis together with the data available in the literature, could be used to develop robust models to predict the strength retention of FRP under harsh environments using machine learning.

References

[1] Bakis CE, Bank LC, Brown V, Cosenza E, Davalos J, Lesko J, et al. Fiber-reinforced polymer composites for construction—State-of-the-art review. Journal of composites for construction. 2002;6(2):73-87.

[2] Christian S, Billington S. Mechanical response of PHB-and cellulose acetate natural fiber-reinforced composites for construction applications. Composites Part B: Engineering. 2011;42(7):1920-8.

[3] Oskouei AV, Jafari A, Bazli M, Ghahri R. Effect of different retrofitting techniques on in-plane behavior of masonry wallettes. Construction and Building Materials. 2018;169:578-90.

[4] Wang Z, Zhao X-L, Xian G, Wu G, Raman RS, Al-Saadi S. Effect of sustained load and seawater and sea sand concrete environment on durability of basalt-and glass-fibre reinforced polymer (B/GFRP) bars. Corrosion Science. 2018;138:200-18.

[5] Nkurunziza G, Debaiky A, Cousin P, Benmokrane B. Durability of GFRP bars: A critical review of the literature. Progress in structural engineering and materials. 2005;7(4):194-209.

[6] Ashrafi H, Bazli M, Oskouei AV. Enhancement of bond characteristics of ribbed-surface GFRP bars with concrete by using carbon fiber mat anchorage. Construction and Building Materials. 2017;134:507-19.

[7] Najafabadi EP, Bazli M, Ashrafi H, Oskouei AV. Effect of applied stress and bar characteristics on the short-term creep behavior of FRP bars. Construction and Building Materials. 2018;171:960-8.

[8] Li Y, Zhao X, Singh RR, Al-Saadi S. Experimental study on seawater and sea sand concrete filled GFRP and stainless steel tubular stub columns. Thin-Walled Structures. 2016;106:390-406.

[9] Xiao J, Qiang C, Nanni A, Zhang K. Use of sea-sand and seawater in concrete construction: Current status and future opportunities. Construction and Building Materials. 2017;155:1101-11.

[10] Mohammed TU, Hamada H, Yamaji T. Performance of seawater-mixed concrete in the tidal environment. Cement and concrete research. 2004;34(4):593-601.

[11] Kupwade-Patil K, Allouche EN. Impact of alkali silica reaction on fly ash-based geopolymer concrete. Journal of materials in Civil Engineering. 2012;25(1):131-9.

[12] Wang Z, Zhao X-L, Xian G, Wu G, Raman RS, Al-Saadi S. Durability study on interlaminar shear behaviour of basalt-, glass-and carbon-fibre reinforced polymer (B/G/CFRP) bars in seawater sea sand concrete environment. Construction and Building Materials. 2017;156:985-1004.

[13] Dong Z, Wu G, Xu Y. Experimental study on the bond durability between steel-FRP composite bars (SFCBs) and sea sand concrete in ocean environment. Construction and Building Materials. 2016;115:277-84.

[14] Cadenazzi T, Nolan S, Mazzocchi G, Stringer Z, Nanni A. Bridge Case Study: What a Contractor Needs to Know on an FRP Reinforcement Project. Journal of Composites for Construction. 2020;24(2):05020001.

[15] Afshar A, Alkhader M, Korach CS, Chiang F-P. Effect of long-term exposure to marine environments on the flexural properties of carbon fiber vinylester composites. Composite Structures. 2015;126:72-7.

[16] Garcia-Espinel J, Castro-Fresno D, Gayo PP, Ballester-Muñoz F. Effects of sea water environment on glass fiber reinforced plastic materials used for marine civil engineering constructions. Materials & Design (1980-2015). 2015;66:46-50.

[17] Bazli M, Ashrafi H, Oskouei AV. Experiments and probabilistic models of bond strength between GFRP bar and different types of concrete under aggressive environments. Construction and Building Materials. 2017;148:429-43.

[18] Micelli F, Nanni A. Durability of FRP rods for concrete structures. Construction and Building materials. 2004;18(7):491-503.

[19] Kodur VK, Bisby LA, Foo SH. Thermal behavior of fire-exposed concrete slabs reinforced with fiber-reinforced polymer bars. ACI structural journal. 2005;102(6):799.

[20] Alsayed S, Al-Salloum Y, Almusallam T, El-Gamal S, Aqel M. Performance of glass fiber reinforced polymer bars under elevated temperatures. Composites Part B: Engineering. 2012;43(5):2265-71.

[21] Manalo A, Surendar S, van Erp G, Benmokrane B. Flexural behavior of an FRP sandwich system with glass-fiber skins and a phenolic core at elevated in-service temperature. Composite Structures. 2016;152:96-105.

[22] Borosnyói A. Influence of service temperature and strain rate on the bond performance of CFRP reinforcement in concrete. Composite Structures. 2015;127:18-27.

[23] Shokrieh MM, Bayat A. Effects of ultraviolet radiation on mechanical properties of glass/polyester composites. Journal of Composite materials. 2007;41(20):2443-55.

[24] Cabral-Fonseca S, Correia J, Rodrigues M, Branco F. Artificial accelerated ageing of GFRP pultruded profiles made of polyester and vinylester resins: characterisation of physical–chemical and mechanical damage. Strain. 2012;48(2):162-73.

[25] Kumar BG, Singh RP, Nakamura T. Degradation of carbon fiber-reinforced epoxy composites by ultraviolet radiation and condensation. Journal of Composite materials. 2002;36(24):2713-33.

[26] Heshmati M, Haghani R, Al-Emrani M. Effects of moisture on the long-term performance of adhesively bonded FRP/steel joints used in bridges. Composites Part B: Engineering. 2016;92:447-62.

[27] Sciolti MS, Frigione M, Aiello MA. Wet lay-up manufactured FRPs for concrete and masonry repair: influence of water on the properties of composites and on their epoxy components. Journal of Composites for Construction. 2010;14(6):823-33.

[28] Kafodya I, Xian G, Li H. Durability study of pultruded CFRP plates immersed in water and seawater under sustained bending: Water uptake and effects on the mechanical properties. Composites Part B: Engineering. 2015;70:138-48.

[29] Kim H-Y, Park Y-H, You Y-J, Moon C-K. Short-term durability test for GFRP rods under various environmental conditions. Composite structures. 2008;83(1):37-47.

[30] Benmokrane B, Elgabbas F, Ahmed EA, Cousin P. Characterization and comparative durability study of glass/vinylester, basalt/vinylester, and basalt/epoxy FRP bars. Journal of Composites for Construction. 2015;19(6):04015008.

[31] Soles CL, Chang FT, Bolan BA, Hristov HA, Gidley DW, Yee AF. Contributions of the nanovoid structure to the moisture absorption properties of epoxy resins. Journal of Polymer Science Part B: Polymer Physics. 1998;36(17):3035-48.

[32] Chin JW, Nguyen T, Aouadi K. Effects of environmental exposure on fiber-reinforced plastic (FRP) materials used in construction. Journal of Composites, Technology and Research. 1997;19(4):205-13.

[33] Aboelseoud MA, Myers JJ. Durability of hybrid composite beam bridges subjected to various environmental conditioning. Journal of Composites for Construction. 2016;20(6):04016045.

[34] Gonenc O. Durability and service life prediction of concrete reinforcing materials: University of Wisconsin--Madison; 2003.

[35] Parnas R, Shaw MT, Liu Q. Basalt fiber reinforced polymer composites. 2007.

[36] Chen Y. Accelerated ageing tests and long-term prediction models for durability of FRP bars in concrete: West Virginia University; 2007.

[37] Bradshaw R, Brinson L. Physical aging in polymers and polymer composites: An analysis and method for time-aging time superposition. Polymer Engineering & Science. 1997;37(1):31-44.

[38] Ashrafi H, Bazli M, Najafabadi EP, Oskouei AV. The effect of mechanical and thermal properties of FRP bars on their tensile performance under elevated temperatures. Construction and Building Materials. 2017;157:1001-10.

[39] Ashrafi H, Bazli M, Vatani Oskouei A, Bazli L. Effect of sequential exposure to UV radiation and water vapor condensation and extreme temperatures on the mechanical properties of GFRP bars. Journal of Composites for Construction. 2017;22(1):04017047.

[40] Hamad RJ, Johari MM, Haddad RH. Mechanical properties and bond characteristics of different fiber reinforced polymer rebars at elevated temperatures. Construction and Building Materials. 2017;142:521-35.

[41] Wang YC, Wong P, Kodur V. An experimental study of the mechanical properties of fibre reinforced polymer (FRP) and steel reinforcing bars at elevated temperatures. Composite Structures. 2007;80(1):131-40.

[42] Robert M, Benmokrane B. Behavior of GFRP reinforcing bars subjected to extreme temperatures. Journal of Composites for Construction. 2009;14(4):353-60.
[43] Hawileh RA, Abu-Obeidah A, Abdalla JA, Al-Tamimi A. Temperature effect on the mechanical properties of carbon, glass and carbon–glass FRP laminates. Construction and Building Materials. 2015;75:342-8.
[44] Lu Z, Xian G, Li H. Effects of elevated temperatures on the mechanical properties of basalt fibers and BFRP plates. Construction and Building Materials. 2016;127:1029-36.
[45] Ou Y, Zhu D, Zhang H, Huang L, Yao Y, Li G, et al. Mechanical characterization of the tensile properties of glass fiber and its reinforced polymer (GFRP) composite under varying strain rates and temperatures. Polymers. 2016;8(5):196.
[46] Dai J-G, Gao W, Teng J. Bond-slip model for FRP laminates externally bonded to concrete at elevated temperature. Journal of Composites for Construction. 2012;17(2):217-28.
[47] Burke PJ, Luke A. Bisby, and Mark F. Green. . Effects of elevated temperature on near surface mounted and externally bonded FRP strengthening systems for concrete. Cement and Concrete Composites. 2013;35(1):190-9.
[48] Nguyen T-C, Bai Y, Zhao X-L, Al-Mahaidi R. Mechanical characterization of steel/CFRP double strap joints at elevated temperatures. Composite Structures. 2011;93(6):1604-12.
[49] Wong P, Davies J, Wang Y. An experimental and numerical study of the behaviour of glass fibre reinforced plastics (GRP) short columns at elevated temperatures. Composite structures. 2004;63(1):33-43.
[50] Wong P, Wang Y. An experimental study of pultruded glass fibre reinforced plastics channel columns at elevated temperatures. Composite structures. 2007;81(1):84-95.
[51] Asaro RJ, Lattimer B, Ramroth W. Structural response of FRP composites during fire. Composite Structures. 2009;87(4):382-93.
[52] Correia JR, Branco FA, Ferreira JG, Bai Y, Keller T. Fire protection systems for building floors made of pultruded GFRP profiles: Part 1: Experimental investigations. Composites Part B: Engineering. 2010;41(8):617-29.
[53] Dodds N, Gibson A, Dewhurst D, Davies J. Fire behaviour of composite laminates. Composites Part A: applied science and manufacturing. 2000;31(7):689-702.
[54] Wang K, Ben Young, and Scott T. Smith. Mechanical properties of pultruded carbon fibre-reinforced polymer (CFRP) plates at elevated temperatures. Engineering structures. 2011;33(7):2154-61.
[55] Shen C, Springer GS. Effects of moisture and temperature on the tensile strength of composite materials. Environmental effects on composite materials. 1981;1:79.

[56] Mouritz A, Mathys Z. Post-fire mechanical properties of glass-reinforced polyester composites. Composites Science and Technology. 2001;61(4):475-90.

[57] Sorathia U, Rollhauser CM, Hughes WA. Improved fire safety of composites for naval applications. Fire and Materials. 1992;16(3):119-25.

[58] Sorathia U, Beck C, Dapp T. Residual strength of composites during and after fire exposure. Journal of Fire Sciences. 1993;11(3):255-70.

[59] Mouritz A. Post-fire flexural properties of fibre-reinforced polyester, epoxy and phenolic composites. Journal of materials science. 2002;37(7):1377-86.

[60] Wu Q, Wen H, Qin Y, Xin S. Perforation of FRP laminates under impact by flat-nosed projectiles. Composites Part B: Engineering. 2012;43(2):221-7.

[61] Pham TM, Hao H. Review of concrete structures strengthened with FRP against impact loading. Structures: Elsevier; 2016. p. 59-70.

[62] Turco A, Bocciarelli M, Nanni A, Poggi C. Influence of width and thickness of composite laminates on the flexural behavior of reinforced concrete beams and slabs. Composite Structures. 2017;178:186-94.

[63] Bazli M, Ashrafi H, Jafari A, Zhao X-L, Gholipour H, Oskouei AV. Effect of thickness and reinforcement configuration on flexural and impact behaviour of GFRP laminates after exposure to elevated temperatures. Composites Part B: Engineering. 2019;157:76-99.

[64] Jafari A, Ashrafi H, Bazli M, Ozbakkaloglu T. Effect of thermal cycles on mechanical response of pultruded glass fiber reinforced polymer profiles of different geometries. Composite Structures. 2019;223:110959.

[65] Mabry NJ, Seracino R, Peters KJ. The effects of accelerated Freeze-Thaw conditioning on CFRP strengthened concrete with pre-existing bond defects. Construction and Building Materials. 2018;163:286-95.

[66] Yan F, Lin Z, Zhang D, Gao Z, Li M. Experimental study on bond durability of glass fiber reinforced polymer bars in concrete exposed to harsh environmental agents: freeze-thaw cycles and alkaline-saline solution. Composites Part B: Engineering. 2017;116:406-21.

[67] McIsaac A, Fam A. Durability under freeze–thaw cycles of concrete beams retrofitted with externally bonded FRPs using bio-based resins. Construction and Building Materials. 2018;168:244-56.

[68] Qiao P, Xu Y. Effects of freeze-thaw and dry-wet conditionings on the mode-I fracture of FRP-concrete interface bonds. Engineering, Construction, and Operations in Challenging Environments: Earth and Space 20042004. p. 601-8.

[69] Dai J-G, Yokota H, Iwanami M, Kato E. Experimental investigation of the influence of moisture on the bond behavior of FRP to concrete interfaces. Journal of Composites for Construction. 2010;14(6):834-44.

[70] Di Ludovico M, Piscitelli F, Prota A, Lavorgna M, Mensitieri G, Manfredi G. Improved mechanical properties of CFRP laminates at elevated temperatures and freeze–thaw cycling. Construction and Building Materials. 2012;31:273-83.

[71] Sousa J, Correia J, Gonilha J, Cabral-Fonseca S, Firmo J, Keller T. Durability of adhesively bonded joints between pultruded GFRP adherends under hygrothermal and natural ageing. Composites Part B: Engineering. 2019;158:475-88.

[72] Dutta PK, Hui D. Low-temperature and freeze-thaw durability of thick composites. Composites Part B: Engineering. 1996;27(3-4):371-9.

[73] Bazli M, Jafari A, Ashrafi H, Zhao X-L, Bai Y, Raman RS. Effects of UV radiation, moisture and elevated temperature on mechanical properties of GFRP pultruded profiles. Construction and Building Materials. 2020;231:117137.

[74] Alkhader M, Zhai X, Chiang F-P. Experimental investigation of the synergistic effects of moisture and freeze-thaw cycles on carbon fiber vinyl-ester composites. Journal of Composite Materials. 2018;52(7):919-30.

[75] Bank L, Cofie E. A modified beam theory for bending and twisting of open-section composite beams—numerical verification. Composite Structures. 1992;21(1):29-39.

[76] Omidvar B. Shear coefficient in orthotropic thin-walled composite beams. Journal of Composites for Construction. 1998;2(1):46-56.

[77] Yan L, Chouw N, Jayaraman K. Effect of UV and water spraying on the mechanical properties of flax fabric reinforced polymer composites used for civil engineering applications. Materials & Design. 2015;71:17-25.

[78] Ching YC, Gunathilake TU, Ching KY, Chuah CH, Sandu V, Singh R, et al. Effects of high temperature and ultraviolet radiation on polymer composites. Durability and Life Prediction in Biocomposites, Fibre-Reinforced Composites and Hybrid Composites: Elsevier; 2019. p. 407-26.

[79] Han L-H, Zhao X-L, Lu H. Concrete-filled tubular members and connections: CRC Press; 2014.

[80] Wium J, Lebet J-P. Force transfer in composite columns. Composite Construction in Steel and Concrete II: ASCE; 1992. p. 840-53.

[81] Xie T, Ozbakkaloglu T. Behavior of steel fiber-reinforced high-strength concrete-filled FRP tube columns under axial compression. Engineering Structures. 2015;90:158-71.

[82] Xie T, Ozbakkaloglu T. Behavior of recycled aggregate concrete-filled basalt and carbon FRP tubes. Construction and Building Materials. 2016;105:132-43.

[83] Li Y, Teng J, Zhao X, Raman RS. Theoretical model for seawater and sea sand concrete-filled circular FRP tubular stub columns under axial compression. Engineering Structures. 2018;160:71-84.

[84] Wu C, Bai Y, Kwon S. Improved bond behavior between GFRP rebar and concrete using calcium sulfoaluminate. Construction and Building Materials. 2016;113:897-904.
[85] Caro M, Jemaa Y, Dirar S, Quinn A. Bond performance of deep embedment FRP bars epoxy-bonded into concrete. Engineering Structures. 2017;147:448-57.
[86] Veljkovic A, Carvelli V, Haffke MM, Pahn M. Concrete cover effect on the bond of GFRP bar and concrete under static loading. Composites Part B: Engineering. 2017;124:40-53.
[87] Zhao X-L, Bai Y, Al-Mahaidi R, Rizkalla S. Effect of dynamic loading and environmental conditions on the bond between CFRP and steel: state-of-the-art review. Journal of Composites for Construction. 2013;18(3):A4013005.
[88] Bai Y, Nguyen T, Zhao X, Al-Mahaidi R. Environment-assisted degradation of the bond between steel and carbon-fiber-reinforced polymer. Journal of Materials in Civil Engineering. 2013;26(9):04014054.
[89] Bai Y, Nguyen T, Zhao X, Al-Mahaidi R. Enhancement of steel/carbon fibre-reinforced polymer adhesively-bonded joints at elevated temperatures through curing. Australian Journal of Structural Engineering. 2014;15(4):367-76.
[90] Biscaia HC, Chastre C. Theoretical analysis of fracture in double overlap bonded joints with FRP composites and thin steel plates. Engineering Fracture Mechanics. 2018;190:435-60.
[91] Teng J, Yu T, Fernando D. Strengthening of steel structures with fiber-reinforced polymer composites. Journal of Constructional Steel Research. 2012;78:131-43.
[92] Yang Y, Biscaia H, Silva MA, Chastre C. Monotonic and quasi-static cyclic bond response of CFRP-to-steel joints after salt fog exposure. Composites Part B: Engineering. 2019;168:532-49.
[93] Wang H-T, Wu G, Dai Y-T, He X-Y. Determination of the bond–slip behavior of CFRP-to-steel bonded interfaces using digital image correlation. Journal of Reinforced Plastics and Composites. 2016;35(18):1353-67.
[94] Davalos JF, Chen Y, Ray I. Long-term durability prediction models for GFRP bars in concrete environment. Journal of Composite Materials. 2012;46(16):1899-914.
[95] Chen Y, Davalos JF, Ray I, Kim H-Y. Accelerated aging tests for evaluations of durability performance of FRP reinforcing bars for concrete structures. Composite Structures. 2007;78(1):101-11.
[96] Wu G, Dong Z-Q, Wang X, Zhu Y, Wu Z-S. Prediction of long-term performance and durability of BFRP bars under the combined effect of sustained load and corrosive solutions. Journal of Composites for Construction. 2014;19(3):04014058.
[97] Robert M, Benmokrane B. Combined effects of saline solution and moist concrete on long-term durability of GFRP reinforcing bars. Construction and Building Materials. 2013;38:274-84.

[98] Chen Y, Davalos JF, Ray I. Durability prediction for GFRP reinforcing bars using short-term data of accelerated aging tests. Journal of composites for construction. 2006;10(4):279-86.
[99] Wang Z, Zhao X-L, Xian G, Wu G, Raman RS, Al-Saadi S, et al. Long-term durability of basalt-and glass-fibre reinforced polymer (BFRP/GFRP) bars in seawater and sea sand concrete environment. Construction and Building Materials. 2017;139:467-89.
[100] Chen M-c, Wen Q-q, Zhu Q, Huang H, Xie L. Simulation of corrosion process for concrete filled steel tubular columns with the cellular automata method. Engineering Failure Analysis. 2017;82:298-307.
[101] Yan L, Chouw N. Behavior and analytical modeling of natural flax fibre-reinforced polymer tube confined plain concrete and coir fibre-reinforced concrete. Journal of Composite Materials. 2013;47(17):2133-48.
[102] Wang J, Feng P, Hao T, Yue Q. Axial compressive behavior of seawater coral aggregate concrete-filled FRP tubes. Construction and Building Materials. 2017;147:272-85.
[103] Bazli M, Zhao X-L, Bai Y, Raman RS, Al-Saadi S. Bond-slip behaviour between FRP tubes and seawater sea sand concrete. Engineering Structures. 2019;197:109421.
[104] Teng J, Yu T, Dai J, Chen G. FRP composites in new construction: current status and opportunities. Proceedings of 7th National Conference on FRP Composites in Infrastructure (Supplementary Issue of Industrial Construction), keynote presentation, Hangzhou, China2011.
[105] Fang H, Bai Y, Liu W, Qi Y, Wang J. Connections and structural applications of fibre reinforced polymer composites for civil infrastructure in aggressive environments. Composites Part B: Engineering. 2018.
[106] Bazli M, Ashrafi H, Jafari A, Zhao X-L, Raman R, Bai Y. Effect of fibers configuration and thickness on tensile behavior of GFRP laminates exposed to harsh environment. Polymers. 2019;11(9):1401.
[107] Kamal A, Boulfiza M. Durability of GFRP rebars in simulated concrete solutions under accelerated aging conditions. Journal of Composites for Construction. 2010;15(4):473-81.
[108] Wu G, Wang X, Wu Z, Dong Z, Xie Q. Degradation of basalt FRP bars in alkaline environment. Science and Engineering of Composite Materials. 2015;22(6):649-57.
[109] Sawpan MA, Mamun AA, Holdsworth PG. Long term durability of pultruded polymer composite rebar in concrete environment. Materials & Design. 2014;57:616-24.
[110] Masmoudi R, Masmoudi A, Ouezdou MB, Daoud A. Long-term bond performance of GFRP bars in concrete under temperature ranging from 20 C to 80 C. Construction and Building Materials. 2011;25(2):486-93.
[111] Wang Z, Zhao X-L, Xian G, Wu G, Raman RS, Al-Saadi S. Effect of sustained load and seawater and sea sand concrete environment on durability of basalt-and glass-fibre reinforced polymer (B/GFRP) bars. Corrosion Science. 2018.

[112] Robert M, Fam A. Long-term performance of GFRP tubes filled with concrete and subjected to salt solution. Journal of Composites for Construction. 2011;16(2):217-24.

[113] Bazli M, Ashrafi H, Oskouei AV. Effect of harsh environments on mechanical properties of GFRP pultruded profiles. Composites Part B: Engineering. 2016;99:203-15.

[114] Feng P, Wang J, Wang Y, Loughery D, Niu D. Effects of corrosive environments on properties of pultruded GFRP plates. Composites Part B: Engineering. 2014;67:427-33.

[115] Korany Y, Drysdale R. Rehabilitation of masonry walls using unobtrusive FRP techniques for enhanced out-of-plane seismic resistance. Journal of Composites for Construction. 2006;10(3):213-22.

[116] Karbhari VM. Materials considerations in FRP rehabilitation of concrete structures. Journal of materials in civil engineering. 2001;13(2):90-7.

[117] Zhao X-L, Zhang L. State-of-the-art review on FRP strengthened steel structures. Engineering Structures. 2007;29(8):1808-23.

[118] Goldston M, Remennikov A, Sheikh MN. Experimental investigation of the behaviour of concrete beams reinforced with GFRP bars under static and impact loading. Engineering Structures. 2016;113:220-32.

[119] Kodur VKR, Baingo D. Fire resistance of FRP reinforced concrete slabs: Institute for Research in Construction; 1998.

[120] Saafi M. Effect of fire on FRP reinforced concrete members. Composite Structures. 2002;58(1):11-20.

[121] Bai Y, Vallée T, Keller T. Modeling of thermal responses for FRP composites under elevated and high temperatures. Composites Science and Technology. 2008;68(1):47-56.

[122] Tseng H-C, Chang R-Y, Hsu C-H. Numerical prediction of fiber orientation and mechanical performance for short/long glass and carbon fiber-reinforced composites. Composites Science and Technology. 2017;144:51-6.

[123] Wu H-C, Fu G, Gibson RF, Yan A, Warnemuende K, Anumandla V. Durability of FRP composite bridge deck materials under freeze-thaw and low temperature conditions. Journal of bridge engineering. 2006;11(4):443-51.

[124] Ali M, Abdullah S, Nuawi MZ, Ariffin A. Correlation of absorbed impact with calculated strain energy using an instrumented Charpy impact test. 2013.

[125] ASTM D7264 / D7264M-15, Standard Test Method for Flexural Properties of Polymer Matrix Composite Materials, ASTM International, West Conshohocken, PA, 2015.

[126] Sutherland L, Soares CG. Impact on low fibre-volume, glass/polyester rectangular plates. Composite structures. 2005;68(1):13-22.

[127] Mahsuli M, Haukaas T. Computer program for multimodel reliability and optimization analysis. Journal of Computing in Civil Engineering. 2012;27(1):87-98.
[128] Keller T, Bai Y, Vallée T. Long-term performance of a glass fiber-reinforced polymer truss bridge. Journal of Composites for Construction. 2007;11(1):99-108.
[129] Jafari A, Oskouei AV, Bazli M, Ghahri R. Effect of the FRP sheet's arrays and NSM FRP bars on in-plane behavior of URM walls. Journal of Building Engineering. 2018;20:679-95.
[130] Oskouei AV, Kivi MP, Araghi H, Bazli M. Experimental study of the punching behavior of GFRP reinforced lightweight concrete footing. Materials and Structures. 2017;50(6):256.
[131] Khaneghahi MH, Najafabadi EP, Shoaei P, Oskouei AV. Effect of intumescent paint coating on mechanical properties of FRP bars at elevated temperature. Polymer Testing. 2018;71:72-86.
[132] Keller T, Theodorou NA, Vassilopoulos AP, De Castro J. Effect of Natural Weathering on Durability of Pultruded Glass Fiber–Reinforced Bridge and Building Structures. Journal of Composites for Construction. 2015;20(1):04015025.
[133] Frigione M, Lettieri M. Durability issues and challenges for material advancements in FRP employed in the construction industry. Polymers. 2018;10(3):247.
[134] Ma G, Yan L, Shen W, Zhu D, Huang L, Kasal B. Effects of water, alkali solution and temperature ageing on water absorption, morphology and mechanical properties of natural FRP composites: plant-based jute vs. mineral-based basalt. Composites Part B: Engineering. 2018;153:398-412.
[135] Nishizaki I, Sakuraba H, Tomiyama T. Durability of pultruded gfrp through ten-year outdoor exposure test. Polymers. 2015;7(12):2494-503.
[136] Wang X, Jiang L, Shen H, Wu Z. Long-Term Performance of Pultruded Basalt Fiber Reinforced Polymer Profiles under Acidic Conditions. Journal of Materials in Civil Engineering. 2018;30(6):04018096.
[137] Dong Z-Q, Wu G, Zhao X-L, Lian J-L. Long-Term Bond Durability of Fiber-Reinforced Polymer Bars Embedded in Seawater Sea-Sand Concrete under Ocean Environments. Journal of Composites for Construction. 2018;22(5):04018042.
[138] Guo F, Al-Saadi S, Raman RS, Zhao X. Durability of Fiber Reinforced Polymer (FRP) in Simulated Seawater Sea Sand Concrete (SWSSC) Environment. Corrosion Science. 2018.
[139] Yan L, Chouw N. Effect of water, seawater and alkaline solution ageing on mechanical properties of flax fabric/epoxy composites used for civil engineering applications. Construction and Building Materials. 2015;99:118-27.
[140] Oskouei AV, Bazli M, Ashrafi H, Imani M. Flexural and web crippling properties of GFRP pultruded profiles subjected to wetting and drying cycles in different sea water conditions. Polymer Testing. 2018.

[141] Fang Y, Wang K, Hui D, Xu F, Liu W, Yang S, et al. Monitoring of seawater immersion degradation in glass fibre reinforced polymer composites using quantum dots. Composites Part B: Engineering. 2017;112:93-102.

[142] Nguyen T-C, Bai Y, Zhao X-L, Al-Mahaidi R. Durability of steel/CFRP double strap joints exposed to sea water, cyclic temperature and humidity. Composite Structures. 2012;94(5):1834-45.

[143] Lu Z, Xie J, Zhang H, Li J. Long-term durability of basalt fiber-reinforced polymer (BFRP) sheets and the epoxy resin matrix under a wet–dry cyclic condition in a chloride-containing environment. Polymers. 2017;9(12):652.

[144] Xin H, Mosallam A, Liu Y, Wang C, Zhang Y. Impact of hygrothermal aging on rotational behavior of web-flange junctions of structural pultruded composite members for bridge applications. Composites Part B: Engineering. 2017;110:279-97.

[145] Xin H, Mosallam A, Liu Y, Yang F, Zhang Y. Hygrothermal aging effects on shear behavior of pultruded FRP composite web-flange junctions in bridge application. Composites Part B: Engineering. 2017;110:213-28.

[146] Wang Z, Xian G, Zhao X-L. Effects of hydrothermal aging on carbon fibre/epoxy composites with different interfacial bonding strength. Construction and Building Materials. 2018;161:634-48.

[147] Hong B, Xian G, Li H. Comparative study of the durability behaviors of epoxy-and polyurethane-based CFRP plates subjected to the combined effects of sustained bending and water/seawater immersion. Polymers. 2017;9(11):603.

[148] Sergi C, Tirillò J, Seghini MC, Sarasini F, Fiore V, Scalici T. Durability of Basalt/Hemp Hybrid Thermoplastic Composites. Polymers. 2019;11(4):603.

[149] Tann D, Delpak R. Influences of freeze and thaw cycles and elevated temperature on the properties of FRP composites. Advanced polymer composites for structural applications in construction: Elsevier; 2004. p. 611-8.

[150] Sheikh SA, Tam S. Effect of Freeze-Thaw Climactic Conditions on Long-Term Durability of FRP Strengthening System. 2007.

[151] Sousa JM, Correia JR, Cabral-Fonseca S, Diogo AC. Effects of thermal cycles on the mechanical response of pultruded GFRP profiles used in civil engineering applications. Composite Structures. 2014;116:720-31.

[152] Nguyen T-C, Bai Y, Zhao X-L, Al-Mahaidi R. Effects of ultraviolet radiation and associated elevated temperature on mechanical performance of steel/CFRP double strap joints. Composite Structures. 2012;94(12):3563-73.

[153] Zhao J, Cai G, Cui L, Si Larbi A, Daniel Tsavdaridis K. Deterioration of basic properties of the materials in FRP-strengthening RC structures under ultraviolet exposure. Polymers. 2017;9(9):402.

[154] Grammatikos SA, Jones RG, Evernden M, Correia JR. Thermal cycling effects on the durability of a pultruded GFRP material for off-shore civil engineering structures. Composite Structures. 2016;153:297-310.
[155] Bank LC, Gentry TR, Barkatt A. Accelerated test methods to determine the long-term behavior of FRP composite structures: environmental effects. Journal of Reinforced Plastics and Composites. 1995;14(6):559-87.
[156] Bai Y, Keller T. Modeling of strength degradation for fiber-reinforced polymer composites in fire. Journal of Composite Materials. 2009;43(21):2371-85.
[157] Yu B, Till V, Thomas K. Modeling of thermo-physical properties for FRP composites under elevated and high temperature. Composites Science and Technology. 2007;67(15-16):3098-109.
[158] Bai Y, Keller T, Vallée T. Modeling of stiffness of FRP composites under elevated and high temperatures. Composites Science and Technology. 2008;68(15-16):3099-106.
[159] Karbhari V, Chin J, Hunston D, Benmokrane B, Juska T, Morgan R, et al. Durability gap analysis for fiber-reinforced polymer composites in civil infrastructure. Journal of composites for construction. 2003;7(3):238-47.
[160] Karbhari V, Rivera J, Zhang J. Low-temperature hygrothermal degradation of ambient cured E-glass/vinylester composites. Journal of applied polymer science. 2002;86(9):2255-60.
[161] Karbhari V, Rivera J, Dutta P. Effect of short-term freeze-thaw cyclingon composite confined concrete. Journal of composites for construction. 2000;4(4):191-7.
[162] Jafari A, Bazli M, Ashrafi H, Oskouei AV, Azhari S, Zhao X-L, et al. Effect of fibers configuration and thickness on tensile behavior of GFRP laminates subjected to elevated temperatures. Construction and Building Materials. 2019;202:189-207.
[163] EN 1504-4. Products and systems for the protection and repair of concrete structures. Definitions, requirements, quality control and evaluation of conformity – Part 4: structural bonding. Brussels: European Committee for Standardization; 2006.
[164] ASTM D6944-15, Standard Practice for Determining the Resistance of Cured Coatings to Thermal Cycling, ASTM International, West Conshohocken, PA, 2015, www.astm.org
[165] da Silva LV, da Silva FW, Tarpani JR, de Camargo Forte MM, Amico SC. Ageing effect on the tensile behavior of pultruded CFRP rods. Materials & Design. 2016;110:245-54.
[166] Ji Y, Kim YJ. Effects of sulfuric acid on durability characteristics of CFRP composite sheets. Journal of Materials in Civil Engineering. 2017;29(10):04017159.
[167] Li H, Xian G, Lin Q, Zhang H. Freeze–thaw resistance of unidirectional-fiber-reinforced epoxy composites. Journal of Applied Polymer Science. 2012;123(6):3781-8.

[168] Carra G, Carvelli V. Ageing of pultruded glass fibre reinforced polymer composites exposed to combined environmental agents. Composite Structures. 2014;108:1019-26.

[169] Sousa JM, Correia JR, Cabral-Fonseca S. Durability of glass fibre reinforced polymer pultruded profiles: comparison between QUV accelerated exposure and natural weathering in a Mediterranean climate. Experimental Techniques. 2016;40(1):207-19.

[170] Aliasghar-Mamaghani M, Khaloo A. Seismic behavior of concrete moment frame reinforced with GFRP bars. Composites Part B: Engineering. 2019;163:324-38.

[171] Bai Y, Post NL, Lesko JJ, Keller T. Experimental investigations on temperature-dependent thermo-physical and mechanical properties of pultruded GFRP composites. Thermochimica Acta. 2008;469(1-2):28-35.

[172] Bai Y, Keller T. Delamination and kink-band failure of pultruded GFRP laminates under elevated temperatures and compression. Composite structures. 2011;93(2):843-9.

[173] Hawileh RA, Naser M, Zaidan W, Rasheed H. Modeling of insulated CFRP-strengthened reinforced concrete T-beam exposed to fire. Engineering Structures. 2009;31(12):3072-9.

[174] Hawileh RA, Abdalla JA, Hasan SS, Ziyada MB, Abu-Obeidah A. Models for predicting elastic modulus and tensile strength of carbon, basalt and hybrid carbon-basalt FRP laminates at elevated temperatures. Construction and Building Materials. 2016;114:364-73.

[175] Bogner B, Borja P. Ultra-violet light resistance of pultruded composites. Composites(France). 1994;34(4):27-30.

[176] Segovia F, Ferrer C, Salvador MD, Amigo V. Influence of processing variables on mechanical characteristics of sunlight aged polyester–glass fibre composites. Polymer degradation and stability. 2000;71(1):179-84.

[177] Najafabadi EP, Khaneghahi MH, Amiri HA, Estekanchi HE, Ozbakkaloglu T. Experimental investigation and probabilistic models for residual mechanical properties of GFRP pultruded profiles exposed to elevated temperatures. Composite Structures. 2019;211:610-29.

[178] Jarrah M, Najafabadi EP, Khaneghahi MH, Oskouei AV. The effect of elevated temperatures on the tensile performance of GFRP and CFRP sheets. Construction and Building Materials. 2018;190:38-52.

[179] Li C, Xian G, Li H. Combined effects of temperature, hydraulic pressure and salty concentration on the water uptake and mechanical properties of a carbon/glass fibers hybrid rod in salty solutions. Polymer Testing. 2019;76:19-32.

[180] Mahato KK, Dutta K, Ray BC. Static and dynamic behavior of fibrous polymeric composite materials at different environmental conditions. Journal of Polymers and the Environment. 2018;26(3):1024-50.

[181] Correia J, Cabral-Fonseca S, Branco F, Ferreira J, Eusébio M, Rodrigues M. Durability of pultruded glass-fiber-reinforced polyester profiles for structural applications. Mechanics of Composite Materials. 2006;42(4):325-38.
[182] Böer P, Holliday L, Kang TH-K. Independent environmental effects on durability of fiber-reinforced polymer wraps in civil applications: a review. Construction and Building Materials. 2013;48:360-70.
[183] Oskouei AV, Bazli M, Ashrafi H, Imani M. Flexural and web crippling properties of GFRP pultruded profiles subjected to wetting and drying cycles in different sea water conditions. Polymer Testing. 2018;69:417-30.
[184] Jacques L. Accelerated and outdoor/natural exposure testing of coatings. Progress in polymer science. 2000;25(9):1337-62.
[185] Bai Y, Keller T. Modeling of mechanical response of FRP composites in fire. Composites Part A: Applied Science and Manufacturing. 2009;40(6-7):731-8.
[186] Del Prete I, Bilotta A, Nigro E. Performances at high temperature of RC bridge decks strengthened with EBR-FRP. Composites Part B: Engineering. 2015;68:27-37.
[187] Correia JR, Bai Y, Keller T. A review of the fire behaviour of pultruded GFRP structural profiles for civil engineering applications. Composite Structures. 2015;127:267-87.
[188] Marouani S, Curtil L, Hamelin P. Ageing of carbon/epoxy and carbon/vinylester composites used in the reinforcement and/or the repair of civil engineering structures. Composites Part B: Engineering. 2012;43(4):2020-30.
[189] Sadler PA, Burn S. Ultraviolet radiation correlation for accelerated and natural weathering. 2005.
[190] ASTM D790-17, Standard Test Methods for Flexural Properties of Unreinforced and Reinforced Plastics and Electrical Insulating Materials, ASTM International, West Conshohocken, PA, 2017.
[191] Zhou J, Lucas JP. Hygrothermal effects of epoxy resin. Part II: variations of glass transition temperature. Polymer. 1999;40(20):5513-22.
[192] Papanicolaou G, Kosmidou TV, Vatalis A, Delides C. Water absorption mechanism and some anomalous effects on the mechanical and viscoelastic behavior of an epoxy system. Journal of Applied Polymer Science. 2006;99(4):1328-39.
[193] Aghababaei M, Mahsuli M. Detailed seismic risk analysis of buildings using structural reliability methods. Probabilistic Engineering Mechanics. 2018;53:23-38.
[194] Azwa Z, Yousif B, Manalo A, Karunasena W. A review on the degradability of polymeric composites based on natural fibres. Materials & Design. 2013;47:424-42.

[195] Hou J, Nie X, Zhang L, Huang Y, Bai Y. Ultimate limit design of composite beams with modular GFRP deck and steel girder. Engineering Structures. 2018;176:337-48.

[196] Chen J, Chouw N. Effect of the interface condition on the bond between flax FRP tube and coconut fibre reinforced concrete composites. Construction and Building Materials. 2018;167:597-604.

[197] Ferdous W, Almutairi AD, Huang Y, Bai Y. Short-term flexural behaviour of concrete filled pultruded GFRP cellular and tubular sections with pin-eye connections for modular retaining wall construction. Composite Structures. 2018;206:1-10.

[198] Acciai A, D'Ambrisi A, De Stefano M, Feo L, Focacci F, Nudo R. Experimental response of FRP reinforced members without transverse reinforcement: failure modes and design issues. Composites Part B: Engineering. 2016;89:397-407.

[199] Li Y, Zhao X, Raman RS. Load-strain model for concrete-filled double-skin circular FRP tubes under axial compression. Engineering Structures. 2019;181:629-42.

[200] Li Y, Zhao X, Raman RS. Mechanical properties of seawater and sea sand concrete-filled FRP tubes in artificial seawater. Construction and Building Materials. 2018;191:977-93.

[201] Yuan JS, Hadi MN. Friction coefficient between FRP pultruded profiles and concrete. Materials and Structures. 2018;51(5):120.

[202] Smith ST, Teng J. FRP-strengthened RC beams. I: review of debonding strength models. Engineering structures. 2002;24(4):385-95.

[203] Biscaia HC, Chastre C, Silva MA. Bond-slip model for FRP-to-concrete bonded joints under external compression. Composites Part B: Engineering. 2015;80:246-59.

[204] Cosenza E, Manfredi G, Realfonzo R. Behavior and modeling of bond of FRP rebars to concrete. Journal of composites for construction. 1997;1(2):40-51.

[205] Achillides Z, Pilakoutas K. Bond behavior of fiber reinforced polymer bars under direct pullout conditions. Journal of Composites for construction. 2004;8(2):173-81.

[206] Yuan JS, Hadi MN. Bond-slip behaviour between GFRP I-section and concrete. Composites Part B: Engineering. 2017;130:76-89.

[207] Li G, Torres S, Alaywan W, Abadie C. Experimental study of FRP tube-encased concrete columns. Journal of composite materials. 2005;39(13):1131-45.

[208] Li Y, Zhao X, Singh RR, Al-Saadi S. Tests on seawater and sea sand concrete-filled CFRP, BFRP and stainless steel tubular stub columns. Thin-Walled Structures. 2016;108:163-84.

[209] Yu B, Kodur V. Effect of temperature on strength and stiffness properties of near-surface mounted FRP reinforcement. Composites Part B: Engineering. 2014;58:510-7.

[210] Feng R, Chen Y, He K, Wei J, Chen B, Zhang X. Push-out tests of concrete-filled stainless steel SHS tubes. Journal of Constructional Steel Research. 2018;145:58-69.

[211] Ji G, Ouyang Z, Li G. Experimental investigation into the interfacial shear strength of AGS-FRP tube confined concrete pile. Engineering structures. 2009;31(10):2309-16.

[212] Yan L, Chouw N, Kasal B. Experimental study and numerical simulation on bond between FFRP and CFRC components. Journal of Reinforced Plastics and Composites. 2017;36(4):305-20.

[213] Aghababaei M, Mahsuli M. Component damage models for detailed seismic risk analysis using structural reliability methods. Structural Safety. 2019;76:108-22.

[214] Zhang Q, Xiao J, Zhang P, Zhang K. Mechanical behaviour of seawater sea-sand recycled coarse aggregate concrete columns under axial compressive loading. Construction and Building Materials. 2019;229:117050.

[215] Xiao J, Zhang Q, Zhang P, Shen L, Qiang C. Mechanical behavior of concrete using seawater and sea-sand with recycled coarse aggregates. Structural Concrete. 2019;20(5):1631-43.

[216] Kaushik S, Islam S. Suitability of sea water for mixing structural concrete exposed to a marine environment. Cement and Concrete Composites. 1995;17(3):177-85.

[217] Zhang Q, Xiao J, Liao Q, Duan Z. Structural behavior of seawater sea-sand concrete shear wall reinforced with GFRP bars. Engineering Structures. 2019;189:458-70.

[218] Ashrafi H, Bazli M, Jafari A, Ozbakkaloglu T. Tensile properties of GFRP laminates after exposure to elevated temperatures: Effect of fiber configuration, sample thickness, and time of exposure. Composite Structures. 2020;238:111971.

[219] Bai Y, Nguyen TC, Zhao XL, Al-Mahaidi R. Environment-assisted degradation of the bond between steel and carbon-fiber-reinforced polymer. Journal of Materials in Civil Engineering. 2013;26(9):04014054.

[220] Khaneghahi MH, Najafabadi EP, Bazli M, Oskouei AV, Zhao X-L. The effect of elevated temperatures on the compressive section capacity of pultruded GFRP profiles. Construction and Building Materials. 2020;249:118725.

[221] Fam A, Greene R, Rizkalla S. Field applications of concrete-filled FRP tubes for marine piles. Special Publication. 2003;215:161-80.

[222] Mirmiran A. Stay-in-place FRP form for concrete columns. Advances in Structural Engineering. 2003;6(3):231-41.

[223] Dong Z, Wu G, Xu B, Wang X, Taerwe L. Bond durability of BFRP bars embedded in concrete under seawater conditions and the long-term bond strength prediction. Materials & Design. 2016;92:552-62.

[224] Altalmas A, El Refai A, Abed F. Bond degradation of basalt fiber-reinforced polymer (BFRP) bars exposed to accelerated aging conditions. Construction and Building Materials. 2015;81:162-71.

[225] Fam A, Schnerch D, Rizkalla S. Rectangular filament-wound glass fiber reinforced polymer tubes filled with concrete under flexural and axial loading: experimental investigation. Journal of Composites for Construction. 2005;9(1):25-33.

[226] Lutz LA, Gergely P. Mechanics of bond and slip of deformed bars in concrete. Journal Proceedings1967. p. 711-21.

[227] Tao Z, Han L-H, Uy B, Chen X. Post-fire bond between the steel tube and concrete in concrete-filled steel tubular columns. Journal of Constructional Steel Research. 2011;67(3):484-96.

[228] Lin Y-W, Biggs D, Wotherspoon L, Ingham JM. In-plane strengthening of unreinforced concrete masonry wallettes using ECC shotcrete. Journal of Structural Engineering. 2014;140(11):04014081.

[229] Jianzhuang Xiao, Qingxiang Liao, Qingtian Zhang, Chengbing Qiang, Xian Liu. Bond behavior between seawater sea-sand recycled aggregate concrete and glass-fiber-reinforced polymer bars. Tongji Daxue Xuebao/Journal of Tongji University, 2018, 46(7): 884-890+971. (in Chinese).

[230] Bazli M, Zhao X-L, Bai Y, Raman RS, Al-Saadi S, Haque A. Durability of pultruded GFRP tubes subjected to seawater sea sand concrete and seawater environments. Construction and Building Materials. 2020;245:118399.

[231] Biscaia HC, Chastre C, Silva MA. Double shear tests to evaluate the bond strength between GFRP/concrete elements. Composite Structures. 2012;94(2):681-94.

[232] Biscaia H. Debonding between external GFRP reinforcement and concrete structural elements: MSc Thesis, Instituto Superior Técnico, Universidade Técnica de Lisboa; 2006.

[233] Zafar A, Bertocco F, Schjødt-Thomsen J, Rauhe J. Investigation of the long term effects of moisture on carbon fibre and epoxy matrix composites. Composites Science and Technology. 2012;72(6):656-66.

[234] Chen Y, Feng R, Shao Y, Zhang X. Bond-slip behaviour of concrete-filled stainless steel circular hollow section tubes. Journal of Constructional Steel Research. 2017;130:248-63.

[235] Choi S, Gartner AL, Etten NV, Hamilton H, Douglas EP. Durability of concrete beams externally reinforced with CFRP composites exposed to various environments. Journal of Composites for Construction. 2011;16(1):10-20.

[236] Teng J, Yu T, Dai J, Chen G. FRP composites in new construction: current status and opportunities. Proceedings of the 7th national conference on FRP composition in infrastructure (Supplementary issue of industrial construction)(Abstract), Hangzhou, China2011.

[237] Katano K, Takeda N, Ishizeki Y, Iriya K. Properties and application of concrete made with sea water and un-washed sea sand. Proceedings of Third International conference on Sustainable Construction Materials and Technologies2013.

[238] Berke N, Bentur A, Diamond S. Steel corrosion in concrete: fundamentals and civil engineering practice: CRC Press; 2014.

[239] Boumarafi A, Abouzied A, Masmoudi R. Harsh environments effects on the axial behaviour of circular concrete-filled fibre reinforced-polymer (FRP) tubes. Composites Part B: Engineering. 2015;83:81-7.

[240] Han L-H, Hou C, Wang Q-L. Square concrete filled steel tubular (CFST) members under loading and chloride corrosion: Experiments. Journal of Constructional Steel Research. 2012;71:11-25.

[241] Hou C-C, Han L-H, Wang Q-L, Hou C. Flexural behavior of circular concrete filled steel tubes (CFST) under sustained load and chloride corrosion. Thin-Walled Structures. 2016;107:182-96.

[242] Han L-H, Hua Y-X, Hou C, Wang Q-L. Circular Concrete-Filled Steel Tubes Subjected to Coupled Tension and Chloride Corrosion. Journal of Structural Engineering. 2017;143(10):04017134.

[243] Ozbakkaloglu T, Xie T. Geopolymer concrete-filled FRP tubes: Behavior of circular and square columns under axial compression. Composites Part B: Engineering. 2016;96:215-30.

[244] Ozbakkaloglu T, Saatcioglu M. Displacement-based model to predict lateral drift capacities of concrete-filled FRP tube columns. Engineering Structures. 2017;147:345-55.

[245] Pando M, Lesko J, Fam A, Rizkalla S. Durability of concrete-filled tubular FRP piles. The 3rd Int Conf on Composites in Infrastructure, ICCI2002. p. 10-2.

[246] Micelli F, Myers J. Durability of FRP-confined concrete. Proceedings of the Institution of Civil Engineers-Construction Materials. 2008;161(4):173-85.

[247] Yang X, Bai Y, Ding F. Structural performance of a large-scale space frame assembled using pultruded GFRP composites. Composite Structures. 2015;133:986-96.

[248] Guo F, Al-Saadi S, Singh R, Zhao X. Durability of Carbon Fiber Reinforced Polymer (Cfrp) With Combined Use Of Seawater Sea Sand Concrete (SWSSC). Proceedings of the Sixth Asia-Pacific Conference on FRP in Structures (APFIS 2017), Singapore2017. p. 19-21.

[249] Guo F, Al-Saadi S, Raman RS, Zhao X. Durability of fiber reinforced polymer (FRP) in simulated seawater sea sand concrete (SWSSC) environment. Corrosion Science. 2018;141:1-13.

[250] Kajorncheappunngam S, Gupta RK, GangaRao HV. Effect of aging environment on degradation of glass-reinforced epoxy. Journal of composites for construction. 2002;6(1):61-9.

[251] Purnell P, Beddows J. Durability and simulated ageing of new matrix glass fibre reinforced concrete. Cement and Concrete Composites. 2005;27(9-10):875-84.

[252] John MJ, Francis B, Varughese K, Thomas S. Effect of chemical modification on properties of hybrid fiber biocomposites. Composites Part A: Applied Science and Manufacturing. 2008;39(2):352-63.
[253] Hoyos CG, Vázquez A. Flexural properties loss of unidirectional epoxy/fique composites immersed in water and alkaline medium for construction application. Composites Part B: Engineering. 2012;43(8):3120-30.
[254] Barjasteh E, Nutt S. Moisture absorption of unidirectional hybrid composites. Composites Part A: Applied Science and Manufacturing. 2012;43(1):158-64.
[255] Blackburn BP, Tatar J, Douglas EP, Hamilton H. Effects of hygrothermal conditioning on epoxy adhesives used in FRP composites. Construction and building materials. 2015;96:679-89.
[256] Wu G, Wang X, Wu Z, Dong Z, Zhang G. Durability of basalt fibers and composites in corrosive environments. Journal of Composite Materials. 2015;49(7):873-87.
[257] Wu P, Xu L, Luo J, Zhang X, Bian W. Influences of long-term immersion of water and alkaline solution on the fatigue performances of unidirectional pultruded CFRP plate. Construction and Building Materials. 2019;205:344-56.
[258] Liao K, Schultheisz C, Hunston DL. Effects of environmental aging on the properties of pultruded GFRP. Composites Part B: Engineering. 1999;30(5):485-93.
[259] Riebel F, Keller T. Long-term compression performance of a pultruded GFRP element exposed to concrete pore water solution. Journal of Composites for Construction. 2007;11(4):437-47.
[260] Nelson WB. Accelerated testing: statistical models, test plans, and data analysis: John Wiley & Sons; 2009.
[261] Bazli M, Zhao X-L, Jafari A, Ashrafi H, Raman RS, Bai Y, et al. Durability of glass-fibre-reinforced polymer composites under seawater and sea-sand concrete coupled with harsh outdoor environments. Advances in Structural Engineering. 2020:1369433220947897.
[262] Bazli M, Zhao X-L, Jafari A, Ashrafi H, Bai Y, Raman RS, et al. Mechanical properties of pultruded GFRP profiles under seawater sea sand concrete environment coupled with UV radiation and moisture. Construction and Building Materials. 2020:120369.
[263] Bazli M, Zhao X-L, Raman RS, Bai Y, Al-Saadi S. Bond performance between FRP tubes and seawater sea sand concrete after exposure to seawater condition. Construction and Building Materials. 2020;265:120342.
[264] Ali AH, Mohamed HM, Benmokrane B, ElSafty A, Chaallal O. Durability performance and long-term prediction models of sand-coated basalt FRP bars. Composites Part B: Engineering. 2019;157:248-58.
[265] Ali AH, Mohamed HM, Benmokrane B. Bar size effect on long-term durability of sand-coated basalt-FRP composite bars. Composites Part B: Engineering. 2020:108059.

[266] Miyano Y, Nakada M. Accelerated testing methodology for durability of CFRP. Composites Part B: Engineering. 2020:107977.

[267] Lau D, Qiu Q, Zhou A, Chow CL. Long term performance and fire safety aspect of FRP composites used in building structures. Construction and building materials. 2016;126:573-85.

[268] Fang H, Bai Y, Liu W, Qi Y, Wang J. Connections and structural applications of fibre reinforced polymer composites for civil infrastructure in aggressive environments. Composites Part B: Engineering. 2019;164:129-43.

[269] Liu T, Liu X, Feng P. A comprehensive review on mechanical properties of pultruded FRP composites subjected to long-term environmental effects. Composites Part B: Engineering. 2020:107958.

[270] Bai Y, Nguyen TC, Zhao XL, Al-Mahaidi R. Environment-assisted degradation of the bond between steel and carbon-fiber-reinforced polymer. Journal of materials in civil engineering. 2014;26(9):04014054.

[271] Zhao X-L, Bai Y, Al-Mahaidi R, Rizkalla S. Effect of dynamic loading and environmental conditions on the bond between CFRP and steel: state-of-the-art review. Journal of Composites for Construction. 2014;18(3):A4013005.

[272] Li YL, Zhao XL, Raman Singh RK, Al-Saadi S. Experimental study on seawater and sea sand concrete filled GFRP and stainless steel tubular stub columns. Thin-Walled Structures. 2016;106:390-406.

[273] Chen GM, He ZB, Jiang T, Chen JF, Teng JG. Axial compression tests on FRP-confined seawater/sea-sand concrete. In: Proceedings of 6th Asia-Pacific Conference on FRP in Structures. Conference, Conference 2017.

[274] Li YL, Teng JG, Zhao XL, Singh Raman RK. Theoretical model for seawater and sea sand concrete-filled circular FRP tubular stub columns under axial compression. Engineering Structures. 2018;160:71-84.

[275] Robert M, Fam A. Long-term performance of GFRP tubes filled with concrete and subjected to salt solution. Journal of Composites for Construction. 2012;16(2):217-24.

[276] Robert M, Wang P, Cousin P, Benmokrane B. Temperature as an accelerating factor for long-term durability testing of FRPs: Should there be any limitations? Journal of Composites for Construction. 2010;14(4):361-7.

[277] ASTM D2990-17, Standard Test Methods for Tensile, Compressive, and Flexural Creep and Creep-Rupture of Plastics , ASTM International, West Conshohocken, PA, 2017.

[278] Lipatov YV, Gutnikov S, Manylov M, Zhukovskaya E, Lazoryak B. High alkali-resistant basalt fiber for reinforcing concrete. Materials & Design. 2015;73:60-6.

[279] Scheffler C, Förster T, Mäder E, Heinrich G, Hempel S, Mechtcherine V. Aging of alkali-resistant glass and basalt fibers in alkaline solutions: Evaluation of the failure stress by Weibull distribution function. Journal of Non-Crystalline Solids. 2009;355(52-54):2588-95.

[280] Rybin V, Utkin A, Baklanova N. Alkali resistance, microstructural and mechanical performance of zirconia-coated basalt fibers. Cement and Concrete Research. 2013;53:1-8.

[281] Rybin V, Utkin A, Baklanova N. Corrosion of uncoated and oxide-coated basalt fibre in different alkaline media. Corrosion Science. 2016;102:503-9.

[282] Bethencourt M, Botana F, Cano M, Marcos M, Sánchez-Amaya J, González-Rovira L. Behaviour of the alloy AA2017 in aqueous solutions of NaCl. Part I: Corrosion mechanisms. Corrosion Science. 2009;51(3):518-24.

[283] Sherif E-SM. Corrosion and corrosion inhibition of aluminum in Arabian Gulf seawater and sodium chloride solutions by 3-amino-5-mercapto-1, 2, 4-triazole. Int J Electrochem Sci. 2011;6(5):1479-92.

[284] Stumm W, Lee GF. Oxygenation of ferrous iron. Industrial & Engineering Chemistry. 1961;53(2):143-6.

[285] Lemire RJ, Berner U, Musikas C, Palmer DA, Taylor P, Tochiyama O, et al. Chemical thermodynamics of iron-Part 1-Chemical thermodynamics volume 13a. Data Bank; 2013.

[286] Strahm U, Patel RC, Matijevic E. Thermodynamics and kinetics of aqueous iron (III) chloride complexes formation. Journal of Physical Chemistry. 1979;83(13):1689-95.

[287] Kumar T, Verma K. A Theory Based on Conversion of RGB image to Gray image. International Journal of Computer Applications. 2010;7(2):7-10.

[288] ASTMD2290-16. Standard Test Method for Apparent Hoop Tensile Strength of Plastic or Reinforced Plastic Pipe. 2016.

[289] Wang Z, Zhao X-L, Xian G, Wu G, Singh Raman RK, Al-Saadi S. Durability study on interlaminar shear behaviour of basalt-, glass- and carbon-fibre reinforced polymer (B/G/CFRP) bars in sea water sea sand concrete environment. Construction & Building Materials. 2017;156:985-1004.

[290] Limeira J, Agulló L, Etxeberria M. Dredged marine sand as a new source for construction materials. Materiales de Construcción. 2012;62(305):7-24.

[291] Peduzzi P. Sand, rarer than one thinks. Environmental Development. 2014;11:208-18.

[292] Bazli M, Zhao XL, Raman RS, Bai Y, Al-Saadi S. Bond strength durability between FRP tubes and seawater sea sand concrete under sea water condition. Asia-Pacific Conference on FRP in Structures 2019: APFIS Conference Series; 2019.

[293] Dong Z, Wu G, Zhao X-L, Zhu H, Wei Y, Yan Z. Mechanical properties of discrete BFRP needles reinforced seawater sea-sand concrete-filled GFRP tubular stub columns. Construction and Building Materials. 2020;244:118330.

[294] Li Y-L, Zhao X-L. Hybrid double tube sections utilising seawater and sea sand concrete, FRP and stainless steel. Thin-Walled Structures. 2020;149:106643.

[295] Zeng J-J, Gao W-Y, Duan Z-J, Bai Y-L, Guo Y-C, Ouyang L-J. Axial compressive behavior of polyethylene terephthalate/carbon FRP-confined seawater sea-sand concrete in circular columns. Construction and Building Materials. 2020;234:117383.

[296] Khezrzadeh H. A statistical micromechanical multiscale method for determination of the mechanical properties of composites with periodic microstructure. Composites Part B: Engineering. 2017;115:138-43.

[297] Khezrzadeh H. Overall properties of particulate composites with fractal distribution of fibers. Mechanics of Materials. 2016;96:1-11.

[298] Ashrafi H, Bazli M, Jafari A, Ozbakkaloglu T. Tensile properties of GFRP laminates after exposure to elevated temperatures: Effect of fiber configuration, sample thickness, and time of exposure. Composite Structures. 2020:111971.

[299] Dong Z, Wu G, Zhao X-L, Zhu H, Lian J-L. The durability of seawater sea-sand concrete beams reinforced with metal bars or non-metal bars in the ocean environment. Advances in Structural Engineering. 2019:1369433219870580.

[300] Dong Z, Wu G, Zhao X-L, Zhu H, Lian J. Bond durability of steel-FRP composite bars embedded in seawater sea-sand concrete under constant bending and shearing stress. Construction and Building Materials. 2018;192:808-17.

[301] Dong Z, Wu G, Zhao X-L, Zhu H, Lian J-L. Durability test on the flexural performance of seawater sea-sand concrete beams completely reinforced with FRP bars. Construction and Building Materials. 2018;192:671-82.

[302] Bai Y, Keller T, Wu C. Pre-buckling and post-buckling failure at web-flange junction of pultruded GFRP beams. Materials and structures. 2013;46(7):1143-54.

[303] ASTM D3039 / D3039M-17, Standard Test Method for Tensile Properties of Polymer Matrix Composite Materials, ASTM International, West Conshohocken, PA, 2017.

[304] Wu C, Zhang L-T, Bai Y, Zhao X-L. Web crippling behavior of pultruded GFRP channel sections under transverse bearing load. Composite Structures. 2019;209:129-42.

[305] Fernandes LA, Gonilha J, Correia JR, Silvestre N, Nunes F. Web-crippling of GFRP pultruded profiles. Part 1: Experimental study. Composite Structures. 2015;120:565-77.

[306] Karbhari VM. Durability of FRP composites for civil infrastructure—myth, mystery or reality. Advances in Structural Engineering. 2003;6(3):243-55.
[307] Jiang X, Kolstein H, Bijlaard F, Qiang X. Effects of hygrothermal aging on glass-fibre reinforced polymer laminates and adhesive of FRP composite bridge: Moisture diffusion characteristics. Composites Part A: Applied Science and Manufacturing. 2014;57:49-58.
[308] Hong B, Xian G, Wang Z. Durability study of pultruded carbon fiber reinforced polymer plates subjected to water immersion. Advances in Structural Engineering. 2018;21(4):571-9.
[309] Ashrafi H, Bazli M, Vatani Oskouei A, Bazli L. Effect of sequential exposure to UV radiation and water vapor condensation and extreme temperatures on the mechanical properties of GFRP bars. Journal of Composites for Construction. 2018;22(1):04017047.
[310] Galgano A, Di Blasi C, Branca C, Milella E. Thermal response to fire of a fibre-reinforced sandwich panel: Model formulation, selection of intrinsic properties and experimental validation. Polymer degradation and stability. 2009;94(8):1267-80.
[311] Khotbehsara MM, Manalo A, Aravinthan T, Reddy KR, Ferdous W, Wong H, et al. Effect of elevated in-service temperature on the mechanical properties and microstructure of particulate-filled epoxy polymers. Polymer Degradation and Stability. 2019;170:108994.
[312] Grammatikos S, Zafari B, Evernden M, Mottram J, Mitchels J. Moisture uptake characteristics of a pultruded fibre reinforced polymer flat sheet subjected to hot/wet aging. Polymer Degradation and Stability. 2015;121:407-19.
[313] Alzeebaree R, Çevik A, Mohammedameen A, Niş A, Gülşan ME. Mechanical performance of FRP-confined geopolymer concrete under seawater attack. Advances in Structural Engineering. 2019:1369433219886964.
[314] Johar M, Chong W, Kang H, Wong K. Effects of moisture absorption on the different modes of carbon/epoxy composites delamination. Polymer degradation and stability. 2019;165:117-25.
[315] Rubino F, Nisticò A, Tucci F, Carlone P. Marine Application of Fiber Reinforced Composites: A Review. Journal of Marine Science and Engineering. 2020;8(1):26.
[316] Gauvin F, Robert M. Durability study of vinylester/silicate nanocomposites for civil engineering applications. Polymer Degradation and Stability. 2015;121:359-68.
[317] Teng J. Performance enhancement of structures through the use of fibre-reinforced polymer (FRP) composites. 2014.

[318] Teng J, Yu T, Dai J, Chen G. FRP composites in new construction: current status and opportunities. Proceedings of 7th National Conference on FRP Composites in Infrastructure (Supplementary Issue of Industrial Construction), keynote presentation2011.

[319] Teng J-G, Xiang Y, Yu T, Fang Z. Development and mechanical behaviour of ultra-high-performance seawater sea-sand concrete. Advances in Structural Engineering. 2019;22(14):3100-20.

[320] Chen GM, Liu PC, Chen JF. Compressive behaviour of sea sand filled CFRP tubular columns. In: Third International Workshop on Seawater Sea-Sand Concrete (SSC) Structures Reinforced with FRP Composites (eds Teng JG, Chen JF, Yu T, et al.), Shenzhen, China. 2020:43-4.

[321] Dong Z, Wu G, Zhao X-L, Zhu H, Lian J-L. The durability of seawater sea-sand concrete beams reinforced with metal bars or non-metal bars in the ocean environment. Advances in Structural Engineering. 2020;23(2):334-47.

[322] Berg AC, Bank LC, Oliva MG, Russell JS. Construction and cost analysis of an FRP reinforced concrete bridge deck. Construction and Building Materials. 2006;20(8):515-26.

[323] Ascione F, Berardi V, Feo L, Giordano A. An experimental study on the long-term behavior of CFRP pultruded laminates suitable to concrete structures rehabilitation. Composites Part B: Engineering. 2008;39(7-8):1147-50.

[324] ElSafty A, Benmokrane B, Rizkalla S, Pour-Ghaz M, Ali AH, Mohamed H, et al. Degradation Mechanisms and Service Life Estimation for Fiber Reinforced Polymer (FRP) Concrete Reinforcements. 2019.

[325] Benmokrane B, Ali AH, Mohamed HM, ElSafty A, Manalo A. Laboratory assessment and durability performance of vinyl-ester, polyester, and epoxy glass-FRP bars for concrete structures. Composites Part B: Engineering. 2017;114:163-74.

[326] Micelli F, Corradi M, Aiello MA, Borri A. Properties of aged GFRP reinforcement grids related to fatigue life and alkaline environment. Applied Sciences. 2017;7(9):897.

[327] Raman R, Guo F, Al-Saadi S, Zhao X-L, Jones R. Understanding fibre-matrix degradation of FRP composites for advanced civil engineering applications: an overview. Corrosion and Materials Degradation. 2020;1(1):27-41.

[328] Bazli M, Zhao X-L, Bai Y, Raman RKS, Al-Saadi S, Haque A. Durability of pultruded GFRP tubes subjected to seawater sea sand concrete and seawater environments. Construction and Building Materials. 2020;245(1).

[329] Standard A. D1141-98: Standard Practice for the Preparation of Substitute Ocean Water. ASTM International, West Conshohocken. 2013.

[330] International A. ASTM G154-16, Standard Practice for Operating Fluorescent Ultraviolet (UV) Lamp Apparatus for Exposure of Nonmetallic Materials. ASTM International West Conshohocken, PA; 2016.
[331] D6944-15(2020) A. Standard Practice for Determining the Resistance of Cured Coatings to Thermal Cycling. ASTM International, West Conshohocken, PA. 2020.
[332] 1504-2 E. EN 1504-2. Products and Systems for the Protection and Repair of concrete Structures. Definitions, Requirements, Quality Control and Evaluation of Conformity – Part 2: surface Protection Systems for Concrete. Brussels: European Committee for Standardization; 2006. 2006.

[333] Karbhari V. E-glass/vinylester composites in aqueous environments: Effects on short-beam shear strength. Journal of Composites for Construction. 2004;8(2):148-56.